

University of Wollongong

Research Online

University of Wollongong Thesis Collection
1954-2016

University of Wollongong Thesis Collections

2016

Di-chromophoric porphyrins: exploring new strategies for enhanced light harvesting and increased photovoltage of dye-sensitized solar cells

Long Zhao

University of Wollongong

Follow this and additional works at: <https://ro.uow.edu.au/theses>

University of Wollongong

Copyright Warning

You may print or download ONE copy of this document for the purpose of your own research or study. The University does not authorise you to copy, communicate or otherwise make available electronically to any other person any copyright material contained on this site.

You are reminded of the following: This work is copyright. Apart from any use permitted under the Copyright Act 1968, no part of this work may be reproduced by any process, nor may any other exclusive right be exercised, without the permission of the author. Copyright owners are entitled to take legal action against persons who infringe their copyright. A reproduction of material that is protected by copyright may be a copyright infringement. A court may impose penalties and award damages in relation to offences and infringements relating to copyright material.

Higher penalties may apply, and higher damages may be awarded, for offences and infringements involving the conversion of material into digital or electronic form.

Unless otherwise indicated, the views expressed in this thesis are those of the author and do not necessarily represent the views of the University of Wollongong.

Recommended Citation

Zhao, Long, Di-chromophoric porphyrins: exploring new strategies for enhanced light harvesting and increased photovoltage of dye-sensitized solar cells, Doctor of Philosophy thesis, School of Chemistry, University of Wollongong, 2016. <https://ro.uow.edu.au/theses/4630>

Research Online is the open access institutional repository for the University of Wollongong. For further information contact the UOW Library: research-pubs@uow.edu.au

**UNIVERSITY OF
WOLLONGONG**



Department of Chemistry

**Di-chromophoric porphyrins: exploring new strategies for enhanced
light harvesting and increased photovoltage of dye-sensitized solar cells**

Long Zhao

Supervisor: Associate Professor Attila J. Mozer

**"This thesis is presented as part of the requirements for the
award of the Degree of
Doctor of Philosophy
of the
University of Wollongong"**

March 2016

ABSTRACT

Although numerous improvements have been achieved in the field of dye-sensitized solar cells (DSSCs), there are still some potential strategies for further development in this technology. In that regard, the most straightforward strategy is to enhance the dye light harvesting properties, in particular, by using low band gap dyes. While such approach would in principle increase the photocurrent, low band gap sensitizers typically yield relatively low photovoltage. This phenomenon is caused by strong intermolecular forces, inherent of low band gap materials. Therefore, to simultaneously increase the photocurrent and photovoltage, new concept of the dye design is required. For instance, a multi-chromophoric dye structure, which is basically a single molecule containing several independent light absorbing units.

Thus, the present thesis concerns with the investigation of different di-chromophoric dyes in DSSCs. As will be shown, these novel dyes can overcome the typical limitations of low band gap dyes in photovoltage, while increasing the photocurrent as a result of the increased light absorption. They not only enhance light absorption and overcome dispersion forces, but also feature other benefits owing to the tri-dimensionality. This is for instance the addition of bulky groups, which can hinder non desired processes such as recombination. The electron lifetimes and consequently the photovoltage of DSSCs increase as a result. Aspects related to the arrangement of the dyes on the photoanode are also benefited from such groups, which enhance the electron injection efficiency and photocurrent. Therefore, in some cases, co-adsorbers such as chenodeoxycholic acid are no longer needed in the di-chromophoric dye sensitization process. The utilization of the cobalt-based electrolyte in DSSCs using di-chromophoric dyes is also investigated in this thesis in terms of photovoltaic performance and dye regeneration. In a specific case, a microsecond component of partial intramolecular hole transfer is observed in a di-chromophoric dye for the first time, and dye regeneration kinetics in this di-chromophoric dye is favoured in respect with the single chromophore of similar driving force.

Attaching an organic chromophore with tuned band gap to extend light absorption of the dyad towards the red may introduce competing electron injection pathways, probing a limitation of di-chromophoric dye using low band gap chromophore. Although the latter effect reduces the photocurrent of DSSCs, the electron lifetimes and photovoltage are

increased. A comparison between di-chromophoric dye and co-sensitization approaches has been carried out. Utilizing intermolecular forces to enhance the electron lifetimes in DSSCs using di-chromophoric dye will be reported for the first time.

Although the power conversion efficiencies of DSSCs using the di-chromophoric dyes still lag behind compared to that of traditional dyes, this thesis provides new prospects in electron transfer mechanisms at the dye-sensitized interfaces. Thus, some of the findings of this work, such as the utilization of dispersion forces and the enhanced dye regeneration kinetics without free energy losses in di-chromophoric dyes, provide new strategies in the further multi-chromophoric dye design. These new insights into the multi-chromophoric dyes behaviour would lead the way to the further development of photovoltaic technology.

ACKNOWLEDGEMENTS

First and foremost, I would like to thank my supervisor A/Prof. A.J. Mozer for his guidance during my PhD thesis. I also would like to thank Dr P. Wagner, who has provided all of the molecules studied in this work. Special thanks as well to Prof. K. C. Gordon and his group (University of Otago) for theoretical calculations. And at last but not least, many thanks to A/Prof. S. Mori (Shinshu University), Dr T. M. Clarke, Dr K. Wagner, Dr A. Nattestad, Dr M. Griffith and others from IPRI photovoltaic group for their fruitful discussions and assistance.

TABLE OF CONTENTS

ABSTRACT.....	i
ACKNOWLEDGEMENTS	iii
TABLE OF CONTENTS	iv
PUBLICATIONS AND PRESENTATIONS	xi
LIST OF FIGURES	xiii
LIST OF TABLES	xxi
LIST OF ABBREVIATIONS	xxiii
CHAPTER 1. INTRODUCTION	1
1.1. Motivation of this study	2
1.2. Scope of this study	4
1.3. Dye-sensitized solar cells (DSSCs).....	9
1.3.1 Design considerations for efficient sensitizers.....	11
1.4. Porphyrins as sensitizers	12
1.4.1 Free-base versus metal complexes.....	15
1.4.2 β -linked versus meso-linked porphyrins	15
1.4.3 Absorption spectrum	16
1.4.4 Single chromophoric porphyrins.....	17
1.4.5 Multi-chromophoric porphyrins.....	20
1.5. Design considerations of additional chromophores	22
1.6. Switch from I^-/I_3^- to Co^{2+}/Co^{3+}	24
1.7. Electron transfer steps in multi-chromophoric DSSCs	25
1.8. Electron injection	27
1.8.1 Physical description	27
1.8.2 Factors affecting electron injection.....	27
1.8.3 Experimental techniques	29
1.9. Förster resonance energy transfer.....	29
1.10. Electron lifetime	31
1.10.1 Physical description	32

1.10.2	Factors affecting electron lifetime	33
1.10.3	Experimental techniques	39
1.10.4	Background of SLIM-PCV measurements	40
1.11.	Dye regeneration	43
1.11.1	Physical description	43
1.11.2	Factors affecting dye regeneration	43
1.11.3	Experimental techniques	45
1.11.4	Conduction band electrons-dye cation recombination	48
1.11.5	Intramolecular hole transfer	49
1.12.	Collaborators contribution	49
1.13.	Summary	50
1.14.	References	51
CHAPTER 2.	EXPERIMENTAL	68
2.1.	Reagents and materials	69
2.2.	Characterization of molecules	70
2.2.1	UV-visible absorption	70
2.2.2	Photoluminescence	70
2.2.3	Electrochemistry	70
2.2.4	Spectroelectrochemistry	72
2.3.	Dye-sensitized solar cells fabrication	74
2.3.1	Photoanode preparation	74
2.3.2	Counter electrode fabrication	75
2.3.3	Device assembling	76
2.4.	Dye-sensitized solar cells characterization	77
2.4.1	Current density-voltage measurements	77
2.4.2	Incident photon-to-current conversion efficiency	77
2.4.3	Light harvesting efficiency measurements	79
2.4.4	Absorbed photon-to-current conversion efficiency calculation	79

2.4.5	Electron lifetime and transport in TiO ₂ films.....	80
2.4.6	Dye loading measurement.....	82
2.5.	Transient absorption spectroscopy	82
2.5.1	INDI laser.....	83
2.5.2	Ekspla laser	84
2.6.	References	85
CHAPTER 3. THREE FAMILIES OF DI-CHROMOPHORIC DYES.....		86
3.1.	Introduction	87
3.2.	Differential pulse voltammetry and energy levels of the three families	89
3.3.	UV-visible absorption	93
3.4.	Photovoltaic performance: current-voltage curves and incident photon-to-current conversion efficiency.....	97
3.5.	Summary and outline of subsequent chapters	103
3.6.	References	104
CHAPTER 4. EFFECT OF ORGANIC CHROMOPHORE SUBSTITUTION ON THE OPTICAL AND ELECTRONIC PROPERTIES OF PORPHYRIN CARBAZOLE DI-CHROMOPHORIC DYES		106
4.1.	Introduction	107
4.2.	Experimental	108
4.2.1	Investigated molecules	108
4.2.2	Spectroscopic and electrochemical characterization.....	108
4.2.3	DSSC fabrication and characterization	108
4.3.	Light absorption in solutions	110
4.4.	Effect of the carbazole substitution on the electrochemical properties of the dyes	113
4.5.	Simultaneously enhanced photocurrent and photovoltage in DSSCs	116
4.6.	Incident photon-to-current conversion efficiency	119
4.7.	Light harvesting efficiency and dye aggregation	120
4.8.	Absorbed photon-to-current conversion efficiency.....	122
4.9.	Increased open circuit voltage using carbazole substituted porphyrin di-chromophoric dyes.....	128

4.10. Conclusions	129
4.11. References	130
CHAPTER 5. FILLING THE ABSORPTION GAP OF PORPHYRIN BY	
CARBAZOLE-FUSED THIOPHENE-SUBSTITUTED DI-CHROMOPHORIC DYES	
AND THE UTILITY OF COBALT ELECTROLYTE	
5.1. Introduction	133
5.2. Experimental	137
5.2.1. Investigated molecules	137
5.2.2. Spectroscopic and electrochemical characterization.....	137
5.2.3. DSSC fabrication and characterization	137
5.3. Light absorption in solution: “filling the gap”	138
5.4. Effect of the carbazole-fused thiophene chromophores on the oxidation and reduction potentials of the di-chromophoric dyes.....	141
5.5. Enhanced photocurrent and photovoltage in DSSCs: The effect of filling the gap	143
5.5.1. Optimization of DSSC fabrication conditions and comparison of iodine / triiodide and cobalt electrolytes	144
5.5.2. Comparison of PorO dyes in DSSC using optimized $\text{Co(dmbpy)}_3^{2+}/\text{Co(dmbpy)}_3^{3+}$ conditions.....	146
5.6. Origin of lower than expected photocurrent.....	149
5.6.1. Incident photon-to-current conversion efficiency	150
5.6.2. Light harvesting efficiency	150
5.6.3. Absorbed photon-to-current conversion efficiency	151
5.6.4. Evidence of charge collection loss in Por-sensitized solar cells using cobalt electrolyte	152
5.6.5. Analysis of the electron injection efficiency.....	153
5.6.6. Insufficient driving force for electron injection	155
5.7. Increased open circuit voltage using carbazole-fused thiophene substituted porphyrin di-chromophoric dyes.....	158
5.8. Conclusions	158

5.9. References	159
CHAPTER 6. A CARBAZOLE-THIOPHENE BENZOTHIADIAZOLE	
THIOPHENE PORPHYRIN: COMPARISON TO SINGLE CHROMOPHORIC DYES	
AND MIXED DYES	162
6.1. Introduction	163
6.2. Experimental	165
6.2.1 Investigated molecules	165
6.2.2 Spectroscopic and electrochemical characterization.....	166
6.2.3 DSSC fabrication and characterization	166
6.3. Purpose one: a comparison to single chromophoric dyes	167
6.3.1 Light absorption in solution	167
6.3.2 Electrochemistry	167
6.3.3 Decreased photovoltaic performance of DSSC using PorR.....	170
6.3.4 Analysis of the photocurrent difference	172
6.3.5 Reduced APCE of DSSC using PorR	174
6.4. Purpose two: a comparison to mixed dyes	177
6.4.1 Light absorption in solution and on TiO ₂ film.....	177
6.4.2 Decreased photocurrent but increased photovoltage of DSSC using PorR ..	
.....	178
6.4.3 Analysis of the photocurrent difference	179
6.5. Analysis of the photovoltage	182
6.6. Conclusions	183
6.7. References	184
CHAPTER 7. PHOTOLUMINESCENCE STUDIES OF DI-CHROMOPHORIC	
PORPHYRIN DYES.....	186
7.1. Introduction	187
7.2. Experimental	190
7.2.1 Investigated molecules	190
7.2.2 Spectroscopic characterization.....	191
7.3. Energy levels of the investigated compounds	192

7.4. Photoluminescence studies of PorY / PorO dyes: energy transfer from the organic chromophore to the porphyrin.....	193
7.4.1 PorY dyes	193
7.4.2 PorO dyes	196
7.5. Photoluminescence of PorR: electron transfer from the porphyrin to the organic chromophore	200
7.6. Correlating photoexcitation pathways with injection efficiency using absorbed photon-to-current conversion measurements	204
7.7. Conclusions	206
7.8. References	207
CHAPTER 8. ENHANCED PHOTOVOLTAGE BY BLOCKING EFFECT AND INTERMOLECULAR FORCES IN DI-CHROMOPHORIC DYE-SENSITIZED SOLAR CELLS	
8.1. Introduction	210
8.2. Experimental	211
8.2.1 Investigated molecules	211
8.2.2 DSSC fabrication and characterization	211
8.3. Photovoltage and photocurrent transients and the calculation of electron lifetime / diffusion coefficient.....	212
8.4. Origin of increased photovoltage of the PorY dyes	217
8.5. Conduction band variation between the iodine and cobalt electrolytes	219
8.6. Origin of increased photovoltage of the PorO dyes	220
8.7. Blocking effect of the PorY and PorO dyes	222
8.8. Similar photovoltage of PorR and Por	224
8.9. Origin of increased photovoltage of PorR compared to mixed dyes.....	225
8.10. Utilization of intermolecular forces by PorR	227
8.11. Conclusions	230
8.12. References	231
CHAPTER 9. FASTER DYE CATION REGENERATION IN DI-CHROMOPHORIC PORPHYRIN DYE DESIGN	
9.1. Introduction	235
9.2. Experimental	237

9.2.1	Investigated molecules	237
9.2.2	Characterization in solution	237
9.2.3	Transient absorption spectroscopy on dyed TiO ₂ films	237
9.3.	Oxidation potentials of the dyes in solution	239
9.4.	Absorption spectrum of the electrochemically generated dye cation radicals in solution.....	239
9.5.	Absorption spectrum of photogenerated dye cation radicals on TiO ₂ electrodes using transient absorption spectroscopy.....	242
9.6.	Intramolecular hole transfer in PorY1	245
9.7.	Conduction band electrons - dye cation recombination in di-chromophoric design	248
9.8.	Faster dye cation regeneration using the iodine-based electrolyte in PorY1 / TiO ₂	249
9.8.1	Redox couple concentration dependence	251
9.8.2	Faster regeneration rate of PorY1 than Por.....	254
9.9.	Faster dye cation regeneration using the cobalt-based electrolyte using the di-chromophoric design.....	256
9.9.1	Redox couple concentration dependence	258
9.9.2	Faster regeneration of PorY1 than Por.....	262
9.10.	Comparison of regeneration rate between iodine- and cobalt-based electrolytes	263
9.11.	Conclusions	264
9.12.	References	266
CHAPTER 10.	CONCLUSIONS AND OUTLOOK	268
10.1.	Conclusions	269
10.2.	Outlook.....	271
APPENDIX	274

PUBLICATIONS AND PRESENTATIONS

Publications

1. Zhao, L.; Wagner, P.; Elliott, A. B. S.; Griffith, M. J.; Clarke, T. M.; Gordon, K. C.; Mori, S.; Mozer, A. J. Enhanced Performance of Dye-Sensitized Solar Cells Using Carbazole-Substituted Di-Chromophoric Porphyrin Dyes. *J. Mater. Chem. A* 2014, 2, 16963-16977.
2. Zhao, L.; Wagner, P.; van der Salm, H.; Clarke, T. M.; Gordon, K. C.; Mori, S.; Mozer, A. J. Dichromophoric Zinc Porphyrins: Filling the Absorption Gap between the Soret and Q Bands. *J. Phys. Chem. C* 2015, 119, 5350-5363.
3. Zhao, L.; Wagner, P.; van der Salm, H.; Gordon, K. C.; Mori, S.; Mozer, A. J. Enhanced Electron Lifetimes in Dye-Sensitized Solar Cells Using a Di-chromophoric Porphyrin: the Utility of Inter-molecular Forces. *ACS. Appl. Mater. Interfaces*. 2015, 7, 22078–22083
4. Ahmed, R.; Zhao, L.; Mozer, A. J.; Will, G.; Bell, J.; Wang, H. Enhanced Electron Lifetime of CdSe/CdS Quantum Dot (QD) Sensitized Solar Cells Using ZnSe Core–Shell Structure with Efficient Regeneration of Quantum Dots. *J. Phys. Chem. C* 2015, 119, 2297-2307.
5. Lin, J.; Zhao, L.; Heo, Y.-U.; Wang, L.; Bijarbooneh, F. H.; Mozer, A. J.; Nattestad, A.; Yamauchi, Y.; Dou, S. X.; Kim, J. H. Mesoporous Anatase Single Crystals for Efficient Co(2+/3+)-Based Dye-Sensitized Solar Cells. *Nano Energy* 2015, 11, 557-567.
6. Zhao, L.; Wagner, P.; Clarke, T. M.; Gordon, K. C.; Mori, S.; Mozer, A. J. Enhancement of Dye Regeneration Kinetics in Di-chromophoric Porphyrin - Carbazole Triphenylamine Dyes Influenced by More Exposed Radical Cation Orbitals. *Chem. Sci.* Accepted. DOI: 10.1039/C6SC00429F, Edge Article.
7. Zhao, L.; Wagner, P.; Clarke, T. M.; Gordon, K. C.; Mori, S.; Mozer, A. J. Effect of Energy and Electron Transfer on Photoelectron Injection Efficiency of Di-chromophoric Porphyrins in Dye-Sensitized Solar Cells (DSSCs). In preparation.

Oral presentations

1. Zhao, L.; Wagner, P.; Clarke, T. M.; Gordon, K. C.; Mori, S.; Mozer, A. J. Porphyrin arrays: Towards 3-D light harvesting. Department of Chemistry – IPRI conference, Nowra, Australia, Oct. 2012,

2. Zhao, L.; Wagner, P.; Clarke, T. M.; Gordon, K. C.; Mori, S.; Mozer, A. J. High efficiency carbazole zinc-porphyrin dyads (Ca-ZnPs) for dye-sensitized solar cells. Dyesol Company, Canberra, Australia, Mar. 2013.
3. Zhao, L.; Wagner, P.; Clarke, T. M.; Gordon, K. C.; Mori, S.; Mozer, A. J. Carbazole derivative zinc porphyrin dyes (Cb-ZnPs) for dye-sensitized solar cells (DSSCs). ACES full centre meeting / Ethics workshop, Hobart, Australia, June 2013.
4. Zhao, L.; Wagner, P.; Clarke, T. M.; Gordon, K. C.; Mori, S.; Mozer, A. J. Charge generation, transport and recombination in di-chromophoric porphyrin-sensitized solar cells. The 7th Advanced Materials & Nanotechnology conference (AMN7), Nelson, New Zealand, Feb. 2015.

Posters

1. Zhao, L.; Wagner, P.; Clarke, T. M.; Gordon, K. C.; Mori, S.; Mozer, A. J. High efficiency carbazole-zinc-porphyrin dyads for dye-sensitized solar cells. ACES full centre meeting, Wollongong, Australia, Feb. 2013.
2. Zhao, L.; Wagner, P.; Clarke, T. M.; Gordon, K. C.; Mori, S.; Mozer, A. J. Interfacial electron transfer kinetics in carbazole zinc porphyrin dyads. ACES full centre meeting, Wollongong, Australia, Feb. 2014.

LIST OF FIGURES

Figure 1.1 Illustration of reduced photovoltage of two D- π -A porphyrins with decreased band gap.	3
Figure 1.2 The porphyrin dyad P10.	5
Figure 1.3 The di-chromophoric dyes studied in this thesis	6
Figure 1.4 The possible electron / energy transfer processes in a di-chromophoric dye D1-D2.....	8
Figure 1.5 Intramolecular charge transfer according to the energy levels.	9
Figure 1.6 Operational mechanism of a dye-sensitized solar cell and the possible electron transfer processes at the electrolyte/dye/TiO ₂ interface.....	10
Figure 1.7 Structures of the single chromophoric porphyrin YD0 and the diporphyrins YDD0-YDD3 and their light absorption spectra.	14
Figure 1.8 Chemical structures of GD2 and P199.	16
Figure 1.9 An example UV-visible absorption spectrum of 5,10,15,20-tetrarylporphyrinato zinc (II) (ZnPor) in solution.....	17
Figure 1.10 Structures of some single chromophoric porphyrins.....	19
Figure 1.11 Structures of some multi-chromophoric porphyrins.....	21
Figure 1.12 Record power conversion efficiencies of DSSCs using single chromophoric porphyrins and multi-chromophoric porphyrins from 1993 to 2014.	22
Figure 1.13 Intramolecular charge transfer and energy transfer in a porphyrin trimer after photoexcitation.....	26
Figure 1.14 A Jablonski diagram	30
Figure 1.15 An illustration of Förster resonance energy transfer from an energy donor to an energy acceptor.....	31
Figure 1.16 The relationship of the parameters in describing electron lifetime and electron diffusion. (a)electron density against open circuit voltage by charge extraction measurement and (b) electron lifetime or electron diffusion coefficient against electron density by small perturbation measurements.	33
Figure 1.17 Illustration of the effect of diffusion coefficient on the electron lifetime ...	34
Figure 1.18 Molecular structure effects on the TiO ₂ (e ⁻)-I ₃ ⁻ recombination process at the TiO ₂ surface.	38

Figure 1.19 Scheme of stepped light-induced transient measurements of photocurrent and voltage.	41
Figure 1.20 Illustration of the mechanism of diffusion coefficient measurement under short circuit condition	42
Figure 1.21 Illustration of the mechanism of electron lifetime measurement under open circuit condition	42
Figure 1.22 Scheme of charge extraction measurement.	43
Figure 1.23 Principle of transient absorption spectroscopy measurement using pump / probe system. (a) the energy levels of the molecule and (b) the response curve of the measurement.	46
Figure 2.1 Differential pulse voltammetry (DPV) and cyclic voltammetry (CV) curves of the freshly prepared Fc/Fc ⁺ redox couple in DCM solution with 0.1 M TBAP using 100 mV s ⁻¹ scan rate.	72
Figure 2.2 An illustration of spectroelectrochemical (SEC) measurement.	73
Figure 2.3 Differential pulse voltammetry of the freshly prepared Fc/Fc ⁺ redox couple in DMF with 0.1 M TBAP using different scan rates.	73
Figure 2.4 Dye-sensitized solar cells (DSSCs) fabrication process diagram.	74
Figure 2.5 Comparison of the Newport and QEX10 IPCE measurement systems. Reference sensitizer: PorR on 2.6 μm TiO ₂ films.	78
Figure 2.6 A diagram for electron lifetime and diffusion coefficient measurements.	80
Figure 2.7 A diagram for switch controlled electron density measurement	81
Figure 2.8 A diagram for shutter controlled electron density at short circuit condition measurement	82
Figure 2.9 A diagram of the dye cation spectrum measurement.	83
Figure 2.10 A diagram of the dye cation kinetics measurement.	84
Figure 3.1 Concept of the di-chromophoric dyes.	89
Figure 3.2 (a) Differential pulse voltammograms and (b) calculated energy levels of the compounds vs. vacuum.	92
Figure 3.3 Molar extinction coefficient (ε) of the compounds measured in DMF.	94
Figure 3.4 FT-Raman (λ _{ex} = 1064 nm, black) and resonance Raman (1 mM CH ₂ Cl ₂ solution, λ _{ex} = 351-448 nm with colours of violet, blue, cyan, green and olive, subsequently) spectra of PorY1 and non-resonant (830 nm, red colour) Raman spectrum of Cb1. Performed by collaborator Prof. Keith C. Gordon.	96

Figure 3.5 Current density-voltage (J - V) curves of DSSCs with the dyes fabricated using thin films under AM 1.5 illumination (solid lines) and in the dark (dashed lines).	97
Figure 3.6 Incident photon-to-current conversion efficiency (IPCE) spectra of the dyes using thin films.	98
Figure 3.7 J - V curves of DSSCs with the dyes fabricated using thick films under AM 1.5 illumination (solid lines) and in the dark (dashed lines).	99
Figure 3.8 IPCE spectra of the dyes using thick films.	102
Figure 4.1 Molar extinction coefficient of the compounds measured in (a) DCM; (b) DMF	111
Figure 4.2 Differential pulse voltammograms of the investigated compounds, (a) negative scan; (b) positive scan.	114
Figure 4.3 Current density-voltage (J - V) curves of DSSCs with the porphyrin dyes fabricated using (a) thin films: $2.2 \pm 0.1 \mu\text{m}$, and thick films: (b) $6 \mu\text{m}$ transparent + $3.2 \mu\text{m}$ scattering TiO_2 , (c) $12 \mu\text{m}$ transparent + $5.5 \mu\text{m}$ scattering TiO_2 , under AM 1.5 illumination (solid lines) and in the dark (dashed lines).	118
Figure 4.4 IPCE spectra of the devices fabricated from the porphyrin dyes on thin TiO_2 films.	119
Figure 4.5 LHE spectra of the porphyrin dyes on thin TiO_2 films.	121
Figure 4.6 Normalized visible absorption spectra at the Q bands of some porphyrins in different solvents.	122
Figure 4.7 APCE spectra of the devices fabricated from the porphyrin dyes on thin TiO_2 films. The inset shows the dye loading.	123
Figure 4.8 Energy level diagram of the compounds.	125
Figure 4.9 IPCE/LHE/APCE spectra of devices fabricated from two dyes with CDCA in dye solution.	127
Figure 4.10 An illustration of the main findings of the chapter.	129
Figure 5.1 Concept of filling the “absorption gap” using the di-chromophoric design.	134
Figure 5.2 Molar extinction coefficient of (a) the carbazole-fused thiophene chromophores and (b) the porphyrins measured in DMF. The 450-550 nm wavelength range was shadowed.	140
Figure 5.3 Differential pulse voltammograms of the PorO dyes and the organic chromophores, (a) positive scan; (b) negative scan.	141

Figure 5.4 Positive scan DPV plots of the PorO dyes dissolved in DMF.....	143
Figure 5.5 Current density-voltage (<i>J</i> - <i>V</i>) curves of DSSCs with the porphyrin dyes fabricated using (a) $2.9\pm0.1\ \mu\text{m}$ transparent and (b) $7.4\pm0.5\ \mu\text{m}$ with $5\ \mu\text{m}$ transparent + $2.5\ \mu\text{m}$ scattering TiO_2 under AM 1.5 illumination (solid lines) and in the dark (dashed lines).....	148
Figure 5.6 IPCE spectra of the devices fabricated from the porphyrin dyes on thin TiO_2 films.	150
Figure 5.7 LHE spectra of the porphyrin dyes on thin TiO_2 films.....	151
Figure 5.8 APCE spectra of the devices fabricated from the porphyrin dyes on thin TiO_2 films.	152
Figure 5.9 Energy level diagram of the compounds.	154
Figure 5.10 (a) IPCE, (b) LHE and (c) APCE spectra of devices fabricated from PorO2 with and without <i>t</i> BP in the cobalt electrolyte and MK2 on thin TiO_2 films.....	156
Figure 5.11 An illustration of the effect of removal <i>t</i> BP on electron injection.	157
Figure 5.12 (a) IPCE, (b) LHE and (c) APCE spectra of devices fabricated from PorO1-3 without <i>t</i> BP in the cobalt electrolyte on thin TiO_2 films.....	157
Figure 6.1 The relative energy levels of the porphyrin (Por) and the organic chromophore (Cb, CbTh and CbBTD1) in the three families of di-chromophoric dyes.	164
Figure 6.2 Molar extinction coefficient (ϵ) of the individual dyes measured in THF. .	167
Figure 6.3 Differential pulse voltammograms of the compounds, (a) positive scan; (b) negative scan.	168
Figure 6.4 Energy level diagram of the compounds.	170
Figure 6.5 Current density-voltage (<i>J</i> - <i>V</i>) curves of DSSCs using the investigated sensitizers under AM 1.5 illumination (solid lines) and in the dark (dashed lines) fabricated with $2.0\pm0.1\ \mu\text{m}$ thick films.....	171
Figure 6.6 (a) Incident photon to converted electron (IPCE), (b) Light harvesting efficiency (LHE) and (c) Absorbed photon to collected electron (APCE) spectra of the DSSCs using the investigated sensitizers on $2.0\pm0.1\ \mu\text{m}$ films.....	174
Figure 6.7 Illustration of two competing electron transfer pathways in PorR DSSCs.	175
Figure 6.8 (a) Current density-voltage curves and (b) IPCE spectra of DSSCs using PorR using the standard electrolyte and the electrolyte without <i>t</i> BP inside fabricated with $7.4\pm0.5\ \mu\text{m}$ thick films.....	176

Figure 6.9 (a) Molar extinction coefficient of PorR and the mixed dyes measured in THF and (b) Absorption of the sensitizers on 2.0 ± 0.1 μm TiO_2 films.	178
Figure 6.10 Current density-voltage curves of DSSCs using PorR and mixed dyes under AM 1.5 illumination (solid lines) and in the dark (dashed lines) fabricated with 2.0 ± 0.1 μm thick films.	179
Figure 6.11 (a) Incident photon to converted electron, (b) Light harvesting efficiency and (c) Absorbed photon to collected electron spectra of the DSSCs using PorR and mixed dyes on 2.0 ± 0.1 μm films.....	182
Figure 7.1 Illustration of (a) energy transfer from D2^* to D1 and (b) the effect on absorbed photon-to-current conversion efficiency of a di-chromophoric dye-sensitized solar cell.	189
Figure 7.2 Energy level diagram of the compounds derived from the peak potentials of differential pulse voltammograms.....	193
Figure 7.3 Absorbance (Abs.) of (a) Por, Cb1, Cb2 and (c) and PorY1, PorY2 and photoluminescence (PL) spectra of (b) Por, Cb1, Cb2 and (d) PorY1, PorY2 in DMF with 1 μM concentration.	195
Figure 7.4 Graphical illustration of the deexcitation pathways in PorY dyes photoexcited at 280 nm and 560 nm.	196
Figure 7.5 Absorbance of (a) the carbazole-fused thiophene chromophores and (c) the PorO dyes and photoluminescence spectra of (b) the carbazole-fused thiophene chromophores and (d) the PorO dyes on 280 nm excitation in DMF with 1 μM concentration.	198
Figure 7.6 Photoluminescence intensities measured by photoexcitation of PorO1-3, CbTh1-3 and Por dissolved in DMF with 1 μM concentration at (a) 480 nm and (b) 560 nm.....	199
Figure 7.7 Graphical illustration of the deexcitation pathways in PorO dyes photoexcited at 280 nm, 480 nm and 560 nm.	199
Figure 7.8 Photoluminescence intensities measured by photoexcitation of PorR and CbBTD-OH dissolved in DMF with 1 μM concentration at 560 nm.	200
Figure 7.9 (a) Absorbance and photoluminescence spectra with (b) 480 nm and (c) 560 nm excitation of PorR and the counterparts in THF with 1 μM concentration.	203
Figure 7.10 Graphical illustration of the deexcitation pathways in PorR photoexcited at 480 nm and 560 nm.....	203

Figure 7.11 Absorbed photon-to-current conversion efficiency (APCE) spectra of the representative dyes using the same iodine-based electrolyte using thin films.....	205
Figure 7.12 Possible energy / electron transfer at the sensitizer/TiO ₂ interface of the three families of di-chromophoric dyes.	206
Figure 8.1 Illustration of enhanced photovoltage by the DSSCs using PorY, PorO and PorR dyes.	211
Figure 8.2 Open circuit voltage decay after stepwise reduction of laser intensity. Four laser intensities were employed: 3.1 V, 2.3 V, 2.0 V and 1.93 V.....	213
Figure 8.3 Short circuit current decay after stepwise reduction of laser intensity. Four laser intensities were employed: 3.1 V, 2.3 V, 2.0 V and 1.93 V.....	214
Figure 8.4 Current decay in the charge extraction measurement. Four laser intensities were employed: 3.1 V, 2.3 V, 2.0 V and 1.93 V.....	215
Figure 8.5 (a) Electron lifetime and (c) diffusion coefficient versus short circuit current density, (b) electron lifetime and (d) open circuit voltage versus electron density for N719-sensitized solar cell using the I ⁻ /I ₃ ⁻ electrolyte. The slope values as well as the calculated parameters are shown in the inset. Film thickness: 2.2 μm.	217
Figure 8.6 (a) Electron lifetime and (c) diffusion coefficient versus short circuit current density, (b) electron lifetime and (d) open circuit voltage versus electron density for DSSCs using Por, PorY1-5 and N719 using the I ⁻ /I ₃ ⁻ electrolyte (two samples for each dye). Film thickness: 2.0±0.1 μm.	218
Figure 8.7 (a) Electron lifetime and (c) diffusion coefficient versus short circuit current density, (b) electron lifetime and (d) open circuit voltage versus electron density for DSSCs using Por using both the I ⁻ /I ₃ ⁻ and the cobalt electrolytes (two samples for each dye). Film thickness: 2.9±0.1 μm.	220
Figure 8.8 (a) Electron lifetime and (c) diffusion coefficient versus short circuit current density density, (b) electron lifetime and (d) open circuit voltage versus electron density for DSSCs using Por, Por1-3 and MK2 using the cobalt electrolyte (two samples for each dye). Film thickness: 2.9±0.1 μm.	222
Figure 8.9 Illustration of the blocking effect in the di-chromophoric porphyrins.	224
Figure 8.10 (a) Electron lifetime and (b) open circuit voltage versus electron density for DSSCs using Por and PorR (four samples for each dye). Film thickness: 2.3±0.1 μm.	225

Figure 8.11 (a) Electron lifetime and (c) diffusion coefficient versus short circuit current density, (b) electron lifetime and open circuit voltage versus electron density for the DSSCs using the investigated sensitizers (two samples for each dye). Film thickness: $2.0 \pm 0.1 \mu\text{m}$	227
Figure 8.12 (a) Electron lifetime and (c) diffusion coefficient versus short circuit current density, (b) electron lifetime and open circuit voltage versus electron density for DSSCs using Por and PorR with different dye loadings. Film thickness: $2.8 \pm 0.1 \mu\text{m}$	229
Figure 8.13 Graphical illustration of the blocking effect in Por and blocking effect + dispersion forces in PorR at full and reduced dye loadings.	230
Figure 9.1 Illustration of the purpose of this chapter.	236
Figure 9.2 Differential pulse voltammetry and the oxidation energy levels of the investigated compounds measured in dichloromethane.	239
Figure 9.3 Spectroelectrochemical (SEC) spectra of (a) Por, (b) Cb1 and (c) PorY1 at different oxidation potentials vs. Fc/Fc^+	242
Figure 9.4 Transient absorption spectra of (a) Por and (b) PorY1 on TiO_2 film with the inert electrolyte (I_0) at different time scales after pulsed 532 nm laser irradiation.	243
Figure 9.5 Transient absorption spectra of (a) Por and (b) PorY1 on TiO_2 film with the redox electrolyte (0.1 M LiI) at different time scales after pulsed 532 nm laser irradiation.	244
Figure 9.6 Time-resolved transient absorption decay and fitted curves of PorY1 / TiO_2 using I_0 after pulsed 532 nm laser irradiation.	246
Figure 9.7 Illustration of partial intramolecular hole transfer in PorY1 / TiO_2 after pulsed 532 nm laser irradiation.	246
Figure 9.8 Time-resolved transient absorption decay and fitted curves of the reduced dye and CDCA-introduced PorY1-sensitized TiO_2 film using I_0 after pulsed 532 nm laser irradiation.	247
Figure 9.9 Time-resolved transient absorption decay and fitted curves of (a) Por / TiO_2 and (b) PorY1 / TiO_2 using I_0 after pulsed 532 nm laser irradiation.	249
Figure 9.10 Time-resolved transient absorption decay and fitted curves of (a) Por / TiO_2 and (b) PorY1 / TiO_2 using 0.1 M LiI (I_1) after pulsed 532 nm laser irradiation.	250
Figure 9.11 Time-resolved transient absorption decay and fitted curves of Por / TiO_2 using the five I^-/I_3^- electrolyte conditions after pulsed 532 nm laser irradiation probing at 800 nm. (a) 0.1 M LiI, (b) 0.01 M LiI, (c) 0.001 M LiI, (d) 0.0001 M LiI and (e) I_0	252

Figure 9.12 Time-resolved transient absorption decay and fitted curves of PorY1 / TiO ₂ using the five I ⁻ /I ₃ ⁻ electrolytes after pulsed 532 nm laser irradiation, probing at 1200 nm and 800 nm, respectively. (a) 0.1 M LiI, (b) 0.01 M LiI, (c) 0.001 M LiI, (d) 0.0001 M LiI and (e) I ₀	253
Figure 9.13 Regeneration rate constant of Por and PorY1 on TiO ₂ films using different concentrated I ⁻ /I ₃ ⁻ electrolytes.	255
Figure 9.14 Time-resolved transient absorption decay and fitted curves of (a) Por / TiO ₂ and (b) PorY1 / TiO ₂ using 0.11 M Co(dmbpy) ₃ ²⁺ (Co_1) after pulsed 532 nm laser irradiation.	257
Figure 9.15 Time-resolved transient absorption decay and fitted curves of Por / TiO ₂ using the five cobalt electrolyte conditions after pulsed 532 nm laser irradiation probing at 800 nm. (a) 0.11 M Co(dmbpy) ₃ ²⁺ , (b) 0.011 M Co(dmbpy) ₃ ²⁺ , (c) 0.0011 M Co(dmbpy) ₃ ²⁺ , (d) 0.00011 M Co(dmbpy) ₃ ²⁺ and (e) Co_0.	259
Figure 9.16 Time-resolved transient absorption decay and fitted curves of PorY1 / TiO ₂ using the five cobalt electrolyte conditions after pulsed 532 nm laser irradiation probing at 1200 nm and 800 nm, respectively. (a) 0.11 M Co(dmbpy) ₃ ²⁺ , (b) 0.011 M Co(dmbpy) ₃ ²⁺ , (c) 0.0011 M Co(dmbpy) ₃ ²⁺ , (d) 0.00011 M Co(dmbpy) ₃ ²⁺ and (e) Co_0.	261
Figure 9.17 Regeneration rate constant of Por and PorY1 on TiO ₂ with different concentrated cobalt electrolytes.	263
Figure 9.18 Regeneration rate constant of Por and PorY1 on TiO ₂ with the I ⁻ /I ₃ ⁻ and cobalt electrolytes.	266
Figure 10.1 Summary of the main findings using di-chromophoric dyes in dye-sensitized solar cells in this thesis	269
Figure 10.2 Molecular structures of further (a) triads and (b) tetrads.	272

LIST OF TABLES

Table 2.1 Reagents and materials information in the study	69
Table 2.2 Solvent and immersing time used for dye sensitization.....	76
Table 3.1 Photovoltaic performance of the sensitizers using both thin and thick films. Device numbers: thin films (3, averaged) and thick films (2, the better ones are shown)	100
Table 3.2 List of topic and questions investigated in the following chapters	104
Table 4.1 Molecular structures of the investigated compounds.....	107
Table 4.2 Oscillator strength (<i>f</i>) of UV-visible absorption spectra of porphyrins in both DCM and DMF.	112
Table 4.3 Electrochemical properties and estimated band gaps of the investigated compounds	115
Table 4.4 Performance of thin film devices (averaged three devices) with porphyrin dyes compared with N719.....	118
Table 4.5 Photocurrent deduced from IPCE in terms of five spectral ranges.....	120
Table 4.6 <i>J-V</i> performance and dye loading of devices fabricated using PorY3 compared to Por in different solvent conditions	128
Table 5.1 Molecular structures of compounds	136
Table 5.2 Summary of spectral and electrochemical data of the compounds.....	142
Table 5.3 DSSCs performance - different dye-sensitization solvents and thickness of TiO ₂ films using the I ⁻ /I ₃ ⁻ electrolyte	145
Table 5.4 DSSCs performance - optimizing the Co(dmbpy) ₃ ²⁺ /Co(dmbpy) ₃ ³⁺ electrolyte	146
Table 5.5 <i>J-V</i> performance of two 2.9 μm thick film devices with porphyrin dyes compared with MK2	148
Table 5.6 <i>J-V</i> performance of three 7.4 μm thick film devices with porphyrin dyes compared with MK2 (two devices).....	148
Table 6.1 Molecular structures of the investigated sensitizers	165
Table 6.2 Summary of spectral and electrochemical data of the compounds.....	168
Table 6.3 Photovoltaic performance of the devices fabricated by the investigated sensitizers	171

Table 6.4 Photovoltaic performance of the devices fabricated by PorR and mixed dyes	179
Table 7.1 Molecular structures of the compounds	190
Table 9.1 Molecular structures of the investigated compounds.....	236
Table 9.2 Electrolytes nomination and components	238

LIST OF ABBREVIATIONS

$^{\circ}\text{C}$	Degree Celcius
μm	micrometre
μM	micromolar
μs	microsecond
Abs.	Absorbance
AC	Alternating current
A_D	The absorbance of dye-sensitized TiO_2 film
A_E	The absorbance of the electrolyte
AM	Air mass
AN	Acetonitrile
APCE	Absorbed photon-to-current conversion efficiency
β	Stretching parameter; trap distribution parameter
CDCA	Chenodeoxycholic acid
CE	Counter electrode
CT	Charge transfer
CV	Cyclic voltammetry
D	Electron diffusion coefficient
D^*	Electronic excited state
D^+	Dye cation
$\text{D}^{\bullet+}$	Dye radical cation
DC	Direct current
DCM	Dichloromethane
DFT	Density functional theory
DMF	Dimethylformamide
DMPII	1,2-dimethyl-3-propylimidazolium iodide
DPO	Digital phosphor oscilloscope
DPV	Differential pulse voltammetry
DSSC	Dye-sensitized solar cell
D- π -A	Donor- π -bridge-acceptor
E_{CB}	Conduction band edge potential
E_{coll}	Electron collection efficiency
ED / n	Electron density
ED_{sc}	Electron density at short circuit condition
EDR	Conduction band electron-dye cation recombination
E_{ele}	Redox couple potential
EER	Conduction band electron-oxidized species in electrolyte recombination
E_{inj}	Electron injection efficiency
EIS	Electrochemical impedance spectroscopy
E_{Ox}	Energy levels of oxidation

E_{Re}	Energy levels of reduction
E_{reg} / ϕ_{reg}	Dye regeneration efficiency
ET	Electron transfer
eV	Electron volt
FF	Fill factor
FRET	Förster resonance energy transfer
fs	femtosecond
FTO	Fluoride-doped tin oxide
PCE / η	Power conversion efficiency
HOMO	Highest occupied molecular orbital
IHT	Intramolecular hole transfer
IMPS	Intensity modulated photocurrent spectroscopy
IMVS	Intensity modulated voltage spectroscopy
IPCE	Incident photon-to-current conversion efficiency
ITO	Indium-doped tin oxide
J_{SC}	Short circuit current density
k	Rate constant
L	Diffusion length
LHE	Light harvesting efficiency
LUMO	Lowest unoccupied molecular orbital
m	The ideality of electron transport and recombination
MHz	Mega Hertz
mM	millimolar
ms	millisecond
mV	millivolt
mW	milliwatt
ND	Neutral density
NIR	Near infrared
nm	nanometre
ns	nanosecond
OC	Open circuit
OD	Optical density
PL	Photoluminescence
Por	Porphyrin
ps	picosecond
Pt	Platinum
RE	Reference electrode
R_{Pt}	Reflectance of platinum covered counter electrode
S_0	Electronic ground state
S_1	The first electronic excited state
S_2	The second electronic excited state
SC	Short circuit

SEC	Spectroelectrochemical
SLIM-PCV	Stepped-light induced transient measurements of photocurrent and voltage
t	time
T	Transmittance
TA	Transient absorption
TAA	Titanium diisopropoxide bis-acetylacetonate
TAS	Transient absorption spectroscopy
TBAOH	Tetrabutylammonium hydroxide
TBAP	Tetrabutylammonium perchlorate
t BP	<i>tert</i> -Butylpyridine
TCO	Transparent conducting oxide
THF	Tetrahydrofuran
UV	Ultraviolet
VB	Valence band
vis	visible
VN	Valeronitrile
V_{OC}	Open circuit voltage
vol	volume
WE	Working electrode
Δ Abs.	Change in absorption
ΔG	Free energy
Δ mOD	milli-change in optical density
Δ OD _{t=0}	The initial change in optical density
ε	Molar extinction coefficient
λ	Wavelength
λ_{onset}	Onset wavelength
τ	Electron lifetime
τ_{SC}	Electron lifetime at short circuit condition
τ_{obs}	The observed lifetime
τ_{WW}	The characteristic stretched relaxation time
ω or d	Thickness
Γ	Dye loading
$\Gamma()$	Gamma function

CHAPTER 1.INTRODUCTION

1.1. Motivation of this study

Sensitizers, the key components affecting the power conversion efficiency (PCE, η) of dye-sensitized solar cells (DSSCs), have been intensively studied over the last three decades.¹⁻²⁷ Among any types of sensitizers, porphyrins have become the highest performing in the last few years.²⁸ The highest power conversion efficiency (13%) was reported in 2014.²⁷

Tailoring porphyrin structure to achieve high solar cell efficiency has two targets:

1. *Lowering the band gap* of the porphyrin to cover more of the solar spectrum and therefore increase the photocurrent. This aim can be achieved by elongating π conjugation and / or attaching electron donating and withdrawing groups to the sensitizer molecules. Electron donors shift the highest occupied molecular orbital (HOMO) level more negatively than the lowest unoccupied molecular orbital (LUMO) level, leading to smaller band gap.^{29,30} Electron acceptors shift the LUMO level more positively than the HOMO level, which also lowers the band gap.³¹ The above effect is often referred to as push-pull effect.^{32,33} For example, a donor- π bridge-acceptor (D- π -A) design has been employed to tailor porphyrins, to achieve panchromatic (visible and near-infrared wavelength) light absorption.³⁴
2. *Maximizing photovoltage*. The photovoltage of a DSSC is determined by the difference of the Fermi level in the TiO_2 and the redox potential of the electrolyte. Increasing the electron density and hence negatively shifting the Fermi level of electrons in the TiO_2 can be achieved by decreasing charge recombination (The charge recombination is referred to the recombination of electrons in TiO_2 conduction band with the acceptor in the electrolyte solution as this process is dominant in DSSCs, unless otherwise stated.) at a given charge photogeneration rate.³⁵ The molecular structure can change charge recombination (the electron lifetime) in DSSCs therefore affecting the photovoltage. Positively shifting the redox potential of the electrolyte can also increase the photovoltage by developing electrolytes with new redox mediators.³⁶

The main shortcoming of lowering the band gap by elongating π -conjugation is the increased polarizability of the electrons. Increased polarizability leads to stronger

intermolecular forces such as induced dipole-induced dipole interactions. The push-pull concept may introduce strong molecular dipoles leading to increased dipole-dipole and dipole-induced dipole forces. Increased intermolecular forces between sensitizers and redox mediators may lead to faster recombination and lower photovoltage as it will be discussed below. For example, two push-pull porphyrins (Fig. 1.1) follow this trend: the photovoltage decreases with band gap of the molecule.²⁹

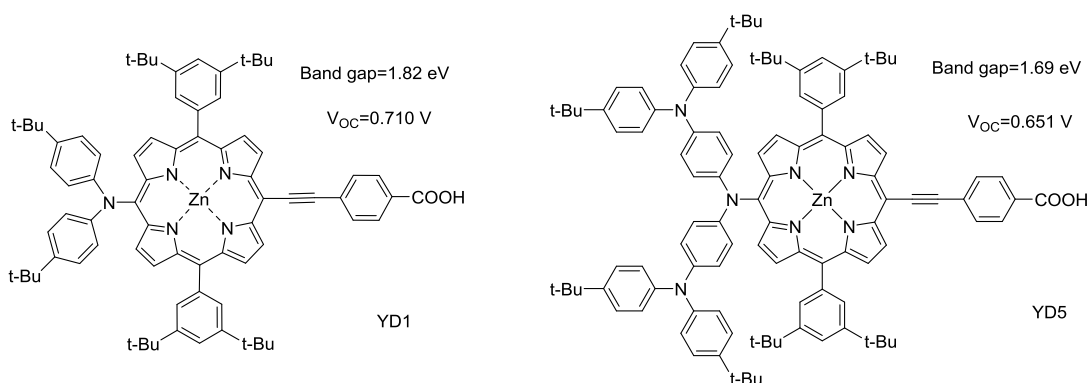


Figure 1.1 Illustration of reduced photovoltage of two D- π -A porphyrins with decreased band gap.

To summarize, the two methodologies to tailor sensitizer structure may be contradictory and lowering the band gap may provide no net benefit to power conversion efficiency. For example, the power conversion efficiency of the DSSC using YD1 was 6.2% while that using YD5 was only 2.1% (structure in Fig. 1.1).²⁹

As will be shown in this thesis, multi-chromophoric sensitizers may enhance the light absorption as well as retard charge recombination. By covalently linking multiple chromophores, a multi-chromophoric sensitizer has the overlapping light absorption of the individual chromophores. By carefully selecting the linker between the chromophores, strong electronic communication between the chromophores can be avoided. Thus, the intermolecular forces in the multi-chromophoric sensitizer are not increased. In fact, as it will be also shown, intermolecular forces can be utilized to *increase* electron lifetime using multi-chromophoric dyes.

The motivation of this thesis is to explore the multi-chromophoric dye sensitizer concept to simultaneously increase photocurrent and photovoltage of dye-sensitized solar cells. In contrast to the above D- π -A concept, the simultaneous increase can be achieved by:

1. Attaching low band gap chromophores, covalently linked to the porphyrin, to

extend and / or to complement the light absorption of the porphyrin.

2. Attaching bulky chromophore to block the approach of the redox mediator to the TiO₂ surface and hence enhance the electron lifetime and photovoltage. The idea of utilizing intermolecular forces to increase electron lifetime by attaching the low band gap chromophore furthest away from the TiO₂ surface will be explored.

1.2. Scope of this study

Most of the international research effort in developing porphyrin dyad sensitizers for dye-sensitized solar cells was focused on developing electronically strongly coupled, fused porphyrin molecules with red-shifted absorption bands.³⁷⁻⁴⁰ In contrast, the research team at the University of Wollongong has described the benefits of using porphyrin dyads containing electronically weakly interacting porphyrin chromophores.⁴¹ An example of such porphyrin dyad (P10 shown in Fig. 1.2) contains two nearly identical chromophores, a phenylethenyl linker and a cyanoacrylic acid anchoring group. 3,5-Dimethylphenyl substituents on the chromophores were attached to the porphyrin themselves to minimize aggregation. It was demonstrated that:^{41,42}

1. The two chromophores are electronically weakly coupled in the ground state. UV-visible absorption spectroscopy showed that the light absorbance of P10 was doubled that of the single porphyrin with no new band observed; resonance Raman spectroscopy and density functional theory (DFT) calculations showed that the orbital energies of P10 were unperturbed compared to the corresponding single porphyrin orbital energies.
2. When photoexcited, both porphyrin chromophores generate photo-electrons by electron injection into TiO₂.
3. The open circuit voltage of the porphyrin dyad has increased compared to the porphyrin monomer dyes. This effect was attributed to the blocking effect from the additional porphyrin. In a follow up study, bulky *tert*-butylpyridine was suggested to play an important role. By coordinating to the Zn porphyrin core, it enhances the blocking effect of a porphyrin dyad containing two Zn porphyrin molecules.⁴²
4. Spectroscopically the two porphyrin chromophores were not distinguishable,

therefore detailed exact charge generation and recombination mechanisms involving the various possible redox states of the di-chromophoric porphyrin was not feasible.

5. Dye uptake did not change so light harvesting in the dimer was nearly doubled. This is the most important point.

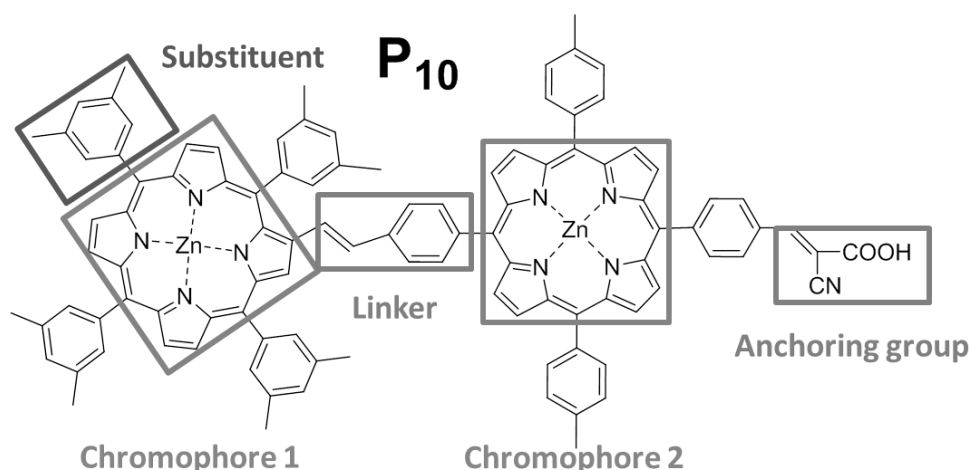


Figure 1.2 The porphyrin dyad P10.

The scope of this study is to explore the di-chromophoric concept by introducing a second chromophore based on carbazole instead of a porphyrin. In this approach, the additional chromophore is spectrally different from the porphyrin (both in the ground and the excited state), therefore some fundamental questions can be answered:

1. How does the energy level offset of the extra chromophore affect the spectroscopic, electrochemical and photovoltaic properties of the di-chromophoric porphyrin?
2. How effective is the extra chromophore in enhancing the photocurrent of the DSSC using the di-chromophoric dyes and what is the mechanism for enhancement?
3. Does the additional chromophore increase electron lifetime?
4. Is there an intramolecular charge transfer following charge injection from the porphyrin to the second chromophore?
5. How does the process, described in point 4, affect charge recombination / regeneration rates?

Fig. 1.3 shows the di-chromophoric porphyrins investigated throughout this thesis.

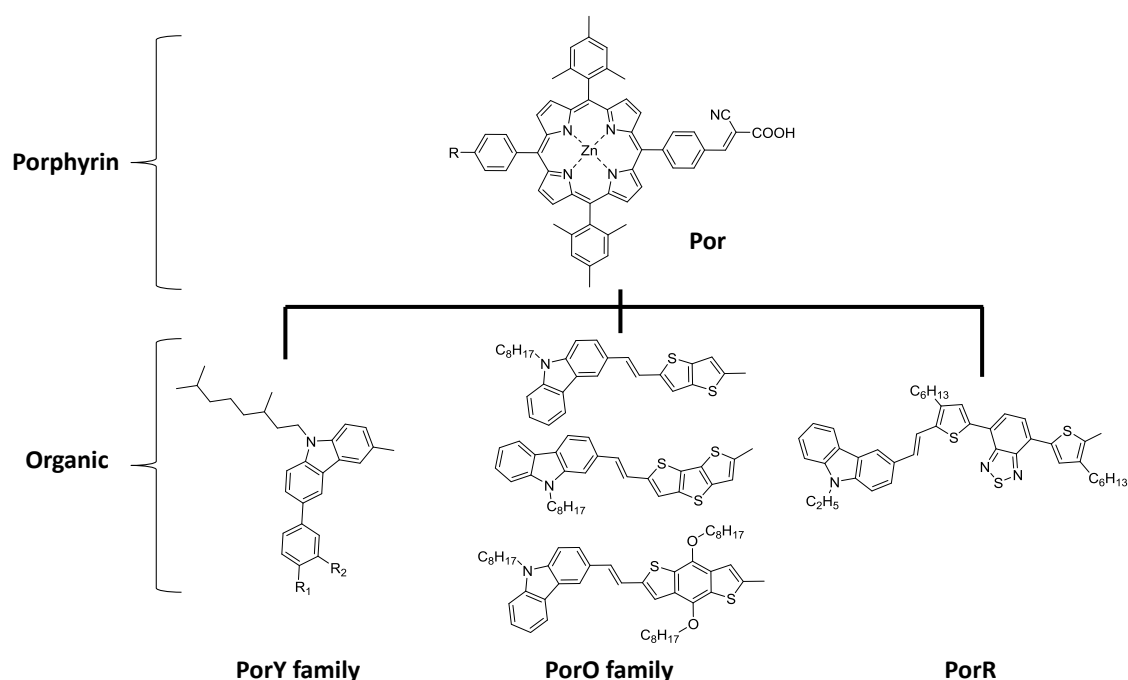


Figure 1.3 The di-chromophoric dyes studied in this thesis

In contrast to Fig. 1.2, the new di-chromophoric dyes investigated in this thesis contain a carbazole derivative with increasingly red-shifted absorption (Y-yellow, O-orange, R-red). The same zinc complex of porphyrin (Por) was used as the building block for all porphyrin dyads. Por is also used as a “reference dye” to compare any performance differences.

The design of the dyes was based on the following principles:

1. The PorY dyads contain carbazole derivatives absorbing light at wavelength shorter than 400 nm. These dyes were designed because of the spectroscopically distinguishable ground state and excited state spectrum of the carbazole and porphyrin chromophores. This allowed to study the effect of carbazole chromophore with various electron donating / withdrawing groups on charge generation and recombination mechanisms. The modification of the electronic structure is achieved by varying R_1 and R_2 groups. The observed effects are investigated in Chapter 4.
2. The PorO family of dyes contain carbazole-oligothiophene chromophores absorbing photons at the 450-500 nm range. These dyes were designed to fill the

light absorption gap between the Soret and Q bands of the porphyrins. Therefore, the light harvesting of the sensitizer and consequently the photocurrent of the DSSCs would be enhanced. This allowed testing experimentally the extent of efficiency improvement due to filling the absorption gap of the porphyrin, which is described in Chapter 5.

3. PorR were designed to further lower the band gap of the sensitizer and red-shift the absorption beyond the band gap of the porphyrin. This is achieved by employing a strong electron acceptor benzothiadiazole in addition to the electron donor - carbazole. This dye structure can be described as D1-A1-P(D2)-A2. It contains two electron acceptors: benzothiadiazole and cyanoacrylic acid linked to the TiO_2 . This design opens up the possibility to study competing charge transfer mechanisms in multi-chromophoric dye sensitizers and its effect on solar cell efficiencies, as discussed in Chapter 6.

In addition, intramolecular charge and energy transfer reactions can be studied in di-chromophoric sensitizers as the relative energy levels of the porphyrin and the additional chromophore is varied.

To illustrate this point, the possible electron transfer reactions in di-chromophoric dyes are depicted in Fig. 1.4. The individual electron transfer steps are also expressed in Eqs. 1.1 to 1.7.

1. A photoexcited state is formed on D2 after photon absorption (Eq. 1.1).
2. An intramolecular energy transfer (IEnT) from D2^* to D1 is followed (Eq. 1.2a).
3. A direct electron injection from D2^* to TiO_2 may be also possible (Eq. 1.2b).
4. The D1 excited state injects electron into TiO_2 (Eq. 1.3).
5. The electrons in TiO_2 ($\text{TiO}_2(\text{e}^-)$) can recombine with the hole on D1 in $\text{TiO}_2(\text{e}^-)$ -dye cation (D^+) recombination (EDR) (Eq. 1.4a).
6. The generated hole on D1 can transfer to D2 via an intramolecular hole transfer (IHT) (Eq. 1.4b).
7. The hole on D1 can be reduced by the reduced species in the electrolyte (Eq. 1.5a), for example, by Co^{2+} . This step is also known as the dye regeneration process (Reg).
8. The hole on D2 can be also reduced by the reduced species in the electrolyte (Eq. 1.5b).
9. The $\text{TiO}_2(\text{e}^-)$ can also recombine with the hole on D2 (Eq. 1.6).

10. Another process that consumes the $\text{TiO}_2(e^-)$ is the $\text{TiO}_2(e^-)$ -acceptor in electrolyte recombination (EER, Eq. 1.7).

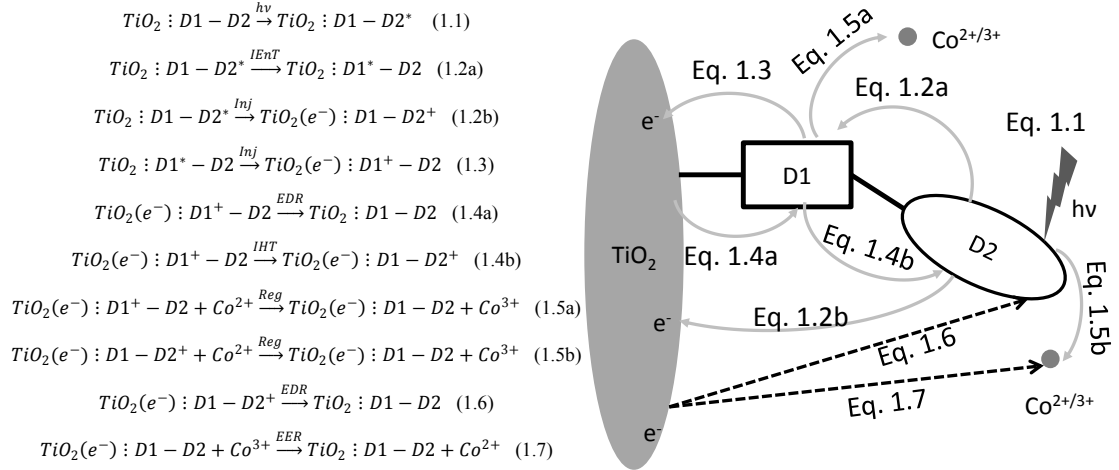


Figure 1.4 The possible electron / energy transfer processes in a di-chromophoric dye D1-D2.

As illustrated in Fig. 1.4, the electron injection, electron recombination and dye regeneration processes in di-chromophoric sensitizers are much more complex compared to those in single chromophores.

The main difference compared to single chromophore sensitizers is the possibility of intramolecular energy and hole transfer (Eq. 1.2a and Eq. 1.4b). The occurrence of the intramolecular hole transfer in a di-chromophore is enabled by any offset in the relevant energy levels (HOMO offset for hole transfer, LUMO offset for electron transfer), as illustrated in Fig. 1.5. It is not recommended to use the LUMO and HOMO when discussing the charge transfer, since that both of them are ground state energy levels. However, the LUMO and HOMO energy levels are used here to demonstrate the charge transfer in a di-chromophoric dye for simplicity.

Energy transfer from D2^* to D1 (Eq. 1.2a) may occur due to the overlapping emission spectra of D2 and absorption spectra of D1 as explained below in more details (Section 1.9).

The intramolecular hole transfer from D1^+ to D2 (Eq. 1.4b) may occur due to an energy offset between the HOMO level (localized on D2) and the HOMO-1 level (localized on D1) (Fig. 1.5).

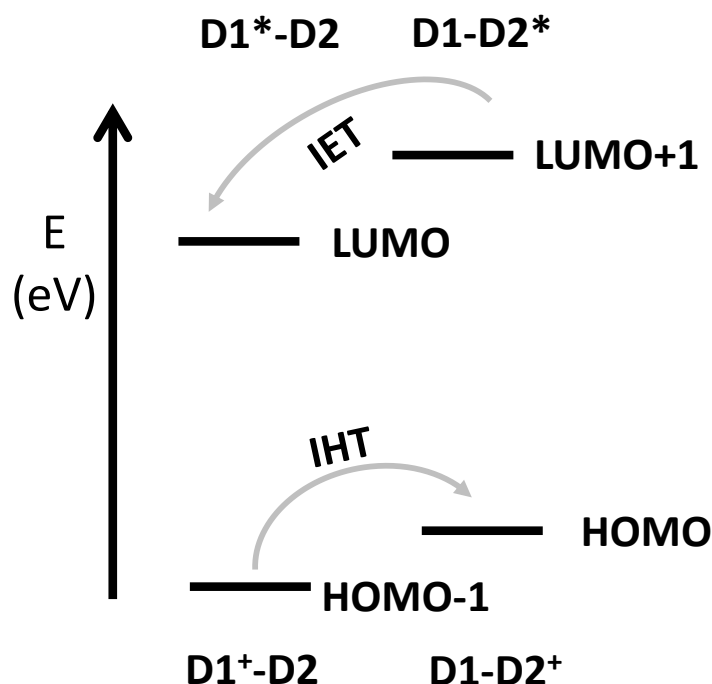


Figure 1.5 Intramolecular charge transfer according to the energy levels.
IET: intramolecular electron transfer; IHT: intramolecular hole transfer.

1.3. Dye-sensitized solar cells (DSSCs)

A dye-sensitized solar cell is a device that utilizes a sensitizer as a light-absorber to transform solar energy into electricity via the photovoltaic effect. Fig. 1.6 demonstrates the operational mechanism of a typical DSSC. Typically a monolayer of the dye is chemisorbed on the surface of a mesoporous TiO_2 layer. The TiO_2 is deposited onto a transparent conducting oxide (TCO) glass.

Photons are absorbed by the dyes (①) and thereafter the excited dyes inject electrons into the conduction band (CB) of the TiO_2 (②). The electrons diffuse through the network of TiO_2 particles and are collected at the conducting oxide glass (③). The oxidized dye is regenerated to its ground state by electron transfer from a redox couple in the electrolyte (④) (for example, I^-/I_3^-).

There are three main recombination processes in DSSCs: i) $\text{TiO}_2(e^-)$ -dye cation recombination (⑤); ii) $\text{TiO}_2(e^-)$ -acceptor in electrolyte recombination (⑥); and iii) excited dye decay to ground state (⑦).⁴³⁻⁴⁶

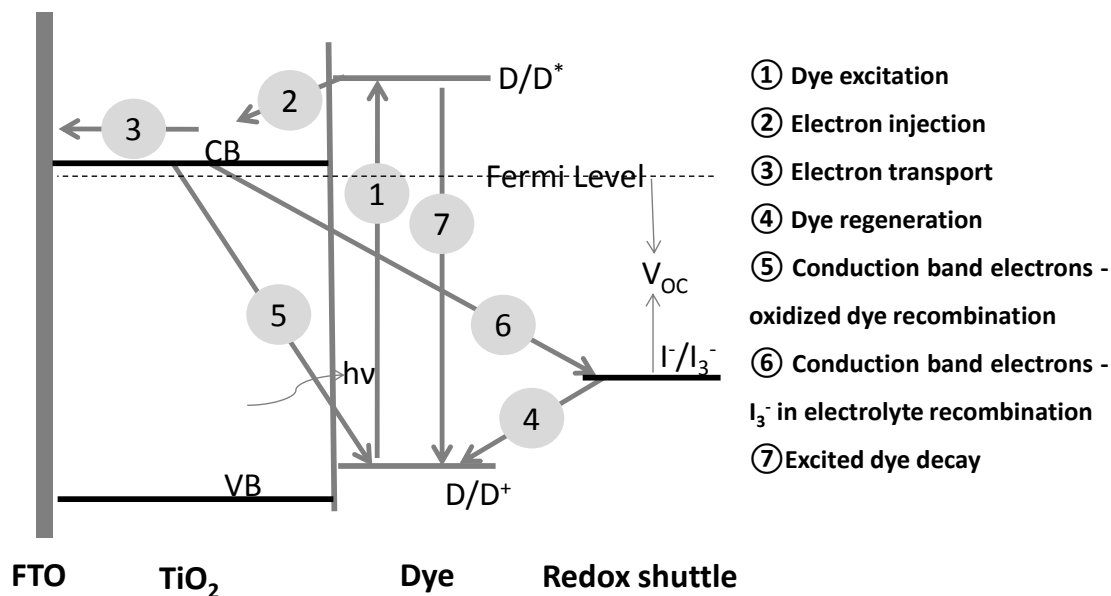


Figure 1.6 Operational mechanism of a dye-sensitized solar cell and the possible electron transfer processes at the electrolyte/dye/ TiO_2 interface

The main components of a typical DSSC are:

1. *Semiconductor* - plays a key role in electron injection, electron recombination and electron collection processes. The photoelectrochemistry of different semiconductor nanoarchitectures in DSSCs and quantum dot solar cells,⁴⁷ various metal oxides as semiconductors and their usage in DSSCs,⁴⁸ the energy levels of different materials and the physical property of the semiconductors^{49,50} are reviewed.
2. *Electrolyte* - reduces the oxidized state of the sensitizer to its ground state and exchanges electron with the counter electrode. The types of redox couples and their function in operational of DSSCs are reviewed in references.^{48,51-53}
3. *Sensitizer* - absorbs photons and injects electrons into the semiconductor from the excited state. The most commonly used sensitizers have been reviewed in the following references.^{48,51,54} Because of the importance of sensitizer development in this thesis, the brief history and current state of the art of sensitizers for DSSCs will be reviewed in detail in the Section 1.4 below.
4. *Current collectors*. The function of the current collectors is to collect the electrons generated in the device active layers and to close the external circuit. The various electrode materials and their effect on the performance of DSSCs have been described in the following studies.^{51,55,56}

1.3.1 Design considerations for efficient sensitizers

The sensitizers employed in typical DSSCs should fulfill the functions of light harvesting and electron injection. It should also help to minimize the recombination processes (⑤ and ⑥ in Fig. 1.6). To achieve these targets, the following aspects in sensitizer design should be considered:

- 1) Light absorption is better to cover the whole visible range towards near infrared wavelengths to increase photocurrent. This is achieved by lowering the HOMO-LUMO gap as explained above. For example, by employing the strong electron withdrawing thiadiazole[3,4-*c*]pyridine to design low band gap chromophores, an organic dye (*E*)-3-(4-(5-(4-(5-(4-(Bis(4-(hexyloxy)phenyl)amino)phenyl)-3-hexylthiophen-2-yl)-[1,2,5]thiadiazolo[3,4-*c*]pyridin-7-yl)-4-hexylthiophen-2-yl)phenyl)-2-cyanoacrylic acid (Y4) extended the light absorption on TiO₂ to 800 nm.⁵⁷
- 2) The HOMO should be more positive than the redox potential of the mediator to allow efficient dye regeneration.
- 3) The LUMO should be more negative than the conduction band potential of TiO₂ to enable efficient electron injection.
- 4) The dye cation radical of the oxidized dye should be localized close to the electrolyte (and further away from the TiO₂) to enable fast regeneration and slow recombination between the injected electrons and the oxidized dyes.^{58,59}
- 5) The LUMO should be localized near the anchoring group into the conduction band of the TiO₂. There are some exceptions to this rule. For example, a long-range electron injection in two rhenium-ruthenium dyads [(4,4'-(CO₂H)₂2,2'-bipyridine)ReI(CO)₃-CN-RuII(2,2'-bipyridine)₂(CN)](PF₆) and [(4,4'-(CO₂H)₂2,2'-bipyridine)ReI(CO)₃-NC-RuII(2,2'-bipyridine)₂(CN)](PF₆) has been reported.⁶⁰
- 6) Units that increase solubility such as long alkyl chains are often utilized to suppress dye aggregation. Long alkyl chains can be also used to shield the surface of the TiO₂ and consequently block the approach of the redox mediator to the surface of TiO₂.^{32,57,61} The disadvantage of introducing bulky chains into the sensitizer is that the dye loading on TiO₂ can decrease.⁶² Hydrophobic side chains may also protect the dye-TiO₂ surface from dye desorption leading to long-term stability.⁶³

- 7) Partial charges on the molecules might increase recombination by attracting oppositely-charged ions. Introducing a metal center which carries a net positive charge, such as the zinc cation in porphyrins or phthalocyanines complexes, may lead to partial charges and increased attraction of I_3^- . On the other hand, the use of *t*BP that can coordinate to the zinc cations may minimize the effect of partial charge on charge recombination.^{42,64} The net negatively-charged oxygen ions in side chains can attract Li^+ from the electrolyte, which consequently attracts I_3^- .^{65,66} This partial charge effect can play an important role in affecting electron lifetime in organic dyes when reducing the dye amount on TiO_2 .⁶⁷
- 8) Finally, strong dispersion forces between highly polarizable segments of dyes and redox mediators may lead to enhanced charge recombination.^{68,69} Specific design rules how to overcome this effect has been proposed for the first time by the work carried out in Chapter 8 of this thesis. It will be shown that dichromophoric dye design can be used to utilize increased dispersion forces to enhance photovoltage.

Several of the above methodologies are contradictory to each other and lead to trade-offs. For example, efficient light harvesting requires low band gap, i.e., more positive LUMO level and more negative HOMO level, while efficient electron injection requires more negative LUMO level and dye regeneration requires more positive HOMO level. Increased light harvesting requires more dyes adsorbed on the TiO_2 surface, while introducing alkyl chains to avoid dye aggregation may lead to lower dye uptake. Low band gap sensitizers extend light absorption to the near infra-red wavelength range but they often easily aggregate due to the highly planar structure and delocalized π -electrons leading to strong π - π interactions. These dyes also induce strong dispersion forces facilitating the recombination. Hence, developing high efficiency sensitizers requires careful optimization.

1.4. Porphyrins as sensitizers

Porphyrins have been extensively used as light harvesters in DSSCs.^{26-28,48,70-74} The progresses in designing porphyrins for DSSCs have been reviewed by Officer *et al.*,⁷² Diau *et al.*,²⁸ Imahori *et al.*³⁴ and Mahammad and Torres *et al.*⁷⁵

In this section, porphyrins for DSSCs will be categorized as (A) the single chromophoric porphyrins and (B) the multi-chromophoric porphyrins. Distinguishing single and multi-chromophoric porphyrins is not often straightforward. The HOMO and LUMO levels of the porphyrins are often altered by adding substituents to the porphyrin ring. The definition of single chromophoric porphyrin dye *in this thesis* is when the changes are so dominant that new light absorption bands and hence a new chromophore is created. In contrast, the absorption spectrum of multi-chromophoric porphyrins can be described by the simple superposition of the added chromophores.

- A. Single chromophoric porphyrins: the porphyrin and its substituents appear to form single chromophore displaying unique absorption characteristics which cannot be described as a simple superposition of the component chromophores. For example, the absorption spectra of substituted, single chromophoric porphyrins often show significantly broadened, or split Soret band and red shifted Q bands.^{29,30,76}
- B. Multi-chromophoric porphyrins: no significant new absorption bands are observed by substitution. The absorption spectrum appears to be a superposition of the component chromophores. The porphyrin Soret and Q bands remain largely unchanged in a multi-chromophoric porphyrin dye.

Investigation of this class of chromophores is the scope of this thesis.

To explain the above categories more clearly, take the diporphyrin series YDD0-YDD3 published by Diau *et al.* as an example (Fig. 1.7).³⁸ YDD0, YDD2 and YDD3 show new absorption bands at the 700 nm-1200 nm wavelength range that is not present in either the porphyrin part or the other component. These dyes are referred as single chromophoric porphyrins. YDD1, on the other hand, displays similar absorption spectrum with double molar extinction coefficients due to the presence of two porphyrin chromophores. YDD1 is therefore a multi-chromophoric porphyrin according to the above definition.

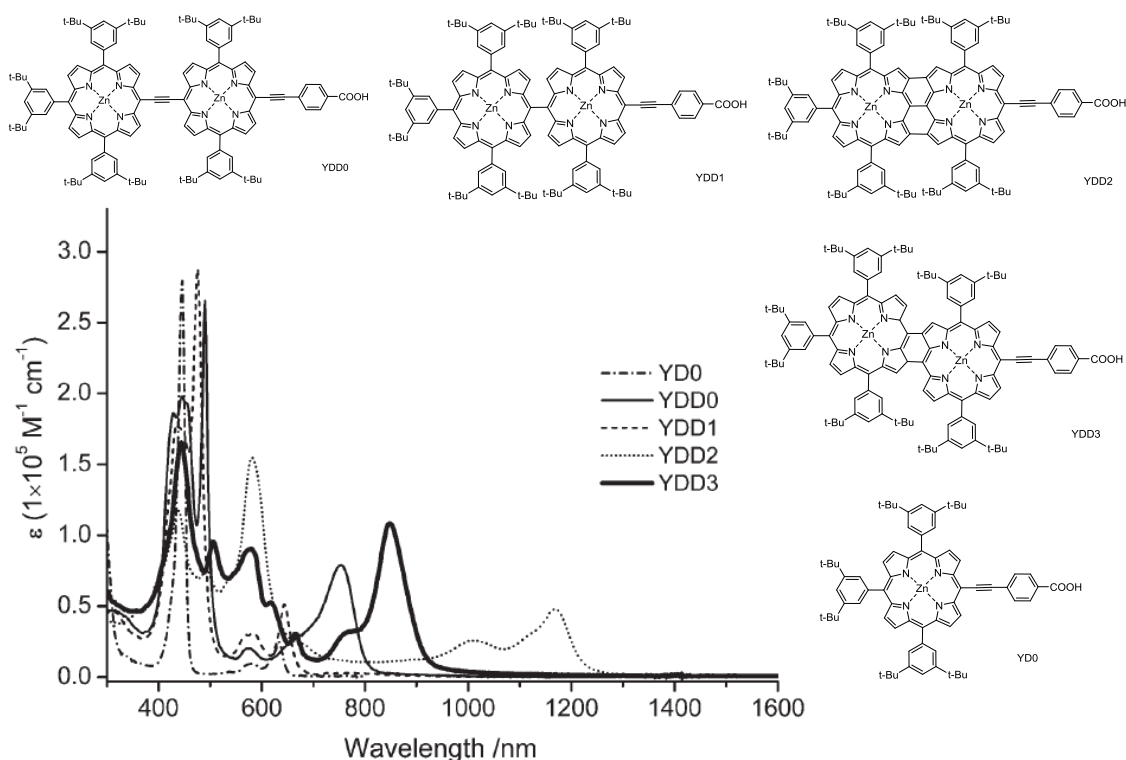


Figure 1.7 Structures of the single chromophoric porphyrin YD0 and the diporphyrins YDD0-YDD3 and their light absorption spectra.
Reproduced from Ref.³⁸

A complementary method of mixing dyes on the surface is introduced too. Typically, this co-sensitization approach is based on the co-adsorption of two or more dyes on TiO_2 electrodes.⁷⁷⁻⁷⁹ Since the chosen dyes usually complement their absorption, the resulting DSSC can give better light absorption and consequently increased photocurrent than that of the individual dyes. Additionally, better electron injection efficiency was found in the case of co-sensitization due to the better dye alignment on TiO_2 surface compared to the individual dyes. The photovoltage becomes slightly improved due to a synergistic effect as well.^{26,28,80-90}

However, the co-sensitization concept does have some limitations. For instance, the extent of dye adsorption onto TiO_2 films is limited by the limited number of binding sites or the surface area in the TiO_2 .^{91,92} Thick films are therefore needed to achieve efficient light harvesting. Using thick TiO_2 films may introduce increased recombination losses and therefore reduce charge collection efficiency. In that regard, multi-chromophoric dyes have an advantage over co-sensitization approach since they

occupy less surface area providing the chromophores are linearly aligned. A comparison to the di-chromophoric dye approach will be made in Chapter 6.

1.4.1 *Free-base versus metal complexes*

The nature of the transition metal in the porphyrin is a key consideration for dye design.^{21,93} Zinc porphyrins are the most studied porphyrins in DSSC applications and achieved the best photovoltaic performance within metalloporphyrins.²⁷ Most zinc porphyrins are photochemically and thermally stable, and are easy to synthesize with high yields.^{94,95}

Compared to their free base analogue, zinc porphyrins used in DSSCs lead to higher photovoltaic performance. This is mainly due to the more suitable HOMO and LUMO levels matching standard DSSCs conditions using TiO₂ nanoparticles and iodine/triiodide organic electrolytes, leading to efficient electron injection and oxidized dye regeneration.⁹⁶ In general, with the same porphyrin, free-base porphyrin possesses a smaller band gap compared to zinc porphyrins.^{97,98} The HOMO level of both free-base and zinc porphyrins is similar and therefore the dye regeneration kinetics is similar.⁹⁶ The LUMO level of free-base porphyrins is therefore slightly more positive compared to their zinc analogue, for example, 0.03-0.15 eV difference in a series of porphyrins with different number of methoxy groups,⁹⁷ leading to a smaller overlap of the TiO₂ acceptor states and loss of electron injection.⁹⁶

1.4.2 *β -linked versus meso-linked porphyrins*

The performance of porphyrins with the linkers at either β or *meso* position was reviewed by Diau *et al.*²⁸ The linker group attaching the dyes to TiO₂ is either at a β -position or at a *meso*-position of the porphyrin ring. For example, GD2 is a β -linked porphyrin²³ and P199 is a *meso*-linked porphyrin (Fig. 1.8).^{41,96} It is not straightforward to draw general rules whether β or *meso* substitution is preferred as it is strongly dependent on the nature and electronic coupling of the substituting group. The *meso*-linked porphyrin SM315 (Fig. 1.10) achieved 13% in DSSCs after introducing push-pull effect, suggesting *meso*-substitution works well for this class of dyes.²⁷ GD2, one of the best single chromophore dyes reaches 7.1% and uses β -linked malonic acid linker,²³ suggesting the utility of β -substitution for this class of dyes.

Meso-substitution on P10 has proved to be resulting in a multi-chromophoric porphyrin category B (see above), which is the main design motive in this thesis. Moreover, the

linker is attached at the *meso*-position of the porphyrin ring, because it is easier to synthesize the di-chromophoric dyes used in this thesis.

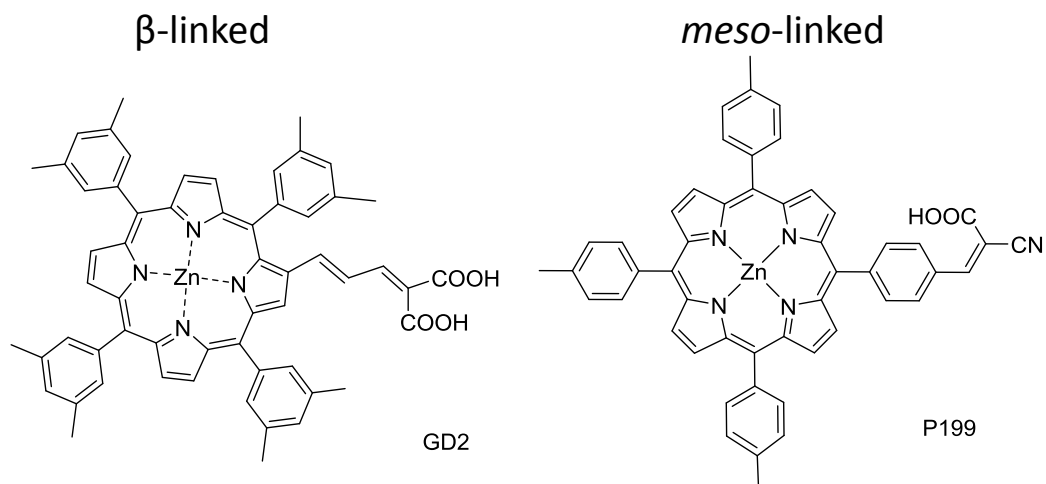


Figure 1.8 Chemical structures of GD2 and P199.

1.4.3 Absorption spectrum

Porphyrins often have several light absorption bands, typically a strong Soret (or B) band and moderate Q bands. The molar extinction coefficients at the Soret band could reach values above $10^5 \text{ M}^{-1} \text{ cm}^{-1}$,⁹⁹ while at the Q bands, they are typically an order of magnitude lower.^{20,100}

The absorption spectrum of porphyrins can be explained by a four-orbital model established by Gouterman.¹⁰¹⁻¹⁰⁴ According to this model, the absorption bands originate from four different transitions between HOMO and HOMO-1 and LUMO and LUMO+1 levels (inset of Fig. 1.9). The symmetry of the HOMO and HOMO-1 orbitals are a_{1u} and a_{2u} , respectively. These orbitals are non-degenerate, but close in energy.¹⁰⁵ The symmetry of the LUMO and LUMO+1 orbitals are e_{gx} and e_{gy} , respectively. These orbitals are degenerate, with even stronger degeneracy in the presence of a coordinating metal ion compared to free-base porphyrin. Electronic transitions from the HOMO and HOMO-1 levels to the non-degenerate / degenerate π^* -orbitals give rise to four possible excitations, the oscillator strength depending on the transition dipole for the transition.^{105,106} Orbital mixing leads to two excited states: a higher energy state with greater oscillator strength (Soret band, S_0 to S_2) and a lower energy state with less oscillator strength (Q bands, S_0 to S_1).

The number of the Q bands depends on the degeneration of e_g orbitals.¹⁰⁵ Metal porphyrins have a set of degenerate e_g orbitals, hence two Q bands are usually observed representing the transition states of Q (1,0) and Q (0,0) (Fig. 1.9). Due to the more asymmetric structure, the non-degenerate e_g orbitals further split into an e_{gx} and an e_{gy} orbital in free-base porphyrins forming four Q bands assigned to the transition states of Q_y (1,0), Q_y (0,0), Q_x (1,0) and Q_x (0,0).

When attached onto the TiO_2 films, porphyrins, similarly to other types of sensitizers, often show slightly broadened light absorption spectra compared to those in solution, which may be due to the different electronic structure bound on the surface compared to solution and / or dye aggregation on TiO_2 .^{41,107-109}

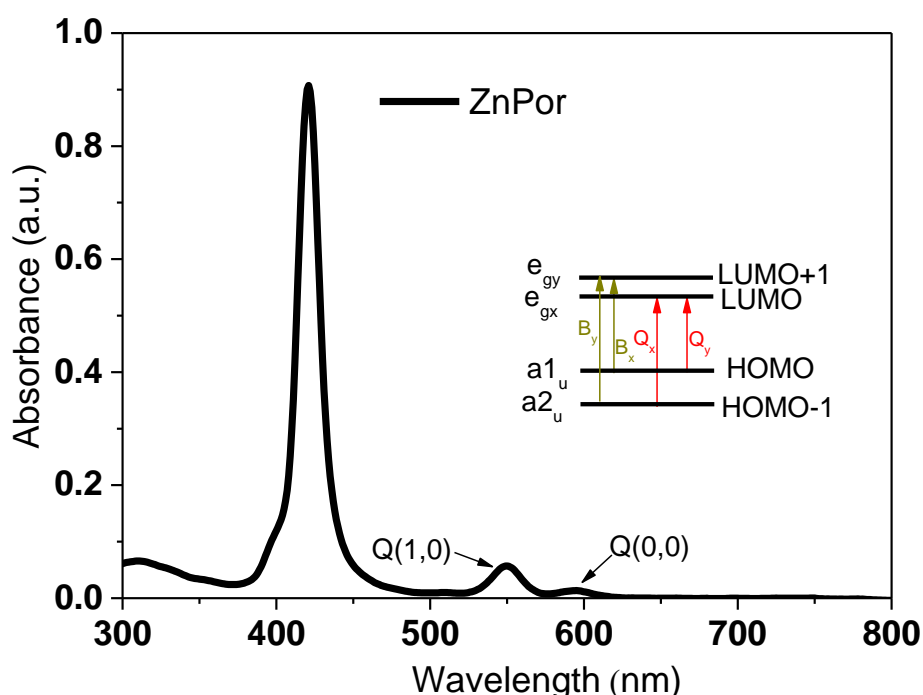


Figure 1.9 An example UV-visible absorption spectrum of 5,10,15,20-tetrarhylporphyrinato zinc (II) (ZnPor) in solution. The inset shows the energy level diagram based on the four-orbital model.

1.4.4 Single chromophoric porphyrins

The definition of single chromophoric porphyrin dye in this thesis is when the changes are so dominant that new light absorption bands and hence a new chromophore is created. The first successful porphyrin used for dye-sensitization was 5,10,15,20-tetrakis(4-carboxyphenyl)porphyrinato zinc(II) (ZnTPPC) in 1987. Efficient electron

injection into TiO₂ electrode from the photoexcited dye was reported.¹¹⁰ Since then, the progress has been enormous:

1. DSSCs using a copper complex Cu-2- α -oxymesoisochlorin achieved the best power conversion efficiency of 2.6% within a series of porphyrins by using cholanic acids as co-adsorbers.¹⁹
2. DSSCs using a free-base porphyrin 5,10,15,20-tetrakis(4-carboxyphenyl)-porphyrin (TCPP) with four anchoring groups achieved 3.5% power conversion efficiency by employing a co-adsorber deoxycholic acid to block dye aggregation as well as to retard recombination.²⁰
3. The use of β -linked zinc porphyrins further enhanced the power conversion efficiency in DSSCs. DSSCs using the porphyrin 4-((*E*)-(2-(5,10,15,20-(tetra3,5-dimethylphenyl)porphyrinato zinc(II)-2-yl)ethen-1-yl)benzoic acid (Zn2),²¹ 1-cyano-2-(5,10,15,20-tetraphenylporphyrinato zinc(II)-2-yl)-acrylic acid (GD1)²² and 3-(5,10,15,20-tetra(3,5-dimethylphenyl)porphyrinato zinc(II)-2-yl)-2-propen-1-ylidenepropandioic acid (GD2)²³ achieved the power conversion efficiencies of 4.8%, 5.6% and 7.1%, respectively.
4. A large increase in power conversion efficiency using porphyrins was obtained by employing the D- π -A (push-pull) porphyrin structure. The concept of a D- π -A structure was developed to modulate the HOMO and the LUMO levels to induce a red-shift of the light absorption.^{25,30,76} Easily tunable band gap by varying donor, spacer, and acceptor moieties, is the key feature of these D- π -A sensitizers.^{111,112}

The YD series porphyrins are based on the D- π -A structure (Fig. 1.10). YD1 achieved 6.0% power conversion efficiency in DSSC by using chenodeoxycholic acid (CDCA) as co-adsorber,¹⁰⁰ and 6.5% by also adding a scattering TiO₂ layer.¹¹³ YD2 exhibited slightly better photovoltaic performance compared to YD1, without using CDCA (6.8%).¹¹³ When co-sensitized with an indoline dye 5-[[4-[4-(2,2-Diphenylethenyl)phenyl]-1,2,3,3a,4,8b-hexahydrocyclopent[*b*]indol-7-yl]methylene]-2-(3-octyl-4-oxo-2-thioxo-5-thiazolidinylidene)-4-oxo-3-thiazolidineacetic acid (D205), YD2 showed more than 11% under one sun standard conditions (AM 1.5G, 100 mW cm⁻² intensity).²⁵ Further modification of the molecular structure by attaching long alkyl chains (YD2-o-C8) as well as improving the DSSC fabrication procedures

resulted in a power conversion efficiency of 12.3%.²⁶ More recently, a single chromophoric porphyrin dye SM315 (Fig. 1.10) achieved 13% with a remarkable photocurrent of up to 18.1 mA cm⁻².²⁷ Some other D- π -A porphyrins with more than 10% power conversion efficiency were developed with an electron donating *N,N*-dialkyl-amino substituted (LD14 and LD16)^{35,76} and pyrenylethynyl unit (LD4)³⁰ (Fig. 1.10).

- Additional chromophores have been attached to the porphyrin via π -conjugated linker to enhance light harvesting by creating new, often red-shifted absorption bands. Note that for this reason, these systems are also categorized as single chromophoric porphyrins in this thesis. The diporphyrin YDD0 (Fig. 1.7) displayed a power conversion efficiency of 4.1%.³⁸ Extended light absorption on TiO₂ to 800 nm was reported by using a π -conjugated *N*-fused carbazole-zinc porphyrin-free-base porphyrin triad (DTBC, Fig. 1.10) with an overall power conversion efficiency of 5.2%.³⁹

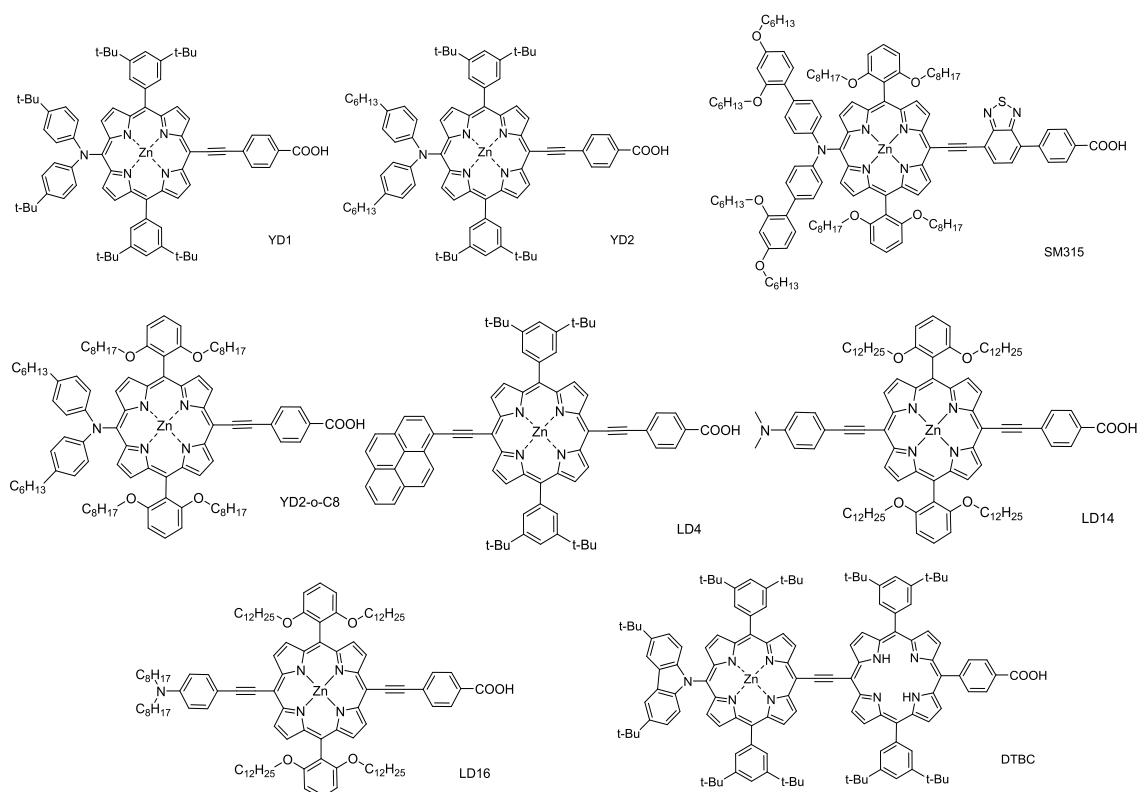


Figure 1.10 Structures of some single chromophoric porphyrins

1.4.5 Multi-chromophoric porphyrins

The definition of multi-chromophoric porphyrin in this thesis is when its absorption spectrum can be described by the simple superposition of the added chromophores. DSSCs using diporphyrins YDD0, YDD2 and YDD3 all showed lower open circuit voltages of 0.60 V, 0.39 V, 0.45 V, respectively, compared to that of YD0 (0.70 V).³⁸ The open circuit voltage of the DSSC using triad DTBC was 0.60 V.³⁹ The low open circuit voltage in these DSSCs using strongly π -conjugated porphyrin systems may originate from increased intermolecular forces. More polarizable π -electrons are anticipated to increase weak intermolecular forces such as London dispersion force, therefore decreasing electron lifetime and photovoltage.⁶⁸

A multi-chromophoric dye design using a non-conjugated arrangement of the chromophores may help to increase open circuit voltage as well as photocurrent. Using the multi-chromophoric approach, light harvesting is extended by using additional chromophores, not through delocalization of π -conjugation.^{40,41,72,114} Using the same chromophores, the extinction coefficient can be also increased. The benefit of increased extinction coefficient to achieve efficient light harvesting is the ability to use thin TiO₂ photoanodes. Thin films have fewer bulk defects as well as shorter electron transport path compared to thick films. The use of thin photoanodes could be also benefit solid state devices and cobalt-based redox mediators with generally faster recombination.^{115,116} This is a definitive point of using multi-chromophoric porphyrins in DSSCs.

The history development of the multi-chromophoric porphyrins is much shorter:

1. The first successful porphyrin dyad DSSC was achieved by a poly(ethylene glycol)-modified dimer (PEG-2b-bd-Zn2, Fig. 1.11) with the power conversion efficiency of 4.2%.¹¹⁷
2. DSSCs using porphyrin dyads P10 and P18 achieved power conversion efficiencies of 3.8% and 3.1% with only 3 μ m thick TiO₂ films, while that using N719 showed a power conversion efficiency of 3.4% under the same fabrication conditions.⁴¹ Further optimization of DSSC based on P10 leads to a power conversion efficiency of 5.5%. This value is amongst the highest value reported for porphyrin arrays.⁴² DSSC using the porphyrin dimer P10 achieved higher open circuit voltage (0.70 V) than the single chromophoric porphyrins P199 or P12 (0.64 V).⁴²

3. DSSC using the porphyrin dyad YDD1 (Fig. 1.7) displayed a power conversion efficiency of 5.2%, which was slightly greater than that using the single chromophoric porphyrin YD0 (5.1%).³⁸
4. By attaching borondipyrromethene (BODIPY) and diketopyrrolopyrrole (DPP) antennas to a zinc porphyrin dyad (D-BODIPY and D-DPP, respectively, Fig. 1.11), a ~30% increase of power conversion efficiency was achieved, from 3.6% of the DSSC using porphyrin dyad to 4.6% of D-BODIPY and 4.4% of DSSC using D-DPP, respectively.⁴⁰ The enhanced photocurrent of the triads was attributed to energy transfer from the antenna chromophores to the main chromophore increasing the photocurrent. DSSC using the triad D-BODIPY showed a 30 mV increase, while that using D-DPP showed similar open circuit voltage compared to the porphyrin dyad.

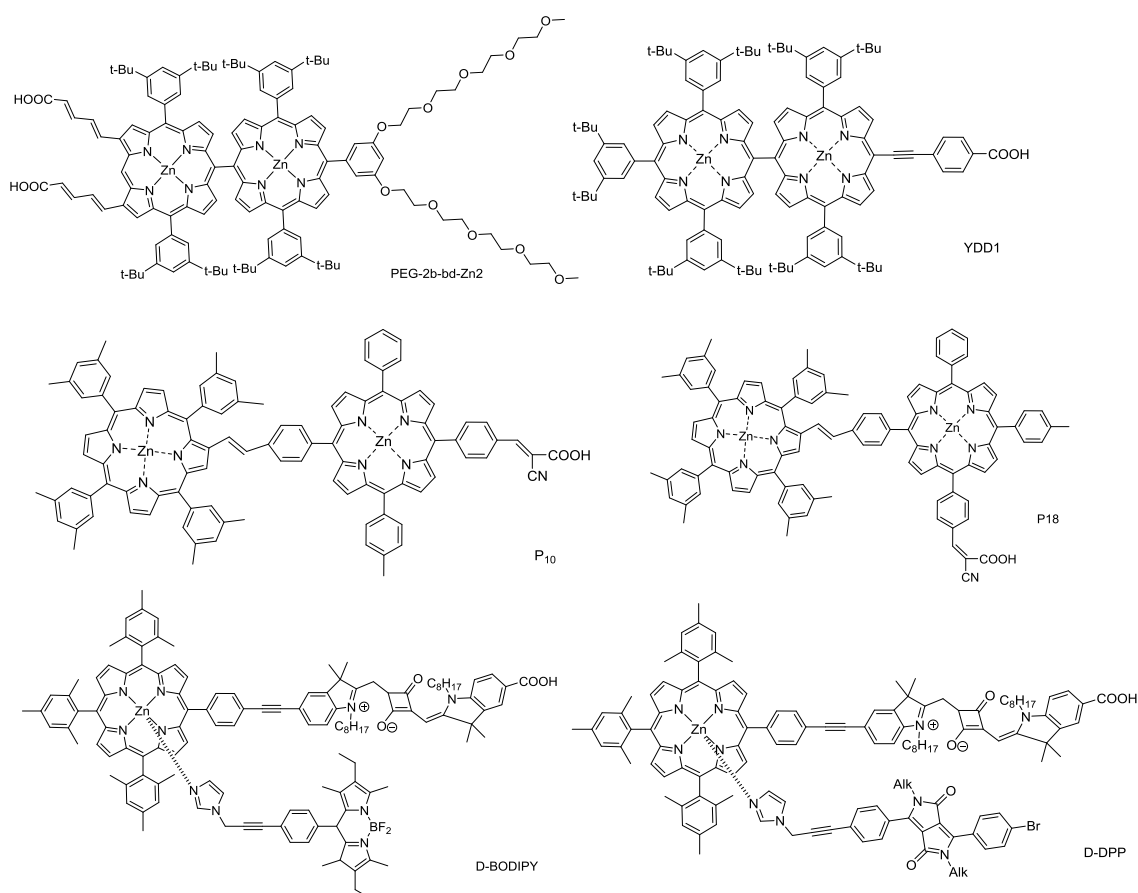


Figure 1.11 Structures of some multi-chromophoric porphyrins

The maximum power conversion efficiencies of DSSCs using multi-chromophoric porphyrins are generally lower compared to single chromophoric porphyrins. A comparison of the power conversion efficiency achieved by the two approaches is shown in Fig. 1.12. The best performing single chromophoric porphyrin SM315 (13%) achieved double the power conversion efficiency of the best multi-chromophoric porphyrin CZP1 (6.2%, named PorY1 in this thesis) in DSSCs. This thesis will focus on the multi-chromophoric systems.

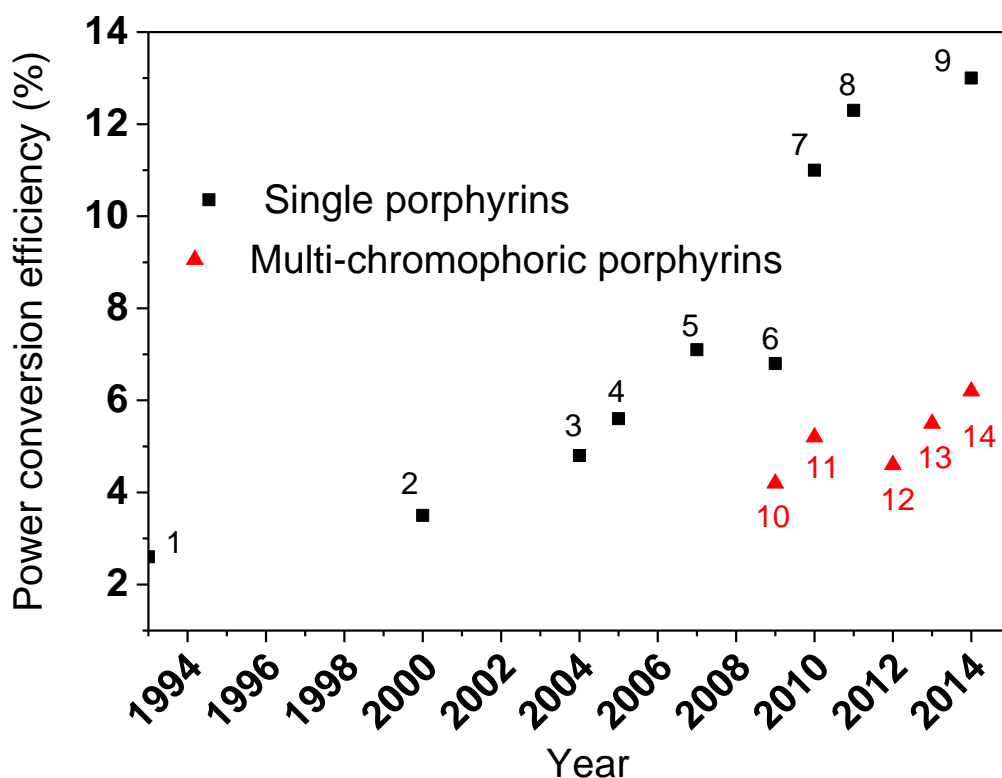


Figure 1.12 Record power conversion efficiencies of DSSCs using single chromophoric porphyrins and multi-chromophoric porphyrins from 1993 to 2014.

(1) Cu-2- α -oxymesoisochlorin,¹⁹ (2) TCPP,²⁰ (3) Zn2,²¹ (4) GD1,²² (5) GD2,²³ (6) YD2,¹¹³ (7) YD2,²⁵ (8) YD2-o-C8,²⁶ (9) SM315,²⁷ (10) PEG-2b-bd-Zn2,¹¹⁷ (11) YDD1,³⁸ (12) D-BODIPY,⁴⁰ (13) P10,⁴² (14) CZP1 (named as PorY1 in this thesis)⁹⁴

1.5. Design considerations of additional chromophores

Carbazole, carbazole-thiophene and carbazole-benzothiadiazole groups are some of the most frequently used building blocks for electronic devices.^{11,14,63,118-134} Therefore, they were chosen as the additional chromophores to build the di-chromophoric dyes in this thesis.

Carbazole moiety is often used as a photochemically and photo-electrochemically stable electron donor group. However, the carbazole moiety itself absorbs light at wavelengths shorter than 400 nm. Extending π -conjugation of the carbazole shifts the light absorption spectrum towards the red. For instance, thiophene can be used to enhance the carbazole light absorption; the longer the conjugated carbazole-thiophene oligomer, the broader the light absorption.¹²² Conducting polymers employed in organic solar cells with even longer π -conjugated segments exhibit light harvesting extended to 700 nm.¹³⁵⁻

137

Thiophene units are often used in organic electronic devices to enhance light absorption due to the delocalization of π -electrons.^{11,138-140} For example, decorating a zinc porphyrin with four polythiophene chains resulted in significantly enhanced light absorption at 440-530 nm wavelength range.¹⁴¹ Polythiophenes, such as poly (3-hexylthiophene) used as the hole transfer material in organic solar cells¹³⁷ and fused-thiophene - bithiophene co-polymers used in semiconductors,¹⁴² can absorb light to 650 nm. Combining thiophene units with carbazole can lead light absorption within 400-450 nm wavelength range, matching the absorption gap between the zinc porphyrin Soret and Q bands, hence were selected for this aspect of the work.^{63,122,123,126,128}

Combining units with different electron donating / withdrawing abilities can lead to a red shift of the light absorption of the carbazole to the visible wavelength range due to a push-pull effect.^{143,144} For example, carbazole conjugated with malonodinitrile - the electron withdrawing group exhibits light absorption to ~470 nm.¹⁴⁴ This effect is successfully used in organic sensitizers. For example, a di-carbazole dye ((*E*)-3-(9-butyl-7-(carbazol-9-yl)-carbazol-2-yl)-2-cyanoacrylic acid) showed light absorption wavelength extended to 500 nm in solution; DSSCs fabricated using this molecule achieved a power conversion efficiency of 1.0%.¹¹⁹ A *tert*-carbazole dye showed light absorption wavelength extended to ~550 nm in tetrahydrofuran (THF) and at ~650 nm on TiO₂ films; DSSCs fabricated using this molecule achieved power conversion efficiency of 6.3%.¹⁴⁵ Adding thiophene moieties between the carbazole donor and the electron accepting group resulted in enhanced photocurrent and photovoltage.¹¹⁹ The high efficiency, commonly studied MK series dyes are good examples of organic dyes with carbazole donor, thiophene as π -linker and cyanoacrylic acid as an acceptor.^{14,146}

2,1,3-benzothiadiazole, being a strong electron acceptor, is often used for low band gap polymers (<1.8 eV or absorption onset wavelength at 700 nm).^{127,130-133} Conductive

polymers consisting of electron-rich 2,5-bis(2-thienyl)-*N*-dodecylpyrrole and electron-deficient benzothiadiazole showed light absorption wavelength longer than 800 nm.¹⁴⁷ The main features of benzothiadiazole used in sensitizers are i) extended light absorption to the near infrared wavelength range; ii) a relatively small blue shift of the absorption peak compared to most D- π -A organic dyes^{16,148} when anchoring to TiO₂ due to weakened deprotonation or H-aggregation;¹³⁴ iii) long-term stability.¹³³ A D-A- π -A structure, in which D is an indoline group, A is benzothiadiazole and the second A is cyanoacrylic acid and dithiophene was a π -linker, has been used as a sensitizer with 8.2% efficiency and light absorption onset wavelength of 700 nm.¹⁴⁹ An organic sensitizer containing benzothiadiazole as the electron deficient moiety and a triphenylamine as the electron donor showed light absorption extended to 800 nm, achieving a power conversion efficiency of more than 6%.¹⁵⁰ An even further red-shifted light absorption to 850 nm was found in an organic dye with D-A- π -A structure, in which D is an indoline group, A is benzothiadiazole and the second A is cyanoacrylic acid and thiophene was a π -linker, exhibiting a power conversion efficiency of 8.7%.¹³³

1.6. Switch from I^-/I_3^- to $\text{Co}^{2+}/\text{Co}^{3+}$

Cobalt mediators have been proved to be the best redox couples for the liquid electrolyte porphyrin-sensitized solar cells.^{27,34} There are some gaps in terms of the scope of this thesis:

1. Cobalt electrolyte in combination with di-chromophoric porphyrins for their use in DSSCs has not been reported in the literature yet. In contrast, cobalt electrolytes are widely used in single chromophoric porphyrin-sensitized solar cells.^{26,27,34,151}
2. Some porphyrins performing well with the I^-/I_3^- redox shuttle perform poorly with the cobalt electrolyte. For example, two zinc porphyrins with three triphenylamine donor groups at the *meso*-position showed ~140 mV increased photovoltages when using the $\text{Co}^{2+}(\text{phen})_3/\text{Co}^{3+}(\text{phen})_3$ redox couple compared to that using the I^-/I_3^- redox shuttle. However, the photocurrents when using the cobalt electrolyte were less than half of that using the iodine electrolyte in most experimental conditions, leading the power conversion efficiencies of these porphyrin dyes using the cobalt electrolyte to less than 2.5%.¹⁵¹

The origin of this apparent incompatibility is not yet clear. Developing di-chromophoric dyes with high performance using cobalt electrolyte is therefore important.

3. The electron recombination reaction using the $\text{Co}^{2+}/\text{Co}^{3+}$ redox mediator compared to the I^-/I_3^- redox shuttle typically proceeds faster. It is interesting to see if the beneficial properties of di-chromophoric dyes enhancing electron lifetime can be also realized using cobalt electrolytes.
4. The combination of di-chromophoric dyes with cobalt electrolytes should improve the performance using thin photoanodes. This is because of that, light harvesting efficiency can be increased using di-chromophoric dyes using thin TiO_2 films; thin TiO_2 electrodes are often necessary when using fast redox shuttles to limit charge recombination.

The next section of the introduction will look at some of the most relevant fundamental photophysical processes that determine the photovoltaic performance of multi-chromophoric dyes. The experimental techniques used to study these processes are also introduced.

1.7. Electron transfer steps in multi-chromophoric DSSCs

To illustrate the importance of the various electron transfer steps in multi-chromophoric DSSCs, a hypothetical porphyrin trimer is depicted in Fig.1.13.

The excitation energy is channelled towards the electron acceptor TiO_2 due to decreasing band gap of the chromophores from right to left ($E_{g1} > E_{g2} > E_{g3}$) by Förster resonance energy transfer (more details in Section 1.9). Alternatively, driving force enabled by a gradually decreasing reduction potential of the chromophores towards the TiO_2 creates an electron transfer cascade. At the TiO_2 /sensitizer interface, electron injection from the photoexcited sensitizer into the TiO_2 conduction band takes place. The photogenerated hole moves towards the electrolyte interface, away from the TiO_2 , which is enabled by a gradually decreasing oxidation potential of the chromophores. Therefore, the distance between the injected electron and hole is elongated. Therefore the charge separated lifetime is increased. Finally, the positive charge on the porphyrin trimer is reduced by the redox mediator in the electrolyte.

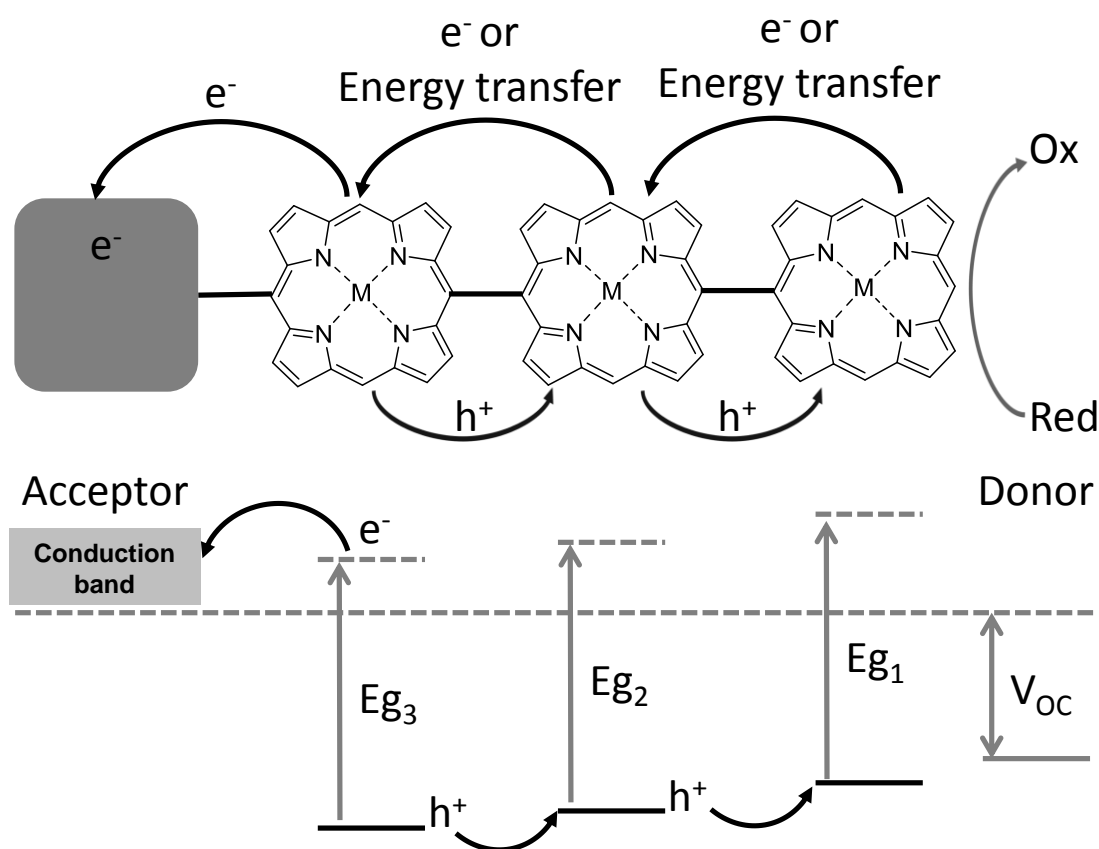


Figure 1.13 Intramolecular charge transfer and energy transfer in a porphyrin trimer after photoexcitation.

The difference in the band gap of the three chromophores in the hypothetical porphyrin trimer leads to a wide wavelength range of light absorption, enhancing the light harvesting efficiency. This should lead to increased short circuit current. However, it is important to recognize that a trade-off, in terms of power conversion efficiency, exists using the hypothetical porphyrin trimer in Fig. 1.13. Due to the driving force required for electron / hole transfer, the electrochemical energy stored in the charge separated state after each electron transfer step is reduced, compromising the maximum available output voltage. Too small of a driving force will lead to slow charge transfer kinetics and loss of photocurrent.

The effect of intramolecular charge transfer in multi-chromophoric dyes on dye regeneration rates has not been reported to date. Chapter 9 will show that in some cases, intramolecular charge transfer in a di-chromophoric porphyrin dye can lead to enhanced dye regeneration kinetics, without compromising the maximum output voltage. This is

achieved by using donor substituents with intrinsically faster dye regeneration kinetics compared to the porphyrin moiety.

1.8. Electron injection

Electron injection is the process, in which the photoexcited dye molecule transfers an electron into the conduction band of TiO₂ leading to a conduction band electron and an oxidized dye.

1.8.1 Physical description

The electron injection efficiency (E_{inj}) can be calculated based on a kinetic competition between the kinetics of the electron injection and the excited state decay (Eq. 1.8).¹⁵²

$$E_{inj} = \frac{k_{inj}}{k_{inj} + k_d} = \frac{k_{inj}}{k_{inj} + k_f + k_{nr}} \quad (1.8)$$

where, k_{inj} is the rate constant for electron injection; k_d is the rate constant for decay of the excited state of the sensitizers; k_f is the rate constant for fluorescence; k_{nr} is the rate constant for non-radiative decay of the excited state.

In the absence of electron transfer, the excited state may decay by emitting a photon (radiative) or through non-radiative channels. The time scale of the excited state decay varies substantially among sensitizers, from a few picoseconds to nanoseconds.

1.8.2 Factors affecting electron injection

The factors which affect the electron injection are:

1. Electronic coupling between the excited state and the acceptor states in TiO₂. For example, delocalization of the LUMO (approximately the lowest energy excited state) orbital (on either the anchoring group or the whole molecule) affects electronic coupling and influences electron injection kinetics in a series of free-base and zinc porphyrins.⁹⁸ The length of the spacer between anchoring group and the chromophore and the angle of orientation of the sensitizers on the TiO₂ surface influences the distance between the electron donor and the electron acceptor states in TiO₂, which in turn influences electronic coupling and the injection kinetics in several zinc porphyrins.¹⁰⁹
2. Driving force, which is the energy difference between the reduction potential ($E_{Re}^* = E_m(D^+/D^*)$) of the excited state of the dye (approximated by the LUMO level) and the conduction band edge potential of the semiconductor is

another important factor influencing electron injection kinetics. More negative excited state reduction potential of the sensitizer and / or more positive conduction band bottom edge of TiO_2 can increase the driving force and enhance the electron injection kinetics.^{153,154} A series of metalloporphyrins with different LUMO level showed large variation in electron injection properties. Only if the LUMO level was more negative compared to the conduction band bottom edge of the semiconductor can electron injection occur. It was found that Zn complex had faster electron injection kinetics compared to Cu and Pd complexes due to its higher lying LUMO level.¹⁵⁵ Adding additives to electrolyte, such as Li^+ , positively shifts the conduction band of TiO_2 therefore increases the electron injection kinetics.^{153,156,157} Changing TiO_2 to other semiconductors with a more positive conduction band potential, such as SnO_2 ,¹⁵⁸ also increases the driving force for electron injection. The minimum driving force to achieve 100% charge injection yield was 0.2 eV using a range of ruthenium complexes, porphyrin and organic dyes and ZnO reported by Katoh *et al.*¹⁵²

3. Excited state lifetime. Longer excited state lifetime may lead to larger electron injection yield. For example, electron injection occurs from both singlet and triplet states in N719-sensitized films.^{98,159-161} The long-lived (sub-picosecond to sub-nanosecond) triplet state enables efficient electron injection even with relatively slow injection rate. In another example, the short-lived excited state lifetime of a Ni complex porphyrin (sub-picoseconds) hinders efficient electron injection to SnO_2 even with 0.5 eV driving force.¹⁵⁵
4. Dye aggregation and dye layer morphology. Dye aggregates and weakly adsorbed dyes on the TiO_2 surface may lead to dyes without electron injection. Such non-injecting dyes show excited state decay to the ground state, rather than participate in electron injection.^{162,163} The morphology of the dye layer on TiO_2 may also affect electron injection. For example, the formation of dye aggregates may quench excited states by decreasing excited state lifetime and / or lowering excited state energy hence leading to lower injection efficiency.⁶³ Sometimes dye aggregation leads to enhanced electron injection, in particular H-aggregates (plane-to-plane π -stacking). This may

originate from the larger driving force for electron injection of the higher-energy H-aggregates excited states or the better electronic coupling between the H-aggregates excited state and the acceptor states in TiO₂.¹⁶⁴

1.8.3 Experimental techniques

Electron injection kinetics can be measured by femtosecond time-resolved transient absorption spectroscopy,^{161,165-167} transient emission spectroscopy^{153,168} as well as terahertz spectroscopy.^{155,169} These measurements were not available experimentally for this thesis.

Another, indirect approach to characterize the electron injection efficiency is the absorbed photon-to-electron conversion efficiency (APCE) quantum yield measurement, which is used in this work instead of the kinetic techniques above.¹⁷⁰ APCE is obtained by dividing incident photon-to-current conversion efficiency with light harvesting efficiency. The former can be measured using standard solar cell measurement techniques, while the latter can be calculated using the absorbance of the film and using an optical model.⁴¹ APCE is the product of electron injection efficiency and charge collection efficiency. By using thin TiO₂ films, the collection efficiency can be 100% and / or the value can be measured by charge extraction measurements.^{170,171} The APCE value divided by charge collection efficiency represents the electron injection efficiency. Characterization of electron injection efficiency using dichromophoric porphyrin dyes using APCE measurements are discussed in Chapter 4, 5 and 6.

1.9. Förster resonance energy transfer

Förster resonance energy transfer (or fluorescence resonance energy transfer, FRET) is a non-radiative, inter or intramolecular, process, in which energy is transferred from an excited donor to a ground state acceptor through space. FRET is a type of excited state dipole-dipole interaction and requires strong overlap of the emission spectra of the donor with the absorption spectra of the acceptor.¹⁷²⁻¹⁷⁴ Since electrons are not transferred in the FRET process, it is not necessary for the wavefunctions of the two molecules to overlap. The distance between the donor and acceptor would be important for an effective energy transfer, but generally occurs over longer distances compared to

electron transfer. The rate of energy transfer is inversely proportional to the sixth power of the distance.¹⁷⁴

The Jablonski diagram describes the typical electronic transitions in a photoexcited molecule and is used to illustrate FRET (Fig. 1.14).¹⁷⁵ After absorption of a photon, molecule is excited to either S_1 or S_2 states. Each electronic excited state has different vibrational states. Internal conversion from the higher energy excited states to the lowest energy excited state is generally a non-radiative process. The S_1 state may undergo intersystem crossing to the first triplet state T_1 via a spin conversion, which is spin forbidden but enabled in the case of strong spin-orbit coupling such as in Ru complexes. Photon is emitted from T_1 back to the ground state (phosphorescence), which typically has lower photon energy and show longer lived emission compared to the fluorescence from S_1 .

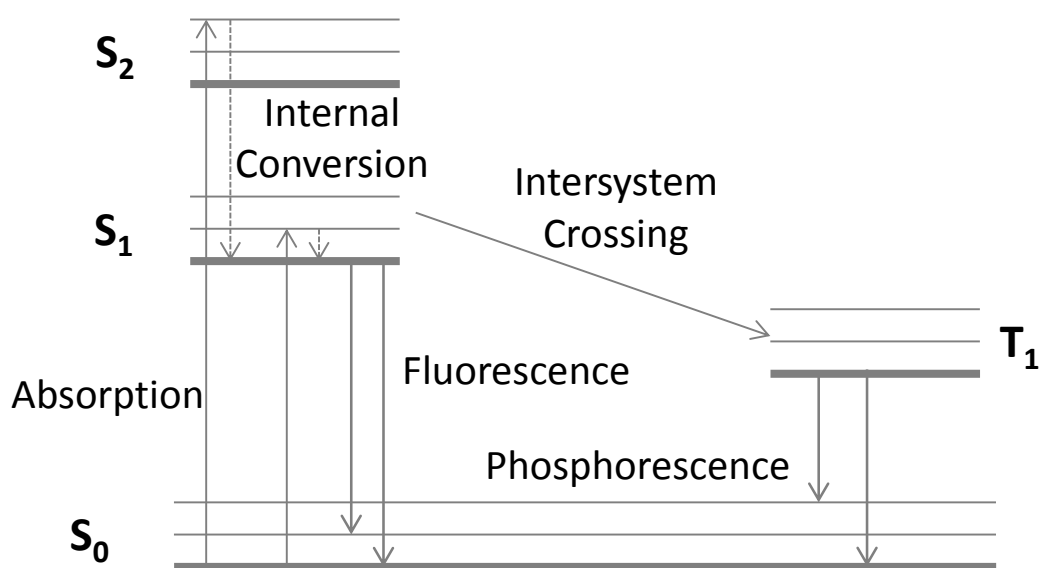


Figure 1.14 A Jablonski diagram

The energy of a photon emitted in fluorescence is lower than the energy of absorbed photon. This difference is known as the Stokes shift and is mainly attributed to the geometric relaxation of the excited state. The fluorescence spectrum is typically independent of the excitation wavelength, known as Kasha's rule. This is due to internal conversion process which is faster (typically 10^{-12} s) than the fluorescence lifetime (typically 10^{-8} s).¹⁷⁵ Contrary to Kasha's rule, in some cases, dual wavelength photoluminescence from both S_2 and S_1 states was observed in some porphyrins.^{105,176}

Fig. 1.15 illustrates FRET between a photoexcited donor and an acceptor based on the Jablonski diagram. The donor has a larger band gap (S_1 to S_0) compared to the acceptor. Photons with high energy excite the donor to the S_1 state. Strong through space coupling and alignment of the transition dipoles allow energy transfer from the excited state donor to the acceptor without photon emission in a non-radiative energy transfer process.

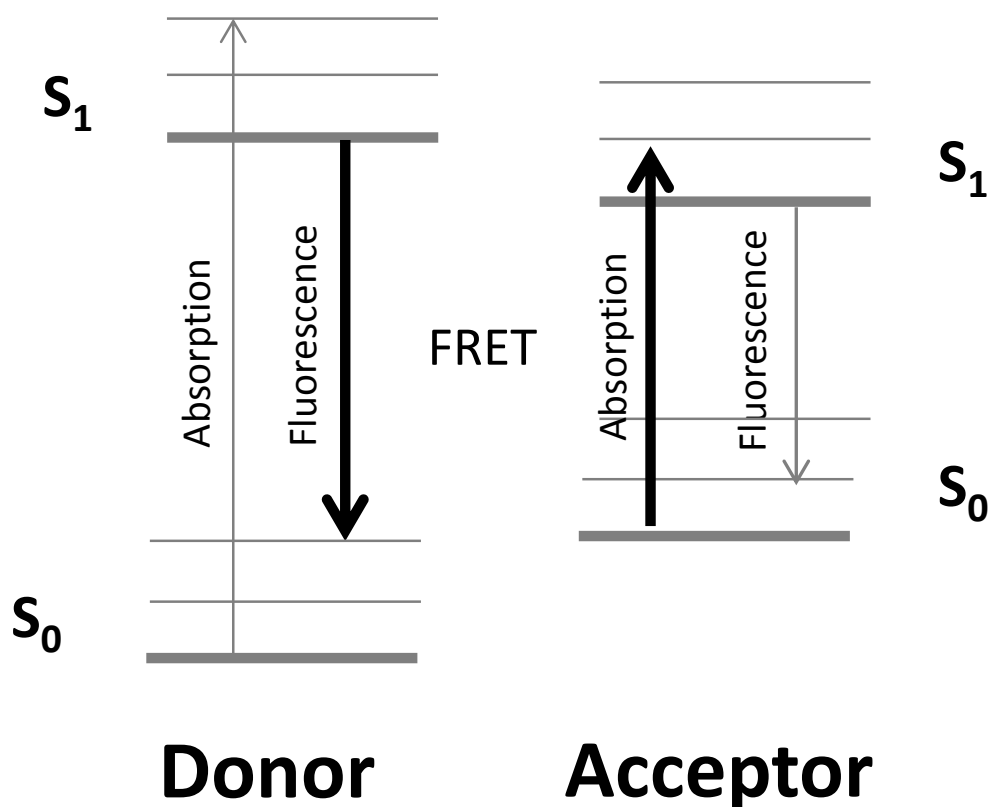


Figure 1.15 An illustration of Förster resonance energy transfer from an energy donor to an energy acceptor

1.10. Electron lifetime

Electron lifetime is an important device property of a solar cell characterizing how long the photoexcited electrons are in the conduction band before they recombine.¹⁷⁷⁻¹⁷⁹ In most DSSCs, fast dye regeneration leads to low concentration of oxidized dye on the TiO_2 surface, therefore the electron lifetime is related to the rate of electron transfer reactions between conduction band electrons and the electron acceptor in the electrolyte

(process ⑥ in Fig. 1.6). Because of its importance to most DSSCs, this will be discussed first.

1.10.1 Physical description

Mathematically, electron lifetime is obtained from the following differential equation (Eq. 1.9), establishing the proportionality between the rate of electron density decay ($\text{cm}^{-3} \text{s}^{-1}$) and electron density (n, cm^{-3}).

$$\frac{dn}{dt} = -\frac{n}{\tau} \quad (1.9)$$

where, n is the total electron density, cm^{-3} ; t is time, s; τ is pseudo first order electron lifetime, s.

Electron lifetime in DSSCs in almost all cases was found to be dependent on charge density. The first order reaction rate equation is modified to describe the small perturbation lifetime (Eq. 1.10).¹⁷¹

$$\tau_n = \frac{n_c}{n} \frac{dn}{dn_c} \tau = m\beta\tau \quad (1.10)$$

where, τ_n is small perturbation electron lifetime, s; n_c is the effective conduction band electron density, cm^{-3} ; m is the ideality of electron transport and recombination; β is trap distribution parameter.

The apparent diffusion coefficient ($D, \text{cm}^2 \text{s}^{-1}$) describes the time that an electron takes to transport across the film. The small perturbation (or the effective) diffusion coefficient ($D_n, \text{cm}^2 \text{s}^{-1}$) characterizes the diffusion of electrons across the film under the concentration gradient. The small perturbation diffusion coefficient relates to the apparent diffusion coefficient by a factor of $m\beta$ (Eq. 1.11).

$$D_n = \frac{n}{n_c} \frac{dn_c}{dn} D = \frac{D}{m\beta} \quad (1.11)$$

The slope β describes the temperature dependence as T/T_0 where T_0 is the characteristic temperature of electron traps. It is derived from the charge density versus open circuit voltage plot measured using a charge extraction method (Fig. 1.16(a)). The reason for the slope is attributed to the presence of an exponential trap state distribution below the conduction band.¹⁸⁰⁻¹⁸²

The factor m describes the deviation of the electron transport and recombination from ideality after introducing the parameter β . It is derived from either the electron lifetime or diffusion coefficient versus electron density plots (Fig. 1.16(b)). It may be affected by a conduction band shift or thermodynamic behavior of free electrons.^{183,184} The

parameter b in Fig. 1.16(b) is the order of free electron recombination. It was introduced since the diffusion length was found to be increased with increasing electron density in some cases,¹⁸⁵⁻¹⁸⁷ which reveals that the electron transport and electron recombination are not of the same order of electron density.

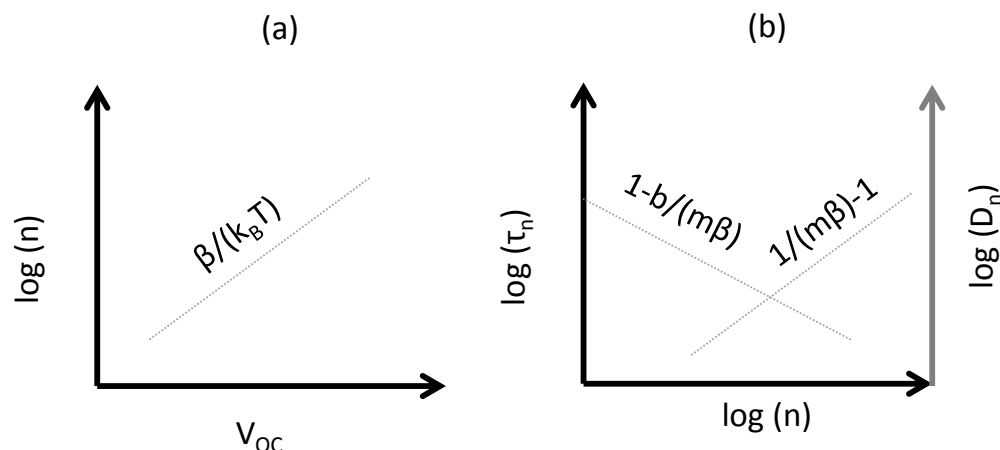


Figure 1.16 The relationship of the parameters in describing electron lifetime and electron diffusion. (a) electron density against open circuit voltage by charge extraction measurement and (b) electron lifetime or electron diffusion coefficient against electron density by small perturbation measurements.

1.10.2 Factors affecting electron lifetime

The following processes may control electron recombination and therefore influence electron lifetime:

1. Electron diffusion.
2. Conduction band edge potential.
3. Dye structure.
4. Internal and solvent reorganization energies.

1.10.2.1 Electron diffusion

Electron diffusion affects the electron lifetime as it determines the probability of an electron to meet with an electron acceptor in the electrolyte if recombination from surface traps are excluded. The faster the electrons are able to move, the faster the recombination is expected to be. This is illustrated in Fig. 1.16 by the opposing dependence of diffusion coefficient and electron lifetime on charge density.

Fig. 1.17 illustrates the effect of electron diffusion coefficient on electron lifetime. This is reproduced from the publication followed by the same logic as Barnes et al.¹⁷¹ The

conduction band edge potential between Cell 1 and Cell 2 is the same as can be seen from the n versus V_{OC} plot (Fig. 1.17(a)). A larger diffusion coefficient in Cell 1 compared to Cell 2 at the same short circuit current (Fig. 1.17(b)) leads to shorter electron lifetime of Cell 1 at the same charge density due to the faster movement of electron towards the acceptor species in the electrolyte (Fig. 1.17(c)). It demonstrates that diffusion coefficient versus charge density needs to be determined when electron lifetime between two cells are compared.

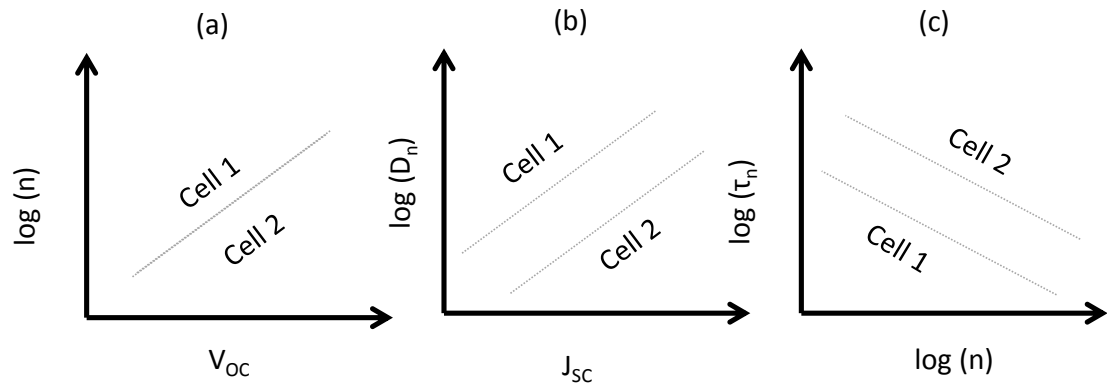


Figure 1.17 Illustration of the effect of diffusion coefficient on the electron lifetime

The larger electron diffusion coefficient could be due to i) fewer concentration of trap states or ii) shallower energy distribution located close to the conduction band bottom edge.¹⁷¹ Electron traps are formed due to the defects in the bulk mesoporous layer, at the electrolyte/TiO₂ interface, and / or at the grain boundaries.^{180,182,188,189} Single crystalline TiO₂ contains fewer defects and shows faster diffusion.^{190,191} ZnO nanorod electrodes showed almost no grain boundaries and showed faster electron transport property compared to the mesoporous ZnO films.¹⁹²

The type of semiconductor material as well as its morphology may affect electron diffusion coefficient. For example, ZnO has superior electron mobility compared to TiO₂, therefore faster electron diffusion to the current collector.^{193,194} The TiO₂ particle size may affect the electron diffusion. It was found that the electron diffusion coefficient increased as the TiO₂ particle size increased from 14 nm to 19 nm then to 32 nm. The increased electron diffusion coefficient was explained by the decreased surface area with larger particle size (therefore less trap states) and the condition of grain boundary.¹⁹⁵ Moreover, the porosity of the TiO₂ can affect the electron diffusion. The

higher the porosity of the TiO₂ network, the slower the electron diffusion may be. This as explained by more “dead ends” or fewer percolation paths for the electrons results in more tortuous electron diffusion paths.¹⁹⁶ Changing the type of cations in the electrolyte also affects the electron diffusion coefficient.^{157,197,198} The electrolyte with Li⁺ showed larger diffusion coefficient values compared to that of tetrabutylammonium cation (TBA⁺) and methylimidazolium cation (HmIm⁺). The Li⁺ concentration, on the other hand, did not affect the diffusion coefficient value, which suggested that the cations did not change the condition of charge traps.¹⁵⁷ The addition of *tert*-butylpyridine in the electrolyte can decrease the diffusion coefficient values in the presence of Li⁺.^{157,197,198}

1.10.2.2 Conduction band edge potential

The potential of the bottom edge of the conduction band of TiO₂ determines the driving force for electron recombination as Fig. 1.6 illustrates and therefore influences the electron lifetime. Although trapped electrons may also recombine with the acceptor species in the electrolyte, this is often ignored assuming that trapped electrons are in quasi-equilibrium with conduction band electrons during recombination.^{171,199}

The conduction band edge potential of TiO₂ is dependent upon the electrolyte/dye/TiO₂ interface property, especially the condition of surface charges. For instance, the electrolyte ingredient *tert*-butylpyridine can negative shift while Li⁺ can positive shift the conduction band edge potential.^{153,156,157,198,200} Adsorbed H⁺ and OH⁻ affect the TiO₂ flatband potential (the electrode potential measured with respect to a reference electrode at an electrolyte/semiconductor interface when the potential drop across the space charge layer becomes zero) following a Nernstian relationship.^{50,201} The conduction band edge potential of TiO₂ might shift by up to 1 V using potential-determining ions (primarily small ions such as H⁺ and Li⁺) in the electrolyte.²⁰² The structure of dye molecules and interactions with TiO₂ may also affect the potential of the conduction band bottom edge of TiO₂ by modulating adsorbed charges on the interface^{46,69,203} or by its dipole on the TiO₂ surface.^{204,205} The dipole moments of solvents can also modulate the conduction band bottom edge potential. By increasing the dipole moments from dimethylformamide (3.82) to 3-methoxypropionitrile (4.04) then to γ -butyrolactone (4.27), the conduction band bottom edge potential of TiO₂ was shifted positively by 74 mV and 18 mV, respectively.²⁰⁶

The conduction band potential of TiO₂ can be affected by TiCl₄ treatment, also employed in this work to prepare DSSCs. In a report by O'Regan *et al.*, it was

downward shifted by 80 mV after a TiCl_4 treatment.²⁰⁷ The $\text{TiO}_2(\text{e}^-)$ -reduced species in the electrolyte recombination rate was reduced by 20 times and therefore the electron lifetime was enhanced.

The common method to find the relative position of the conduction band edge potential is to measure the electron density versus open circuit voltage using charge extraction measurement^{42,177,207-210} or measuring the chemical capacitance using electrochemical impedance spectroscopy (EIS) measurement.^{211,212} In this thesis, charge extraction measurement is employed. The technique is described in Section 1.10.3.

1.10.2.3 Dye structure

Although the sensitizer is electrochemically not involved in the electron recombination reaction (it does not get reduced or oxidized), its structure has been shown to have a large effect on it.

Generally, organic dyes have shorter electron lifetimes than the Ru-based dyes when using the I/I_3^- redox couple. This is mainly due to the high concentration of I_3^- at the vicinity of the TiO_2 surface in the organic-sensitized devices.⁶⁹ Porphyrins, either free-base or zinc complexes, generally have shorter electron lifetimes than N719 when using the iodine-based electrolyte.⁹⁶

Fig. 1.18 illustrates the effect of the sensitizer structure on the electron recombination reaction. Molecules and ions adsorbed on the TiO_2 surface can influence the recombination reaction by either blocking the approach of I_3^- ions or attracting I_3^- ions through various interactions.

- a) Blocking effect. The blocking effect is that, by adding bulky groups, the distance between the TiO_2 surface and the electrolyte is increased and the conduction band electrons-oxidized species in electrolyte recombination is therefore retarded (Fig. 1.18(a)). The blocking effect is dependent on the packing density of the sensitizers on the TiO_2 surface, for example, devices with full surface coverage of the TiO_2 were reported to obtain larger photovoltage than devices with reduced dye-loading.^{42,213} Larger molecular size as well as alkyl chains both contribute to the blocking effects of organic dyes, resulting in longer electron lifetimes. Covalently linking bulky chains on the substituents of the porphyrin to add a steric effect has been widely used to increase the electron lifetime and photovoltage.^{27,34,94,214,215}
- b) Partial charges. Partial charges are the net charges (either negatively or

positively charged) on the dye molecules due to the asymmetric distribution of electrons. The negative partial charges in the molecule, for example partial charged oxygen can attract Li^+ and consequently I_3^- to closer to the TiO_2 surface, therefore reducing the electron lifetime (Fig. 1.18(b)).^{69,216,217} In the case of N719, negative partial charges, localized on the NCS ligands or nonbonded carboxyl groups at the ligand unit, attract positive cations in the electrolyte and pushing I_3^- from the TiO_2 surface.⁶⁹

- c) Dipole-dipole forces, dipole-induced dipole forces and dispersion forces (induced dipole-induced dipole forces). These intermolecular forces are weak attractive forces between the negative side of one molecule and the positive side of another molecule. For molecules having permanent dipoles, both dipole-dipole and dipole-induced dipole interactions can occur. When mixing one polar molecule and another nonpolar molecule, the dipole-induced dipole forces dominate. Dispersion forces are present in all molecules whether they are polar or nonpolar. This thesis will focus on dispersion forces as they change with increasing polarizability of electrons.

Dispersion forces are related to the polarizability of sensitizers and the distance between the two species. In DSSCs, the dyes may attract redox couples in electrolyte solution because of dispersion forces (Fig. 1.18(c)), and this may trigger faster recombination kinetics. Stronger dispersion forces between the dye and acceptors in the electrolyte was reported with longer π -conjugation unit in a series of triphenylamine-based dyes linked by different numbers of vinylene and thiophene units. The short electron lifetime and low photovoltage was consequently obtained.⁶⁸ A new di-chromophoric porphyrin was designed in this thesis to utilize the dispersion force to elongate electron lifetime (see Chapter 8).

- d) Coordination. A coordination complex can be formed when the coordination center (typically transition metal ions) and the ligands can share covalent bonds. Similar to the blocking effect, the coordination complex can block the conduction band electrons-oxidized species in electrolyte recombination pathway. For example, the additive in the electrolyte, *t*BP, may coordinate with the zinc porphyrin thus blocking the recombination process and increasing the electron lifetime (Fig. 1.18(d)).^{42,64}

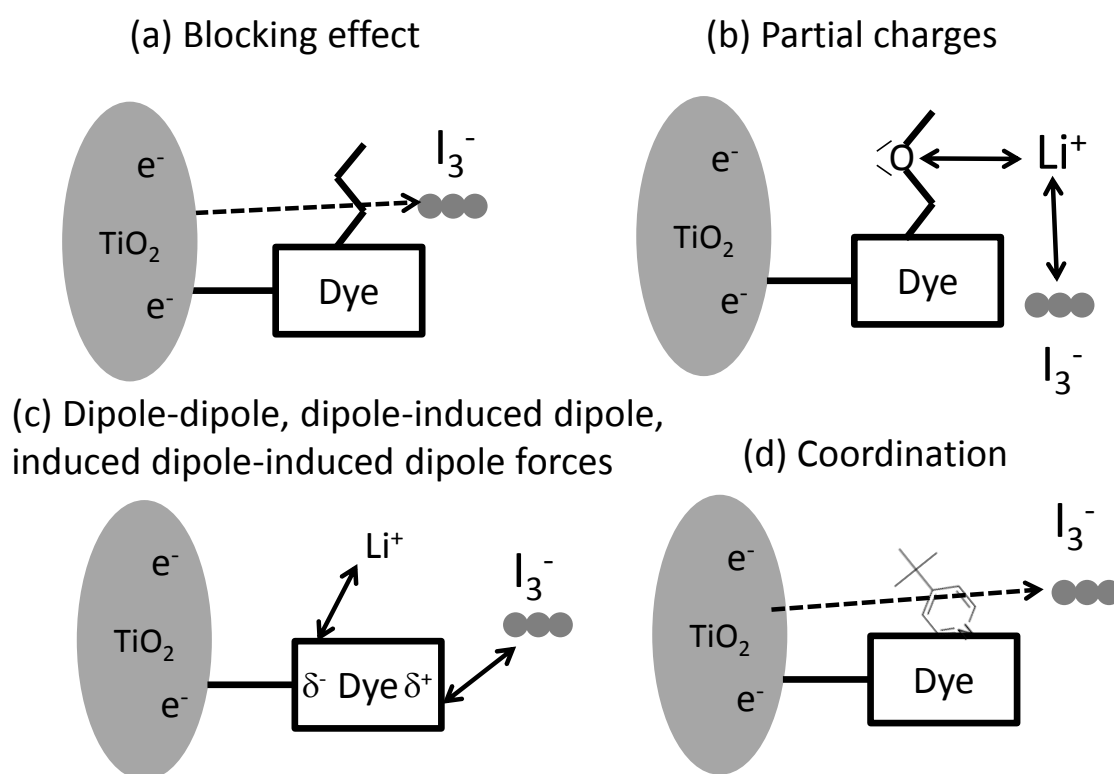


Figure 1.18 Molecular structure effects on the $\text{TiO}_2(e^-)\text{-I}_3^-$ recombination process at the TiO_2 surface.

1.10.2.4 Internal and solvent reorganization energies

According to Marcus theory, the reorganization energy during electron transfer is related to the change of the geometry during the electron transfer process.²¹⁸ A smaller reorganization energy typically leads to faster electron transfer rate in the normal Marcus regime. In terms of the electron lifetime, the reorganization energy of the redox species in the electrolyte may affect the recombination kinetics. The reduction of I_3^- to I^- is a two-electron reaction during the recombination process, which may require a larger reorganization energy compared to the one electron redox couple, such as Fc^+ to Fc ²¹⁹⁻²²¹ and Co^{3+} to Co^{2+} .^{26,27,191,222-224} The structure of the cobalt redox couple did not affect the reorganization energy. For example, a series of cobalt polypyridine redox couples was reported to show similar reorganization energy of 0.6 eV.²²⁵ The $\text{TiO}_2(e^-)\text{-Fc}^+$ or -Co^{3+} recombination reaction was reported to be faster than the $\text{TiO}_2(e^-)\text{-I}_3^-$ recombination, especially in some of the ruthenium based sensitizers.²²⁵ Another contribution to the reorganization energy is the solvation shell surrounding the redox mediator. The energy levels of the redox mediator are distributed to some extent due to

the fluctuations of the solvation shell, which in turn affects the reorganization energy of the redox mediator.²²⁶

The above four effects could influence electron lifetime simultaneously. Establishing the dominant mechanism is often quite elaborative. Reduced dye loading experiment can be used to distinguish dye blocking effect from the effect of attracting forces. The blocking effect diminishes at low dye coverages at large exposed TiO₂ surfaces, while attraction forces should still be operable at lower dye loading condition.^{42,213} Varying the concentration and nature of electrolyte components such as Li (nature size of cation), *t*BP and the redox couple concentrations are often employed to determine the effect of conduction band edge potential and electron diffusion coefficient on electron lifetime.^{157,198,200,227}

1.10.3 Experimental techniques

1.10.3.1 Small perturbation techniques

The presence of electron traps states leading to large dispersion of charge carrier lifetimes makes charge carrier lifetime measurements using large signal modulation or large signal decays difficult. Small perturbation techniques were introduced to measure the electron transport and electron recombination without affecting the steady state trap state distribution significantly. The transient signal is triggered by an optical (light intensity) or electrical (current or voltage) perturbation on a background signal. The background signal relates to a steady state; by changing the background signal, electron transport and recombination under various background steady states and consequently, electron densities can be studied. Two main small perturbation techniques to measure electron recombination (electron lifetime) and electron transport (electron diffusion coefficient) are intensity-modulated photovoltage/photocurrent spectroscopy (IMPS/IMVS) measurements^{181,195,228,229} and stepped light-induced transient measurements of photocurrent and voltage (SLIM-PCV).^{41,96,230,231}

- IMPS measures the modulation of photocurrent in response to the modulation of the incident light intensity at short circuit condition. Electron extraction from the TiO₂ is the main pathway to change the electron density in TiO₂, thus the electron diffusion time constant (the parameter used to calculate the diffusion coefficient) can be obtained from the breakpoint frequency ($f_p=1/(2\pi\tau)$). IMVS

measures the modulation of photovoltage in response to the modulation of incident light intensity at open circuit condition. In the absence of charge extraction, electron recombination is the main pathway to change the electron density in TiO_2 , thus the electron lifetime can be obtained from the breakpoint frequency.

- SLIM-PCV measures the photocurrent/photovoltage transient in response to a stepwise reduction in light intensity. The photocurrent transient is obtained at short circuit condition, and therefore the electron transport dynamics (electron diffusion coefficient) is obtained. The photovoltage transient is obtained at open circuit condition, and therefore the electron recombination dynamics (electron lifetime) is obtained.

In this thesis, SLIM-PCV and charge extraction measurements will be employed to measure the electron lifetime and diffusion. There are two advantages of SLIM-PCV compared to the IMPS/IMVS measurements:

1. Faster to measure. The transient SLIM-PCV method measures one transient at a time, while the frequency modulated IMPS/IMVS requires to measure the current response to light modulation at various frequencies. Any long-term drift in device performance may affect these latter measurements and may cause dispersion in the measured time constants.
2. Simpler to fit the curves to get time constant. The plots obtained from the SLIM-PCV measurements are photocurrent/photovoltage versus time. Using small modulation, almost all cases a simple mono-exponential equation is sufficient to obtain good quality fitting. The plots obtained from the IMPS/IMVS measurements often represented as EIS equivalent Nyquist or Bode plots. In case of dispersion, non-ideal circuit elements may lead to the requirement of a complicated equivalent circuit to obtain good quality fitting.²³²⁻²³⁴

1.10.4 Background of SLIM-PCV measurements

The SLIM-PCV measurement was introduced in 2005 by Mori *et al.*²³⁰ An illustration of the SLIM-PCV measurement is shown in Fig. 1.19. Typically, it employs a diode laser as the light source for modulating the light intensity. The small stepwise-reduced laser intensity by a function generator induces the photocurrent or photovoltage decay. The photocurrent and photovoltage transients are recorded by a digital multimeter.

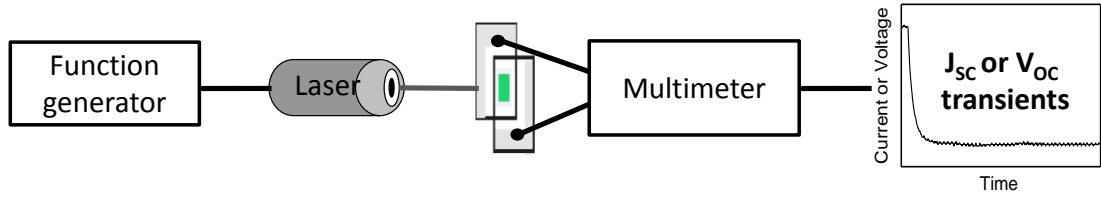


Figure 1.19 Scheme of stepped light-induced transient measurements of photocurrent and voltage.

The transient curves are typically fitted by a mono-exponential decay.^{230,235} The time constant is consequently obtained as the fitting parameter. The electron diffusion coefficient is calculated from this time constant and the electron lifetime is the fitted time constant.

The processes during diffusion coefficient measurement are illustrated in Fig. 1.20. At short circuit condition, injected electrons in TiO₂ can diffuse through the TiO₂ layer. The dye cation D⁺ concentration is negligible due to the fast regeneration; the TiO₂(e⁻)-dye cation recombination is therefore ignored. If recombination time constant of the conduction band electrons with the oxidized species in the electrolyte is slower by 2-3 orders of magnitude than the electron transport time, recombination during charge extraction can be ignored. The photocurrent decay is characterized by the time constant τ_c , which corresponds to electron diffusion. The electron diffusion coefficient is further derived from this time constant following Eq. 1.12 by solving a one-dimensional diffusion equation.²³⁰

$$D_n = \frac{\omega^2}{2.77\tau_c} \quad (1.12)$$

where, ω is the thickness of TiO₂ film.

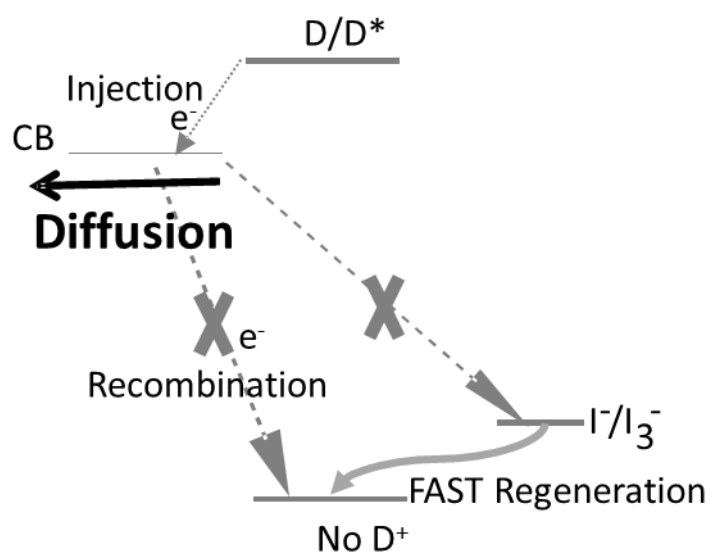


Figure 1.20 Illustration of the mechanism of diffusion coefficient measurement under short circuit condition

The electron transfer mechanism during the electron lifetime measurement is illustrated in Fig. 1.21. At open circuit condition, injected electrons in TiO_2 cannot be extracted due to the high external resistance. If the dye cation D^+ concentration is negligible due to the fast regeneration, the photovoltage transient is characterized by the time constant τ_n which corresponds to the electron recombination.

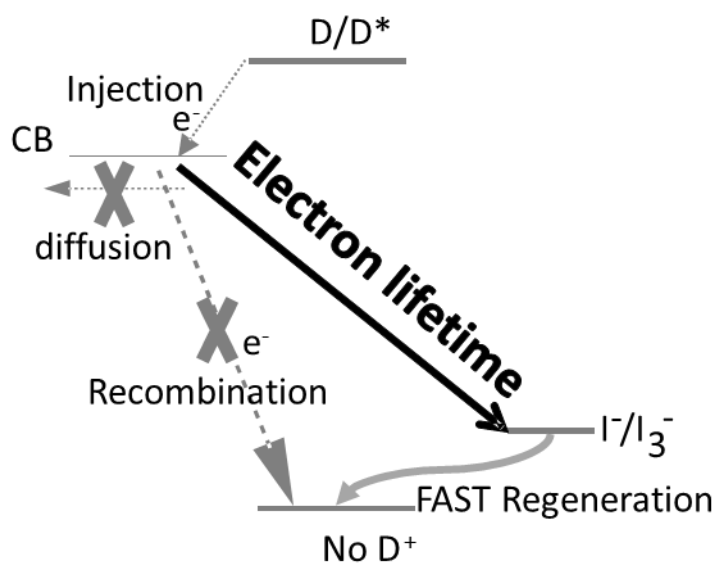


Figure 1.21 Illustration of the mechanism of electron lifetime measurement under open circuit condition

Electron density in TiO_2 is obtained by integrating the photocurrent transient in a charge extraction measurement.^{208,236} An illustration of the charge extraction measurement is shown in Fig. 1.22. The laser, same as used in the SLIM-PCV measurement and the sample is held at open circuit condition by using a fast switch. The laser intensity is completely turned off (controlled by a function generator), meanwhile, the switch is closed leading to short circuit condition. By integrating the resulting photocurrent detected by the multimeter, the charge at the initial light intensity is obtained.

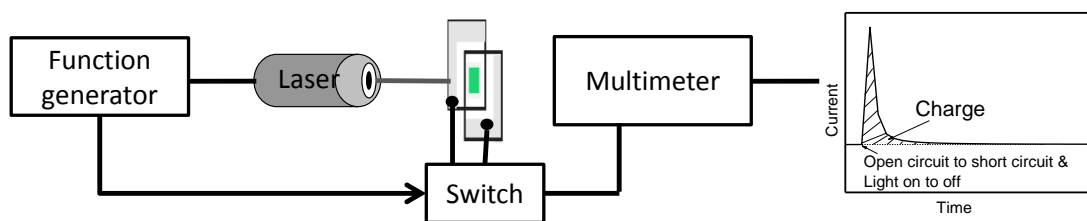


Figure 1.22 Scheme of charge extraction measurement.

1.11. Dye regeneration

Dye regeneration in a DSSC is the electron transfer step in which the oxidized dye returns to its reduced state, while an electron donor in the electrolyte is oxidized (process ④ in Fig. 1.6)

1.11.1 Physical description

From the point of view of DSSC efficiency, dye regeneration can be characterized by the dye regeneration yield (ϕ_{reg}), which describes the kinetic competition between the conduction band electrons-dye cation recombination and the dye regeneration. Mathematically, it can be calculated as Eq. 1.13, where, k_{reg} is the regeneration rate constant; k_{edr} is the recombination rate constant between $\text{TiO}_2(e^-)$ and dye cation.

$$\phi_{reg} = \frac{k_{reg}}{k_{reg} + k_{edr}} \quad (1.13)$$

1.11.2 Factors affecting dye regeneration

Dye regeneration kinetics is mainly dependent on the energy gap between the HOMO of the sensitizer and the electrochemical potential of the electrolyte.²³⁷⁻²⁴⁰ To achieve a fast dye regeneration rate, the ground-state oxidation potential $E_{Ox} = E_m(D^+/D)$, approximated

by the HOMO of the sensitizer should be positive enough to gain sufficient free energy difference with respect to the electrolyte redox potential. The requirement for the lowest driving force has been studied in several dye systems.^{219,220,241} The motivation of minimizing the driving force for dye regeneration is to aid the improvement of low band gap sensitizers and new redox couples.^{26,220} This is because a trade-off between the driving force for dye regeneration and light absorption / photovoltage exists as described in Section 1.7. Increased driving force based on a positive shift of the HOMO level of the sensitizer (or a negative shift of the electrolyte potential) means reduced light absorption (or reduced photovoltage).²⁴² The driving force requirement has been investigated in a series of carbazole-thiophene organic dyes using Fc/Fc⁺ derivatives as the redox mediators, which suggested that a driving force of 0.20-0.25 eV ($\Delta G=20-25$ kJ mol⁻¹) is sufficient to obtain nearly 100% dye regeneration yield.²¹⁹ A driving force of 0.18 eV ($\Delta G=18$ kJ mol⁻¹) was too small for efficient regeneration due to the relative fast recombination between the TiO₂(e⁻) and the dye cation.²²⁰ Driving forces as large as 0.70 eV are required to overcome the activation energy in the two-electron reaction I/I₃⁻ redox couple.²⁴³⁻²⁴⁵ In another report, driving force as low as 0.3 eV was sufficient for an efficient dye regeneration of thirty ruthenium dyes using the I/I₃⁻ redox couple.²³⁷ In terms of altering the driving force for dye regeneration, two possible approaches can be used.

1. Adjusting the HOMO level of the sensitizer. For example, adding electron withdrawing groups on the porphyrin core positively shifted the HOMO level,³¹ while attaching electron donor on the porphyrin core typically negatively shifted the HOMO level.^{30,76}
2. Choosing the redox couple. Regeneration of dye cations by the typical I/I₃⁻ electrolyte is generally fast, while the one-electron reaction redox mediators, such as ferrocene^{219,246} and Cobalt(II)-bis[2,6-bis(1'-butylbenzimidazol-2'-yl)pyridine],²⁴⁷ showed even faster regeneration kinetics with sufficient driving force. Changing the structure of the redox couple to tune the electrochemical potential can also affect the regeneration kinetics.^{219,241}

Additional considerations affecting dye regeneration kinetics are:

1. Steric hindrance on the sensitizer. The effect of alkyl chains on the regeneration kinetics is under debate.^{219,248} Slower regeneration rate was observed in a series of Ru-based sensitizers when the length of the alkyl chains increased. For alkyl

chains longer than C₁₃H₂₇, the regeneration kinetics was even slower than the TiO₂(e⁻)-dye cation recombination kinetics.²⁴⁸ Slower regeneration rate was also observed in a series of π -conjugated organic dyes with alkyl chains compared to those without.²⁴⁹ While in a series of organic sensitizers, the alkyl chains played negligible role in affecting the regeneration rate.²¹⁹

2. The electrolyte solvent. Electrolyte viscosity affects ionic diffusion.^{250,251} In general, the lower the viscosity of the solvent, the faster the diffusion of the ions / cations in the electrolyte leading to faster regeneration.⁴⁸
3. Solvation energy may influence the reorganization energy of the dye regeneration reaction influencing the reaction kinetics.²⁵²
4. Changing the concentration of the reduced species in the redox shuttle.²⁵³ The higher concentration of the reduced species in electrolyte, the faster the regeneration of the sensitizer. However, if the ion diffusivity in the electrolyte reaches the limit, increasing the concentration of redox shuttle makes no difference on the regeneration rate.²¹⁹ In particular, the positively charged components in the electrolyte that could adsorb on TiO₂, such as Li⁺, accelerates the regeneration as they can change the actual concentration of redox couple at the proximity of the sensitizers.²⁵⁴

1.11.3 Experimental techniques

The TiO₂(e⁻)-dye cation recombination, dye regeneration and intramolecular hole transfer kinetics can be characterized by transient absorption spectroscopy (TAS). TAS is a pump / probe technique. The probe light excites the sample promoting electrons from the ground state S₀ to the first singlet excited state S₁. The pump laser further excites the first singlet excited state S₁ to the singlet excited states with higher energy S₂, S₃, etc. If an intersystem crossing occurs after the excitation, the pump laser can also excite the first triplet excited state T₁ to the triplet excited states with higher energy T₂, T₃, etc. The absorption by photoexcited states is the transient absorption (Fig. 1.23(a)). The typical response of a pump / probe system using a photodetector is shown in Fig. 1.23(b). The probe light establishes a background signal, showing a constant voltage of the photodetector. Following photoexcitation by the pump laser, the transient state is formed. The additional absorption of the transient state causes a negative voltage

transient (less photons are detected, Fig. 1.23(b)). The changing of voltage versus the recording time is converted to the change in optical density (ΔOD) using the Eq. 1.14.

$$\Delta OD = -\log\left(\frac{V_t}{V_{t=0}}\right) \quad (1.14)$$

where, $V_{t=0}$ is the response voltage before laser illumination, V ; V_t is the response voltage after laser illumination, V .

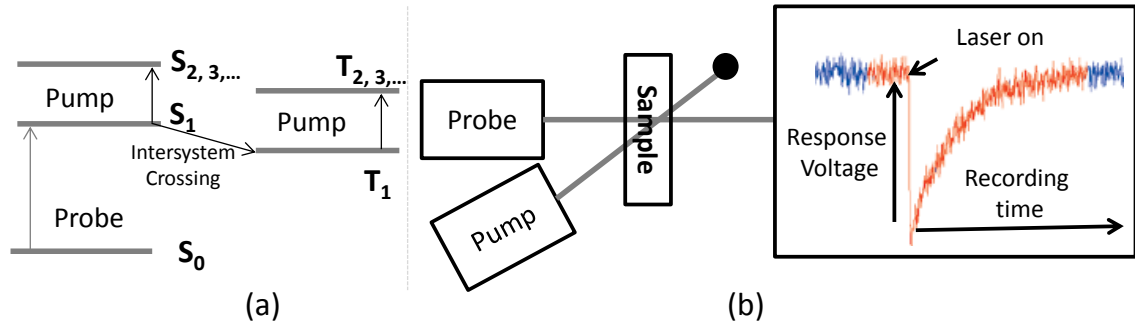


Figure 1.23 Principle of transient absorption spectroscopy measurement using pump / probe system. (a) the energy levels of the molecule and (b) the response curve of the measurement.

The ΔOD may have contribution from various processes as shown in Eq. 1.15.

$$\Delta OD = \Delta OD(D^+) + \Delta OD(TiO_2(e^-)) + \Delta OD(I_2^-) + \Delta OD(PL) + \Delta OD(Tri) + \Delta OD(EA) \quad (1.15)$$

$\Delta OD(D^+)$ is the absorption of dye cation; $\Delta OD(TiO_2(e^-))$ is absorption of the electrons in TiO_2 film; $\Delta OD(I_2^-)$ is the absorption by the intermediate product I_2^- ; $\Delta OD(PL)$ is photoluminescence; $\Delta OD(Tri)$ is absorption of triplet state; $\Delta OD(EA)$ is electroabsorption (Stark effect) caused by a local electric field.^{255,256}

Photoluminescence lifetime is around several nanoseconds, therefore it cannot be detected in a microsecond time scale dye regeneration measurement used in this study. $\Delta OD(Tri)$ is also negligible in typical DSSCs with large incident photon-to-current efficiency due to efficient charge injection.²⁵⁷ Electroabsorption appears at onset of the ground state absorption range. $\Delta OD(I_2^-)$ is difficult to detect due to low concentration of I_2^- and weak absorption. $\Delta OD(TiO_2(e^-))$ is typically observed as a long-lived signal which can be correlated with electron lifetime measurements performed electrically. A simplified equation Eq. 1.16 is often used to fit the transient species decay curves for well performing DSSCs.

$$\Delta OD = \Delta OD(D^+) + \Delta OD(TiO_2(e^-)) \quad (1.16)$$

A stretched exponential, rather than mono-exponential, equation is employed due to a distribution of different time constants.^{219,258} This is because the concentrations of the D^+ , $TiO_2(e^-)$, I^- and I_3^- around the electrolyte/dye/ TiO_2 interface is not uniform. Furthermore, the condition of charge traps may change as the concentration of the cations varied and affects the time constants.¹⁵⁷ The observed lifetime (τ_{obs}) is introduced instead of the characteristic stretched relaxation time (τ_{WW}) to better describe the dye cation decay kinetics. The stretching parameter β reflects the deviation of the decay from single exponential character. The relations of the parameters in Eq. 1.17 are shown in Eqs. 1.18 to 1.21.

$$\Delta OD(t) = \Delta OD_{t=0} e^{-(t/\tau_{WW})^\beta} \quad (1.17)$$

$$\tau_{obs} = \frac{\tau_{WW}}{\beta} \Gamma\left(\frac{1}{\beta}\right) \quad (1.18)$$

$$\Gamma\left(\frac{1}{\beta}\right) = \int_0^\infty u^{\frac{1}{\beta}-1} e^{-u} du \quad (1.19)$$

$$k_{obs} = \frac{1}{\tau_{obs}} \quad (1.20)$$

$$k_{reg} = (k_{obs} - k_{rec}) \times \frac{1}{[M]} \quad (1.21)$$

where, $\Delta OD(t)$ is the change of optical density with time (t); $\Delta OD_{t=0}$ is the initial absorption magnitude of dye cation or $TiO_2(e^-)$; β is the stretching parameter; τ_{WW} is the characteristic stretched relaxation time, s; $\Gamma()$ is the gamma function; τ_{obs} is the observed lifetime, s; k_{obs} is the observed rate constant, s^{-1} ; k_{rec} is the observed recombination rate constant, s^{-1} ; k_{reg} is the observed regeneration rate constant, $M^{-1} s^{-1}$; $[M]$ is the concentration of reduced species in the redox shuttle, M.

Transient absorption spectrum of the sensitizer can be used to probe if intramolecular charge transfer occurs in a multi-chromophoric dye molecule. Sensitizers with multiple chromophores may show multiple dye cation absorption bands.²⁵⁹⁻²⁶² For the YD2-o-C8 in acetonitrile, the transient absorption band in the visible wavelength range is assigned to vibrational relaxation from S_2 to S_1 states. The absorption band in the near infrared wavelength range was attributed to the intramolecular charge separated state, created by the electron transfer from the donor (the diarylamino unit) to the acceptor (the carboxylic acid group).²⁶⁰ While for the porphyrins with phenylethenyl linkers on TiO_2 , the absorption band in the near infrared wavelength range up to 900 nm was assigned to formation of the porphyrin cation radical.²⁶³

1.11.4 Conduction band electrons-dye cation recombination

The $\text{TiO}_2(\text{e}^-)$ -dye cation recombination typically occurs on the millisecond timescale and is limited by slow release of electrons from electron traps. More broadly, the recombination kinetics influenced by the following parameters:

1. Electron diffusion. This is mainly related to electron density and trap states, which is similar to its effect on electron lifetime in Section 1.10.2.
2. Thermodynamic driving force, which is the electrochemical energy difference between the conduction band bottom edge of the TiO_2 (assuming the recombination is dominated by free electrons in the TiO_2 conduction band) and the oxidation potential (approximated by the HOMO level) of the sensitizer. The change in conduction band bottom edge of the TiO_2 has been discussed in Section 1.10.2. The modulation of the HOMO level of the sensitizer can be achieved by attaching electron donating / withdrawing groups onto the sensitizer as described above in Section 1.1.
3. The distance between the two reacting species that influences the electronic coupling for electron transfer. Longer linkers between the donor and the anchoring group^{264,265} can slow down the $\text{TiO}_2(\text{e}^-)$ -dye cation recombination kinetics. Porphyrins with conjugated and non-conjugated linker or tilt angles of molecules on the TiO_2 surface (by changing the number of phenyl between the porphyrin and the carboxylic group) both altered the distance between the dye and the TiO_2 surface.¹⁰⁹
4. The barrier height for recombination, which is influenced by the chemical / physical nature of the medium between the reacting species. For example, a dielectric layer formed at the TiO_2 surface by ionic additives in the solid-state electrolyte slowed down the recombination kinetics.²⁶⁶ Electron recombination with the dye cations could occur through space, not only through chemical bond, which could be the reason for the poor photovoltaic performance of a porphyrin dye with a longer linker compared to that with a shorter linker.²⁶³
5. In some cases, sub-nanosecond component of recombination is observed, attributed to recombination with electrons in surface traps.^{96,109,263} It is possible that electrons are injected not into the TiO_2 conduction band, but to localized surface states near the dye molecule. Strong coupling between the surface trap state and the oxidized dye leads to faster recombination.²⁶⁷ From temperature

dependent measurements, it was concluded that the recombination kinetics was controlled by a distribution of barrier heights present at the interface of the adsorbed dyes and the TiO₂ surface.²⁶⁸

1.11.5 Intramolecular hole transfer

Intramolecular hole transfer, also referred to as cascaded hole transfer, or intramolecular dye regeneration, is a hole transfer step between two parts of the molecule covalently linked. It is distinguished from intermolecular hole transfer predominantly due to the possibility of the through bond character as well as controlled distance between electron donor and acceptor species.

The motivation to use sensitizers with an intramolecular hole transfer is to increase the distance between the positive charge and the TiO₂ and therefore achieve long-lived charge-separation state.⁴⁴ Such design is thought to mimic the photosynthetic process in natural plants, which utilizes a cascaded electron transfer step following charge separation to increase the lifetime of the charge separated state.²⁶⁹⁻²⁷⁴

Molecular dyads, triads, and various designs of supramolecular assemblies with cascaded electron and energy transfer pathways have been intensively studied.^{262,270,272,275-279} For example, in triphenylamine substituted Ru-based dyads, long-lived charge separation state with a half lifetime of 300 μ s has been achieved.²⁸⁰

Due to the close proximity and relatively strong coupling, the timescale of intramolecular charge transfer is typically in the nanosecond time domain.^{262,277,279,280}

For example, the electron transfer rate from the phenothiazine (PTZ) to the Ru(III) in a PTZ-substituted Ru-based dye was faster than the instrument resolution (50 ns) of the setup.²⁷⁷ Faster than 20 ns intramolecular electron transfer was obtained with Ru-based heterotriads with a trialkylamine donor.²⁸⁰ N845, another Ru-based heterotriad showed nanosecond electron transfer from the donor to the Ru ligand.²⁷⁹ More recently, a ~5 ns intramolecular hole transfer was reported in a triarylamine-substituted π -conjugated Ru-based dyad at -45 °C.²⁶²

1.12. Collaborators contribution

The collaborators of ARC Discovery Project (main funding for work summarized in this thesis) are acknowledged. The experimental details for their contribution to this thesis are contained here.

All the compounds (except N719 and MK2) employed in this study were synthesized and chemical characterization performed by Dr Pawel Wagner at Intelligent Polymer Research Institute (IPRI), University of Wollongong (Australia). Density functional theory (DFT) calculations, FT-Raman spectra and resonance Raman spectroscopy were performed by Prof. Keith Gordon group at the University of Otago (New Zealand).

1.13. Summary

The motivation of this study is to explore the multi-chromophoric porphyrin concept to simultaneously increase photocurrent and photovoltage of dye-sensitized solar cells. This design is contrasted to the single chromophore design, currently producing higher performance DSSC results, in which new absorption bands are introduced through the push-pull effect of substituents. The scope is to build on previous studies using a porphyrin dimer and to investigate more fundamentally important questions related to electron and energy transfer pathways using chromophores based on carbazole. This is enabled by the spectrally distinguishable characteristic of carbazole and its derivatives used in this thesis.

The main mechanism of DSSC operation was described, with particular focus on sensitizer design. A brief history of porphyrin dye development was presented, highlighting the fact that porphyrin dyes are one of the most successful dyes to date. However, there may be limits to further increases by decreasing the band gap, due to a decrease in the achievable open circuit voltage. This introduction also highlighted the complexity of using multi-chromophoric dyes in terms of electron injection, electron recombination and dye regeneration. Due to the importance of these processes to the result of this thesis, these were reviewed in more detail.

This review identified the following gaps in the existing literature:

1. The exact dye regeneration / recombination mechanisms in multi-chromophoric dyes are not clear.
2. The effect of tuning the energy levels on the photovoltaic performance using multi-chromophoric dyes is not obvious due to the lack of strong electronic coupling between the chromophores. Particularly interesting is the effect of attaching lower band gap chromophores to the porphyrin and its effect on photovoltaic performance. This should show what limit of the di-chromophoric

dye approach is compared to single chromophore or mixed dyes.

3. The effect of the additional chromophores on the electron lifetime in the multi-chromophoric dyes distinguishing the various factors is not clear.
4. The effect of intramolecular charge transfer in multi-chromophoric dyes on dye regeneration rates has not been reported to date.
5. Comparison of co-sensitization and di-chromophoric dye approaches.
6. Utility of di-chromophoric dyes with cobalt electrolyte.

This thesis advances knowledge in the above areas by using state-of-the-art spectroscopic techniques, including stepped light-induced transient measurements of photocurrent and voltage, transient absorption, photoluminescence, differential pulse voltammetry and spectroelectrochemical measurements. These spectroscopic tools are combined with detailed photovoltaic device fabrication and testing methodology.

1.14. References

- (1) O'Regan, B.; Grätzel, M. *Nature* **1991**, *353*, 737.
- (2) Nazeeruddin, M. K.; Kay, A.; Rodicio, I.; Humphry-Baker, R.; Mueller, E.; Liska, P.; Vlachopoulos, N.; Grätzel, M. *J. Am. Chem. Soc.* **1993**, *115*, 6382.
- (3) Nazeeruddin, M. K.; De Angelis, F.; Fantacci, S.; Selloni, A.; Viscardi, G.; Liska, P.; Ito, S.; Takeru, B.; Grätzel, M. *J. Am. Chem. Soc.* **2005**, *127*, 16835.
- (4) Wang, Q.; Ito, S.; Grätzel, M.; Fabregat-Santiago, F.; Mora-Seró, I.; Bisquert, J.; Bessho, T.; Imai, H. *J. Phys. Chem. B* **2006**, *110*, 25210.
- (5) Gao, F.; Wang, Y.; Shi, D.; Zhang, J.; Wang, M.; Jing, X.; Humphry-Baker, R.; Wang, P.; Zakeeruddin, S. M.; Grätzel, M. *J. Am. Chem. Soc.* **2008**, *130*, 10720.
- (6) Chen, C.-Y.; Wang, M.; Li, J.-Y.; Pootrakulchote, N.; Alibabaei, L.; Ngoc-le, C.-h.; Decoppet, J.-D.; Tsai, J.-H.; Grätzel, C.; Wu, C.-G.; Zakeeruddin, S. M.; Grätzel, M. *Acs Nano* **2009**, *3*, 3103.
- (7) Yu, Q.; Wang, Y.; Yi, Z.; Zu, N.; Zhang, J.; Zhang, M.; Wang, P. *Acs Nano* **2010**, *4*, 6032.
- (8) Han, L.; Islam, A.; Chen, H.; Malapaka, C.; Chiranjeevi, B.; Zhang, S.; Yang, X.; Yanagida, M. *Energy Environ. Sci.* **2012**, *5*, 6057.
- (9) Horiuchi, T.; Miura, H.; Sumioka, K.; Uchida, S. *J. Am. Chem. Soc.*

2004, *126*, 12218.

(10) Hara, K.; Wang, Z.-S.; Sato, T.; Furube, A.; Katoh, R.; Sugihara, H.; Dan-oh, Y.; Kasada, C.; Shinpo, A.; Suga, S. *J. Phys. Chem. B* **2005**, *109*, 15476.

(11) Kim, S.; Lee, J. K.; Kang, S. O.; Ko, J.; Yum, J. H.; Fantacci, S.; De Angelis, F.; Di Censo, D.; Nazeeruddin, M. K.; Grätzel, M. *J. Am. Chem. Soc.* **2006**, *128*, 16701.

(12) Ito, S.; Zakeeruddin, S. M.; Humphry-Baker, R.; Liska, P.; Charvet, R.; Comte, P.; Nazeeruddin, M. K.; Péchy, P.; Takata, M.; Miura, H.; Uchida, S.; Grätzel, M. *Adv. Mater.* **2006**, *18*, 1202.

(13) Hwang, S.; Lee, J. H.; Park, C.; Lee, H.; Kim, C.; Park, C.; Lee, M.-H.; Lee, W.; Park, J.; Kim, K.; Park, N.-G.; Kim, C. *Chem. Commun.* **2007**, 4887.

(14) Wang, Z.-S.; Koumura, N.; Cui, Y.; Takahashi, M.; Sekiguchi, H.; Mori, A.; Kubo, T.; Furube, A.; Hara, K. *Chem. Mater.* **2008**, *20*, 3993.

(15) Ito, S.; Miura, H.; Uchida, S.; Takata, M.; Sumioka, K.; Liska, P.; Comte, P.; Pechy, P.; Grätzel, M. *Chem. Commun.* **2008**, 5194.

(16) Zeng, W.; Cao, Y.; Bai, Y.; Wang, Y.; Shi, Y.; Zhang, M.; Wang, F.; Pan, C.; Wang, P. *Chem. Mater.* **2010**, *22*, 1915.

(17) Tsao, H. N.; Yi, C.; Moehl, T.; Yum, J.-H.; Zakeeruddin, S. M.; Nazeeruddin, M. K.; Grätzel, M. *ChemSusChem* **2011**, *4*, 591.

(18) Xu, M.; Zhang, M.; Pastore, M.; Li, R.; De Angelis, F.; Wang, P. *Chem. Sci.* **2012**, *3*, 976.

(19) Kay, A.; Grätzel, M. *J. Phys. Chem.* **1993**, *97*, 6272.

(20) Cherian, S.; Wamser, C. C. *J. Phys. Chem. B* **2000**, *104*, 3624.

(21) Nazeeruddin, M. K.; Humphry-Baker, R.; Officer, D. L.; Campbell, W. M.; Burrell, A. K.; Grätzel, M. *Langmuir* **2004**, *20*, 6514.

(22) Wang, Q.; Campbell, W. M.; Bonfantani, E. E.; Jolley, K. W.; Officer, D. L.; Walsh, P. J.; Gordon, K.; Humphry-Baker, R.; Nazeeruddin, M. K.; Grätzel, M. *J. Phys. Chem. B* **2005**, *109*, 15397.

(23) Campbell, W. M.; Jolley, K. W.; Wagner, P.; Wagner, K.; Walsh, P. J.; Gordon, K. C.; Schmidt-Mende, L.; Nazeeruddin, M. K.; Wang, Q.; Grätzel, M.; Officer, D. L. *J. Phys. Chem. C* **2007**, *111*, 11760.

(24) Park, J. K.; Lee, H. R.; Chen, J.; Shinokubo, H.; Osuka, A.; Kim, D. *J. Phys. Chem. C* **2008**, *112*, 16691.

- (25) Bessho, T.; Zakeeruddin, S. M.; Yeh, C. Y.; Diau, E. W. G.; Grätzel, M. *Angew. Chem. Int. Ed.* **2010**, *49*, 6646.
- (26) Yella, A.; Lee, H.-W.; Tsao, H. N.; Yi, C.; Chandiran, A. K.; Nazeeruddin, M. K.; Diau, E. W.-G.; Yeh, C.-Y.; Zakeeruddin, S. M.; Grätzel, M. *Science* **2011**, *334*, 629.
- (27) Mathew, S.; Yella, A.; Gao, P.; Humphry-Baker, R.; Curchod, B. F. E.; Ashari-Astani, N.; Tavernelli, I.; Rothlisberger, U.; Nazeeruddin, M. K.; Grätzel, M. *Nat. Chem.* **2014**, *6*, 242.
- (28) Li, L.-L.; Diau, E. W.-G. *Chem. Soc. Rev.* **2013**, *42*, 291.
- (29) Hsieh, C.-P.; Lu, H.-P.; Chiu, C.-L.; Lee, C.-W.; Chuang, S.-H.; Mai, C.-L.; Yen, W.-N.; Hsu, S.-J.; Diau, E. W.-G.; Yeh, C.-Y. *J. Mater. Chem.* **2010**, *20*, 1127.
- (30) Wang, C.-L.; Chang, Y.-C.; Lan, C.-M.; Lo, C.-F.; Diau, E. W.-G.; Lin, C.-Y. *Energy Environ. Sci.* **2011**, *4*, 1788.
- (31) Giraudeau, A.; Callot, H. J.; Gross, M. *Inorg. Chem.* **1979**, *18*, 201.
- (32) Koumura, N.; Wang, Z.-S.; Mori, S.; Miyashita, M.; Suzuki, E.; Hara, K. *J. Am. Chem. Soc.* **2006**, *128*, 14256.
- (33) Wu, S.-L.; Lu, H.-P.; Yu, H.-T.; Chuang, S.-H.; Chiu, C.-L.; Lee, C.-W.; Diau, E. W.-G.; Yeh, C.-Y. *Energy Environ. Sci.* **2010**, *3*, 949.
- (34) Higashino, T.; Imahori, H. *Dalton Trans.* **2015**, *44*, 448.
- (35) Wang, C.-L.; Lan, C.-M.; Hong, S.-H.; Wang, Y.-F.; Pan, T.-Y.; Chang, C.-W.; Kuo, H.-H.; Kuo, M.-Y.; Diau, E. W.-G.; Lin, C.-Y. *Energy Environ. Sci.* **2012**, *5*, 6933.
- (36) Yanagida, S.; Yu, Y.; Manseki, K. *Acc. Chem. Res.* **2009**, *42*, 1827.
- (37) Koehorst, R. B. M.; Boschloo, G. K.; Savenije, T. J.; Goossens, A.; Schaafsma, T. J. *J. Phys. Chem. B* **2000**, *104*, 2371.
- (38) Mai, C.-L.; Huang, W.-K.; Lu, H.-P.; Lee, C.-W.; Chiu, C.-L.; Liang, Y.-R.; Diau, E. W.-G.; Yeh, C.-Y. *Chem. Commun.* **2010**, *46*, 809.
- (39) Liu, Y.; Lin, H.; Dy, J. T.; Tamaki, K.; Nakazaki, J.; Nakayama, D.; Uchida, S.; Kubo, T.; Segawa, H. *Chem. Commun.* **2011**, *47*, 4010.
- (40) Warnan, J.; Pellegrin, Y.; Blart, E.; Odobel, F. *Chem. Commun.* **2012**, *48*, 675.
- (41) Mozer, A. J.; Griffith, M. J.; Tsekouras, G.; Wagner, P.; Wallace, G. G.; Mori, S.; Sunahara, K.; Miyashita, M.; Earles, J. C.; Gordon, K. C.; Du, L.; Katoh, R.;

- Furube, A.; Officer, D. L. *J. Am. Chem. Soc.* **2009**, *131*, 15621.
- (42) Sunahara, K.; Griffith, M. J.; Uchiyama, T.; Wagner, P.; Officer, D. L.; Wallace, G. G.; Mozer, A. J.; Mori, S. *ACS Appl. Mater. Interfaces* **2013**, *5*, 10824.
- (43) Koval, C. A.; Howard, J. N. *Chem. Rev.* **1992**, *92*, 411.
- (44) Ardo, S.; Meyer, G. J. *Chem. Soc. Rev.* **2009**, *38*, 115.
- (45) Haque, S. A.; Palomares, E.; Cho, B. M.; Green, A. N. M.; Hirata, N.; Klug, D. R.; Durrant, J. R. *J. Am. Chem. Soc.* **2005**, *127*, 3456.
- (46) O'Regan, B. C.; Durrant, J. R. *Acc. Chem. Res.* **2009**, *42*, 1799.
- (47) Kamat, P. V.; Tvrdy, K.; Baker, D. R.; Radich, J. G. *Chem. Rev.* **2010**, *110*, 6664.
- (48) Hagfeldt, A.; Boschloo, G.; Sun, L.; Kloo, L.; Pettersson, H. *Chem. Rev.* **2010**, *110*, 6595.
- (49) Halme, J.; Vahermaa, P.; Miettunen, K.; Lund, P. *Adv. Mater.* **2010**, *22*, E210.
- (50) Xu, Y.; Schoonen, M. A. A. *Am. Mineral.* **2000**, *85*, 543.
- (51) Hamann, T. W.; Jensen, R. A.; Martinson, A. B. F.; Van Ryswyk, H.; Hupp, J. T. *Energy Environ. Sci.* **2008**, *1*, 66.
- (52) Hamann, T. W.; Ondersma, J. W. *Energy Environ. Sci.*, *4*, 370.
- (53) Bella, F.; Gerbaldi, C.; Barolo, C.; Grätzel, M. *Chem. Soc. Rev.* **2015**, *44*, 3431.
- (54) Bignozzi, C. A.; Argazzi, R.; Boaretto, R.; Busatto, E.; Carli, S.; Ronconi, F.; Caramori, S. *Coord. Chem. Rev.* **2013**, *257*, 1472.
- (55) Grätzel, M. *J. Photochem. Photobiol. C: Photochem. Rev.* **2003**, *4*, 145.
- (56) Thomas, S.; Deepak, T. G.; Anjusree, G. S.; Arun, T. A.; Nair, S. V.; Nair, A. S. *J. Mater. Chem. A* **2014**, *2*, 4474.
- (57) Hua, Y.; He, J.; Zhang, C.; Qin, C.; Han, L.; Zhao, J.; Chen, T.; Wong, W.-Y.; Wong, W.-K. R.; Zhu, X. *J. Mater. Chem. A* **2014**.
- (58) Poddutoori, P. K.; Zarrabi, N.; Moiseev, A. G.; Gumbau-Brisa, R.; Vassiliev, S.; van der Est, A. *Chem. Eur. J.* **2013**, *19*, 3148.
- (59) El-Khouly, M. E.; Ryu, J. B.; Kay, K.-Y.; Ito, O.; Fukuzumi, S. *J. Phys. Chem. C* **2009**, *113*, 15444.
- (60) Argazzi, R.; Bignozzi, C. A.; Heimer, T. A.; Meyer, G. J. *Inorg. Chem.* **1997**, *36*, 2.

- (61) Murakami, T. N.; Koumura, N.; Uchiyama, T.; Uemura, Y.; Obuchi, K.; Masaki, N.; Kimura, M.; Mori, S. *J. Mater. Chem. A* **2013**, *1*, 792.
- (62) Cheng, M.; Yang, X.; Zhang, F.; Zhao, J.; Sun, L. *J. Phys. Chem. C* **2013**, *117*, 9076.
- (63) Mishra, A.; Fischer, M. K. R.; Bäuerle, P. *Angew. Chem. Int. Ed.* **2009**, *48*, 2474.
- (64) Liu, Y.; Lin, H.; Dy, J. T.; Tamaki, K.; Nakazaki, J.; Nishiyama, C.; Uchida, S.; Segawa, H.; Li, J. *J. Phys. Chem. C* **2014**, *118*, 1426.
- (65) Furube, A.; Katoh, R.; Hara, K.; Sato, T.; Murata, S.; Arakawa, H.; Tachiya, M. *J. Phys. Chem. B* **2005**, *109*, 16406.
- (66) Yano, J.; Koga, T.; Yamasaki, S. *J. Mater. Sci.* **1998**, *33*, 2817.
- (67) Uemura, Y.; Mori, S.; Hara, K.; Koumura, N. *Jpn. J. Appl. Phys.* **2012**, *51*, 10NE14/1.
- (68) Marinado, T.; Nonomura, K.; Nissfolk, J.; Karlsson, M. K.; Hagberg, D. P.; Sun, L.; Mori, S.; Hagfeldt, A. *Langmuir* **2009**, *26*, 2592.
- (69) Miyashita, M.; Sunahara, K.; Nishikawa, T.; Uemura, Y.; Koumura, N.; Hara, K.; Mori, A.; Abe, T.; Suzuki, E.; Mori, S. *J. Am. Chem. Soc.* **2008**, *130*, 17874.
- (70) Darwent, J. R.; Douglas, P.; Harriman, A.; Porter, G.; Richoux, M.-C. *Coord. Chem. Rev.* **1982**, *44*, 83.
- (71) Martinez-Diaz, M. V.; de la Torre, G.; Torres, T. *Chem. Commun.* **2010**, *46*, 7090.
- (72) Campbell, W. M.; Burrell, A. K.; Officer, D. L.; Jolley, K. W. *Coord. Chem. Rev.* **2004**, *248*, 1363.
- (73) Walter, M. G.; Rudine, A. B.; Wamser, C. C. *J. Porphyrins Phthalocyanines* **2010**, *14*, 759.
- (74) Giribabu, L.; Kanaparthi, R. K. *Curr. Sci.* **2013**, *104*, 847.
- (75) Urbani, M.; Grätzel, M.; Nazeeruddin, M. K.; Torres, T. *Chem. Rev.* **2014**, *114*, 12330.
- (76) Chang, Y.-C.; Wang, C.-L.; Pan, T.-Y.; Hong, S.-H.; Lan, C.-M.; Kuo, H.-H.; Lo, C.-F.; Hsu, H.-Y.; Lin, C.-Y.; Diau, E. W.-G. *Chem. Commun.* **2011**, *47*, 8910.
- (77) Ehret, A.; Stuhl, L.; Spitler, M. T. *J. Phys. Chem. B* **2001**, *105*, 9960.
- (78) Cid, J.-J.; Yum, J.-H.; Jang, S.-R.; Nazeeruddin, M. K.; Martínez-

Ferrero, E.; Palomares, E.; Ko, J.; Grätzel, M.; Torres, T. *Angew. Chem. Int. Ed.* **2007**, *46*, 8358.

(79) Funaki, T.; Koumura, N.; Sayama, K. *Chem. Lett.* **2013**, *42*, 1371.

(80) Sun, X.; Wang, Y.; Li, X.; Agren, H.; Zhu, W.; Tian, H.; Xie, Y. *Chem. Commun.* **2014**, *50*, 15609.

(81) Chang, S.; Wang, H.; Lee, L. T. L.; Zheng, S.; Li, Q.; Wong, K. Y.; Wong, W.-K.; Zhu, X.; Wong, W.-Y.; Xiao, X.; Chen, T. *Journal of Materials Chemistry C* **2014**, *2*, 3521.

(82) Kang, M. S.; Kang, S. H.; Kim, S. G.; Choi, I. T.; Ryu, J. H.; Ju, M. J.; Cho, D.; Lee, J. Y.; Kim, H. K. *Chem. Commun.* **2012**, *48*, 9349.

(83) Kang, S. H.; Choi, I. T.; Kang, M. S.; Eom, Y. K.; Ju, M. J.; Hong, J. Y.; Kang, H. S.; Kim, H. K. *J. Mater. Chem. A* **2013**, *1*, 3977.

(84) Clifford, J. N.; Martinez-Ferrero, E.; Viterisi, A.; Palomares, E. *Chem. Soc. Rev.* **2011**, *40*, 1635.

(85) Ogura, R. Y.; Nakane, S.; Morooka, M.; Orihashi, M.; Suzuki, Y.; Noda, K. *Appl. Phys. Lett.* **2009**, *94*, 073308.

(86) Wu, H.-P.; Ou, Z.-W.; Pan, T.-Y.; Lan, C.-M.; Huang, W.-K.; Lee, H.-W.; Reddy, N. M.; Chen, C.-T.; Chao, W.-S.; Yeh, C.-Y.; Diau, E. W.-G. *Energy Environ. Sci.* **2012**, *5*, 9843.

(87) Matthew, J. G.; Attila, J. M.; George, T.; Ying, D.; Pawel, W.; Klaudia, W.; Gordon, G. W.; Shogo, M.; David, L. O. *Appl. Phys. Lett.* **2011**, *98*, 163502.

(88) Wang, Y.; Chen, B.; Wu, W.; Li, X.; Zhu, W.; Tian, H.; Xie, Y. *Angew. Chem. Int. Ed.* **2014**, *53*, 10779.

(89) Ogomi, Y.; Pandey, S. S.; Kimura, S.; Hayase, S. *Thin Solid Films* **2010**, *519*, 1087.

(90) Magne, C.; Urien, M.; Pauporte, T. *RSC Advances* **2013**, *3*, 6315.

(91) Siegers, C.; Hohl-Ebinger, J.; Zimmermann, B.; Würfel, U.; Mülhaupt, R.; Hinsch, A.; Haag, R. *ChemPhysChem* **2007**, *8*, 1548.

(92) Odobel, F.; Pellegrin, Y.; Warnan, J. *Energy Environ. Sci.* **2013**, *6*, 2041.

(93) Shalabi, A. S.; El Mahdy, A. M.; Taha, H. O. *J. Nanopart. Res.* **2013**, *15*.

(94) Zhao, L.; Wagner, P.; Elliott, A. B. S.; Griffith, M. J.; Clarke, T. M.; Gordon, K. C.; Mori, S.; Mozer, A. J. *J. Mater. Chem. A* **2014**, *2*, 16963.

(95) Burrell, A. K.; Officer, D. L.; Plieger, P. G.; Reid, D. C. W. *Chem. Rev.*

2001, *101*, 2751.

(96) Griffith, M. J.; Sunahara, K.; Wagner, P.; Wagner, K.; Wallace, G. G.; Officer, D. L.; Furube, A.; Katoh, R.; Mori, S.; Mozer, A. J. *Chem. Commun.* **2012**, *48*, 4145.

(97) Jagadeeswari, S.; Paramaguru, G.; Renganathan, R. *J. Photochem. Photobiol., A* **2014**, *276*, 104.

(98) Santos, T. D.; Morandeira, A.; Koops, S.; Mozer, A. J.; Tsekouras, G.; Dong, Y.; Wagner, P.; Wallace, G.; Earles, J. C.; Gordon, K. C.; Officer, D.; Durrant, J. R. *J. Phys. Chem. C* **2010**, *114*, 3276.

(99) Rimington, C. *Biochem. J* **1960**, *75*, 620.

(100) Lee, C.-W.; Lu, H.-P.; Lan, C.-M.; Huang, Y.-L.; Liang, Y.-R.; Yen, W.-N.; Liu, Y.-C.; Lin, Y.-S.; Diao, E. W.-G.; Yeh, C.-Y. *Chem. Eur. J.* **2009**, *15*, 1403.

(101) Gouterman, M. *J. Chem. Phys.* **1959**, *30*, 1139.

(102) Gouterman, M. *J. Mol. Spectrosc.* **1961**, *6*, 138.

(103) Gouterman, M.; Wagnière, G. H.; Snyder, L. C. *J. Mol. Spectrosc.* **1963**, *11*, 108.

(104) Weiss, C.; Kobayashi, H.; Gouterman, M. *J. Mol. Spectrosc.* **1965**, *16*, 415.

(105) Morandeira, A. *Thesis, Universite DE Geneve* **2003**, 319.

(106) Uddin, J. 2012, p 87.

(107) Kasha, M. *Radiat. Res.* **1963**, *20*, 55.

(108) Si, L.; He, H. *J. Phys. Chem. A* **2014**, *118*, 3410.

(109) Imahori, H.; Kang, S.; Hayashi, H.; Haruta, M.; Kurata, H.; Isoda, S.; Canton, S. E.; Infahsaeng, Y.; Kathiravan, A.; Pascher, T.; Chabera, P.; Yartsev, A. P.; Sundstrom, V. *J. Phys. Chem. A* **2011**, *115*, 3679.

(110) Kalyanasundaram, K.; Vlachopoulos, N.; Krishnan, V.; Monnier, A.; Graetzel, M. *J. Phys. Chem.* **1987**, *91*, 2342.

(111) Haid, S.; Marszalek, M.; Mishra, A.; Wielopolski, M.; Teuscher, J.; Moser, J.-E.; Humphry-Baker, R.; Zakeeruddin, S. M.; Grätzel, M.; Baeuerle, P. *Adv. Funct. Mater.* **2012**, *22*, 1291.

(112) Akhtaruzzaman, M.; Seya, Y.; Asao, N.; Islam, A.; Kwon, E.; El-Shafei, A.; Han, L.; Yamamoto, Y. *J. Mater. Chem.* **2012**, *22*, 10771.

(113) Lu, H.-P.; Tsai, C.-Y.; Yen, W.-N.; Hsieh, C.-P.; Lee, C.-W.; Yeh, C.-Y.;

- Diau, E. W.-G. *J. Phys. Chem. C* **2009**, *113*, 20990.
- (114) Imahori, H. *J. Phys. Chem. B* **2004**, *108*, 6130.
- (115) Bach, U.; Lupo, D.; Comte, P.; Moser, J. E.; Weissortel, F.; Salbeck, J.; Spreitzer, H.; Gratzel, M. *Nature* **1998**, *395*, 583.
- (116) Feldt, S. M.; Lohse, P. W.; Kessler, F.; Nazeeruddin, M. K.; Gratzel, M.; Boschloo, G.; Hagfeldt, A. *Phys. Chem. Chem. Phys.* **2013**, *15*, 7087.
- (117) Park, J. K.; Chen, J.; Lee, H. R.; Park, S. W.; Shinokubo, H.; Osuka, A.; Kim, D. *J. Phys. Chem. C* **2009**, *113*, 21956.
- (118) Murakami, T. N.; Koumura, N.; Kimura, M.; Mori, S. *Langmuir* **2014**, *30*, 2274.
- (119) Venkateswararao, A.; Thomas, K. R. J.; Lee, C.-P.; Li, C.-T.; Ho, K.-C. *ACS Appl. Mater. Interfaces* **2014**, *6*, 2528.
- (120) Fischer, M. K. R.; Wenger, S.; Wang, M.; Mishra, A.; Zakeeruddin, S. M.; Grätzel, M.; Bäuerle, P. *Chem. Mater.* **2010**, *22*, 1836.
- (121) Kim, S.; Choi, H.; Baik, C.; Song, K.; Kang, S. O.; Ko, J. *Tetrahedron* **2007**, *63*, 11436.
- (122) Kato, S.-i.; Shimizu, S.; Kobayashi, A.; Yoshihara, T.; Tobita, S.; Nakamura, Y. *J. Org. Chem.* **2014**, *79*, 618.
- (123) Zhang, X.; Côté, A. P.; Matzger, A. J. *J. Am. Chem. Soc.* **2005**, *127*, 10502.
- (124) He, M.; Zhang, F. *J. Org. Chem.* **2006**, *72*, 442.
- (125) Roncali, J. *Chem. Rev.* **1992**, *92*, 711.
- (126) Grimsdale, A. C.; Chan, K. L.; Martin, R. E.; Jokisz, P. G.; Holmes, A. B. *Chem. Rev.* **2009**, *109*, 897.
- (127) Zhou, P.; Zhang, Z.-G.; Li, Y.; Chen, X.; Qin, J. *Chem. Mater.* **2014**, *26*, 3495.
- (128) Lee, J.-Y.; Shin, W.-S.; Haw, J.-R.; Moon, D.-K. *J. Mater. Chem.* **2009**, *19*, 4938.
- (129) Katz, H. E.; Bao, Z.; Gilat, S. L. *Acc. Chem. Res.* **2001**, *34*, 359.
- (130) Neto, B. A. D.; Lapis, A. A. M.; da Silva Junior, E. N.; Dupont, J. *Eur. J. Org. Chem.* **2013**, 228.
- (131) Wu, Y.; Zhu, W. *Chem. Soc. Rev.* **2013**, *42*, 2039.
- (132) Velusamy, M.; Justin Thomas, K. R.; Lin, J. T.; Hsu, Y.-C.; Ho, K.-C.

Org. Lett. **2005**, 7, 1899.

(133) Zhu, W.; Wu, Y.; Wang, S.; Li, W.; Li, X.; Chen, J.; Wang, Z.-s.; Tian, H. *Adv. Funct. Mater.* **2011**, 21, 756.

(134) Wu, Y.; Marszalek, M.; Zakeeruddin, S. M.; Zhang, Q.; Tian, H.; Grätzel, M.; Zhu, W. *Energy Environ. Sci.* **2012**, 5, 8261.

(135) Blouin, N.; Michaud, A.; Gendron, D.; Wakim, S.; Blair, E.; Neagu-Plesu, R.; Belletête, M.; Durocher, G.; Tao, Y.; Leclerc, M. *J. Am. Chem. Soc.* **2007**, 130, 732.

(136) Kim, J.-H.; Park, J. B.; Shin, S. A.; Hyun, M. H.; Hwang, D.-H. *Polymer* **2014**, 55, 3605.

(137) Günes, S.; Neugebauer, H.; Sariciftci, N. S. *Chem. Rev.* **2007**, 107, 1324.

(138) Wu, Y.; Zhang, X.; Li, W.; Wang, Z.-S.; Tian, H.; Zhu, W. *Adv. Energy Mater.* **2012**, 2, 149.

(139) Katoh, R.; Furube, A.; Mori, S.; Miyashita, M.; Sunahara, K.; Koumura, N.; Hara, K. *Energy Environ. Sci.* **2009**, 2, 542.

(140) Wang, Z.-S.; Cui, Y.; Dan-oh, Y.; Kasada, C.; Shinpo, A.; Hara, K. *J. Phys. Chem. C* **2008**, 112, 17011.

(141) Liu, Y.; Guo, X.; Xiang, N.; Zhao, B.; Huang, H.; Li, H.; Shen, P.; Tan, S. *J. Mater. Chem.* **2010**, 20, 1140.

(142) He, M.; Li, J.; Tandia, A.; Sorensen, M.; Zhang, F.; Fong, H. H.; Pozdin, V. A.; Smilgies, D.-M.; Malliaras, G. G. *Chem. Mater.* **2010**, 22, 2770.

(143) Asiri, A. M.; Marwani, H. M.; Khan, S. A. *J. Saudi Chem. Soc.* **2014**, 18, 392.

(144) Asiri, A. M.; Khan, S. A.; Al-Amoudi, M. S.; Alamry, K. A. *Bull. Korean Chem. Soc.* **2014**, 33, 1900.

(145) Lai, H.; Hong, J.; Liu, P.; Yuan, C.; Li, Y.; Fang, Q. *RSC Advances* **2012**, 2, 2427.

(146) Zhang, X.-H.; Wang, Z.-S.; Cui, Y.; Koumura, N.; Furube, A.; Hara, K. *J. Phys. Chem. C* **2009**, 113, 13409.

(147) Dhanabalan, A.; van Duren, J. K. J.; van Hal, P. A.; van Dongen, J. L. J.; Janssen, R. A. J. *Adv. Funct. Mater.* **2001**, 11, 255.

(148) Yang, J.; Ganesan, P.; Teuscher, J.; Moehl, T.; Kim, Y. J.; Yi, C.; Comte, P.; Pei, K.; Holcombe, T. W.; Nazeeruddin, M. K.; Hua, J.; Zakeeruddin, S. M.; Tian, H.;

Grätzel, M. *J. Am. Chem. Soc.* **2014**, *136*, 5722.

(149) Zhu, H.; Li, W.; Wu, Y.; Liu, B.; Zhu, S.; Li, X.; Agren, H.; Zhu, W. *Acs Sustain. Chem. Eng.* **2014**, *2*, 1026.

(150) Tang, Z.-M.; Lei, T.; Jiang, K.-J.; Song, Y.-L.; Pei, J. *Chem. Asian J.* **2010**, *5*, 1911.

(151) Aljarilla, A.; Clifford, J. N.; Pelleja, L.; Moncho, A.; Arrechea, S.; de la Cruz, P.; Langa, F.; Palomares, E. *J. Mater. Chem. A* **2013**, *1*, 13640.

(152) Katoh, R.; Furube, A. *J. Photochem. Photobiol. C: Photochem. Rev.* **2014**, *20*, 1.

(153) Koops, S. E.; O'Regan, B. C.; Barnes, P. R. F.; Durrant, J. R. *J. Am. Chem. Soc.* **2009**, *131*, 4808.

(154) Ning, Z.; Fu, Y.; Tian, H. *Energy Environ. Sci.*, *3*, 1170.

(155) Milot, R. L.; Moore, G. F.; Crabtree, R. H.; Brudvig, G. W.; Schmittenmaer, C. A. *J. Phys. Chem. C* **2013**, *117*, 21662.

(156) Liu, Y.; Hagfeldt, A.; Xiao, X.-R.; Lindquist, S.-E. *Sol. Energy Mater. Sol. Cells* **1998**, *55*, 267.

(157) Nakade, S.; Kanzaki, T.; Kubo, W.; Kitamura, T.; Wada, Y.; Yanagida, S. *J. Phys. Chem. B* **2005**, *109*, 3480.

(158) Fukai, Y.; Kondo, Y.; Mori, S.; Suzuki, E. *Electrochem. Commun.* **2007**, *9*, 1439.

(159) Damrauer, N. H.; Cerullo, G.; Yeh, A.; Boussie, T. R.; Shank, C. V.; McCusker, J. K. *Science* **1997**, *275*, 54.

(160) Tachibana, Y.; Haque, S. A.; Mercer, I. P.; Moser, J. E.; Klug, D. R.; Durrant, J. R. *J. Phys. Chem. B* **2001**, *105*, 7424.

(161) Asbury, J. B.; Hao, E.; Wang, Y. Q.; Ghosh, H. N.; Lian, T. Q. *J. Phys. Chem. B* **2001**, *105*, 4545.

(162) Dos Santos, T.; Morandeira, A.; Koops, S.; Mozer, A. J.; Tsekouras, G.; Dong, Y.; Wagner, P.; Wallace, G.; Earles, J. C.; Gordon, K. C.; Officer, D.; Durrant, J. R. *J. Phys. Chem. C* **2010**, *114*, 3276.

(163) Lim, J.; Kwon, Y. S.; Park, T. *Chem. Commun.* **2011**, *47*, 4147.

(164) Mulhern, K. R.; Detty, M. R.; Watson, D. F. *J. Phys. Chem. C* **2011**, *115*, 6010.

(165) Durrant, J. R.; Haque, S. A.; Palomares, E. *Chem. Commun.* **2006**, 3279.

- (166) Hannappel, T.; Burfeindt, B.; Storck, W.; Willig, F. *J. Phys. Chem. B* **1997**, *101*, 6799.
- (167) Benkö, G.; Kallioinen, J.; Korppi-Tommola, J. E. I.; Yartsev, A. P.; Sundström, V. *J. Am. Chem. Soc.* **2001**, *124*, 489.
- (168) Bram, O.; Cannizzo, A.; Chergui, M. *Phys. Chem. Chem. Phys.* **2012**, *14*, 7934.
- (169) Pijpers, J. J. H.; Ulbricht, R.; Derossi, S.; Reek, J. N. H.; Bonn, M. *J. Phys. Chem. C* **2011**, *115*, 2578.
- (170) Halme, J.; Boschloo, G.; Hagfeldt, A.; Lund, P. *J. Phys. Chem. C* **2008**, *112*, 5623.
- (171) Barnes, P. R. F.; Miettunen, K.; Li, X.; Anderson, A. Y.; Bessho, T.; Grätzel, M.; O'Regan, B. C. *Adv. Mater.* **2013**, *25*, 1881.
- (172) Forster, T. *Discuss. Faraday Soc.* **1959**, *27*, 7.
- (173) Jares-Erijman, E. A.; Jovin, T. M. *Nat Biotech* **2003**, *21*, 1387.
- (174) Basham, J. I.; Mor, G. K.; Grimes, C. A. *ACS Nano* **2010**, *4*, 1253.
- (175) Lakowicz, J. R. *Principles of fluorescence spectroscopy, 3rd Edition* **2008**.
- (176) Quimby, D. J.; Longo, F. R. *J. Am. Chem. Soc.* **1975**, *97*, 5111.
- (177) Mozer, A. J.; Wagner, P.; Officer, D. L.; Wallace, G. G.; Campbell, W. M.; Miyashita, M.; Sunahara, K.; Mori, S. *Chem. Commun.* **2008**, *0*, 4741.
- (178) Bisquert, J.; Fabregat-Santiago, F.; Mora-Sero, I.; Garcia-Belmonte, G.; Gimenez, S. *J. Phys. Chem. C* **2009**, *113*, 17278.
- (179) Zaban, A.; Greenshtein, M.; Bisquert, J. *ChemPhysChem* **2003**, *4*, 859.
- (180) Bisquert, J.; Vikhrenko, V. S. *J. Phys. Chem. B* **2004**, *108*, 2313.
- (181) Fisher, A. C.; Peter, L. M.; Ponomarev, E. A.; Walker, A. B.; Wijayantha, K. G. U. *J. Phys. Chem. B* **2000**, *104*, 949.
- (182) Bisquert, J. *J. Phys. Chem. B* **2004**, *108*, 2323.
- (183) Jennings, J. R.; Ghicov, A.; Peter, L. M.; Schmuki, P.; Walker, A. B. *J. Am. Chem. Soc.* **2008**, *130*, 13364.
- (184) Barnes, P. R. F.; Anderson, A. Y.; Durrant, J. R.; O'Regan, B. C. *Phys. Chem. Chem. Phys.* **2011**, *13*, 5798.
- (185) Barnes, P. R. F.; Anderson, A. Y.; Koops, S. E.; Durrant, J. R.; O'Regan, B. C. *J. Phys. Chem. C* **2008**, *113*, 1126.

- (186) Barnes, P. R. F.; O'Regan, B. C. *J. Phys. Chem. C* **2010**, *114*, 19134.
- (187) Bisquert, J.; Mora-Sero, I. *J. Phys. Chem. Lett.* **2010**, *1*, 450.
- (188) Peter, L. *Acc. Chem. Res.* **2009**, *42*, 1839.
- (189) Nakade, S.; Matsuda, M.; Kambe, S.; Saito, Y.; Kitamura, T.; Sakata, T.; Wada, Y.; Mori, H.; Yanagida, S. *J. Phys. Chem. B* **2002**, *106*, 10004.
- (190) Forro, L.; Chauvet, O.; Emin, D.; Zuppiroli, L.; Berger, H.; Lévy, F. *J. Appl. Phys.* **1994**, *75*, 633.
- (191) Lin, J.; Zhao, L.; Heo, Y.-U.; Wang, L.; Bijarbooneh, F. H.; Mozer, A. J.; Nattestad, A.; Yamauchi, Y.; Dou, S. X.; Kim, J. H. *Nano Energy* **2015**, *11*, 557.
- (192) Galoppini, E.; Rochford, J.; Chen, H.; Saraf, G.; Lu, Y.; Hagfeldt, A.; Boschloo, G. *J. Phys. Chem. B* **2006**, *110*, 16159.
- (193) Williams, V. O.; Jeong, N. C.; Prasittichai, C.; Farha, O. K.; Pellin, M. J.; Hupp, J. T. *ACS Nano* **2012**, *6*, 6185.
- (194) Martinson, A. B. F.; McGarrah, J. E.; Parpia, M. O. K.; Hupp, J. T. *Phys. Chem. Chem. Phys.* **2006**, *8*, 4655.
- (195) Nakade, S.; Saito, Y.; Kubo, W.; Kitamura, T.; Wada, Y.; Yanagida, S. *J. Phys. Chem. B* **2003**, *107*, 8607.
- (196) Benkstein, K. D.; Kopidakis, N.; van de Lagemaat, J.; Frank, A. J. *J. Phys. Chem. B* **2003**, *107*, 7759.
- (197) Fredin, K.; Gorlov, M.; Pettersson, H.; Hagfeldt, A.; Kloo, L.; Boschloo, G. *J. Phys. Chem. C* **2007**, *111*, 13261.
- (198) Boschloo, G.; Häggman, L.; Hagfeldt, A. *J. Phys. Chem. B* **2006**, *110*, 13144.
- (199) van de Lagemaat, J.; Park, N. G.; Frank, A. J. *J. Phys. Chem. B* **2000**, *104*, 2044.
- (200) Jennings, J. R.; Wang, Q. *J. Phys. Chem. C* **2009**, *114*, 1715.
- (201) Hagfeldt, A.; Grätzel, M. *Chem. Rev.* **1995**, *95*, 49.
- (202) Redmond, G.; O'Keeffe, A.; Burgess, C.; MacHale, C.; Fitzmaurice, D. *J. Phys. Chem.* **1993**, *97*, 11081.
- (203) Rühle, S.; Cahen, D. *J. Phys. Chem. B* **2004**, *108*, 17946.
- (204) Ronca, E.; Pastore, M.; Belpassi, L.; Tarantelli, F.; De Angelis, F. *Energy Environ. Sci.* **2013**, *6*, 183.
- (205) Chen, P.; Yum, J. H.; Angelis, F. D.; Mosconi, E.; Fantacci, S.; Moon, S.-

- J.; Baker, R. H.; Ko, J.; Nazeeruddin, M. K.; Grätzel, M. *Nano Lett.* **2009**, *9*, 2487.
- (206) Hao, F.; Jiao, X.; Li, J.; Lin, H. *Nanoscale* **2013**, *5*, 726.
- (207) O'Regan, B. C.; Durrant, J. R.; Sommeling, P. M.; Bakker, N. J. *J. Phys. Chem. C* **2007**, *111*, 14001.
- (208) Duffy, N. W.; Peter, L. M.; Rajapakse, R. M. G.; Wijayantha, K. G. U. *Electrochem. Commun.* **2000**, *2*, 658.
- (209) Barnes, P. R. F.; Liu, L.; Li, X.; Anderson, A. Y.; Kisserwan, H.; Ghaddar, T. H.; Durrant, J. R.; O'Regan, B. C. *Nano Lett.* **2009**, *9*, 3532.
- (210) Listorti, A.; Creager, C.; Sommeling, P.; Kroon, J.; Palomares, E.; Fornelli, A.; Breen, B.; Barnes, P. R. F.; Durrant, J. R.; Law, C.; O'Regan, B. *Energy Environ. Sci.* **2011**, *4*, 3494.
- (211) Jennings, J. R.; Liu, Y.; Wang, Q.; Zakeeruddin, S. M.; Grätzel, M. *Phys. Chem. Chem. Phys.* **2011**, *13*, 6637.
- (212) Barea, E. M.; Gonzalez-Pedro, V.; Ripolles-Sanchis, T.; Wu, H.-P.; Li, L.-L.; Yeh, C.-Y.; Diau, E. W.-G.; Bisquert, J. *J. Phys. Chem. C* **2011**, *115*, 10898.
- (213) Griffith, M. J.; Sunahara, K.; Furube, A.; Mozer, A. J.; Officer, D. L.; Wagner, P.; Wallace, G. G.; Mori, S. *J. Phys. Chem. C* **2013**, *117*, 11885.
- (214) Xue, X.; Zhang, W.; Zhang, N.; Ju, C.; Peng, X.; Yang, Y.; Liang, Y.; Feng, Y.; Zhang, B. *Rsc Advances* **2014**, *4*, 8894.
- (215) Koumura, N.; Wang, Z.-S.; Miyashita, M.; Uemura, Y.; Sekiguchi, H.; Cui, Y.; Mori, A.; Mori, S.; Hara, K. *J. Mater. Chem.* **2009**, *19*, 4829.
- (216) Reynal, A.; Forneli, A.; Martinez-Ferrero, E.; Sañchez-Dilaz, A.; Vidal-Ferran, A. n.; O'Regan, B. C.; Palomares, E. *J. Am. Chem. Soc.* **2008**, *130*, 13558.
- (217) O'Regan, B. C.; López-Duarte, I.; Martínez-Díaz, M. V.; Forneli, A.; Albero, J.; Morandeira, A.; Palomares, E.; Torres, T.; Durrant, J. R. *J. Am. Chem. Soc.* **2008**, *130*, 2906.
- (218) Marcus, R. A.; Sutin, N. *Biochim. Biophys. Acta* **1985**, *811*, 265.
- (219) Daeneke, T.; Mozer, A. J.; Uemura, Y.; Makuta, S.; Fekete, M.; Tachibana, Y.; Koumura, N.; Bach, U.; Spiccia, L. *J. Am. Chem. Soc.* **2012**, *134*, 16925.
- (220) Daeneke, T.; Mozer, A. J.; Kwon, T.-H.; Duffy, N. W.; Holmes, A. B.; Bach, U.; Spiccia, L. *Energy Environ. Sci.* **2012**, *5*, 7090.
- (221) Daeneke, T.; Kwon, T.-H.; Holmes, A. B.; Duffy, N. W.; Bach, U.; Spiccia, L. *Nat Chem* **2011**, *3*, 211.

- (222) Zhang, J.; Yang, L.; Zhang, M.; Wang, P. *Acta Polym. Sin.* **2013**, 619.
- (223) Polander, L. E.; Yella, A.; Curchod, B. F. E.; Ashari Astani, N.; Teuscher, J.; Scopelliti, R.; Gao, P.; Mathew, S.; Moser, J.-E.; Tavernelli, I.; Rothlisberger, U.; Grätzel, M.; Nazeeruddin, M. K.; Frey, J. *Angew. Chem. Int. Ed.* **2013**, 52, 8731.
- (224) Yum, J.-H.; Baranoff, E.; Kessler, F.; Moehl, T.; Ahmad, S.; Bessho, T.; Marchioro, A.; Ghadiri, E.; Moser, J.-E.; Yi, C.; Nazeeruddin, M. K.; Grätzel, M. *Nat Commun* **2012**, 3, 631.
- (225) Mosconi, E.; Yum, J.-H.; Kessler, F.; Gomez Garcia, C. J.; Zuccaccia, C.; Cinti, A.; Nazeeruddin, M. K.; Grätzel, M.; De Angelis, F. *J. Am. Chem. Soc.* **2012**, 134, 19438.
- (226) Feldt, S. M.; Lohse, P. W.; Kessler, F.; Nazeeruddin, M. K.; Gratzel, M.; Boschloo, G.; Hagfeldt, A. *Phys. Chem. Chem. Phys.* **2013**, 15, 7087.
- (227) Zhao, L.; Wagner, P.; van der Salm, H.; Clarke, T. M.; Gordon, K. C.; Mori, S.; Mozer, A. J. *J. Phys. Chem. C* **2015**, 119, 5350.
- (228) Schlichthörl, G.; Huang, S. Y.; Sprague, J.; Frank, A. J. *J. Phys. Chem. B* **1997**, 101, 8141.
- (229) Dloczik, L.; Ileperuma, O.; Lauermann, I.; Peter, L. M.; Ponomarev, E. A.; Redmond, G.; Shaw, N. J.; Uhlendorf, I. *J. Phys. Chem. B*, 101, 10281.
- (230) Nakade, S.; Kanzaki, T.; Wada, Y.; Yanagida, S. *Langmuir* **2005**, 21, 10803.
- (231) Nishida, J.-i.; Masuko, T.; Cui, Y.; Hara, K.; Shibuya, H.; Ihara, M.; Hosoyama, T.; Goto, R.; Mori, S.; Yamashita, Y. *J. Phys. Chem. C* **2010**, 114, 17920.
- (232) Bisquert, J. *J. Phys. Chem. B* **2001**, 106, 325.
- (233) Mastroianni, S.; Lanuti, A.; Penna, S.; Reale, A.; Brown, T. M.; Di Carlo, A.; Decker, F. *ChemPhysChem* **2012**, 13, 2925.
- (234) Bisquert, J. *J. Electroanal. Chem.* **2010**, 646, 43.
- (235) Agnaldo de Souza, G.; Marian, R. D.; Naruhiko, M.; Shozo, Y.; Shogo, M.; Ana, F. N. *J. Appl. Phys.* **2009**, 106, 064316.
- (236) Bailes, M.; Cameron, P. J.; Lobato, K.; Peter, L. M. *J. Phys. Chem. B* **2005**, 109, 15429.
- (237) Funaki, T.; Otsuka, H.; Onozawa-Komatsuzaki, N.; Kasuga, K.; Sayama, K.; Sugihara, H. *J. Mater. Chem. A* **2014**, 2, 15945.
- (238) Reddy, N. M.; Pan, T.-Y.; Rajan, Y. C.; Guo, B.-C.; Lan, C.-M.; Diao, E.

W.-G.; Yeh, C.-Y. *Phys. Chem. Chem. Phys.* **2013**, *15*, 8409.

(239) Teng, C.; Yang, X.; Li, S.; Cheng, M.; Hagfeldt, A.; Wu, L.-z.; Sun, L. *Chem. Eur. J.* **2010**, *16*, 13127.

(240) Hua, Y.; Chang, S.; He, J.; Zhang, C.; Zhao, J.; Chen, T.; Wong, W.-Y.; Wong, W.-K.; Zhu, X. *Chem. Eur. J.* **2014**, *20*, 6300.

(241) Feldt, S. M.; Wang, G.; Boschloo, G.; Hagfeldt, A. *J. Phys. Chem. C* **2011**, *115*, 21500.

(242) Sun, Z.; Liang, M.; Chen, J. *Acc. Chem. Res.* **2015**, *48*, 1541.

(243) Boschloo, G.; Hagfeldt, A. *Acc. Chem. Res.* **2009**, *42*, 1819.

(244) Clifford, J. N.; Palomares, E.; Nazeeruddin, M. K.; Grätzel, M.; Durrant, J. R. *J. Phys. Chem. C* **2007**, *111*, 6561.

(245) Oskam, G.; Bergeron, B. V.; Meyer, G. J.; Searson, P. C. *J. Phys. Chem. B* **2001**, *105*, 6867.

(246) Cazzanti, S.; Caramori, S.; Argazzi, R.; Elliott, C. M.; Bignozzi, C. A. *J. Am. Chem. Soc.* **2006**, *128*, 9996.

(247) Nusbaumer, H.; Moser, J.-E.; Zakeeruddin, S. M.; Nazeeruddin, M. K.; Grätzel, M. *J. Phys. Chem. B* **2001**, *105*, 10461.

(248) Kroeze, J. E.; Hirata, N.; Koops, S.; Nazeeruddin, M. K.; Schmidt-Mende, L.; Grätzel, M.; Durrant, J. R. *J. Am. Chem. Soc.* **2006**, *128*, 16376.

(249) Ogawa, J.; Koumura, N.; Hara, K.; Mori, S. *Jpn. J. Appl. Phys.* **2014**, *53*, 127301.

(250) Haque, S. A.; Palomares, E.; Upadhyaya, H. M.; Otley, L.; Potter, R. J.; Holmes, A. B.; Durrant, J. R. *Chem. Commun.* **2003**, 3008.

(251) Shi, D.; Pootrakulchote, N.; Li, R.; Guo, J.; Wang, Y.; Zakeeruddin, S. M.; Grätzel, M.; Wang, P. *J. Phys. Chem. C* **2008**, *112*, 17046.

(252) Kebede, Z.; Lindquist, S.-E. *Sol. Energy Mater. Sol. Cells* **1999**, *57*, 259.

(253) Montanari, I.; Nelson, J.; Durrant, J. R. *J. Phys. Chem. B* **2002**, *106*, 12203.

(254) Pelet, S.; Moser, J.-E.; Grätzel, M. *J. Phys. Chem. B* **2000**, *104*, 1791.

(255) Bublitz, G. U.; Boxer, S. G. *Annu. Rev. Phys. Chem.* **1997**, *48*, 213.

(256) Cappel, U. B.; Feldt, S. M.; Schöneboom, J.; Hagfeldt, A.; Boschloo, G. *J. Am. Chem. Soc.* **2010**, *132*, 9096.

(257) Tran Thi, T. H.; Desforge, C.; Thiec, C.; Gaspard, S. *J. Phys. Chem.*

1989, 93, 1226.

(258) Anderson, A. Y.; Barnes, P. R. F.; Durrant, J. R.; O'Regan, B. C. *J. Phys. Chem. C* **2011**, 115, 2439.

(259) Piatkowski, P.; Martin, C.; di Nunzio, M. R.; Cohen, B.; Pandey, S.; Hayse, S.; Douhal, A. *J. Phys. Chem. C* **2014**, 118, 29674.

(260) di Nunzio, M. R.; Cohen, B.; Pandey, S.; Hayse, S.; Piani, G.; Douhal, A. *J. Phys. Chem. C* **2014**, 118, 11365.

(261) Hu, K.; Robson, K. C. D.; Johansson, P. G.; Berlinguette, C. P.; Meyer, G. J. *J. Am. Chem. Soc.* **2012**, 134, 8352.

(262) Hu, K.; Robson, K. C. D.; Beauvilliers, E. E.; Schott, E.; Zarate, X.; Arratia-Perez, R.; Berlinguette, C. P.; Meyer, G. J. *J. Am. Chem. Soc.* **2013**, 136, 1034.

(263) Chang, C.-W.; Luo, L.; Chou, C.-K.; Lo, C.-F.; Lin, C.-Y.; Hung, C.-S.; Lee, Y.-P.; Diao, E. W.-G. *J. Phys. Chem. C* **2009**, 113, 11524.

(264) Lin, C.-Y.; Lo, C.-F.; Luo, L.; Lu, H.-P.; Hung, C.-S.; Diao, E. W.-G. *J. Phys. Chem. C* **2009**, 113, 755.

(265) Rochford, J.; Chu, D.; Hagfeldt, A.; Galoppini, E. *J. Am. Chem. Soc.* **2007**, 129, 4655.

(266) Fabregat-Santiago, F.; García-Cañadas, J.; Palomares, E.; Clifford, J. N.; Haque, S. A.; Durrant, J. R.; Garcia-Belmonte, G.; Bisquert, J. *J. Appl. Phys.* **2004**, 96, 6903.

(267) Johansson, P. G.; Kopecky, A.; Galoppini, E.; Meyer, G. J. *J. Am. Chem. Soc.* **2013**, 135, 8331.

(268) Katoh, R.; Furube, A. *J. Phys. Chem. Lett.* **2011**, 2, 1888.

(269) Gust, D.; Moore, T. A. *Science* **1989**, 244, 35.

(270) Gust, D.; Moore, T. A.; Moore, A. L. *Acc. Chem. Res.* **1993**, 26, 198.

(271) Sykora, M.; Maxwell, K. A.; DeSimone, J. M.; Meyer, T. J. *Proc. Natl. Acad. Sci.* **2000**, 97, 7687.

(272) Bignozzi, C. A.; Argazzi, R.; Kleverlaan, C. J. *Chem. Soc. Rev.* **2000**, 29, 87.

(273) D'Souza, F.; Smith, P. M.; Zandler, M. E.; McCarty, A. L.; Itou, M.; Araki, Y.; Ito, O. *J. Am. Chem. Soc.* **2004**, 126, 7898.

(274) Wasielewski, M. R. *Chem. Rev.* **1992**, 92, 435.

(275) Indelli, M. T.; Bignozzi, C. A.; Harriman, A.; Schoonover, J. R.;

Scandola, F. *J. Am. Chem. Soc.* **1994**, *116*, 3768.

(276) Kleverlaan, C. J.; Indelli, M. T.; Bignozzi, C. A.; Pavanin, L.; Scandola, F.; Hasselman, G. M.; Meyer, G. J. *J. Am. Chem. Soc.* **2000**, *122*, 2840.

(277) Argazzi, R.; Bignozzi, C. A.; Heimer, T. A.; Castellano, F. N.; Meyer, G. J. *J. Am. Chem. Soc.* **1995**, *117*, 11815.

(278) Haque, S. A.; Handa, S.; Peter, K.; Palomares, E.; Thelakkat, M.; Durrant, J. R. *Angew. Chem. Int. Ed.* **2005**, *44*, 5740.

(279) Hirata, N.; Lagref, J.-J.; Palomares, E. J.; Durrant, J. R.; Nazeeruddin, M. K.; Grätzel, M.; Di Censo, D. *Chem. Eur. J.* **2004**, *10*, 595.

(280) Bonhôte, P.; Moser, J.-E.; Humphry-Baker, R.; Vlachopoulos, N.; Zakeeruddin, S. M.; Walder, L.; Grätzel, M. *J. Am. Chem. Soc.* **1999**, *121*, 1324.

CHAPTER 2. EXPERIMENTAL

2.1. Reagents and materials

Table 2.1 Reagents and materials information in the study

Name	Company	Purity
Dichloromethane (DCM)	Chem-Supply	99.8%, further dried
DCM	RCI Labscan	99.8%, further dried
Dimethylformamide (DMF)	Honeywell	99.99%
DMF	RCI Labscan	99.8%, further dried
Ethanol (EtOH)	Sigma-Aldrich	99.8%, anhydrous
Tetrahydrofuran (THF)	Ajax	97%, further dried
THF	Honeywell	99.99%
THF	Sigma-Aldrich	99.9%, anhydrous, inhibitor free
Toluene	Honeywell	99.99%
Toluene	RCI Labscan	99.9%, further dried
Acetonitrile (AN)	Sigma-Aldrich	99.8%, anhydrous
Valeronitrile (VN)	Sigma-Aldrich	99.5%, anhydrous
<i>tert</i> -Butanol (t-BuOH)	Aldrich	99.0%
Platinic acid (H ₂ PtCl ₆)	Sigma-Aldrich	38% Pt
Titanium diisopropoxide bis(acetylacetonate) (TAA).	Aldrich	75% in isopropanol
1,2-dimethyl-3-propylimidazolium iodide (DMPII)	Synthesized in house	-
Lithium Iodide (LiI)	Aldrich	99.9%
Iodine (I ₂)	Aldrich	99.99%
Lithium perchlorate (LiClO ₄)	Aldrich	95%
<i>tert</i> -Butylpyridine (<i>t</i> -BP)	Aldrich	96%
Tetrabutylammonium perchlorate (TBAP)	Fluka	99.0%
Tetrabutylammonium hydroxide solution (TBAOH)	Fluka	40 wt% in water
Ferrocene (Fc)	Aldrich	98%
Chenodeoxycholic acid (CDCA)	Solaronix	-
Titanium tetrachloride (TiCl ₄)	Sigma-Aldrich	99.0%
Cobalt tris(4,4'-dimethyl-2,2'-bipyridine)	Synthesized in	-

	house	
Transparent TiO ₂ paste	Dyesol	18-NRT
Scattering TiO ₂ paste	Dyesol	WER2-O
FTO glass, 3 mm	Nippon Sheet Glass	8 Ω /square
FTO glass, 2.2 mm	TEC [®]	7 Ω /square
N719	Solaronix	-
MK2	Sigma-Aldrich	95%
All new molecules and dyes in this study	Synthesized in house	-

2.2. Characterization of molecules

2.2.1 UV-visible absorption

UV-visible (UV-vis) absorption spectroscopy was performed both in solutions and on TiO₂ films using a Shimadzu UV-3600 spectrophotometer using 1 cm length quartz cuvettes. The concentration of porphyrin solutions was 1 μ M in DCM, THF and DMF solutions, while higher concentrations, such as 5 μ M or 10 μ M were chosen for non-porphyrin molecules, discussed in Chapter 5 and 6, due to their generally low molecular extinction coefficient values.

The calculations of light harvesting efficiency were based on absorption / transmission measurements of dye-sensitized TiO₂ films.

2.2.2 Photoluminescence

Photoluminescence (PL) spectroscopy was recorded with a fluorescence (Fluorolog[®] FL3-221, Horiba) spectrometer. The same solutions as in Section 2.2.1 and a 1 cm Quartz cuvette were employed. The monochromator slit width in the front of the detector was set to obtain 3 nm bandwidth. The integral time was 0.1 s and the signal intensity was $\sim 10^4$ - 10^6 Counts Per Second (CPS).

2.2.3 Electrochemistry

Differential pulse voltammetry (DPV) and cyclic voltammetry (CV) were carried out with a three-electrode system using a potentiostat (eDAQ instrument).

All compounds were dissolved in DCM, DMF, and THF solution as required. The solvents were dried by going through a column of activated alumina. Prior to each

experiment, the solvents were purged with dry argon for 30 minutes, and placed in a glove bag (Atmosbag, Sigma-Aldrich). The concentration of the dissolved dyes was 0.5 mM and tetrabutylammonium perchlorate (TBAP), used as supporting electrolyte, was 0.1 M.

Measurements were performed using a Pt wire with 0.5 mm diameter as the working electrode (WE), Pt mesh as the counter electrode (CE) and a Ag/AgCl wire as the pseudo reference electrode (RE).

The Ag/AgCl wire was fabricated by oxidizing a silver wire in an HCl solution. First, a silver wire with a 1-2 cm length was polished with sand-paper. Second, the silver wire was immersed into 3 M HCl solution. Third, the silver wire as the WE and a Pt mesh as the CE and RE, 10 mA (galvanostatic) current was applied for 10 minutes to oxidize the surface Ag to AgCl. Fourth, the Ag/AgCl wire was washed by water and ethanol. Fifth, the Ag/AgCl wire was sealed using a glass tube to leave a ~3 mm tip exposed.

The RE potential was calibrated using 1 mM ferrocene dissolved in the same solution as the dye. The redox potential of the ferrocene/ferrocenium couple (Fc/Fc^+) was measured within 15 mins after solution preparation. The current-voltage plots measured using the 1 mM Fc/Fc^+ solution using both DPV and CV techniques are shown in Fig. 2.1. The peak potential in the DPV plot is identical to the half wave potential of the CV curve $((0.37+0.47)/2 \text{ V})$ at ~0.42 V. The DPV technique was typically used in this thesis due to the easier identification of multi-electron redox processes in di-chromophoric dyes.

The Pt wire was polished with polishing paper prior to use, and sealed by an approximately 10 mm glass tube to leave an exposed area of 6.6 mm^2 .

The scan rate was 100 mV s^{-1} , the pulse amplitude was $\pm 25 \text{ mV}$, and the potential step (step E) was $\pm 10 \text{ mV}$ in DPV experiments.

The scan rate was 100 mV s^{-1} in CV measurements.

The CV results of all the compounds are shown in Appendix Figs. A1-A3. The difference between the DPV and CV of a reference dye is also shown in Appendix Fig. A4.

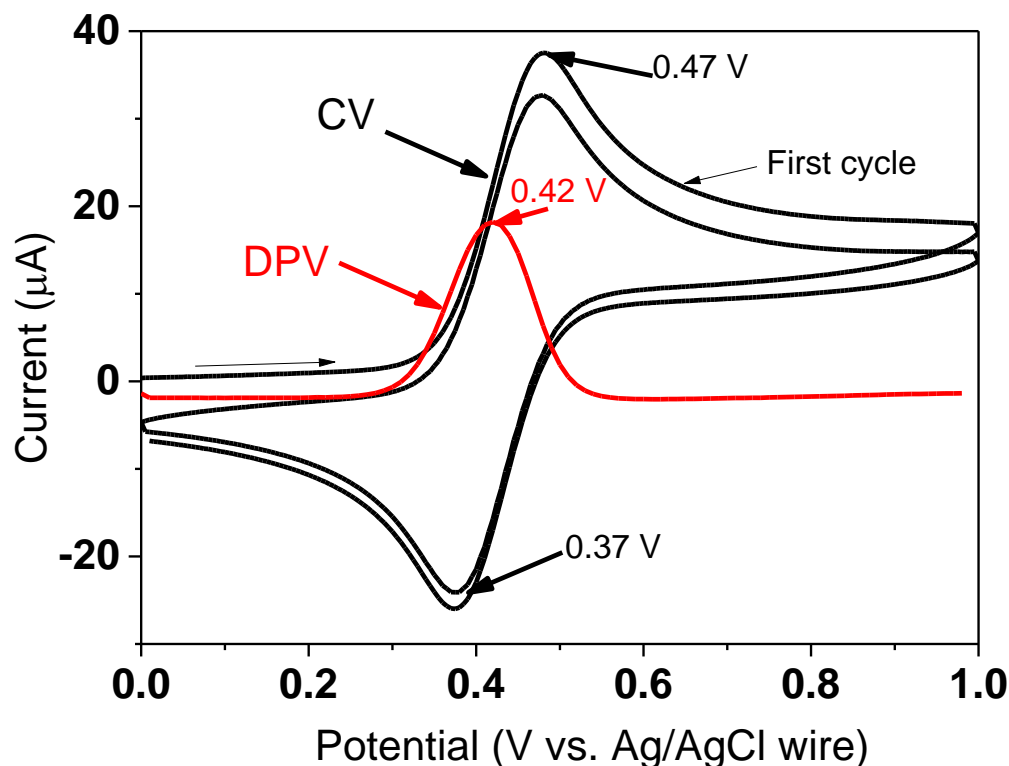


Figure 2.1 Differential pulse voltammetry (DPV) and cyclic voltammetry (CV) curves of the freshly prepared Fc/Fc^+ redox couple in DCM solution with 0.1 M TBAP using 100 mV s^{-1} scan rate.

2.2.4 Spectroelectrochemistry

Spectroelectrochemical (SEC) spectroscopy of each compound was measured by monitoring the change of absorption during the oxidation and reduction reaction controlled by a potentiostat. The setup used a UV-3600 spectrometer and an eDAQ potentiostat, as shown in Fig. 2.2. A three-electrode, optically transparent thin-layer electrochemical (OTTLE) cell was used as the working chamber, with the optical path length 0.2 mm. The solution contained 0.2 mM of a compound and 0.1 M of TBAP (supporting electrolyte), respectively, in solutions such as DCM (for compounds in Chapter 9) and DMF (for compounds in Chapter 6, shown in Appendix Fig. A5).

Before undertaking the SEC spectra measurement, the potential of the reference electrode, such as a silver wire or Pt wire, was calibrated with 1 mM freshly prepared Fc/Fc^+ using 10 mV s^{-1} scan rate. The calibration curves are shown in Fig. 2.3. A larger noise and a broader oxidation peak is observed employing 100 mV s^{-1} scan rate as compared to 10 mV s^{-1} scan rate. Since a rather broad oxidation peak was observed at

10 mV s⁻¹, the onset potential was used for the calibration (versus the onset potential of oxidation of Fc/Fc⁺).

The baseline of absorption spectrum for each sample was obtained by applying -0.2 to -0.4 V vs. Fc/Fc⁺, at which potential neither oxidation nor reduction reactions could occur. Between the applied potential steps, 2-5 minutes elapsed before obtaining an absorption spectrum. This was sufficient to get to near steady state condition at each applied potential.

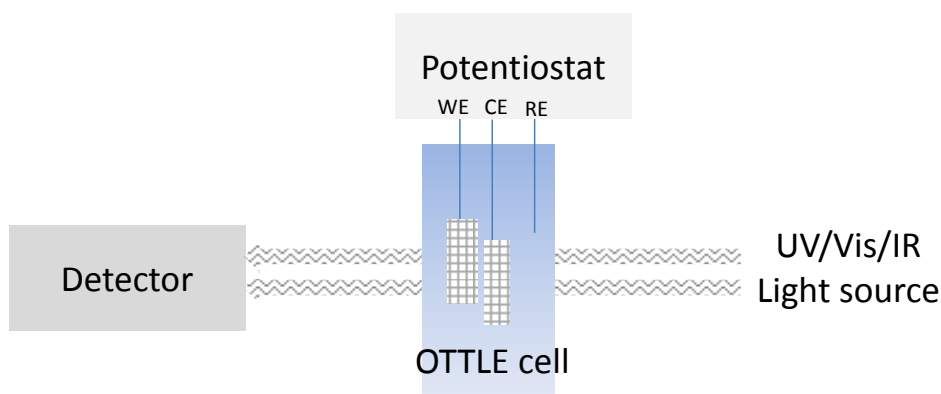


Figure 2.2 An illustration of spectroelectrochemical (SEC) measurement

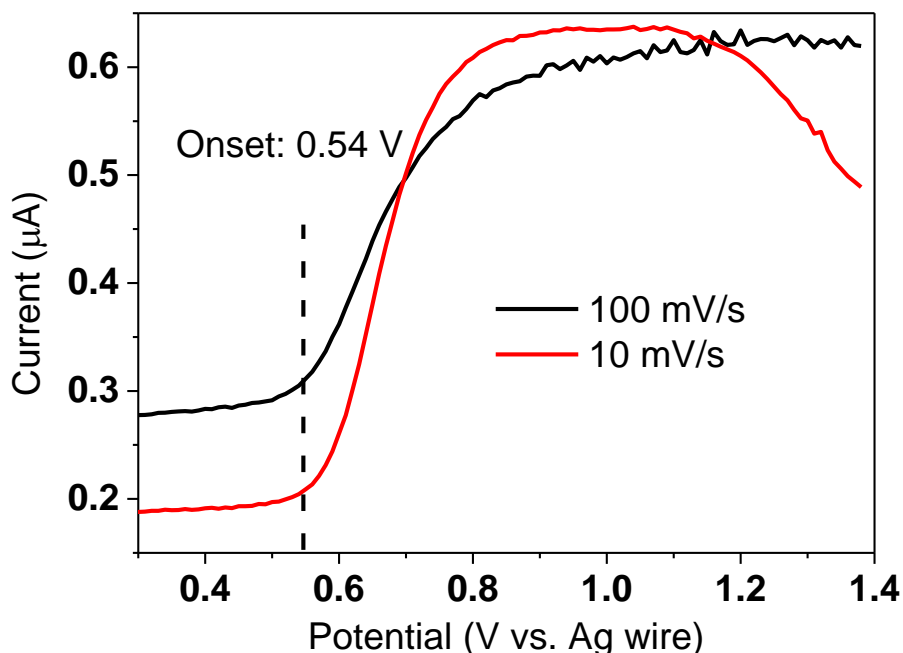


Figure 2.3 Differential pulse voltammetry of the freshly prepared Fc/Fc⁺ redox couple in DMF with 0.1 M TBAP using different scan rates.

2.3. Dye-sensitized solar cells fabrication

Fig. 2.4 illustrates the fabrication process of dye-sensitized solar cells (DSSCs).

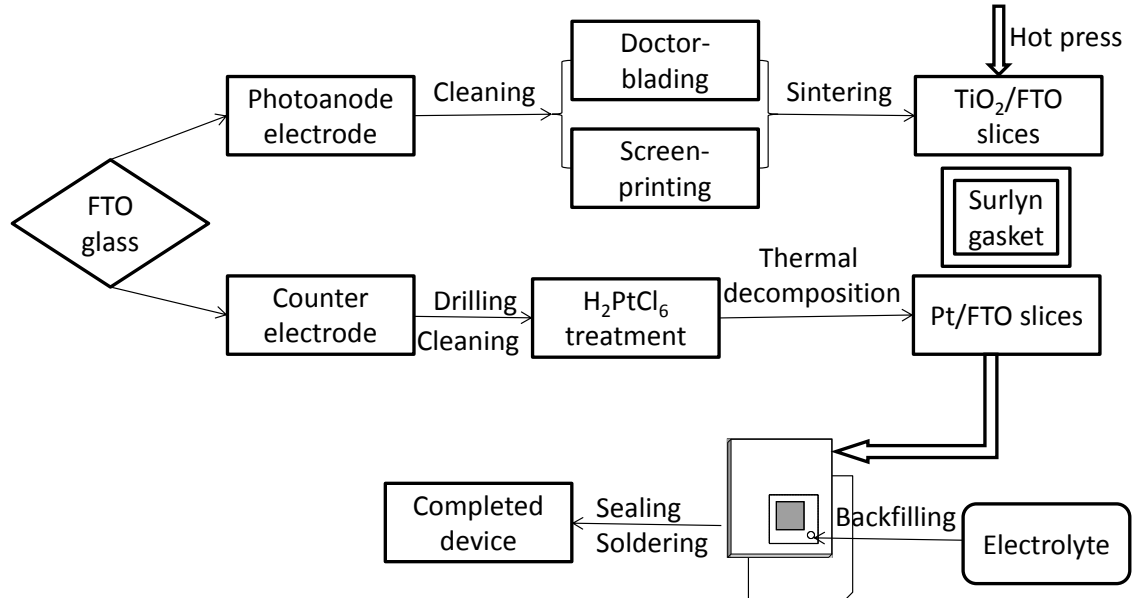


Figure 2.4 Dye-sensitized solar cells (DSSCs) fabrication process diagram

2.3.1 Photoanode preparation

2.3.1.1 Screen printing method

- 1) Cleaning. Sonicating the fluorine doped tin oxide glass (FTO glass) first in soap water, then in acetone, and last in ethanol, each for 20 minutes.
- 2) TiO₂ compact layer. A TiO₂ compact layer was prepared by spray coating of titanium diisopropoxide bis(acetylacetonate) (TAA).¹ The TAA was dissolved in ethanol with 1: 9 (vol) ratio. The precursor was sprayed onto the FTO glass, held at 400 °C, and kept for another 30 minutes on the hotplate at the same temperature. 12 spraying cycles were employed.
- 3) Screen printing. The TiO₂ thickness was controlled by changing the screen mesh density and the number of printing cycles. Films using both transparent TiO₂ paste (18-NRT, Dyesol) as well as scattering TiO₂ paste (WER2-O, Dyesol) were fabricated with the same screen under the same position. For the transparent paste, 2~3 μm and 5~6 μm TiO₂ layer after sintering would be obtained when using the 90T screen and 43T screen, respectively. For the scattering paste, similar thickness was obtained as the transparent paste using the same screen. When preparing multilayers, 15 minutes at room

temperature, 10 minutes on the hotplate at 120°C, and another 10 minutes to allow to cool down was applied before printing the next layer.

- 4) Sintering the mesoporous TiO₂ layer. The sintering program for the printed TiO₂ layer was: 325 °C for 5 minutes, 375 °C for 5 minutes, 450 °C for 30 minutes, 500 °C for 15 minutes, followed by cooling down to the room temperature.
- 5) TiCl₄ treatment. The sintered TiO₂ films were immersed in 0.02 M TiCl₄ solution in water at 70°C for 30 minutes. After being rinsed by water and ethanol, the films were heated to 500 °C, and held for 30 minutes.
- 6) Cutting the TiO₂/FTO glass sheets to slices with the size 1.3 cm × 1.7 cm for future use.
- 7) The thickness of the films was measured by a stylus profilometer (DekTek).

2.3.1.2 Doctor-blading method

- 1) Cutting FTO glass into a 10 cm × 5 cm strip and cleaning following the aforementioned procedure at section 2.3.1.1.
- 2) Doctor-blading. The cleaned FTO glass was fastened using 3M scotch tape which also works as the spacer. The TiO₂ paste was then deposited onto the FTO glass using a glass roller.
- 3) Sintering. Leaving the doctor-bladed layer at room temperature for 20 minutes. The sintering procedure was same as the screen printing method.
- 4) Cutting the FTO photoanode into the 1.5 cm × 1.7 cm size. A glass slide was then used to scrape the extra TiO₂ particles away from the edge of each substrate to produce a film area of 4 × 4 mm². The TiO₂ film was placed towards a corner of the substrate, with 2.5 mm clearances towards two edges.
- 5) The actual surface area of the photoanode was measured by scanning the shape of substrates using Excon image software. The thickness of the films was measured by DekTek.

2.3.2 Counter electrode fabrication

- 1) The FTO glass was cut into the size 1.7 cm × 2 cm.
- 2) A hole was drilled 2.5 mm × 2.5 mm from the edges.
- 3) The FTO glass was cleaned following the same procedure as FTO glass for photoanode fabrication.

4) A platinum layer was coated on the counter electrode surface by a thermal decomposition method. 10 mM platinum acid (H_2PtCl_6) in ethanol was used as the precursor. One drop of the solution was needed for one slice of counter electrode, which was then sintered at 400 °C for 30 minutes.

2.3.3 Device assembling

1) Anode side cleaning and dye sensitization. All the TiO_2/FTO glass films were put onto the hotplate and re-sintered at 450°C for 30 minutes to remove any adsorbed organic contaminants or moisture. Once the films had cooled to < 80 °C, they were immersed into a dye solution. Both the dye solvent and the immersing time depend on the sensitizers, and are summarized in Table 2.2.

Table 2.2 Solvent and immersing time used for dye sensitization

Sensitizers	Solvent	Immersing time	Concentration
The PorY dyes and PorR	THF	1.5 hours	0.2 mM
The PorO dyes	0.1 mM CDCA in Ethanol: toluene=1:1 (vol)	1.5 hours	0.2 mM
N719	AN: <i>t</i> -BuOH=1:1 (vol)	18~24 hours	0.3-0.5 mM
MK2	AN:toluene=1:1 (vol)	6 hours	0.2 mM

2) Assembling. The dye-absorbed TiO_2/FTO film was rinsed with AN and was dried with air. A counter electrode, a Surlyn gasket and the photoanode were sandwiched and put on the hotplate for sealing. The temperature for sealing was ~120 °C and the pressure was ~2 bars. Parafilm was used to cover the injection hole for short time storage to keep away the air moisture.

3) Electrolyte backfilling. Both iodine-based electrolyte and cobalt-based electrolyte have been used in this work. The electrolyte injection into the sandwiched device was achieved by using a vacuum pump controlled by a vacuum controller V-850 (BUCHI®). Pressure was set to 65 mbar and the device was filled twice. The injection hole was sealed thereafter by a piece of Surlyn attached aluminium foil or a piece of Surlyn attached microscope glass for a transparent device.

- 4) External connectors soldering. Both photoanode and photocathode were soldered with copper wires.
- 5) The surface of devices was cleaned with ethanol and stored in dark.

2.4. Dye-sensitized solar cells characterization

To stabilize the devices, a 20-minute light soaking process was applied before photovoltaic measurements.^{2,3}

2.4.1 Current density-voltage measurements

Current density-voltage (J-V) measurements were performed using two systems. In Chapter 4 and 8, a simulated 100 mW cm⁻² air mass (AM) 1.5G solar simulation (Newport) and a Keithley 2400 source measure unit was used. For the work shown in Chapter 5, a new solar simulator (TriSOL, OAI) was installed and used.

After the light soaking, the devices based on the I⁻/I₃⁻ electrolyte, were measured once in the dark followed by a measurement under 1 sun illumination. The reproducibility between measurements was very good when using the iodine electrolyte, while slight larger variation was noticed with the cobalt electrolyte. Hence, devices with the cobalt electrolyte were measured three times (J-V measurements) and were kept in dark for 30 seconds to allow the devices to cool down to room temperature before the last recording.

A 6 mm × 6 mm mask was employed in all J-V measurements to define the illumination area. The power conversion efficiency (*PCE*, η) was calculated according to Eq. 2.1.

$$\eta = \frac{J_{SC} \times V_{OC} \times FF}{P_{in}} \quad (2.1)$$

Where J_{SC} , short-circuit current density, mA cm⁻²; V_{OC} , open-circuit voltage, V; FF , fill factor; P_{in} , intensity of incident light, mW cm⁻² (for one sun with AM 1.5 G, the value is 100 mW cm⁻²).

2.4.2 Incident photon-to-current conversion efficiency

Incident photon-to-current conversion efficiency (IPCE) is the monochromatic quantum efficiency of the solar cell as illustrated by Eq. 2.2.

$$J_{SC} = \int IPCE(\lambda) \phi_{photon}(\lambda) d\lambda \quad (2.2)$$

where, ϕ_{photon} is the photon flux at the standard one sun condition, mA cm⁻² nm⁻¹. It has been recorded using two different systems in this work.

In Chapter 4, a 300 W Xe lamp coupled to a monochromator with long pass filters was used. The light output was focused on a $\sim 2 \text{ mm}^2$ spot with additional optics (Newport). The photocurrent response of the devices was recorded in 5 nm wavelength steps using a Keithley 2400. The measured currents were referenced to a calibrated Si diode (PECCELL).

In Chapter 5 and 6, IPCE was recorded using a QEX10 quantum efficiency measurement system (PV measurements). Both the entrance and exit slit widths for the monochromator were set to obtain bandwidth of 6 nm, resulting in a $0.8 \text{ mm} \times 0.8 \text{ mm}$ beam dimensions (smaller than the active area of the devices). The photocurrent response of the devices was recorded in 5 nm wavelength steps. The program parameters were set to the default values towards the delay time (0 before change λ , 0 between readings, 5 ms after change filter / gratings) and measurements (0.3 s time period, 3 readings per λ). The delay after changing wavelength was set to 50 ms to allow the devices to stabilize. The measured currents were referenced to a calibrated Si diode (THORLABS, LMR1/M).

Comparison between the Newport and QEX10 IPCE measurement systems is shown in Fig. 2.5. The IPCE plot measured by the Newport system showed a 5 nm red-shifted spectrum compared to that of the QEX10 system.

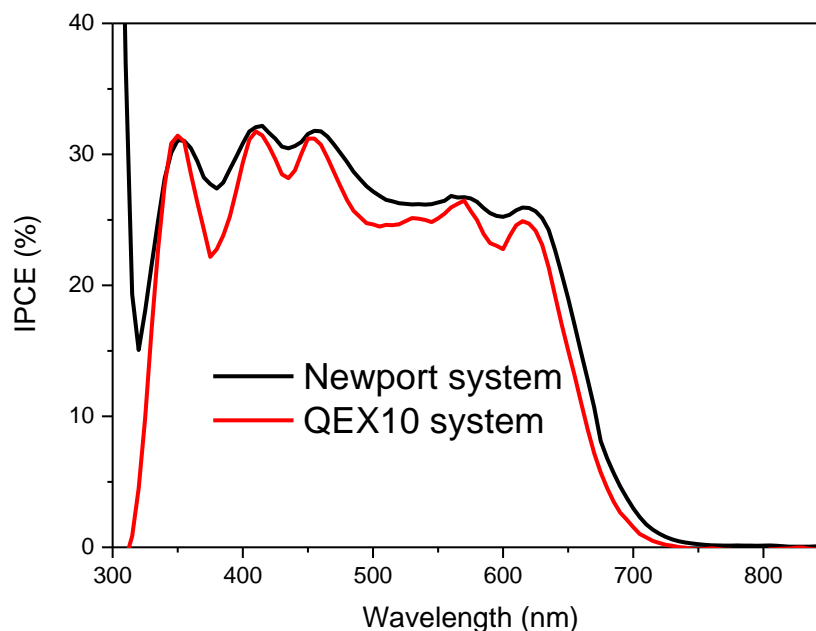


Figure 2.5 Comparison of the Newport and QEX10 IPCE measurement systems.
Reference sensitizer: PorR on $2.6 \mu\text{m}$ TiO_2 films.

2.4.3 Light harvesting efficiency measurements

The UV-vis absorption of the sensitized films was measured by Shimadzu UV-3600 spectrophotometer. Microscope cover slides were placed over the sensitized films, and a drop of the electrolyte was injected into the space between the photoanode and the cover slide to mimic device conditions during IPCE measurements. Transmittance of the photoanode FTO glass and reflectance of the counter electrode were obtained by the UV-3600 spectrophotometer with the integrating sphere attachment. Light harvesting efficiency (LHE) of the dyes on TiO₂ was calculated using the following Eqs. 2.3-2.6.^{4,5}

$$LHE_{forward} = T_{FTO}(1 - 10^{-(A_D + A_E P)}) \frac{A_D}{A_D + A_E P} \quad (2.3)$$

$$LHE_{backward} = R_{Pt} 10^{-(A_D + A_E P + 2A_E \frac{d}{\omega})} LHE_{forward} \quad (2.4)$$

$$d = d_{Surlyn} - \omega \quad (2.5)$$

$$LHE = LHE_{backward} + LHE_{backward} \quad (2.6)$$

where T_{FTO} is the transmittance of the conducting glass substrate containing the effect of light reflection loss at an air/substrate glass interface; A_D is the absorbance of the dye-sensitized TiO₂ film; A_E is the absorbance of the electrolyte when the pathlength is equal to the thickness of the TiO₂ film; R_{Pt} is the reflectance of Pt covered CE; d is the thickness of the bulk electrolyte between the TiO₂ layer and the CE; d_{Surlyn} is the thickness of the device sealing material; ω is the thickness of the TiO₂ layer; P is the porosity of the TiO₂ electrode.

In the equations, A_E was obtained by the method stated as follows. A 25 μ m Surlyn gasket was made to a rectangle with the size of 12 mm \times 8 mm outside and 8 mm \times 4 mm inside. Two slices of microscopic glass were sealed using this gasket with a pre-drilled hole at the corner in one of them for electrolyte backfilling. Electrolyte was injected and the absorbance was measured.

Another parameter in the equations, A_D , was obtained by measuring the transmittance of dye-TiO₂/FTO glass with a drop of electrolyte. A slice of FTO glass was set as the reference.

2.4.4 Absorbed photon-to-current conversion efficiency calculation

Absorbed photon-to-current conversion efficiency (APCE) was calculated from IPCE and LHE values according to Eq. 2.7:

$$APCE(\lambda) = \frac{IPCE(\lambda)}{LHE(\lambda)} = E_{inj}(\lambda) \times E_{coll}(\lambda) \times E_{reg}(\lambda) \quad (2.7)$$

where E_{inj} is electron injection efficiency, E_{coll} is charge collection efficiency and E_{reg} is regeneration efficiency.

2.4.5 Electron lifetime and transport in TiO_2 films

Stepped light-induced measurements of photocurrent and photovoltage (SLIM-PCV) were used to determine electron lifetime (τ) and electron diffusion coefficient (D) (Fig. 2.6).⁶ A 635 nm diode laser was employed as the light source. A lens was used to control the spot size of the laser beam on the device covering the whole active area. A data acquisition board (DAQ board) was used as the digital / analog converter, connected to a personal computer (PC). By varying the laser intensity, J_{SC} or V_{OC} decays were obtained. The current or voltage transient mode was selected by V - I mode switch box (V means voltage and I means current). The resistances under current and voltage mode were $0.5\ \Omega$ and $10\ M\Omega$, respectively. A multimeter (ADCMT 7461A) was employed to record the small photocurrent or photovoltage perturbations triggered the laser intensity change. The measurement was controlled by a home-built Labview program.

For τ measurements, the laser intensity was decreased to give a less than 1 mV change in the photovoltage under an open circuit condition (the V mode). The τ as well as the steady state V_{OC} at that light intensity were obtained.

For D measurements, the laser intensity was reduced to obtain less than 10% change in the photocurrent under a short circuit condition (the I mode). The D and the steady state J_{SC} at that light intensity was obtained.

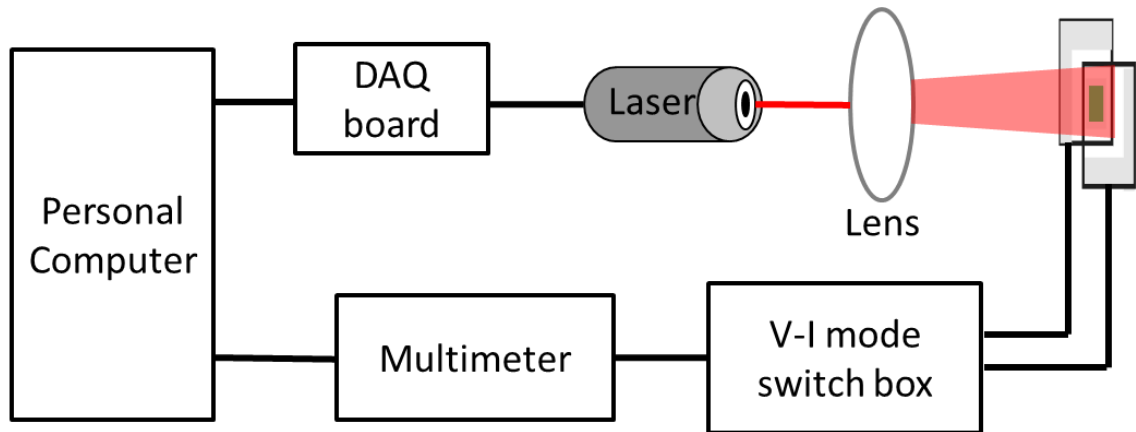


Figure 2.6 A diagram for electron lifetime and diffusion coefficient measurements.

Electron density (ED) in TiO_2 films at open circuit condition was determined by a charge extraction method (Fig. 2.7).⁷ A fast switch (AsamaLab) was used to connect the DAQ board and the device. The laser intensity was switched off completely, while the device was simultaneously switched from open circuit to short circuit using this switch to measure charge density at open circuit condition. The porosity of the semiconductor was not taken into account for the calculation of electron density (Eq. 2.8).

$$ED = \frac{\int Idt \times 6.24 \times 10^{18}}{A \times \omega} \quad (2.8)$$

where, A is the area of TiO_2 film; ω is the thickness of TiO_2 film.

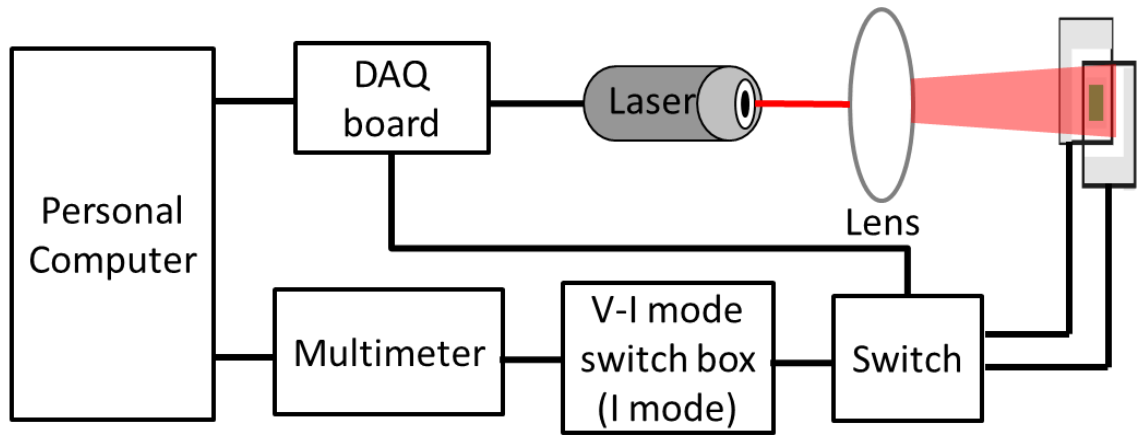


Figure 2.7 A diagram for switch controlled electron density measurement

Electron diffusion length (L) was obtained by measuring the ED at short circuit condition (ED_{sc}). The ED_{sc} was determined by switching off the laser light using a shutter between the lens and the laser while keeping the device at short circuit (Fig. 2.8). The electron lifetime at short circuit condition (τ_{sc}) was calculated by fitting the $\log \tau$ versus $\log(ED)$ plot and introduced ED_{sc} into the fitted mathematical equation. The electron diffusion length (L) was obtained using Eq. 2.9:

$$L = \sqrt{D\tau_{sc}} \quad (2.9)$$

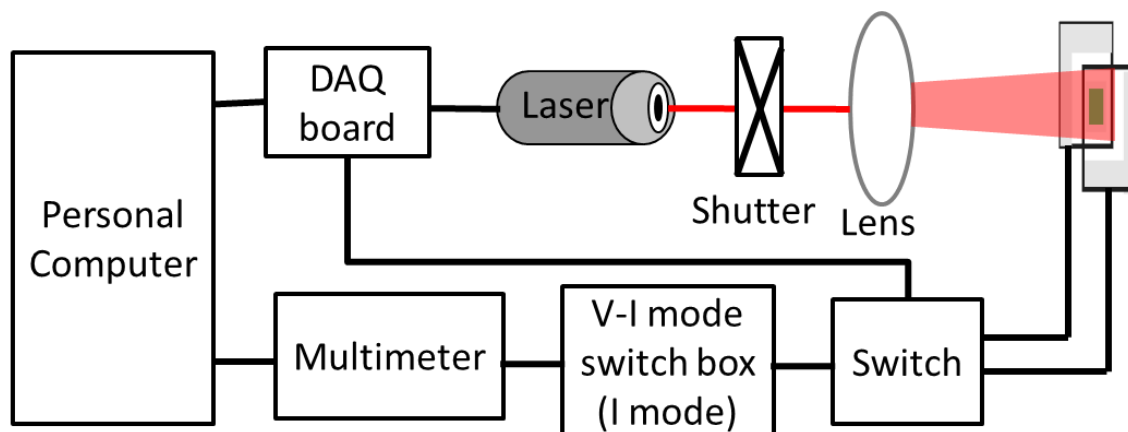


Figure 2.8 A diagram for shutter controlled electron density at short circuit condition measurement

2.4.6 Dye loading measurement

The amount of dye adsorbed on the TiO_2 was determined using thin dye-sensitized TiO_2 films ($\sim 3 \mu\text{m}$). 3 ml of 0.1 M tetra-butylammonium hydroxide solution (TBAOH) in DMF was used to desorb the sensitizers from the surface of the TiO_2 films. To obtain larger volume for UV-vis absorption measurements, the solutions were further diluted to 0.033 M.

2.5. Transient absorption spectroscopy

Transient absorption spectroscopy (TAS) was employed to measure the dye cation absorption spectrum and monitor the decay kinetics of the oxidized dye reaction with the injected TiO_2 electron. A transparent TiO_2 film, with $\sim 3 \mu\text{m}$ thickness and $8 \text{ mm} \times 8 \text{ mm}$ active area, was coated on FTO glass using either screen printing or doctor-blading method. A TiCl_4 post-treatment was also employed following the procedure outlined in device fabrication above. Dye-sensitized films were covered by a piece of microscope cover glass (1 mm) and sandwiched with $25 \mu\text{m}$ Surlyn. Two types of electrolytes were used in the TAS measurements: inert electrolyte and redox electrolyte. The former not containing redox mediator was used for characterizing the recombination between electrons in TiO_2 and the oxidized dye and the latter was used to study the dye regeneration processes. Exact composition of the electrolytes is specified in the experimental section of the relevant chapters.

2.5.1 INDI laser

A Q-switched Nd-YAG laser (532 nm, 10 Hz, INDI Quanta-Ray, Spectra-Physics) was employed as the excitation light source (the pump). The probe beam was provided by a current-controlled (BENTHAM 605) quartz halogen lamp (IL1), which was spectrally optimized by a series of filters, including band pass filters, longpass (LP) and neutral density filters, before passing through the sample. The detection system was comprised of a monochromator (CM110, SP), a silicon or InGaAs photoreceiver (HCA-S-200M-IN, Germany) and a digital phosphor oscilloscope (DPO 4054). TAS signal was averaged by 512 times for both dye cation spectrum and kinetics measurements. Pump laser intensity was measured by a pyroelectric energy sensor (ES111C, THORLABS).

Fig. 2.9 shows a diagram for the oxidized dye spectrum measurement using TAS technique. The photovoltage signal on the photodetector was amplified by a voltage amplifier DHPVA-200 in AC mode (10 Hz cut-off frequency) and a 200 MHz high frequency filter. The spectra at 950-1000 nm wavelength region were measured using grating 1 (monochromator) and InGaAs detector. The output of the voltage amplifier was connected to a digitalizing oscilloscope. A home-built Labview program was used to calculate the change in optical density (ΔOD) versus time, and versus wavelength.

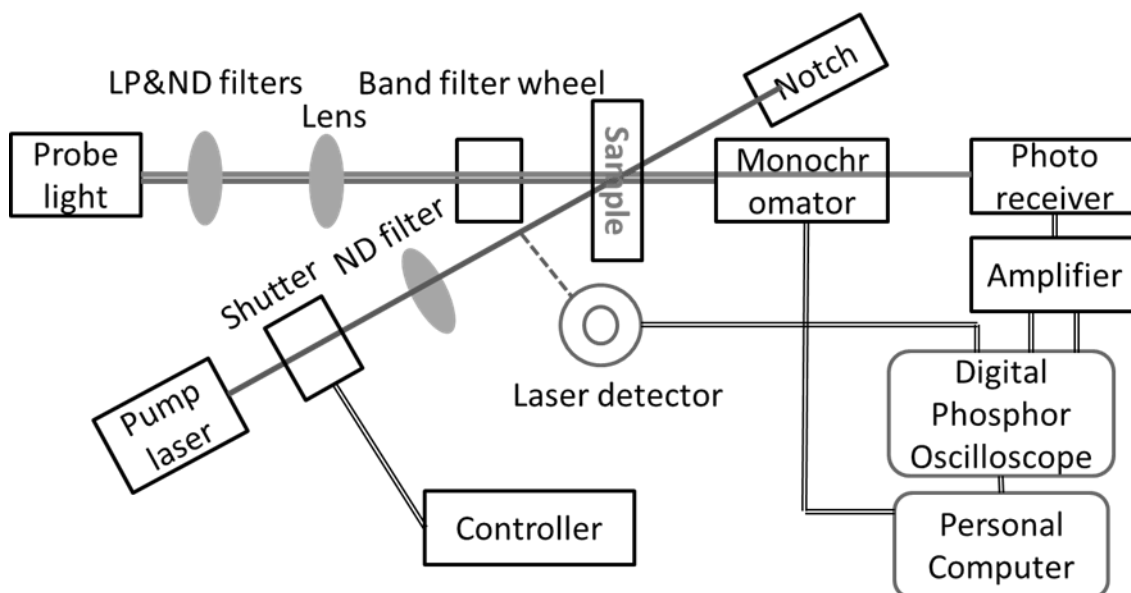


Figure 2.9 A diagram of the dye cation spectrum measurement

For kinetics measurements (Fig. 2.10), the TA signal was obtained at 1 Hz by choosing one pulse out of a 10 Hz pulse train using a digital delay/pulse generator (DG535, Stanford Research) and a beam shutter (SH05, Thorlabs). Since the porphyrin dye cation decay kinetics would last up to millisecond (ms) time scale and the amplifier in AC mode influenced decay kinetics beyond ~ 2 ms, the amplifier was not used in the kinetic mode measurements. The laser intensities $45\text{--}50\text{ }\mu\text{J s}^{-1}\text{ pulse}^{-1}$ were used for porphyrins and $6\text{--}8\text{ }\mu\text{J s}^{-1}\text{ pulse}^{-1}$ for organic dyes, to result the initial ΔOD value in the range of $0.2\text{--}1 \times 10^{-3}$. Each sample was measured by three different time scales to obtain enough points in all time range when the traces are plotted on a logarithmic scale. The time resolution of the TAS set up was around 40 ns.

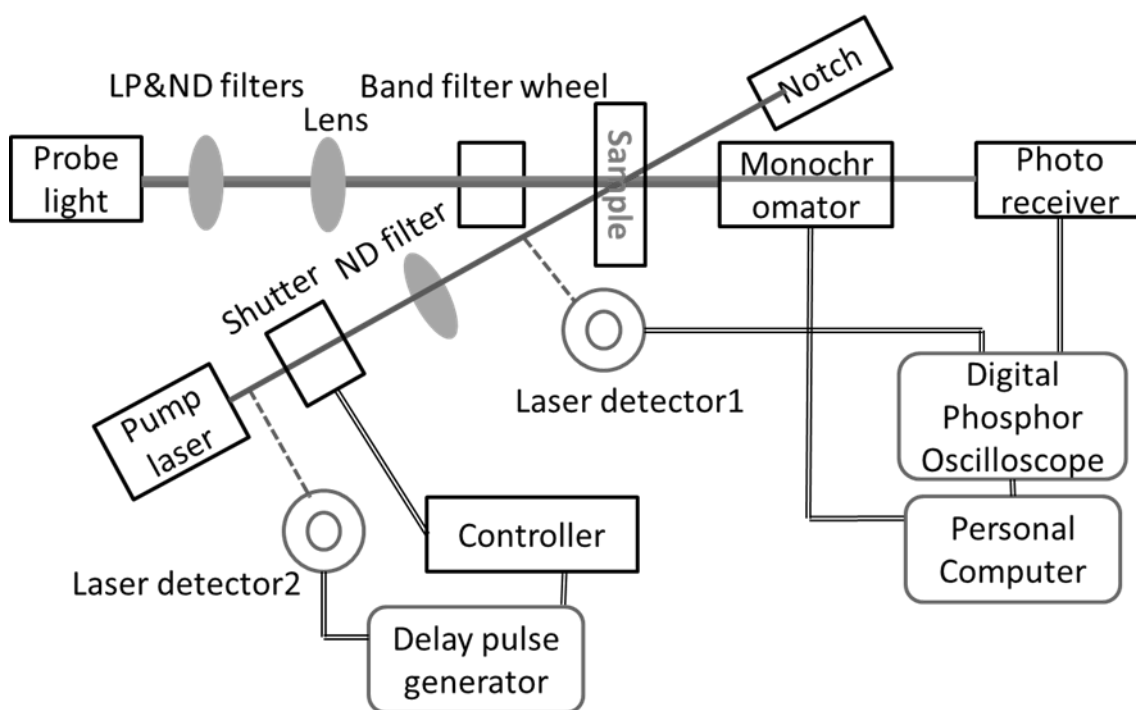


Figure 2.10 A diagram of the dye cation kinetics measurement

2.5.2 Ekspla laser

A Nd-YAG laser (SL230, Ekspla[®]) was employed as excitation light source (the pump), producing a 100 ps pulse at 532nm, with a repetition frequency of 1 Hz. The probe beam was provided by a current-controlled (Xe900) halogen lamp (XP920, EDINBURGH INSTRUMENTS) with a XP920 pulse generator interface (current 8(60), width 3(30)), which was spectrally optimized by longpass filters, before passing

the sample. A monochromator (Newport) was used to control the wavelength and a silicon or InGaAs photoreceiver (High-speed photoreceiver, 1601&1611, New focus) was used to detect changes in the optical signal intensity. For kinetics measurements, another digital delay generator (DG645, Standard research systems) was used to control the laser master oscillator to 1 Hz output. A 2 GHz digital phosphor oscilloscope (DPO 5204) was used to record the voltage transient from the photodetectors. 80-200 measurements were averaged. Laser intensity was recorded by high power detector (818P-015-18HP, Newport).

2.6. References

- (1) Kavan, L.; Grätzel, M. *Electrochim. Acta* **1995**, *40*, 643.
- (2) Wagner, K.; Griffith, M. J.; James, M.; Mozer, A. J.; Wagner, P.; Triani, G.; Officer, D. L.; Wallace, G. G. *J. Phys. Chem. C* **2011**, *115*, 317.
- (3) Griffith, M. J.; Sunahara, K.; Furube, A.; Mozer, A. J.; Officer, D. L.; Wagner, P.; Wallace, G. G.; Mori, S. *J. Phys. Chem. C* **2013**, *117*, 11885.
- (4) Kubo, W.; Sakamoto, A.; Kitamura, T.; Wada, Y.; Yanagida, S. *J. Photochem. Photobiol., A* **2004**, *164*, 33.
- (5) Mozer, A. J.; Griffith, M. J.; Tsekouras, G.; Wagner, P.; Wallace, G. G.; Mori, S.; Sunahara, K.; Miyashita, M.; Earles, J. C.; Gordon, K. C.; Du, L.; Katoh, R.; Furube, A.; Officer, D. L. *J. Am. Chem. Soc.* **2009**, *131*, 15621.
- (6) Nakade, S.; Kanzaki, T.; Wada, Y.; Yanagida, S. *Langmuir* **2005**, *21*, 10803.
- (7) Duffy, N. W.; Peter, L. M.; Rajapakse, R. M. G.; Wijayantha, K. G. U. *Electrochem. Commun.* **2000**, *2*, 658.

CHAPTER 3. THREE FAMILIES OF DI-CHROMOPHORIC DYES

3.1. Introduction

The electrochemical properties, UV-visible absorption and the photovoltaic performance of a series of di-chromophoric dyes consisting of a porphyrin and an additional organic chromophore linked via phenylethenyl group are investigated throughout this thesis. The band gap of the organic chromophores is tuned to investigate its effects on the properties of dye molecules and their photovoltaic performance in dye-sensitized solar cells (DSSCs).

By using multi-chromophoric sensitizers DSSCs, a simultaneous increase in the photocurrent and photovoltage could be achieved. The guidelines influence photocurrent and photovoltage in DSSCs have been described in Chapter 1. The photocurrent can be increased by introducing complementary absorption by the chromophores, or if thin photoanodes are used, by increasing the extinction coefficient at the same wavelength range.¹ The photovoltage can be increased by preventing the approach of the redox mediator to the TiO₂ surface, for example, by attaching bulky substituents to the dye, hence blocking recombination.²⁻⁴

The three families of dyes (PorY, PorO and PorR, Fig. 3.1) contain a carbazole derivative with increasingly red-shifted absorption (Y-yellow, O-orange, R-red) as the second chromophore. They were designed based on the following principles:

1. **PorY family:** The main purpose of this family was to be able to photoexcite the organic chromophore, independently of the porphyrin, and thus obtain spectroscopic insights into charge generation and recombination mechanisms. Furthermore, to study the steric effect of bulky organic chromophore on the performance of solar cells independent of the light harvesting efficiency. For this purpose, carbazole was chosen as a chromophore, which does not absorb strongly at the main porphyrin absorption bands and therefore does not contribute significantly to the light harvesting of the di-chromophoric dyes. Carbazole chromophore was modified with substituents with different electron donating and withdrawing abilities to investigate their influence on the energy levels of the dyads and thereafter the photovoltaic performance of the molecules.
2. **PorO family:** Carbazole-thiophene conjugate was chosen as the organic chromophore to fill the absorption gap (450-550 nm) between the Soret and Q

bands of the porphyrin. The importance of improving the light harvesting efficiency within this wavelength range is demonstrated.

3. **PorR**, where two competing electron transfer paths are possible, was created by incorporating an additional electron acceptor. This design is referred to as D1-A1-P(D2)-A2 structure, where A1 is 2,1,3-benzothiadiazole and A2 is cyanoacrylic acid. Porphyrin (P) plays a role of an electron donor (D2). The path leading to electron transfer to the benzothiadiazole unit away from the interface should lead to lower injection efficiency into the TiO₂ interface. This design, somewhat unexpectedly, has opened up the possibility to utilize dispersion forces by D1-A1 to increase the electron lifetime. This topic will be discussed in detail in Chapter 8.

The rationale for using zinc porphyrins and carbazole substituents as the additional chromophore in the three families of di-chromophoric dyes has been introduced in Chapter 1.

In this chapter, for simplicity and ease of comparison, each family of di-chromophoric dyes are represented by one dye, namely 5-(4-(2-cyano-2-carboxyethenyl)phenyl)-15-(4-(2-(6-(4-(*N,N*-diphenylamino)phenyl-9-(3,7-dimethyloctyl)-carbazol-3-yl)ethenyl)phenyl)-10,20-bis(2,4,6-trimethylphenyl)porphyrinato zinc (II) (PorY1), 5-(4-(2-cyano-2-carboxyethenyl)phenyl)-15-(4-(2-(5-(2-(6-(2-(9-octylcarbazol-3-yl)ethenyl)dithieno[3,2-*b*:2',3'-*d*]thiophen-2-yl)ethenyl)phenyl)-10,20-bis(2,4,6-trimethylphenyl)porphyrinato zinc(II) (PorO2) and (5-(4-(2-cyano-2-carboxyethenyl)phenyl)-15-(2-(5-(7-(5-(2-(9-ethylcarbazol-3-yl)ethenyl)-4-hexylthien-2-yl)benzo-2,1,3-thiadiazol-4-yl)-3-hexylthien-2-yl)ethenyl)-10,20-bis(2,4,6-trimethylphenyl)porphyrinato zinc(II) (PorR). Detailed comparisons within the families of dyes, such as tuning the energy levels within the PorY family, are discussed in subsequent chapters. The three families of di-chromophoric dyes are distinguished by the colour of the organic chromophore. As shown in Fig. 3.1, PorY1 contains a carbazole chromophore (yellow), PorO2 contains a carbazole-fused thiophene chromophore with an orange colour and PorR contains a carbazole-thiophene benzothiadiazole-thiophene chromophore with moderate light absorption in the red (Y for yellow, O for orange and R for red, respectively).

In this chapter, the energy levels and the light absorption properties of the di-chromophoric dyes are investigated using differential pulse voltammetry, followed by

UV-vis spectroscopy. The results are explained using resonance Raman spectroscopy performed by the project collaborators: Prof. K. C. Gordon, Dr A. B. S. Elliott and Dr H. van der Salm from the University of Otago (Dunedin, New Zealand). Finally, the photovoltaic performance of the investigated molecules in dye-sensitized solar cells was compared using either thin (2.0-2.6 μm) or thick (consisted of both 5-12 μm transparent layer and 2.5-5.5 μm scattering layer) TiO_2 layers using current-voltage and incident photon-to-current conversion efficiency (IPCE) measurements. These high level comparisons between the dye families provide some simple general design rules for di-chromophoric dyes and also raise some important scientific questions. These are listed at the end of the chapter, setting the scene for subsequent, more detailed chapters of this thesis.

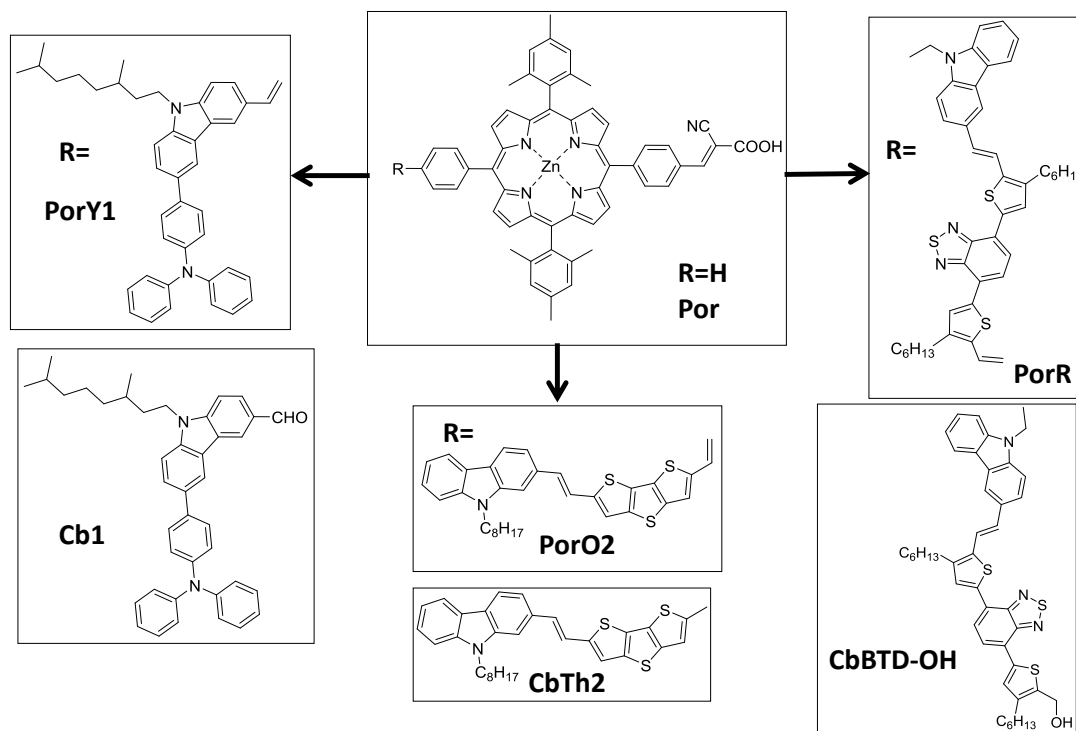


Figure 3.1 Concept of the di-chromophoric dyes.

3.2. Differential pulse voltammetry and energy levels of the three families

A differential pulse voltammetry (DPV) technique was used to measure the oxidation and reduction reactions of the three families of di-chromophoric dyes (Fig. 3.2(a)).

The first oxidation peaks of Por, CbTh2 and CbBTD-OH (structure displayed in Fig. 3.1) are very similar at +0.3 V vs Fc/Fc⁺, while that of Cb1 is ~0.1 V more positive compared to the others (Fig. 3.2(a)). Clear second oxidation reaction peaks are observed in Por and Cb1. CbTh2 and CbBTD-OH show featureless tail at potentials >0.3 V.

Only Por and CbBTD-OH show reduction reactions in the applied potential window of -1.2 V to -2.4 V vs Fc/Fc⁺. The reduction peak of CbBTD-OH at -1.67 V vs Fc/Fc⁺ is ~0.2 V more positive compared to the first reduction peak of Por at -1.89 V vs Fc/Fc⁺.

The oxidation of PorY1, PorO2 and PorR show two broad peaks, with the first oxidation peaks showing similar potential at +0.3 V vs Fc/Fc⁺ (Fig. 3.2(a)). Compared to that of Por, the organic chromophores, the first oxidation peak of the di-chromophoric dyes appears to be a simple superposition of the Por and organic chromophores. Similarly, the second oxidation peak of PorY1 appears to be a superposition of the second Por and Cb1 peaks, appearing at less positive potentials compared to those of the other two di-chromophoric dyes.

Reduction of PorY1 results in two peaks similar to that of Por (Fig. 3.2(a)). PorO2 and PorR are also observed the same cathodic peak at -1.97 V vs Fc/Fc⁺. Moreover, another more positive reduction peak at -1.67 V vs Fc/Fc⁺ is observed in PorR, which is identical to that of CbBTD-OH.

The first oxidation peaks of CbTh2, CbBTD-OH and the three di-chromophoric dyes are very similar (Fig. 3.2). The broad oxidation in di-chromophoric dyes can be explained by the superposition of Por oxidation and the organic chromophore oxidation, indicating that the chromophores in PorY1, PorO2 and PorR are not electronically coupled in the ground state. This non-interacting nature of the di-chromophoric dyes is important for the purposes of the thesis. It suggests the multi-chromophoric nature of the dyes: weakly interaction consisting of individual chromophore.

The first reduction reaction peaks of PorY1 and PorO2 are similar to that of Por, which indicates that reduction of the porphyrin part is more accessible compared to the second chromophore. In contrast, reduction of PorR results in a first peak assigned to the organic chromophore and a second peak originating from the reduction of the porphyrin. In this case, it is easier to reduce the organic chromophore than the porphyrin due to the strong electron withdrawing property of the benzothiadiazole unit. This is an important result with significant consequences to the photophysics and solar cell performance (Chapters 6 and 7)

Different solvents were used to prepare solutions of the three families di-chromophoric dyes for the DPV measurements. Por and PorY1 were measured in dichloromethane (DCM), while PorO2 and PorR were measured in dimethylformamide (DMF). DCM is better for electrochemical characterization especially reduction reactions since it is easier to get rid of water compared to DMF. However, PorO2 does not dissolve in DCM very well possibly due to the more planar structure of the carbazole fused-thiophene. Although carefully dried solvents were used in this study (see Chapter 2), DMF is harder to keep dry compared to DCM, resulting in a reduction feature attributed to water reduction at -1.5 V vs Fc/Fc⁺ (Fig. 3.2(a)).

The first oxidation peak of the three di-chromophoric dyes is similar, independent of the solvent, while the first reduction peaks of PorY1 and PorO2 originate from the reduction of the porphyrin showing a ~0.1 V negative shift changing from DCM to DMF. This reduction potential variation within the three di-chromophoric porphyrins is due to the solvent effect rather than the dye molecule structure property.

The energy levels were calculated from the peak potentials of the DPV plots as shown in Fig. 3.2(b). No clear differences are observed in either the first oxidation potential or the first reduction potential of Por, PorY1 and PorO2. On the other hand, the first reduction potential of PorR has positively shifted compared to the other porphyrins. This lower reduction potential of the organic chromophore enables a pathway for an intramolecular electron transfer from the photoexcited porphyrin to the organic chromophore. The organic chromophore in PorR is positioned opposite to the anchoring unit and away from the TiO₂, therefore electron injection to TiO₂ might be affected. The loss of excitation energy without electron injection to TiO₂ may lead to decreased photovoltaic performance of PorR.

The potential difference between the conduction band edge potential (E_{CB}) of TiO₂ and the first reduction potential is often used to describe the driving force for electron injection from the photoexcited porphyrin to TiO₂ (Chapter 1 Section 1.8.2). The driving force for electron injection is similar between PorY1 and PorO2, both of which are larger than PorR (Fig. 3.2(b)). Detailed studies of electron injection will be discussed in Chapter 4 and 5.

The difference between the redox potential of the mediator and the first oxidation potential of sensitizers is often used to describe the driving force for dye cation radical reduction (Chapter 1 Section 1.11.2). In addition to driving force, some other factors,

such as reorganization energy, the electron donor group and packing on the TiO_2 surface may affect dye regeneration kinetics. This topic is investigated in detail in Chapter 9.

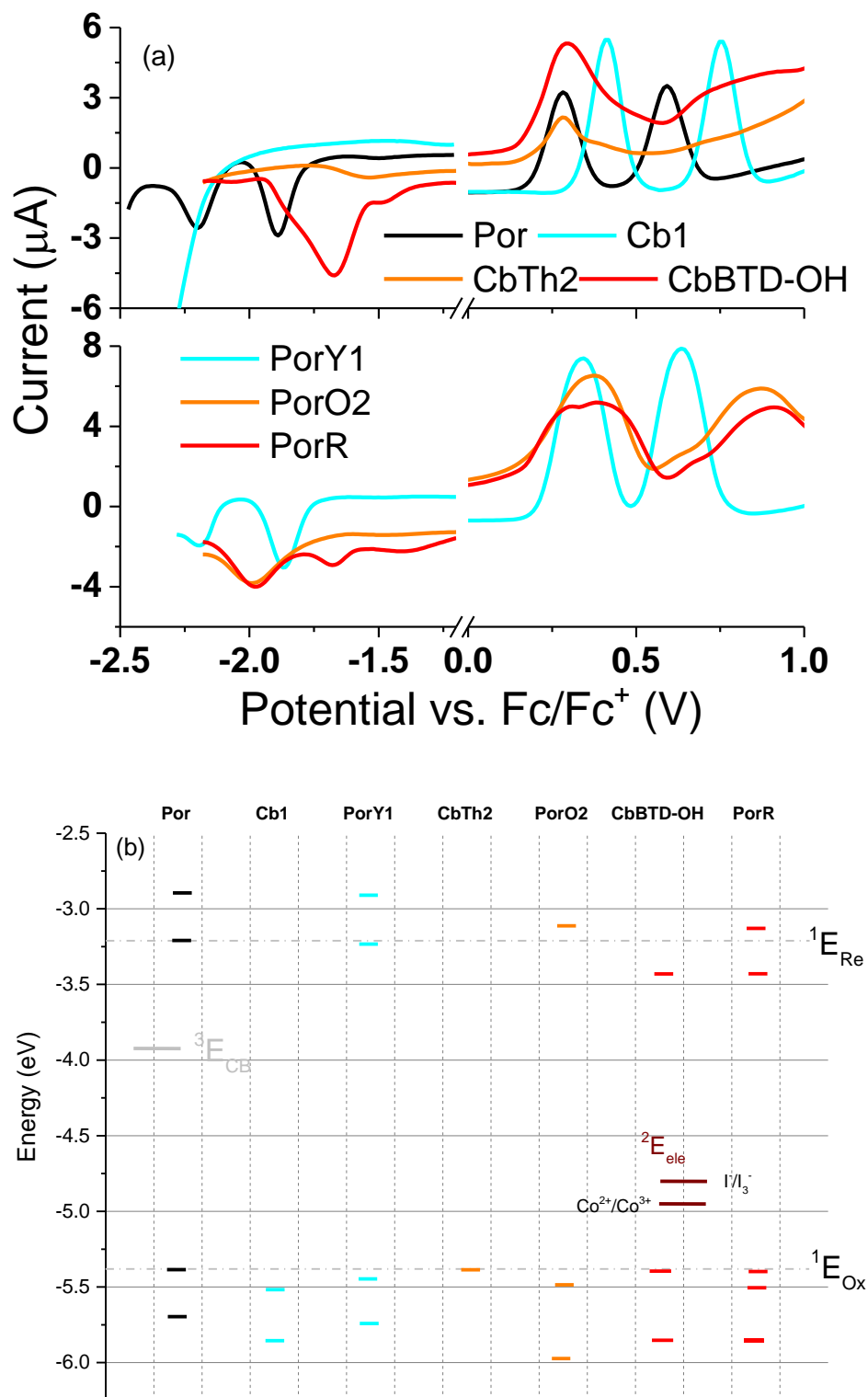


Figure 3.2 (a) Differential pulse voltammograms and (b) calculated energy levels of the compounds vs. vacuum.

Por, Cb1 and PorY1 were measured in DCM, while CbTh2, PorO2, CbBTD-OH and PorR were measured in DMF. 1. The energy levels of oxidation (E_{Ox}) and the energy levels of reduction (E_{Re}) were calculated from the peak potentials of oxidation (E_{Ox} vs. Fc/Fc^+) and reduction (E_{Re} vs. Fc/Fc^+) as $E_{Ox} = - (E_{Ox \text{ vs. } Fc/Fc^+} + 5.1)$ (eV) and $E_{Re} = - (E_{Re \text{ vs. } Fc/Fc^+} + 5.1)$ (eV), respectively. The potential of the Fc/Fc^+ redox couple was assumed to be -5.1 eV vs. vacuum⁵. 2. The redox couple potential (E_{ele}) using I^-/I_3^- was adopted from Ref⁶ and that using $Co(dmbpy)_3^{2+/3+}$ was adopted from Ref.^{7,8} 3. E_{CB} was adopted from Ref,⁹ with the value being calibrated to the absolute energy based on the assumption $E_{Fc/Fc^+} = +0.63$ V vs. NHE.

3.3. UV-visible absorption

PorY1 has increased light absorption in the 300-400 nm wavelength range due to the light absorption by the carbazole-triphenylamine unit, while PorO2 absorbs strongly in the 450-500 nm wavelength range (Fig. 3.3). The complementary light absorption by the organic chromophore CbTh2, effectively, although not completely, fills the absorption gap between the porphyrin Soret and Q band peaks. The effect of filling the absorption gap on photovoltaic performance will be described in detail in Chapter 5. PorR containing a carbazole-thiophene benzothiadiazole thiophene substituent extends the light absorption to slightly beyond 650 nm in solution.

PorY1 and PorO2 show broader Soret band and small increases in the absorption intensity in the Q bands relative to Por. These small differences in light absorption are attributed to the geometric distortion of the porphyrin part caused by attaching bulky substituents. Further evidence is provided in Chapter 4.

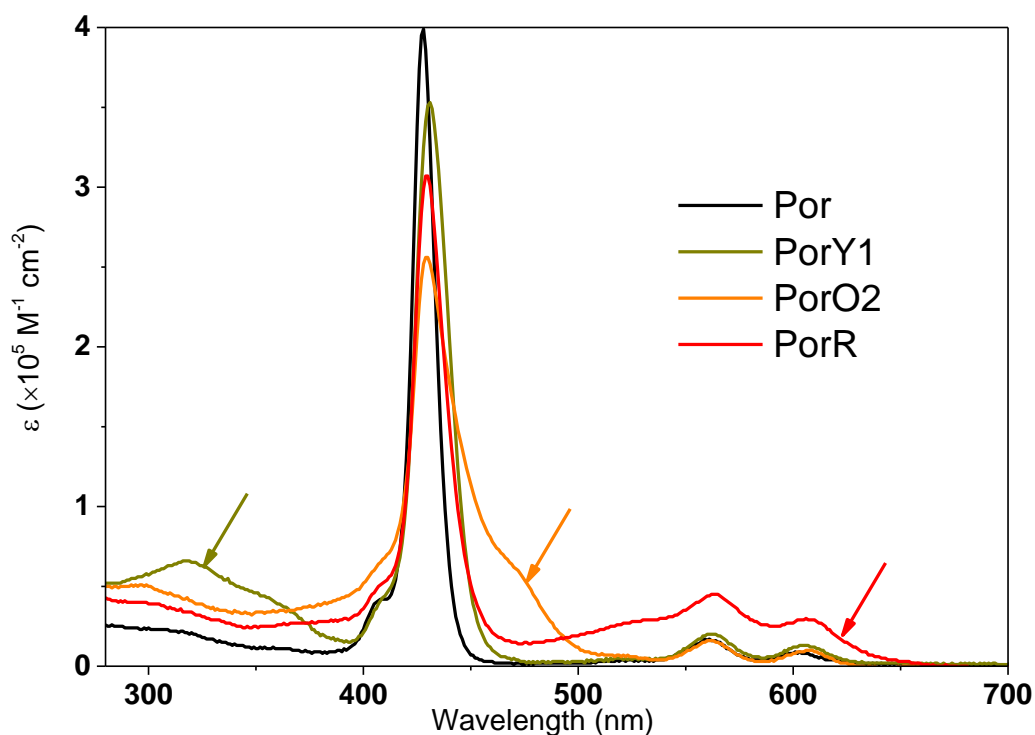


Figure 3.3 Molar extinction coefficient (ϵ) of the compounds measured in DMF.

The three arrows indicate the main change in each di-chromophoric dye compared to Por.

Employing the phenylethenyl unit as the bridge to covalently link the two chromophores in di-chromophoric dyes resulted in limited electronic communication in the ground state. This is due to a large dihedral angle (64 degree in PorR for example), which distorts the overlap of π -electron orbitals between the chromophores.

This lack of strong electronic communication is supported by the UV-vis characteristic (Fig. 3.3). Apart from the smaller, non-specific differences above, light absorption spectra of the di-chromophoric dyes are the superposition of the porphyrin and organic chromophore absorptions. Strong electronic coupling leading to larger delocalization typically induces red-shifted light absorption or even leads to the splitting of the Soret band.¹⁰⁻¹⁵

Further support for the negligible electronic communication between the two chromophores in the di-chromophoric dyes is given by the resonance Raman. The result was performed by project collaborators at the University of Otago.

The FT-Raman and resonance Raman spectra of PorY1 are shown in Fig. 3.4. An organic chromophore Cb1, electronically similar to the organic chromophore of PorY1,

was also measured and was used to distinguish the Raman bands originating from the carbazole or from the porphyrin (Fig. 3.4). Non-resonance Raman spectroscopy, therefore, helps to identify the extent of electronic delocalization following photoexcitation of the di-chromophoric dyes. For example, by exciting at 830 nm wavelength (non-resonance condition), the carbazole Cb1 shows strong Raman bands at 1003, 1599 and 1613 cm^{-1} (Fig. 3.4). When excited at 407 and 413 nm (resonance with the Soret band), Por shows intense bands at 1233, 1356 and 1549 cm^{-1} . When excited at 351 and 364 nm (carbazole is excited, resonance condition), PorY1 shows the most intense Raman bands at 1599, 1613 and 1632 cm^{-1} , which are similar to Cb1. When excited at 407 and 413 nm (porphyrin is excited, resonance condition), PorY1 shows the intense bands at 1233, 1356 and 1549 cm^{-1} , which are identical to Por. The enhancements of either (but not both) carbazole or porphyrin Raman bands indicate the lack of electronic communication and electron delocalization between the two units in photoexcited PorY1.

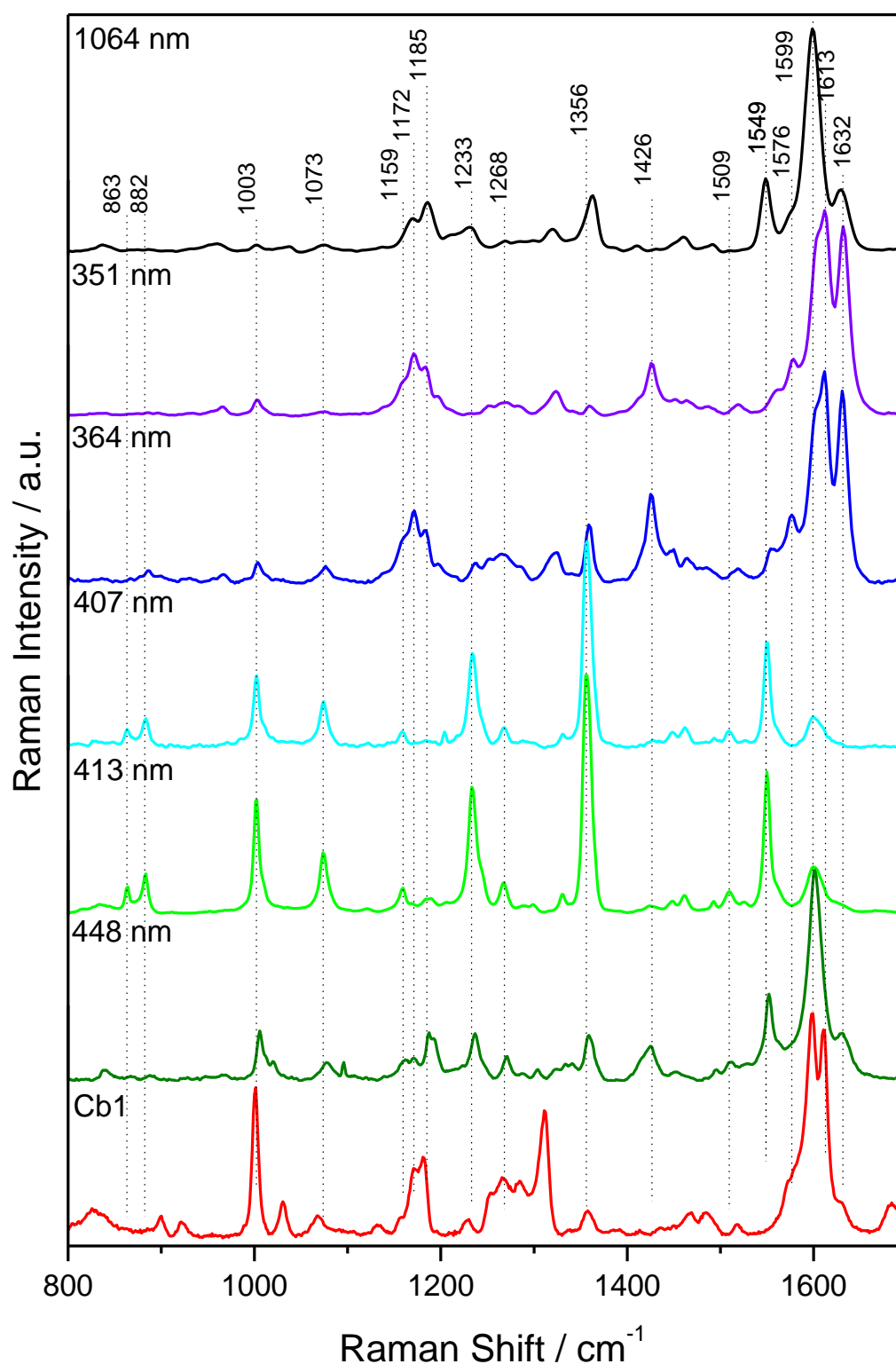


Figure 3.4 FT-Raman ($\lambda_{\text{ex}} = 1064 \text{ nm}$, black) and resonance Raman (1 mM CH_2Cl_2 solution, $\lambda_{\text{ex}} = 351\text{-}448 \text{ nm}$ with colours of violet, blue, cyan, green and olive, subsequently) spectra of PorY1 and non-resonant (830 nm, red colour) Raman spectrum of Cb1. Performed by collaborator Prof. Keith C. Gordon.

3.4. Photovoltaic performance: current-voltage curves and incident photon-to-current conversion efficiency

Thin film (2-2.6 μm) devices were fabricated to avoid charge collection losses, making it possible to compare the light harvesting properties and the electron injection efficiency of the di-chromophoric dyes.

Current density-voltage (J - V) curves of DSSCs of the porphyrin dye Por and the three di-chromophoric dyes are shown in Fig. 3.5. The average photovoltaic performance of three devices is listed in Table 3.1, suggesting good reproducibility.

A 20% improvement in short circuit current density (J_{SC}) is observed in DSSCs using PorY1 (7.37 mA cm^{-2}) or PorO2 (7.68 mA cm^{-2}) compared to Por (6.06 mA cm^{-2}). The open circuit voltage (V_{OC}) of DSSC using PorY1 (770 mV) is 80 mV higher than that of Por (690 mV). The V_{OC} increase of DSSC using PorO2 (710 mV) is much less significant (20 mV) compared to that of PorY1. Similar V_{OC} , but lower J_{SC} is observed in DSSC using PorR (695 mV and 3.22 mA cm^{-2} , respectively) compared to Por. Fill factors among devices are not clearly different. As clearly shown in Table 3.1, DSSCs using both PorY1 and PorO2 show better performance compared to Por. DSSC using PorR shows the lowest performance among the three families of di-chromophoric dyes.

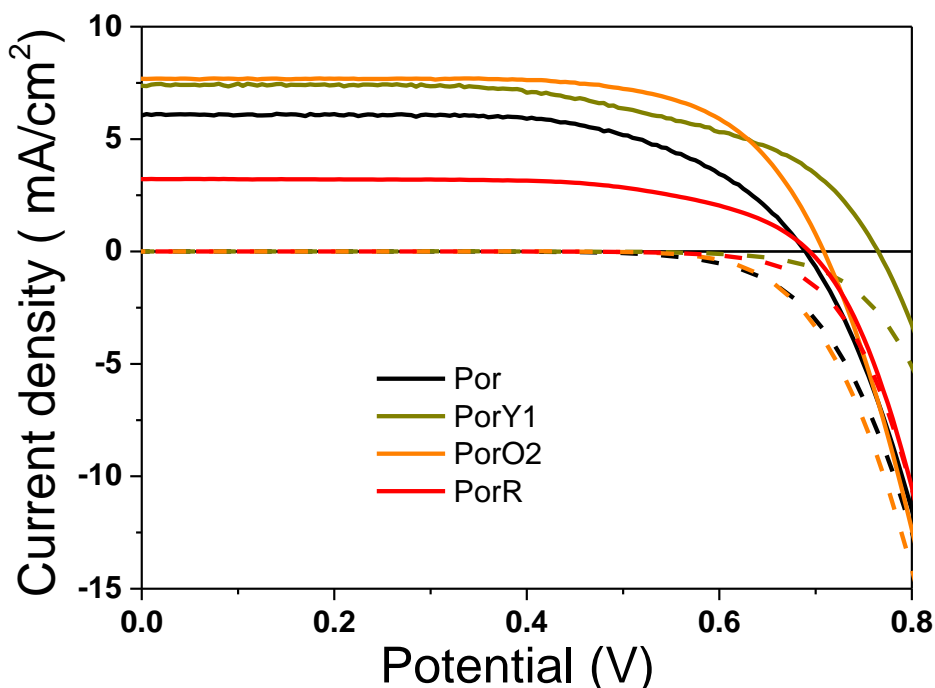


Figure 3.5 Current density-voltage (J - V) curves of DSSCs with the dyes fabricated using thin films under AM 1.5 illumination (solid lines) and in the dark (dashed lines).

The incident photon-to-current conversion efficiency (IPCE) spectra of the four porphyrins using thin TiO_2 films are shown in Fig. 3.6. Compared to Por, PorY1 shows increased IPCE values in the 350-650 nm wavelength range, and a 10 nm broader Soret band. PorO2 exhibits increased IPCE values at the “absorption gap” between the Soret and Q bands, and also enhanced IPCE values at the Q bands. PorR shows the lowest IPCE values in most of the wavelengths, however, the IPCE onset wavelength extends to more than 700 nm, making it the most promising dye considering light harvesting efficiency.

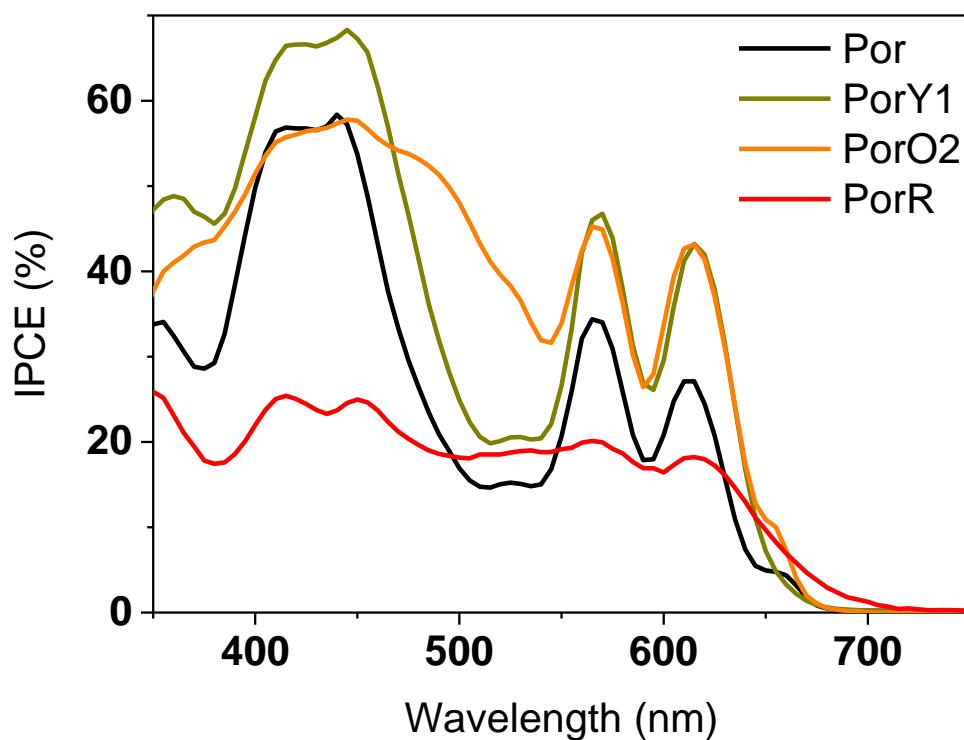


Figure 3.6 Incident photon-to-current conversion efficiency (IPCE) spectra of the dyes using thin films.

Increased light absorption using thicker TiO_2 films should lead to increased light harvesting and therefore increased photovoltaic performance. However, limitations in charge collection due to slow diffusion or short electron lifetime may influence the thickness dependence and limit the benefit of increased light absorption.

To check the above, thick films using 5-12 μm transparent and 2.5-5.5 μm scattering TiO_2 layers were also fabricated. Various TiO_2 thicknesses have been used for the

fabrication of devices (see subsequent chapters); the optimized thickness using each sensitizer with the best power conversion efficiency is shown here for comparison. Fig. 3.7 plots the J - V curves of the porphyrins using thick films. The photovoltaic performance for each device is listed in Table 3.1.

The highest power conversion efficiency of 6.23% was achieved by PorY1. This is one of the highest efficiency amongst the di-chromophoric dyes studied in this thesis and is also among the best reported for all porphyrin sensitizers.^{2,11,16,17} Even more interesting is that this enhanced photovoltaic performance is achieved without significant changes to the electronic levels compared to that of the simple porphyrin Por (Fig. 3.2(b)). The increased photocurrent may originate from the enhanced electron injection efficiency and to some extent from the increased light harvesting efficiency due to the distorted structure and the additional carbazole chromophore. Detailed electrochemical characterization and light harvesting efficiency / absorbed photon-to-current conversion efficiency measurements are discussed in Chapter 4 and suggest that improved dye morphology preventing dye aggregation in the more bulky PorY1 is primarily responsible for the enhanced injection efficiency and better photocurrent.

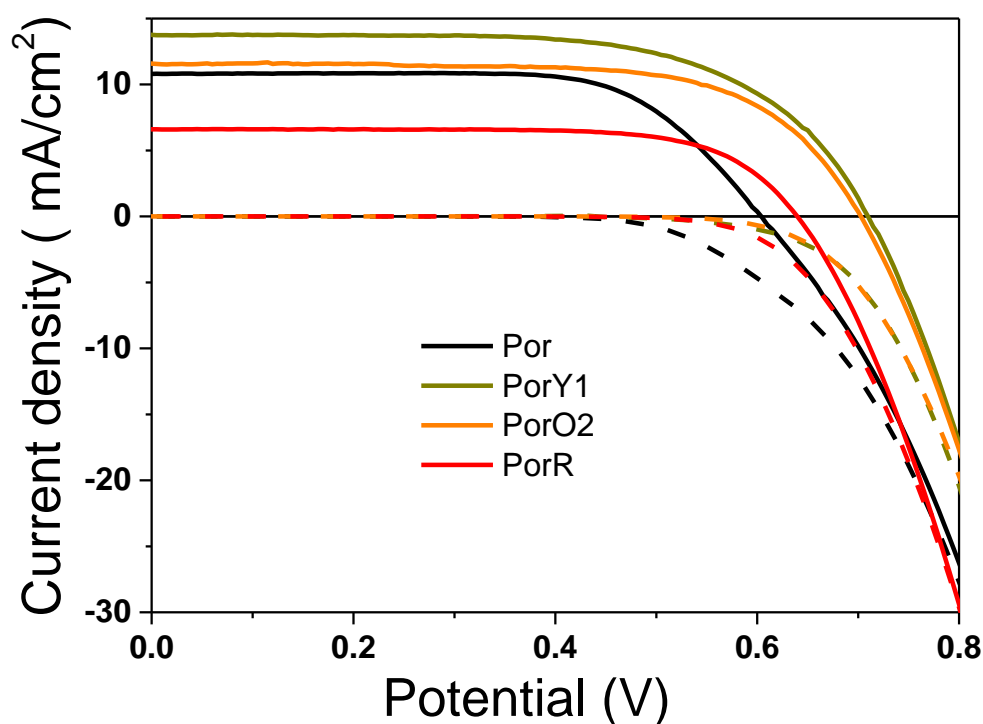


Figure 3.7 J - V curves of DSSCs with the dyes fabricated using thick films under AM 1.5 illumination (solid lines) and in the dark (dashed lines).

Table 3.1 Photovoltaic performance of the sensitizers using both thin and thick films. Device numbers: thin films (3, averaged) and thick films (2, the better ones are shown)

Dye	J_{sc} mA/cm ²	V_{oc} mV	FF	η %	Thickness (μ m)	Films condition
Por	6.0±0.2	690±10	0.62±0.01	2.6±0.1	2.2	Transparent TiO ₂ layer only, TAA layer and TiCl ₄ post-treatment applied (Chapter 2)
PorY1	7.0±0.4	770±10	0.60±0.03	3.3±0.2	2.2	
PorO2	7.4±0.3	700±10	0.69±0.01	3.6±0.1	2.6	
PorR	3.2±0.1	700±5	0.63±0.01	1.4±0.1	2	
Por	10.81	605	0.68	4.44	12+5.5	Transparent + scattering TiO ₂ layers, TAA layer and TiCl ₄ post-treatment applied (Chapter 2)
PorY1	13.76	710	0.64	6.23	12+5.5	
PorO2	11.58	705	0.67	5.48	5+2.5	
PorR	6.6	640	0.71	3.01	5+2.5	
Electrolyte: 0.6 M 1,2-dimethyl-3-propylimidazolium iodide (DMPII), 0.1 M LiI, 0.05 M I ₂ , 0.5 M <i>tert</i> -butylpyridine (<i>t</i> BP) in acetonitrile (AN): valeronitrile (VN)=85:15 (vol.). Device fabrication conditions: Solvent: tetrahydrofuran (THF); dye concentration: 0.2 mM; dye up-taking time: 1.5 hours; light soaking before testing: 20 minutes.						

The increased photocurrent in PorO2 may originate from enhanced light harvesting efficiency by filling the porphyrin absorption gap between the Soret and Q bands and / or increased charge injection or collection efficiencies. Detailed electrochemical characterization, light harvesting efficiency / absorbed photon-to-current conversion efficiency measurements and tuning electrolyte components in Chapter 5 suggest that the increased light harvesting is mainly responsible for the increased photocurrent. The performance, however, is limited by efficient electron injection due to a first reduction potential that is too positive. This limitation in electron injection of PorO2 devices, although similar energy levels of PorO2 and PorY1, may relate to the weak electronic coupling of PorO2 to TiO₂.

Despite the fact that light harvesting of PorR is the most red-shifted, the photocurrent obtained using this dye is the lowest. The decreased photocurrent originates from electron injection losses, which are attributed to energy / electron transfer from the

porphyrin to the organic chromophore, competing with electron injection to the TiO₂. This is supported by photoluminescence measurements in Chapter 7 and light harvesting efficiency / absorbed photon-to-current conversion efficiency measurements discussed in Chapter 6.

The photocurrents using the thick films are nearly doubled compared to those using thin films using all sensitizers. The open circuit voltages, however, decrease 50-90 mV in Por, PorY1 and PorR. PorO2 exhibits similar open circuit voltage when using thick films, from 710 mV to 705 mV. This indicates that the charge recombination compromise the benefit of enhanced light harvesting in thicker films.

The IPCE spectra using thick films are displayed in Fig. 3.8. DSSC using PorY1 exhibits larger IPCE values compared to the other porphyrins in the 350-650 wavelength range. DSSC using PorO2 shows increased IPCE values at the absorption gap and Q bands compared to Por, similarly to using thin films. However, the IPCE values of device using PorO2 within the 450-550 nm wavelength range are lower compared to that of PorY1. This trend is different from the results obtained using thin films, which may indicate increased charge collection losses in DSSC using PorO2. The optimized thicknesses for devices using PorO2 and PorR are less than that of PorY is mainly due to more charge collection losses. Furthermore, the IPCE peak value of DSSC using PorO2 at the Soret band (60%) are 10% less than that of Por (70%), which may suggest electron injection losses or charge collection losses. DSSC using PorR shows relatively poor IPCE (~30%) but with an extended wavelength coverage.

It should be pointed out that the dye loading on TiO₂ within the films sensitized with the four porphyrins are similar (as shown in the following chapters, $1.1-1.6 \times 10^{-4}$ mole cm⁻³). Therefore, the dye amount should not be accounted for the light harvesting and the IPCE differences in these devices.

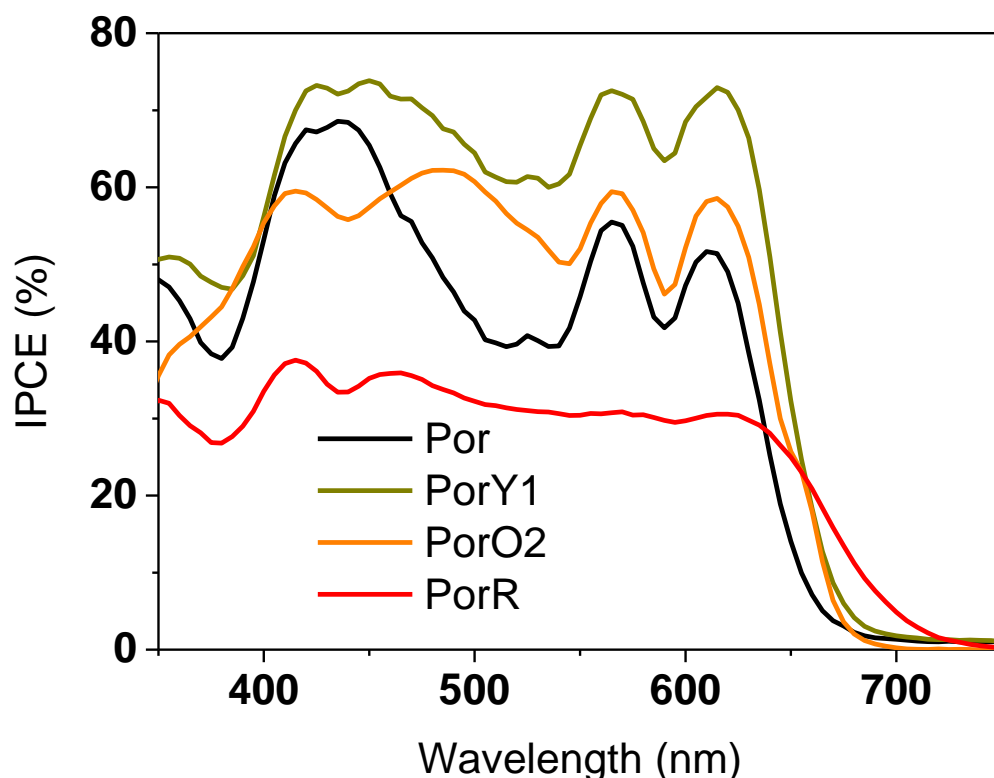


Figure 3.8 IPCE spectra of the dyes using thick films.

Because of the importance of electron lifetime in these three families of di-chromophoric dyes, detailed investigations of electron lifetime and electron diffusion coefficient using stepped light-induced transient photocurrent and photovoltage techniques, will be carried out in Chapter 8. The increased photovoltages using PorY1 and PorO2 are attributed to increased electron lifetime, which originates from the bulky, tridimensional organic chromophores blocking the approach of the electron accepting species in the electrolyte to the TiO_2 interface.

PorR constitutes a special case as it contains a highly polarizable, low band gap chromophore. For the first time, dispersion forces between highly polarizable dye segments and acceptor species in the electrolyte are exploited to enhance electron lifetime in a di-chromophoric dye design. Chapter 8 will discuss this aspect of the thesis.

3.5. Summary and outline of subsequent chapters

To summarize, a simple comparison, focusing on electrochemical properties, UV-vis absorption and photovoltaic performance in DSSCs of the three families of di-chromophoric dyes, were presented. The main findings are:

- i) Electrochemistry, UV-visible absorption and resonance Raman spectroscopy suggest that there is very weak electronic communication in the ground state between the porphyrin and organic chromophore of the di-chromophoric dyes.
- ii) UV-visible absorption measurement demonstrates that the light absorption gap between the Soret and Q bands of Por can be partly filled by the carbazole-fused thiophene chromophore of the PorO2.
- iii) The carbazole-thiophene benzothiadiazole thiophene chromophore shows lower reduction potential and lower band gap compared to that of the porphyrin in PorR. Therefore, an intramolecular electron / energy transfer from the excited porphyrin to the organic chromophore is possible, which leads to the low photovoltaic performance of devices using PorR.
- iv) DSSCs using PorY1 and PorO2 exhibit higher, while that of using PorR lower, photocurrent than the porphyrin component. IPCE measurement suggests increased IPCE values in the 350-650 nm wavelength range in PorY1, enhanced IPCE values at the “absorption gap” and the Q bands in PorO2, and decreased IPCE values in most of the wavelengths but extended IPCE onset wavelength to more than 700 nm in PorR, compare to Por. Detail analysis of the origin of these differences in photocurrent of devices will be discussed in the following chapters.
- v) All DSSCs using the three di-chromophoric dyes show similar or enhanced photovoltage compared to that using the single chromophoric porphyrin.

The comparisons lead to some important scientific questions. These questions are listed below in Table 3.2, setting out the structure of the thesis.

Table 3.2 List of topic and questions investigated in the following chapters

Chapters	Topic / Questions investigated
4	What is the origin of increased photocurrent in a series carbazole-substituent porphyrin dyes (PorY family)?
5	What limits the IPCE values in the PorO family using organic chromophores thieno[3,2-b]thiophene, dithieno[3,2-b:2',3'-d]thiophene and 4,8-dicecyloxybenzo[1,2-b:4,5-b']dithiophene? How about the utility of cobalt electrolyte in the di-chromophoric dyes?
6	How is the photovoltaic performance of the di-chromophoric dye (PorR) influenced by two competing electron transfer pathways? How about if compared to the co-sensitization (mixed dyes) system?
7	Energy / electron transfer pathways within the three families of di-chromophoric dyes.
8	Correlation of dye structure and electron lifetime in di-chromophoric dyes.
9	How does intramolecular hole transfer influence dye regeneration and recombination kinetics?

3.6. References

- (1) Mozer, A. J.; Griffith, M. J.; Tsekouras, G.; Wagner, P.; Wallace, G. G.; Mori, S.; Sunahara, K.; Miyashita, M.; Earles, J. C.; Gordon, K. C.; Du, L.; Katoh, R.; Furube, A.; Officer, D. L. *J. Am. Chem. Soc.* **2009**, *131*, 15621.
- (2) Sunahara, K.; Griffith, M. J.; Uchiyama, T.; Wagner, P.; Officer, D. L.; Wallace, G. G.; Mozer, A. J.; Mori, S. *ACS Appl. Mater. Interfaces* **2013**, *5*, 10824.
- (3) Ohta, M.; Koumura, N.; Hara, K.; Mori, S. *Electrochem. Commun.* **2011**, *13*, 778.
- (4) Lee, M.-W.; Kim, J.-Y.; Lee, D.-H.; Ko, M. J. *ACS Appl. Mater. Interfaces* **2014**, *6*, 4102.
- (5) Cardona, C. M.; Li, W.; Kaifer, A. E.; Stockdale, D.; Bazan, G. C. *Adv. Mater.* **2011**, *23*, 2367.
- (6) Boschloo, G.; Hagfeldt, A. *Acc. Chem. Res.* **2009**, *42*, 1819.
- (7) Feldt, S. M.; Wang, G.; Boschloo, G.; Hagfeldt, A. *J. Phys. Chem. C* **2011**, *115*, 21500.
- (8) Mosconi, E.; Yum, J.-H.; Kessler, F.; Gomez Garcia, C. J.; Zuccaccia, C.;

Cinti, A.; Nazeeruddin, M. K.; Grätzel, M.; De Angelis, F. *J. Am. Chem. Soc.* **2012**, *134*, 19438.

(9) Hagfeldt, A.; Boschloo, G.; Sun, L.; Kloo, L.; Pettersson, H. *Chem. Rev.* **2010**, *110*, 6595.

(10) Angiolillo, P. J.; Lin, V. S. Y.; Vanderkooi, J. M.; Therien, M. J. *J. Am. Chem. Soc.* **1995**, *117*, 12514.

(11) Mai, C.-L.; Huang, W.-K.; Lu, H.-P.; Lee, C.-W.; Chiu, C.-L.; Liang, Y.-R.; Diau, E. W.-G.; Yeh, C.-Y. *Chem. Commun.* **2010**, *46*, 809.

(12) Lin, C.-Y.; Lo, C.-F.; Luo, L.; Lu, H.-P.; Hung, C.-S.; Diau, E. W.-G. *J. Phys. Chem. C* **2009**, *113*, 755.

(13) Lo, C.-F.; Hsu, S.-J.; Wang, C.-L.; Cheng, Y.-H.; Lu, H.-P.; Diau, E. W.-G.; Lin, C.-Y. *J. Phys. Chem. C* **2010**, *114*, 12018.

(14) Lu, H.-P.; Tsai, C.-Y.; Yen, W.-N.; Hsieh, C.-P.; Lee, C.-W.; Yeh, C.-Y.; Diau, E. W.-G. *J. Phys. Chem. C* **2009**, *113*, 20990.

(15) Hsieh, C.-P.; Lu, H.-P.; Chiu, C.-L.; Lee, C.-W.; Chuang, S.-H.; Mai, C.-L.; Yen, W.-N.; Hsu, S.-J.; Diau, E. W.-G.; Yeh, C.-Y. *J. Mater. Chem.* **2010**, *20*, 1127.

(16) Liu, Y.; Lin, H.; Dy, J. T.; Tamaki, K.; Nakazaki, J.; Nakayama, D.; Uchida, S.; Kubo, T.; Segawa, H. *Chem. Commun.* **2011**, *47*, 4010.

(17) Warnan, J.; Pellegrin, Y.; Blart, E.; Odobel, F. *Chem. Commun.* **2012**, *48*, 675.

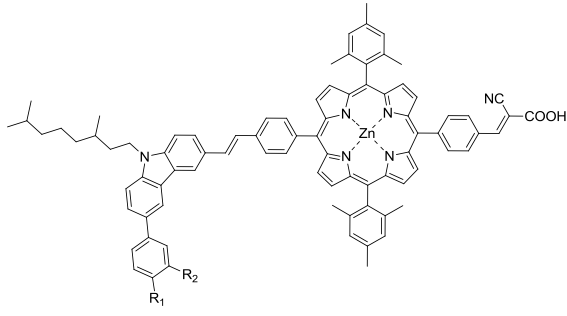
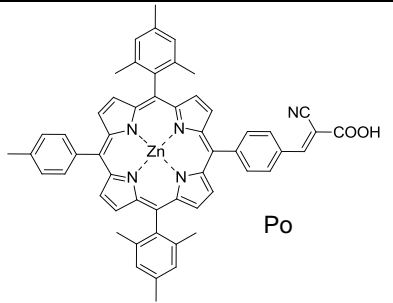
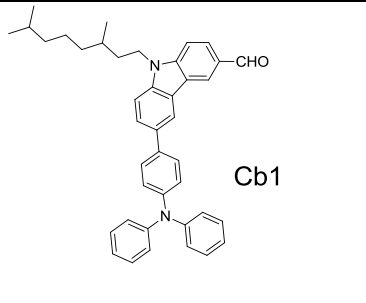
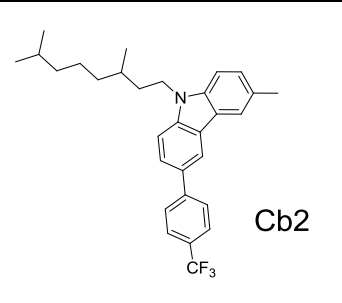
**CHAPTER 4.EFFECT OF ORGANIC CHROMOPHORE SUBSTITUTION ON
THE OPTICAL AND ELECTRONIC PROPERTIES OF PORPHYRIN
CARBAZOLE DI-CHROMOPHORIC DYES**

4.1. Introduction

The influence of electron withdrawing / donating substituents, at the carbazole unit, on the optical and electrochemical properties of the di-chromophoric porphyrin-carbazole dyes (PorY family, Table 4.1) is investigated in this chapter. The PorY dyes are compared to a single chromophoric porphyrin dye (Por) and two carbazole chromophores (Cb1 and Cb2).

The aim of this comparison is to understand how the organic chromophore electronic levels influence the photovoltaic performance in dye-sensitized solar cell. Using light harvesting efficiency (LHE), incident photon-to-current conversion efficiency (IPCE) and absorbed photon-to-current conversion efficiency (APCE) measurements, it is shown that the organic chromophore substitution does not affect the photovoltaic performance. However, improvements in photovoltage and photocurrent for all dyes have been observed compared to the single chromophoric porphyrin dye. Detailed measurements to understand the origin of these improvements and the utility of using bulky carbazole units in the di-chromophoric approach will be discussed.

Table 4.1 Molecular structures of the investigated compounds

						
	Name	PorY1	PorY2	PorY3	PorY4	PorY5
	R1	Ph ₂ N	CF ₃	Me	MeO	H
	R2	H	H	H	H	CF ₃
 <p>Po</p>	 <p>Cb1</p>					
	 <p>Cb2</p>					

4.2. Experimental

4.2.1 Investigated molecules

The following abbreviations are used for the compounds in Table 4.1: 5-(4-(2-cyano-2-carboxyethenyl)phenyl)-15-(4-(2-(6-(4-(N,N-diphenylamino)phenyl)-9-(3,7-dimethyloctyl)carbazol-3-yl)ethenyl)phenyl)-10,20-bis(2,4,6-trimethylphenyl)porphyrinato zinc (II) (PorY1); 5-(4-(2-cyano-2-carboxyethenyl)phenyl)-15-(4-(2-(6-(4-trifluoromethylphenyl)-9-(3,7-dimethyloctyl)carbazol-3-yl)ethenyl)phenyl)-10,20-bis(2,4,6-trimethylphenyl)porphyrinato zinc (II) (PorY2); 5-(4-(2-cyano-2-carboxyethenyl)phenyl)-15-(4-(2-(6-(4-methylphenyl)-9-(3,7-dimethyloctyl)carbazol-3-yl)ethenyl)phenyl)-10,20-bis(2,4,6-trimethylphenyl)porphyrinato zinc (II) (PorY3); 5-(4-(2-cyano-2-carboxyethenyl)phenyl)-15-(4-(2-(6-(4-methoxyphenyl)-9-(3,7-dimethyloctyl)carbazol-3-yl)ethenyl)phenyl)-10,20-bis(2,4,6-trimethylphenyl)porphyrinato zinc (II) (PorY4); 5-(4-(2-cyano-2-carboxyethenyl)phenyl)-15-(4-(2-(6-(3-trifluoromethylphenyl)-9-(3,7-dimethyloctyl)carbazol-3-yl)ethenyl)phenyl)-10,20-bis(2,4,6-trimethylphenyl)porphyrinato zinc (II) (PorY5); 5-(4-(2-cyano-2-carboxyethenyl)phenyl)-15-(4-methylphenyl)-10,20-bis(2,4,6-trimethylphenyl)porphyrinato zinc (II) (Por); 6-(4-(N,N-diphenylamino)phenyl)-(9-(3,5-dimethyloctyl)carbazole-3-carboxaldehyde (Cb1); 9-(3,7-dimethyloctyl)-6-methyl-3-(4-trifluoromethylphenyl)carbazole (Cb2).

4.2.2 Spectroscopic and electrochemical characterization

UV-visible (UV-vis) absorption spectroscopy was performed using a Shimadzu UV-3600 spectrophotometer in both dichloromethane (DCM) and dimethylformamide (DMF) with 1 μ M concentration.

Differential Pulse Voltammetry (DPV) was carried out using an eDAQ potentiostat in DCM. The dye concentration was 0.5 mM and the supporting electrolyte tetrabutylammonium perchlorate (TBAP,) was 0.1 M. The reference electrode (RE) potential was calibrated using 1 mM ferrocene/ferrocenium couple (Fc/Fc^+).

4.2.3 DSSC fabrication and characterization

Both photoanode and counter electrode consisted of fluorine doped tin oxide glass (FTO glass, 3 mm, 8 Ω /square, Nippon Sheet Glass) substrate. A platinum layer was coated

on the counter electrode surface by a thermal decomposition method as illustrated in Chapter 2. The photoanode contained an approximately 100 nm TiO₂ compact titanium diisopropoxide bis(acetylacetonate) (TAA) layer and a mesoporous TiO₂ layer. The mesoporous TiO₂ layer was screen-printed using both transparent TiO₂ paste (18-NRT, Dyesol) and scattering paste (WER2-O, Dyesol). TiCl₄ post-treatment was applied to the photoanodes after the sintering of the mesoporous layer.

The pre-cut TiO₂/FTO glass substrates were sensitized by immersing into 0.2 mM dye solution in anhydrous tetrahydrofuran (THF) for 1.5 hours. To employ 2 mM chenodeoxycholic acid (CDCA, Solaronix) as co-adsorber, ethanol was used as the solvent.

The standard electrolyte for the device characterization was composed of 0.6 M 1,2-dimethyl-3-propylimidazolium iodide (DMPII), 0.1 M LiI, 0.05 M I₂, 0.5 M *tert*-butylpyridine (*t*BP) in acetonitrile (AN): valeronitrile (VN)=85:15 (vol).

The benchmark ruthenium dye N719 was employed as a marker. N719 dye solution was 0.4 mM in AN:*t*BuOH=1:1 (vol) solvent, where *t*BuOH was *tert*-Butanol.

The finished devices were exposed to 100 mW cm⁻² AM 1.5 illumination for 20 minutes before current density-voltage (*J*-*V*) measurements. *J*-*V* measurements were performed using a simulated 100 mW cm⁻² air mass 1.5G solar simulation (Newport) and a Keithley 2400 source measure unit. The size of the sensitized area was 4 mm × 4 mm.

Incident photon-to-current conversion efficiency (IPCE) was recorded after the *J*-*V* measurements using a 300 W Xe lamp coupled to a monochromator with long pass filters. Light harvesting efficiency (LHE) was calculated from the UV-vis absorbance of the sensitizers on TiO₂ films.^{1,2} Small amount of electrolyte was used during the measurement to better match the UV-vis absorption measurement conditions to device operating conditions. The absorbed photon-to-current conversion efficiency (APCE) was thereafter calculated as the ratio of IPCE and LHE (APCE=IPCE/LHE).

For dye loading test, 0.1 M tetrabutylammonium hydroxide solution (TBAOH) in DMF was used for dye desorption from the semiconductor. For quantitative analysis, the UV-visible absorption spectroscopy was employed. The peak molar extinction coefficient values of the compounds at the Soret band are shown in Appendix Table A1.

4.3. Light absorption in solutions

The molar extinction coefficients (ϵ) of the single chromophoric porphyrin Por and the PorY dyes in DCM and DMF are shown in Fig. 4.1(a) and (b), respectively. The molar extinction coefficients of the two carbazole chromophores, Cb1 and Cb2, were also measured in DCM (Fig. 4.1(a)).

As seen in Fig. 4.1(a), the addition of the carbazole moieties to the porphyrin resulted in an increased absorbance in the 270-370 nm wavelength range in all PorY dyes. This is in accordance with the absorption profile of Cb1 and Cb2, which shows light absorption at the 260-400 nm wavelength range. PorY1 shows slightly increased absorption in this high energy region. This is due to the presence of the triphenylamine (TPA) unit in PorY1, adding additional light absorption at 320-380 nm wavelength range as compared to PorY2-5.

The absorption bands of the PorY dyes appear to be a simple superposition of the porphyrin and carbazole absorption bands. Furthermore, no significant variation in the UV-vis absorption spectra is observed by changing the electron withdrawing / donating substituents in PorY1 to PorY5. The molar extinction coefficient of Por is 5-15% higher at the Soret band and 20~40% lower at the Q bands compared to PorY dyes. Additionally, about 10 nm broadening of the Soret band is observed in the PorY dyes relative to Por.

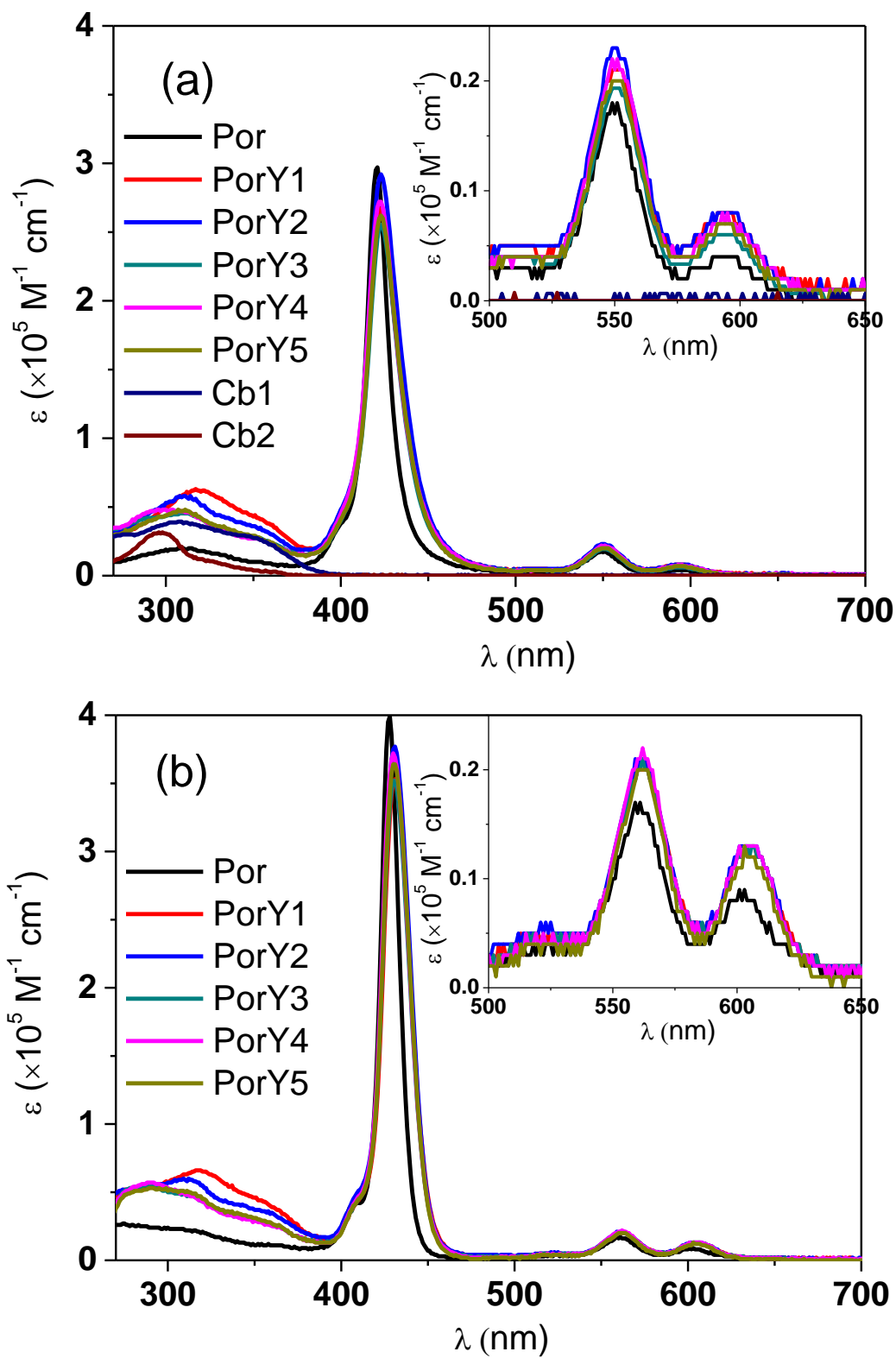


Figure 4.1 Molar extinction coefficient of the compounds measured in (a) DCM; (b) DMF

The UV-vis absorption spectra of the PorY dyes slightly differ between DCM and DMF. The Soret band intensity is 30% higher in DMF compared to in DCM. The molar extinction coefficient in DMF was nearly doubled in the 570-620 nm wavelength region compared to DCM. The oscillator strength (f) calculated from the integrated area encompassing the Soret band (380-500 nm) and the Q bands (520-630 nm) shows larger values in DMF than that in DCM (Table 4.2).

Because the dielectric constants are very different: 9.1 for DCM and 38 for DMF, the difference in the solvation energies of the dyes may cause the small changes in the UV-vis absorption.^{3,4}

In summary, the UV-vis absorption data reveals that there are no marked changes in the intensity and position of the Soret and Q bands when comparing Por and PorY1-5. Thus, it is reasonable to conclude that there is little electronic interaction between the substituent carbazole chromophore and the porphyrin. The origin of the weak interaction is a significant dihedral twist along the phenylethynyl bridge between the two chromophores (a dihedral angle of 117 degrees estimated by DFT calculation).² The small observed changes are all consistent with the effect of geometric distortion of the porphyrin as suggested in previous reports.⁵⁻⁷

Table 4.2 Oscillator strength (f) of UV-visible absorption spectra of porphyrins in both DCM and DMF.

Dyes	(f) [#] in DCM		(f) [#] in DMF		(DMF-DCM)/DCM	
	380-500 nm	520-630 nm	380-500 nm	520-630 nm	380-500 nm	520-630 nm
Por	1.52	0.08	1.56	0.10	5%	30%
PorY1	1.88	0.12	1.92	0.13	4%	16%
PorY2	2.07	0.12	2.07	0.14	2%	14%
PorY3	1.77	0.10	1.90	0.13	9%	40%
PorY4	1.91	0.12	1.98	0.13	6%	21%
PorY5	1.81	0.10	1.92	0.12	8%	19%
Max.	38%	56%	34%	38%	(PorY2-Por)/Por	
Min.	18%	23%	23%	22%*	(PorY3-Por)/Por	
#calculated by 4.32×10 ⁻⁹ ×A, where A=integrated area of the absorption band in each solution. Using the plot of molar extinction coefficient (ε, M ⁻¹ cm ⁻¹) versus wavenumbers (cm ⁻¹) to obtain A [#] . *calculated by (PorY5-Por)/Por						

4.4. Effect of the carbazole substitution on the electrochemical properties of the dyes

The reduction / oxidation voltammograms, measured by differential pulse voltammetry (DPV), of the investigated compounds are shown in Fig. 4.2, and summarized peak potentials are in Table 4.3.

There are no quantitative differences in the first reduction and first oxidation peak potentials (E_{Re}^{1st} and E_{Ox}^{1st}) of the PorY dyes respect to the reference Por. This is in agreement with the optical characterization. The functionalization of carbazole-substituent porphyrin dyes did not affect the band gap or the relative band positions. The carbazole substituents with different electron donating / withdrawing abilities do not affect the E_{Re}^{1st} and E_{Ox}^{1st} significantly.

The carbazole substituent appears to influence the high lying oxidation potentials of the PorY dyes (Fig. 4.2(b)). New oxidation peaks appear in the PorY dyes as compared to Por. Por displays two oxidation peaks at +0.28 V vs Fc/Fc⁺ and +0.59 V vs Fc/Fc⁺. PorY2-5 show three or four potentials with the first oxidation peak potentials are identical to Por as described above. Interestingly, PorY1 shows two oxidation peaks of more than double the current compared to Por. Since the concentration is the same, it suggests that PorY1 oxidation consist of the overlapping one-electron oxidation reactions of the two chromophores.

The new oxidation features in PorY dyes can be analysed when looking at the oxidative voltammograms of the organic chromophore Cb1 (+0.41 V vs Fc/Fc⁺ and +0.75 V vs Fc/Fc⁺) and Cb2 (+0.78 V vs Fc/Fc⁺ and +1.05 V vs Fc/Fc⁺). In the case of PorY1 and Cb1, there is a clear overlap in the second oxidation potential. In the case of Por2-5, there are new oxidation reactions that do not present in the constituting chromophores. The new oxidative features can be explained by two different configurations of the single-oxidized PorY2-5 with a delocalized (negative shift) and localized cation radical (positive shift).

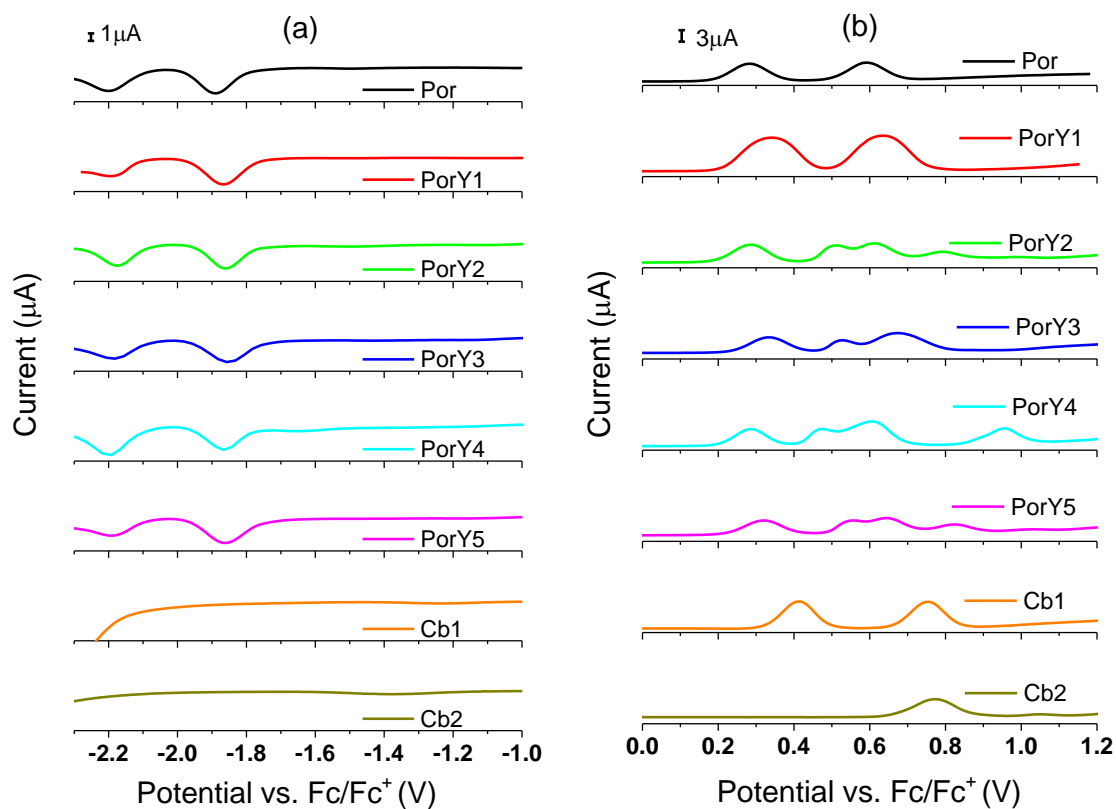


Figure 4.2 Differential pulse voltammograms of the investigated compounds, (a) negative scan; (b) positive scan.
Sample concentration: 0.5mM; solvent: DCM; supporting electrolyte: TBAP; Pt wire surface area: 6.6 mm²; scan rate: 100 mV s⁻¹.

Table 4.3 Electrochemical properties and estimated band gaps of the investigated compounds

Dye	Peak Potential vs. Fc/Fc ⁺		Onset Potential vs. Fc/Fc ⁺		^a ΔE_1 /eV	^b ΔE_2 /eV
	E_{Re}/V	E_{Ox}/V	E_{RO}/V	E_{OO}/V		
Por	-1.89	0.28	-1.78	0.18	2.17	2.00
	-2.20	0.59	-2.08	0.49		
PorY1	-1.86	0.34	-1.75	0.21	2.21	2.00
	-2.19	0.64	-2.09	0.51		
PorY2	-1.86	0.29	-1.76	0.18	2.15	1.98
	-2.18	0.51	-2.06	0.45		
	-	0.61	-	0.50		
	-	0.79	-	0.68		
PorY3	-1.86	0.33	-1.75	0.23	2.19	1.99
	-2.18	0.53	-2.06	0.47		
	-	0.67	-	0.54		
PorY4	-1.86	0.28	-1.76	0.18	2.13	1.99
	-2.20	0.47	-2.07	0.42		
	-	0.61	-	0.51		
	-	0.95	-	0.84		
PorY5	-1.86	0.32	-1.75	0.22	2.18	1.98
	-2.19	0.56	-2.10	0.49		
	-	0.64	-	0.53		
	-	0.82	-	0.72		
Cb1	-	0.42	-	0.32	-	3.04
	-	0.75	-	0.66		
Cb2	-	0.77	-	0.65	-	3.31
	-	1.05	-	0.96		

Notes: ^a Band gap from DPV, $\Delta E_1 = E_{Ox}^{1st} - E_{Re}^{1st}$; ^b Band gap from UV-vis absorption spectrum in DCM, $\Delta E_2 = 1243/\lambda_{onset}$, where λ_{onset} is the onset wavelength.

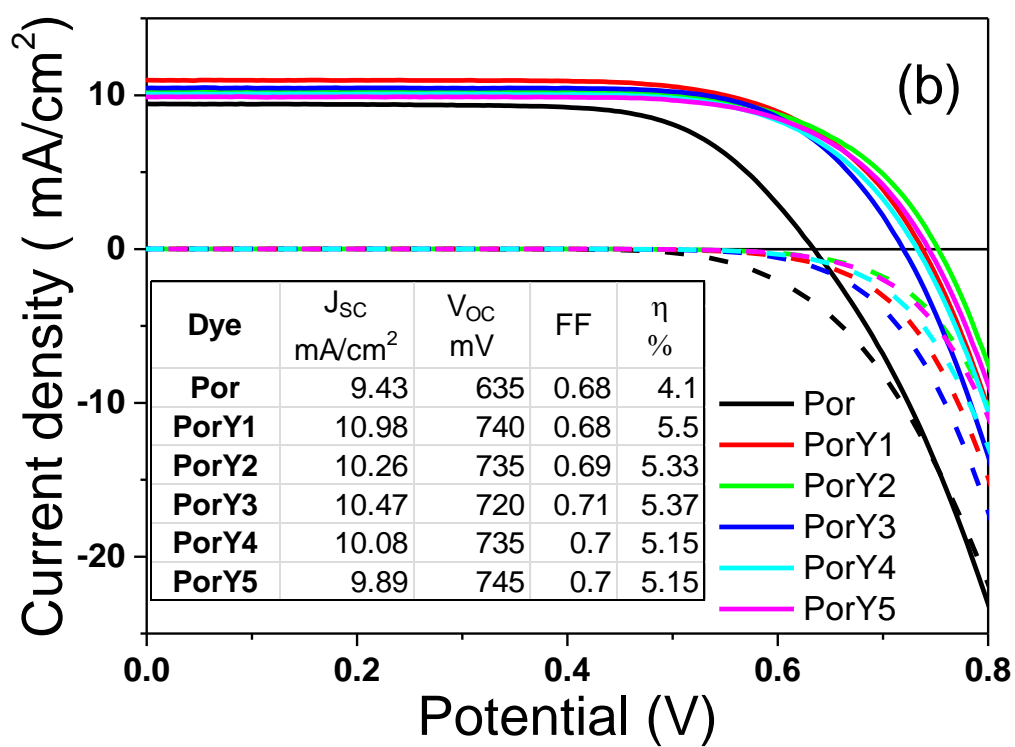
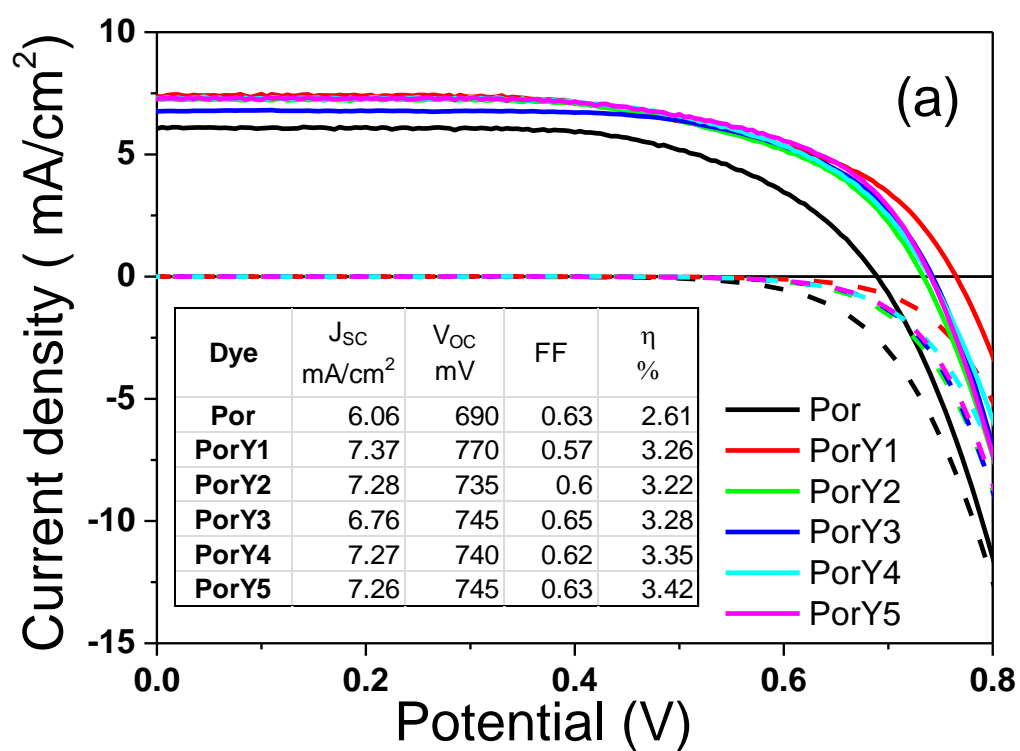
4.5. Simultaneously enhanced photocurrent and photovoltage in DSSCs

The measurements described above suggested that the electronic structure of the PorY dyes was not significantly affected by the substitution on the carbazole. Moreover, no significant electronic interaction in the ground state has been observed between the porphyrin and the carbazole chromophores. Therefore, no major differences, apart from the slightly increased and broadened light absorption are expected when the dyes are used in DSSCs.

Current density-voltage (J - V) curves of DSSCs comprising the porphyrin dyes and three different TiO_2 thicknesses are shown in Fig. 4.3 (the averaged data from three devices are shown in Table 4.4). Typically, thin films were used to avoid charge collection loss, enabling APCE and charge collection measurements, while thick films with more complete light harvesting were used to evaluate the potential of the new dyes as sensitizers for DSSCs.

Significant increase in the short circuit current density (J_{SC}) and open circuit voltage (V_{OC}) are observed using the PorY dyes in DSSCs compared to Por on 2.2 μm films (Fig. 4.3(a)). DSSCs using the PorY dyes show a 20% improvement in J_{SC} (J_{SC} of Por is 6 mA cm^{-2}), except that using PorY3, which shows a 10% increase. Furthermore, all the DSSCs using the PorY dyes showed higher V_{OC} values (740 to 770 mV) compared to that of Por (690 mV). No systematic variation in the fill factors was observed. To summarize, the power conversion efficiencies (η) of the DSSCs using the PorY dyes show 30% increase compared to that of Por, which is unexpected and significant considering no major effects on the electronic structure has been observed as explained above.

Thick TiO_2 films of 9 μm and 17.5 μm were also employed to fabricate DSSCs and the J - V data is shown in Fig. 4.3(b) and (c). A 15~20% increase in short circuit current and a 70 mV to 100 mV increase in open circuit voltage are observed for DSSCs using the PorY dyes. The highest power conversion efficiencies have been achieved by PorY1 and PorY2 with values above 6%, while PorY3 to PorY5 show 5.5%.



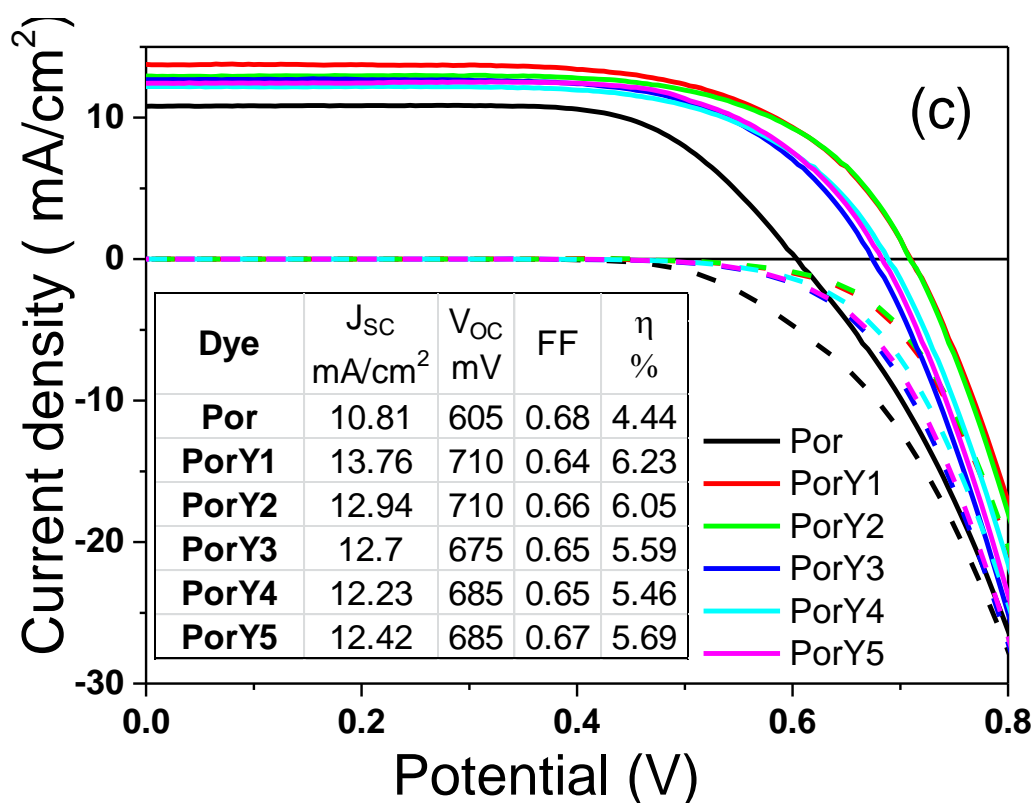


Figure 4.3 Current density-voltage (J - V) curves of DSSCs with the porphyrin dyes fabricated using (a) thin films: $2.2 \pm 0.1 \mu\text{m}$, and thick films: (b) $6 \mu\text{m}$ transparent + $3.2 \mu\text{m}$ scattering TiO_2 , (c) $12 \mu\text{m}$ transparent + $5.5 \mu\text{m}$ scattering TiO_2 , under AM 1.5 illumination (solid lines) and in the dark (dashed lines).

The inset shows the photovoltaic performance for each device.

Table 4.4 Performance of thin film devices (averaged three devices) with porphyrin dyes compared with N719

Dye	Thickness / μm	J_{sc} mA/cm ²	V_{oc} mV	FF	η %	Note	Γ mol/cm ³
Por	2.2 ± 0.1	6.0 ± 0.2	690 ± 10	0.62 ± 0.01	2.6 ± 0.1	After light soaking 20 mins	1.2×10^{-4}
PorY1		7.0 ± 0.4	770 ± 10	0.60 ± 0.03	3.3 ± 0.2		1.2×10^{-4}
PorY2		7.0 ± 0.3	730 ± 10	0.63 ± 0.03	3.2 ± 0.1		1.0×10^{-4}
PorY3		6.9 ± 0.2	740 ± 10	0.64 ± 0.01	3.3 ± 0.1		1.4×10^{-4}
PorY4		7.3 ± 0.4	750 ± 10	0.63 ± 0.02	3.4 ± 0.1		1.2×10^{-4}
PorY5		7.1 ± 0.5	750 ± 10	0.63 ± 0.01	3.4 ± 0.2		1.1×10^{-4}
N719	2.2 ± 0.1	7.2 ± 0.1	800 ± 10	0.67 ± 0.02	3.9 ± 0.1	As-prepared	0.9×10^{-42}
	18	16.66	735	0.69	8.44		-

4.6. Incident photon-to-current conversion efficiency

The increased J_{SC} of the PorY dyes compared to Por can be explained by taking into account of the IPCE spectra (Fig. 4.4). DSSCs using the PorY dyes all show increased IPCE values at all wavelengths compared to Por. No clear differences are observed within the PorY dyes, which is consistent with the similar photocurrent of the thin film DSSCs.

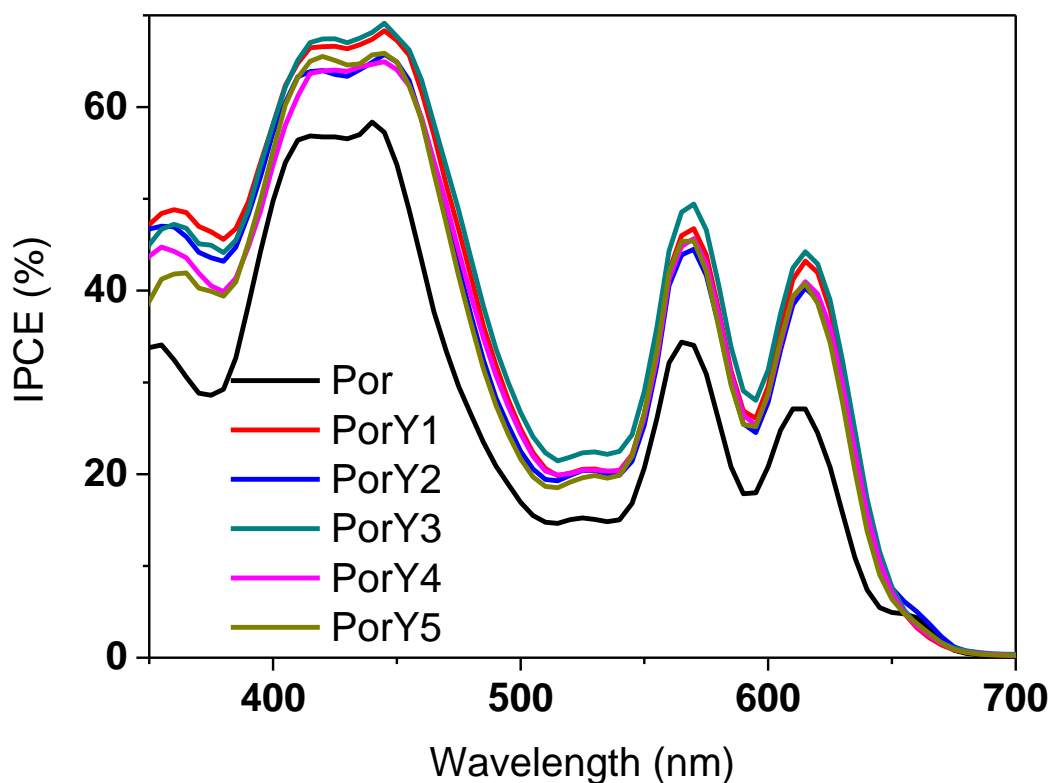


Figure 4.4 IPCE spectra of the devices fabricated from the porphyrin dyes on thin TiO_2 films.

Film thickness: $2.0 \pm 0.1 \mu\text{m}$.

The J_{SC} improvement (ΔJ_{SC}) is evaluated by dividing the IPCE wavelength range into five regions, namely 315-380 nm, 385-440 nm, 445-510 nm, 515-540 nm and 545-700 nm. The dominant effect to improved photocurrent is identified (Table 4.5).

- i) carbazole chromophore absorption overlapped with TiO_2 and electrolyte absorption (315-380 nm) – The effect of extra light absorption by the carbazole can contribute to less than 10% increase to the J_{SC} .

- ii) porphyrin absorption at the Soret band (385-440 nm) – This contributes to less than 10% increase to the J_{SC} .
- iii) porphyrin absorption broadening at the red edge of Soret band (445-510 nm) – The broadening of the Soret band contributes to more than 30% increase to the J_{SC} , which is one of the major contribution.
- iv) the absorption gap between the Soret and Q bands (515-540 nm) – The enhancement in this wavelength range contributes to less than 10% increase to the J_{SC} .
- v) porphyrin absorption at the Q bands (545-700 nm) – The effect of the enhanced Q bands can contribute to nearly 50% increase to the J_{SC} , which is one of the major contribution.
- vi) overall increase of IPCE – This is normalized as 100%.

Table 4.5 Photocurrent deduced from IPCE in terms of five spectral ranges

Specification	Dye relationship	Wavelength range/nm					Total
		315~380	385~440	445~510	515~540	545~700	
ΔJ_{SC} mA/cm ²	PorY1-Por [#]	0.14	0.12	0.62	0.1	0.83	1.81
	PorY3-Por [#]	0.12	0.12	0.69	0.14	0.97	2.04
	PorY3-Por*	0.1	0.08	0.54	0.19	1.01	1.92
Percentage %	PorY1-Por [#]	8	7	34	6	46	100
	PorY3-Por [#]	6	6	34	7	48	100
	PorY3-Por*	5	4	28	10	53	100
[#] THF as solvent; * 2 mM CDCA in ethanol as solvent.							

The major contributions to the increased IPCE are points (iii) and (v). Those findings lead to the conclusion that light absorption by the additional chromophore is not the major factor increasing the photocurrent. Geometric distortion leading to broadening of the Soret band and enhance Q bands leads to overall 80% of the improvement.

4.7. Light harvesting efficiency and dye aggregation

Due to a red-shifted and broadened Soret band compared to Por (Fig. 4.5), the PorY dyes on TiO₂ show increased light harvesting. However, this light harvesting

enhancement by the carbazole chromophore only contributes to 5-8% of the increased photocurrent as discussed above. The LHE values in the whole wavelength range within the films fabricated using PorY1-5 are very similar. In all the cases, the LHE peak values are close to 70%, which is limited by the reflection and transmission of the photoanode glass.

An absorption band at ~660 nm is observed in Por-sensitized TiO_2 film. No such band was observed in the PorY dyes-sensitized TiO_2 films. However, this band no longer appears if chenodeoxycholic acid is added to ethanol to prepare the sensitizing dye solution (Fig. 4.6).

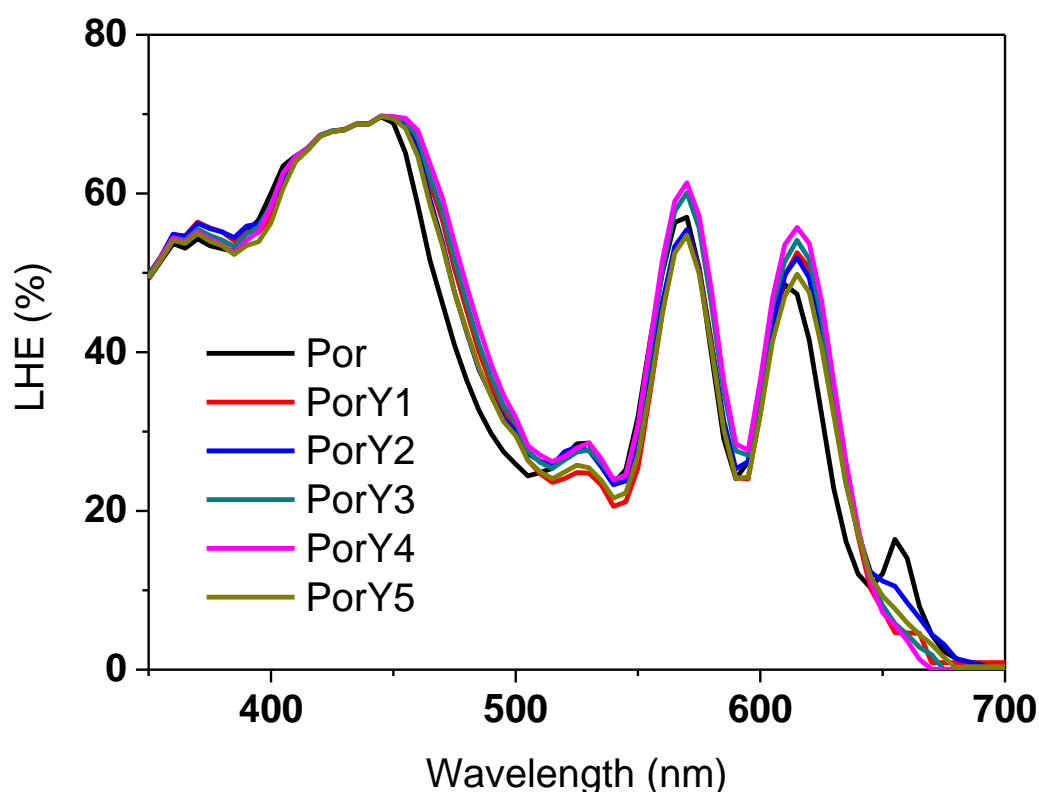


Figure 4.5 LHE spectra of the porphyrin dyes on thin TiO_2 films.
Film thickness: $2.0 \pm 0.1 \mu\text{m}$.

CDCA in THF, on the other hand, does not have the same effect; the absorption peak is visible at 660 nm in solution. These results can be explained by aggregation of Por on TiO_2 leading to the absorption band at 660 nm, which is prevented by adding CDCA. This is an important observation (see below) to understand the effect of carbazole substituent on the photovoltaic efficiency of the dyes studied in this chapter.

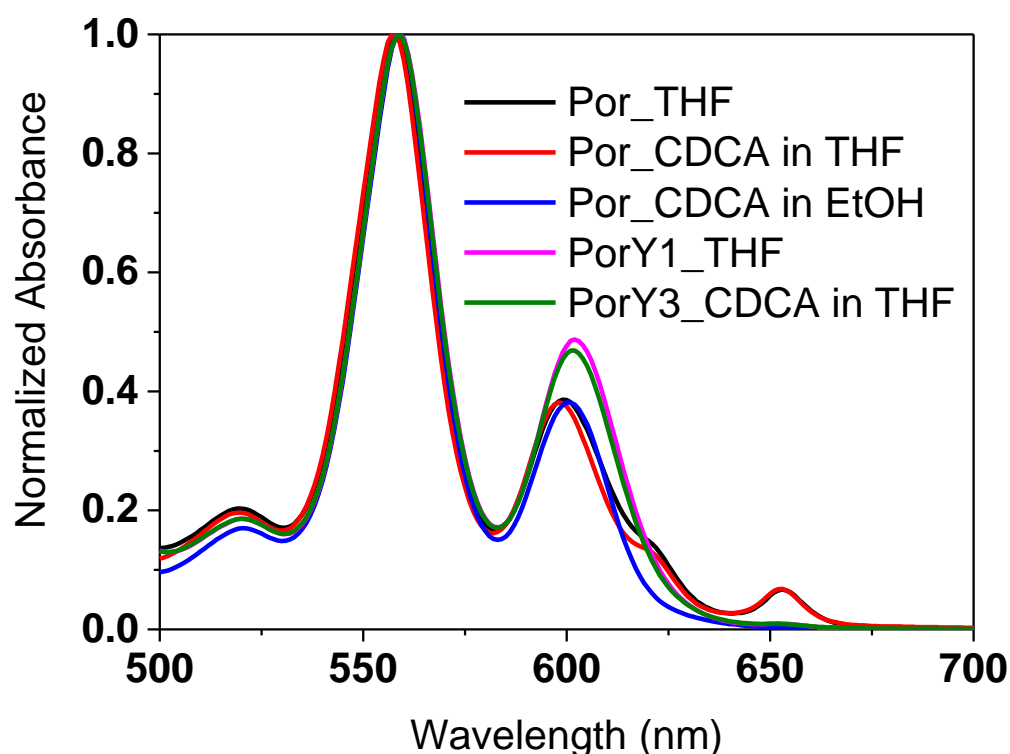


Figure 4.6 Normalized visible absorption spectra at the Q bands of some porphyrins in different solvents.
Dye concentration: 30 μ M.

4.8. Absorbed photon-to-current conversion efficiency

The APCE values are calculated (by dividing the IPCE values by the LHE values at the corresponding wavelength) for DSSCs using the PorY dyes (Fig. 4.7). All PorY dyes show approximately 10-15% higher values compared to Por in the 350-700 nm wavelength range. There is no clear difference in APCE values between DSSCs by changing the substitution on the carbazole. The maximum APCE values for DSSCs using the PorY dyes are close to 100% in the Soret band, while somewhat lower around 75% for the Q bands. The origin of different APCE values between the Soret band and the Q bands is not clear. The difference can be either assigned to wavelength dependent injection or collection efficiency.^{9,10} The latter was investigated using front and back illumination IPCE measurements, but the results were inconclusive due to the coexisting absorption of the electrolyte with the porphyrin Q bands.⁹ The APCE “peaks” within the Q bands (over 100%) are due to slight wavelength shifts between the IPCE and LHE spectra.

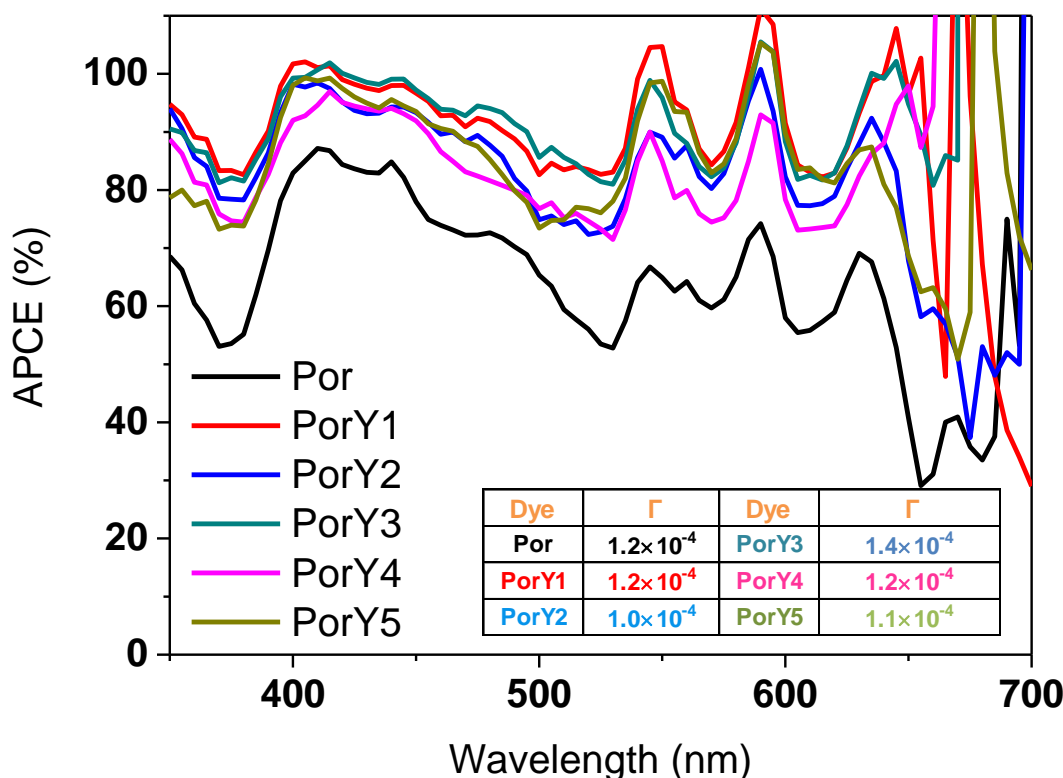


Figure 4.7 APCE spectra of the devices fabricated from the porphyrin dyes on thin TiO_2 films. The inset shows the dye loading.

Film thickness: $2.0 \pm 0.1 \mu\text{m}$; the unit of dye loading (Γ) is mol cm^{-3} .

The increased APCE measured for DSSCs using thin films and the PorY dyes compared to Por suggests improved electron injection efficiency. Note that collection efficiency is close to 100% for DSSCs using these porphyrins as shown in Appendix Fig. A7. As described in Chapter 1 Section 1.8.2, injection efficiency depends on:

- 1) Electronic coupling between the excited state and the acceptor states in TiO_2 .
- 2) Driving force, which is the energy difference between the reduction potential and the conduction band edge potential of the semiconductor.
- 3) Excited state lifetime.
- 4) Dye aggregation and dye layer morphology.

1). Electronic coupling between the excited state and the acceptor states in TiO_2

This is very similar within the porphyrin dyes. First, the same anchoring unit was used for all the porphyrins and second, the organic chromophore in the PorY dyes does not

alter the dihedral angle of the porphyrin and the cyanoacrylic anchoring group as suggested by DFT calculations (contributed by collaborators).¹¹ Therefore, the electronic coupling cannot be an important factor influencing electron injection differences between the PorY dyes and Por.

2). *Driving force.*

The energy level diagram illustrating the DSSCs, derived from the DPV measurements and literature values, is plotted in Fig. 4.8. The driving force is defined by the difference between the conduction band bottom edge potential of TiO₂ and the electrochemical energy of the first excited state of the sensitizer. The latter can be approximated by the first reduction potential.¹² The conduction band edge potential of TiO₂ in all DSSCs using Por and PorY dyes was nearly identical (Chapter 8 Section 8.4). The identical position of the first reduction potentials (Fig. 4.8) suggests that the driving force of electron injection is not responsible for the difference in APCE and injection efficiency. According to literature, driving force of ~0.2 eV was estimated to be sufficient for 100% electron injection efficiency for some organic dyes, Ru-based dyes and single chromophoric porphyrins on ZnO films.¹³ The driving force values of all the porphyrins should be sufficient for 100% injection as supported by the ~100% electron injection efficiency of PorY dyes in the wavelength range of 350-700 nm (Fig. 4.7). The 20-40% increase in electron injection efficiency of DSSCs using PorY1-5 cannot be explained by driving force.

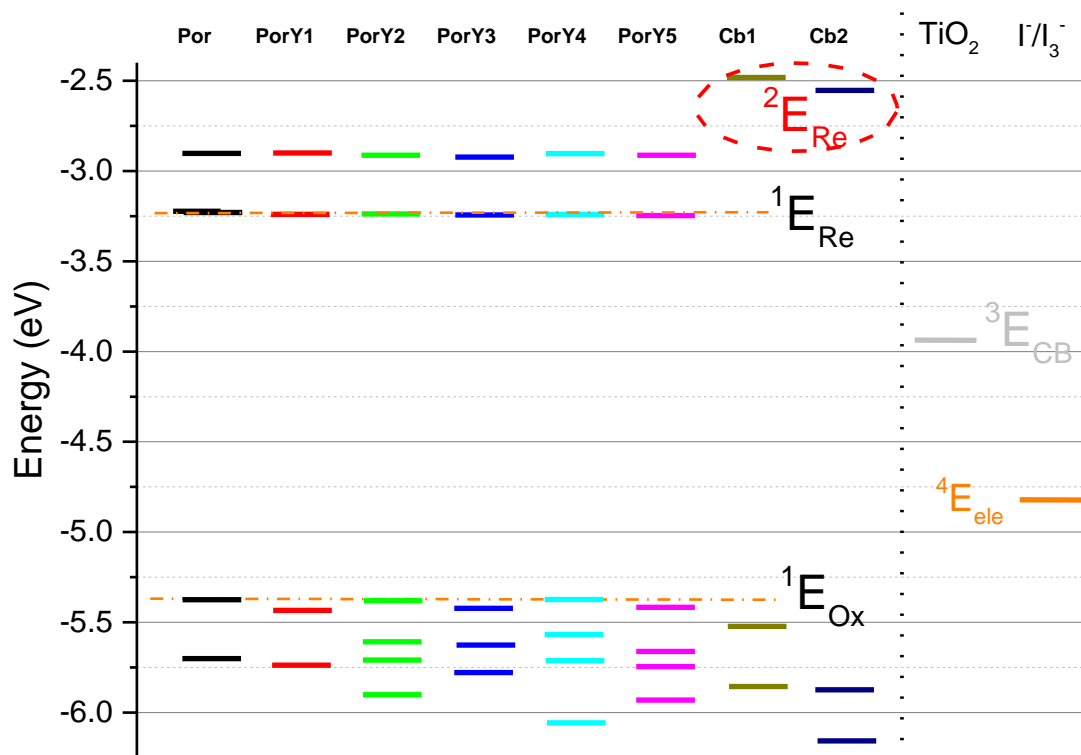


Figure 4.8 Energy level diagram of the compounds.

1. The energy levels of oxidation (E_{Ox}) and the energy levels of reduction (E_{Re}) were calculated from the peak potentials of oxidation (E_{Ox} vs. Fc/Fc^+) and reduction (E_{Re} vs. Fc/Fc^+) as $E_{Ox} = -(E_{Ox}$ vs. $Fc/Fc^+ + 5.1)$ (eV) and $E_{Re} = -(E_{Re}$ vs. $Fc/Fc^+ + 5.1)$ (eV), respectively. The potential of the Fc/Fc^+ redox couple was assumed to be -5.1 eV vs. vacuum¹⁴.
2. E_{Re} of Cb1 and Cb2 were calculated from UV-vis absorption spectra by the equation $E_{Re} = \Delta E + E_{Ox}$, where the band gap (ΔE) was calculated by the equation $\Delta E = 1243/\lambda_{onset}$.
3. E_{CB} was adopted from Ref.¹⁵.
4. The I^-/I_3^- redox couple potential (E_{ele}) was adopted from Ref.¹⁶. Both values of point 3 and point 4 were calibrated to the absolute energy based on the assumption $E_{Fc/Fc^+} = +0.63$ V vs. NHE.

3). Excited state lifetime.

The excited state lifetime of the investigated dyes was not measured due to the lack of access to photoluminescence lifetime measurement. However, ultrafast electron injection of most porphyrins (<200 femtoseconds) with similar structure suggests that electron injection efficiency is not limited by excited state lifetime.¹⁷ Furthermore, steady state photoluminescence studies suggest similar photoluminescence intensity of Por and PorY dyes, which may suggest similar quantum yield and lifetime (Chapter 7).

4). Dye aggregation and dye layer morphology

Taking all the factors into consideration, the 20-40% increase in electron injection efficiency of DSSCs using PorY1-5 should originate from better dye alignment and

improved dye layer morphology. The non-injecting dyes adsorbed on TiO₂ surface in Por DSSCs originate from dye aggregates and weakly adsorbed dyes; they do not participate in electron injection, but instead the excited state decays to the ground state by either radiative or non-radiative pathways.^{18,19}

To test this hypothesis, DSSCs using Por and PorY3 dyes and CDCA in ethanol as the dye solvent were prepared. The photovoltaic data of these DSSCs are shown in Table 4.6 and the IPCE/LHE/APCE plots are shown in Fig. 4.9.

The peak IPCE values at the Soret band of the two dyes are same at 72% (Fig. 4.9(a)), approaching nearly 100% APCE values (Fig. 4.9(c)). The increased IPCE/APCE for the DSSCs with the single chromophoric porphyrin Por suggests that the Por aggregates (note the absence of the 660 nm aggregate peak in the IPCE spectrum) limit the electron injection efficiency at the Soret band.

The LHE of film sensitized by PorY3 is higher compared to that of Por at the Q bands. This is due to the more dye amount loaded on TiO₂ of PorY3 compared to that of Por (inset of Fig. 4.9(c)). Compared to the dye uptake in THF (1.2×10^{-4} mol cm⁻³, Table 4.4) or pure ethanol (1.2×10^{-4} mol cm⁻³, Table 4.6), Por with CDCA (0.8×10^{-4} mol cm⁻³, Table 4.6) leads to only ~70% of the coverage achieved without CDCA, while dye uptake of PorY3 does not show any difference in these solvents.

The APCE of devices using PorY3 exhibit values close to 100% in the Q bands, while that of Por is only ~85% (Fig. 4.9(c)). The origin of injection efficiency loss even in the absence of dye aggregates is unclear. One possibility is the presence of non-injecting dyes, non-uniformly distributed in the TiO₂ film towards the electrolyte side, which decreases the APCE at weakly absorbed photon wavelengths.

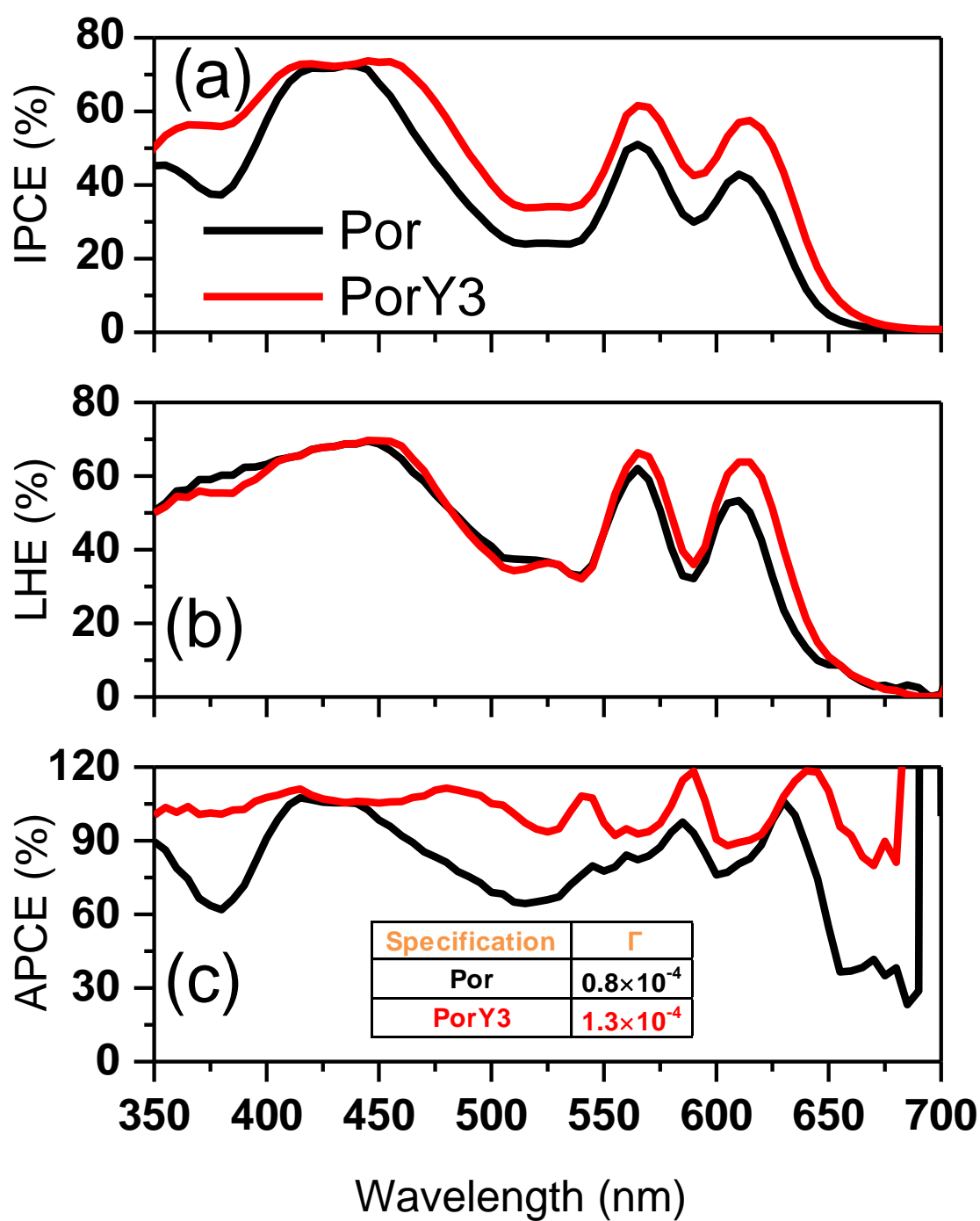


Figure 4.9 IPCE/LHE/APCE spectra of devices fabricated from two dyes with CDCA in dye solution.

Solvent: ethanol; film thickness: $2.7 \pm 0.1 \mu\text{m}$; CDCA concentration: 2 mM; the unit of Γ is mol cm^{-3} .

Table 4.6 *J-V* performance and dye loading of devices fabricated using PorY3 compared to Por in different solvent conditions

Solvent	Dye	J_{sc} mA/cm ²	V_{oc} mV	FF	η %	Dye loading Γ / mol/cm ³
2mM CDCA in THF	Por	5.32	620	0.67	2.21	0.9×10^{-4}
	PorY3	6.55	695	0.67	3.03	1.2×10^{-4}
2mM CDCA in ethanol	Por	6.75	685	0.67	3.08	0.8×10^{-4}
	PorY3	8.42	765	0.66	4.23	1.3×10^{-4}
Pure ethanol	Por	6.27	700	0.58	2.53	1.2×10^{-4}
	PorY3	8.41	750	0.58	3.63	1.4×10^{-4}
Film thickness: 2.7 ± 0.1 μ m; dye concentration 0.2 mM.						

The important point is that carbazole substitution eliminates the need for co-adsorber like CDCA to achieve close to 100% injection efficiency (using CDCA may be restricted from the choice of dye solvent, elaborate optimization and reduced dye loading on TiO₂, etc.). This is beneficial because higher dye loading can be obtained as compared to using CDCA; this allows the use of thinner TiO₂ films.

4.9. Increased open circuit voltage using carbazole substituted porphyrin di-chromophoric dyes

As data in Fig. 4.4 and Table 4.4 suggest, the benefit of using carbazole substituted porphyrin dyes in DSSC is not only increased photocurrent, but equally importantly, increased open circuit voltage. Because of the importance of this topic and the underlying complexity identifying the improvement mechanism, this will be discussed in Chapter 8, which is assigned to the blocking effect from the additional organic chromophore using electron lifetime measurements.

It is suggested that improved dye layer morphology using bulky substituents not only improves injection efficiency, but also enhances electron lifetime by improved blocking effect. This leads to simultaneously increased photocurrent and photovoltage using PorY1-5 dyes in DSSCs.

4.10. Conclusions

No clear change in the optical and electrochemical properties of a series of di-chromophoric dyes with various electron withdrawing / donating substituents attached to the carbazole has been observed. This is explained by the limited electronic communication between the carbazole and the porphyrin chromophores due to geometric distortion (a dihedral angle of 117 degrees estimated by DFT calculation). However, simultaneously increased photocurrent and photovoltage and consequently 20 to 30% improvement in the power conversion efficiency of DSSCs using the PorY dyes has been observed compared to that of Por. These main findings are illustrated in Fig. 4.10. No significant differences in DSSC performance within the di-chromophoric dyes were observed.

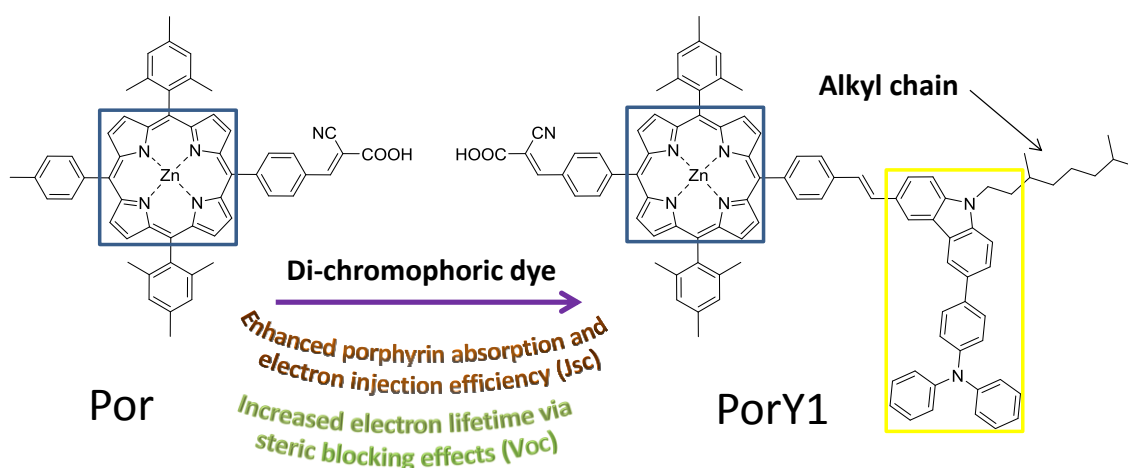


Figure 4.10 An illustration of the main findings of the chapter.

The improved performance to up to 6% is interesting and is analysed in more detail. This chapter focused on investigation of the origin of photocurrent enhancements using incident photon-to-current conversion efficiency / light harvesting efficiency / absorbed photon-to-current conversion efficiency measurements, that the results suggested that:

1. The enhancement of photocurrent was mainly ascribed to the enhanced electron injection efficiency.

2. The enhanced light harvesting, originating from a broadened Soret band absorption and slightly enhanced Q bands due to non-planar structure of the di-chromophoric dye, contributed less than 10% of the increased photocurrent.
3. The increased electron injection efficiency of the di-chromophoric dyes was due to the elimination of the dye aggregation and the non-injecting dyes on the TiO₂ surface.

4.11. References

- (1) Kubo, W.; Sakamoto, A.; Kitamura, T.; Wada, Y.; Yanagida, S. *J. Photochem. Photobiol., A* **2004**, *164*, 33.
- (2) Mozer, A. J.; Griffith, M. J.; Tsekouras, G.; Wagner, P.; Wallace, G. G.; Mori, S.; Sunahara, K.; Miyashita, M.; Earles, J. C.; Gordon, K. C.; Du, L.; Katoh, R.; Furube, A.; Officer, D. L. *J. Am. Chem. Soc.* **2009**, *131*, 15621.
- (3) Weinkauf, J. R.; Cooper, S. W.; Schweiger, A.; Wamser, C. C. *J. Phys. Chem. A* **2002**, *107*, 3486.
- (4) Chen, K.-F.; Chang, C.-W.; Lin, J.-L.; Hsu, Y.-C.; Yeh, M.-C. P.; Hsu, C.-P.; Sun, S.-S. *Chem. Eur. J.* **2010**, *16*, 12873.
- (5) Cramariuc, O.; Hukka, T. I.; Rantala, T. T. *Chem. Phys.* **2004**, *305*, 13.
- (6) Kim, D.; Osuka, A. *Acc. Chem. Res.* **2004**, *37*, 735.
- (7) Cho, H. S.; Song, N. W.; Kim, Y. H.; Jeoung, S. C.; Hahn, S.; Kim, D.; Kim, S. K.; Yoshida, N.; Osuka, A. *J. Phys. Chem. A* **2000**, *104*, 3287.
- (8) Quimby, D. J.; Longo, F. R. *J. Am. Chem. Soc.* **1975**, *97*, 5111.
- (9) Halme, J.; Boschloo, G.; Hagfeldt, A.; Lund, P. *J. Phys. Chem. C* **2008**, *112*, 5623.
- (10) Asbury, J. B.; Anderson, N. A.; Hao, E.; Ai, X.; Lian, T. *J. Phys. Chem. B* **2003**, *107*, 7376.
- (11) Zhao, L.; Wagner, P.; Elliott, A. B. S.; Griffith, M. J.; Clarke, T. M.; Gordon, K. C.; Mori, S.; Mozer, A. J. *J. Mater. Chem. A* **2014**, *2*, 16963.
- (12) Santos, T. D.; Morandeira, A.; Koops, S.; Mozer, A. J.; Tsekouras, G.; Dong, Y.; Wagner, P.; Wallace, G.; Earles, J. C.; Gordon, K. C.; Officer, D.; Durrant, J. R. *J. Phys. Chem. C* **2010**, *114*, 3276.

- (13) Katoh, R.; Furube, A. *J. Photochem. Photobiol. C: Photochem. Rev.* **2014**, *20*, 1.
- (14) Cardona, C. M.; Li, W.; Kaifer, A. E.; Stockdale, D.; Bazan, G. C. *Adv. Mater.* **2011**, *23*, 2367.
- (15) Hagfeldt, A.; Boschloo, G.; Sun, L.; Kloo, L.; Pettersson, H. *Chem. Rev.* **2010**, *110*, 6595.
- (16) Boschloo, G.; Hagfeldt, A. *Acc. Chem. Res.* **2009**, *42*, 1819.
- (17) Griffith, M. J.; Sunahara, K.; Wagner, P.; Wagner, K.; Wallace, G. G.; Officer, D. L.; Furube, A.; Katoh, R.; Mori, S.; Mozer, A. J. *Chem. Commun.* **2012**, *48*, 4145.
- (18) Dos Santos, T.; Morandeira, A.; Koops, S.; Mozer, A. J.; Tsekouras, G.; Dong, Y.; Wagner, P.; Wallace, G.; Earles, J. C.; Gordon, K. C.; Officer, D.; Durrant, J. R. *Journal of Physical Chemistry C* **2010**, *114*, 3276.
- (19) Lim, J.; Kwon, Y. S.; Park, T. *Chem. Commun.* **2011**, *47*, 4147.

**CHAPTER 5. FILLING THE ABSORPTION GAP OF PORPHYRIN BY
CARBAZOLE-FUSED THIOPHENE-SUBSTITUTED DI-
CHROMOPHORIC DYES AND THE UTILITY OF COBALT
ELECTROLYTE**

5.1. Introduction

This chapter has two purposes: the first is to investigate the effect of filling the “absorption gap” between the Soret and Q bands in porphyrins on their photovoltaic performance and the second is to determine the utility of cobalt electrolyte in di-chromophoric dye-sensitized solar cells. The first purpose was achieved by using the additional chromophore (di-chromophoric design approach) with complementary absorption in the wavelength range from 450 nm to 550 nm. The second purpose was achieved by characterizing the photovoltaic performance of the devices using these di-chromophoric dyes.

Described by the four-orbital model in Chapter 1 Section 1.4.3,¹⁻⁴ the “absorption gap” in typical porphyrins is due to their unique electronic structure leading to optically narrow transitions (the Soret and Q bands) separated by a rather large energy gap with no or very low oscillator strength transitions.

Two approaches can be followed to fill the “absorption gap” in the porphyrin dyes as introduced in Chapter 1 Section 1.4:

- 1) The single chromophoric porphyrin approach. For example, a push-pull effect is utilized to modulate the electronic structure and the UV-vis absorption.^{5,6} This approach is the most commonly used and achieves broad light harvesting spectrum, including filling the absorption gap and red-shifted spectrum.
- 2) The multi-chromophoric dye approach - by introducing additional chromophores that absorb photons at the 450 nm to 550 nm wavelength range. The absorption spectrum of the di-chromophoric dye closely resembles the superposition of the absorption spectrum of the individual chromophores. This approach is less frequently explored and is the subject of this chapter.

There are several potential candidates as the second chromophore, such as metal complexes or π -conjugated systems involving carbazoles, thiophenes, triphenylamines, Bodipy and fluorenes.⁷⁻¹² Carbazole - fused thiophene oligomers were chosen because of their light absorption bands in the 250-550 nm wavelength range.¹³⁻¹⁶ Other factors were relatively well developed chemistry and ease of functionalization.

Motivation:

The expected increase in efficiency by filling the porphyrin “absorption gap” (without shifting the absorption edge) is illustrated in Fig. 5.1. The black curve shown in Fig. 5.1

is the molar extinction coefficient of Por in DCM solvent on a logarithmic scale. The 350-450 nm wavelength range is the Soret band and the 550-650 nm wavelength range is the Q band. The incident photon to current conversion efficiency (IPCE) values (the shaded areas) in both wavelength ranges are relatively higher compared to that of the 450-550 nm wavelength range, which is known as the absorption gap. The increased IPCE from the typical 30% to 80% within the 450 nm to 550 nm wavelength region would lead to a 30% increase in power conversion efficiency assuming that the open circuit voltage (V_{OC}) = 750 mV and fill factor (FF) = 0.75 and remain constant.

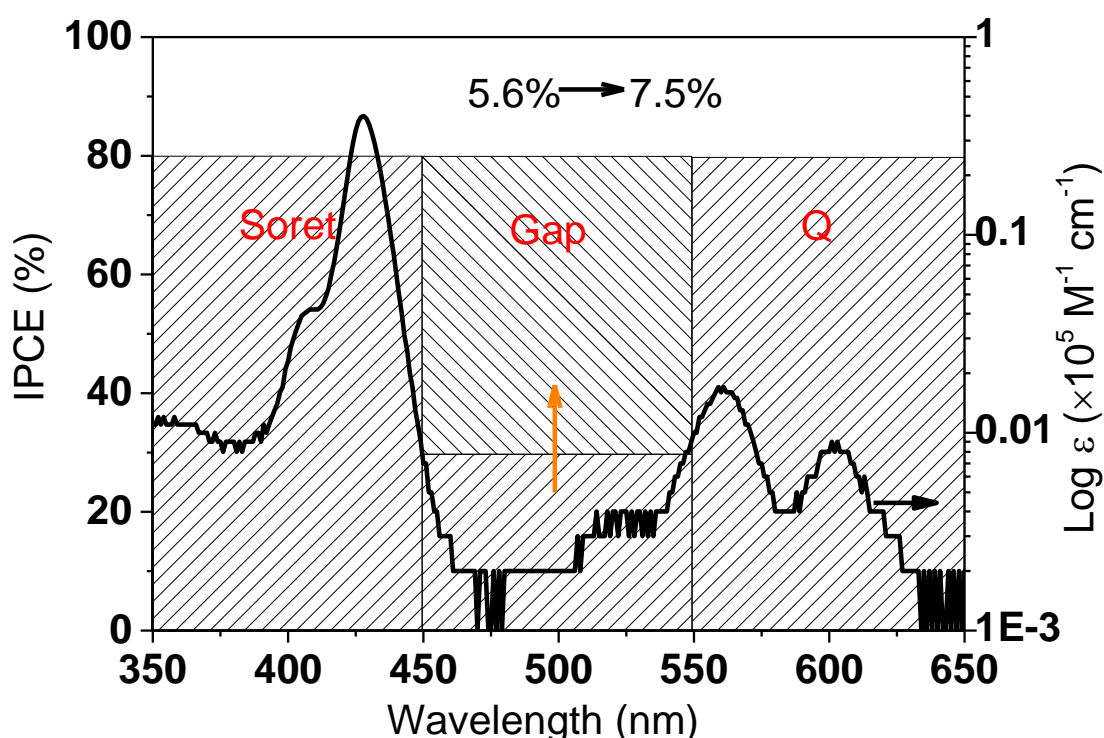


Figure 5.1 Concept of filling the “absorption gap” using the di-chromophoric design. If the IPCE in the 450 nm to 550 nm wavelength range was assumed to rise from the typical 30% to 80%, the IPCE in Soret and Q bands was kept at 80%, the V_{OC} and FF were assumed to be 750 mV and 0.75, respectively, the power conversion efficiency would increase from 5.6% to 7.5%.

As demonstrated in Chapter 4, by using the di-chromophoric porphyrins with carbazole as additional chromophore (PorY family), a photovoltage increase has been achieved in addition to the photocurrent improvements. It is also the purpose of this chapter to explore if such photovoltage increase can be achieved using carbazole-fused thiophene dyes, in addition to the anticipated benefits in increased light harvesting. Such increase

in photovoltage, if realized, should translate to even higher increase in power conversion efficiency compared to that in Fig. 5.1.

To achieve the objective of the chapter, three fused thiophene units were used as the organic chromophores. By covalently linking to a porphyrin dye Por, three di-chromophoric porphyrins were synthesized: PorO1 with thieno[3,2-b]thiophene, PorO2 with dithieno[3,2-b:2',3'-d]thiophene and PorO3 with 4,8-dicecyloxybenzo[1,2-b:4,5-b']dithiophene (Table 5.1).

A cobalt redox couple (cobalt tris(4,4'-dimethyl-2,2'-bipyridine), Table 5.1) was also used in addition to the iodine / triiodide (I/I_3^-) electrolyte used in Chapter 4 to fabricate DSSCs using the PorY dyes. The rationale of using cobalt electrolytes has been introduced in Chapter 1 Section 1.6.

This chapter will first look at the light absorption and electrochemical properties of the three new di-chromophoric dyes PorO1-3. The ability of the carbazole-fused thiophene chromophores to fill the “absorption gap” of the porphyrin is analysed. Photovoltaic devices are prepared and characterized, showing that the above aims are achieved, although not completely. Good performance DSSCs using the new dyes and cobalt electrolyte with respectable photovoltage are achieved. The organic dye MK2, which shows benchmark photovoltaic performance using cobalt-based electrolytes,¹⁷ was introduced as a reference. Some limitations in the absorbed photon-to-current conversion efficiency (APCE) are found in PorO1-3 dyes DSSCs, which are attributed to decreased charge injection efficiency due to insufficient driving force for charge injection. This lack of driving force for electron injection is mainly caused by the negatively shifted conduction band bottom edge potential of TiO_2 when using the optimized cobalt electrolyte.

Table 5.1 Molecular structures of compounds

Parental porphyrin	R	Name
<p>(Por)</p>	<p>(CbTh1)</p>	PorO1
	<p>(CbTh2)</p>	PorO2
	<p>(CbTh3)</p>	PorO3

<p>Co²⁺</p>	<p>Co³⁺</p>
------------------------	------------------------

MK2

5.2. Experimental

5.2.1. Investigated molecules

The following abbreviations are used for the compounds displayed in Table 5.1: (*E, E*) 5-(4-(2-cyano-2-carboxyethenyl)phenyl)-15-(4-(2-(5-(2-(9-octylcarbazol-3-yl)ethenyl)thieno[3,2-*b*]thiophen-2-yl)ethenyl)phenyl)-10,20-bis(2,4,6-trimethylphenyl)porphyrinato zinc(II) (PorO1), (*E, E*) 5-(4-(2-cyano-2-carboxyethenyl)phenyl)-15-(4-(2-(5-(2-(6-(2-(9-octylcarbazol-3-yl)ethenyl)dithieno[3,2-*b*:2',3'-*d*]thiophen-2-yl)ethenyl)phenyl)-10,20-bis(2,4,6-trimethylphenyl)porphyrinato zinc(II) (PorO2), (*E, E*) 5-(4-(2-cyano-2-carboxyethenyl)phenyl)-15-(4-(2-(5-(2-(6-(2-(9-octylcarbazol-3-yl)ethenyl)-4,8-dioctyloxybenzo[1,2-*b*:5,4-*b'*]dithiophen-2-yl)ethenyl)phenyl)-10,20-bis(2,4,6-trimethylphenyl)porphyrinato zinc(II) (PorO3), (*E*) 2-Methyl-5-(2-(9-octylcarbazol-3-yl)ethenyl)thieno[3,2-*b*]thiophene (CbTh1), (*E*) 2-Methyl-6-(2-(9-octylcarbazol-3-yl)ethenyl)dithieno[3,2-*b*:2',3'-*d*]thiophene (CbTh2), (*E*) 2-Methyl-6-(2-(9-octylcarbazol-3-yl)ethenyl)-4,8-dioctyloxybenzo[1,2-*b*:5,4-*b'*]dithiophene (CbTh3), 5-(4-(2-cyano-2-carboxyethenyl)phenyl)-15-(4-methylphenyl)-10,20-bis(2,4,6-trimethylphenyl)porphyrinato zinc(II) (Por).

5.2.2. Spectroscopic and electrochemical characterization

UV-visible (UV-vis) absorption spectroscopy was performed using a Shimadzu UV-3600 spectrophotometer using 1 cm length quartz cuvettes and 1 μ M solutions in dimethylformamide (DMF).

Differential pulse voltammetry (DPV) was measured using 0.5 mM solutions of the compounds with 0.1 M tetrabutylammonium perchlorate (TBAP, supporting electrolyte) in DMF. The potential of the reference electrode (RE) was calibrated using 1 mM ferrocene/ferrocenium couple (Fc/Fc⁺) as an internal standard.

5.2.3. DSSC fabrication and characterization

Both photoanode and photocathode used fluorine doped tin oxide glass (FTO glass, 2.2 mm, 7 Ω /square, TEC[®]) as the substrate. The photoanode was comprised of a compact TiO₂ layer (titanium diisopropoxide bis(acetylacetonate)) and a mesoporous TiO₂ layer, following by a TiCl₄ solution post-treatment. Mesoporous TiO₂ layer was deposited using screen-printed transparent TiO₂ layer (18-NRT, Dyesol). A scattering layer (WER2-O, Dyesol) was further printed to prepare thick TiO₂ electrodes. The TiO₂/FTO

glass substrates, with 4 mm × 4 mm active area, were immersed into a mixed solvent dye solution with 0.2 mM dyes for 1.5 hours to achieve dye-sensitization. The mixed solvent was ethanol: toluene =1: 1 (vol) with 0.1 mM chenodeoxycholic acid (CDCA) as co-adsorber.

The I[−]/I₃[−] electrolyte used in optimization process was composed of 0.6 M 1,2-dimethyl-3-propylimidazolium iodide (DMPII), 0.1 M LiI, 0.05 M I₂, 0.1 M LiClO₄, and 0.5 M *tert*-butylpyridine (*t*BP) in acetonitrile (AN):valeronitrile (VN)=85:15 (vol). The cobalt electrolyte used for most of the comparison was composed of 0.22 M Co(dmbpy)₃²⁺ / 0.05 M Co(dmbpy)₃³⁺, 0.05 M LiClO₄, 0.1 M *t*BP and 1 mM CDCA in AN.

For comparison, DSSCs sensitized with an organic dye MK2 (Table 5.1) were fabricated. The dye solution was 0.2 mM in AN:toluene =1:1 (vol) with 6 hours dye-sensitization.

Current density-voltage (*J-V*) measurements were performed using a simulated 100 mW cm^{−2} AM 1.5G solar simulator (TriSOL, OAI) coupled to a Keithley 2400 source measure unit. A 20 minutes light soaking and three successive *J-V* measurements were applied to the finished devices before the last recording. A 6 mm × 6 mm mask was employed during the measurements.

Incident photon-to-current conversion efficiency (IPCE) was recorded using a QEXPor quantum efficiency measurement system (PV measurements). Light harvesting efficiency (LHE) was calculated from the UV-vis absorbance of the sensitizers on 2.9 μm TiO₂ films.^{18,19} A small amount of electrolyte was used during the measurement to better match the UV-vis absorption measurement conditions to device operating conditions.

The amount of dye loading on TiO₂ was determined using 2.9 μm TiO₂ films. 0.1 M tetra-butylammonium hydroxide solution (TBAOH) in DMF was used to desorb the sensitizers from the surface of the TiO₂ films. The peak molar extinction coefficient values of the compounds at the Soret band are shown in Appendix Table A1.

5.3. Light absorption in solution: “filling the gap”

Fig. 5.2 shows the molar extinction coefficients (ϵ) of the carbazole-fused thiophene chromophores CbTh1-3, the single chromophoric porphyrin Por and the carbazole-fused thiophene substituent di-chromophoric porphyrins PorO1-3 in DMF. The wavelength of

the maximum absorption (λ_{max}^{abs}) and the ϵ values of the investigated compounds are listed in Table 5.2.

The carbazole-fused thiophene chromophores CbTh1-3 exhibit UV-vis absorption peaks extended till ~500 nm wavelength with the highest ϵ value of $\sim 6 \times 10^4 \text{ M}^{-1} \text{ cm}^{-1}$ measured using CbTh3 (Fig. 5.2(a)). The ϵ values of CbTh1-3 at 450-500 nm are less than $\sim 1 \times 10^4 \text{ M}^{-1} \text{ cm}^{-1}$ with the highest obtained by CbTh2, which is mainly due to its red-shifted spectrum compared to the other two chromophores.

The “absorption gap” of the porphyrin used in this work (low molar extinction coefficients between the Soret and Q bans at 450-550 nm wavelength range) is shown in Fig. 5.2(b) by the shaded area. In comparison to Fig. 5.2(a), the “absorption gap” can be partly filled using the carbazole-fused thiophene chromophores if attached to the porphyrin in a di-chromophoric design within the 450 nm to 500 nm wavelength range. However, simple superposition of the new carbazole-fused thiophene chromophore and the porphyrin contribute only part of the required improvement within the 450 nm to 550 nm wavelength range, suggesting that the band gap of the organic chromophores is not low enough if a simple superposition of absorptions is assumed.

The absorption intensity at the 450-500 nm wavelength region is enhanced more in the di-chromophoric PorO1-3 compared to the assumed simple superposition of the absorption of CbTh1-3 and of Por (Table 5.2). This may be due to the extension of π -conjugation between the organic chromophores and the porphyrin through the phenylethenyl linker.

It is the light absorption by the carbazole-fused thiophene chromophores that contributes to light absorption at 450-500 nm in the PorO dyes as revealed by the density functional theory (DFT) calculation as well as the resonance Raman spectroscopy characterization (performed by collaborators).²⁰ The ϵ values in the 300-400 nm wavelength region are also increased. Although DFT calculation also suggested that the carbazole-fused thiophene chromophores do not alter the LUMO of the porphyrins, the calculations suggested that a limited electronic communication between the chromophores is possible.

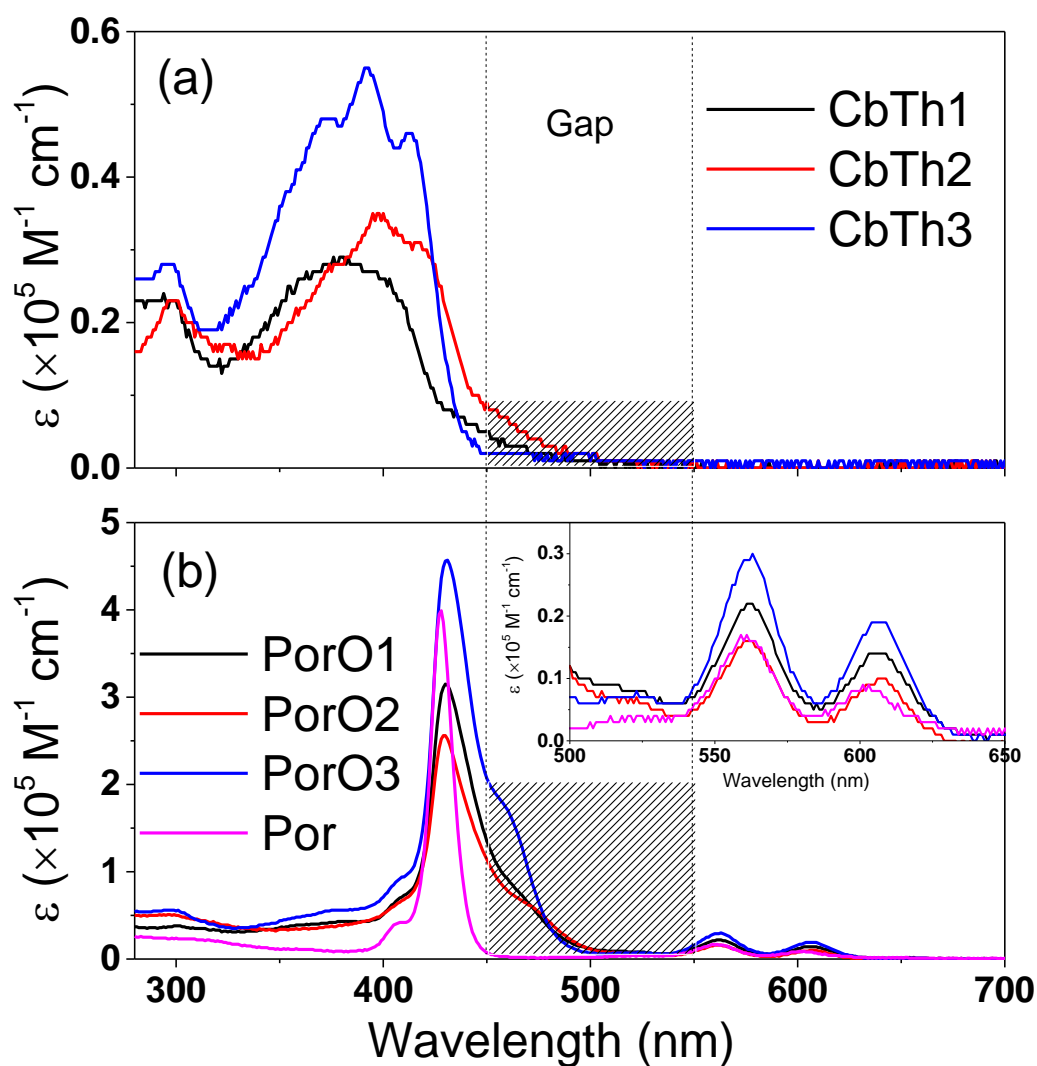


Figure 5.2 Molar extinction coefficient of (a) the carbazole-fused thiophene chromophores and (b) the porphyrins measured in DMF. The 450-550 nm wavelength range was shadowed.

The definition of single chromophoric porphyrins and multi-chromophoric porphyrins in Chapter 1 Section 1.4 is not straightforward to apply to these PorO dyes, because some new absorption features are detected that are not present in the individual chromophores.

5.4. Effect of the carbazole-fused thiophene chromophores on the oxidation and reduction potentials of the di-chromophoric dyes

The oxidation and reduction reactions of the carbazole-fused thiophene chromophores CbTh1-3, the single chromophoric porphyrin Por and the carbazole-fused thiophene substituent di-chromophoric porphyrins PorO1-3 are shown in Fig. 5.3(a) and (b), respectively. Peak potentials as well as the band gaps are calculated from the difference in the first oxidation potentials (E_{Ox}^{1st}) and the first reduction potentials (E_{Re}^{1st}), shown in Table 5.2.

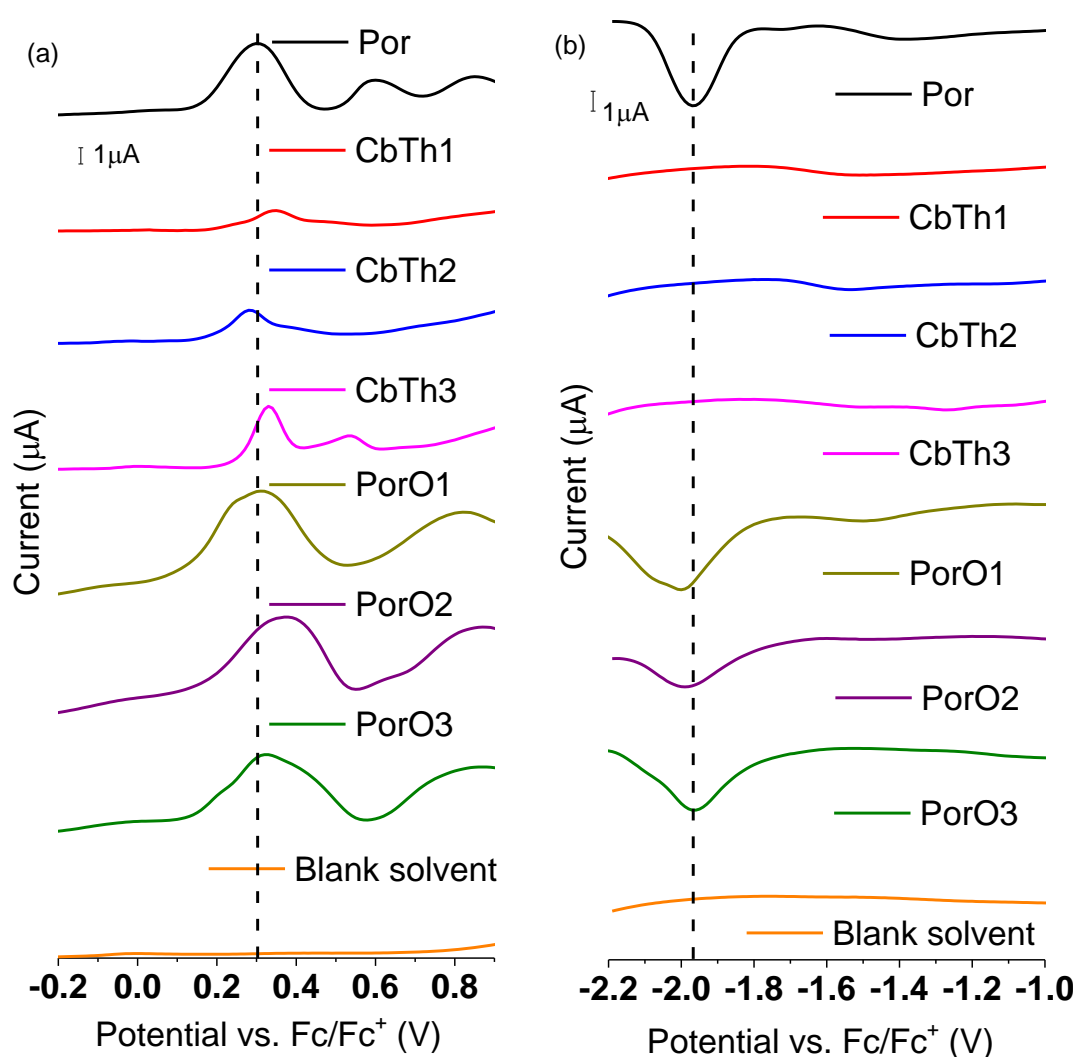


Figure 5.3 Differential pulse voltammograms of the PorO dyes and the organic chromophores, (a) positive scan; (b) negative scan.

Sample concentration: 0.5mM; solvent: DMF; supporting electrolyte: TBAP; Pt wire surface area: 6.6 mm²; scan rate: 100 mV s⁻¹.

The carbazole-fused thiophene chromophores CbTh1-3 and the single chromophoric porphyrin Por show the first oxidation potentials with less than 0.1 V difference (Fig. 5.3(a)). The organic compounds do not show any reduction reaction in the applied potential window of up to -2.2 V vs. Fc/Fc⁺.

PorO1-3 show broad first oxidation reactions. Simply overlapping the oxidations of the porphyrin and carbazole-fused thiophene chromophores does not exactly resemble the oxidation peaks of the corresponding dyad (Fig. 5.4). Moreover, PorO1-3 show 0.1 V more negative onset potentials compared to Por. Both phenomena suggest that the energy level of porphyrin in the dyads is slightly different from that in Por. Weak electronic coupling between the two chromophores in the PorO dyes is therefore feasible.

The reduction of the porphyrins all show only one peak at the same similar potentials ~-2.00 V vs. Fc/Fc⁺, suggesting the addition of the carbazole-fused thiophene organic chromophore do not significantly affect the reduction of the porphyrin in the PorO dyes.

Table 5.2 Summary of spectral and electrochemical data of the compounds

Dye	^[a] λ_{onset} (nm)	λ_{max} (nm)	ε (10 ⁵ M ⁻¹ cm ⁻¹)	Peak Potential vs. Fc/Fc ⁺		^[b] ΔE /eV
				E_{Re} /V	E_{Ox} /V	
CbTh1	470	298, 381	0.19, 0.27	--	0.35	--
CbTh2	489	298, 397	0.24, 0.34	--	0.28	--
CbTh3	447	298, 371, 392, 413	0.22, 0.40, 0.46, 0.39	--	0.33, 0.54	--
PorO1	502	430, 562, 606	3.10, 0.22, 0.15	-2.00	0.31, 0.82	2.31
PorO2	514	430, 562, 606	2.59, 0.20, 0.14	-1.99	0.38, 0.87	2.37
PorO3	496	430, 562, 606	4.49, 0.33, 0.23	-1.97	0.32, 0.86	2.29
Por	451	428, 561, 603	3.97, 0.17, 0.09	-1.97	0.30, 0.59, 0.85	2.27

Note: ^[a] the porphyrins PorO1-3 and Por used the Soret band onset absorption wavelength (λ_{onset}); ^[b] calculated by the equation of $\Delta E = E_{Ox}^{1st} - E_{Re}^{1st}$.

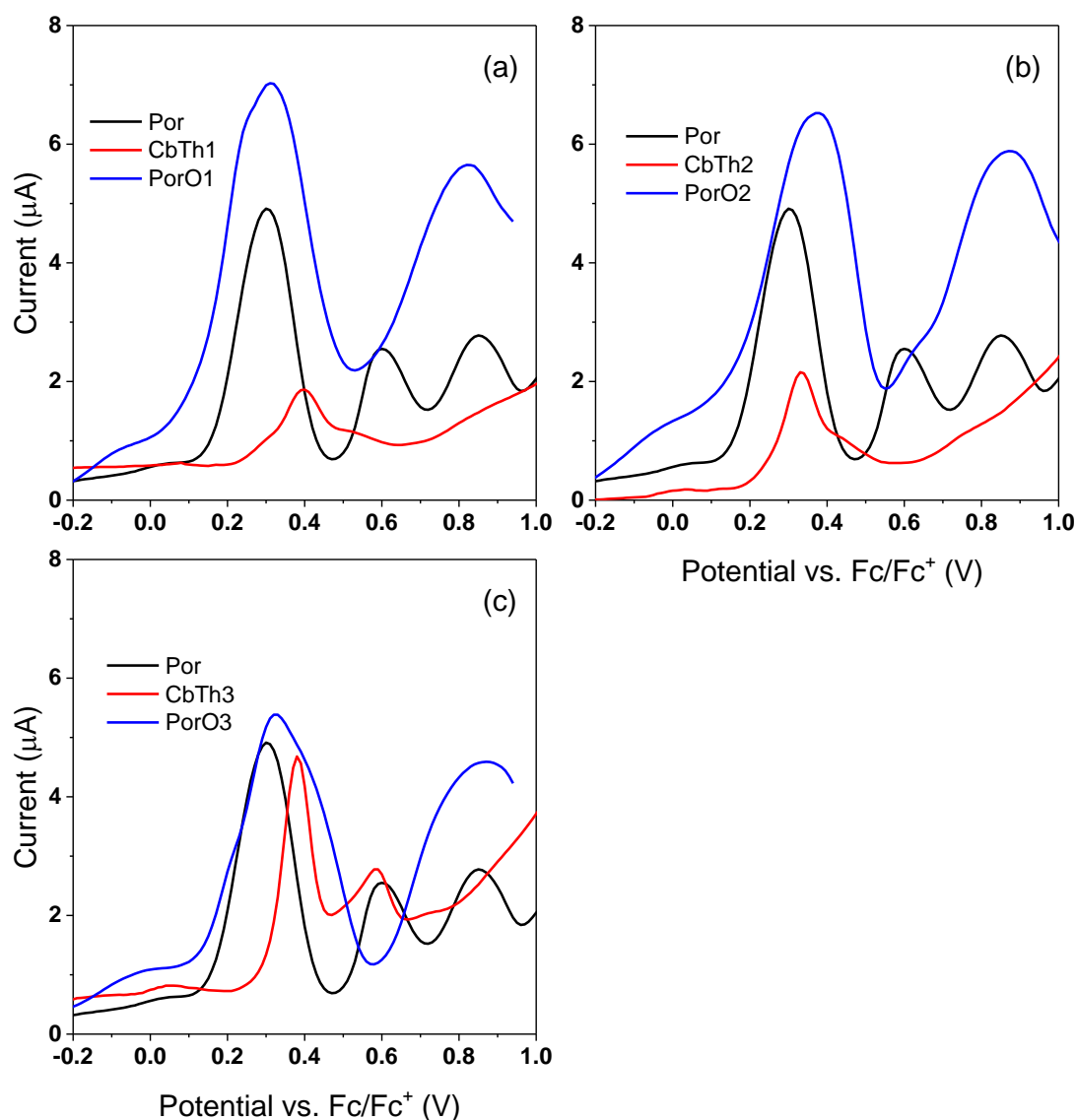


Figure 5.4 Positive scan DPV plots of the PorO dyes dissolved in DMF.

5.5. Enhanced photocurrent and photovoltage in DSSCs: The effect of filling the gap

The “absorption gap” in the single chromophoric porphyrin dye Por was partly filled by covalently linking thieno[3,2-b]thiophene, dithieno[3,2-b:2',3'-d]thiophene and 4,8-dicecyloxybenzo[1,2-b:4,5-b']dithiophene to the porphyrin using a phenylethenyl linker. The light absorption at the “absorption gap” of Por was enhanced in the dichromophoric porphyrins in solution as suggested by UV-vis absorption measurement. When fabricated in DSSCs, the enhanced light harvesting and therefore the photocurrent

of the PorO dyes would be expected. The results are compared to MK2 DSSCs as references.

5.5.1. Optimization of DSSC fabrication conditions and comparison of iodine / triiodide and cobalt electrolytes

To achieve high efficiency DSSCs, the fabrication conditions were optimized (Table 5.3 and 5.4).

The first attempt was using THF as the dye uptake solvent, which is same as used for the PorY dyes in Chapter 4. A low open circuit voltage (V_{OC}) of 630 mV was obtained in DSSC using PorO2 and the I/I_3^- electrolyte (Table 5.3).

Change of solvent for dye solution. No significant difference was found when changing the dye bath solvent to either *tert*-Butanol: AN: DCM=1.5:1.5:2 (vol) or ethanol: toluene = 1:1 (vol). The open circuit voltages were the same at ~630 mV.

Adding CDCA to the solution. The V_{OC} is increased by 30 mV. Moreover, the short circuit current density (J_{SC}) is increased by ~10%.

Increasing the CDCA concentration. A decreased fill factor (FF) is observed when the CDCA concentration is increased to 5 mM without affecting the V_{OC} and J_{SC} significantly.

Change of TiO_2 thickness. The optimized TiO_2 thickness was determined using both PorO1 and PorO2. The devices using the 7.4 μm thick TiO_2 electrodes achieved higher short circuit current densities and open circuit voltages compared to those using either thinner (2.9 μm) or thicker (17.5 μm) films.

Best fabrication condition using the I/I_3^- electrolyte. Using ethanol: toluene =1: 1 (vol) as the solvent and 0.1 mM CDCA as co-adsorber with 7.4 μm thick TiO_2 films, PorO1 and PorO2 showed similar power conversion efficiencies of 5.5%.

These optimized conditions developed for the I/I_3^- electrolyte were further tuned for the use of the $Co(dmbpy)_3^{2+}/Co(dmbpy)_3^{3+}$ electrolyte (Table 5.4).

The first attempt was using 0.11 M $Co(dmbpy)_3^{2+}$ and 0.025 M $Co(dmbpy)_3^{3+}$ in the electrolyte (0.05 M $LiClO_4$ and 0.1 M *t*BP in acetonitrile), with low FF (0.61) obtained by DSSC using PorO1. This may indicate that the concentration of the redox couple was not high enough for sufficient regeneration.

Increasing the concentration of $Co(dmbpy)_3^{2+}/Co(dmbpy)_3^{3+}$. Doubling the concentration of $Co(dmbpy)_3^{2+}$ and $Co(dmbpy)_3^{3+}$ in the electrolyte enhanced the FF .

However, the J_{SC} and V_{OC} were lower, indicating more recombination occurred with high concentration of redox shuttle.

Adding 1 mM CDCA to the $Co(dmbpy)_3^{2+}/Co(dmbpy)_3^{3+}$ electrolyte resulted in 10% increased J_{SC} and slightly decreased V_{OC} in DSSCs using PorO1 and PorO2.

The further optimized $Co(dmbpy)_3^{2+}/Co(dmbpy)_3^{3+}$ electrolyte comprised of 0.22 M $Co(dmbpy)_3^{2+}$, 0.05 M $Co(dmbpy)_3^{3+}$, 0.05 M $LiClO_4$, 0.1 M *t*BP and 1 mM CDCA in AN. The best power conversion efficiencies of 4.4% and 4.7% are obtained by DSSCs using PorO1 and PorO2 with 7.4 μm TiO_2 films, respectively.

In summary, good performance DSSC using both I^-/I_3^- electrolyte and $Co(dmbpy)_3^{2+}/Co(dmbpy)_3^{3+}$ electrolyte were achieved. The former showed higher photocurrent (by 20%) but lower photovoltage (by 3%).

Table 5.3 DSSCs performance - different dye-sensitization solvents and thickness of TiO_2 films using the I^-/I_3^- electrolyte

Sensitizer	Solvent	Thickness/ μm	$J_{SC}/$ $mA\ cm^{-2}$	$V_{OC}/$ mV	FF	$\eta\%$
PorO2	THF	Transparent (Scattering) ~12 (5.5)	10.05	630	0.74	4.66
	EtOH: Toluene=1:1		9.58	635	0.74	4.47
	<i>tert</i> -butanol: AN: DCM=1.5:1.5:2		10.15	640	0.73	4.71
	EtOH: THF=2:1 with 0.1 mM CDCA		10.15	660	0.73	4.88
	EtOH: Toluene=1:1 with 0.1 mM CDCA		11.08	660	0.73	5.36
	EtOH: Toluene=1:1 with 0.5 mM CDCA		11.11	650	0.73	5.25
	EtOH: Toluene=1:1 with 1 mM CDCA		11	660	0.73	5.26
	EtOH: Toluene=1:1 with 5 mM CDCA		11.56	660	0.7	5.37
PorO1	EtOH: Toluene=1:1 with 0.1 mM CDCA	5 (2.5)	11.16	700	0.71	5.52
PorO2	EtOH: Toluene=1:1 with 0.1 mM CDCA		11.58	705	0.67	5.48
PorO1	EtOH: Toluene=1:1 with 0.1 mM CDCA	2.9 (0)	7.28	695	0.68	3.46
PorO2	EtOH: Toluene=1:1 with 0.1 mM CDCA		7.04	705	0.64	3.19

Table 5.4 DSSCs performance - optimizing the $\text{Co(dmbpy)}_3^{2+}/\text{Co(dmbpy)}_3^{3+}$ electrolyte

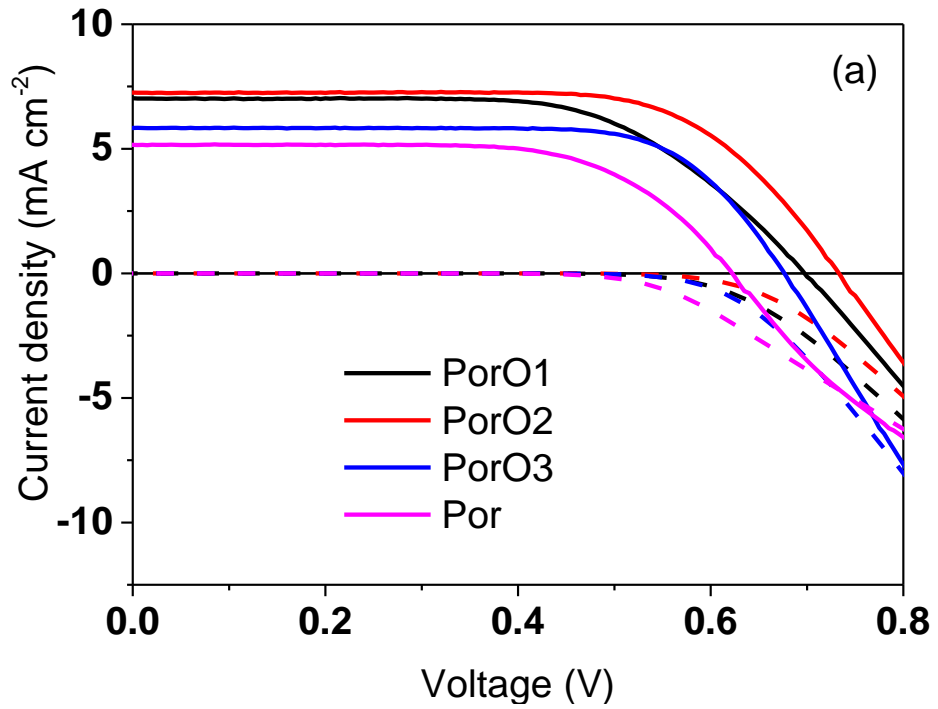
Thickness/ μm	Sensitizer	Electrolyte	$J_{sc}/$ mA cm ⁻²	$V_{oc}/$ mV	FF	$\eta\%$
7.4±0.5	PorO1	Electrolyte A	8.43	740	0.61	3.8
		Electrolyte B	7.13	715	0.73	3.71
		Electrolyte B + 1 mM CDCA	8.66	710	0.71	4.37
	PorO2	Electrolyte A + Saturated CDCA	11.85	670	0.58	4.59
		Electrolyte B	8.23	730	0.65	3.92
		Electrolyte B + 1 mM CDCA	9.25	725	0.71	4.73
Note: Electrolyte A: 0.11 M Co(dmbpy) ₃ ²⁺ / 0.025 M Co(dmbpy) ₃ ³⁺ , 0.05 M LiClO ₄ and 0.1 M <i>t</i> BP in AN.						
Electrolyte B: 0.22 M Co(dmbpy) ₃ ²⁺ / 0.05 M Co(dmbpy) ₃ ³⁺ , 0.05 M LiClO ₄ and 0.1 M <i>t</i> BP in AN.						

5.5.2. Comparison of PorO dyes in DSSC using optimized $\text{Co(dmbpy)}_3^{2+}/\text{Co(dmbpy)}_3^{3+}$ conditions

Fig. 5.5(a) and (b) shows the DSSCs using the PorO dyes compared to that using Por fabricated by both thin (2.9 \pm 0.1 μm) and thick (7.4 \pm 0.5 μm) TiO_2 films using the optimized $\text{Co(dmbpy)}_3^{2+}/\text{Co(dmbpy)}_3^{3+}$ electrolyte, respectively. Simultaneously enhanced photocurrent and photovoltage are observed by DSSCs using the PorO dyes compared to that using Por using both TiO_2 thicknesses. Several devices have been fabricated using each sensitizer using either thickness, suggesting good reproducibility (Table 5.5 and Table 5.6).

When using the 2.9 \pm 0.1 μm films, the best power conversion efficiency of 3.6% was achieved by DSSC using PorO2, with a 40% increase in J_{sc} and a 100 mV higher V_{oc} compared to Por under the same condition. The other two dyads, with photocurrents and photovoltages lower than PorO2, still show an overall ~40% increased power conversion efficiency in relative to Por. PorO3 shows the lowest J_{sc} among the di-chromophoric dyes. The FF of PorO1 is slightly lower (0.62) than the other porphyrins (0.69 \pm 0.04).

When using the $7.4 \pm 0.5 \text{ }\mu\text{m}$ films, similar J - V trend is observed. The best power conversion efficiency of 4.73% is achieved by DSSC using PorO2 (Table 5.6). Compared to DSSC using Por, DSSC using PorO2 attains a 55% increase in J_{SC} (9.25 mA cm^{-2}) and 85 mV in V_{OC} (725 mV), leading to a nearly twice the power conversion efficiency. The difference in J_{SC} between the DSSCs using PorO dyes and Por was further enhanced in thick films compared to that in thin films, which may suggest less collection losses in PorO dyes.



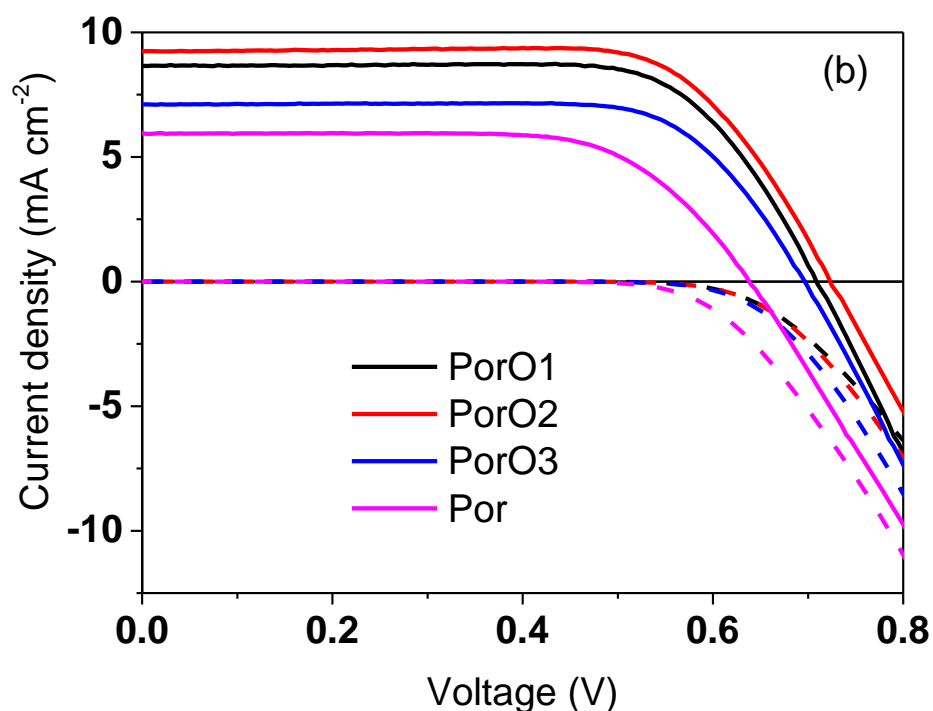


Figure 5.5 Current density-voltage (J - V) curves of DSSCs with the porphyrin dyes fabricated using (a) $2.9 \pm 0.1 \mu\text{m}$ transparent and (b) $7.4 \pm 0.5 \mu\text{m}$ with $5 \mu\text{m}$ transparent + $2.5 \mu\text{m}$ scattering TiO_2 under AM 1.5 illumination (solid lines) and in the dark (dashed lines).

Table 5.5 J - V performance of two $2.9 \mu\text{m}$ thick film devices with porphyrin dyes compared with MK2

Device	$J_{sc}/\text{mA cm}^{-2}$	V_{oc}/mV	FF	$\eta\%$
PorO1_1	7.03	700	0.62	3.03
PorO1_2	6.43	675	0.63	2.73
PorO2_1	7.26	735	0.68	3.6
PorO2_2	6.48	735	0.66	3.14
PorO3_1	5.75	685	0.68	2.67
PorO3_2	5.84	680	0.71	2.83
Por_1	5.16	625	0.65	2.1
Por_2	4.84	615	0.73	2.16
MK2_1	11.1	810	0.60	5.39
MK2_2	12.18	795	0.55	5.37

Table 5.6 J - V performance of three $7.4 \mu\text{m}$ thick film devices with porphyrin dyes compared with MK2 (two devices)

Device	$J_{sc}/\text{mA cm}^{-2}$	V_{oc}/mV	FF	$\eta\%$
PorO1_1	8.47	700	0.65	3.87
PorO1_2	8.25	720	0.69	4.11
PorO1_3	8.66	710	0.71	4.37
PorO2_1	9.25	725	0.71	4.73
PorO2_2	8.11	735	0.7	4.19
PorO2_3	8.71	720	0.63	3.94
PorO3_1	6.37	705	0.74	3.34
PorO3_2	7.11	700	0.72	3.56
PorO3_3	7.44	675	0.66	3.33
Por_1	6.15	645	0.63	2.5
Por_2	5.95	640	0.68	2.58
Por_3	5.36	615	0.63	2.08
MK2_1	13.5	805	0.52	5.67
MK2_2	13.6	805	0.49	5.35

5.6. Origin of lower than expected photocurrent

The best power conversion efficiency of the DSSCs using the PorO dyes is 4.73% using the cobalt electrolyte, which is less than expected if using the simple calculation in Fig. 5.1 (7.5%). This is mainly due to the lower photocurrent (the highest photocurrent of the DSSC using PorO2 is 9.25 mA cm^{-2} , while the expected photocurrent of the DSSC using sensitizers with IPCE value of 80% at 350-650 nm wavelength range is 13.34 mA cm^{-2}).

The origin of lower than expected photocurrent by DSSC using the PorO dyes compared to Por is investigated next by incident photon-to-current conversion efficiency (IPCE), light harvesting efficiency (LHE) and absorbed photon-to-current conversion efficiency (APCE) measurements using $2.9\text{ }\mu\text{m}$ transparent TiO_2 electrodes. The dye regeneration efficiency of the PorO dyes does not limit the photocurrent of the DSSCs by investigating the transient absorption kinetics of all the di-chromophoric dyes (recombination kinetics, regeneration kinetics and the calculation of dye regeneration efficiency are shown in Appendix Fig. A11 and Tables A3-A4).

5.6.1. Incident photon-to-current conversion efficiency

Fig. 5.6 displays the IPCE plots of DSSCs using the PorO dyes compare to Por. DSSCs using the PorO dyes show enhanced IPCE values beyond 450 nm, but lower values at the peak of Soret band at the 400-440 nm wavelength range, compared to Por. The IPCE values at the “absorption gap” between the Soret and Q bands in DSSC using Por are increased in DSSCs using the PorO dyes, which reveal that the extra chromophore benefits the photocurrent. DSSC using PorO2 shows a broader IPCE spectrum at the red edge of the Soret band compared to DSSC using PorO1 and PorO3. The peak IPCE value of DSSC using Por at the Soret band is 60%, which is 5% higher than those using the PorO dyes.

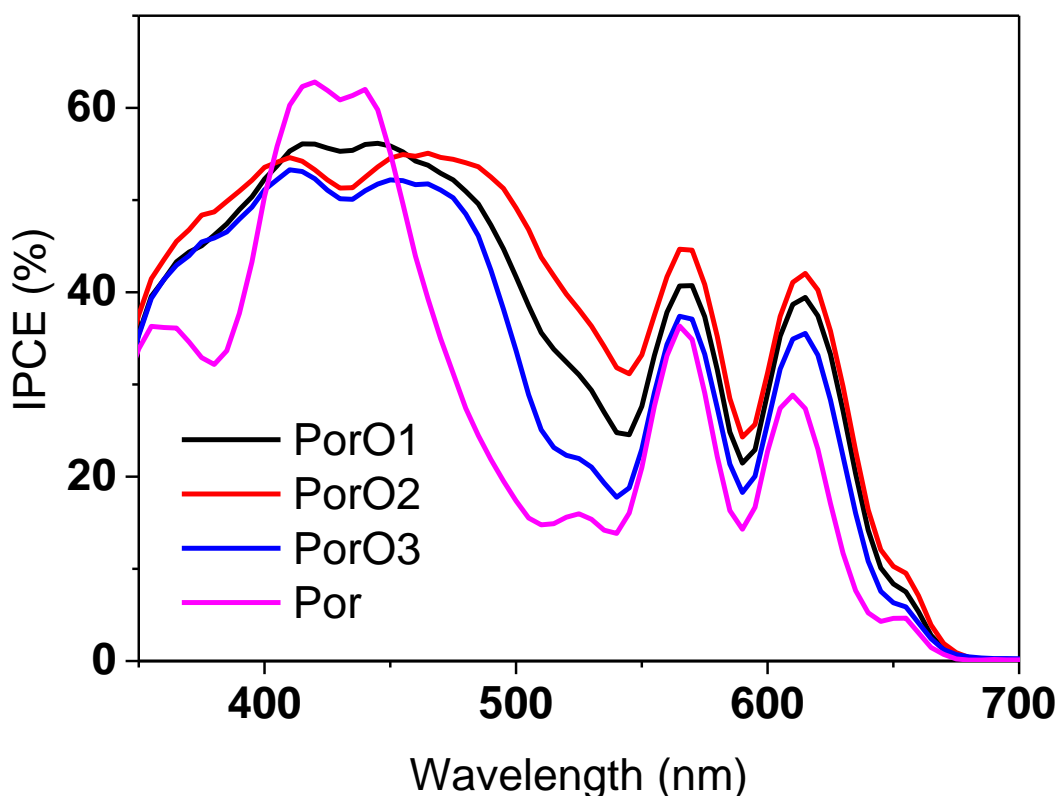


Figure 5.6 IPCE spectra of the devices fabricated from the porphyrin dyes on thin TiO_2 films.

5.6.2. Light harvesting efficiency

The LHE plot clearly suggests the filling of light “absorption gap” between the Soret and Q bands by the PorO dyes (Fig. 5.7). All DSSCs using PorO dyes show 40-80 nm broadened LHE at the 450-550 nm wavelength range with more than 40% LHE values.

Moreover, the DSSCs using PorO dyes attain 10% increased LHE values at Q bands compared to that using Por. These features are generally consistent with the UV-vis absorption spectra in solution. However, even more red-shifted and broadened absorptions are observed within the “absorption gap” when attached to TiO₂ compared to in dilute solutions. The cause of this can be dye interaction and / or dye-TiO₂ electronic interactions.²¹

Although the amount of PorO3 on TiO₂ ($0.9 \times 10^4 \text{ mol cm}^{-3}$) is only half of PorO1 and PorO2 ($1.7 \times 10^4 \text{ mol cm}^{-3}$), the LHE values at the Soret and Q bands within the DSSCs using the three dyads are very similar. This is mainly due to the larger molar extinction coefficient of PorO3 compared to that of PorO1 and PorO2 (see the UV-vis absorption in solution).

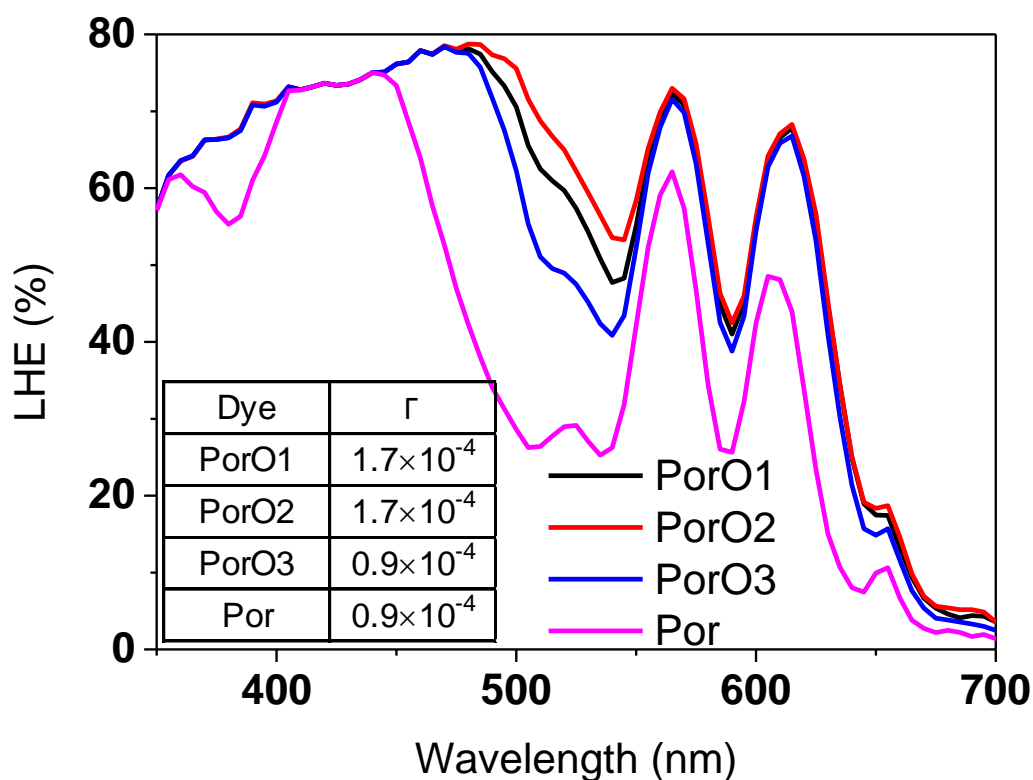


Figure 5.7 LHE spectra of the porphyrin dyes on thin TiO₂ films.
The inset shows the dye loading (Γ), with the unit mol cm^{-3} .

5.6.3. Absorbed photon-to-current conversion efficiency

The APCE value of DSSC using Por is 85% at the peak of Soret band, which is ~10% higher than that using the PorO dyes (Fig. 5.8). At the “absorption gap” and Q bands,

i.e. in 450-700 nm wavelength region, the APCE values among DSSCs using Por, PorO1 and PorO2 are very similar. DSSC using PorO3, however, is found to be 5-10% lower than the other porphyrins in the 450-700 nm wavelength region.

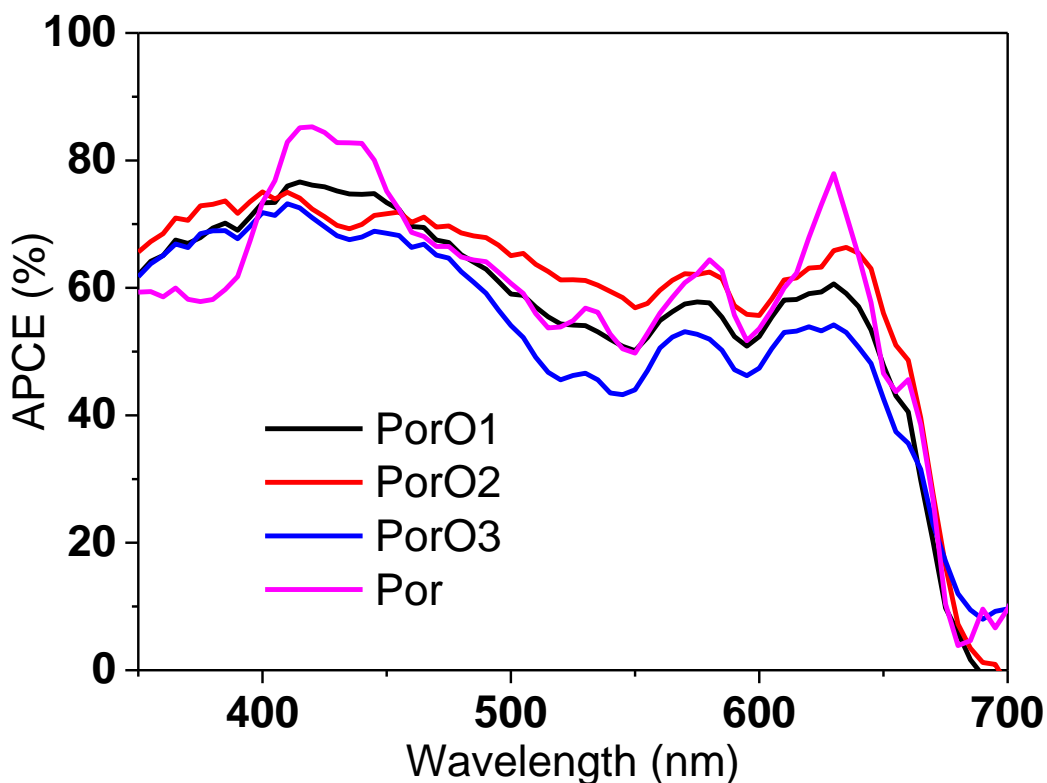


Figure 5.8 APCE spectra of the devices fabricated from the porphyrin dyes on thin TiO_2 films.

5.6.4. Evidence of charge collection loss in Por-sensitized solar cells using cobalt electrolyte

It was proposed (Chapter 1 Section 1.10.3) that using thin TiO_2 films ($2.9 \mu\text{m}$), recombination at short circuit condition can be avoided, therefore the APCE measurement reflects changes in the injection efficiency between dyes. This assumption needs to be carefully checked using cobalt electrolyte exhibiting generally faster recombination kinetics.

As the charge collection efficiency is affected by the semiconductor thickness, comparison of the photocurrent between $2.9 \mu\text{m}$ and $7.4 \mu\text{m}$ TiO_2 films can reveal the presence of charge collection losses at short circuit conditions. When changing the TiO_2 film thickness from $2.9 \mu\text{m}$ to $7.4 \mu\text{m}$, DSSCs using Por showed smaller increase in

photocurrent (from 5.2 mA cm⁻² to 6.0 mA cm⁻², 15% increase) compared to DSSCs using the PorO dyes (for example, PorO2, from 7.3 mA cm⁻² to 9.3 mA cm⁻², 30% increase). This different magnitude increasing in photocurrent, other than the differences in increased LHE, suggests more charge collection losses in DSSCs using Por compared to that using the PorO dyes in thicker films.

The charge collection efficiencies of DSSCs using Por and PorO1-3 can be calculated from the measurement of diffusion length, showing values close to 90% for DSSC using Por and ~95% for DSSCs using the di-chromophoric dyes. These measurements are discussed separately in Appendix Fig. A8.

Devices using Por face more charge collection losses compared to that using the PorO dyes when using thick films. It is a significant outcome of this chapter that thicker films can be used with increased performance of DSSCs using the novel di-chromophoric porphyrin dyes compared to that using the single chromophoric porphyrin dye with cobalt electrolyte.

5.6.5. Analysis of the electron injection efficiency

A 5-10% charge collection loss is suggested in the devices using the porphyrins when using 2.9 μm TiO₂ films (Appendix Fig. A8). The total losses in the APCE of the DSSCs using porphyrins are ~20% at the Soret band and ~40% at the Q bands. Consequently, the ~15% loss at the Soret band and the ~35% loss at the Q bands are not accounted for by charge collection losses are assigned to the losses in electron injection efficiency. Injection losses may originate from the following factors introduced in Chapter 1 Section 1.8.2.

- 5) Electronic coupling between the excited state and the acceptor states in TiO₂.
- 6) Driving force, which is the energy difference between the reduction potential and the conduction band edge potential of the semiconductor.
- 7) Excited state lifetime.
- 8) Dye aggregation and dye layer morphology.

Electronic coupling between the excited state and the acceptor states in TiO₂ may affect the electron injection efficiency in PorO dyes DSSCs. Although the organic chromophore in the PorO dyes does not alter the dihedral angle of the porphyrin and the cyanocarboxylate anchoring group as suggested by DFT calculations (performed by

collaborators),²⁰ UV-visible absorption spectroscopy and electrochemical spectroscopy results suggested weakly electronic communication between the two chromophores in PorO dyes. The electron density may shift away from TiO₂, reducing the electronic coupling between the dye and TiO₂.

Driving force

Using the peak potentials, an energy level diagram is obtained (Fig. 5.9). The energy level diagram suggests that the driving force for electron injection among the porphyrins is similar. A driving force of ~0.2 eV was estimated to be sufficient for 100% electron injection efficiency for some organic dyes, Ru-based dyes and single chromophoric porphyrins on ZnO films.²² It is very difficult to measure the exact conduction band edge potential since it strongly depends on the electrolyte (a negatively shifted 0.1 eV was observed when using the Co(dmbpy)₃²⁺/Co(dmbpy)₃³⁺ electrolyte compared to that using the I⁻/I₃⁻ electrolyte, this will be discussed in Chapter 8 Section 8.5 in detail). Hence the driving force for the electron injection in the porphyrins may not be sufficient for 100% injection as that the APCE values are only 60-75% for PorO1-3 and 50-85% for Por (Fig. 5.8).

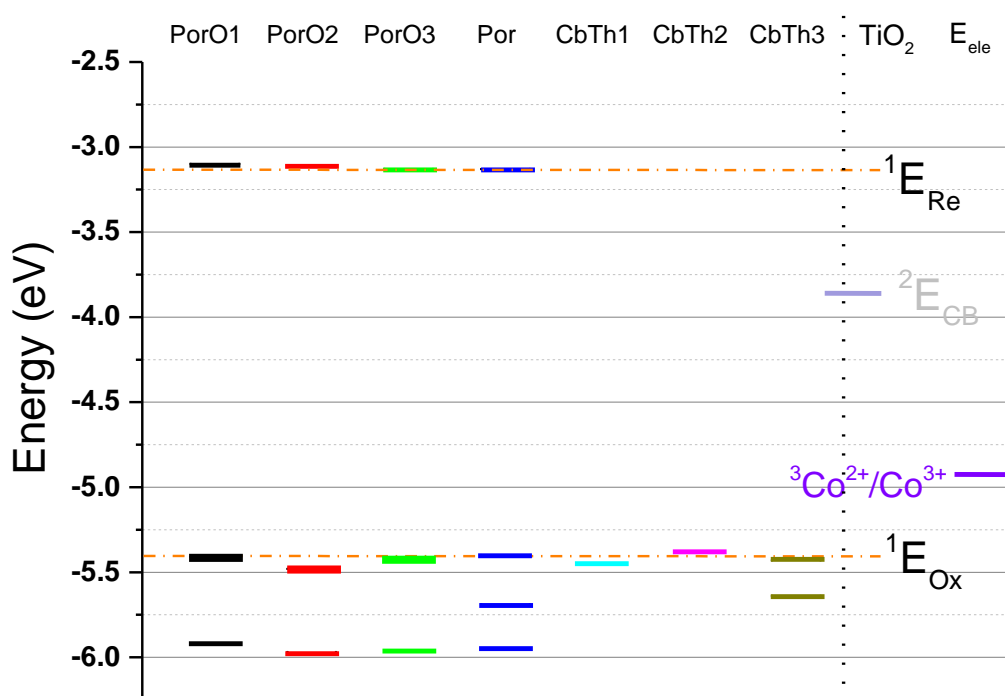


Figure 5.9 Energy level diagram of the compounds.

¹ The energy levels of oxidation (E_{Ox}) and the energy levels of reduction (E_{Re}) were calculated from the peak potentials of oxidation (E_{Ox} vs. Fe/Fe^+) and reduction (E_{Re} vs.

$_{Fc/Fc^+}$) as $E_{Ox} = - (E_{Ox \text{ vs. } Fc/Fc^+} + 5.1) \text{ (eV)}$ and $E_{Re} = - (E_{Re \text{ vs. } Fc/Fc^+} + 5.1) \text{ (eV)}$, respectively. The potential of the Fc/Fc^+ redox couple was assumed to be -5.1 eV vs. vacuum²³. ² E_{CB} was adopted from Ref.²⁴ plus a ~0.1 eV negative shift when using the $Co(dmbpy)_3^{2+}/Co(dmbpy)_3^{3+}$ electrolyte.³ The $Co(dmbpy)_3^{2+}/Co(dmbpy)_3^{3+}$ redox couple potential (E_{ele}) was adopted from Ref.^{25,26} The values of ² and ³ were calibrated to the absolute energy based on the assumption $E_{Fc/Fc^+} = +0.63 \text{ V vs. NHE}$.

Excited state lifetimes

As discussed in Chapter 4 and the steady state photoluminescence results in Chapter 7, the excited state lifetime should not contribute to the difference in electron injection efficiency of Por and PorO dyes DSSCs.

Dye aggregation and dye layer morphology

Chapter 4 suggested that dye aggregation and / or the presence of non-injecting dyes on the TiO_2 surface limited Por to obtain unity electron injection yield. In this chapter, DSSC using Por showed the peak APCE value of ~80% (Fig. 5.8). The charge collection measurement suggested a 10% loss in charge collection at most (Appendix Fig. A8). The other 10% of APCE may assign to the presents of non-injecting dyes on TiO_2 .

The APCE values of DSSC using PorO3 were 5-10% lower compared to that using PorO1 and PorO2. The dye uptake amount of PorO3 was only half compared to the other two di-chromophoric dyes (Fig. 5.7). This may imply that PorO3 cannot strongly bind to TiO_2 or occupies more space of one molecule due to the octyloxy chains at the organic chromophore. This binding / morphology problem of PorO3 may lead to the decreased APCE.

5.6.6. Insufficient driving force for electron injection

The possibility of insufficient driving force for electron injection was checked by removing *tert*-butylpyridine from the electrolyte. As a typical additive in the electrolyte for DSSCs, *t*BP can be adsorbed on the TiO_2 surface and negatively shift the TiO_2 conduction band bottom edge, leading the energy difference between the first reduction potential and the conduction band edge potential smaller (but *t*BP gives larger photovoltage).²⁷⁻³⁰ The significance of *t*BP in the cobalt electrolyte on the TiO_2 conduction band bottom edge is measured by stepped light-induced transient measurements of photocurrent and photovoltage and charge extraction measurements.

By removing *t*BP from the electrolyte, a 130 mV positive shift of the conduction band potential is suggested (Appendix Fig. A10).

The removal of *t*BP resulted in an intense enhancement of IPCE and APCE in the whole visible wavelength range using PorO2 in DSSCs with cobalt electrolyte (Fig. 5.10). The LHE spectra between the optimized electrolyte and the *t*BP free electrolyte do not show any significant difference, suggesting the *t*BP does not change the absorption property of the sensitizers. The organic dye MK2 is again used here as a reference. The IPCE/APCE values at the Soret band of DSSC using the electrolyte without *t*BP exhibit similar values as that of the MK2-sensitized solar cells. This suggests that by positively shifting the conduction band of TiO₂ (by removal of *t*BP), the electron injection efficiency of PorO2 devices is enhanced due to the larger driving force (Fig. 5.11).

The APCE values of DSSC using PorO2 are 80-90% in the 350-600 nm wavelength range, using the cobalt electrolyte without *t*BP, which is more than 20% higher than that using the optimized cobalt electrolyte. This more than 20% enhanced APCE is assigned to the increased electron injection efficiency.

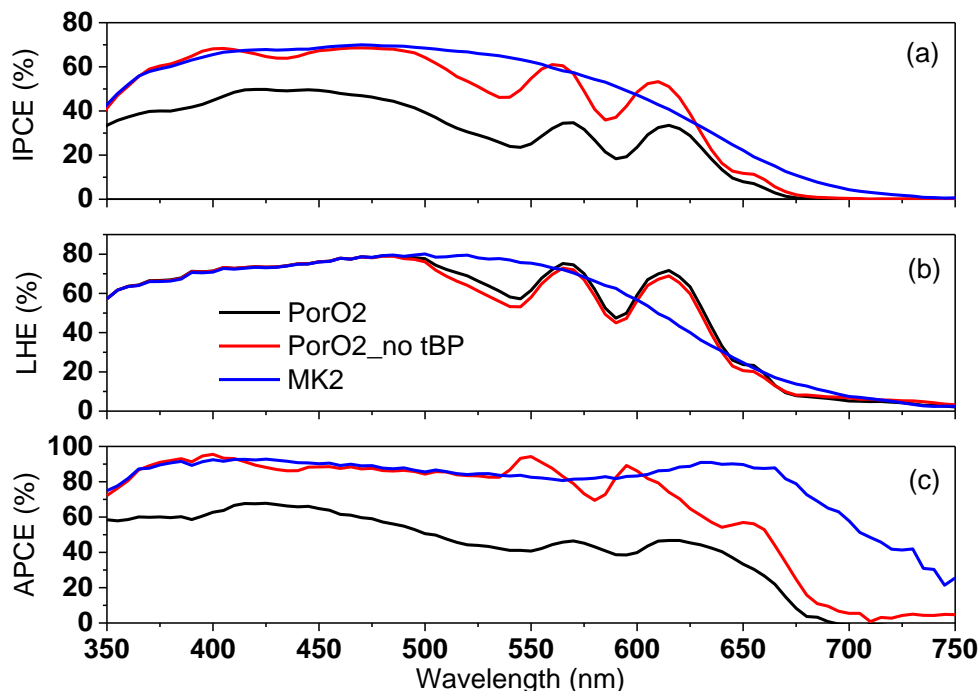


Figure 5.10 (a) IPCE, (b) LHE and (c) APCE spectra of devices fabricated from PorO2 with and without *t*BP in the cobalt electrolyte and MK2 on thin TiO₂ films. Film thickness: 3.2 ± 0.2 μm for PorO2, 2.9 ± 0.1 μm for MK2.

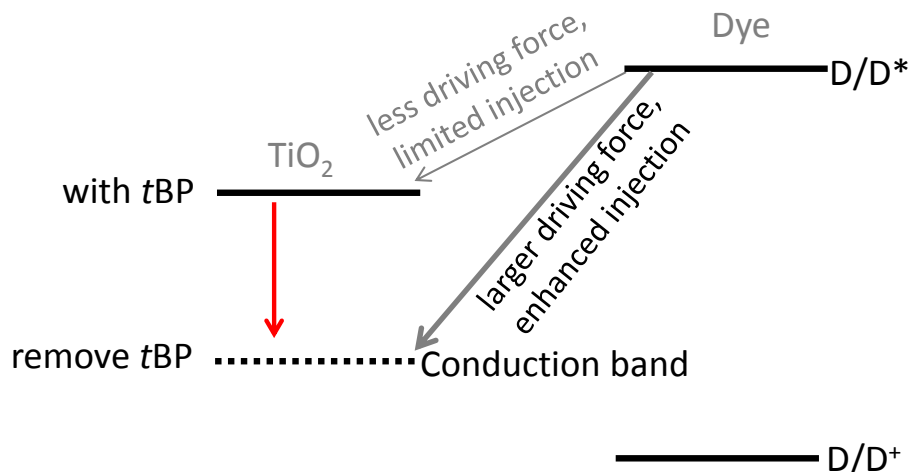


Figure 5.11 An illustration of the effect of removal *t*BP on electron injection.

Similar to DSSC using PorO2, DSSCs using PorO1 and PorO3 both lead to significantly increased IPCE/APCE values by omission of *t*BP from the electrolyte (Fig. 5.12). The IPCE/APCE peak values at the Soret band within DSSCs using the three dichromophoric dyes are very similar (70%/95%). It is noted that DSSC using PorO3 shows 5% less IPCE/APCE values at the Q bands compared to that using PorO1 and PorO2, which is consistent with the result using the optimized cobalt electrolyte.

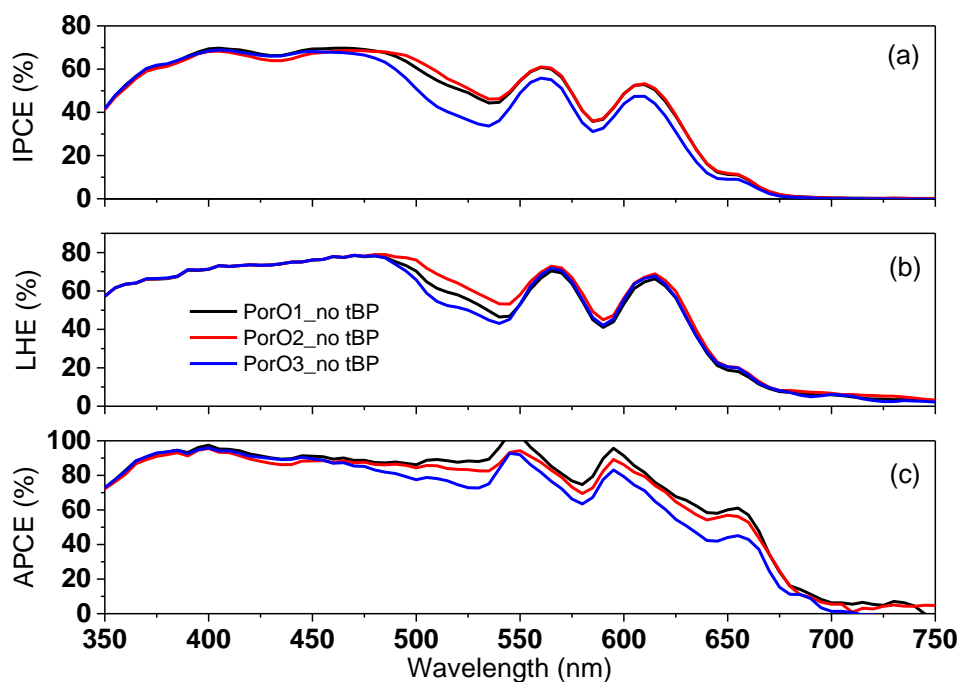


Figure 5.12 (a) IPCE, (b) LHE and (c) APCE spectra of devices fabricated from PorO1-3 without *t*BP in the cobalt electrolyte on thin TiO_2 films.
Film thickness: $3.2 \pm 0.2 \mu\text{m}$.

5.7. Increased open circuit voltage using carbazole-fused thiophene substituted porphyrin di-chromophoric dyes

As Fig. 5.5 and Table 5.5 suggest, the benefit of using carbazole-fused thiophene substituted porphyrin dyes in DSSC is not only increased photocurrent compared to Por, but also increased open circuit voltage. Such increased open circuit voltage as an additional benefit to the filling of the “absorption gap” to enhance light harvesting strongly supports the utility of the di-chromophoric approach in achieving high efficiency photovoltaic devices. The origin of this enhanced open circuit voltage will be discussed in Chapter 8, and is assigned to the blocking effect from the additional organic chromophore.

5.8. Conclusions

Di-chromophoric concept was used to fill the light “absorption gap” in typical porphyrins between the Soret and Q bands. By using three carbazole-fused thiophene substituted di-chromophoric porphyrins (the PorO dyes), the “absorption gap” between the Soret and Q bands in the single chromophoric porphyrin Por was partly filled. The electrochemistry results suggested that the organic chromophores did not affect the reduction reactions of the di-chromophoric dyes, while showed their influence on the oxidation reactions. Weak electronic coupling between the two components in the PorO dyes was suggested by the electrochemical results.

The photovoltaic performance of DSSCs using cobalt electrolyte and incident photon-to-current conversion efficiency / light harvesting efficiency / absorbed photon-to-current conversion efficiency measurements were carried out to investigate the effect of the filling “absorption gap”. These measurements showed that:

1. Both photocurrent and photovoltage of DSSCs using the PorO dyes were enhanced in relative to that using Por.
2. The best power conversion efficiencies of 4.7% using the $\text{Co(dmbpy)}_3^{2+}/\text{Co(dmbpy)}_3^{3+}$ electrolyte and 5.5% using the I^-/I_3^- electrolyte were achieved by DSSCs using PorO2, which were nearly doubled respect to DSSCs using Por.

3. The light harvesting efficiencies of the PorO dyes were enhanced by partly, although not completely, filling the “absorption gap” between the Soret and Q bands and increasing light absorption at the Q bands.
4. Towards filling the “absorption gap” using the di-chromophoric concept, PorO2 shows better performance while PorO3 is worse compared to PorO1.
5. Enhanced charge collection was found in DSSCs using the PorO dyes compared to that using Por.
6. The limitation in photovoltaic performance of the DSSCs using the PorO dyes with the optimized cobalt electrolyte is the insufficient driving force for electron injection. This is due to excessively positive reduction potentials of the PorO dyes, demonstrated with IPCE/LHE/APCE measurements using the cobalt electrolyte without *t*BP. The reason of the limited driving force for electron injection in di-chromophoric dyes is still unclear.
7. DSSC using PorO3 achieved 5% lower IPCE/APCE values at the Q bands compared to those using PorO1 and PorO2, which may be due to its weakly binding on TiO₂/ occupying more TiO₂ space of one molecule morphology.
8. Most importantly, the utility of cobalt electrolyte in di-chromophoric dye-sensitized solar cells is demonstrated.

5.9. References

- (1) Gouterman, M. *J. Chem. Phys.* **1959**, *30*, 1139.
- (2) Gouterman, M. *J. Mol. Spectrosc.* **1961**, *6*, 138.
- (3) Gouterman, M.; Wagnière, G. H.; Snyder, L. C. *J. Mol. Spectrosc.* **1963**, *11*, 108.
- (4) Weiss, C.; Kobayashi, H.; Gouterman, M. *J. Mol. Spectrosc.* **1965**, *16*, 415.
- (5) Koumura, N.; Wang, Z.-S.; Mori, S.; Miyashita, M.; Suzuki, E.; Hara, K. *J. Am. Chem. Soc.* **2006**, *128*, 14256.
- (6) Wu, S.-L.; Lu, H.-P.; Yu, H.-T.; Chuang, S.-H.; Chiu, C.-L.; Lee, C.-W.; Diau, E. W.-G.; Yeh, C.-Y. *Energy Environ. Sci.* **2010**, *3*, 949.
- (7) Grätzel, M. *J. Photochem. Photobiol. C: Photochem. Rev.* **2003**, *4*, 145.
- (8) Baheti, A.; Singh, P.; Lee, C.-P.; Thomas, K. R. J.; Ho, K.-C. *J. Org.*

Chem. **1981**, 76, 4910.

- (9) Xu, W.; Peng, B.; Chen, J.; Liang, M.; Cai, F. *J. Phys. Chem. C* **2008**, 112, 874.
- (10) Nazeeruddin, M. K.; Kay, A.; Rodicio, I.; Humphry-Baker, R.; Mueller, E.; Liska, P.; Vlachopoulos, N.; Grätzel, M. *J. Am. Chem. Soc.* **1993**, 115, 6382.
- (11) Wang, Z.-S.; Koumura, N.; Cui, Y.; Takahashi, M.; Sekiguchi, H.; Mori, A.; Kubo, T.; Furube, A.; Hara, K. *Chem. Mater.* **2008**, 20, 3993.
- (12) Lazarides, T.; Kuhri, S.; Charalambidis, G.; Panda, M. K.; Guldi, D. M.; Coutsolelos, A. G. *Inorg. Chem.* **2012**, 51, 4193.
- (13) Kato, S.-i.; Shimizu, S.; Kobayashi, A.; Yoshihara, T.; Tobita, S.; Nakamura, Y. *J. Org. Chem.* **2014**, 79, 618.
- (14) Zhang, X.; Côté, A. P.; Matzger, A. J. *J. Am. Chem. Soc.* **2005**, 127, 10502.
- (15) He, M.; Zhang, F. *J. Org. Chem.* **2006**, 72, 442.
- (16) Katoh, R.; Furube, A. *J. Phys. Chem. Lett.* **2011**, 2, 1888.
- (17) Lin, J.; Zhao, L.; Heo, Y.-U.; Wang, L.; Bijarbooneh, F. H.; Mozer, A. J.; Nattestad, A.; Yamauchi, Y.; Dou, S. X.; Kim, J. H. *Nano Energy* **2015**, 11, 557.
- (18) Kubo, W.; Sakamoto, A.; Kitamura, T.; Wada, Y.; Yanagida, S. *J. Photochem. Photobiol., A* **2004**, 164, 33.
- (19) Mozer, A. J.; Griffith, M. J.; Tsekouras, G.; Wagner, P.; Wallace, G. G.; Mori, S.; Sunahara, K.; Miyashita, M.; Earles, J. C.; Gordon, K. C.; Du, L.; Katoh, R.; Furube, A.; Officer, D. L. *J. Am. Chem. Soc.* **2009**, 131, 15621.
- (20) Zhao, L.; Wagner, P.; van der Salm, H.; Clarke, T. M.; Gordon, K. C.; Mori, S.; Mozer, A. J. *J. Phys. Chem. C* **2015**, 119, 5350.
- (21) Wu, Y.; Zhang, X.; Li, W.; Wang, Z.-S.; Tian, H.; Zhu, W. *Adv. Energy Mater.* **2012**, 2, 149.
- (22) Katoh, R.; Furube, A. *J. Photochem. Photobiol. C: Photochem. Rev.* **2014**, 20, 1.
- (23) Cardona, C. M.; Li, W.; Kaifer, A. E.; Stockdale, D.; Bazan, G. C. *Adv. Mater.* **2011**, 23, 2367.
- (24) Hagfeldt, A.; Boschloo, G.; Sun, L.; Kloo, L.; Pettersson, H. *Chem. Rev.* **2010**, 110, 6595.
- (25) Feldt, S. M.; Wang, G.; Boschloo, G.; Hagfeldt, A. *J. Phys. Chem. C*

2011, *115*, 21500.

(26) Mosconi, E.; Yum, J.-H.; Kessler, F.; Gomez Garcia, C. J.; Zuccaccia, C.; Cinti, A.; Nazeeruddin, M. K.; Grätzel, M.; De Angelis, F. *J. Am. Chem. Soc.* **2012**, *134*, 19438.

(27) Nakade, S.; Makimoto, Y.; Kubo, W.; Kitamura, T.; Wada, Y.; Yanagida, S. *J. Phys. Chem. B* **2005**, *109*, 3488.

(28) Huang, S. Y.; Schlichthörl, G.; Nozik, A. J.; Grätzel, M.; Frank, A. J. *J. Phys. Chem. B* **1997**, *101*, 2576.

(29) Zhang, S.; Yang, X.; Zhang, K.; Chen, H.; Yanagida, M.; Han, L. *Phys. Chem. Chem. Phys.* **2011**, *13*, 19310.

(30) Nakade, S.; Kanzaki, T.; Kubo, W.; Kitamura, T.; Wada, Y.; Yanagida, S. *J. Phys. Chem. B* **2005**, *109*, 3480.

**CHAPTER 6.A CARBAZOLE-THIOPHENE BENZOTHIADIAZOLE
THIOPHENE PORPHYRIN: COMPARISON TO SINGLE
CHROMOPHORIC DYES AND MIXED DYES**

6.1. Introduction

Since the light harvesting property of the porphyrin strongly influences the performance of dye-sensitized solar cells (DSSCs), lowering the band gap of the porphyrin should increase the efficiency. This is known as the single chromophoric porphyrin approach according to the definition in Chapter 1 Section 1.4. Such approach has been widely implemented in other reports,¹⁻⁵ and involves the extension of the π conjugation at the porphyrin, typically, by using a donor- π bridge-acceptor (D- π -A) design. The main shortcoming of elongating π -conjugation is the increased polarizability of the electrons. In general, increased polarizability leads to stronger intermolecular forces and lower photovoltage in DSSCs.

The other two approaches can be followed to extend the light absorption as introduced in Chapter 1 Section 1.4 are listed below:

- 3) The multi-chromophoric dye approach - by introducing additional low band chromophores that absorb photons towards red. The multi-chromophoric dye concept can be used to enhance light harvesting without increasing the intermolecular forces. Chapter 5 has demonstrated the significance of filling the absorption gap between the Soret and Q bands in porphyrins on photovoltaic performance of DSSCs. Further extending light absorption to the red is expected to enhance light harvesting and therefore increase photovoltaic performance.
- 4) Co-sensitization approach (mixed dyes) – by co-adsorbing several chromophores on TiO₂ electrodes. A comparison between the multi-chromophoric dye and co-sensitization approaches has not been reported.

However, low band gap organic chromophore is needed in the multi-chromophoric dye to extend the light absorption to lower energy. This may induce an electron transfer from the porphyrin to the organic chromophore as suggested from the energy level diagram shown in Fig. 6.1. The organic chromophores in Chapter 4 and 5 possess larger band gap and more negative first reduction potential compared to the porphyrin, leading electrons to channel to the TiO₂. On the contrary, the organic chromophore in this chapter, as will show below, possesses lower band gap as well as more positive first reduction potential compared to the porphyrin, leading partial electrons to channel to the organic chromophore as a competing pathway to the electron injection to TiO₂. Chapter 3 already showed that competition pathways are possible. The effect of these two

competing electron injection pathways on photovoltaic performance of di-chromophoric dye-sensitized solar cells will be investigated in this chapter in more detail.

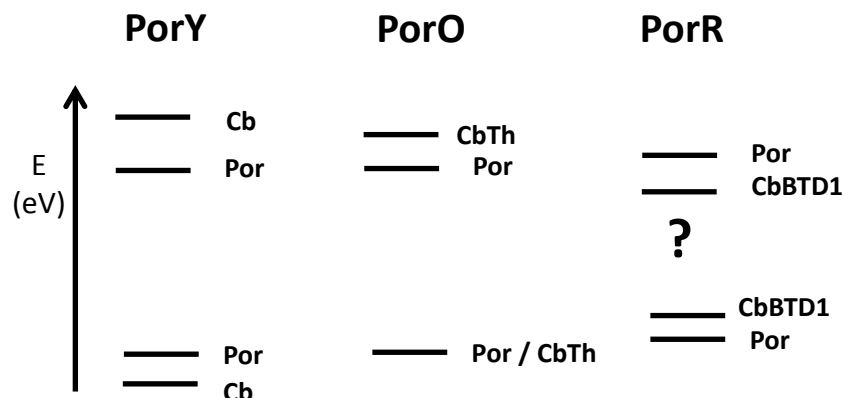


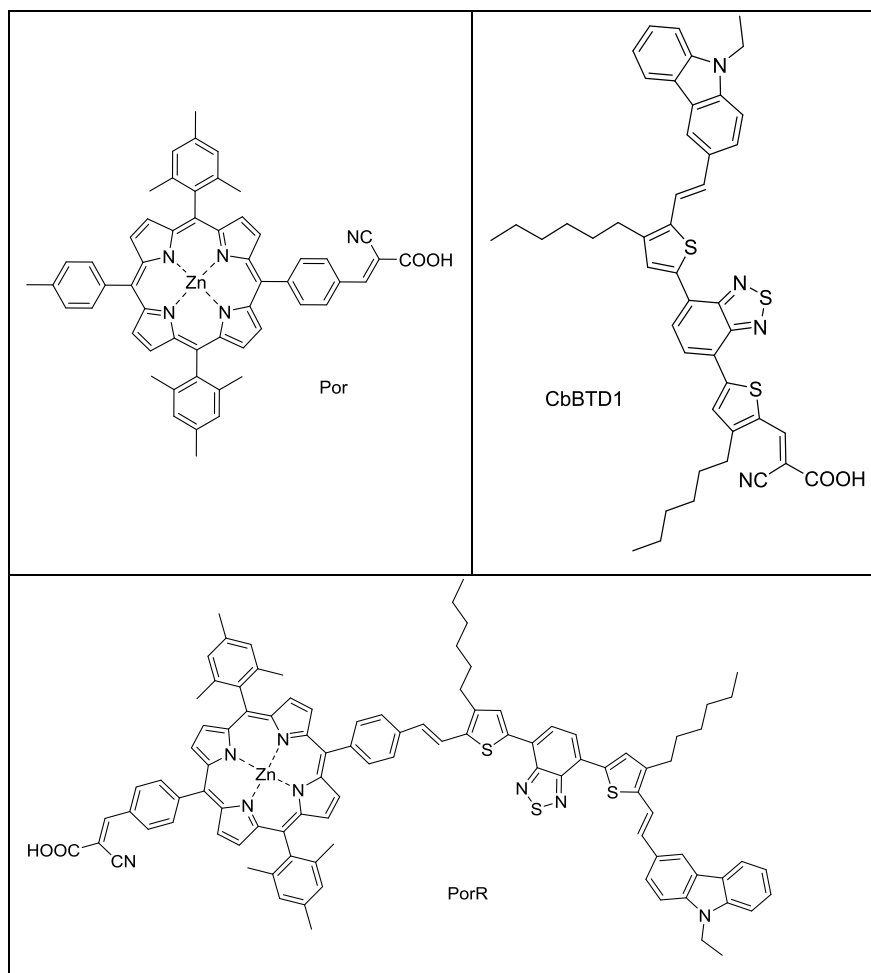
Figure 6.1 The relative energy levels of the porphyrin (Por) and the organic chromophore (Cb, CbTh and CbBTD1) in the three families of di-chromophoric dyes.

Two purposes are included in this chapter:

- 1) The di-chromophoric dye (carbazole-thiophene benzothiadiazole thiophene-substituted porphyrin PorR) and its counterparts, a single chromophoric porphyrin Por and an organic dye CbBTD1 are characterized (Table 6.1);
- 2) Three different molar ratios of dye mixtures comprised of Por and CbBTD1 (1:3, 1:1 and 3:1) are investigated.

Decreased photocurrent was obtained by the di-chromophoric porphyrin compared to the individual dyes and the mixed dyes in DSSCs. The di-chromophoric porphyrin DSSC showed only slightly more than half of power conversion efficiency compared to that of the single chromophoric dyes and the mixed dyes. The origin of the decreased photocurrent in DSSCs using PorR was analysed using incident photon-to-current conversion efficiency (IPCE), light harvesting efficiency (LHE) and absorbed photon-to-current conversion efficiency (APCE) measurements, and was attributed to the reduced electron injection efficiency. The photovoltage of the di-chromophoric dye was similar to the single chromophoric porphyrin and much larger as compared to the organic dye and the mixed dyes. The origin of these differences in photovoltage will be discussed in Chapter 8.

Table 6.1 Molecular structures of the investigated sensitizers



6.2. Experimental

6.2.1 Investigated molecules

The structures of single zinc porphyrin Por, carbazole-thiophene benzothiadiazole thiophene organic dye CbBTD1 and carbazole-thiophene benzothiadiazole thiophene substituent di-chromophoric zinc porphyrin PorR are shown in Table 6.1.

2-cyano-3-(5-(7-(5-(2-(9-ethylcarbazol-3-yl)ethenyl)-4-hexylthien-2-yl)benzo-2,1,3-thiadiazol-4-yl)-3-hexylthien-2-yl)acrylic acid (CbBTD1); 5-(4-(2-cyano-2-carboxyethenyl)phenyl)-15-(2-(5-(7-(5-(2-(9-ethylcarbazol-3-yl)ethenyl)-4-hexylthien-2-yl)benzo-2,1,3-thiadiazol-4-yl)-3-hexylthien-2-yl)ethenyl)-10,20-bis(2,4,6-trimethylphenyl)porphyrinato zinc(II) (PorR); 5-(7-(5-(2-(9-Ethylcarbazol-3-yl)ethenyl)-4-hexylthien-2-yl)benzo-2,1,3-thiadiazol-4-yl)-3-hexylthien-2-ylmethanol

(CbBTD-OH). 5-(4-(2-cyano-2-carboxyethenyl)phenyl)-15-(4-methylphenyl)-10,20-bis(2,4,6-trimethylphenyl)porphyrinato zinc(II) (Por).

6.2.2 Spectroscopic and electrochemical characterization

UV-visible (UV-vis) absorption spectroscopy was recorded in tetrahydrofuran (THF). Differential pulse voltammetry (DPV) and spectroelectrochemical (SEC) spectroscopy were measured using 0.5 mM of each compound in dimethylformamide (DMF).

6.2.3 DSSC fabrication and characterization

The photoanode employed fluorine doped tin oxide glass (FTO glass, 3 mm, 8 Ω /square, Nippon Sheet Glass) as the substrate. Fabrication of the photoanode and photocathode was under the same procedure in Chapter 4. The thin TiO₂ films (~2.0 μ m) was comprised of only one transparent layer, while the thick TiO₂ films consisted of one transparent (~5 μ m) and one scattering (~2.5 μ m) layers.

For dye-sensitization, THF was employed as the solvent with 1.5 h immersing time. The concentration of the individual dyes Por, PorR and CbBTD1 was 0.2 mM. For the mixed dyes consisted of Por and CbBTD1, three different molar ratios with the total concentration of 0.2 mM were chosen. Therefore, the concentrations of Por and CbBTD1 in the mixed 1:3, the mixed 1:1 and the mixed 3:1 were 0.05 mM and 0.15 mM, 0.1mM and 0.1 mM and 0.15 mM and 0.05 mM, respectively.

The electrolyte for the device characterization was comprised of 0.6 M 1,2-dimethyl-3-propylimidazolium iodide (DMPII, synthesized in house), 0.1 M LiI (99.9%, Aldrich), 0.05 M I₂ (99.99%, Aldrich), 0.5 M *tert*-butylpyridine (*t*BP, 96%, Aldrich) in acetonitrile (AN, 99.8%, Sigma-Aldrich): valeronitrile (VN, 99.5%, Sigma-Aldrich) = 85:15 (vol).

Current density-voltage (*J-V*) measurements, Incident photon-to-current conversion efficiency (IPCE)-Light harvesting efficiency (LHE)-Absorbed photon-to-current conversion efficiency (APCE) measurement and the dye loading on TiO₂ were characterized by the same procedures in Chapter 5.

One additional experiment compared to Chapter 5 is determining the dye uptake on the mixed dye-sensitized TiO₂ films. For the mixed dyes, two wavelengths were chosen for the calculation of the dye loading where the main absorbance was attributed to CbBTD1 and Por respectively. These wavelengths were 388 nm and 432 nm. The peak molar

extinction coefficient values of the compounds at the Soret band are shown in Appendix Table A1.

6.3. Purpose one: a comparison to single chromophoric dyes

6.3.1 Light absorption in solution

Fig. 6.2 shows the molar extinction coefficient (ϵ) of the single chromophoric porphyrin Por, the organic dye CbBTD1, and the di-chromophoric porphyrin PorR in THF. The light absorption spectrum of the di-chromophoric dye is simply a superposition of that of Por and CbBTD1 in most of the visible wavelength region. The onset of absorption of PorR is close to that of CbBTD1. Moreover, the di-chromophoric porphyrin PorR shows the same maximum, but 10 nm broader, absorption at the Soret band as compared to Por. A marked change is the increased absorption of PorR at the Q bands.

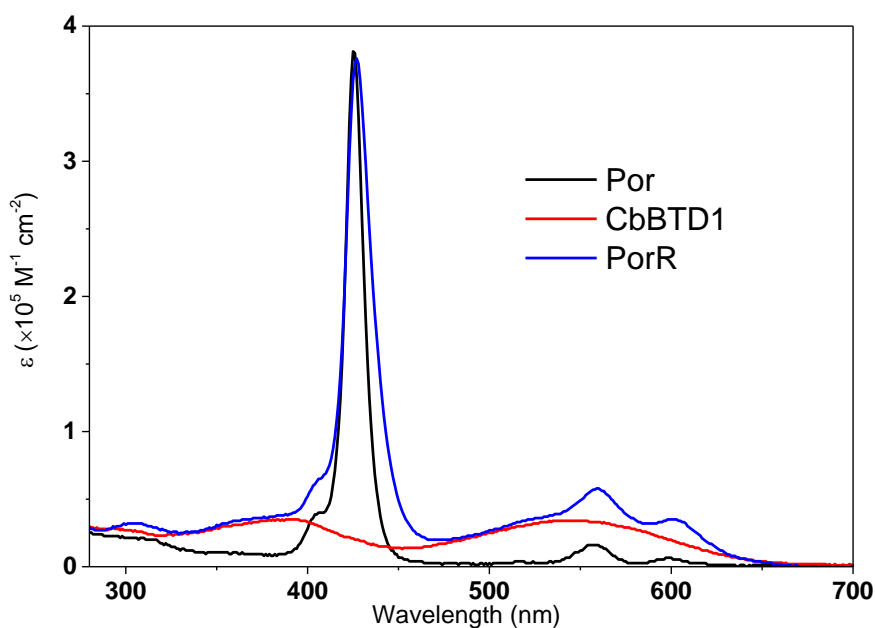


Figure 6.2 Molar extinction coefficient (ϵ) of the individual dyes measured in THF.

6.3.2 Electrochemistry

The oxidation and reduction reactions of the single chromophoric porphyrin Por, the organic dye CbBTD1 and the di-chromophoric porphyrin PorR were measured in DMF using differential pulse voltammetry (DPV, Fig. 6.3(a) and (b), respectively). Peak

potentials in the DPV plots and the energy gaps calculated using both electrochemical method and optical spectroscopy are listed in Table 6.2.

The first oxidation potentials (positive scan) of the porphyrin dye Por and the organic dye CbBTD1 show identical value at 0.30 V vs. Fc/Fc^+ (Fig. 6.3(a)). The dichromophore porphyrin PorR shows a broad first oxidation which is formed by two one-electron reactions at 0.30 V and 0.40 V vs. Fc/Fc^+ . CbBTD1 shows a second oxidation potential at ~ 0.80 V vs. Fc/Fc^+ .

Cathodic sweep of PorR results in two reactions: the first reduction peak potential is at -1.67 V vs. Fc/Fc^+ which is identical to the reduction peak potential of CbBTD1, and the second peak potential at -1.97 V vs. Fc/Fc^+ , which is identical to the reduction peak potential of Por (Fig. 6.3(b)). This clearly suggests that the porphyrin and the organic chromophore in PorR did not electronically affect each other. Reducing Por and CbBTD1 shows only one reaction peak in the potential window. CbBTD1 is ~ 0.3 V easier to be reduced compared to Por.

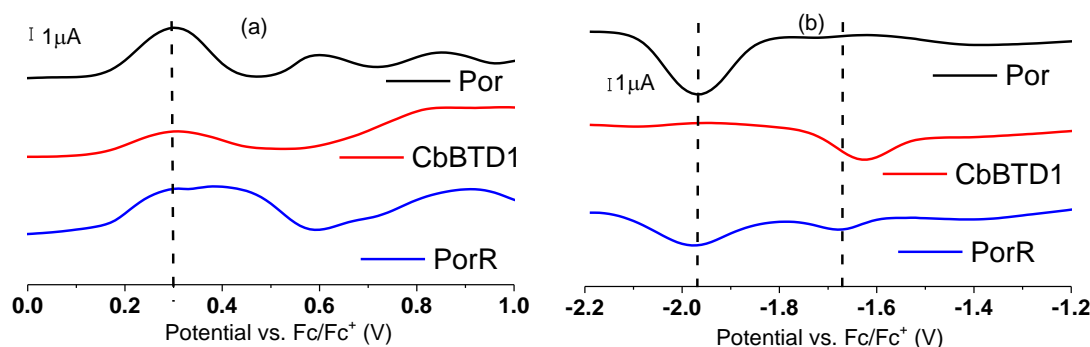


Figure 6.3 Differential pulse voltammograms of the compounds, (a) positive scan; (b) negative scan.

Sample concentration: 0.5 mM; solvent: DMF; supporting electrolyte: TBAP; Pt wire surface area: 6.6 mm^2 ; scan rate: 100 mV s^{-1} .

Table 6.2 Summary of spectral and electrochemical data of the compounds

Compound	Abs. λ_{max} (nm)	ε ($\times 10^5 \text{ M}^{-1} \text{ cm}^{-1}$)	Peak Potential vs. Fc/Fc^+		ΔE (eV)
			E_{Re} (V)	E_{Ox} (V)	
Por	426, 557, 599	3.80, 0.16, 0.07	-1.97	0.30, 0.59, 0.85	2.27
CbBTD1	392, 548	0.35, 0.34	-1.62	0.30, 0.83	1.92
PorR	427, 560, 602	3.78, 0.58, 0.35	-1.67, -1.97	0.30, 0.40, 0.91	1.97

An energy level diagram including all the compounds is obtained from the electrochemical measurements (Fig. 6.4). The energy levels of the two-electron reaction of the broad first oxidation peak of PorR were assigned to the organic chromophore as the first and the porphyrin part as the second component (determined by spectroelectrochemistry, shown in Appendix Fig. A5). The conduction band edge potential (E_{CB}) of TiO_2 and the electrolyte potential (E_{ele}) are shown as well.

The first reduction potential of PorR originates from the reduction of the organic chromophore. The reduction energy level of Por is closer to the vacuum energy compared to that of CbBTD1. The more negative energy level of the Por than CbTBD1 in PorR suggests that electron transfer from the photoexcited porphyrin to the organic chromophore is possible. When applied in DSSC, this intramolecular electron transfer in PorR may reduce the electron injection efficiency to TiO_2 and consequently reduce the photovoltaic performance.

The first oxidation potential of PorR originates from the oxidation of the organic chromophore. The oxidation energy level of Por is more positive compared to that of CbBTD1. The more positive energy level of the Por than CbTBD1 in PorR suggests that the driving force for dye regeneration is reduced. Moreover, if an intramolecular hole transfer occurred from the porphyrin to the organic chromophore after electron injection, the distance between the injected electrons in the conduction band of TiO_2 and the dye cation would be enlarged, which may lead to long-lived charge separation state. The long-lived charge separation state, in turn, benefits the dye regeneration efficiency and may increase the photovoltaic performance of DSSC if dye regeneration kinetics limited charge transfer.

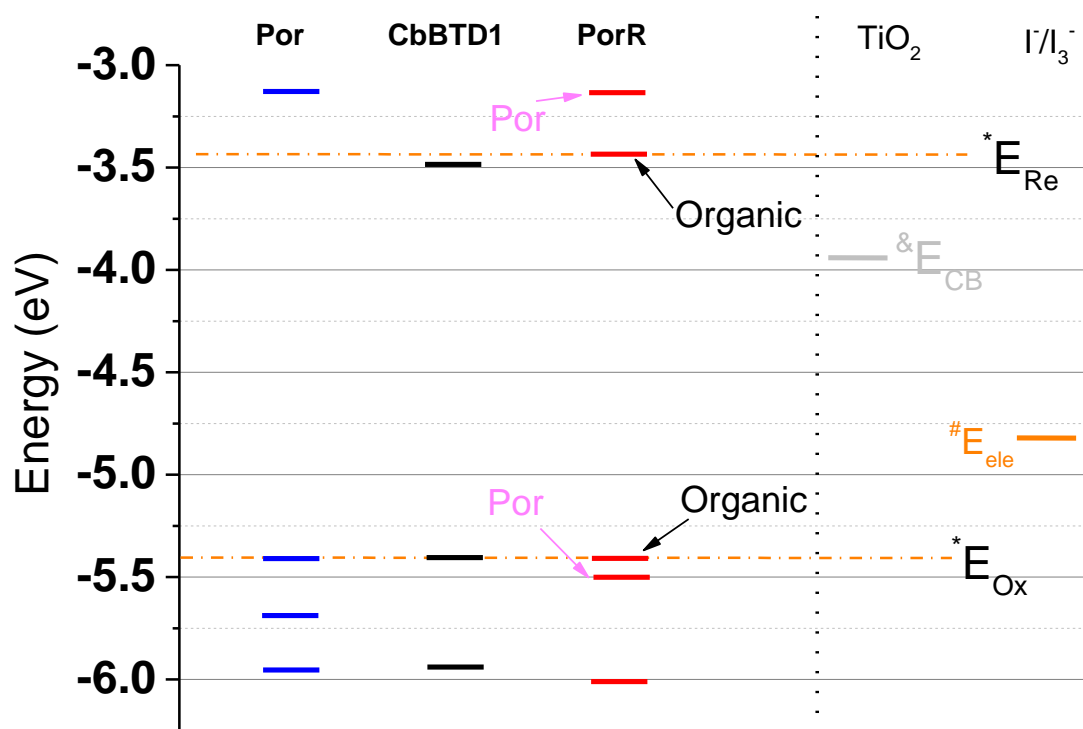


Figure 6.4 Energy level diagram of the compounds.

* The energy levels of oxidation (E_{Ox}) and the energy levels of reduction (E_{Re}) were calculated from the peak potentials of oxidation ($E_{Ox\text{ vs. }Fc/Fc^+}$) and reduction ($E_{Re\text{ vs. }Fc/Fc^+}$) as $E_{Ox} = -(E_{Ox\text{ vs. }Fc/Fc^+} + 5.1)$ (eV) and $E_{Re} = -(E_{Re\text{ vs. }Fc/Fc^+} + 5.1)$ (eV), respectively. The potential of the Fc/Fc^+ redox couple was assumed to be -5.1 eV vs. vacuum⁷. E_{CB} was adopted from Ref.⁸. # The I^-/I_3^- redox couple potential (E_{ele}) was adopted from⁹. Both values of E_{CB} and E_{ele} were calibrated to the absolute energy based on the assumption $E_{Fc/Fc^+} = +0.63$ V vs. NHE.

6.3.3 Decreased photovoltaic performance of DSSC using PorR

The di-chromophoric dye PorR and the two single chromophoric dyes, Por and CbBTD1, were characterized in DSSCs. The current density-voltage ($J-V$) curves comprising the single chromophoric porphyrin Por, the organic dye CbBTD1, and the di-chromophoric porphyrin PorR are shown in Fig. 6.5. The parameters of the photovoltaic performance are listed in Table 6.3.

DSSC using PorR exhibits a photocurrent of 3.22 mA cm^{-2} , which is only half of the DSSCs using the single chromophoric dyes. The photovoltage of DSSC using PorR is 20 mV less than that of Por, while 100 mV larger compared to that of CbBTD1. Fill factors (FF) are slightly varied within the sensitizers. Consequently, DSSC using the di-chromophoric porphyrin PorR shows lower efficiency compared to that of the porphyrin dye Por and the organic dye CbBTD1.

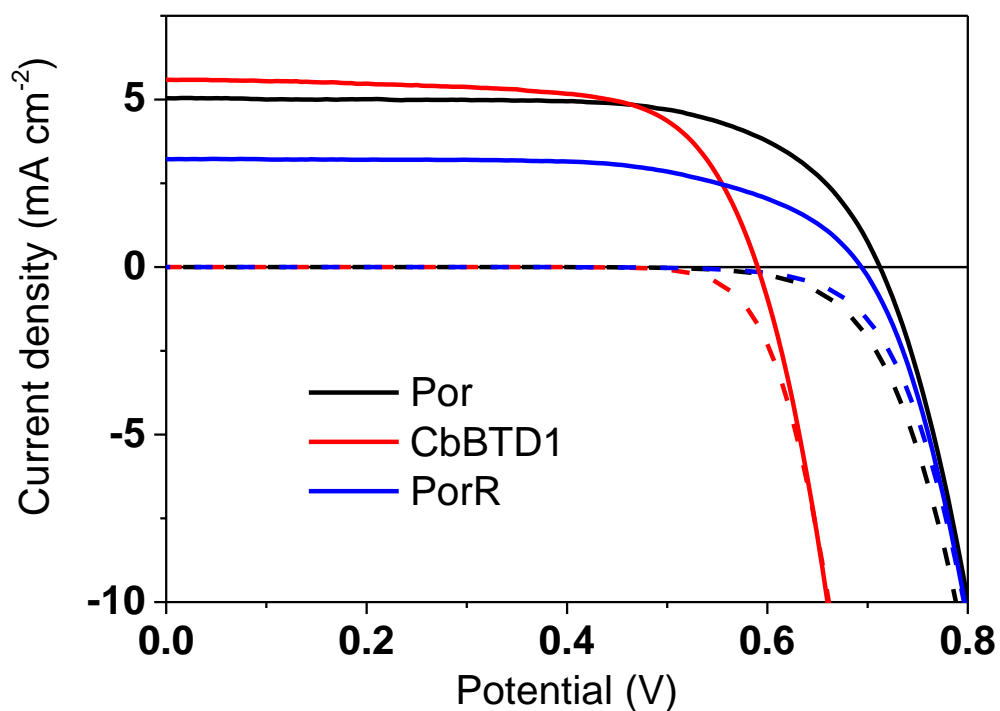


Figure 6.5 Current density-voltage (J-V) curves of DSSCs using the investigated sensitizers under AM 1.5 illumination (solid lines) and in the dark (dashed lines) fabricated with 2.0 ± 0.1 μm thick films.

Table 6.3 Photovoltaic performance of the devices fabricated by the investigated sensitizers

Thickness (μm)	Dye	J_{sc} mA cm^{-2}	V_{oc} mV	FF	η %	Dye loading Γ ($\times 10^{-4} \text{ mol cm}^{-3}$)
2.0	Por	5.04	715	0.66	2.39	1.1
	CbBTD1	5.59	595	0.68	2.25	1.2
	PorR	3.22	695	0.64	1.43	1.3

6.3.4 Analysis of the photocurrent difference

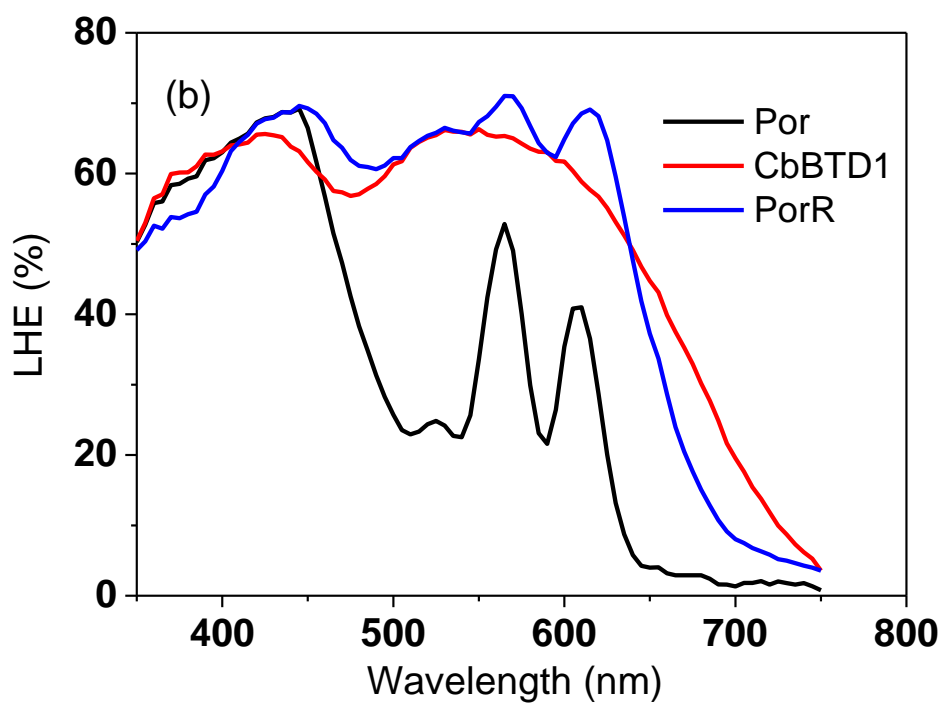
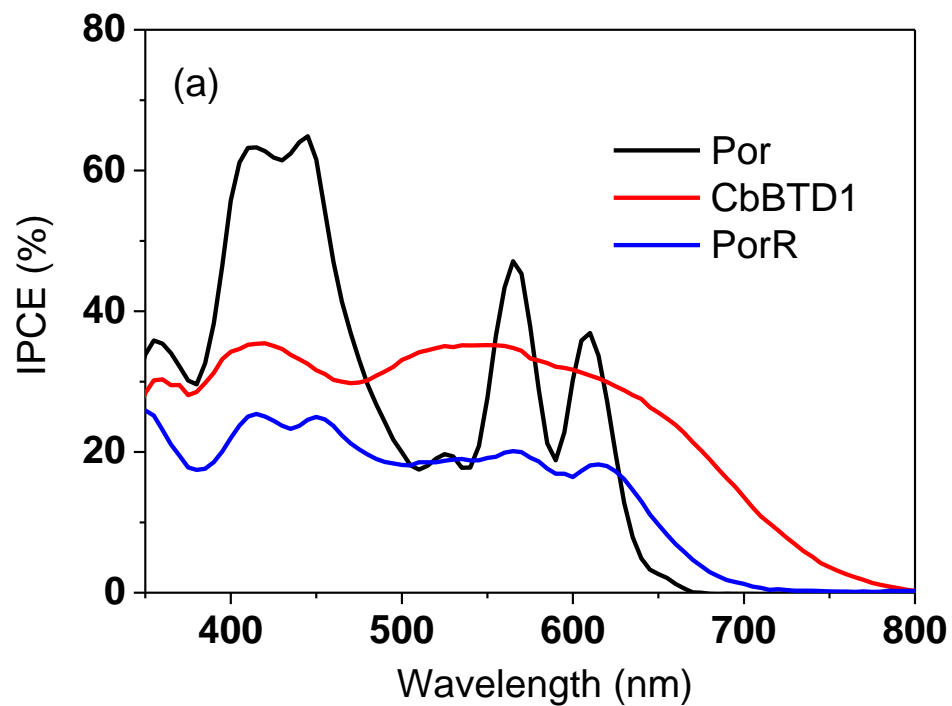
Incident photon-to-current conversion efficiency (IPCE) / light harvesting efficiency (LHE) / absorbed photon-to-current conversion efficiency (APCE) of the DSSCs using Por, CbBTD1, and PorR were recorded on $\sim 2.0\ \mu\text{m}$ films (Figs. 6.6(a)-(c)).

The typical IPCE value of DSSC using PorR is $\sim 20\%$ in the 350-650 nm wavelength region, which is only half compared to that of the organic dye CbBTD1 (Fig. 6.7(a)). The IPCE spectrum of DSSC using PorR terminates at 720 nm, which is 50 nm red-shifted compared to that using Por but 80 nm blue-shifted compared to that using the organic dye CbBTD1.

PorR-sensitized film exhibits enhanced LHE values at the 450-750 nm wavelength range compared to Por-sensitized film (Fig. 6.7(b)). The LHE of PorR-sensitized film decreases sharply after 650 nm, resulting in a narrower spectrum compared to CbBTD1-sensitized films. The differences in the LHE of the individual dyes are not originated from the dye uptake as suggested by the similar dye loading amount in Table 6.3.

DSSCs using PorR shows APCE value of only 30% in the 350-650 nm wavelength region (Fig. 6.7(c)). The reason of the low APCE of DSSC using PorR will be discussed later. DSSC using Por exhibits the highest APCE value, typically 80-90%, in the 400-650 nm wavelength range. DSSC using the organic dye CbBTD1 shows APCE value of 50% in the 400-650 nm wavelength range with a rising tail afterwards.

The results suggest that the reduced photocurrent of DSSC using PorR is due to the limited electron injection efficiency. The light harvesting efficiency of the PorR-sensitized films, on the other hand, is much increased compared to the Por-sensitized films.



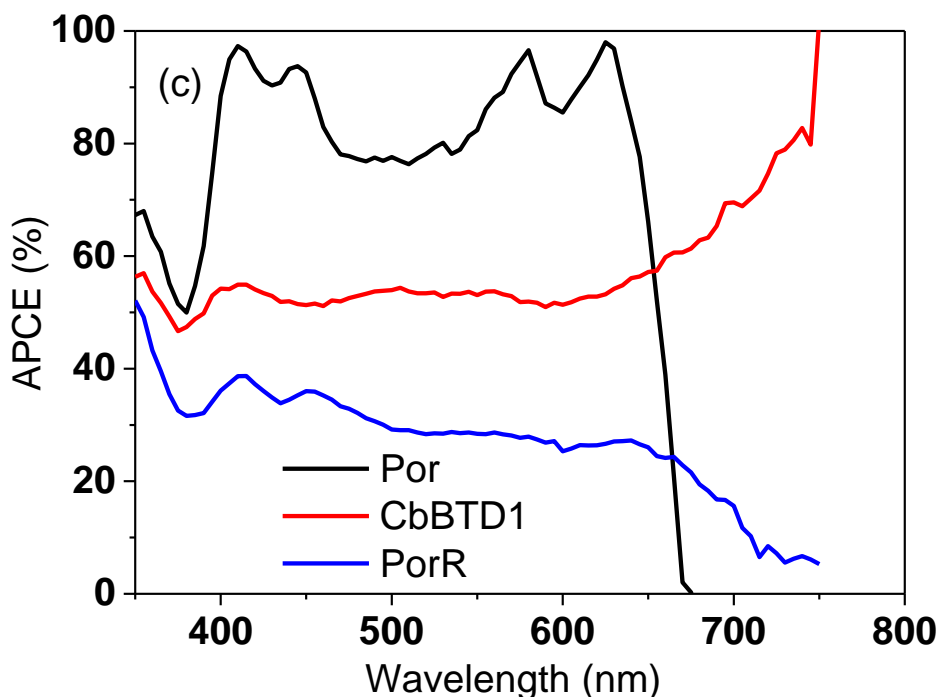


Figure 6.6 (a) Incident photon to converted electron (IPCE), (b) Light harvesting efficiency (LHE) and (c) Absorbed photon to collected electron (APCE) spectra of the DSSCs using the investigated sensitizers on $2.0 \pm 0.1 \mu\text{m}$ films.

6.3.5 Reduced APCE of DSSC using PorR

The charge collection efficiencies of both conditions are nearly uniform as revealed by the diffusion length measurements shown in Appendix Fig. A9. Hence, the less than 100% of APCE is mainly attributed to the electron injection losses.

The electron injection efficiency of the Por DSSC is ~85% while that of the PorR DSSC is 30% (Fig. 6.7(a) and Fig. 6.7(b)). As revealed by the energy level diagram in Fig. 6.4 and the photoluminescence measurements in Chapter 7 Section 7.5, an electron transfer from the excited porphyrin to the organic chromophore is possible in PorR (Fig. 6.7(b)). The photocurrent (3.22 mA cm^{-2}) as well as the APCE value of 30% in the 350-650 nm wavelength range of PorR suggest that the electron injection to TiO_2 and electron transfer to the organic chromophore from the photoexcited porphyrin are two competing processes rather than predominated by one of them.

A hypothesis is therefore raised: the low APCE of DSSC using PorR is mainly due to that the two electron transfer pathways leads to reduced electron injection to TiO_2 .

To check this hypothesis, electrolyte without *tert*-butylpyridine (*t*BP) inside was employed. The downward shifted (positive shifted) conduction band of TiO_2 after

removal of tBP^{10-13} should increase the driving force for electron injection (Fig. 6.7(c)). The driving force for the intramolecular electron transfer from the porphyrin to the organic in PorR should not be affected significantly with change of tBP . Therefore more electrons can be channeled to TiO_2 rather than transfer to the organic chromophore (electron injection efficiency of >30% in Fig. 6.7(c)). Consequently, the photocurrent as well as the IPCE is expected to increase.

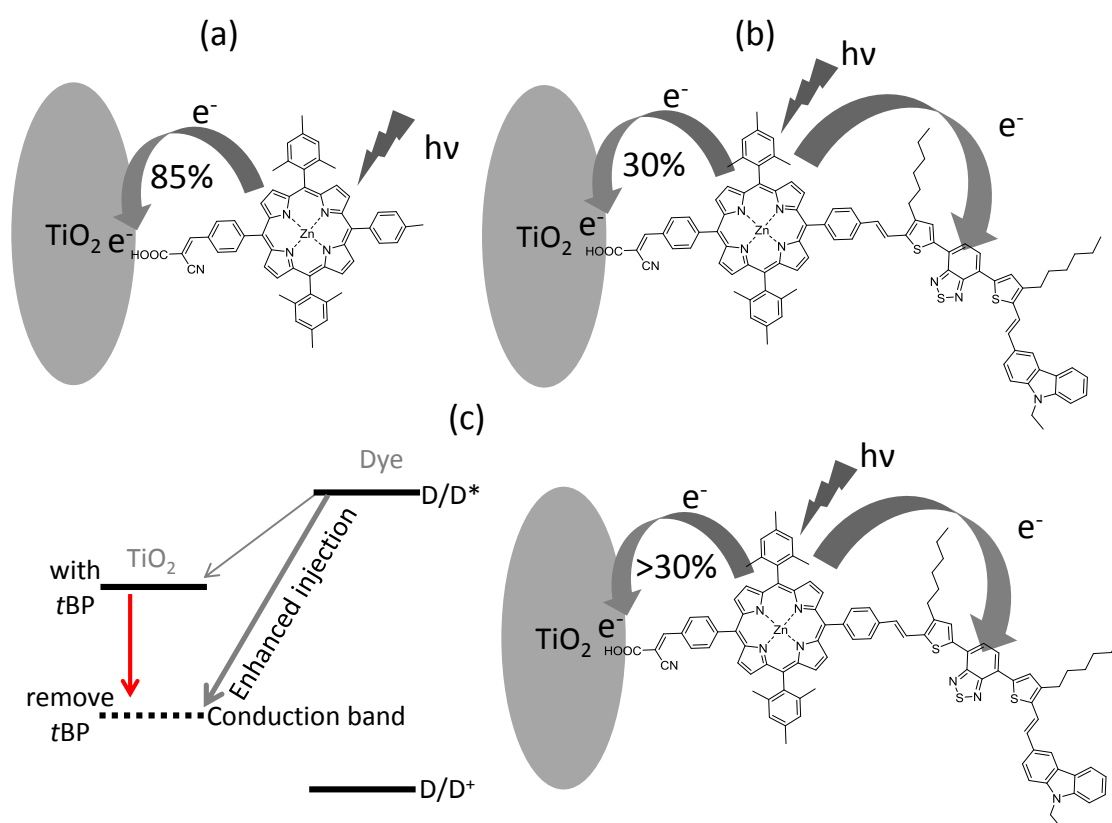


Figure 6.7 Illustration of two competing electron transfer pathways in PorR DSSCs. (a) electron injection efficiency of 85% in Por DSSC; (b) electron injection efficiency of 30% in PorR DSSC since two electron transfer pathways and (c) electron injection efficiency of >30% in PorR DSSC by removal of tBP from the electrolyte.

Figs. 6.8(a) and (b) show the photovoltaic performance and the IPCE curves of DSSCs using PorR, with and without tBP in the electrolyte using thick films ($7.4 \pm 0.5 \mu m$, with $\sim 5 \mu m$ transparent and $\sim 2.5 \mu m$ scattering layers), respectively. The photocurrent and IPCE values are both nearly doubled after removal of tBP . Although decreased open circuit voltage and fill factor are observed, the better power conversion efficiency of 3.7% is obtained using the electrolyte without tBP .

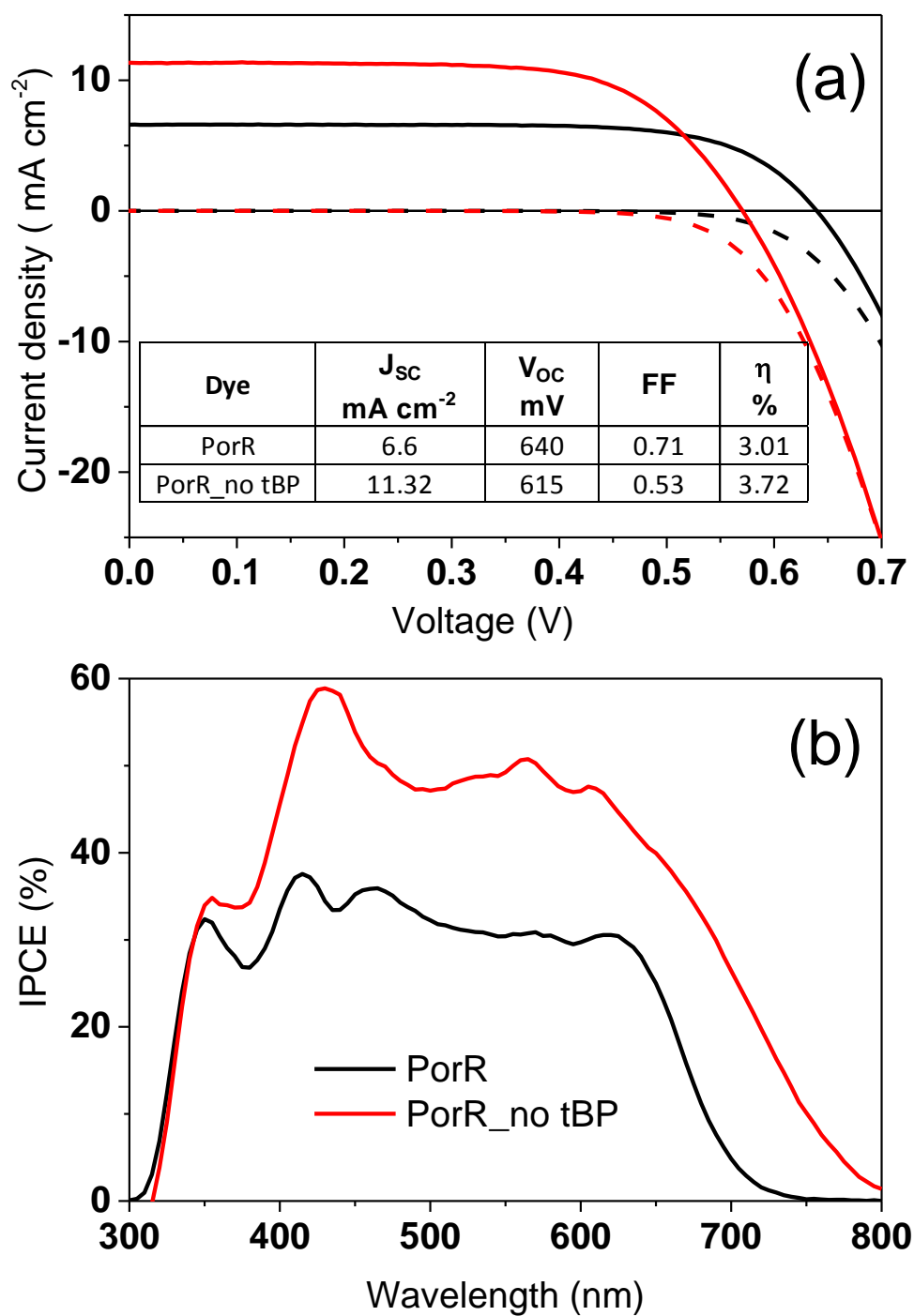


Figure 6.8 (a) Current density-voltage curves and (b) IPCE spectra of DSSCs using PorR using the standard electrolyte and the electrolyte without *t*BP inside fabricated with 7.4 ± 0.5 μm thick films.

The significantly increased photocurrent and IPCE values after omission of *t*BP clearly support the hypothesis that the two electron transfer paths decrease the photocurrent of

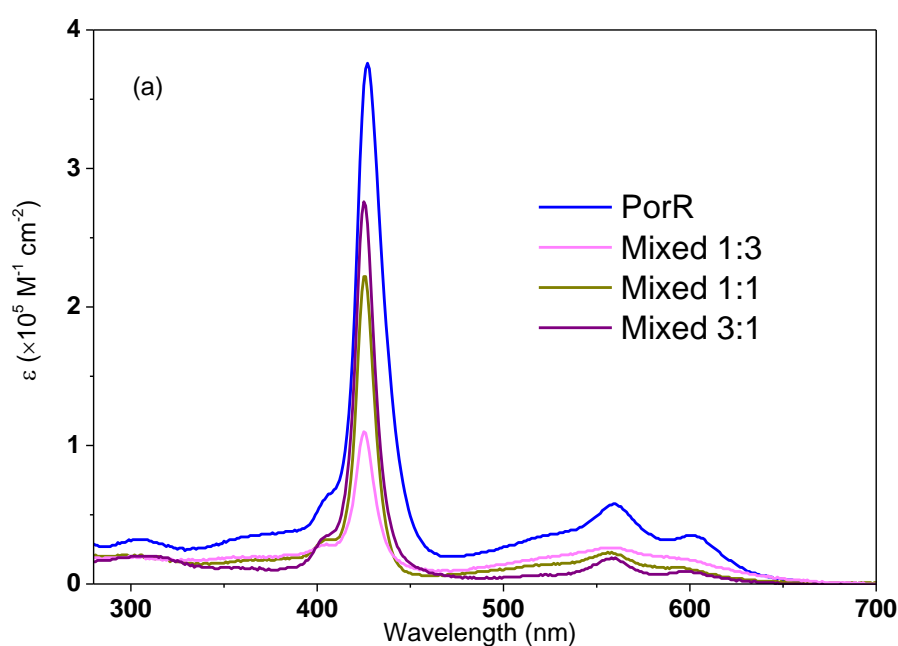
DSSCs using PorR. By enlarging the driving force for the electron injection to TiO_2 , the electron transfer quantum yield at this side is increased.

6.4. Purpose two: a comparison to mixed dyes

6.4.1 Light absorption in solution and on TiO_2 film

Fig. 6.9(a) shows the ε of the di-chromophoric porphyrin PorR and three mixtures of Por and CbBTD1 (1:3, 1:1, 3:1) in THF. The mixed dyes show larger ε values at the Soret band with more Por component in the solution (mixed 3:1>mixed 1:1>mixed 1:3), while they show larger ε values at the Q bands with more CbBTD1 component in the solution (mixed 1:3>mixed 1:1>mixed 3:1). Compared to the di-chromophoric porphyrin PorR, the three dye mixtures show lower molar extinction coefficient values in the 280-650 nm wavelength range.

Fig. 6.9(b) shows the absorption of PorR and the three dye mixtures on TiO_2 films. The di-chromophoric porphyrin PorR exhibits larger absorbance at the Soret band and similar absorbance at the Q bands compared to the mixed 1:1 and the mixed 1:3. With less CbBTD1 in solution and on TiO_2 films (see dye loading in Table 6.5), the mixed 3:1 shows the lowest absorbance at 450-650 nm wavelength range. The absorption of PorR- TiO_2 film terminates at ~ 700 nm, which is 50 nm blue shifted compared to those of the mixed dye- TiO_2 films.



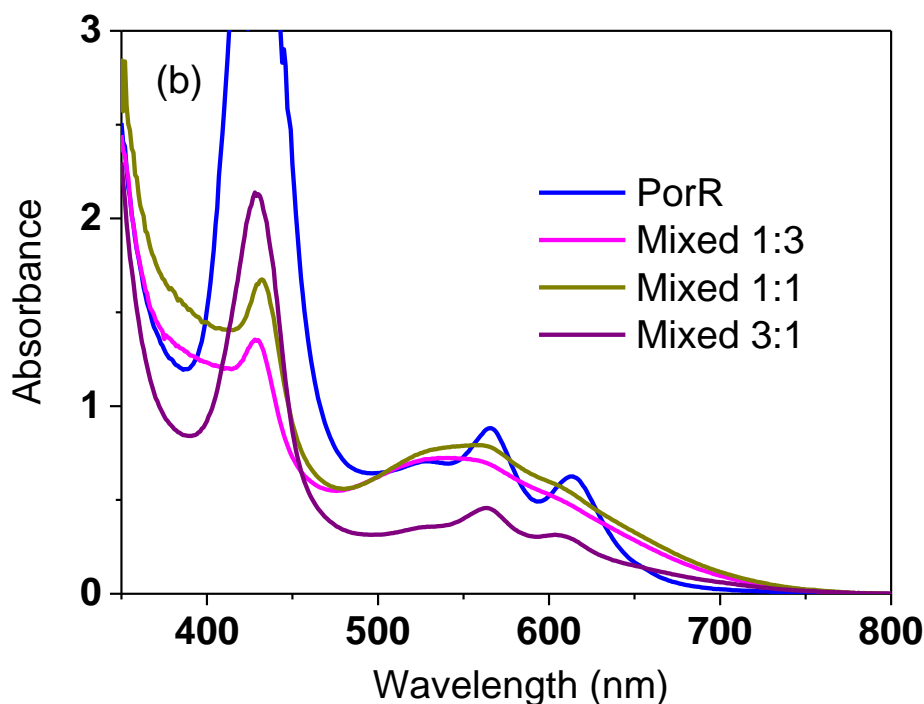


Figure 6.9 (a) Molar extinction coefficient of PorR and the mixed dyes measured in THF and (b) Absorption of the sensitizers on $2.0 \pm 0.1 \mu\text{m}$ TiO_2 films.

6.4.2 Decreased photocurrent but increased photovoltage of DSSC using PorR

The di-chromophoric dye PorR and the three mixed dyes were characterized in DSSCs. The J - V curves comprising the di-chromophoric porphyrin PorR and three mixtures of Por and CbBTD1 are shown in Fig. 6.10. The parameters of the photovoltaic performance are listed in Table 6.5.

The DSSCs using mixed dyes show better performance than that using PorR. The DSSC using mixed 1:3 (Por:CbBTD1) performs the best with the highest J_{SC} of 6.47 mA cm^{-2} , while similar V_{OC} as DSSCs using the other mixtures, yielding a η of 2.63%. The lowest performing DSSC using PorR shows only half of the photocurrent compared to DSSCs using the mixtures.

DSSCs using the mixtures show 80~95 mV lower photovoltage compared to that using the di-chromophoric dye. The remarkably decreased photovoltage of the mix dye DSSCs indicates that the organic sensitizer CbBTD1 limits the photovoltage. As will be explained in Chapter 8, this is due to the organic dye has increased dispersion forces compared to the porphyrin, which attracts I_3^- to the proximity of TiO_2 .

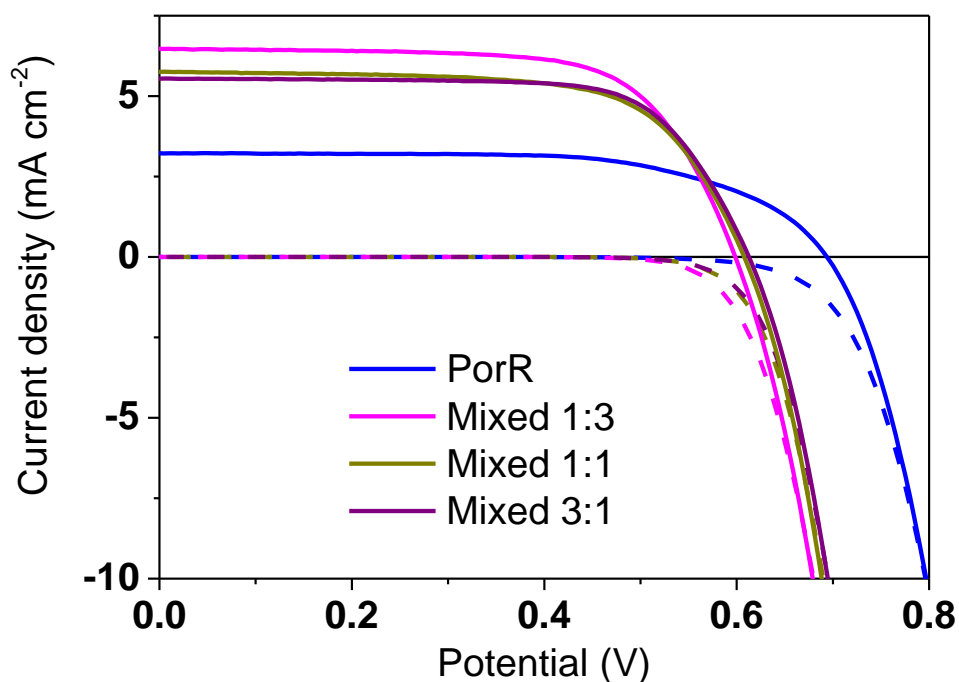


Figure 6.10 Current density-voltage curves of DSSCs using PorR and mixed dyes under AM 1.5 illumination (solid lines) and in the dark (dashed lines) fabricated with 2.0 ± 0.1 μm thick films.

Table 6.4 Photovoltaic performance of the devices fabricated by PorR and mixed dyes

Thickness (μm)	Dye	J_{SC} mA cm^{-2}	V_{OC} mV	FF	η %	Dye loading Γ ($\times 10^{-4} \text{ mol cm}^{-3}$)
2.0	PorR	3.22	695	0.64	1.43	1.3
	Mixed 1:3	6.47	600	0.68	2.63	0.2+1.1
	Mixed 1:1	5.75	610	0.67	2.34	0.3+0.8
	Mixed 3:1	5.54	615	0.71	2.4	0.5+0.4

Note: Dye loading amounts of the mixed dyes are Por+CbBTD1.

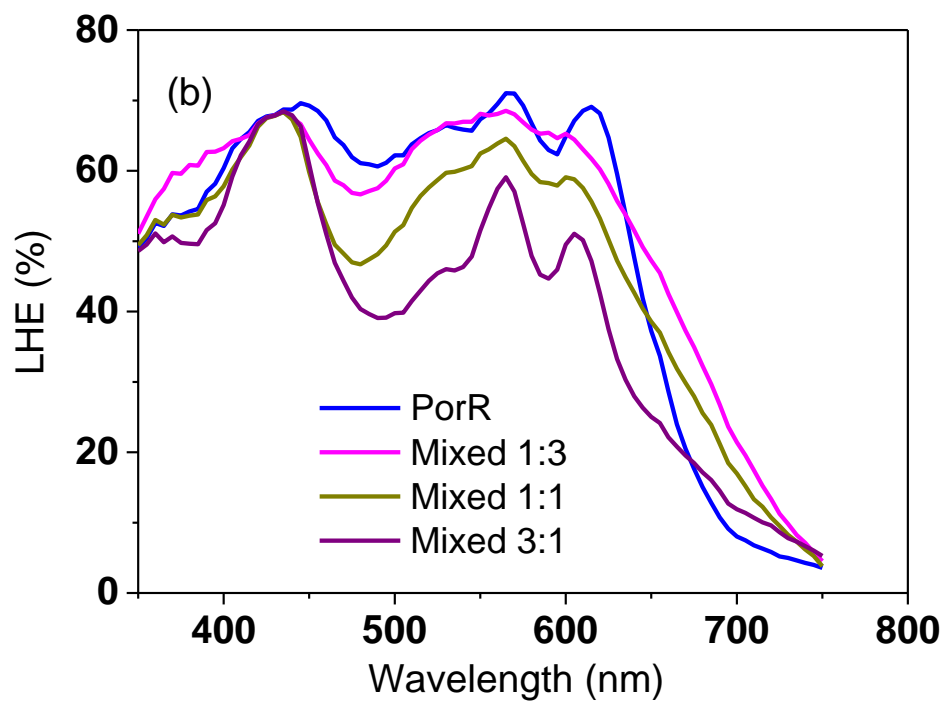
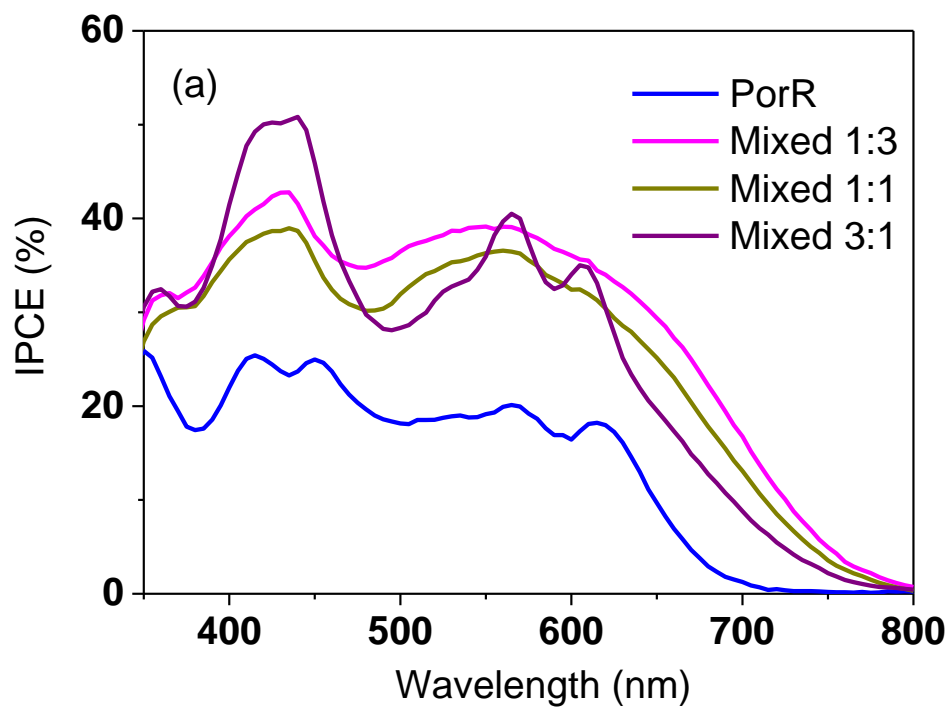
6.4.3 Analysis of the photocurrent difference

Figs. 6.13(a)-(c) show the IPCE / LHE / APCE of DSSCs using PorR and the mixed dyes using ~ 2.0 μm films.

The typical IPCE value of DSSC using PorR (~20%) is only half of that using the mixed dyes in the 350-650 nm wavelength region (Fig. 6.13(a)). The IPCE spectrum of DSSC using PorR terminates at 720 nm, which is 80 nm blue-shifted compared to that using the mixed dyes. The IPCE values within DSSC using the mixed dyes varied with the ratio of the two chromophores. The DSSC using mixed 3:1 (Por:CbBTD1), with more Por in the mixture, shows higher IPCE values at the Soret and Q bands but lower at the wavelengths of 480-540 nm and 620-800 nm compared to that using the mixed 1:1 and 1:3 (Por:CbBTD1).

The LHE values of the mixed dye-sensitized films are less than the PorR-sensitized film at the 450-650 nm wavelength region, while larger at the wavelengths afterwards (Fig. 6.7(b)). The enhanced LHE of PorR-TiO₂ film is mainly contributed to the larger dye loading compared to the mixed dye-TiO₂ film (Table 6.5), suggesting the utility of the di-chromophoric dye using thin photoanodes. The LHE of PorR-sensitized film decreases sharply after 650 nm, resulting in a narrower spectrum compared to mixed dye-sensitized films. Within the mixed dye-sensitized films, the LHE values vary mainly at the 450-750 nm wavelength region, which is assigned to the different amount of the organic dye on TiO₂ films (Table 6.5). The mixed 1:3-sensitized film, with more CbBTD1 on TiO₂ films, shows larger LHE values at the wavelengths after 450 nm compared to the other two mixed dye-sensitized films.

DSSCs using the mixed dyes typically show doubled APCE values of that using PorR in the 350-750 nm wavelength region (Fig. 6.7(c)). Within the mixtures, DSSC using the mixed 3:1 exhibits the highest APCE values of 70%, while DSSCs using the mixed 1:1 and the mixed 1:3 show similar APCE values of 60%. Moreover, the APCE spectra of DSSCs using the mixed 1:3 and the mixed 1:1 are observed a rise feature, while that using PorR shows a decline shape after 650 nm. This may suggest that CbBTD1 in the mixed dyes injects electron into TiO₂, while the organic chromophore in PorR does no photoelectron injection.



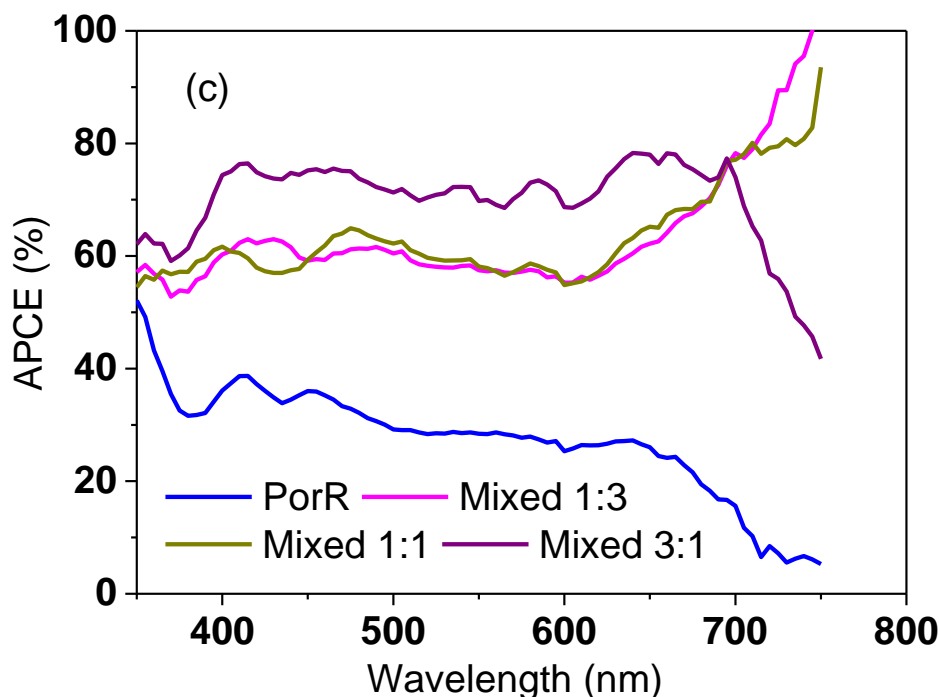


Figure 6.11 (a) Incident photon to converted electron, (b) Light harvesting efficiency and (c) Absorbed photon to collected electron spectra of the DSSCs using PorR and mixed dyes on $2.0 \pm 0.1 \mu\text{m}$ films.

To sum up, DSSC using the di-chromophoric dye showed less photocurrent and power conversion efficiency compared to DSSCs using the mixed dyes. Although the former exhibited larger light harvesting efficiency in most of the visible wavelength ranges due to the larger dye loading on TiO_2 , its electron injection efficiency was significantly reduced due to the two competing electron transfer pathways.

6.5. Analysis of the photovoltage

The open circuit voltage in DSSC using PorR is similar to that using Por but more than 80 mV larger than those using the organic dye and the mixed dyes.

The similar photovoltage of DSSCs using PorR and Por is due to that the blocking effect from the coordination with *t*BP in both conditions which controls the TiO_2 conduction band electrons - I_3^- recombination kinetics. The larger photovoltage of DSSCs using PorR compared to those using mixed dyes is explained by the utilization of dispersion forces that elongates electron lifetime.

The organic chromophore in PorR possesses lower band gap and therefore increases dispersion forces compared to the porphyrin. The stronger dispersion forces between the polarizable organic chromophore and I_3^- attract I_3^- to the organic chromophore where is further away from the TiO_2 surface. The TiO_2 conduction band electrons - I_3^- recombination is hence retarded and the photovoltage is increased. The role of dispersion force in affecting the electron lifetime is further proved by reducing the dye loading of Por and PorR in DSSCs, in which, the photovoltage of DSSC using Por is much more decreased compared to that using PorR.

The utilization of dispersion forces to enhance the photovoltage of DSSC is, for the first time, demonstrated by this work. Detailed experiments and explanations will be discussed in Chapter 8.

6.6. Conclusions

Further extending light absorption of porphyrin to red using the di-chromophoric concept was achieved by covalently linking a carbazole-thiophene benzothiadiazole thiophene organic chromophore to a porphyrin (PorR). Differential pulse voltammetry revealed that the organic chromophore was easier to be oxidized and reduced compared to the porphyrin in the di-chromophoric dye. DSSCs using the di-chromophoric dye, the single chromophoric porphyrin, the organic dye and the mixed dyes were characterized. The origin of the photocurrent differences was investigated by the incident photon-to-current conversion efficiency / light harvesting efficiency / absorbed photon-to-current conversion efficiency measurements. The main findings are:

- 1) DSSC using the di-chromophoric dye achieved similar open circuit voltage as that using the single chromophoric porphyrin but more than 80 mV larger than those using the organic dye and the mixed dyes.
- 2) The light harvesting efficiency of DSSC using the di-chromophoric dye was much higher than that of the single chromophoric porphyrin in the 350-750 nm wavelength range.
- 3) The low photocurrent of DSSC using PorR was because of the two competing electron transfer pathways at the di-chromophoric dye-sensitized TiO_2 film interface. The electron transfer from the photoexcited porphyrin to the organic chromophore decreases the electron injection efficiency to TiO_2 .

- 4) DSSC using the di-chromophoric dye showed larger light harvesting efficiency values at the 450-650 nm wavelength range as compared to those of the mixed dyes due to the larger dye loading on TiO₂, suggesting the utility of di-chromophoric dye using thin films.
- 5) DSSC using the di-chromophoric dye showed only half of power conversion efficiency compared to DSSCs using the mixed dyes.

6.7. References

- (1) Hsieh, C.-P.; Lu, H.-P.; Chiu, C.-L.; Lee, C.-W.; Chuang, S.-H.; Mai, C.-L.; Yen, W.-N.; Hsu, S.-J.; Diau, E. W.-G.; Yeh, C.-Y. *J. Mater. Chem.* **2010**, *20*, 1127.
- (2) Wang, C.-L.; Chang, Y.-C.; Lan, C.-M.; Lo, C.-F.; Diau, E. W.-G.; Lin, C.-Y. *Energy Environ. Sci.* **2011**, *4*, 1788.
- (3) Giraudeau, A.; Callot, H. J.; Gross, M. *Inorg. Chem.* **1979**, *18*, 201.
- (4) Koumura, N.; Wang, Z.-S.; Mori, S.; Miyashita, M.; Suzuki, E.; Hara, K. *J. Am. Chem. Soc.* **2006**, *128*, 14256.
- (5) Wu, S.-L.; Lu, H.-P.; Yu, H.-T.; Chuang, S.-H.; Chiu, C.-L.; Lee, C.-W.; Diau, E. W.-G.; Yeh, C.-Y. *Energy Environ. Sci.* **2010**, *3*, 949.
- (6) Ehret, A.; Stuhl, L.; Spitler, M. T. *J. Phys. Chem. B* **2001**, *105*, 9960.
- (7) Cid, J.-J.; Yum, J.-H.; Jang, S.-R.; Nazeeruddin, M. K.; Martínez-Ferrero, E.; Palomares, E.; Ko, J.; Grätzel, M.; Torres, T. *Angew. Chem. Int. Ed.* **2007**, *46*, 8358.
- (8) Funaki, T.; Koumura, N.; Sayama, K. *Chem. Lett.* **2013**, *42*, 1371.
- (9) Sun, X.; Wang, Y.; Li, X.; Agren, H.; Zhu, W.; Tian, H.; Xie, Y. *Chem. Commun.* **2014**, *50*, 15609.
- (10) Chang, S.; Wang, H.; Lee, L. T. L.; Zheng, S.; Li, Q.; Wong, K. Y.; Wong, W.-K.; Zhu, X.; Wong, W.-Y.; Xiao, X.; Chen, T. *Journal of Materials Chemistry C* **2014**, *2*, 3521.
- (11) Kang, M. S.; Kang, S. H.; Kim, S. G.; Choi, I. T.; Ryu, J. H.; Ju, M. J.; Cho, D.; Lee, J. Y.; Kim, H. K. *Chem. Commun.* **2012**, *48*, 9349.
- (12) Kang, S. H.; Choi, I. T.; Kang, M. S.; Eom, Y. K.; Ju, M. J.; Hong, J. Y.; Kang, H. S.; Kim, H. K. *J. Mater. Chem. A* **2013**, *1*, 3977.

- (13) Clifford, J. N.; Martinez-Ferrero, E.; Viterisi, A.; Palomares, E. *Chem. Soc. Rev.* **2011**, *40*, 1635.
- (14) Ogura, R. Y.; Nakane, S.; Morooka, M.; Orihashi, M.; Suzuki, Y.; Noda, K. *Appl. Phys. Lett.* **2009**, *94*, 073308.
- (15) Wu, H.-P.; Ou, Z.-W.; Pan, T.-Y.; Lan, C.-M.; Huang, W.-K.; Lee, H.-W.; Reddy, N. M.; Chen, C.-T.; Chao, W.-S.; Yeh, C.-Y.; Diau, E. W.-G. *Energy Environ. Sci.* **2012**, *5*, 9843.
- (16) Matthew, J. G.; Attila, J. M.; George, T.; Ying, D.; Pawel, W.; Klaudia, W.; Gordon, G. W.; Shogo, M.; David, L. O. *Appl. Phys. Lett.* **2011**, *98*, 163502.
- (17) Wang, Y.; Chen, B.; Wu, W.; Li, X.; Zhu, W.; Tian, H.; Xie, Y. *Angew. Chem. Int. Ed.* **2014**, *53*, 10779.
- (18) Yella, A.; Lee, H.-W.; Tsao, H. N.; Yi, C.; Chandiran, A. K.; Nazeeruddin, M. K.; Diau, E. W.-G.; Yeh, C.-Y.; Zakeeruddin, S. M.; Grätzel, M. *Science* **2011**, *334*, 629.
- (19) Li, L.-L.; Diau, E. W.-G. *Chem. Soc. Rev.* **2013**, *42*, 291.
- (20) Ogomi, Y.; Pandey, S. S.; Kimura, S.; Hayase, S. *Thin Solid Films* **2010**, *519*, 1087.
- (21) Magne, C.; Urien, M.; Pauporte, T. *RSC Advances* **2013**, *3*, 6315.
- (22) Siegers, C.; Hohl-Ebinger, J.; Zimmermann, B.; Würfel, U.; Mülhaupt, R.; Hinsch, A.; Haag, R. *ChemPhysChem* **2007**, *8*, 1548.
- (23) Odobel, F.; Pellegrin, Y.; Warnan, J. *Energy Environ. Sci.* **2013**, *6*, 2041.
- (24) Bessho, T.; Zakeeruddin, S. M.; Yeh, C. Y.; Diau, E. W. G.; Grätzel, M. *Angew. Chem. Int. Ed.* **2010**, *49*, 6646.
- (25) Hardin, B. E.; Snaith, H. J.; McGehee, M. D. *Nature Photon.* **2012**, *6*, 162.
- (26) Marinado, T.; Nonomura, K.; Nissfolk, J.; Karlsson, M. K.; Hagberg, D. P.; Sun, L.; Mori, S.; Hagfeldt, A. *Langmuir* **2009**, *26*, 2592.

**CHAPTER 7. PHOTOLUMINESCENCE STUDIES OF DI-CHROMOPHORIC
PORPHYRIN DYES**

7.1. Introduction

This chapter focuses on steady-state photoluminescence spectroscopy of the PorY, PorO and PorR dyes in solution to examine photoinduced energy / electron transfer pathways. These measurements aid the understanding of charge generation mechanisms in dye-sensitized solar cells using di-chromophoric dyes.

Energy and electron transfer:

The theory of Förster resonance energy transfer (or fluorescence resonance energy transfer, FRET) and electron transfer has been described in Chapter 1 Section 1.9. The efficiency or quantum yield of FRET depends on the distance between energy donor and acceptor to the sixth power. Another key requirement for efficient FRET is that the emission spectrum of the donor must overlap with the absorption spectrum of the acceptor.¹⁻³ The energy transfer is dipole induced interaction, therefore, unlike electron transfer, the electron orbitals of the energy donor and the acceptor do not need to overlap. Instead, the transition dipoles for emission / photoexcitation need to align.

Photoinduced electron transfer, affected by the overlap of electronic wave functions on the donor and acceptor is a short range interaction, exponentially dependent on distance.⁴ Electron transfer is more effective at shorter distances compared to energy transfer. A key requirement for charge transfer is the driving force for charge transfer, i.e. the offset of the redox potential of the first excited state (approximated by the lowest unoccupied molecular orbital energy, LUMO) between the donor and the acceptor, or the offset of the oxidation potential of the first excited state (approximated by the highest occupied molecular orbital energy, HOMO), as illustrated in Chapter 1 Fig. 1.5. In the di-chromophoric dyes examined here, this is approximated by the difference between the first reduction and oxidation potentials of the porphyrin part and the additional chromophore for electron and hole transfer, respectively.

The efficiency of energy / electron transfer in a di-chromophoric dye can affect the electron injection efficiency when the second chromophore (further away from the TiO₂ surface) is photoexcited. An illustration of an energy / electron transfer cascade at the di-chromophoric dye/TiO₂ interface is shown in Fig. 7.1(a) (both D1 and D2 are chromophores). When D2 is selectively photoexcited to D2*, the excitation energy can be transferred to D1 (form D1*) by an energy transfer. Alternatively, the exciton may dissociate to create D1^{•-} and the cation radical D2^{•+}. In the next step, D1* may inject an

electron to TiO_2 before it can, radiatively or nonradiatively, relax to the ground state. Alternatively, $\text{D1}^{\bullet-}$ may transfer its electron to TiO_2 before it recombines with $\text{D2}^{\bullet+}$. An interesting case is the one when the direction of energy or electron transfer is reversed due to change in overlap of photoluminescence and absorption spectra or change in the driving force for electron transfer, as is the case for PorR which has a lower band gap chromophore attached to the porphyrin. In this case, energy and electron transfer from D1^* to D2 may decrease the electron injection yield from D1^* to TiO_2 conduction band due to a kinetic competition between the two “opposite” pathways.

Characterization techniques:

Typically, femto to picosecond time-resolved transient absorption or photoluminescence lifetime studies are required to identify the dominating mechanism and their timescale.⁵⁻

¹¹ Such specialized facilities were not available for this thesis. Steady state photoluminescence measurements at various excitation wavelengths selectively exciting the two different chromophores within the di-chromophoric dyes are employed. Both energy and electron transfer are expected to quench the photoluminescence of the donor chromophore D2 . In the case of energy transfer, increased photoluminescence of the D1^* is expected due to the increased concentration of D1^* through the energy transfer pathway. Electron transfer, on the other hand, is not expected to increase photoluminescence intensity of D1^* . Recombination of $\text{D1}^{\bullet-}$ and $\text{D2}^{\bullet+}$ may lead to photoluminescence with a strong charge transfer characteristics, i.e. weak and broad emission features, typically lower in energy than the emissions of the constituting chromophores.

As explained in Chapter 1 Section 1.8.3, absorbed photon-to-current conversion efficiency (APCE) measurements coupled with charge extraction measurements can yield information on injection quantum yield in an operational DSSC. These measurements are relatively straightforward and used frequently in this thesis. Typically, thin TiO_2 films are used to ensure close to 100% charge collection yield. Under these conditions, it is expected that <100% energy or electron transfer yield will lead to lower APCE values at wavelength where the second chromophore is selectively photoexcited. Assuming that the quantum yield for energy transfer from D2^* to D1 is φ_a and injection yield for electron transfer from D1^* to the conduction band of TiO_2 is φ_b , APCE values at wavelength range of photon absorption of D1 will equal φ_b , while for

the wavelength range corresponding to photon absorption by D2 will equal $\phi_a \times \phi_b$ (Fig. 7.1(b)). A similar diagram for electron transfer from D2* to D1 can be drawn with the modification that injection yield from D1* to TiO₂ conduction band could be different from the injection yield of D1* to TiO₂ conduction band.¹²

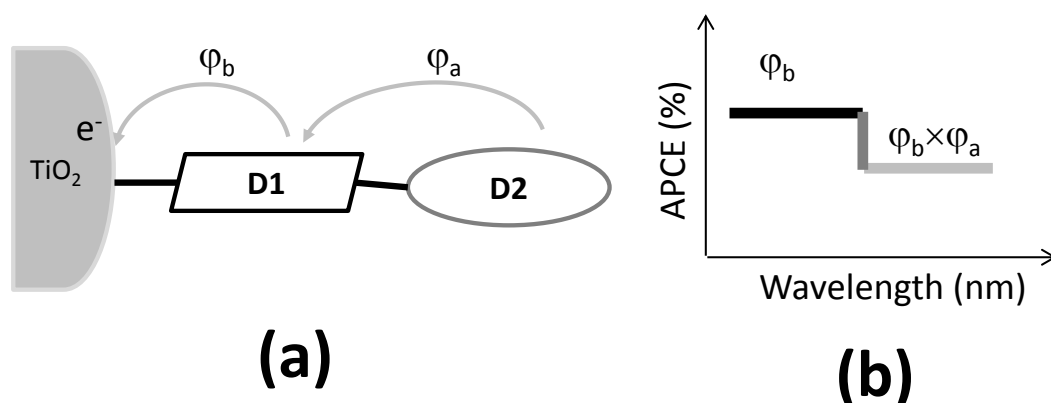


Figure 7.1 Illustration of (a) energy transfer from D2* to D1 and (b) the effect on absorbed photon-to-current conversion efficiency of a di-chromophoric dye-sensitized solar cell.

In the first part of this chapter, steady state photoluminescence (PL) spectroscopy measurement is employed to investigate the possibility of energy / electron transfer pathways in di-chromophoric dyes in solution. Following Fig. 7.1, D1 is a porphyrin, while D2 is one of carbazole chromophores (the PorY dyes), carbazole-fused thiophene chromophores (the PorO dyes) and carbazole-thiophene benzothiadiazole thiophene chromophore (PorR), linked by a phenylethynyl unit (structures in Table 7.1). By changing the excitation wavelength either the chromophores are both excited or are selectively excited: 280 nm to excite the porphyrin and all the organic chromophores; 480 nm to excite the organic chromophores in PorY and PorR dyes and 560 nm to excite the porphyrin and the organic chromophore in PorR. The emission spectra are analysed in terms of spectral changes, quenching or enhancement of photoluminescence bands attributed to the constituting chromophores. Possible energy and / or electron transfer paths are discussed using energy diagrams obtained by differential pulse voltammetry.

In the second part of the chapter, APCE spectra of DSSCs prepared by the same di-chromophoric dyes are analysed and the efficiency of charge photogeneration from D2

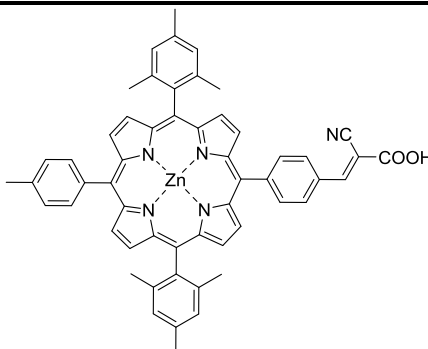
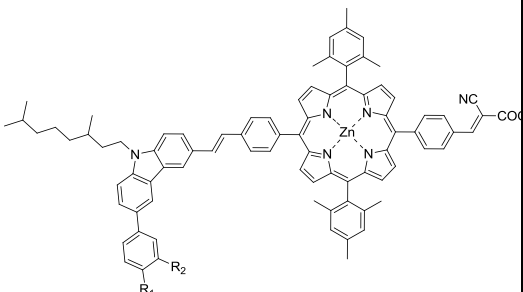
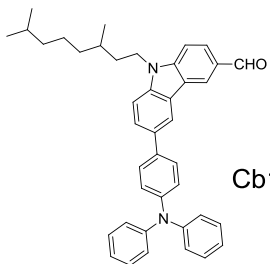
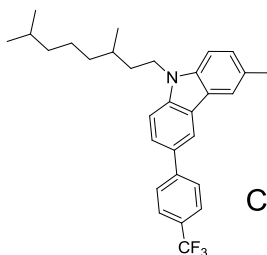
and D1 chromophores is discussed as the band gap of D2 is tuned to lower energies from PorY to PorR.

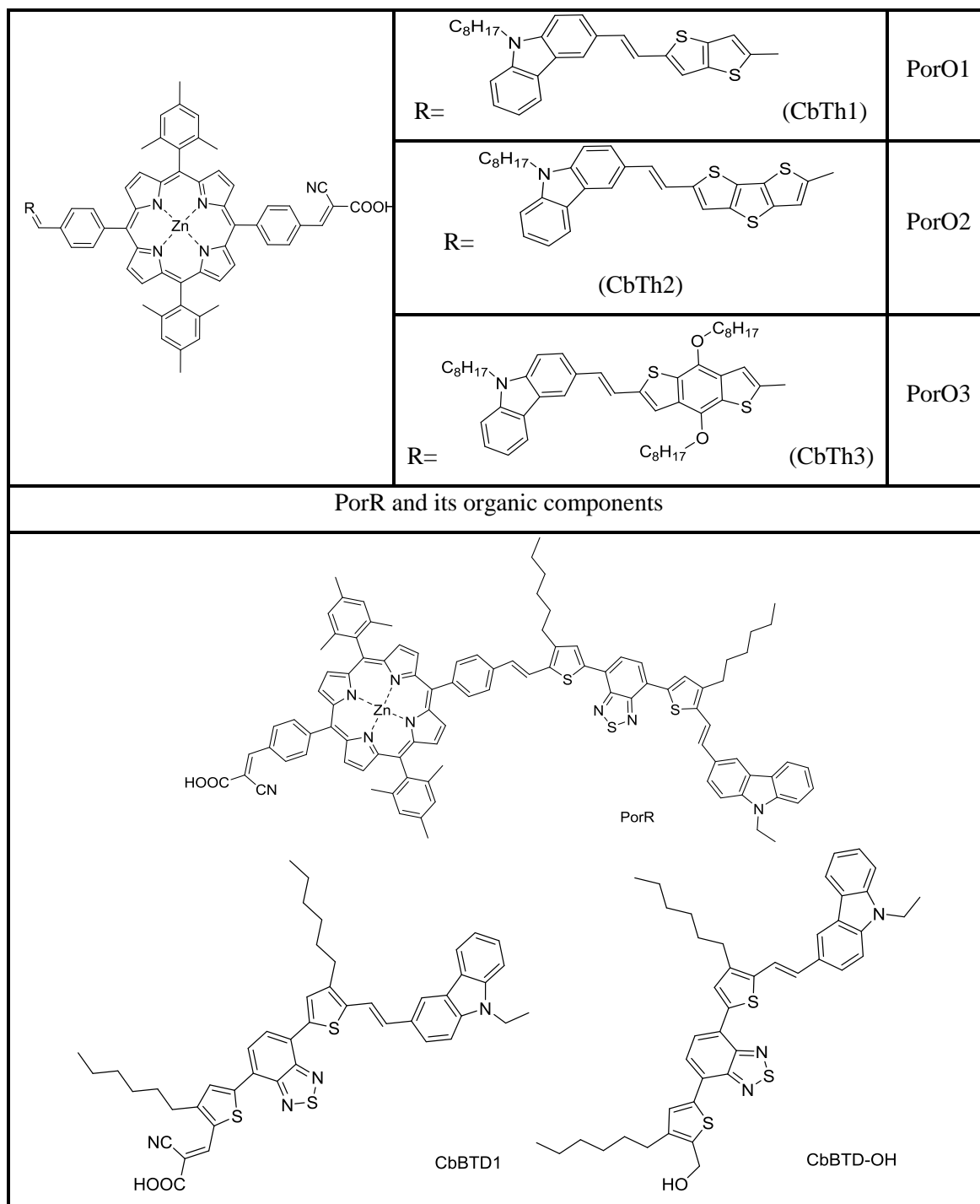
7.2. Experimental

7.2.1 Investigated molecules

The structures of Por, the PorY dyes, the PorO dyes, PorR and the organic chromophores are displayed in Table 7.1.

Table 7.1 Molecular structures of the compounds

Por						
						
The PorY dyes and their organic components						
	Nam	PorY	PorY	PorY	PorY	
	e	1	2	3	4	5
	R1	Ph ₂ N	CF ₃	Me	MeO	H
	R2	H	H	H	H	CF ₃
	Cb1					
						
Cb2						
The PorO dyes and their organic components (to be continued)						



7.2.2 Spectroscopic characterization

UV-visible (UV-vis) absorption spectroscopy and photoluminescence spectroscopy were performed in solution using the procedure described in Chapter 2. Dimethylformamide (DMF) was employed as the solvent for the PorY and PorO dyes and their organic components, and tetrahydrofuran (THF) was used for PorR and its

organic component. All the measurements were carried out using 1 cm length Quartz cuvettes and 1 μ M solutions.

7.3. Energy levels of the investigated compounds

The energy levels of all the di-chromophoric dyes (as well as the constituent chromophores) obtained from the peak potentials of differential pulse voltammograms are shown in Fig. 7.2. These results were presented in Chapters 4, 5 and 6 but collected here again for ease of comparison. The organic chromophores could not be reduced in the measured potential window. Instead, the excited state reduction potentials were estimated from the onset of the absorption spectrum and the oxidation potentials.

The organic chromophores in the PorY and PorO dyes possess more negative first reduction potentials and similar first oxidation potentials in respect to Por. The band gaps of these chromophores are larger as compared to the porphyrin chromophore band gap. As will be shown, the photoluminescence from the organic chromophore overlaps with the absorption of the porphyrin. Therefore, both electron and energy transfer from the photoexcited organic chromophore to the porphyrin in the PorY dyes and the PorO dyes are feasible.

Organic chromophore represented here by the structurally similar (CbBTD-OH) in PorR has a more positive first reduction potential and a similar first oxidation potential. Consequently it has lower energy band gap as compared to the porphyrin. As will be shown, emission of the porphyrin overlaps with the absorption of the organic chromophore. Therefore, both electron and energy transfer from the porphyrin to the organic chromophore in PorR are feasible. This is opposite to the direction of possible energy / electron transfer in PorY and PorO dyes.

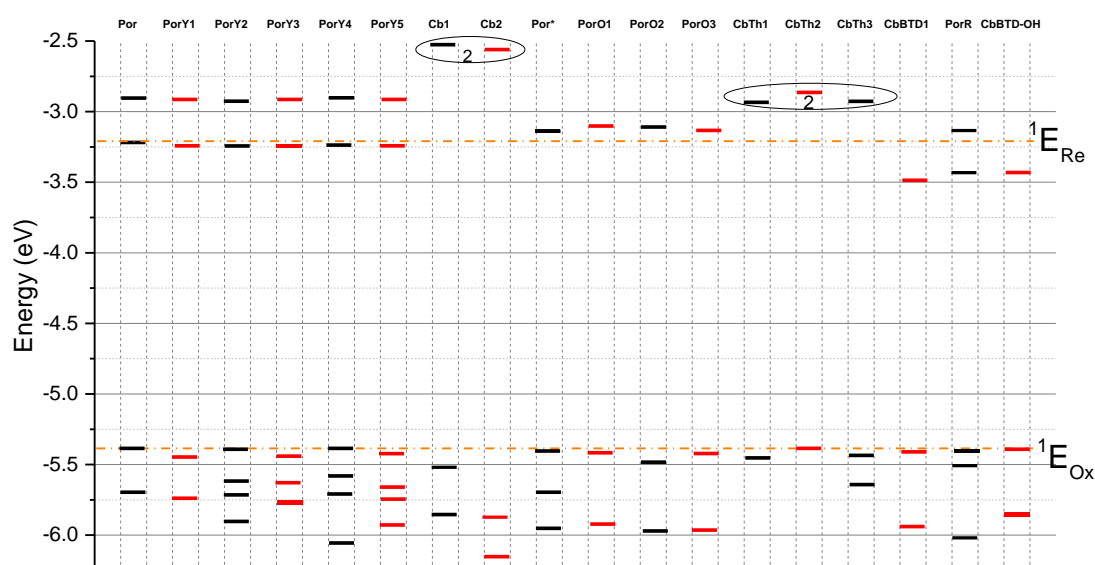


Figure 7.2 Energy level diagram of the compounds derived from the peak potentials of differential pulse voltammograms.

From left to right: Por to Cb2 were measured in dichloromethane; Por* to CbBTD-OH were measured in dimethylformamide.¹ The energy levels of oxidation (E_{Ox}) and the energy levels of reduction (E_{Re}) were calculated from the peak potentials of oxidation ($E_{Ox \text{ vs. } Fc/Fc^+}$) and reduction ($E_{Re \text{ vs. } Fc/Fc^+}$) as $E_{Ox} = -(E_{Ox \text{ vs. } Fc/Fc^+} + 5.1)$ (eV) and $E_{Re} = -(E_{Re \text{ vs. } Fc/Fc^+} + 5.1)$ (eV), respectively. The potential of the Fc/Fc^+ redox couple was assumed to be -5.1 eV vs. vacuum¹³.² Energy levels calculated from UV-vis absorption spectra by the equation $E_{Re} = \Delta E + E_{Ox}$, where the band gap (ΔE) can get from the absorption of onset wavelength (λ_{onset}) by the equation $\Delta E = 1243/\lambda_{onset}$.

7.4. Photoluminescence studies of PorY / PorO dyes: energy transfer from the organic chromophore to the porphyrin

7.4.1 PorY dyes

UV-vis absorption spectra of Por, Cb1, Cb2, PorY1 and PorY2 dissolved in DMF are shown in Fig. 7.3(a) and (c). The photoluminescence (PL) spectra obtained by photoexcitation at 280 nm using the same concentration solutions are shown in Fig. 7.3(b) and (d). At this wavelength, both porphyrin part and carbazole chromophores are photoexcited. The absorbance values of Por, Cb1, Cb2, PorY1 and PorY2 at 280 nm are 0.029, 0.055, 0.022, 0.071 and 0.044, respectively (Fig. 7.3(a) and (c)).

Photoexcitation of Por leads to two PL bands between 570 nm and 700 nm (Fig. 7.3(b)). These bands are assigned to the radiative decay from the porphyrin S_1 to the ground state S_0 . Such a spectrum is characteristic of a Zn porphyrin chromophore as reported in literature.^{14,15} Cb1 contains an electron donating group triphenylamine (TPA),

covalently linked to the carbazole unit. The emission peak of Cb1 is at 530 nm. Cb2, with an electron withdrawing group CF_3 attached on the carbazole moiety, shows strong emission bands at the 350-480 nm wavelength range, which is ~ 150 nm blue-shifted compared to Cb1. Moreover, the PL intensity of Cb2 is ten times higher compared to that of Cb1. The emissions from the porphyrin and the carbazole moieties are clearly separated in terms of wavelength region of the bands.

Photoexcitation of PorY1 leads to weak PL bands at 350-480 nm with peak intensity value of 0.05×10^5 CPS assigned to the emission of the Cb-TPA unit (Fig. 7.3(d)). In addition, relatively strong bands with peak intensity value of 1.4×10^5 CPS at 600-700 nm assigned to the emission from the porphyrin are observed. PorY2 shows similar PL spectrum as PorY1, but with higher peak intensity value of 0.25×10^5 CPS at 350-480 nm and lower peak intensity value of 1.2×10^5 CPS at 600-700 nm.

The photoluminescence spectra of both Cb1 and Cb2 (440-650 nm and 350-480 nm, respectively) have overlap with the absorption spectrum of the Q bands and the Soret band of the porphyrin, respectively. This suggests that FRET is possible. The photoluminescence intensities of both PorY1 and PorY2 photoexcited at 280 nm and emission measured at 400 nm are reduced by five times compared to that of the Cb1 and Cb2. This is partially due to absorption of the porphyrin ($\sim 6\%$ of light is absorbed at 400 nm using the absorbance value of 0.025 of both PorY1 and PorY2). The absorption of Cb1 and Cb2 at 400 nm is negligible. The significantly reduced emission of the carbazole chromophore in PorY1 and PorY2 suggests the energy and / or electron transfer is operating, however, with not 100% efficiency since emissions from carbazole chromophore in PorY1 and PorY2 are still observed.

Photoluminescence of the porphyrin in the 600-700 nm wavelength range in both of photoexcited PorY1 and PorY2 show four times increased intensity as compared to Por, with slightly shifted peak wavelengths. A significant percentage (75% and 50% in PorY1 and PorY2, respectively) of the photons at 280nm wavelength is absorbed by the carbazole chromophore. Because of this, the concentration of photoexcited porphyrin, promptly generated at 280 nm, is expected to be lower in PorY1 and PorY2 as compared to that in Por. The increased PL intensity suggests energy transfer is a more reasonable mechanism for the quenched Cb1 and Cb2 emissions than electron transfer.

However, these steady state PL measurements do not provide a definitive evidence that energy transfer is operating.

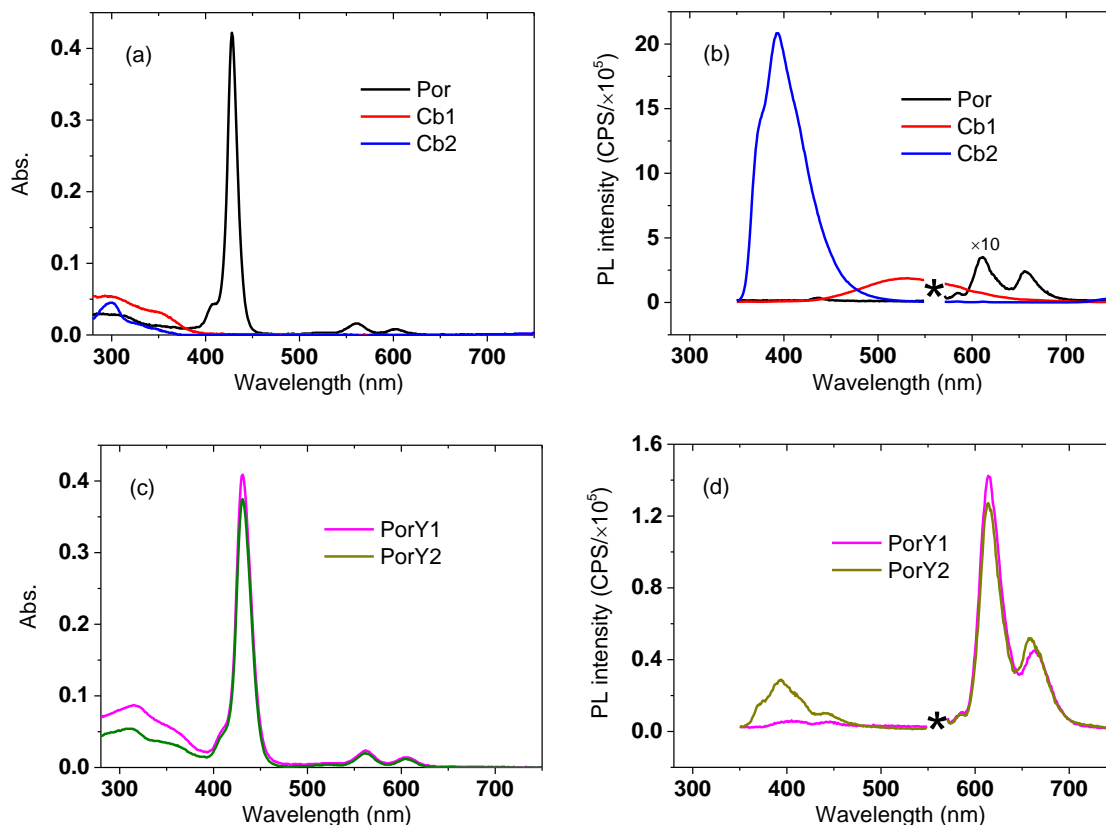


Figure 7.3 Absorbance (Abs.) of (a) Por, Cb1, Cb2 and (c) and PorY1, PorY2 and photoluminescence (PL) spectra of (b) Por, Cb1, Cb2 and (d) PorY1, PorY2 in DMF with 1 μ M concentration.

Excitation wavelength for PL: 280 nm. The PL intensity of Por in (b) was multiplied by 10. The second harmonic of the excitation wavelength at 560 nm was deleted (indicated by a star) from the spectra.

The photoluminescence spectra of the remaining dyes in the PorY series, namely PorY3-5 were also measured (Appendix Fig. A6). When photoexcited at both 280 nm and 560 nm, PorY3-5 in solution show very similar spectrum to PorY2. Within the PorY series, the substitution on the carbazole chromophore is varied with the aim of tuning the energy levels of the chromophore, as illustrated in Table 7.1. As discussed in Chapter 4, the effect of carbazole substitution did not affect the energy levels of the porphyrin because of the lack of significant electronic communication through the phenylethenyl linker. Analysis of PorY3-5 spectra did not yield any significant new

insight: quenched photoluminescence of the carbazole and enhanced emission (three times higher intensity) at wavelengths assigned to the porphyrin emission is observed, similarly to the case of PorY2. This suggests energy transfer from the carbazole chromophore to the porphyrin may be operable to some extent within the entire PorY series, independent of substitution.

The proposed mechanism is illustrated in Fig. 7.4. Both porphyrin (D1) and carbazole chromophore (D2) are photoexcited at 280 nm. Energy transfer from D2* to D1 increases the concentration of D1*. It leads to enhanced emission from D1* and quenched emission from D2*. At 560 nm excitation, only the porphyrin D1 is photoexcited. The organic chromophore alone does not emit, therefore, the photoluminescence spectrum only shows the characteristic emission of the porphyrin. The PL intensities of PorY1-5 are nearly doubled as compared to that of Por, which may mainly originate from the increased light absorbance at 560 nm (0.020-0.025 of PorY dyes and 0.016 of Por at 560 nm).

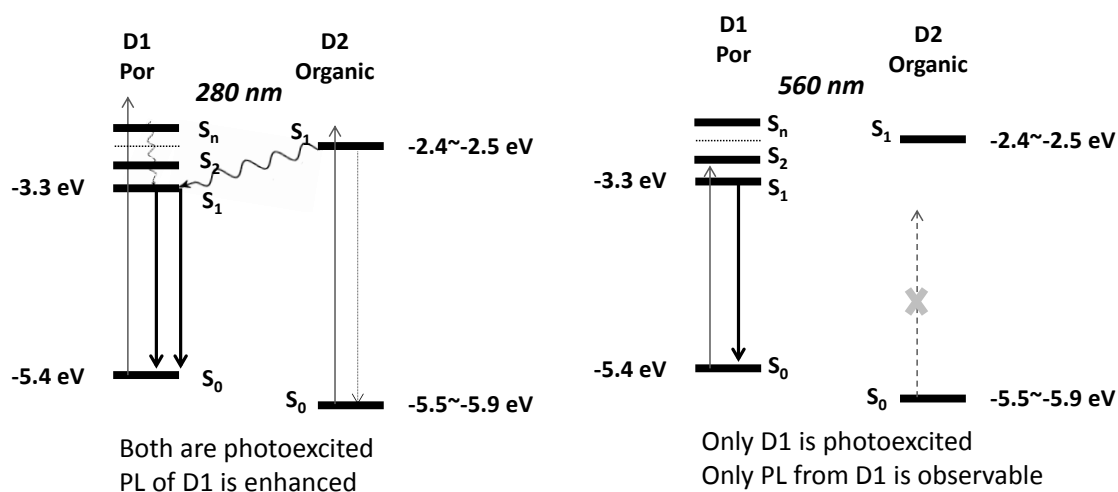


Figure 7.4 Graphical illustration of the deexcitation pathways in PorY dyes photoexcited at 280 nm and 560 nm.

7.4.2 PorO dyes

Fig. 7.5 shows the UV-vis absorption and photoluminescence spectra of the carbazole-fused thiophene organic chromophores CbTh1-3, the di-chromophoric dyes PorO1-3 and the single chromophoric porphyrin Por dissolved in DMF. The excitation wavelength was again 280 nm, where both the porphyrin and the carbazole-fused

thiophene chromophores are photoexcited. The absorbance values of CbTh1-3, PorO1-3 and Por at 280 nm are 0.023, 0.016, 0.026, 0.037, 0.05, 0.054 and 0.026, respectively (Fig. 7.5(a) and (c)).

The photoexcited carbazole-fused thiophene chromophores CbTh1-3 typically show two emission bands: a weaker one at wavelengths shorter than 400 nm and a more intense one within the 440-500 nm wavelength range (Fig. 7.5(b)). CbTh2 shows a slightly red-shifted PL band as compared to bands of CbTh1 and CbTh3. This red shift is consistent with the red shifted UV-vis absorption band of CbTh2 (Fig. 7.5(a)). The order of emission intensity from highest to lowest is CbTh1 (0.51×10^6 CPS), CbTh2 (0.35×10^6 CPS) and CbTh3 (0.20×10^6 CPS), which does not follow the trend in light absorption at the excitation wavelength, suggesting higher quantum yield of emission of CbTh1 compared to CbTh3.

The photoluminescence peaks assigned to emissions by the carbazole-fused thiophene chromophores in PorO1-3 are not found in the photoluminescence of PorO1 and PorO3 dyes (Fig. 7.5(d)). Photoexcitation of PorO2, on the other hand, leads to a weak emission at 500 nm. The PL intensities of the porphyrin in PorO1-3, i.e. 600-720 nm, are all enhanced by two to three times compared to that in Por, despite the lower concentration of promptly generated excited chromophores due to the competitive absorption by the carbazole-fused thiophene chromophore and the porphyrin. This result, similar to the PorY dyes, suggests that energy transfer from the carbazole-fused thiophene chromophores to the porphyrin in the PorO dyes occurs as illustrated in Fig. 7.7. The emission of the organic chromophores (350-650 nm) overlaps with the absorption wavelength region of the porphyrin (280-630 nm), which suggests that FRET is possible. Compared to the PorY dyes, the PorO dyes have better overlap of the emission of the organic chromophores and the absorption of the porphyrin, which may explain the more pronounced quenching observed, at least for PorO1 and PorO3.

The order of PL peak intensities from highest to lowest within the series CbTh1-3 are consistent with the UV-vis absorbance at 480 nm excitation: CbTh2 shows the highest intensity, followed by CbTh1 and CbTh3 (Fig. 7.6). The porphyrin does not significantly absorb light at 480 nm, therefore, photoexcitation at 480 nm almost exclusively excites the organic chromophore within PorO1-3. Despite this, the dichromophoric dyes PorO1-3 all show emission assigned to the porphyrin chromophore. This very strongly indicates energy transfer from the organic chromophore to the

porphyrin as illustrated in Fig. 7.7. PorO2 shows a PL intensity of 0.05×10^6 CPS at 500-580 nm where the organic chromophore is expected to emit (Fig. 7.6(a)). This suggests that the excited state of the organic chromophore in PorO2 is not completely quenched and that the energy transfer efficiency is not 100%.

When photoexcited at 560 nm, all PorO1-3 exhibit the characteristic two PL bands assigned to porphyrin emission (Fig. 7.6(b)). No energy transfer from the porphyrin to the organic chromophore occurs as illustrated in Fig. 7.7. The differences in PL intensities within the porphyrins are consistent with the differences in UV-vis absorbance at 560 nm (Fig. 7.5).

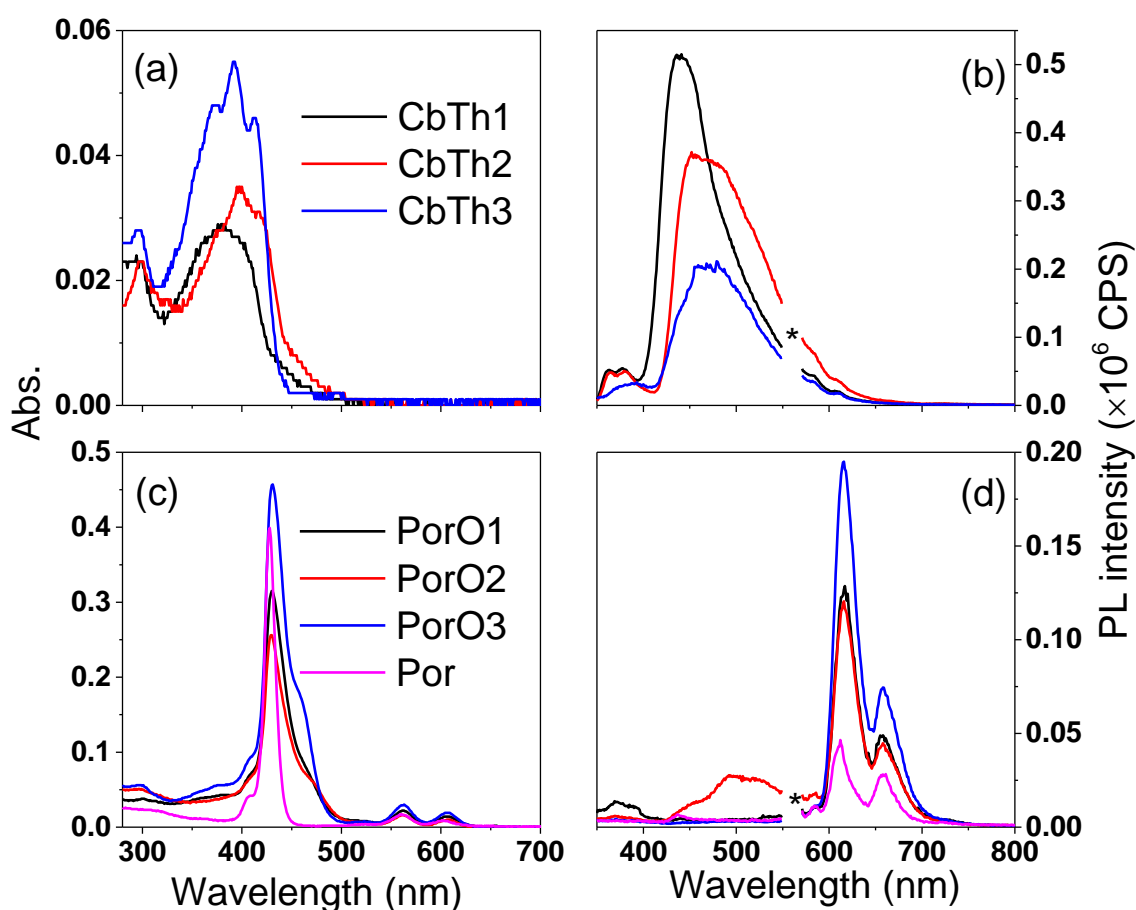


Figure 7.5 Absorbance of (a) the carbazole-fused thiophene chromophores and (c) the PorO dyes and photoluminescence spectra of (b) the carbazole-fused thiophene chromophores and (d) the PorO dyes on 280 nm excitation in DMF with 1 μ M concentration.

The second harmonic of the excitation wavelength at 560 nm was deleted (indicated by a star) from the PL spectra.

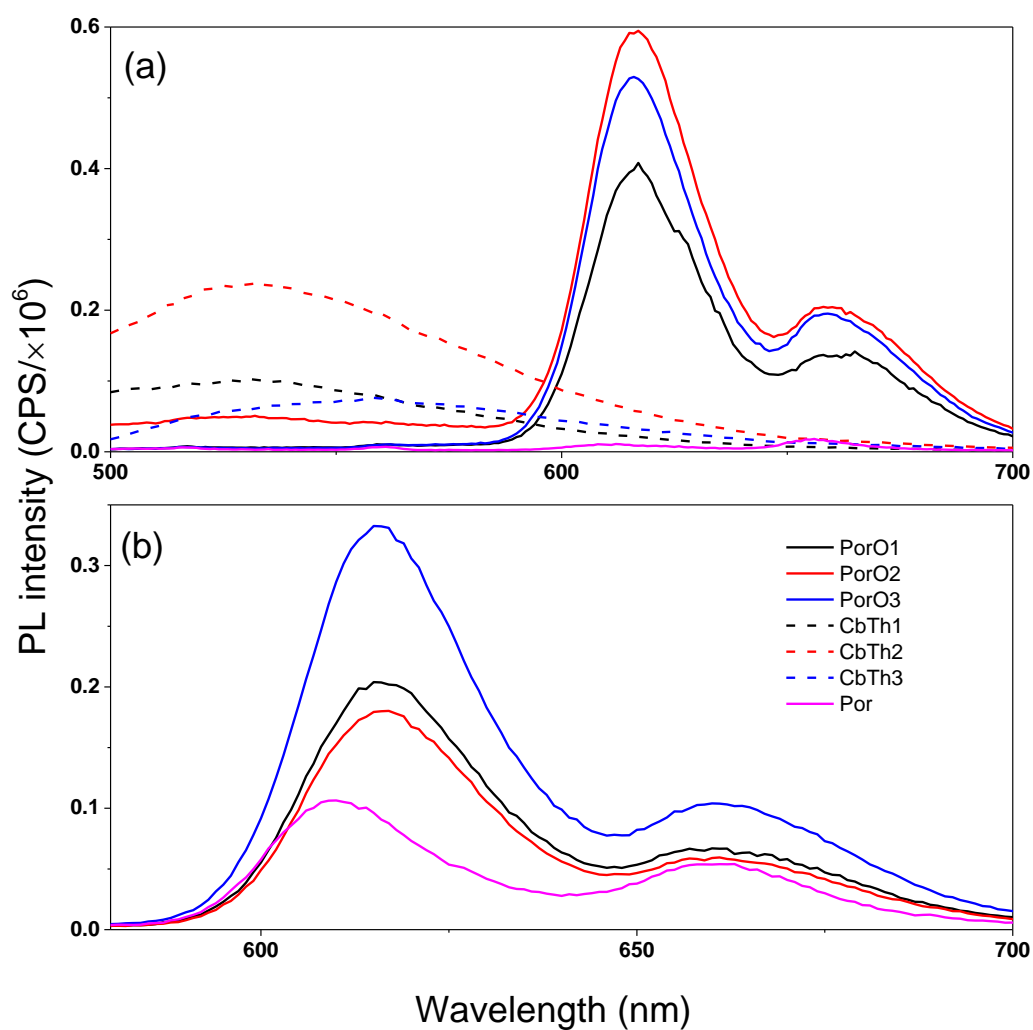


Figure 7.6 Photoluminescence intensities measured by photoexcitation of PorO1-3, CbTh1-3 and Por dissolved in DMF with 1 μM concentration at (a) 480 nm and (b) 560 nm.

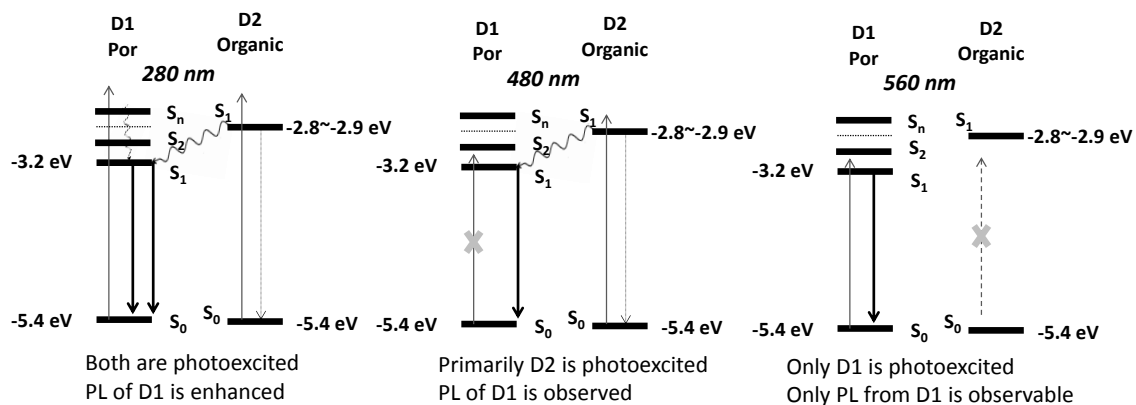


Figure 7.7 Graphical illustration of the deexcitation pathways in PorO dyes photoexcited at 280 nm, 480 nm and 560 nm.

7.5. Photoluminescence of PorR: electron transfer from the porphyrin to the organic chromophore

Fig. 7.8 shows the photoluminescence spectrum of PorR consisting of a carbazole-thiophene benzothiadiazole thiophene and porphyrin chromophores as well as the carbazole-thiophene benzothiadiazole thiophene organic alcohol CbBTD-OH as measured in DMF. CbBTD-OH, which is structurally similar to the organic chromophore in PorR was used to provide a comparative emission spectra. Photoexcited at 560 nm, both CbBTD-OH and PorR show a weak emission with peak intensities of 0.06×10^5 CPS and 0.15×10^5 CPS, respectively. These values are only one twentieth as strong compared to in THF (Fig. 7.9). Such a strong solvent effect suggests the charge transfer nature of the emissive state in both molecules. In more polar DMF, the charge transfer state is more stabilized leading to less emission, compared to less polar THF.¹⁶ To increase sensitivity, THF solutions were used to investigate energy transfer in the di-chromophoric dye.

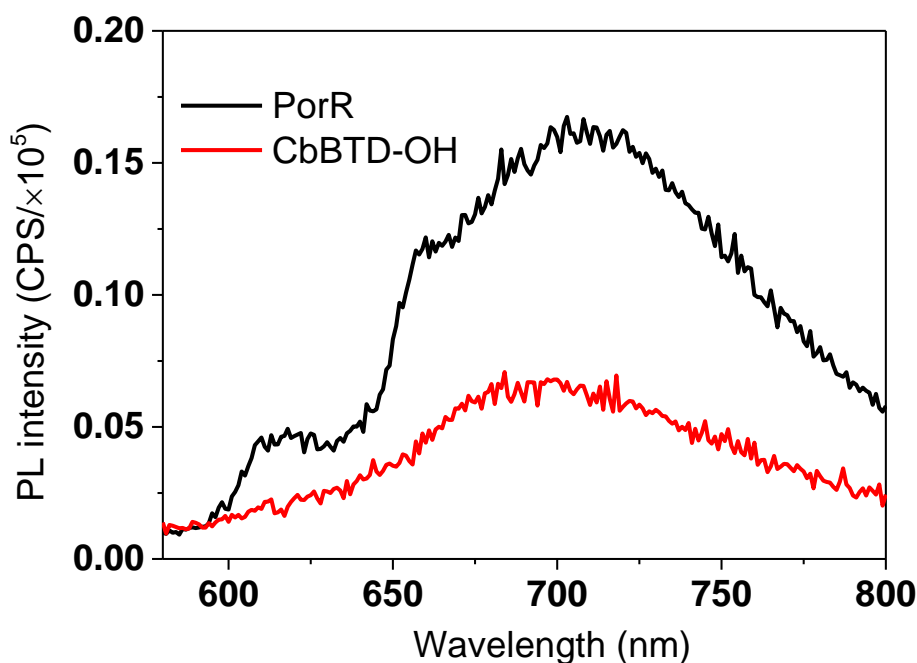


Figure 7.8 Photoluminescence intensities measured by photoexcitation of PorR and CbBTD-OH dissolved in DMF with 1 μ M concentration at 560 nm.

Fig. 7.9 shows the absorbance and photoluminescence spectra of the single chromophoric porphyrin Por, the di-chromophoric porphyrin PorR and the carbazole-thiophene benzothiadiazole thiophene organic alcohol CbBTD-OH recorded at two excitation wavelengths (480 nm and 560 nm) in THF.

At 480 nm, assuming that the absorption of PorR is a simple superposition of the absorption of the individual chromophores, the organic chromophore in PorR is dominantly photoexcited. The porphyrin absorption at this wavelength is very weak, also indicated by two very weak emission bands assigned in Fig. 7.9(b). Photoexcited at 480 nm, the organic alcohol CbBTD-OH shows a broad PL band from 580 nm to beyond 800 nm. The di-chromophoric porphyrin PorR shows a similarly featured spectrum, but with slightly stronger PL intensities beyond 650 nm as compared to CbBTD-OH. The peak PL intensities of PorR and CbBTD-OH are 2.1 and 1.4×10^5 CPS, respectively. Considering that the UV-vis absorbance of PorR and CbBTD-OH are 0.021 and 0.011 with 1 μ M concentration, respectively, PorR shows a lower fluorescence quantum yield compared to CbBTD-OH. Moreover, a small shoulder at ~ 610 nm coinciding with the first porphyrin emission band, is observed in the PL spectra of PorR which is absent in that of CbBTD-OH. This may suggest that some porphyrin emission is superimposed on the emission from the photoexcited carbazole-thiophene benzothiadiazole thiophene at 480 nm excitation.

At 560 nm, both the organic chromophore and the porphyrin are photoexcited in PorR (Fig. 7.9(c)). Similarly to Section 7.3 above, the photoexcited Por shows two strong PL bands at 606 nm and 657 nm. The spectrum of the photoexcited CbBTD-OH recorded at 560 nm photoexcitation is similar to the spectrum recorded at 480 nm. The spectrum of photoexcited PorR also shows a similar shape of PL bands as compared to CbBTD-OH, but with three times greater intensities. PorR shows five times larger absorbance (0.058) compared to CbBTD-OH (0.012) at 560 nm, which indicates that the difference in PL intensity can be attributed to the differences in the absorption coefficients at the excitation wavelength.

The spectrum of PorR photoexcited at 560 nm is significantly different from that of the PorY and PorO dyes. While PorY and PorO dyes show characteristics porphyrin emission, PorR did not. While the emission of the organic chromophore is prominent in the PL of photoexcited PorR, its emission intensity was not noticeably enhanced compared to that of CbBTD-OH.

Moreover, when the organic chromophore was photoexcited at 280 nm in PorY and PorO dyes, the emission from the porphyrin chromophore was enhanced by two to three times in both series compared to Por. When the organic chromophore was photoexcited (480 nm) in PorR, no clear signatures of the porphyrin emission could be observed. While energy transfer from the organic chromophore to porphyrin in PorY and PorO dyes was plausible, no evidence for energy transfer from the organic chromophore to the porphyrin was found in Fig. 7.9. This suggests that electron transfer, rather than energy transfer, from the porphyrin to the organic chromophore is responsible for the quenching of the porphyrin photoluminescence in PorR. A further indication of the presence of a charge separated state, rather than a neutral state, is the presence of a strong solvent polarity effect on the emission intensity (from DMF to THF).

The emission spectrum of the porphyrin at 580-700 nm (Fig. 7.9(c)) overlaps with the absorption spectrum of the organic chromophore (280-650 nm, Fig. 7.9(a)), which suggests the FRET is possible. Electron transfer from the porphyrin to the organic component in PorR, as another possible way, is also suggested as discussed below.

As illustrated in Fig. 7.10, electron transfer may proceed from the photoexcited porphyrin to the organic chromophore leading to an oxidized porphyrin cation radical and a reduced carbazole-thiophene benzothiadiazole thiophene moiety. The back electron transfer is non-radiative (excess energy dissipated as heat) and hence no fluorescence is observed. Due to less stabilization of the charge transfer state in less polar solvent, the electron transfer yield is lower, hence more intense luminescence is observed. Based on this data alone, however, energy transfer from the porphyrin to the organic chromophore cannot be ruled out completely.

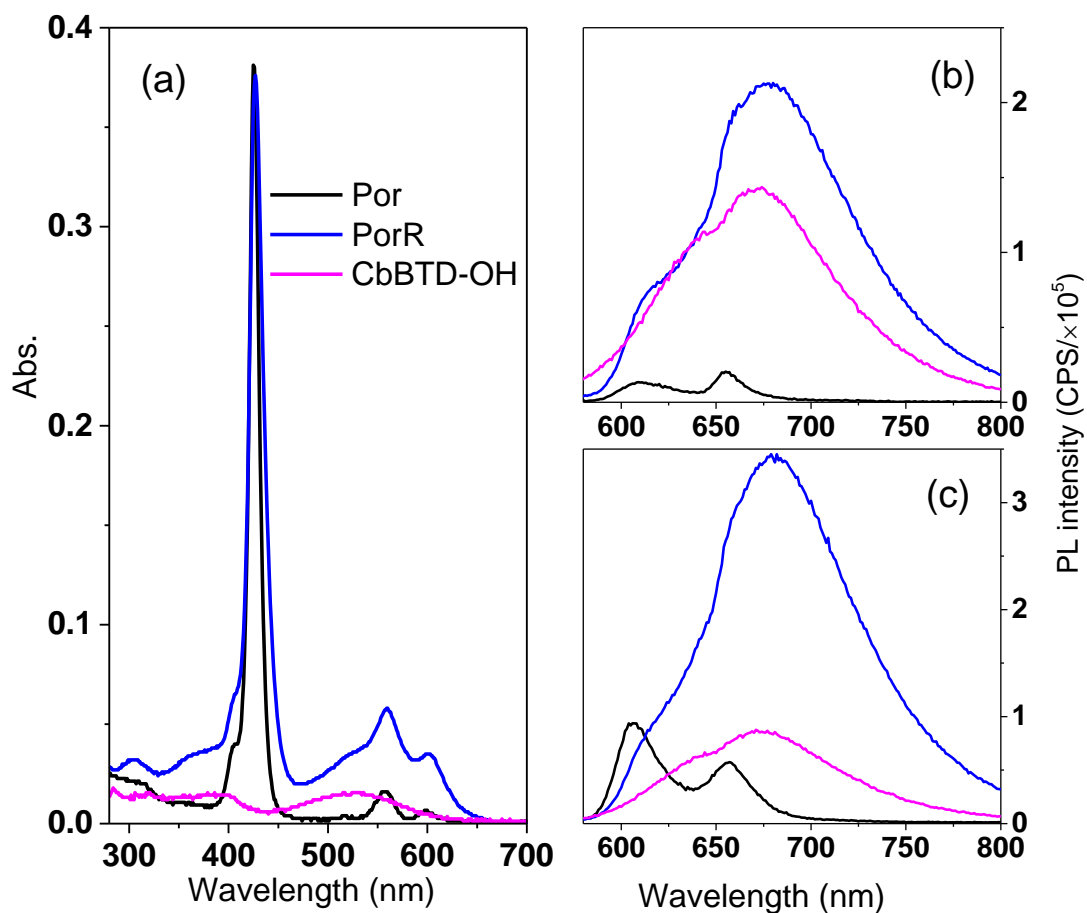


Figure 7.9 (a) Absorbance and photoluminescence spectra with (b) 480 nm and (c) 560 nm excitation of PorR and the counterparts in THF with 1 μ M concentration.

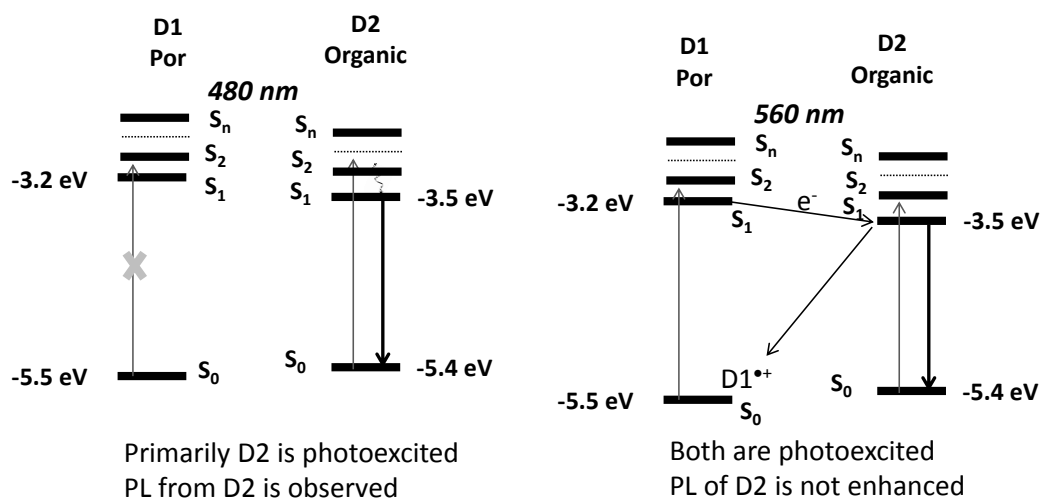


Figure 7.10 Graphical illustration of the deexcitation pathways in PorR photoexcited at 480 nm and 560 nm.

7.6. Correlating photoexcitation pathways with injection efficiency using absorbed photon-to-current conversion measurements

Energy transfer from the organic chromophore to the porphyrin in either PorY and PorO sensitized TiO_2 should contribute to charge generation mechanism at wavelengths where the organic chromophore are selectively excited, as explained in the introduction. Photoinduced electron transfer or energy transfer from the porphyrin to the organic chromophore (away from the TiO_2 interface) is expected to decrease the charge injection efficiency leading to lower APCE in dye-sensitized solar cells using PorR.

The APCE spectra of DSSCs using Por, PorY1, PorO2 and PorR are shown in Fig. 7.11. The APCE value of DSSC using Por at the Q bands is 60%. The APCE value of DSSC using PorY1 is 90%, a 30% increase compared to that using Por. This has been attributed to increased injection efficiency due to increased bulkiness of the dye and lower concentration of “non-injecting dye” as explained in Chapter 4 Section 4.8. Since porphyrin, electrolyte and TiO_2 all absorb at around 400 nm, selective photoexcitation of the organic chromophore in DSSC is not feasible. Therefore, discussion of the effect of possible energy transfer from the organic chromophore on charge photogeneration is not straightforward. The relative values of APCE below 400 nm did not decrease for DSSCs sensitized with PorY1 compared to that of Por, which suggest that energy transfer does lead to photogeneration with the same overall quantum yield (Fig. 7.11).

The APCE values of the DSSC using PorO2 shows 60% at the Q bands, which is similar to that in DSSC using Por (Fig. 7.11). As explained in Chapter 5, the APCE of DSSC using PorO dyes is limited by the insufficient driving force and to some extent by the presence of non-injecting dyes. The broad shoulder between 450 nm and 500 nm is attributed to photoexcitation of the organic chromophore. The APCE values at this wavelength range are lower compared to the Soret band, but on average, higher than that in the Q bands suggesting similarly efficient photogeneration from the photoexcited organic chromophore compared to the photoexcited porphyrin. It is noted that while energy transfer from the photoexcited organic chromophore to the porphyrin was suggested by the photoluminescence data in solution, this does not mean energy transfer is the dominating mechanism when the dye is attached to TiO_2 . If the photoexcited state wave function of the excited organic chromophore has sufficient overlap with TiO_2 acceptor states, electron transfer to TiO_2 , faster than energy transfer to the porphyrin, is

possible (Fig. 7.12). The results in this chapter alone cannot answer the exact mechanism, it is only suggested that the injection yield from both chromophores is similar.

The DSSC using PorR shows much lower APCE values, around 30% at the 400-650 nm wavelength range, less than half the value compared to that of using Por. The decreased electron injection efficiency at the Soret band clearly suggest that another process, electron transfer to the organic chromophore, competes with electron injection into the conduction band of TiO_2 (Fig. 7.12). Moreover, the APCE values decrease even further above 660 nm where the organic chromophore is selectively excited.

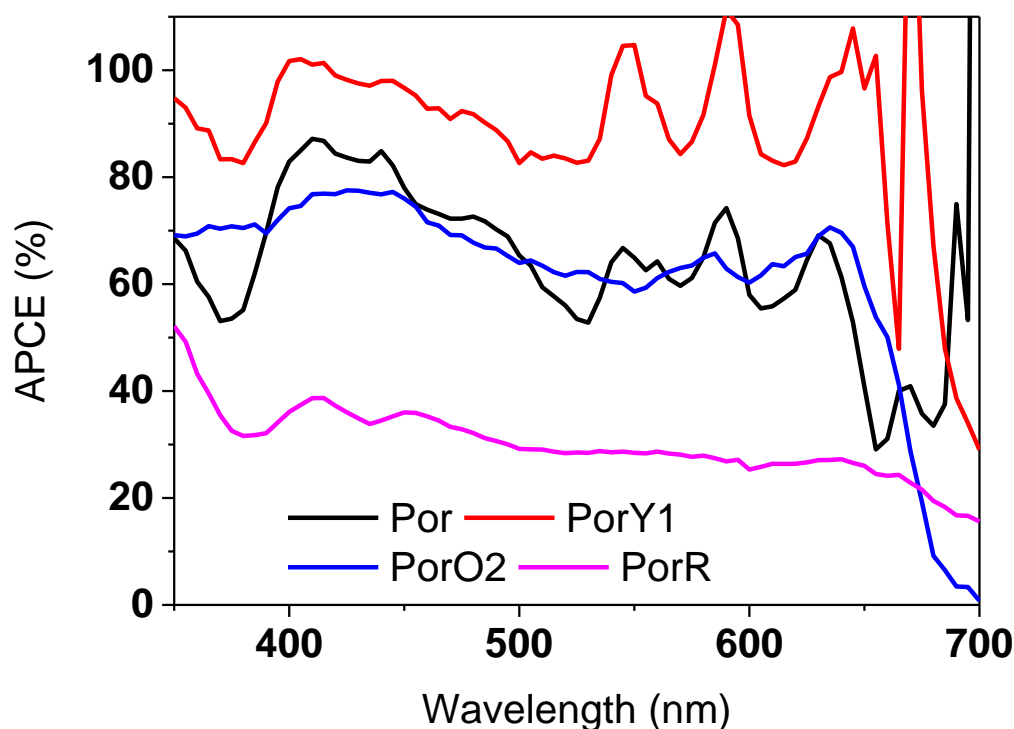


Figure 7.11 Absorbed photon-to-current conversion efficiency (APCE) spectra of the representative dyes using the same iodine-based electrolyte using thin films. Electrolyte components: 0.6 M 1,2-dimethyl-3-propylimidazolium iodide (DMPII), 0.1 M LiI, 0.05 M I_2 , 0.5 M *tert*-butylpyridine (*t*BP) in acetonitrile (AN): valeronitrile (VN)=85:15 (vol).

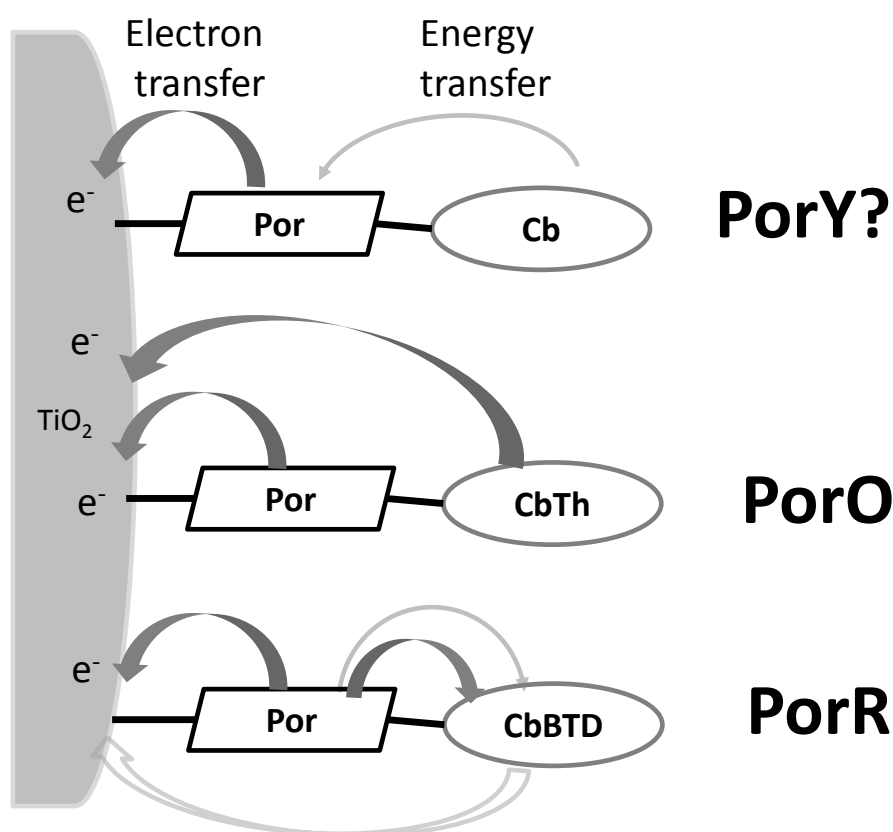


Figure 7.12 Possible energy / electron transfer at the sensitizer/TiO₂ interface of the three families of di-chromophoric dyes.

The above systematic studies, while not conclusive, due to the experimental techniques available, provide interesting insights into the charge photogeneration mechanism of di-chromophoric dyes, which should aid the design of new systems with increased efficiency. This shows a limit of the di-chromophoric (non-conjugated) dyes. However, single chromophore with lower lying LUMO cannot be attached to porphyrin. It is not a problem to use mixed dyes, as the low band gap unit can inject into TiO₂ (Chapter 6).

7.7. Conclusions

The possible photoexcitation pathways (energy and electron transfer) between the organic chromophore with varied band gaps (Y, O and R) and porphyrin were examined for three families of the di-chromophoric dyes, using photoluminescence measurements. Energy transfer from the organic chromophore to the porphyrin was suggested in the

PorY and PorO dyes. In the di-chromophoric dye PorR, electron transfer from the porphyrin to the organic chromophore appeared to occur.

The above photoexcitation pathways were correlated with the charge generation yields using absorbed photon-to-current conversion efficiency measurements using the above dyes in DSSCs. The APCE at the absorption wavelength of the organic chromophore did not change compared to the wavelength where the porphyrin absorbs, which suggests that energy transfer from the organic chromophore to the porphyrin in PorY1 or PorO2 is near unity leading to the same electron injection efficiency. It was noted that electron injection directly from the photoexcited carbazole-fused thiophene chromophore into the conduction band of TiO₂ is also possible. Electron transfer from the porphyrin to the carbazole-thiophene benzothiadiazole thiophene chromophore in PorR is detrimental to the electron injection efficiency in DSSC using this dye, clearly identified by the low APCE values obtained, which suggests a limit of the di-chromophoric dyes using low band gap chromophore.

7.8. References

- (1) Forster, T. *Discuss. Faraday Soc.* **1959**, 27, 7.
- (2) Jares-Erijman, E. A.; Jovin, T. M. *Nat Biotech* **2003**, 21, 1387.
- (3) Basham, J. I.; Mor, G. K.; Grimes, C. A. *ACS Nano* **2010**, 4, 1253.
- (4) Williams, R. *University of Amsterdam, PhD thesis* **1996**.
- (5) Durrant, J. R.; Haque, S. A.; Palomares, E. *Chem. Commun.* **2006**, 3279.
- (6) Asbury, J. B.; Hao, E.; Wang, Y. Q.; Ghosh, H. N.; Lian, T. Q. *J. Phys. Chem. B* **2001**, 105, 4545.
- (7) Hannappel, T.; Burfeindt, B.; Storck, W.; Willig, F. *J. Phys. Chem. B* **1997**, 101, 6799.
- (8) Benkö, G.; Kallioinen, J.; Korppi-Tommola, J. E. I.; Yartsev, A. P.; Sundström, V. *J. Am. Chem. Soc.* **2001**, 124, 489.
- (9) Bram, O.; Cannizzo, A.; Chergui, M. *Phys. Chem. Chem. Phys.* **2012**, 14, 7934.
- (10) Koops, S. E.; O'Regan, B. C.; Barnes, P. R. F.; Durrant, J. R. *J. Am. Chem. Soc.* **2009**, 131, 4808.

- (11) Santos, T. D.; Morandeira, A.; Koops, S.; Mozer, A. J.; Tsekouras, G.; Dong, Y.; Wagner, P.; Wallace, G.; Earles, J. C.; Gordon, K. C.; Officer, D.; Durrant, J. R. *J. Phys. Chem. C* **2010**, *114*, 3276.
- (12) Berhe, S. A.; Gobeze, H. B.; Pokharel, S. D.; Park, E.; Youngblood, W. J. *ACS Appl. Mater. Interfaces* **2014**, *6*, 10696.
- (13) Cardona, C. M.; Li, W.; Kaifer, A. E.; Stockdale, D.; Bazan, G. C. *Adv. Mater.* **2011**, *23*, 2367.
- (14) Lin, C.-Y.; Lo, C.-F.; Luo, L.; Lu, H.-P.; Hung, C.-S.; Diau, E. W.-G. *J. Phys. Chem. C* **2009**, *113*, 755.
- (15) Xue, X.; Zhang, W.; Zhang, N.; Ju, C.; Peng, X.; Yang, Y.; Liang, Y.; Feng, Y.; Zhang, B. *Rsc Advances* **2014**, *4*, 8894.
- (16) Debnath, T.; Maity, P.; Lobo, H.; Singh, B.; Shankarling, G. S.; Ghosh, H. N. *Chem. Eur. J.* **2014**, *20*, 3510.

**CHAPTER 8. ENHANCED PHOTOVOLTAGE BY BLOCKING EFFECT AND
INTERMOLECULAR FORCES IN DI-CHROMOPHORIC DYE-
SENSITIZED SOLAR CELLS**

8.1. Introduction

The purpose of this chapter is to investigate the reason for the increased photovoltage in the dye-sensitized solar cells (DSSCs) using di-chromophoric dyes. In particular, PorY and PorO dyes display blocking effect in DSSCs. The elongated electron lifetime of PorR in DSSCs is attributed to dispersion forces. The use of blocking effect to enhance electron lifetime has been well studied.¹⁻⁵ The utilization of intermolecular forces to enhance photovoltage in DSSCs, however, is demonstrated in DSSCs for the first time.

The open circuit voltage (V_{OC}) of the photovoltaic devices is mainly dependent on two factors:

1. Energy level difference. The electrochemical potential difference between the conduction band edge potential (E_{CB}) of TiO_2 and the redox potential of the redox couple.
2. Electron lifetime. The recombination kinetics of the conduction band electrons in TiO_2 with the oxidized species in the electrolyte, such as I_3^- and Co^{3+} . This recombination decreases the electron density in TiO_2 therefore decreasing the Fermi level.

These two factors will be checked to investigate the origin of the enhanced photovoltage in DSSCs using the di-chromophoric dyes. The energy level difference is only dependent on the conduction band edge potential of TiO_2 once using the same redox mediator. The conduction band edge potential of TiO_2 is determined using charge extraction measurement.^{6,7} The electron lifetime is investigated using the stepped light-induced measurements of photocurrent and photovoltage (SLIM-PCV).⁸⁻¹⁰ As one of the factors that affects the electron lifetime, electron diffusion coefficient is also measured (see Chapter 1 Section 1.10.2).

The open circuit voltage of the DSSCs using the single chromophoric porphyrin Por (690 mV) increased to 735-770 mV of PorY dyes using an I/I_3^- redox mediator (Fig. 8.1). The open circuit voltage of the DSSCs using the single chromophoric porphyrin Por (625 mV) increased to 680-735 mV of PorO dyes using a $\text{Co}(\text{dmbpy})_3^{2+}/\text{Co}(\text{dmbpy})_3^{3+}$ redox mediator (Fig. 8.1). The open circuit voltage of the DSSC using PorR (695 mV) was more than 80 mV larger compared to that of the mixed dyes using the two monomers Por and CbBTD1 (Fig. 8.1). The elongated electron

lifetimes in the di-chromophoric dyes will be explained in this chapter using SLIM-PCV measurements.

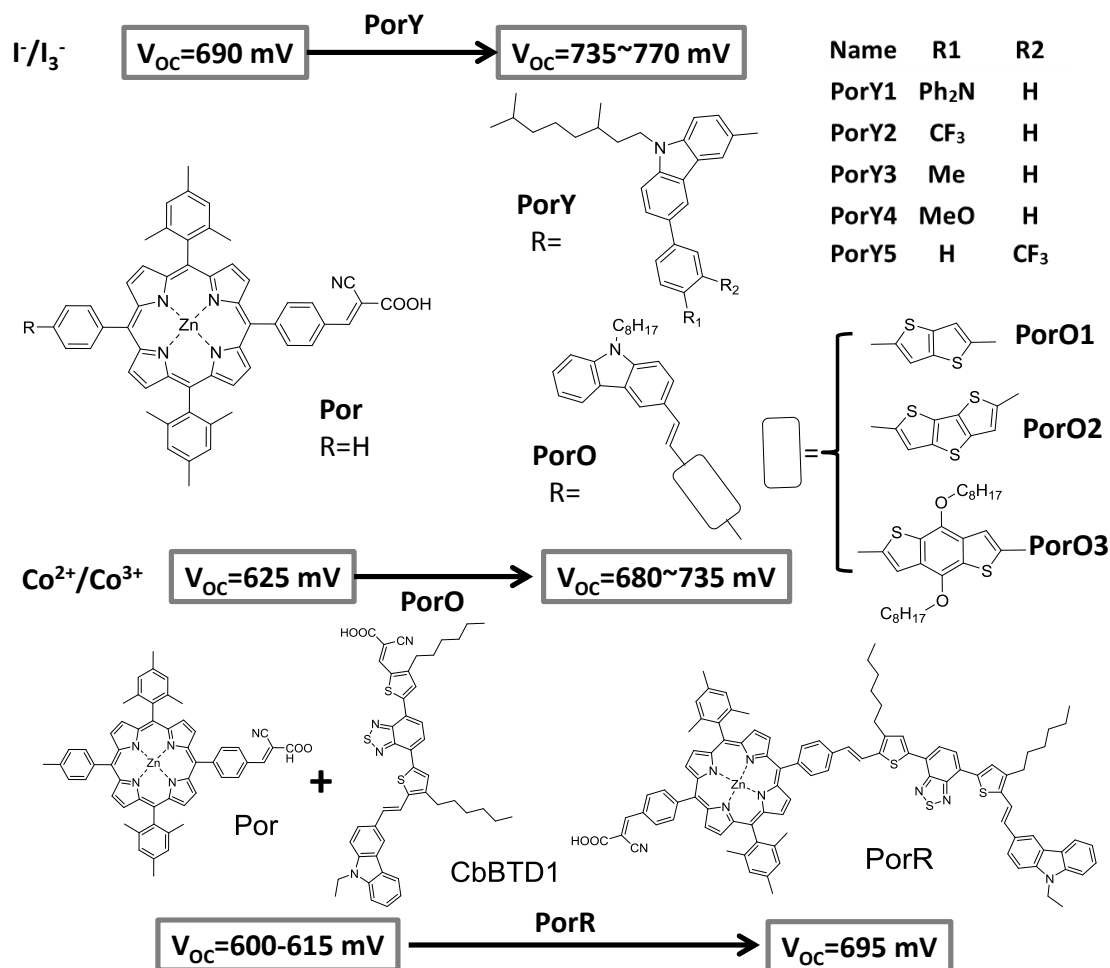


Figure 8.1 Illustration of enhanced photovoltage by the DSSCs using PorY, PorO and PorR dyes.

8.2. Experimental

8.2.1 Investigated molecules

The chemical structures of the sensitizers are displayed in Fig. 8.1.

8.2.2 DSSC fabrication and characterization

The fabrication of devices using PorY1-5, PorO1-3 and PorR was described in Chapter 4, 5 and 6, respectively. The thickness of TiO₂ photoanodes is 2-3 μm to avoid of significant charge collection losses.

For the mixed dyes measurement, the mole ratios in solution were used (detail in Chapter 6). For the reduced dye loading measurements (PorR and Por), 0.005 mM and 0.01 mM dye concentration in THF with 1.5 h immersing time were employed.

The I^-/I_3^- electrolyte employed for characterization of PorY1-5 and PorR was composed of 0.6 M 1,2-dimethyl-3-propylimidazolium iodide (DMPII), 0.1 M LiI, 0.05 M I_2 , 0.5 M *tert*-butylpyridine (*t*BP) in acetonitrile (AN): valeronitrile (VN)=85:15 (vol). The ruthenium dye N719 with excellent photovoltaic performance was used as a reference.

The $Co(dmbpy)_3^{2+}/Co(dmbpy)_3^{3+}$ electrolyte employed for characterization of PorO1-3 was composed of 0.22 M $Co(dmbpy)_3^{2+}$ / 0.05 M $Co(dmbpy)_3^{3+}$, 0.05 M $LiClO_4$, 0.1 M *t*BP and 1 mM chenodeoxycholic acid (CDCA) in AN. The organic dye MK2 with excellent photovoltaic performance was used as a reference.

Stepped light-induced measurements of photocurrent and photovoltage (SLIM-PCV) were used to determine electron lifetime (τ) and electron diffusion coefficient (D). The electron lifetime and diffusion coefficient were obtained corresponding to the transient photovoltage and photocurrent changes, respectively. Electron density (ED) in TiO_2 films was determined by a charge extraction method. Both measurements were performed using a 635 nm diode laser as the light source.

8.3. Photovoltage and photocurrent transients and the calculation of electron lifetime / diffusion coefficient

The stepped light-induced transient measurements of photocurrent and photovoltage and the charge extraction measurement are used to obtain the electron lifetime and diffusion coefficient. This section will present data that is obtained from SLIM-PCV and charge extraction measurement using a N719-sensitized DSSC on 2.2 μm TiO_2 film to establish a baseline before investigate the new porphyrins.

Electron lifetime measurement. The electron lifetime of the device is measured under open circuit condition using four different laser intensities (by changing the applied voltage to the laser diode, Fig. 8.2). Fitting each plot using a mono-exponential equation obtains a time constant. This time constant is the electron lifetime at the corresponding laser intensity. For example, the electron lifetime is 0.024 s when the applied laser voltage is 3.1 V. The open circuit voltage at this laser intensity is 0.77 V.

When the laser intensity is lower, for example, by tuning the applied laser voltage from 3.1 V to 3.07 V, a V_{OC} decay is observed (Fig. 8.2). Less than 1 mV difference is obtained between the original V_{OC} (at 3.1 V) and the steady state V_{OC} (at 3.07 V). The time constant of this V_{OC} decay is the electron lifetime.

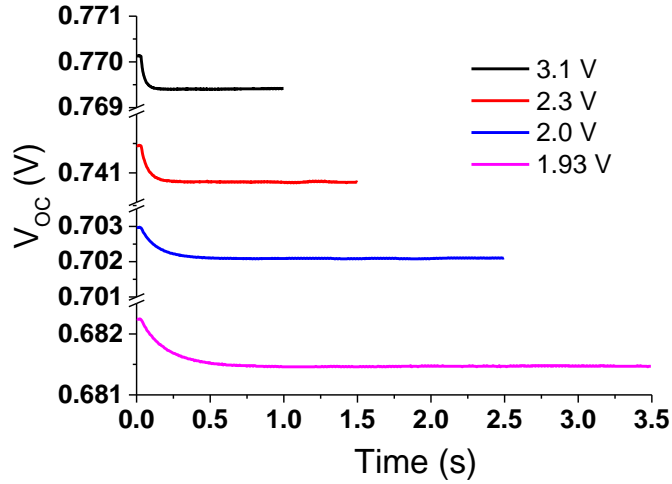


Figure 8.2 Open circuit voltage decay after stepwise reduction of laser intensity. Four laser intensities were employed: 3.1 V, 2.3 V, 2.0 V and 1.93 V.

Diffusion coefficient measurement. The electron diffusion coefficient in TiO_2 is measured under short circuit condition using four different laser intensities (Fig. 8.3). Fitting each plot using a mono-exponential equation obtains a time constant. The electron diffusion coefficient is calculated from this time constant following the Eq. 8.1 by solving a one-dimensional diffusion equation.¹¹

$$D_n = \frac{\omega^2}{2.77\tau_c} \quad (8.1)$$

where, τ_c is the time constant; ω is the thickness of TiO_2 film.

For example, the time constant at 3.1 V applied laser voltage is 0.0013 s. The calculated diffusion coefficient is $13.7 \times 10^{-6} \text{ cm}^2 \text{ s}^{-1}$. The short circuit current density is calculated from the measured current (0.40 mA) by dividing by the active area of the photoanode (0.16 cm^2), leading to 2.5 mA cm^{-2} .

When the laser intensity is lower, for example, by tuning the applied laser voltage from 3.1 V to 3.04 V, a current decay is observed (Fig. 8.3). Less than 10% difference is obtained between the original current (at 3.1 V) and the steady state current (at 3.04 V). The time constant of this current decay is used for calculation of diffusion

coefficient. The constant 50 Hz noise, especially at lower response current, originates from the noise of laser power supply.

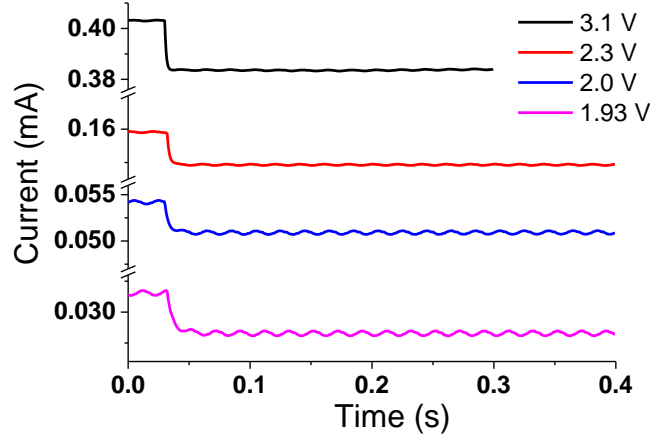


Figure 8.3 Short circuit current decay after stepwise reduction of laser intensity. Four laser intensities were employed: 3.1 V, 2.3 V, 2.0 V and 1.93 V.

Charge extraction measurement. The electron density of the device is measured under open circuit condition using four different laser intensities (Fig. 8.4). By changing the device from open circuit condition to short circuit condition and simultaneously switching off the illumination, the photon-generated electrons are extracted. Integrating the current over time leads to the number of charges. Dividing by the geometric volume of TiO₂ film, the electron density is obtained (Eq. 8.2).

$$ED = \frac{\int Idt \times 6.24 \times 10^{18}}{A \times \omega} \quad (8.2)$$

where, ED is the electron density; A is the area of TiO₂ film.

For example, the integrated area ($\int Idt$, number of charges) at 3.1 V applied laser voltage is 4.2×10^{-3} (Coulomb, C). The calculated electron density is $7.5 \times 10^{18} \text{ cm}^{-3}$.

When the laser intensity is switched off, for example, by tuning the applied laser voltage from 3.1 V to 1.0 V (laser off), meanwhile, change the circuit from open circuit to short circuit, the charges in TiO₂ flow through the circuit and a trace of current change is observed (Fig. 8.4). By measuring the current long enough, almost all of the charges stored in TiO₂ are accumulated.

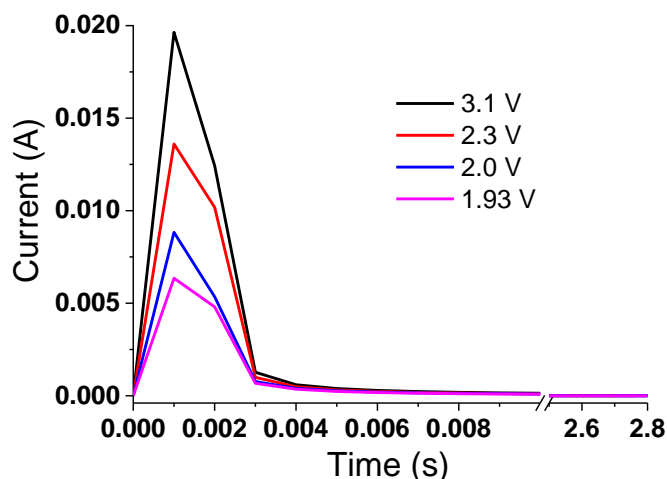


Figure 8.4 Current decay in the charge extraction measurement. Four laser intensities were employed: 3.1 V, 2.3 V, 2.0 V and 1.93 V.

The results of the above measurements are shown in Fig. 8.5(a)-(d).

Fig. 8.5(a) illustrates the relationship between electron lifetime and short circuit current density. The electron lifetime decreases as the short circuit current density increases. The electron lifetime was measured under open circuit condition and it depends on electron density. The electron density at open circuit voltage cannot be directly obtained from the short circuit density and needs to be determined from charge extraction plots at same charge density.

Fig. 8.5(b) is the electron lifetime-electron density plot. Both parameters are measured under open circuit condition. The electron lifetime decreases as the electron density increases. The higher the electron density in TiO_2 , the faster electron diffusion is. From this plot, the electron lifetime under a certain electron density can be obtained, for example, at $ED = 5 \times 10^{18} \text{ cm}^{-3}$, the electron lifetime of N719 is $\sim 0.07 \text{ s}$. This value is very similar to the reported value of 0.05 s under similar condition.⁸

The plot of electron lifetime versus electron density (or short circuit current density) is important to understand the origin of V_{OC} of DSSC.^{8,12,13} The electron lifetime comparison at the same electron density is necessary.

The other two parameters that could affect the electron lifetime are electron diffusion coefficient and conduction band edge potential of TiO_2 as introduced in Chapter 1 Section 1.10.2. Larger electron diffusion coefficient means faster movement of electrons towards recombination sites leading to faster recombination and shorter electron lifetime.^{14,15} More positive versus vacuum (downward shift) conduction band

edge potential reduces the recombination driving force and may lead to longer electron lifetime. Both factors need to be taken into account to analyse the origin of electron lifetime in DSSCs.^{9,16,17}

Fig. 8.5(c) shows the electron diffusion coefficient versus short circuit current density plot. Both parameters were measured under short circuit conditions. The factors that can affect the diffusion coefficient have been introduced in Chapter 1 Section 1.10.2. The diffusion coefficient values of the TiO₂ in the experiment are $1-10 \times 10^{-6} \text{ cm}^2 \text{ s}^{-1}$ at short circuit current density of $0.1-1 \text{ mA cm}^{-2}$. These values are similar to the reported values ($7-20 \times 10^{-6} \text{ cm}^2 \text{ s}^{-1}$ at $0.2-1 \text{ mA cm}^{-2}$).⁸ The slope of this plot $((1-m\beta)/b)$ reveals the Density of States (DOS) distribution of trap states in TiO₂ near the conduction band.¹⁵

Fig. 8.5(d) shows the open circuit voltage versus electron density plot. Both parameters were measured under open circuit condition. The intercept of the plot at the y-axis gives the information of the conduction band edge position. However, this is only a relative position under certain electron density, for example, at $ED = 5 \times 10^{18} \text{ cm}^{-3}$, the intercept on y-axis (the open circuit voltage) of N719 is $\sim 0.73 \text{ V}$. The slope of this plot (β , trap distribution parameter) reveals the same information as Fig. 8.5(c), which is the trap states distribution in TiO₂ near the conduction band.

The slope values as well as the calculated parameters are shown in the inset of Figs. 8.5(b), (c) and (d). The physical explanation of the parameters has been explained in Chapter 1 Section 1.10.1. The parameter β value of 0.20 is obtained from the slope of Fig. 8.5(d). From the slope value of -1.94 in Fig. 8.5(b), the value of m/b is calculated (1.70). Using β , m/b , and the slope of Fig. 8.5(c) values, the parameter b is calculated to be 1.10. In turn, the parameter m is calculated to be 1.87 from the slope value of Fig. 8.5(b).

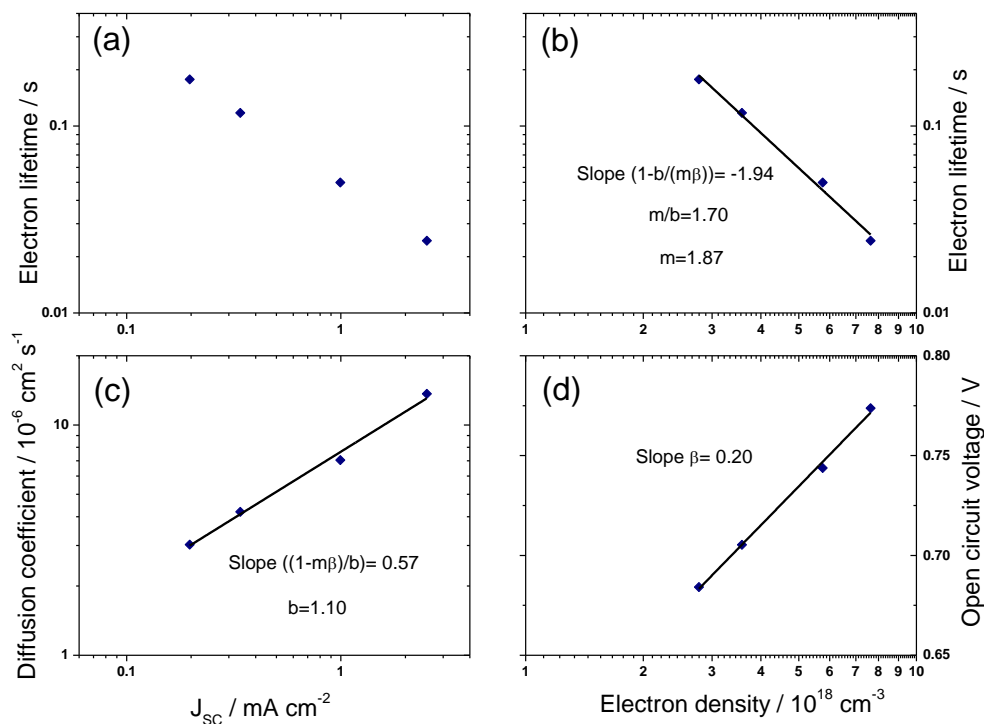


Figure 8.5 (a) Electron lifetime and (c) diffusion coefficient versus short circuit current density, (b) electron lifetime and (d) open circuit voltage versus electron density for N719-sensitized solar cell using the I^-/I_3^- electrolyte. The slope values as well as the calculated parameters are shown in the inset. Film thickness: 2.2 μm .

8.4. Origin of increased photovoltage of the PorY dyes

The DSSCs using the PorY dyes achieved 50-80 mV higher open circuit voltages than using Por (photovoltaic performance in Chapter 4, Fig. 8.1). The reason for these enhanced photovoltages was investigated by the SLIM-PCV technique and the charge extraction method below (Fig. 8.6).

More than two times longer electron lifetimes are observed by the DSSCs using PorY dyes compared to that using Por under either the same short circuit current density (Fig. 8.6(a)) or electron density (Fig. 8.6(b)). For example, at $ED = 2 \times 10^{18} \text{ cm}^{-3}$, the electron lifetimes of DSSCs using PorY1, PorY2 and Por are 0.2 s, 0.04 s and 0.02 s, respectively. This increased electron lifetime is not due to the faster electron transport in TiO_2 , as no significant difference was found in electron diffusion coefficient at the same short circuit current density (Fig. 8.6(c)). Moreover, no significant change is observed in Fig. 8.6(d) neither in the y-axis intercept nor in the slope of V_{oc} vs. $\log ED$ plot. The

similar y-axis intercept in all porphyrins suggests that the conduction band edge potential of TiO_2 is also similar within DSSCs using the porphyrins.

The electron lifetimes within the DSSCs using PorY dyes do not varied significantly. PorY1, with the largest organic substituent, shows slightly longer electron lifetimes compared to PorY2-5 in DSSCs. This suits well with the blocking effect which affects the electron lifetimes.

The increased open circuit voltages of the DSSCs using PorY dyes compared to that using Por is attributed to the increased electron lifetimes. The electron lifetimes of DSSCs using PorY1 are half that of N719 at matched electron density. This is one of the longest electron lifetimes reported for porphyrins. Due to this significant enhanced electron lifetime, the open circuit voltage of DSSCs using PorY1 was 770 mV, which is very close to that using N719 (800 mV, Chapter 4 Section 4.5).

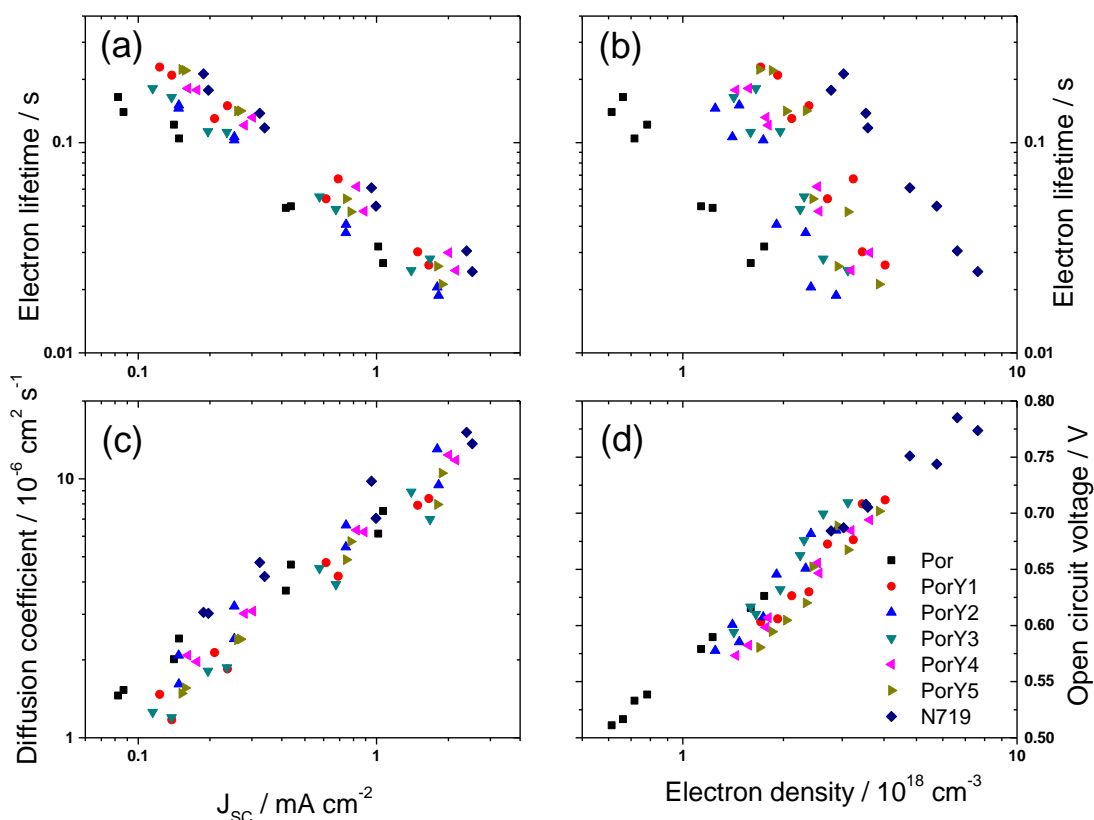


Figure 8.6 (a) Electron lifetime and (c) diffusion coefficient versus short circuit current density, (b) electron lifetime and (d) open circuit voltage versus electron density for DSSCs using Por, PorY1-5 and N719 using the I^-/I_3^- electrolyte (two samples for each dye). Film thickness: $2.0 \pm 0.1 \mu\text{m}$.

8.5. Conduction band variation between the iodine and cobalt electrolytes

The utility of di-chromophoric porphyrin dyes to use with cobalt electrolyte is demonstrated in Chapter 5. Good performance DSSCs using PorO dyes and cobalt electrolyte with respectable photovoltage are achieved. The best power conversion efficiency of 4.7% was achieved by PorO2.

Electron lifetime, diffusion coefficient and the conduction band bottom edge potential of TiO_2 may be affected by the concentration of the components (such as $t\text{BP}$ and Li^+) in the electrolyte.^{12,18,19} DSSCs using PorY dyes using the I^-/I_3^- electrolyte (Chapter 4) achieved nearly 100% absorbed photon-to-current conversion efficiency (APCE), while DSSCs using PorO dyes using the optimized cobalt electrolyte achieved only 80% APCE mainly due to a limited driving force for electron injection. Therefore, comparing the conduction band potential of the devices using the two electrolytes is beneficial for the analysis of the driving force for electron injection.

The iodine electrolyte and the cobalt electrolyte are compared in respect to electron lifetime, diffusion coefficient and electron density using Por as the reference sensitizer (Fig. 8.7). The electron lifetime in DSSCs using the cobalt electrolyte is more than 10 times shorter compared to that using the I^-/I_3^- electrolyte under either the same short circuit current or the same electron density (Fig. 8.7(a) and Fig. 8.7(b)). This is mainly attributed to a 0.15 V upward shifted in the intercept at the y-axis (negative shifted the conduction band edge potential of TiO_2) in DSSCs using the cobalt electrolyte compared to the I^-/I_3^- electrolyte (Fig. 8.7(d)). This 0.15 eV difference between the iodine and cobalt electrolytes in Fig. 8.7(d) may origin partly from the electrolyte components. The difference in redox potential is also a factor which contributes to this 0.15 eV shift as the device is a two-electrode system.

The ~50% larger diffusion coefficient values of the DSSCs using the cobalt electrolyte compared to the I^-/I_3^- electrolyte under the matched short circuit current density is possibly due to the different concentrations of $t\text{BP}$ in the electrolytes (Fig. 8.7(c)). The component $t\text{BP}$ can decrease the diffusion coefficient values in the presence of Li^+ .^{12,19,20} The concentration of $t\text{BP}$ in the cobalt electrolyte is less than that in the iodine electrolyte, which contributes to a larger diffusion coefficient. The upward shifted conduction band edge potential of the DSSCs using the cobalt electrolyte

compared to the I^-/I_3^- electrolyte may also attribute to a few percentage of the larger diffusion coefficient.

The faster recombination in the case of the cobalt electrolyte compared to those of the I^-/I_3^- electrolyte may due to the one-electron reaction of the former. The faster electron diffusion may also contribute to this faster recombination to some extent. The longer electron lifetimes of the PorO dyes compared to Por in DSSCs using the cobalt electrolyte (shows in Fig. 8.8) suggests the utility of di-chromophric dyes for DSSCs.

It is noted that the slopes of the two conditions in Fig. 8.7(d) are different. This is mainly due to the different concentrations of electrolyte components, especially Li^+ which may affect the trap energy.

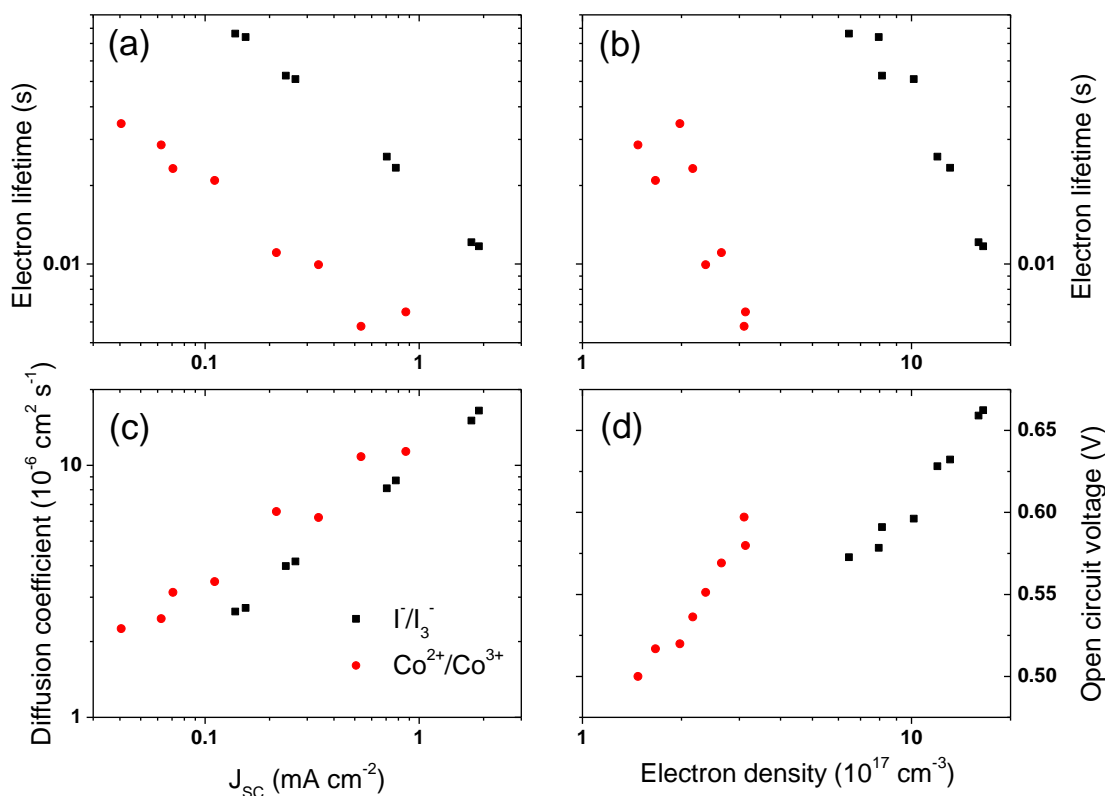


Figure 8.7 (a) Electron lifetime and (c) diffusion coefficient versus short circuit current density, (b) electron lifetime and (d) open circuit voltage versus electron density for DSSCs using Por using both the I^-/I_3^- and the cobalt electrolytes (two samples for each dye). Film thickness: $2.9 \pm 0.1 \mu\text{m}$.

8.6. Origin of increased photovoltage of the PorO dyes

The SLIM-PCV and charge extraction measurements results of the DSSCs using the PorO dyes and Por using the cobalt electrolyte are shown in Fig. 8.8. Larger electron lifetimes are observed in DSSCs using PorO1-3 compared to that using Por at both

matched short circuit current density and electron density (Fig. 8.8(a) and Fig. 8.8(b)). In particular, DSSCs using PorO2 exhibit the longest electron lifetimes within the di-chromophoric dyes, which are more than an order of magnitude longer than the DSSCs using Por, for instance, 0.08 s versus 0.006 s at $ED = 3 \times 10^{17} \text{ cm}^{-3}$. The electron diffusion coefficients of the DSSCs within porphyrins are identical at matched short circuit current density (Fig. 8.8(c)), indicating that the origin of the electron lifetime increase is not due to changes in electron transport. The relationship between open circuit voltage and electron density in Fig. 8.8(d) also shows very similar slope and y-axis intercept, implying the similar trap states distribution as well as the similar conduction band edge potential in all DSSCs.

It is the larger electron lifetimes that contribute to the enhanced open circuit voltages of the DSSCs using PorO dyes compared to that using Por. DSSCs using PorO3 show the shortest electron lifetimes and consequently the lowest open circuit voltages within the di-chromophoric dyes. Using MK2 as a reference, the electron lifetimes of the DSSCs using the di-chromophoric dyes are still reduced. This may be assigned to the positive shifted conduction band edge potential of the MK2-sensitized devices, as suggested by a $\sim 80 \text{ mV}$ downward shift of y-axis intercept in Fig. 8.8(d).

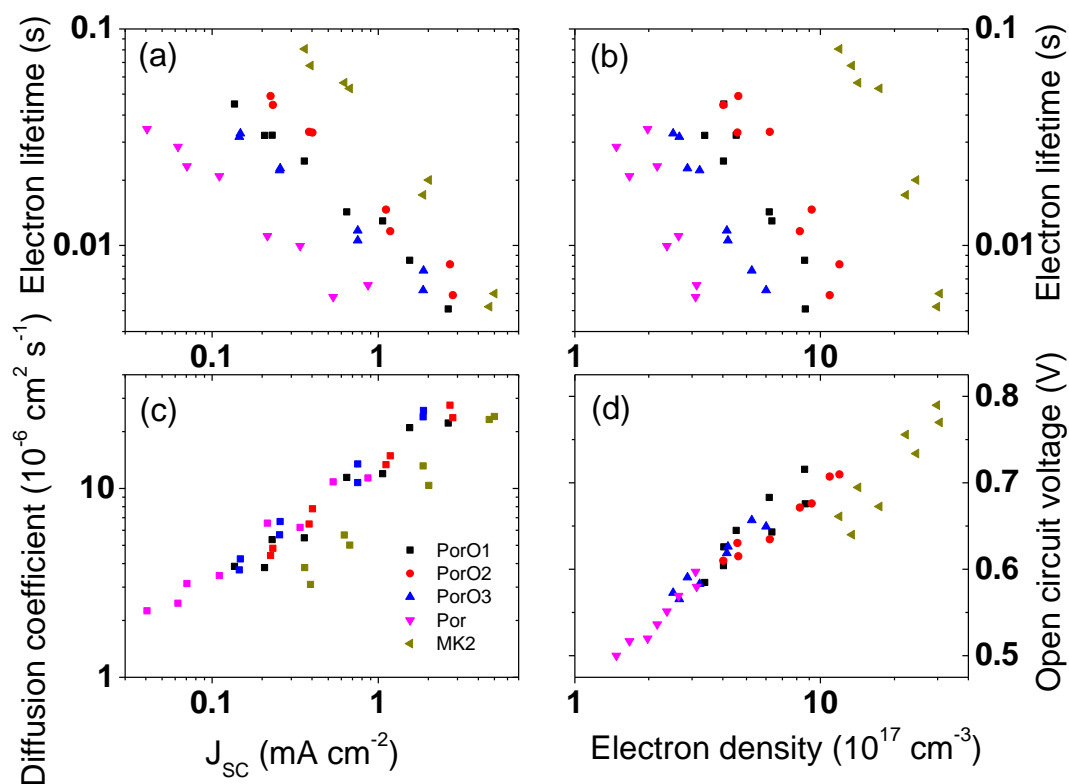


Figure 8.8 (a) Electron lifetime and (c) diffusion coefficient versus short circuit current density density, (b) electron lifetime and (d) open circuit voltage versus electron density for DSSCs using Por, Por1-3 and MK2 using the cobalt electrolyte (two samples for each dye). Film thickness: $2.9 \pm 0.1 \mu\text{m}$.

8.7. Blocking effect of the PorY and PorO dyes

The electron lifetimes of the DSSCs using the PorY and PorO dyes were much longer compared to that using Por. As introduced in Chapter 1 Section 1.10.2, the following processes may influence electron lifetime:

5. Electron diffusion.
6. Conduction band edge potential.
7. Dye structure.
8. Internal and solvent reorganization energies.

As suggested by the results above, the elongated electron lifetimes in the DSSCs using the PorY and PorO dyes were due to neither the *electron diffusion* nor the shifted *conduction band edge potential* of TiO_2 . Due to the same electrolyte employed in each comparison, the *reorganization energy of the redox species* in the electrolyte did not contribute to the elongated electron lifetimes of DSSCs using the di-chromophoric dyes. The *internal reorganization energy* may affect the electron lifetime if the dye structure changes significantly after electron injection, which is unlikely in these di-chromophoric dyes.

Consequently, the elongated electron lifetimes in DSSCs using the di-chromophoric dyes are assigned to *dye structure*.

The *dye structure* affects the electron lifetime by the following four effects (Chapter 1 Section 1.10.2):

1. Blocking effect.
2. Partial charges.
3. Dipole-dipole forces, dipole-induced dipole forces and dispersion forces (induced dipole-induced dipole forces).
4. Coordination.

The oxygen atom was employed in the organic chromophore in PorY4 and PorO3. This may attribute to shorter electron lifetimes of the two di-chromophoric dyes. However,

this *partial charge* effect cannot explain the longer electron lifetimes in the DSSCs using the other di-chromophoric dyes compared to that using Por.

The band gaps of the organic chromophores employed in the PorY and PorO dyes are larger than the porphyrin, therefore, the *dispersion forces* between the organic chromophore and the electrolyte are negligible in affecting the electron lifetime.

The *coordination* of *t*BP with the zinc ion in all the porphyrins is related to the dye amount on TiO₂. Since there is one zinc porphyrin core in one molecule in Por, PorY1-5 and PorO1-3, the coordination effect should be same with similar dye amount on TiO₂. Dye uptake of Por and the PorY dyes are similar ($1.0\text{--}1.4 \times 10^4 \text{ mol cm}^{-3}$, Chapter 4 Section 4.8). Therefore, the coordination cannot explain the longer electron lifetime of DSSCs using the PorY dyes compared to that using Por. Dye uptake of Por was less compared to that of PorO1 and PorO2 when changing the dye solvent in Chapter 5 Section 5.6.2 (Por of $0.9 \times 10^4 \text{ mol cm}^{-3}$, PorO1 and PorO2 of $1.7 \times 10^4 \text{ mol cm}^{-3}$). This may contribute to some extent of the longer electron lifetime of the DSSCs using the latter dyes. Dye uptake of Por was identical to that of PorO3 ($0.9 \times 10^4 \text{ mol cm}^{-3}$). The longer electron lifetime of DSSCs using PorO3 compared to that using Por cannot be explained by coordination.

Consequently, the *blocking effect* from the *dye structure* is the main reason that contributes to the longer electron lifetimes of the DSSCs using the PorY and PorO dyes compared to that using Por. For the DSSCs using the PorY dyes, the size of the carbazole moieties, especially the 3,7-dimethyloctyl chain on the carbazole units, impedes the access of I₃[−] to the TiO₂ surface. Among DSSCs using these di-chromophoric porphyrins, DSSCs using PorY1 possessing the bulkiest side chromophore, achieved the longest electron lifetimes, which is also among the longest electron lifetimes reported for porphyrin sensitized solar cells.

For DSSCs using the PorO dyes, similar blocking effect to the PorY dyes was obtained and was attributed to their longer electron lifetimes compared to the DSSCs using Por. This is mainly caused by the octyl chain in these di-chromophoric dyes.

The blocking effect in DSSCs using the PorY and PorO dyes is illustrated in Fig. 8.9. The organic chromophore at the top of the di-chromophoric dyes blocks the pathway of I₃[−] to the TiO₂ surface and therefore elongating the electron lifetime. The importance of

this finding is that by using the di-chromophoric dye design, not only the photocurrent can be enhanced, but also the photovoltage of DSSCs can be maximized.

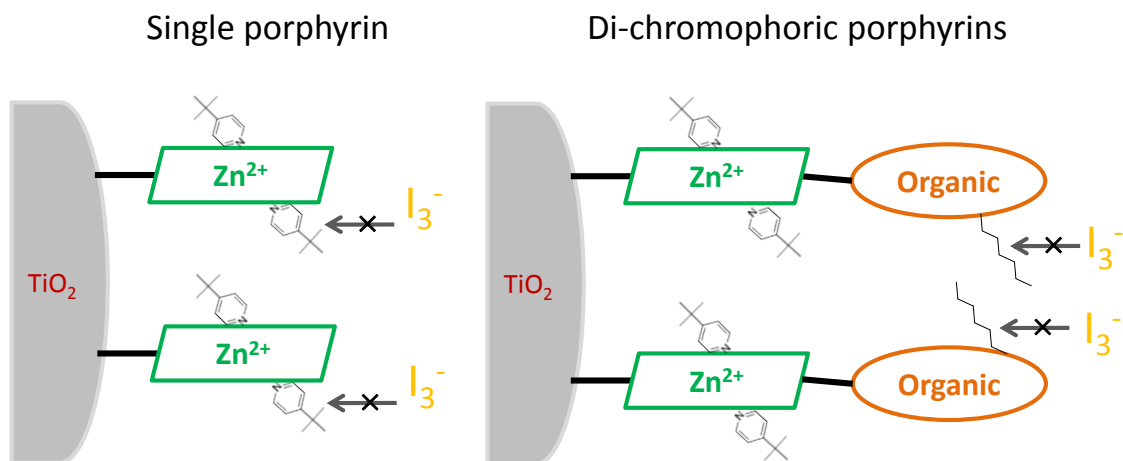


Figure 8.9 Illustration of the blocking effect in the di-chromophoric porphyrins.

8.8. Similar photovoltage of PorR and Por

The SLIM-PCV and charge extraction measurements results of the DSSCs using PorR and Por are shown in Fig. 8.10. The di-chromophoric dye PorR shows nearly two times longer electron lifetimes as compared to Por in DSSCs (Fig. 8.10(a)). The conduction band edge potential of TiO₂ shows very similar position between the two porphyrins as the intercepts of y-axis in Fig. 8.10(b) are not significantly varied.

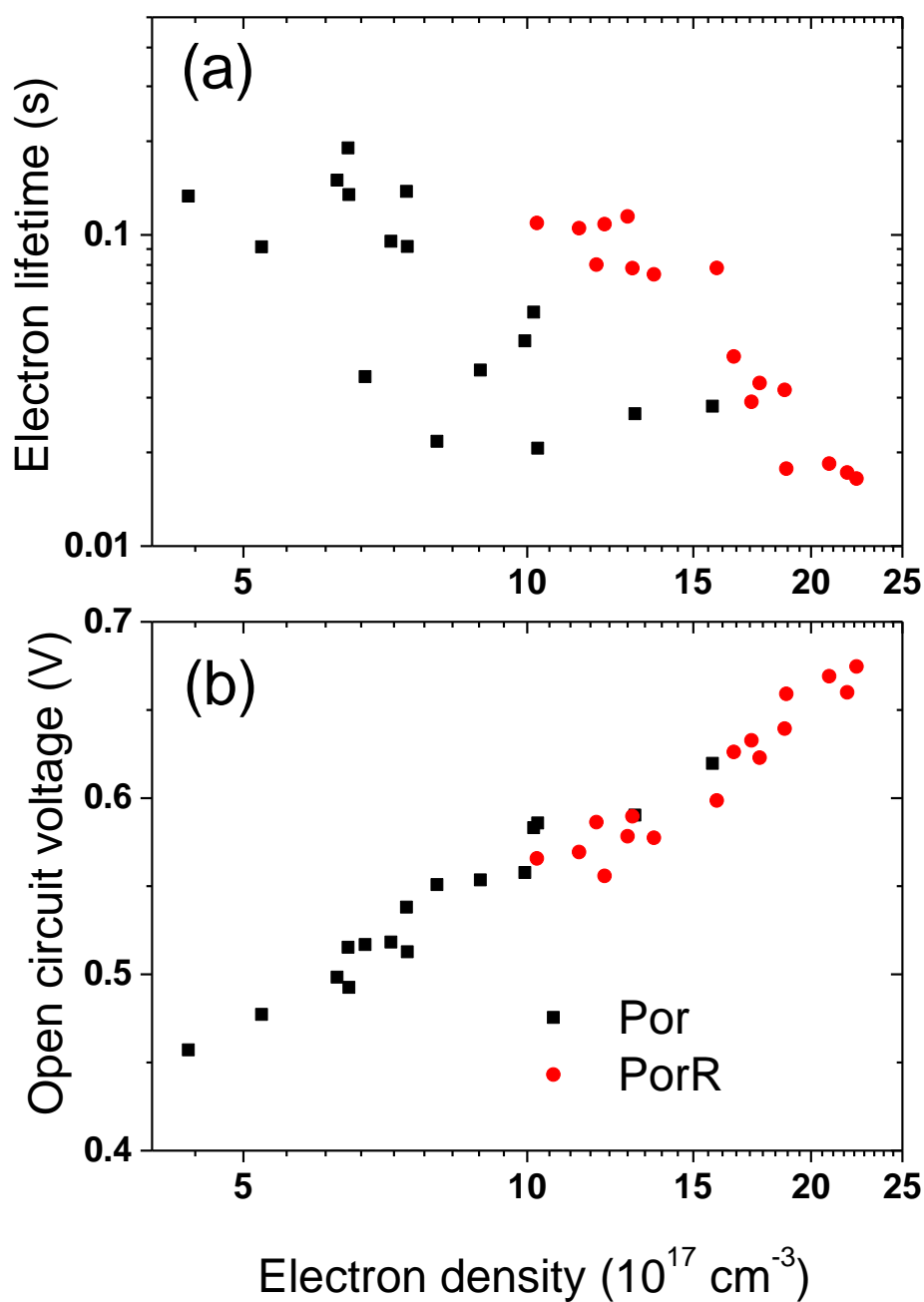


Figure 8.10 (a) Electron lifetime and (b) open circuit voltage versus electron density for DSSCs using Por and PorR (four samples for each dye). Film thickness: $2.3 \pm 0.1 \text{ } \mu\text{m}$.

8.9. Origin of increased photovoltage of PorR compared to mixed dyes

It is noted that the di-chromophoric dye PorR introduced an organic chromophore carbazole-thiophene benzothiadiazole thiophene with lower band gap compared to the porphyrin. The dispersion force is increased as the band gap of dyes is decreased.²¹ The low band gap organic dye has stronger dispersion forces compared to the zinc

porphyrin. As discussed in Chapter 1, increased dispersion forces between sensitizers and redox mediators typically lead to faster recombination and lower photovoltage of DSSCs. However, introducing low band gap organic chromophore in PorR at the top of the molecule did not show this phenomenon. Instead, the dispersion forces can be utilized to enhance the photovoltage. For this specific topic, mixed dyes comprised of the single chromophoric porphyrin Por and the organic dye CbBTD1 were employed for comparison.

Fig. 8.11 shows the SLIM-PCV and charge extraction measurements results of the DSSCs using Por, CbBTD1, PorR and mixed dyes with three different ratios (Por:CbBTD1=1:3, 1:1 and 3:1, respectively, ratios are in solution).

DSSCs using the porphyrin dyes Por and PorR show longer electron lifetimes compared to that using either the mixtures or the organic dye CbBTD1 under either the same short circuit current densities (Fig. 8.11(a)) or electron densities (Fig. 8.11(b)). For example, at electron density of $10 \times 10^{17} \text{ cm}^{-3}$, DSSCs using Por and PorR achieve a similar electron lifetime of 0.07 s, which is more than ten times longer compared to the DSSCs using either the mixtures or CbBTD1. Slightly longer electron lifetime is observed in DSSCs using PorR compared to Por. DSSCs using the mixed dyes all show very similar electron lifetimes as that using the organic dye.

The electron diffusion coefficient within DSSCs using the sensitizers does not vary significantly since the $\log D$ versus $\log J_{SC}$ plots are in similar slope with quite close intercepts on y-axis (Fig. 8.11(c)). This suggests that the electron diffusion does not contribute to the difference in electron lifetimes. The $\log V_{OC}$ versus $\log ED$ in Fig. 8.11(d) shows similar slope. The intercepts on y-axis under the same electron density do not show significant variation amongst the DSSCs, suggesting that the conduction band edge potential of TiO_2 does not shift. The unchanged diffusion coefficient and the conduction band edge potential reveal that the larger photovoltages of the porphyrins compared to the mixed dyes and CbBTD1 originates from the longer electron lifetimes.

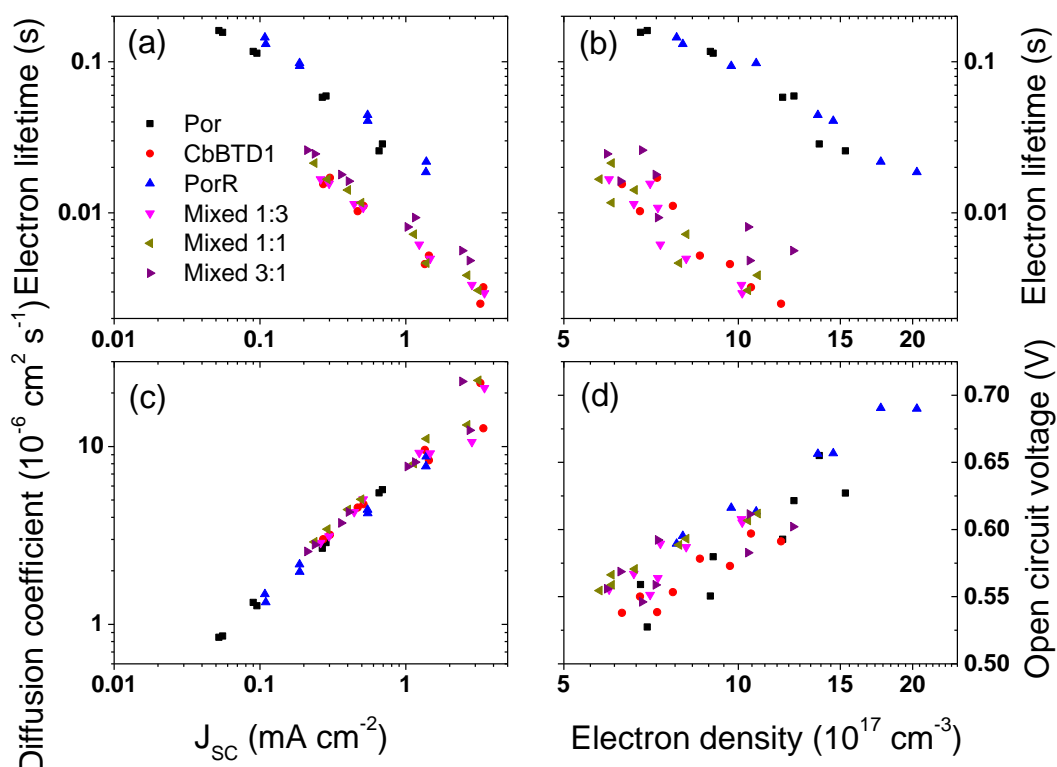


Figure 8.11 (a) Electron lifetime and (c) diffusion coefficient versus short circuit current density, (b) electron lifetime and open circuit voltage versus electron density for the DSSCs using the investigated sensitizers (two samples for each dye). Film thickness: $2.0 \pm 0.1 \mu\text{m}$.

8.10. Utilization of intermolecular forces by PorR

The electron lifetimes of PorR DSSCs were much longer compared to that using the mixed dyes. The utilization of intermolecular forces, especially dispersion forces, to enhance the electron lifetime was demonstrated by PorR.

No *partial charge* effect exists in either PorR or the mixed dyes.

The *coordination* of *tBP* with the zinc ion in DSSCs using PorR may contribute to its longer electron lifetime compared to that using the mixed dyes since the zinc ions numbers are different (caused by different dye loading amount). The *blocking effect* may also play a role in affecting the electron lifetimes since the *dye structures* of the PorR and the mixed dyes are different. Both effects are strongly related to the dye amount on TiO_2 .

The *dispersion forces* between the chromophore and the electrolyte can also affect the electron lifetime. The organic chromophore with smaller band gap has stronger

dispersion forces compared to the zinc porphyrin, which attracts more I_3^- to its surroundings. The different position of the organic chromophore at the TiO_2 surface influences the electron lifetime. This effect is negligibly related to the dye amount on TiO_2 .

To identify whether the dye-loading-related *blocking effect* / *coordination* or structure-related *dispersion forces* contributes to the elongated electron lifetimes in PorR, devices using reduced dye loaded films were employed (photovoltaic performance is shown in Appendix Table A7). SLIM-PCV as well as charge extraction measurements were carried out on DSSCs using PorR and Por.

Significant longer electron lifetimes are observed in DSSCs using PorR compared to that using Por with reduced dye loadings (Fig. 8.12(a) and (b)). The less the dye loading, the more difference in electron lifetimes between PorR and Por. Four times and thirty times longer electron lifetimes are observed in DSSCs using PorR compared to that using Por with 12% and 4% of full dye loading condition at the same electron density, respectively (0.053 versus 0.012 and 0.03 versus 0.001 , respectively, at $ED = 1.5 \times 10^{18} \text{ cm}^{-3}$, Appendix Table A7). The diffusion coefficient (Fig. 8.12(c)) as well as the conduction band edge potential (indicated by the intercept on y-axis in Fig. 8.12(d)) between the two dyes are similar.

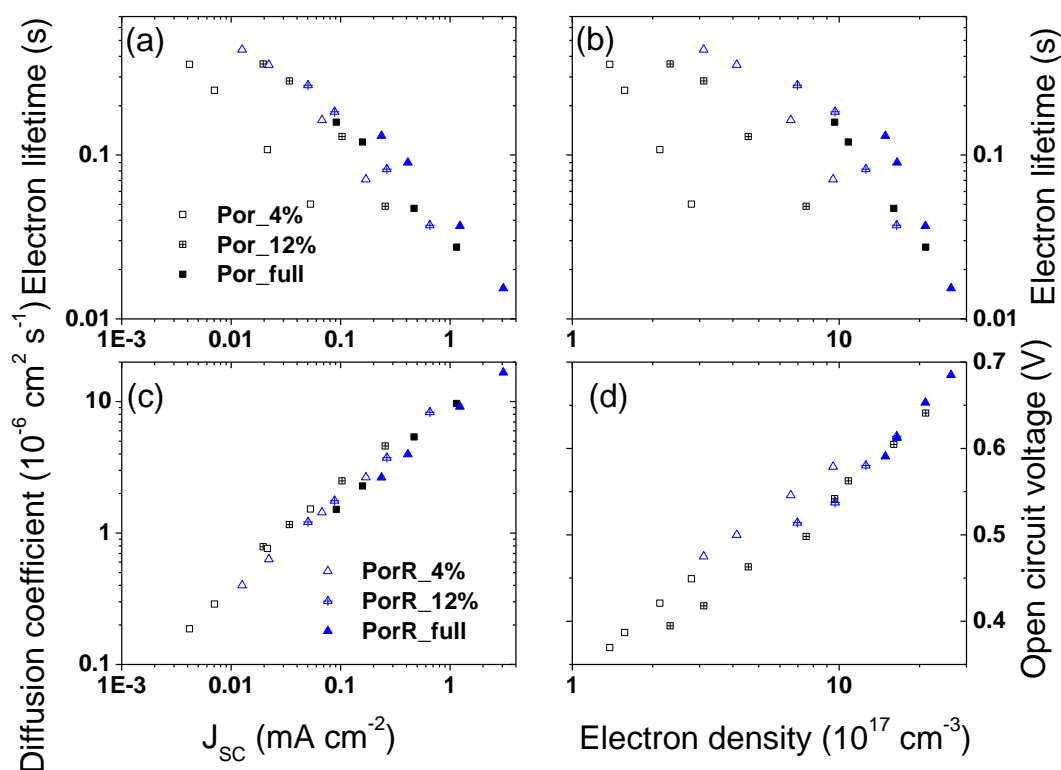


Figure 8.12 (a) Electron lifetime and (c) diffusion coefficient versus short circuit current density, (b) electron lifetime and open circuit voltage versus electron density for DSSCs using Por and PorR with different dye loadings. Film thickness: $2.8 \pm 0.1 \mu\text{m}$.

The greatly reduced electron lifetime of DSSCs using Por with reducing dye loadings is mainly due to the decreased blocking effect. The blocking effect in Por is mainly caused by the dye amount and the coordination with *t*BP (Fig. 8.13). The less the Por molecules on the TiO_2 surface, the fewer the numbers of *t*BP-Por molecules, and the more pathways for I_3^- to go closer to the TiO_2 surface. In contrast, the electron lifetime of PorR using reduced dye loadings is not significantly affected. This suggests the dispersion forces functioning in the di-chromophoric dye: with full dye loading condition, both the blocking effect and the dispersion forces benefit the electron lifetime of PorR; with reduced dye amount, the blocking effect in the di-chromophoric dye is negligible while dispersion forces play the key role in retarding the recombination (Fig. 8.13). The stronger dispersion forces between the polarized organic chromophore and I_3^- , which are not affected by the dye loading, attract the I_3^- to the organic chromophore and enlarge the recombination distance.

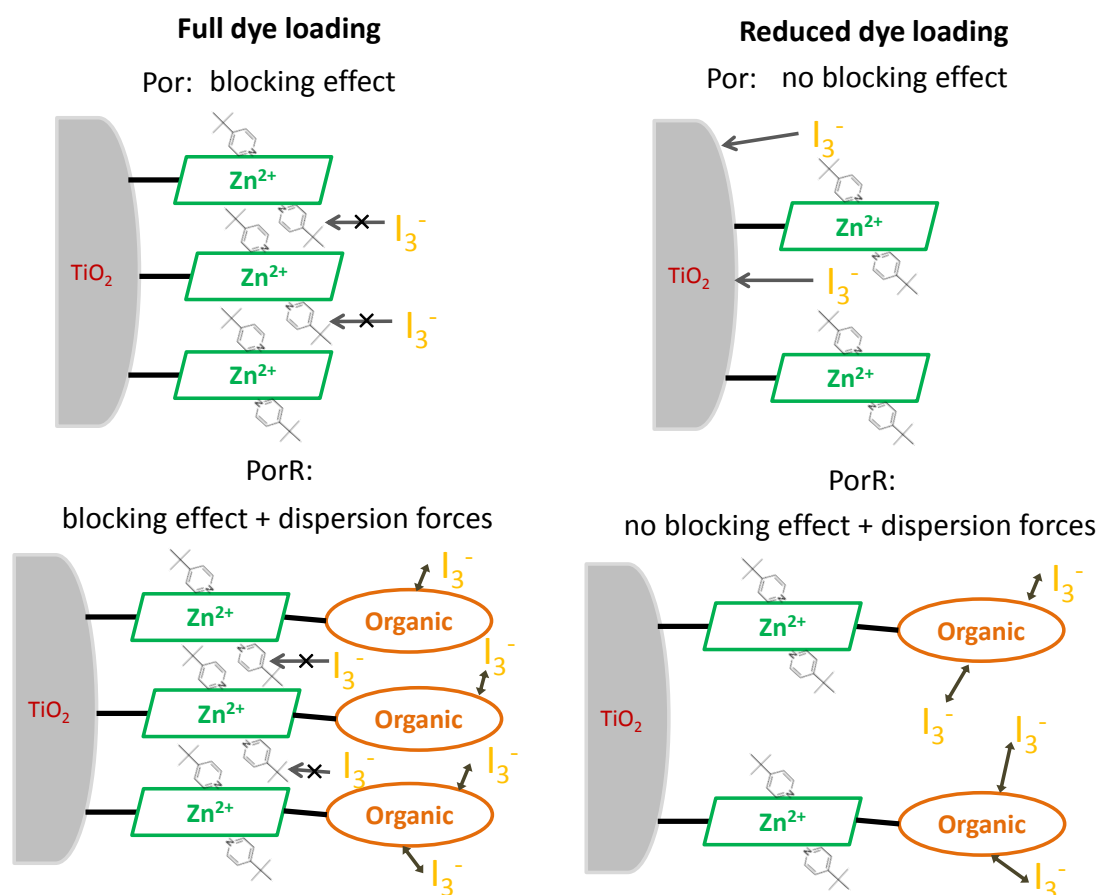


Figure 8.13 Graphical illustration of the blocking effect in Por and blocking effect + dispersion forces in PorR at full and reduced dye loadings.

The utilizing of dispersion forces in di-chromophoric design to enhance the electron lifetime in DSSCs is reported for the first time by this work. The importance of this finding is that by rational molecular design, the “*detrimental*” intermolecular forces can be used to *enhance* the photovoltage of DSSCs.

8.11. Conclusions

This chapter has clarified the origin of the improved photovoltage in di-chromophoric dyes by employing stepped light-induced transient measurements of photocurrent and photovoltage and charge extraction measurements. The main findings are:

1. The increased photovoltage of the di-chromophoric dyes was assigned to the longer electron lifetimes.

2. The longer electron lifetimes of the DSSCs using the PorR and PorO dyes compared to that using Por were mainly due to the blocking effect from the additional organic chromophores.
3. Faster recombination was implied by both larger diffusion coefficient and negatively shifted TiO₂ conduction band potential in DSSCs using the cobalt electrolyte compared to that using the I⁻/I₃⁻ electrolyte. The longer electron lifetimes of the PorO dyes compared to Por in DSSCs using the cobalt electrolyte suggest the utility of di-chromophoric dyes in DSSCs.
4. By comparing to the mixed dyes, the di-chromophoric dye PorR demonstrated the utilization of dispersion forces to enhance the electron lifetimes in DSSCs: the organic dyes with stronger dispersion forces attracted more I₃⁻ from the electrolyte compared to the porphyrin enlarging the distance between the conduction band electrons and I₃⁻.
5. Reduced dye loading measurement was used to support the finding in point 4: with negligible blocking effect in both cases but stronger dispersion forces in the latter case, the single chromophoric porphyrin showed much shorter electron lifetimes compared to the di-chromophoric dye.

These findings suggest the di-chromophoric dye design that is a very useful strategy for the sensitizer engineer in DSSCs. Not only the photocurrent of the DSSCs can be enhanced, but also the photovoltage can be maximized using di-chromophoric dyes. DSSCs using one of the di-chromophoric dyes, PorY1, achieved almost the same electron lifetime as well as the open circuit voltage as N719. Even in cobalt electrolyte, the photovoltages of the DSSCs using the di-chromophoric dyes were still much higher compared to that using the single chromophoric porphyrin due to the elongated electron lifetimes.

8.12. References

- (1) Higashino, T.; Imahori, H. *Dalton Trans.* **2015**, 44, 448.
- (2) Xue, X.; Zhang, W.; Zhang, N.; Ju, C.; Peng, X.; Yang, Y.; Liang, Y.; Feng, Y.; Zhang, B. *Rsc Advances* **2014**, 4, 8894.
- (3) Mathew, S.; Yella, A.; Gao, P.; Humphry-Baker, R.; Curchod, B. F. E.;

Ashari-Astani, N.; Tavernelli, I.; Rothlisberger, U.; Nazeeruddin, M. K.; Grätzel, M. *Nat. Chem.* **2014**, *6*, 242.

(4) Zhao, L.; Wagner, P.; Elliott, A. B. S.; Griffith, M. J.; Clarke, T. M.; Gordon, K. C.; Mori, S.; Mozer, A. J. *J. Mater. Chem. A* **2014**, *2*, 16963.

(5) Koumura, N.; Wang, Z.-S.; Miyashita, M.; Uemura, Y.; Sekiguchi, H.; Cui, Y.; Mori, A.; Mori, S.; Hara, K. *J. Mater. Chem.* **2009**, *19*, 4829.

(6) Duffy, N. W.; Peter, L. M.; Rajapakse, R. M. G.; Wijayantha, K. G. U. *Electrochem. Commun.* **2000**, *2*, 658.

(7) Bailes, M.; Cameron, P. J.; Lobato, K.; Peter, L. M. *J. Phys. Chem. B* **2005**, *109*, 15429.

(8) Mozer, A. J.; Wagner, P.; Officer, D. L.; Wallace, G. G.; Campbell, W. M.; Miyashita, M.; Sunahara, K.; Mori, S. *Chem. Commun.* **2008**, *0*, 4741.

(9) Bisquert, J.; Fabregat-Santiago, F.; Mora-Sero, I.; Garcia-Belmonte, G.; Gimenez, S. *J. Phys. Chem. C* **2009**, *113*, 17278.

(10) Zaban, A.; Greenshtein, M.; Bisquert, J. *ChemPhysChem* **2003**, *4*, 859.

(11) Nakade, S.; Kanzaki, T.; Wada, Y.; Yanagida, S. *Langmuir* **2005**, *21*, 10803.

(12) Nakade, S.; Kanzaki, T.; Kubo, W.; Kitamura, T.; Wada, Y.; Yanagida, S. *J. Phys. Chem. B* **2005**, *109*, 3480.

(13) Nakade, S.; Makimoto, Y.; Kubo, W.; Kitamura, T.; Wada, Y.; Yanagida, S. *J. Phys. Chem. B* **2005**, *109*, 3488.

(14) Bisquert, J.; Zaban, A.; Salvador, P. *J. Phys. Chem. B* **2002**, *106*, 8774.

(15) Barnes, P. R. F.; Miettunen, K.; Li, X.; Anderson, A. Y.; Bessho, T.; Grätzel, M.; O'Regan, B. C. *Adv. Mater.* **2013**, *25*, 1881.

(16) Miyashita, M.; Sunahara, K.; Nishikawa, T.; Uemura, Y.; Koumura, N.; Hara, K.; Mori, A.; Abe, T.; Suzuki, E.; Mori, S. *J. Am. Chem. Soc.* **2008**, *130*, 17874.

(17) Griffith, M. J.; Sunahara, K.; Wagner, P.; Wagner, K.; Wallace, G. G.; Officer, D. L.; Furube, A.; Katoh, R.; Mori, S.; Mozer, A. J. *Chem. Commun.* **2012**, *48*, 4145.

(18) Jennings, J. R.; Wang, Q. *J. Phys. Chem. C* **2009**, *114*, 1715.

(19) Boschloo, G.; Häggman, L.; Hagfeldt, A. *J. Phys. Chem. B* **2006**, *110*, 13144.

(20) Fredin, K.; Gorlov, M.; Pettersson, H.; Hagfeldt, A.; Kloo, L.; Boschloo,

G. J. Phys. Chem. C **2007**, *111*, 13261.

(21) Marinado, T.; Nonomura, K.; Nissfolk, J.; Karlsson, M. K.; Hagberg, D. P.; Sun, L.; Mori, S.; Hagfeldt, A. *Langmuir* **2009**, *26*, 2592.

**CHAPTER 9. FASTER DYE CATION REGENERATION IN DI-
CHROMOPHORIC PORPHYRIN DYE DESIGN**

9.1. Introduction

The purpose of this chapter is to evaluate whether dye cation radical generated on the porphyrin chromophore can be ‘internally’ regenerated by hole transfer by the carbazole organic chromophore and furthermore, whether such internal hole transfer affects the recombination / regeneration kinetics between conduction band TiO_2 electrons, dye cations and redox mediators. For this view, PorY1 containing a carbazole triphenylamine (Cb-TPA) chromophore will be used. Fig. 9.1 describes the possible electron transfer pathways in di-chromophoric dye-sensitized solar cell. The green arrow represents the hole transfer from one dye chromophore to the other. The red arrows show the electron transfer steps that will be specifically investigated in this chapter:

1. TiO_2 conduction band electron recombination with dye cation: The kinetics of this reaction may be affected due to the increased charge separation following internal hole transfer within the sensitizer molecule (see Chapter 1 Section 1.2).
2. The dye regeneration kinetics may be affected by internal hole transfer due to i) better electronic coupling between the extra dye cation radical orbitals with the electron donor orbitals of the redox mediator; ii) change in driving force for the regeneration step (see Chapter 1 Section 1.11.2).

The recombination reaction between TiO_2 conduction band electron and oxidized species in the electrolyte (triiodide, cobalt tris(4,4'-dimethyl-2,2'-bipyridine)) may also be affected.

The di-chromophoric dye PorY1 contains a porphyrin and a Cb-TPA moiety (Table 9.1). By design (see Chapter 1 Section 1.2), the dye cation radical spectra of porphyrin and Cb-TPA are distinguishable from each other, hence can be selectively probed using TAS. Dye cation decay kinetics at two probe wavelengths, corresponding to dye cation located at porphyrin and Cb-TPA moieties, were measured in the absence of redox mediator. The intramolecular hole transfer kinetics were also measured and found to be on sub-nanosecond to microsecond time scale. By adding and increasing the concentration of either the iodine or cobalt redox mediator, the dye regeneration kinetics are determined using stretching exponential fitting and kinetic equations introduced in Chapter 1 Section 1.11.3. It was found that charge regeneration rate constant of the Cb-TPA by redox mediator is enhanced compared to Por / TiO_2 . A slight enhancement of

regeneration kinetics from the porphyrin part was also observed in the di-chromophoric dye, which is attributed to the partial intramolecular hole transfer. The importance of these findings is discussed in terms of new design rules for di-chromophoric sensitizers with faster regeneration.

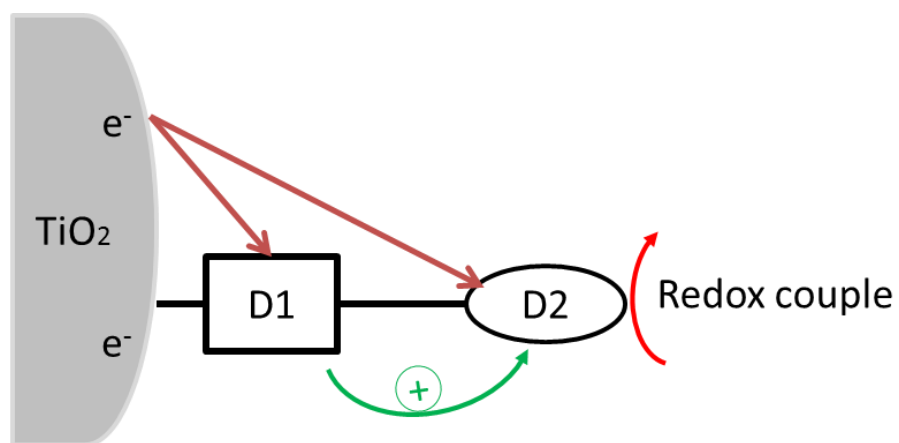
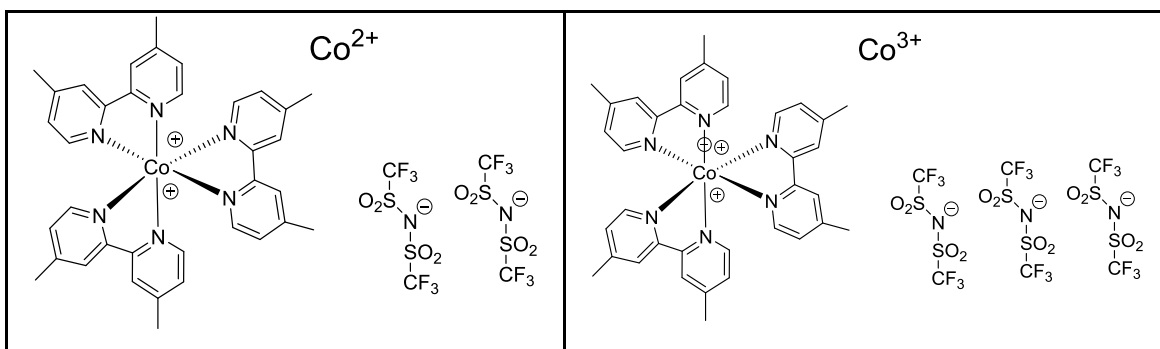


Figure 9.1 Illustration of the purpose of this chapter.

Table 9.1 Molecular structures of the investigated compounds

<p>Por</p>	<p>Cb1</p>
<p>PorY1</p> <p>(to be continued)</p>	



9.2. Experimental

9.2.1 Investigated molecules

The structure of molecules for this study is shown in Table 9.1. The structure of the cobalt couple is also shown.

9.2.2 Characterization in solution

Spectroelectrochemical (SEC) spectroscopy and differential pulse voltammetry (DPV) of each compound was measured in dichloromethane (DCM). The SEC setup combined UV-3600 spectrometer and a potentiostat (eDAQ), and used optically transparent thin-layer electrochemical (OTTLE) cell as the working chamber. The solvent contained 0.1 M tetrabutylammonium perchlorate (TBAP) as supporting electrolyte. The baseline of spectrum for each sample was obtained by applying -0.2 V vs. Fc/Fc^+ .

9.2.3 Transient absorption spectroscopy on dyed TiO_2 films

The photoanode was prepared using the procedure described in Chapter 2. A TiO_2 compact layer, mesoporous TiO_2 layer and a TiCl_4 post-treatment were employed to fabricate the films. The thickness of the films is 2.8-3.2 μm .

The doctor-bladed TiO_2 films with $\sim 10 \mu\text{m}$ thick in Fig. 9.7 were fabricated on a slice of 1 mm microscopic glass with neither compact layer nor the TiCl_4 post-treatment. The reduced dye loading amount film was obtained using 0.1 mM dye solution in THF for 90 minutes for dye-sensitizing. The chenodeoxycholic acid (CDCA)-introduced film in the same figure was obtained using 0.1 mM dye solution with 2 mM CDCA in ethanol for 90 minutes for dye-sensitizing.

The TiO_2/FTO slices were placed into a 0.2 mM dye solution in THF for 90 minutes for dye-sensitizing to fabricate full coverage films. PorY1/ TiO_2 films with 35% dye amount

in Fig. 9.13 were made using a 0.05 mM dye solution in THF and 90 minutes for dye-sensitizing.

Components of the electrolytes are listed in Table 9.2.

Table 9.2 Electrolytes nomination and components

Electrolyte	Components and concentration
Inert I_0	0.1 M LiClO ₄ , and 0.5 M <i>t</i> BP in AN: VN=85:15 (vol)
I_0.001	0.0006 M DMPII, 0.0001 M LiI and 0.05 mM I ₂ in I_0
I_0.01	0.006 M DMPII, 0.001 M LiI and 0.5 mM I ₂ in I_0
I_0.1	0.06 M DMPII, 0.01 M LiI and 5 mM I ₂ in I_0
I_1	0.6 M DMPII, 0.1 M LiI and 50 mM I ₂ in I_0
Inert Co_0	0.05 M LiClO ₄ , and 0.1 M <i>t</i> BP in AN
Co_0.001	0.00011 M Co(dmbpy) ₃ ²⁺ and 0.025 mM Co(dmbpy) ₃ ³⁺ in Co_0
Co_0.01	0.0011 M Co(dmbpy) ₃ ²⁺ and 0.25 mM Co(dmbpy) ₃ ³⁺ in Co_0
Co_0.1	0.011 M Co(dmbpy) ₃ ²⁺ and 2.5 mM Co(dmbpy) ₃ ³⁺ in Co_0
Co_1	0.11 M Co(dmbpy) ₃ ²⁺ and 25 mM Co(dmbpy) ₃ ³⁺ in Co_0
Note: DMPII for 1,2-dimethyl-3-propylimidazolium iodide; AN for acetonitrile; VN for valeronitrile, <i>t</i> BP for <i>tert</i> -butylpyridine.	

TAS was performed on the aforementioned samples in transmission mode using a pump/probe system (INDI Quanta-Ray laser system). Transient absorption spectrum measurements were performed using further amplification of the signals using a voltage amplifier (DHPVA-200) and at a repetition rate of 10 Hz. The laser intensity was 24-26 $\mu\text{J cm}^{-2}$ pulse⁻¹. Kinetic measurements were performed without the amplifier at a repetition rate of 1 Hz. The laser intensity was 45-50 $\mu\text{J cm}^{-2}$ pulse⁻¹. TAS signal was averaged by 512 times for both dye cation spectrum and kinetic measurements.

Fitting equations and procedures of the TAS curves were introduced to Chapter 1 Section 1.11.3. The fitted parameters of all the plots are shown in Appendix Table A5.

9.3. Oxidation potentials of the dyes in solution

Fig. 9.2 plots the differential pulse voltammograms as well as the energy levels of the investigated samples obtained from the peak potential of the first oxidation reactions. This is the same data mentioned in Chapter 4, replotted for clarity.

This has been discussed in Chapter 4. The first broad oxidation feature of PorY1 appears to be a superposition of that of Por and Cb1, which suggests two one-electron reactions. Based on the energy diagram of the individual chromophores, it is easier to oxidize Por than the Cb-TPA moiety. The experimental obtained first oxidation energy level of PorY1 is -5.43 eV versus vacuum, which is between the energy level of the zinc porphyrin part (-5.37 eV of Por) and the carbazole moiety (-5.52 eV of Cb1). The data implies similar, and therefore experimentally difficult to distinguish, energy levels of the two chromophores in the di-chromophoric dye.

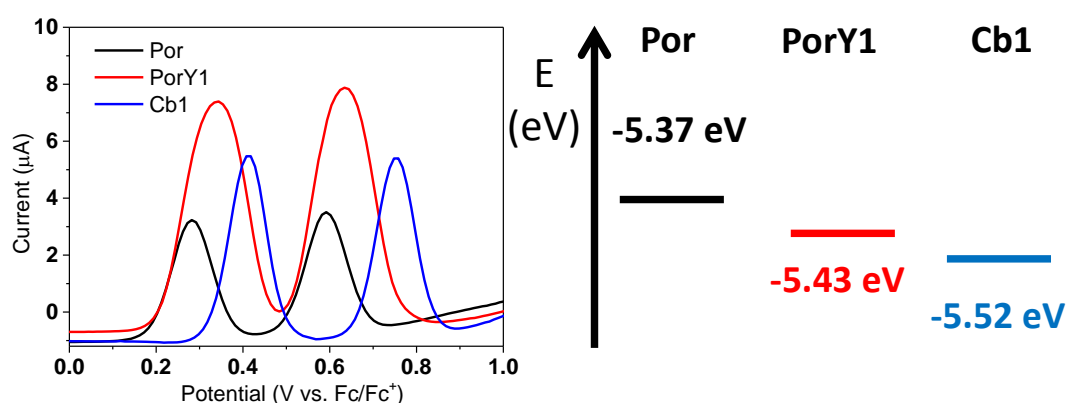


Figure 9.2 Differential pulse voltammetry and the oxidation energy levels of the investigated compounds measured in dichloromethane.

9.4. Absorption spectrum of the electrochemically generated dye cation radicals in solution

To measure the absorption spectra of dye cation radicals in solution, a spectroelectrochemical (SEC) technique was employed.

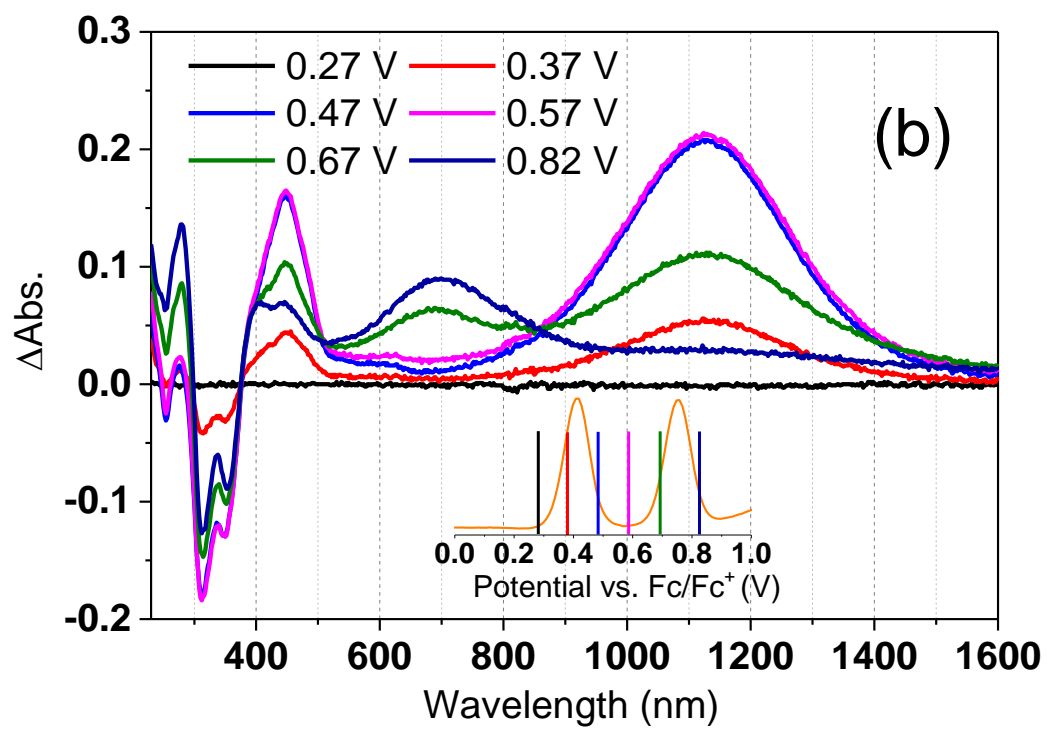
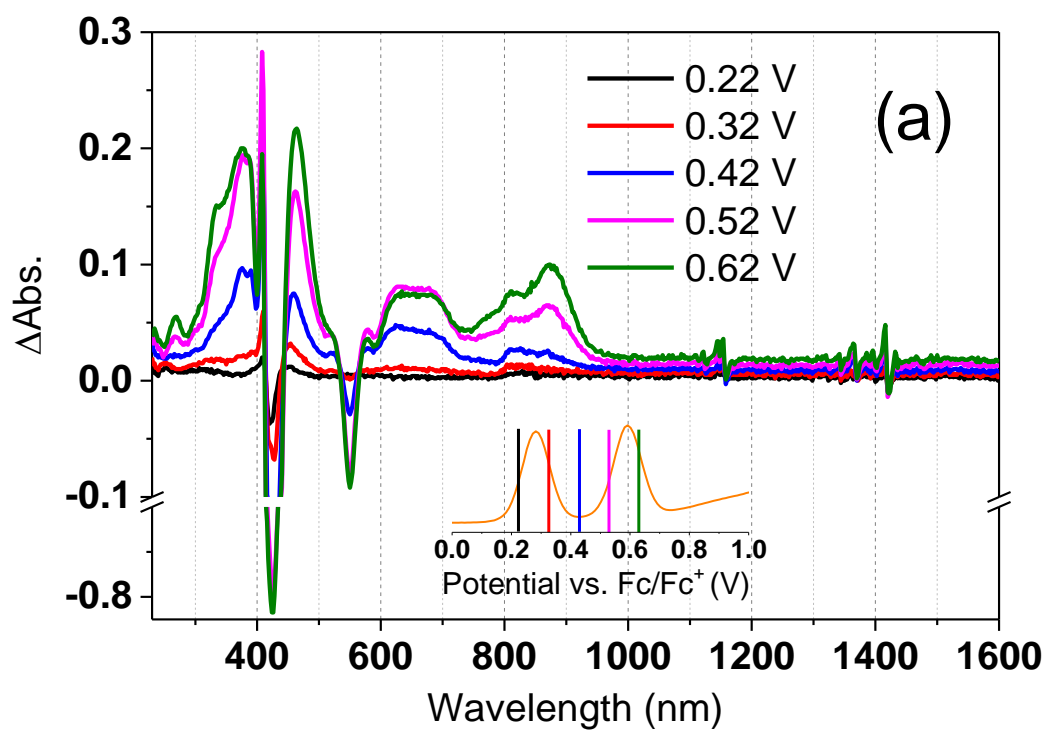
Figs. 9.3(a)-(c) show the spectroelectrochemical spectra of Por, Cb1 and PorY1, respectively, under various applied potentials. These applied potentials are selected based on the differential potential voltammetry plots in the insets. The change in

absorption ($\Delta\text{Abs.}$) indicates the change in light absorption between the radical cation and the dye ground state. It depends on the extinction coefficient of the generated species and their concentration.

The porphyrin radical cation ($\text{Por}^{\bullet+}$) absorbs light at different wavelengths compared to the carbazole radical cation ($\text{Cb-TPA}^{\bullet+}$) as shown in Figs. 9.3(a)-(b). The oxidation of the porphyrin Por results in the bleaching of the Soret (400-440 nm) and Q bands (530-560 nm) (Fig. 9.3(a)). The oxidized porphyrin shows an absorption spectrum with features at 280-400 nm, 430-500 nm, 600-700 nm and 700-900 nm. The carbazole radical cation absorbs at 230-280 nm and 320-500 nm (Fig. 9.3(b)) and an intense absorption spectrum is observed at 800-1500 nm wavelength range. This near infrared wavelength absorption of $\text{Cb-TPA}^{\bullet+}$ is spectrally distinguishable from the features of $\text{Por}^{\bullet+}$ (Fig. 9.3(a) and (b)).

Absorption features of both porphyrin radical cation and the carbazole radical cation are featured in PorY1 from potentials higher than 0.47 V (Fig. 9.3(c)). Based on the individual SEC spectra, the absorption in the 1000-1600 nm wavelength range is assigned to $\text{Cb-TPA}^{\bullet+}$, while that at the 260-1000 nm wavelength range is attributed to $\text{Por}^{\bullet+}$, with some contribution from $\text{Cb-TPA}^{\bullet+}$. The porphyrin is oxidized first at 0.27 V while the Cb-TPA is oxidized latter after 0.37 V.

The $\Delta\text{Abs.}$ plots of PorY1 all show a step increase of the intensity at ~950 nm, which is due to the instrument noise from the change of gratings.



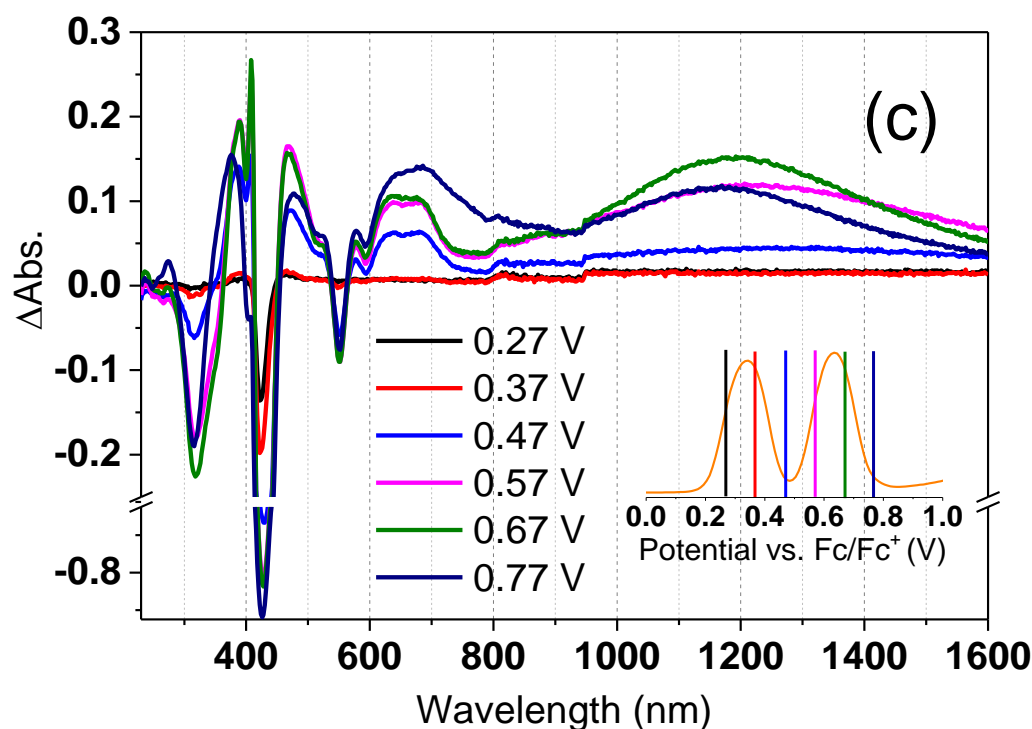


Figure 9.3 Spectroelectrochemical (SEC) spectra of (a) Por, (b) Cb1 and (c) PorY1 at different oxidation potentials vs. Fc/Fc^+ . The inset gives the differential potential voltammetry oxidation plots and indicates the applied potentials by colourful lines.

9.5. Absorption spectrum of photogenerated dye cation radicals on TiO_2 electrodes using transient absorption spectroscopy

In the TAS experiments conducted here, the sample is photoexcited at 532 nm with short (8 ns) laser pulses. The transient absorption (TA) spectrum is represented by the change in optical density (ΔOD) as a function of probe wavelength for a given delay time, as described in Chapter 1 and 2. Similar to SEC measurements, the change in absorption is proportional to the extinction coefficient and the concentration of the photogenerated species.

TAS was employed to measure the absorption of dye cations of Por and PorY1 on TiO_2 films using the inert electrolyte (I_0). Features are observed in the 550-950 nm wavelength range (Fig. 9.4(a)). These match well with the SEC produced Por cation (Por^+). The two negative transient absorption signal bands at 570 nm and 620 nm are assigned to the bleaching of the Q bands and its recovery to ground state. The transient

absorption signal value of ~ 0.05 in the 950-1600 nm wavelength range is assigned to the absorption of injected electrons in TiO_2 ($\text{TiO}_2(\text{e}^-)$).^{1,2}

The PorY1 / TiO_2 cation shows an intense absorption band in the near infrared wavelength range, i.e. 1000 nm-1600 nm (Fig. 9.4(b)). The PorY1 / TiO_2 cation spectrum matches well the electrochemically generated PorY1⁺ spectrum (SEC) in solution (Fig. 9.3(c)). The new absorption band observed in PorY1 / TiO_2 compared to that in Por / TiO_2 is assigned to the formation of Cb-TPA⁺. This suggests that both porphyrin radical cation and Cb-TPA radical cation are present on the TiO_2 films following photoexcitation at 532 nm where porphyrin absorbs.

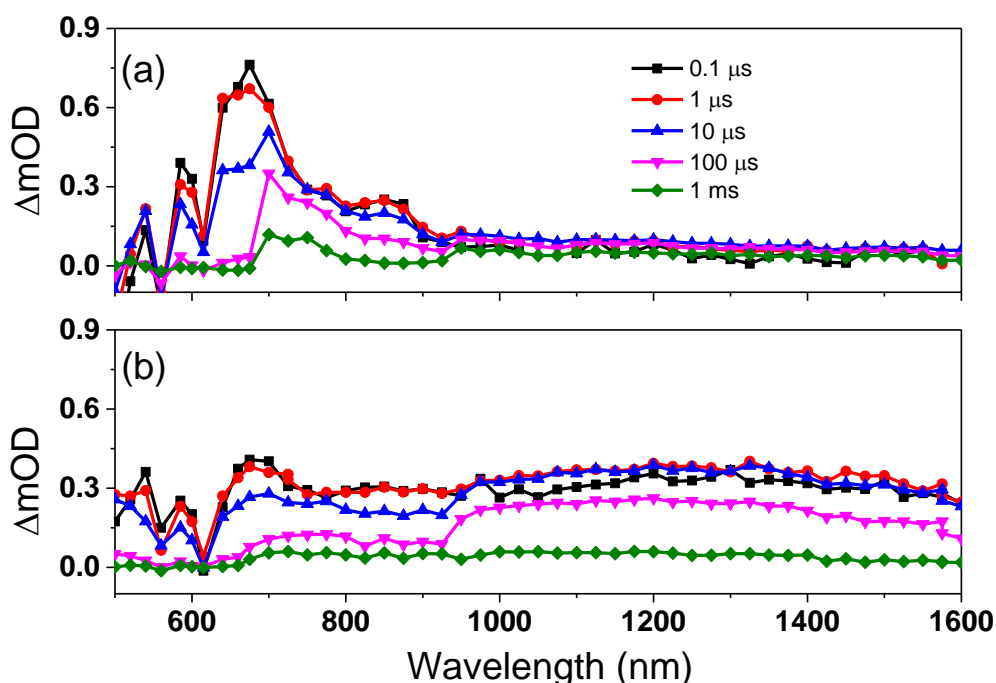


Figure 9.4 Transient absorption spectra of (a) Por and (b) PorY1 on TiO_2 film with the inert electrolyte (I_0) at different time scales after pulsed 532 nm laser irradiation. TiO_2 film thickness: $3 \pm 0.1 \mu\text{m}$.

The dye cation spectra of both sensitizers on TiO_2 films with the iodine redox couple added to the electrolyte are very similar to that with the inert electrolyte at 0.1 μs (Fig. 9.5). It reveals that the addition of the redox mediator does not affect the dye cation spectrum significantly. The TA signals of both sensitizers decay much faster after 0.1 μs in the presence of the redox mediator, which suggest that dye cation regeneration (the red arrow in Fig. 9.1) is faster than the $\text{TiO}_2(\text{e}^-)$ -dye cation recombination (one of the brown arrow in Fig. 9.1).

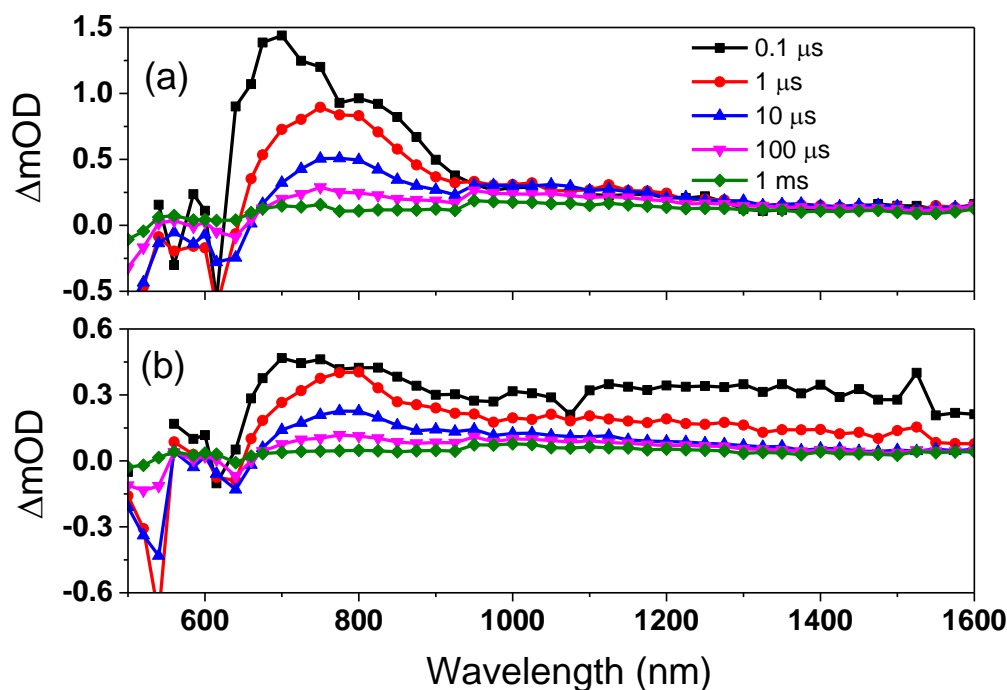
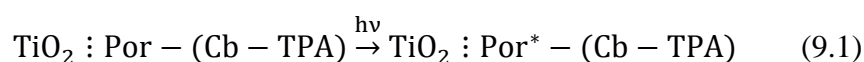
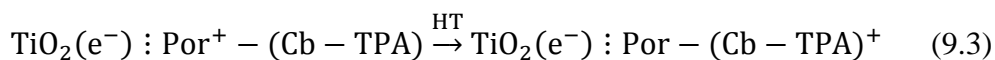
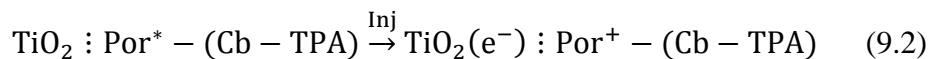


Figure 9.5 Transient absorption spectra of (a) Por and (b) PorY1 on TiO₂ film with the redox electrolyte (0.1 M LiI) at different time scales after pulsed 532 nm laser irradiation.
TiO₂ film thickness: 3±0.1 μm.

The clear difference in dye cation spectra of Por / TiO₂ and PorY1 / TiO₂ using both inert and redox electrolytes suggests that the two cation locations (Por⁺ and Cb-TPA⁺) from PorY1 can be selectively probed. Wavelengths of 800 nm and 1200 nm were chosen to probe Por⁺ decay (of both Por and PorY1) and the Cb-TPA⁺ decay (of PorY1), respectively.

Cb-TPA⁺ is generated by a hole transfer (HT) from Por⁺ in PorY1. An illustration of the processes forming Cb-TPA⁺ is shown in equations 9.1-9.3. 532 nm photons can only excite the porphyrin part to Por^{*}; the organic chromophore does not absorb photons at this wavelength (Eq. 9.1). Energy transfer is not favourable from Por to Cb-TPA as suggested by Chapter 7 Section 7.4. The only mechanism is hole transfer from Por⁺, itself generated following electron injection from excited porphyrin to TiO₂ (Eq. 9.2). The hole on Por⁺ transfers to the organic chromophore via either an intramolecular or intermolecular transfer path (Eq. 9.3).





9.6. Intramolecular hole transfer in PorY1

Fig. 9.6 displays the transient absorption decay curves of PorY1 probed at 1200 nm and 800 nm using the inert electrolyte I_0. A rise is observed in the curve probed at 1200 nm, which occurs with an observed lifetime (τ_{obs}) of 0.9 μs . This was also checked using the sub-ns laser setup (see Appendix Fig. A13). This rise feature demonstrates increased amount of $\text{Por}-(\text{Cb}-\text{TPA})^+$ with time.

More importantly, only a certain percentage of the holes on the porphyrin is transferred to the carbazole chromophore in PorY1 / TiO_2 . This can be suggested by the strong absorption at 800 nm (the initial ΔmOD value of 0.4). A small rise component is also observed in PorY1 on TiO_2 at 800 nm probe wavelength (the red curve in Fig. 9.6). These observations are consistent with hole transfer from Por to Cb-TPA leading to Cb-TPA^+ (Eq. 9.3).

The hole transfer yield is estimated to be 31% providing two assumptions: 1) ΔmOD at 800 nm was only attributed by $\text{Por}^+-(\text{Cb}-\text{TPA})$; 2) the ratios of $\Delta\text{Abs}(\text{Por})^{*+} / \Delta\text{Abs}(\text{Cb-TPA})^{*+}$ (the ΔAbs peak values obtained from SEC spectra of Por at 0.42 V vs Fc/Fc^+ and Cb1 at 0.57 V vs Fc/Fc^+ , respectively, in the 700-900 nm wavelength range) and $\Delta\text{mOD}(\text{Por}^+-(\text{Cb}-\text{TPA})) / \Delta\text{mOD}(\text{Por}-(\text{Cb}-\text{TPA})^+)$ (obtained from TAS spectra of PorY1 / TiO_2 probed at 800 nm and 1200 nm, respectively) are same (see Appendix Table A6).

An explanation of the partial hole transfer is shown in Fig. 9.7. Only some of the PorY1 dyes transfer their holes from the porphyrin to the Cb-TPA moiety, while the others do not transfer their holes. This is reasonable as the driving force for hole transfer is very small as suggested by the energy levels in Fig. 9.2.

Some of the hole transfer occurs on a microsecond time scale. Previously hole transfer on the nanosecond scale has been reported in chromophores with strong conjugation,³⁻⁶ see Chapter 1 Section 1.11.5. This is the first time that a microsecond component of intramolecular hole transfer is reported. Intermolecular hole transfer was reported between dye molecules on TiO_2 .^{6,7}

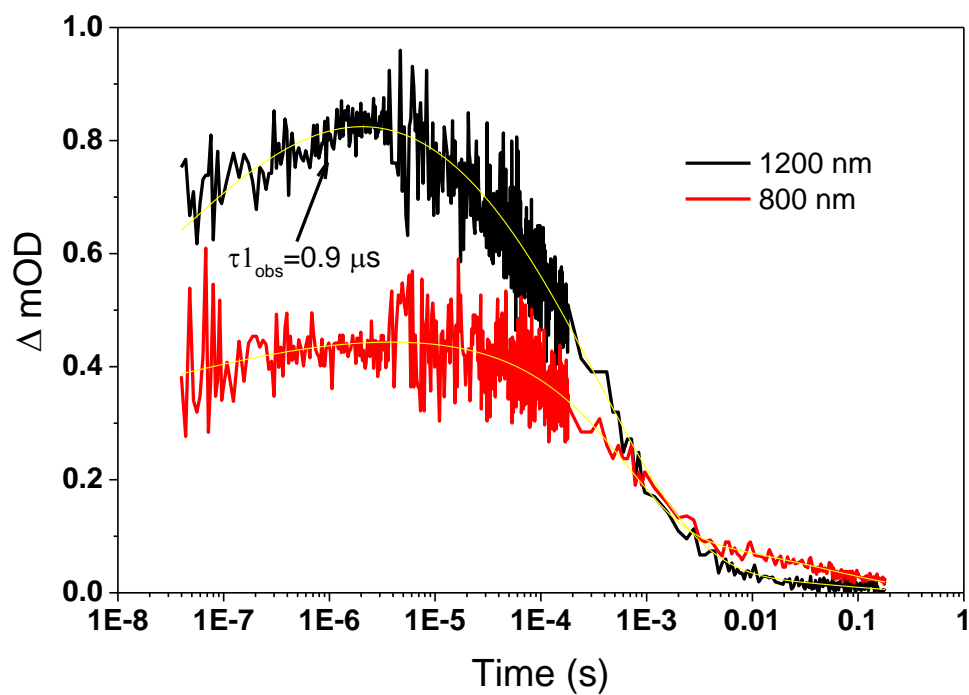


Figure 9.6 Time-resolved transient absorption decay and fitted curves of PorY1 / TiO₂ using I₀ after pulsed 532 nm laser irradiation.

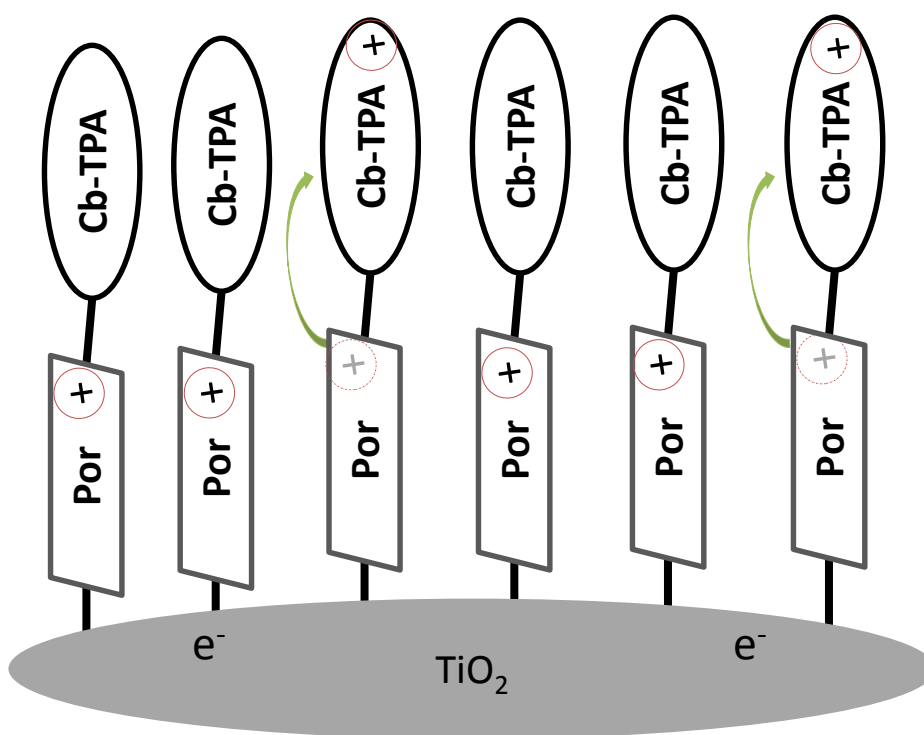


Figure 9.7 Illustration of partial intramolecular hole transfer in PorY1 / TiO₂ after pulsed 532 nm laser irradiation.

Fig. 9.8 shows the transient absorption spectrum decay of PorY1 with reduced dye loading or using co-adsorber CDCA on TiO₂ films. Both reduced dye loading and CDCA should increase the intermolecular distance between the di-chromophoric dyes, leading to slower or diminishing intermolecular hole transfer. The measurement in Fig 9.8 suggests very small changes in the transient signal decay (0.9 μ s of the hole transfer at full dye loading, 0.3~0.4 μ s at reduced dye loading or using CDCA), which in turn suggests that the main component of the hole transfer in this time scale is intramolecular, i.e. occurs within the di-chromophoric dye. The larger transient absorption intensity of CDCA-introduced film after 0.01 s indicates that the electrons in TiO₂ can live much longer compared to the reduced dye film.

The intramolecular hole transfer in the di-chromophoric dye was slower than reported before. Two contributing factors are i) the driving force for this hole transfer is very small based on peak potentials (see Fig. 9.2); ii) the weak electronic coupling due to the dihedral angle between Por and the Cb-TPA (see Chapter 3).

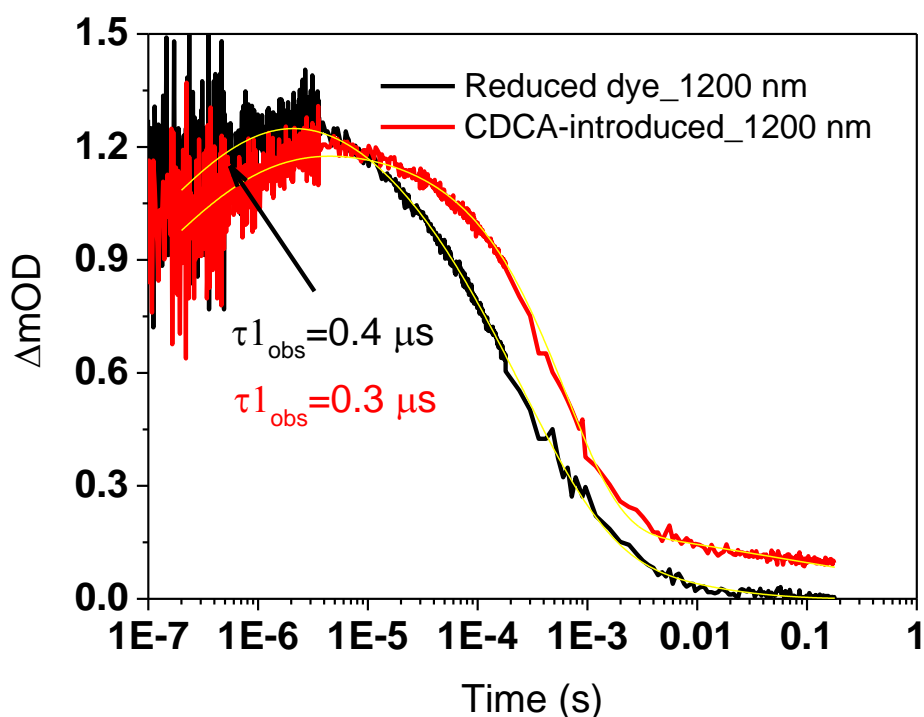


Figure 9.8 Time-resolved transient absorption decay and fitted curves of the reduced dye and CDCA-introduced PorY1-sensitized TiO₂ film using I₀ after pulsed 532 nm laser irradiation.

Dye amounts of the reduced dye and the CDCA-introduced conditions are $6 \times 10^{-5} \text{ mol cm}^{-3}$ and $3 \times 10^{-5} \text{ mol cm}^{-3}$, respectively.

9.7. Conduction band electrons - dye cation recombination in di-chromophoric design

Fig. 9.9(a) and (b) display the transient absorption decay curves of Por and PorY1, respectively, on TiO_2 using the inert electrolyte I_0. The fitted lines and the observed lifetimes are also shown.

The transient absorption decay observed for Por on TiO_2 at 1200 nm in Fig. 9.9(a) is assigned to the decay of TiO_2 conduction band electrons. The transient absorption decay at 800 nm is assigned to the recombination of Por^+ with TiO_2 conduction band electrons. The observed lifetime of this reaction is 2.3 ms. This is four times longer than that of $\text{TiO}_2(\text{e}^-) \text{Por}^+(\text{Cb-TPA})$ recombination (observed lifetime of 0.8 ms, Fig. 9.9(b)). However, it is not straightforward to resolve small differences in recombination kinetics on this timescale. First, the recombination kinetics should depend on electron density and trap distribution, which is not measured or carefully controlled in these experiments. Secondly, some portion of electrons can be trapped for longer than 1 s. The repetition rate of the laser is 1 s, so some of the long-lived charges may accumulate in the TiO_2 during the measurement causing a Fermi level shift and change in the recombination kinetics. Note that the lifetime is obtained from fitting to a stretched exponential. At these long time delays the stretching factor is small and has a strong influence on the calculated lifetime.¹ There is some ambiguity in this procedure to obtain comparable lifetime, so direct comparisons are not straightforward.

The important point is that internal hole transfer does not lead to significantly increased lifetime in PorY1 sensitized TiO_2 films. The $\text{TiO}_2(\text{e}^-) \text{Por}(\text{Cb-TPA})^+$ recombination lifetime is 0.9 ms as probed at 1200 nm, while the $\text{TiO}_2(\text{e}^-) \text{Por}^+(\text{Cb-TPA})$ recombination is 0.8 ms when probed at 800 nm (Fig. 9.9(b)). No change in the recombination kinetics has been reported in porphyrin-triphenylamine dyads with an intramolecular hole transfer.⁸ This is likely due to the fact the recombination is controlled by release of electron from electron traps, and not by the change in distance between the two chromophores in the dyads.⁴ In other words, the recombination is electron diffusion limited, and not limited by interfacial electron transfer. The electron

density in these experiments was around $6 \times 10^{17} \text{ cm}^{-3}$, calculated based on the laser intensity and light harvesting efficiency at 532 nm (Appendix Table A2). It is probably too low to observe recombination kinetics controlled by interfacial electron transfer.

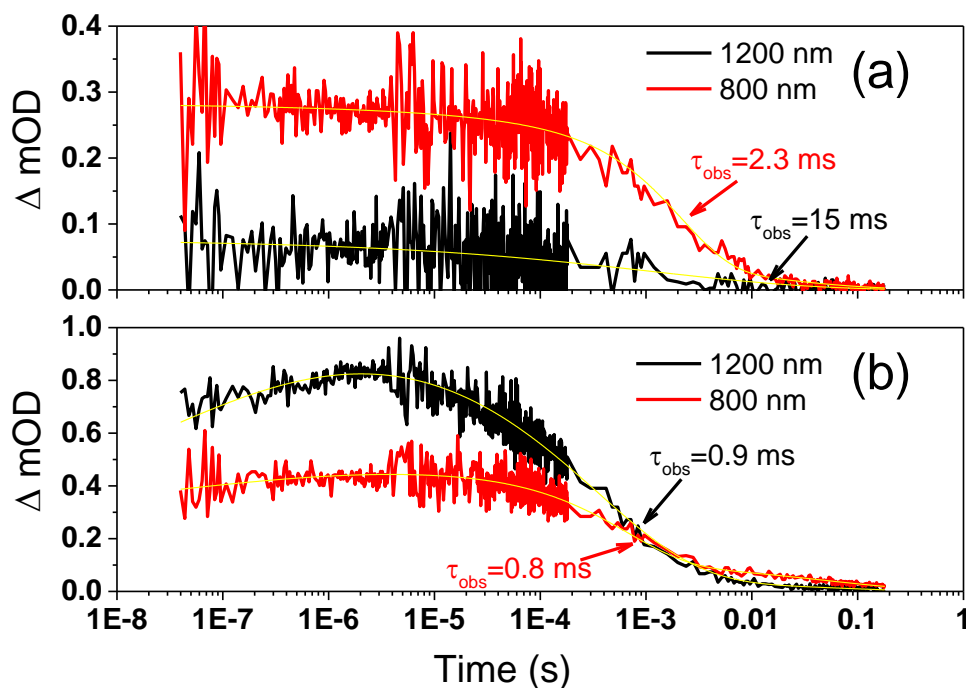


Figure 9.9 Time-resolved transient absorption decay and fitted curves of (a) Por / TiO₂ and (b) PorY1 / TiO₂ using I₀ after pulsed 532 nm laser irradiation.

9.8. Faster dye cation regeneration using the iodine-based electrolyte in PorY1 / TiO₂

Fig. 9.10(a) and (b) show the transient absorption decay of Por and PorY1 using 0.1 M LiI (I₁) as the electrolyte. A fast decay of the transient absorption signal is observed before 0.1 ms, corresponding to regeneration of the dye cation. The long-lived signal beyond 0.1 ms is assigned to the absorption by trapped electrons in TiO₂.

The transient absorption signal of Por⁺ / TiO₂ decays similar as that of Por⁺-(Cb-TPA) / TiO₂ probed at 800 nm (Fig. 9.10(a) and (b)). The fitted lifetimes of Por⁺ / TiO₂ and Por⁺-(Cb-TPA) / TiO₂ are 3.2 μs and 1.9 μs, respectively. Regeneration of Por-(Cb-TPA)⁺ / TiO₂ (PorY1_1200 nm), with an observed lifetime of 0.3 μs, is an order of magnitude faster compared to that of Por⁺ / TiO₂ or Por⁺-(Cb-TPA) / TiO₂. This

suggests that faster regeneration occurs at the Cb-TPA chromophore compared to the porphyrin.

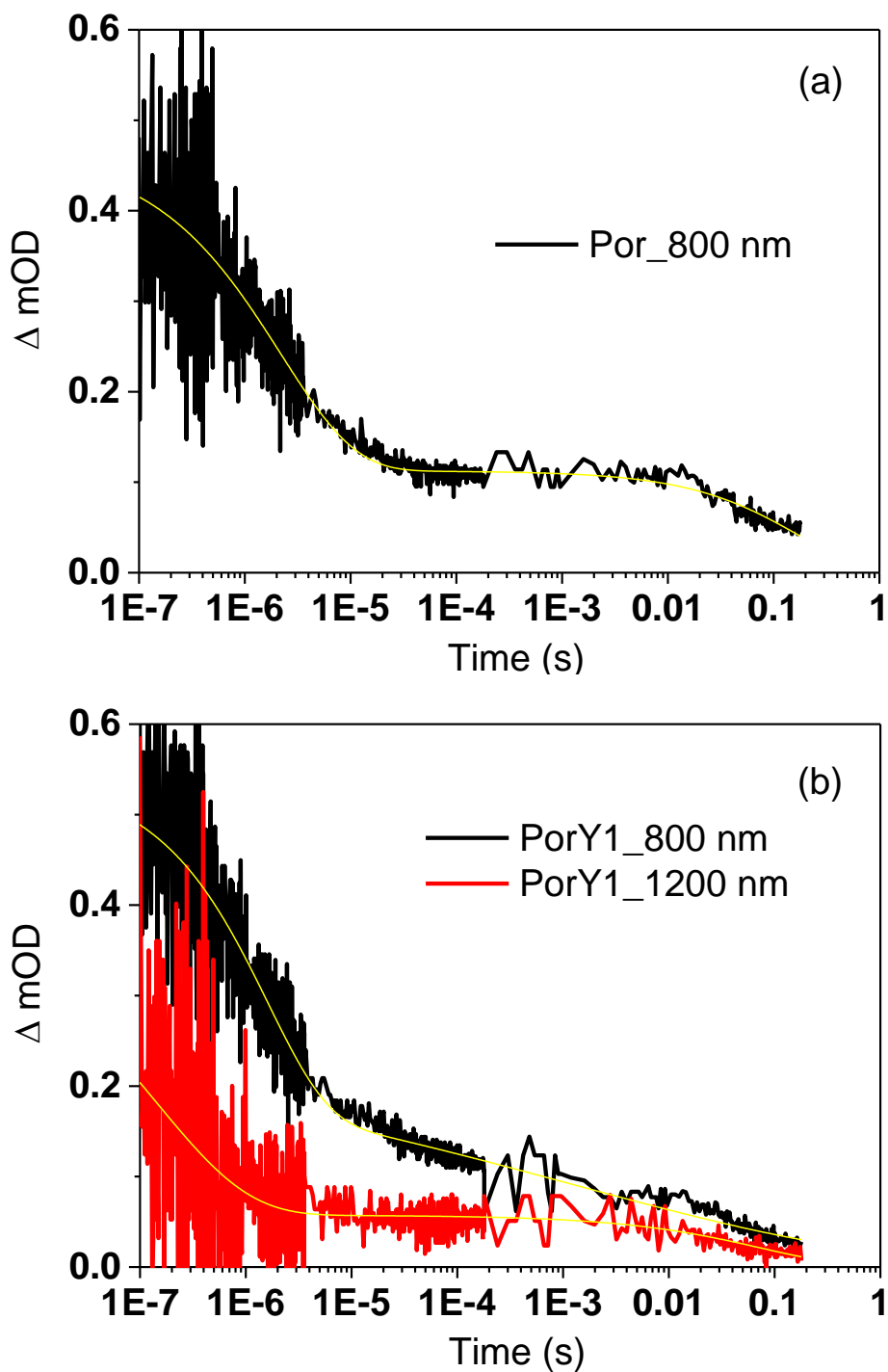


Figure 9.10 Time-resolved transient absorption decay and fitted curves of (a) Por / TiO_2 and (b) PorY1 / TiO_2 using 0.1 M LiI (I_1) after pulsed 532 nm laser irradiation.

9.8.1 Redox couple concentration dependence

A series of I^-/I_3^- electrolytes with different concentrations of the redox couple were employed to measure the regeneration rate constant and its possible dependence on redox couple concentration.

Figs. 9.11(a)-(e) show the transient absorption signal decay for Por^+ / TiO_2 using a series of I^-/I_3^- electrolytes with various concentrations. The decay gets faster with increasing concentration of the redox shuttle. The regeneration of Por cation occurs on microsecond time scale using both 0.1 M LiI (I_{-1}) and 0.01 M LiI ($I_{-0.1}$). The regeneration rate decreases when the electrolyte changes to 0.001 M LiI ($I_{-0.01}$), showing an observed lifetime of 0.5 ms. Further reducing the concentration to 0.0001 M LiI ($I_{-0.001}$) results in an observed lifetime of 1 ms. which is close to the observed lifetime of using electrolyte without redox mediator I_0 (2.2 ms).

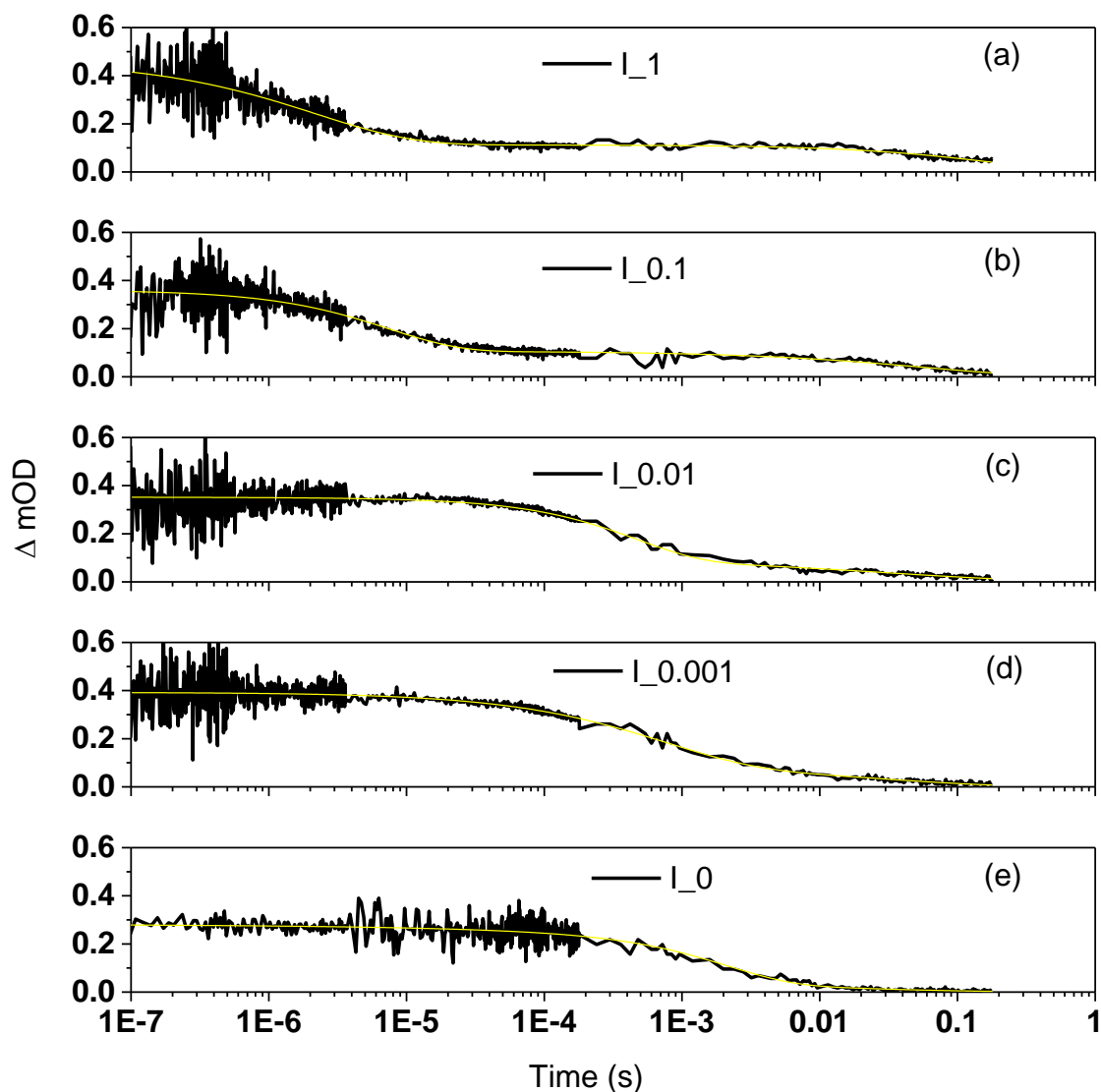


Figure 9.11 Time-resolved transient absorption decay and fitted curves of Por / TiO₂ using the five I⁻/I₃⁻ electrolyte conditions after pulsed 532 nm laser irradiation probing at 800 nm. (a) 0.1 M LiI, (b) 0.01 M LiI, (c) 0.001 M LiI, (d) 0.0001 M LiI and (e) I₀.

Figs. 9.12(a)-(e) show the transient absorption signal decays of Por-(Cb-TPA)⁺ / TiO₂ (probed at 1200 nm) and Por⁺-(Cb-TPA) / TiO₂ (probed at 800 nm) using I⁻/I₃⁻ electrolytes. In all I⁻/I₃⁻ containing electrolytes (0.1 M LiI to 0.0001 M LiI), faster decay was observed at 1200 nm than at 800 nm. This faster decay at 1200 nm than 800 nm indicates the faster regeneration kinetics of Por-(Cb-TPA)⁺ than Por⁺-(Cb-TPA) in PorY1 / TiO₂.

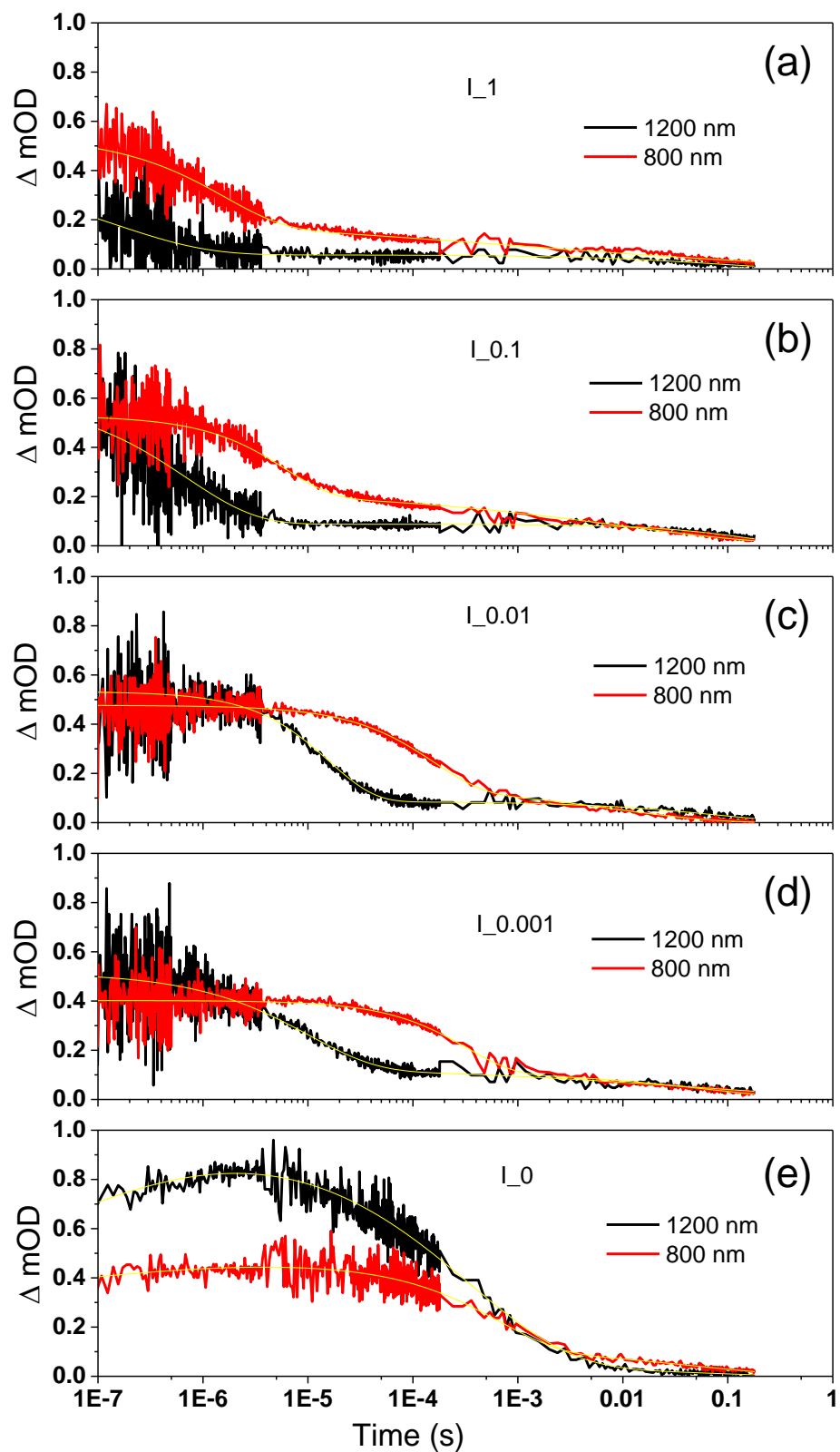


Figure 9.12 Time-resolved transient absorption decay and fitted curves of PorY1 / TiO_2 using the five I^-/I_3^- electrolytes after pulsed 532 nm laser irradiation, probing at 1200 nm and 800 nm, respectively. (a) 0.1 M LiI, (b) 0.01 M LiI, (c) 0.001 M LiI, (d) 0.0001 M LiI and (e) I_0 .

9.8.2 Faster regeneration rate of PorY1 than Por

The regeneration rate constants (k_{reg}) of Por^+ , $\text{Por}^+(\text{Cb-TPA})$ and $\text{Por}-(\text{Cb-TPA})^+$ using different iodine-based electrolytes were calculated as the ratio of observed rate constant and the concentration of I^- (Eq. 9.4).

$$k_{reg} = (k_{obs} - k_{rec}) \times \frac{1}{[M]} \quad (9.4)$$

where, k_{reg} is the observed regeneration rate constant with the unit $\text{M}^{-1} \text{S}^{-1}$; k_{obs} is the observed rate constant with the unit S^{-1} ; k_{rec} is the observed recombination rate constant with the unit S^{-1} ; $[M]$ is the concentration of reduced species in the redox shuttle.

Fig. 9.13 shows the regeneration rate constant versus the I^- concentration of the two porphyrins (Por_800 nm for Por^+ , PorY1_800 nm for $\text{Por}^+(\text{Cb-TPA})$ and PorY1_1200 nm for $\text{Por}-(\text{Cb-TPA})^+$). The regeneration rate constants of each species do not vary significantly with the I^- concentrations in most cases (10% variation). The averaged regeneration rate constants of Por^+ , $\text{Por}^+(\text{Cb-TPA})$ and $\text{Por}-(\text{Cb-TPA})^+$ are $\sim 6 \times 10^5 \text{ M}^{-1} \text{ s}^{-1}$, $\sim 2 \times 10^6 \text{ M}^{-1} \text{ s}^{-1}$ and $\sim 1 \times 10^7 \text{ M}^{-1} \text{ s}^{-1}$, respectively.

The regeneration rate constants of $\text{Por}^+(\text{Cb-TPA})$ are slightly larger than that of Por^+ . On one hand, the hole transfer in PorY1 might contribute to this slightly faster regeneration kinetics. Note that the hole transfer is partial, i.e. only happens in some dye molecules. A large fraction of dye molecules did not undergo hole transfer, but instead, regenerated by the redox mediator..

The regeneration rate constants of $\text{Por}-(\text{Cb-TPA})^+$ are five times larger than that of $\text{Por}^+(\text{Cb-TPA})$. The similar energy levels calculated from the peak potentials of the porphyrin (either in Por or PorY1, Fig. 9.2) and organic chromophore suggest that free energy driving force is not responsible for enhanced regeneration kinetic using the organic chromophore.

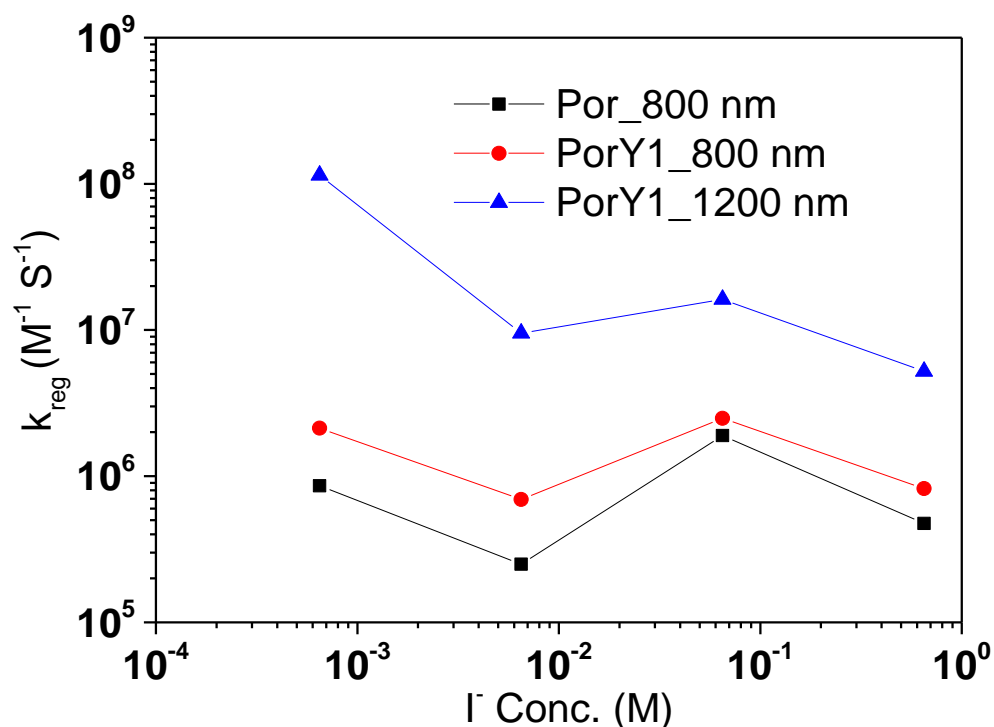


Figure 9.13 Regeneration rate constant of Por and PorY1 on TiO₂ films using different concentrated I⁻/I₃⁻ electrolytes.

As discussed in Chapter 1, regeneration kinetics are influenced by four factors in addition to driving force using the same redox mediator:

1. Steric hindrance on the sensitizer – affects the distance / electronic coupling between the electrolyte and the sensitizer.
2. The electrolyte solvent – affects the ionic mobility in the electrolyte, i.e. diffusion limitation. In either iodine or cobalt electrolyte, the solvent is same within the five different concentrations.
3. Solvation energy (the reorganization energy) – affects the driving force for dye cation regeneration.
4. The concentration of the reduced species in the redox shuttle – alters the probability of reactions between the reduced species in the electrolyte and the dye cation. By using the regeneration rate constant, this factor is no longer considered.

The *steric hindrance* of the carbazole moiety should not contribute to the faster regeneration of PorY1 / TiO₂. The similar regeneration rate of the porphyrin cation in

PorY1 compared with that in Por implies that the alkyl chain on carbazole moiety does not hamper regeneration. Reduced dye loading of PorY1 on TiO₂ films (35% of the full coverage) with diluted electrolytes (0.001 M LiI) showed similar regeneration rate constants as full coverage PorY1 / TiO₂, which suggest that the steric hindrance of Cb-TPA should not affect the regeneration (Appendix, Fig. A12). In some cases, slower regeneration was reported by adding alkyl chains on the sensitizers.^{9,10}

The faster regeneration of Por-(Cb-TPA)⁺ compared to that of Por⁺-(Cb-TPA) may relate to the 3D structure or *the reorganization energies* of the two chromophores. Density functional theory calculated by collaborators suggested that there are more exposed dye cation radical orbitals in the di-chromophoric dye compared to the single chromophoric porphyrin, which may explain the faster regeneration kinetics of the former.

The results suggest a new concept for designing molecules for dye-sensitized solar cells, which is developing the regeneration of sensitizers by attaching molecules with faster regeneration.

9.9. Faster dye cation regeneration using the cobalt-based electrolyte using the di-chromophoric design

The dye regeneration kinetics using cobalt-based electrolytes were also investigated. Cobalt electrolytes are interesting with porphyrins: some porphyrins achieved prominent photovoltaic performance while some did not as introduced in Chapter 1 Section 1.6. Therefore it is worthwhile to study cobalt electrolytes in di-chromophoric dye.

Regeneration kinetics of both Por and PorY1 on TiO₂ films were determined using cobalt electrolytes with systematically varied concentrations. Similar to the results using the I⁻/I₃⁻ electrolytes, faster regeneration rate was found in PorY1 / TiO₂ compared to that in Por / TiO₂.

Fig. 9.14(a) and (b) show the transient absorption decay for Por and PorY1 on TiO₂ using 0.11 M Co(dmbpy)₃²⁺ (Co_1) as the electrolyte. A fast decay of the transient absorption signal is observed before 0.1 ms, suggesting fast regeneration of the dye cation. The absorption of the trapped electrons in TiO₂ is indicated by the above zero values of transient absorption signal at the tail of the transient decay curves.

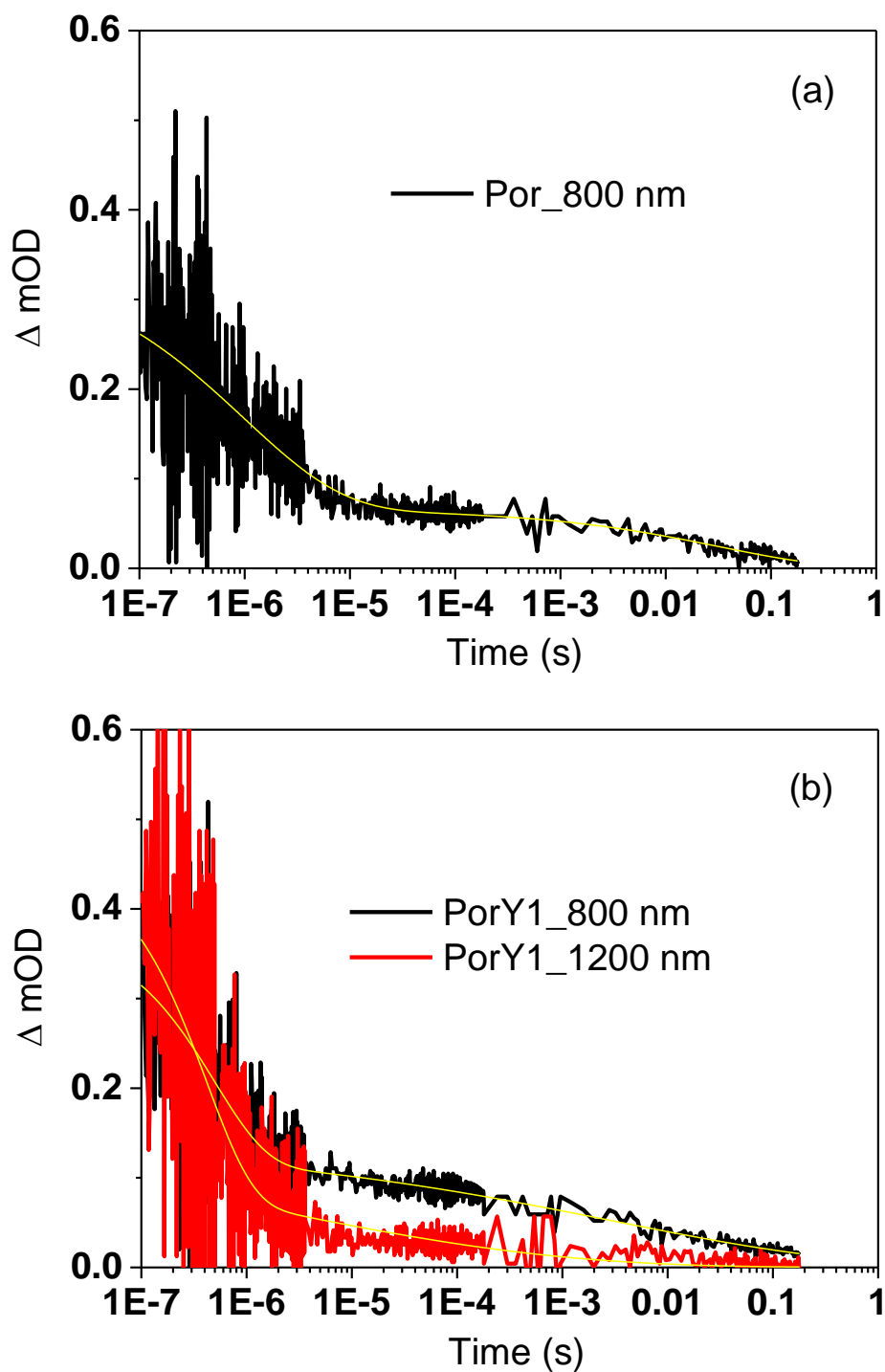


Figure 9.14 Time-resolved transient absorption decay and fitted curves of (a) Por / TiO₂ and (b) PorY1 / TiO₂ using 0.11 M Co(dmbpy)₃²⁺ (Co_1) after pulsed 532 nm laser irradiation.

Faster dye regeneration is observed of PorY1 / TiO₂ compared to Por / TiO₂. Por⁺ / TiO₂ probed at 800 nm shows slower dye regeneration decay (before 10 μ s) compared to

either $\text{Por}^+(\text{Cb-TPA}) / \text{TiO}_2$ probed at 800 nm or $\text{Por}-(\text{Cb-TPA})^+ / \text{TiO}_2$ probed at 1200 nm. The observed lifetimes of $\text{Por}_{800 \text{ nm}}$, $\text{PorY1}_{800 \text{ nm}}$ and $\text{PorY1}_{1200 \text{ nm}}$ are 2.3 μs , 0.5 μs and 0.4 μs , respectively. The transient absorption signal values at 0.1 μs are very similar in the three curves in Fig. 9.14(a) and (b).

9.9.1 Redox couple concentration dependence

Fig. 9.15 shows the transient absorption signal decay for $\text{Por}^+ / \text{TiO}_2$ using a series of cobalt electrolytes with various concentrations of the redox couple. Faster decay of the transient absorption signal is observed with higher concentration of the redox couple, which is similar to the regeneration kinetic trend of $\text{Por}^+ / \text{TiO}_2$ using the iodine-based electrolytes. The observed lifetimes are an order of magnitude longer when diluted by the inert electrolyte to one tenth of the highest concentration, from 2.3 μs using 0.11 M Co(dmbpy)_3^{2+} (Co_1) to 16.5 μs using 0.011 M Co(dmbpy)_3^{2+} (Co_0.1) then to 161 μs using 0.0011 M Co(dmbpy)_3^{2+} (Co_0.01). The decay curves of 0.00011 M Co(dmbpy)_3^{2+} (Co_0.001) and inert electrolyte Co_0 are very similar, which suggests that the recombination of the trapped electrons in TiO_2 and dye cation (the observed lifetimes of 3.9 ms using 0.00011 M Co(dmbpy)_3^{2+} and 2.9 ms using Co_0, respectively) control the transient absorption decay.

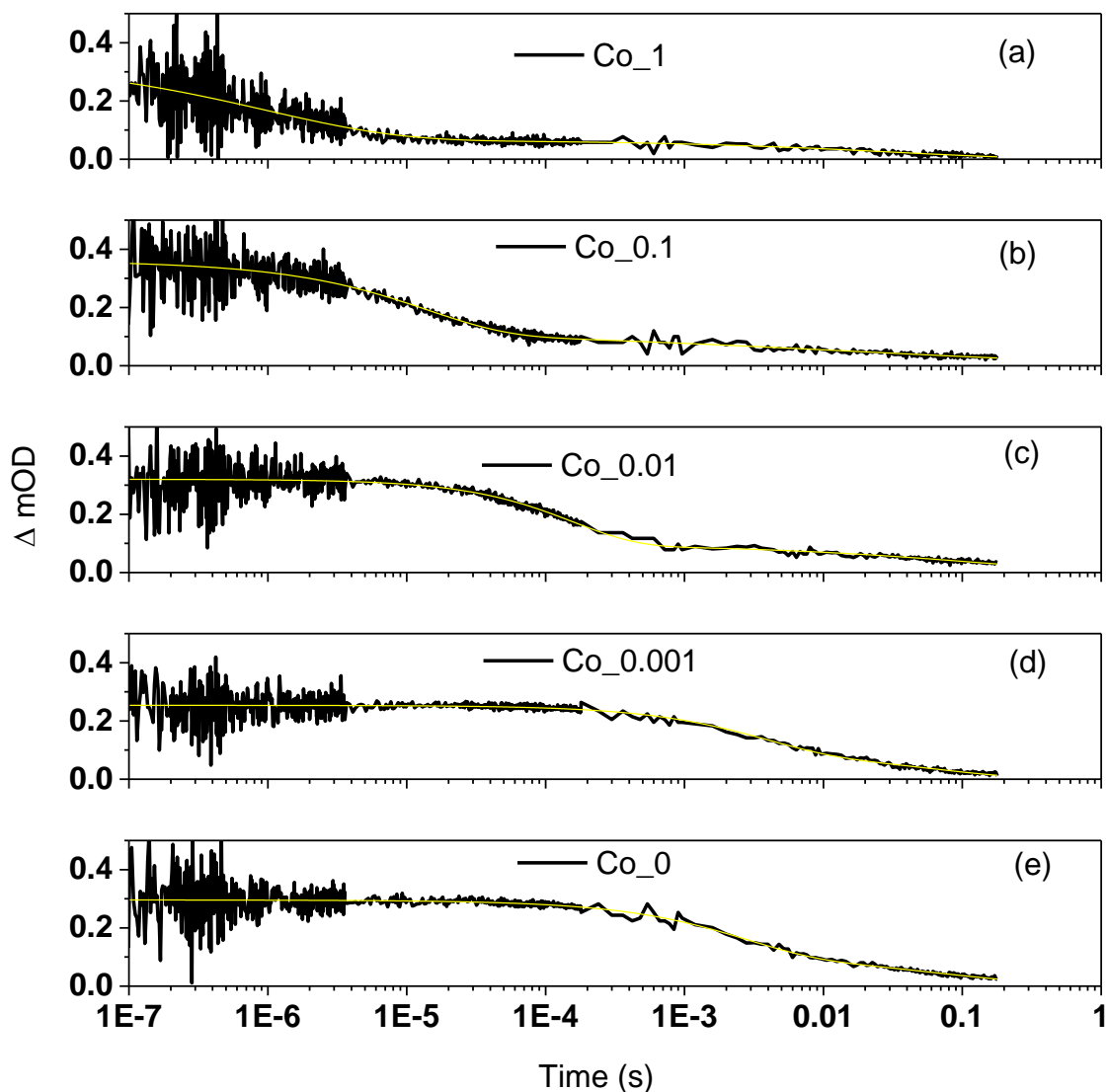


Figure 9.15 Time-resolved transient absorption decay and fitted curves of Por / TiO₂ using the five cobalt electrolyte conditions after pulsed 532 nm laser irradiation probing at 800 nm. (a) 0.11 M Co(dmbpy)₃²⁺, (b) 0.011 M Co(dmbpy)₃²⁺, (c) 0.0011 M Co(dmbpy)₃²⁺, (d) 0.00011 M Co(dmbpy)₃²⁺ and (e) Co₀.

Figs. 9.16(a)-(e) show the transient absorption signal decay of PorY1 / TiO₂ using the cobalt-based electrolytes. Typically, the higher the concentration of the redox shuttle, the faster the decay of transient absorption signal. Faster decay of PorY1_1200 nm than PorY1_800 nm is observed when using 0.0011 M Co(dmbpy)₃²⁺ and 0.00011 M Co(dmbpy)₃²⁺. However, the transient absorption signal decay of Por-(Cb-TPA)⁺ / TiO₂ is very similar to that of Por⁺-(Cb-TPA) / TiO₂ when using 0.11 M Co(dmbpy)₃²⁺ and 0.011 M Co(dmbpy)₃²⁺, which suggests similar dye regeneration kinetics of the two components.

No clear difference in kinetics is observed when using $0.00011 \text{ M Co(dmbpy)}_3^{2+}$ compared to using the inert electrolyte Co_0 at either wavelength. The observed lifetimes using $0.00011 \text{ M Co(dmbpy)}_3^{2+}$ are 0.1 ms and 1.6 ms at 1200 nm and 800 nm, respectively, which are very similar to that using Co_0 (0.2 ms and 1.7 ms at 1200 nm and 800 nm, respectively). Therefore, the regeneration kinetics of PorY1 / TiO_2 using $0.00011 \text{ M Co(dmbpy)}_3^{2+}$ cannot be measured.

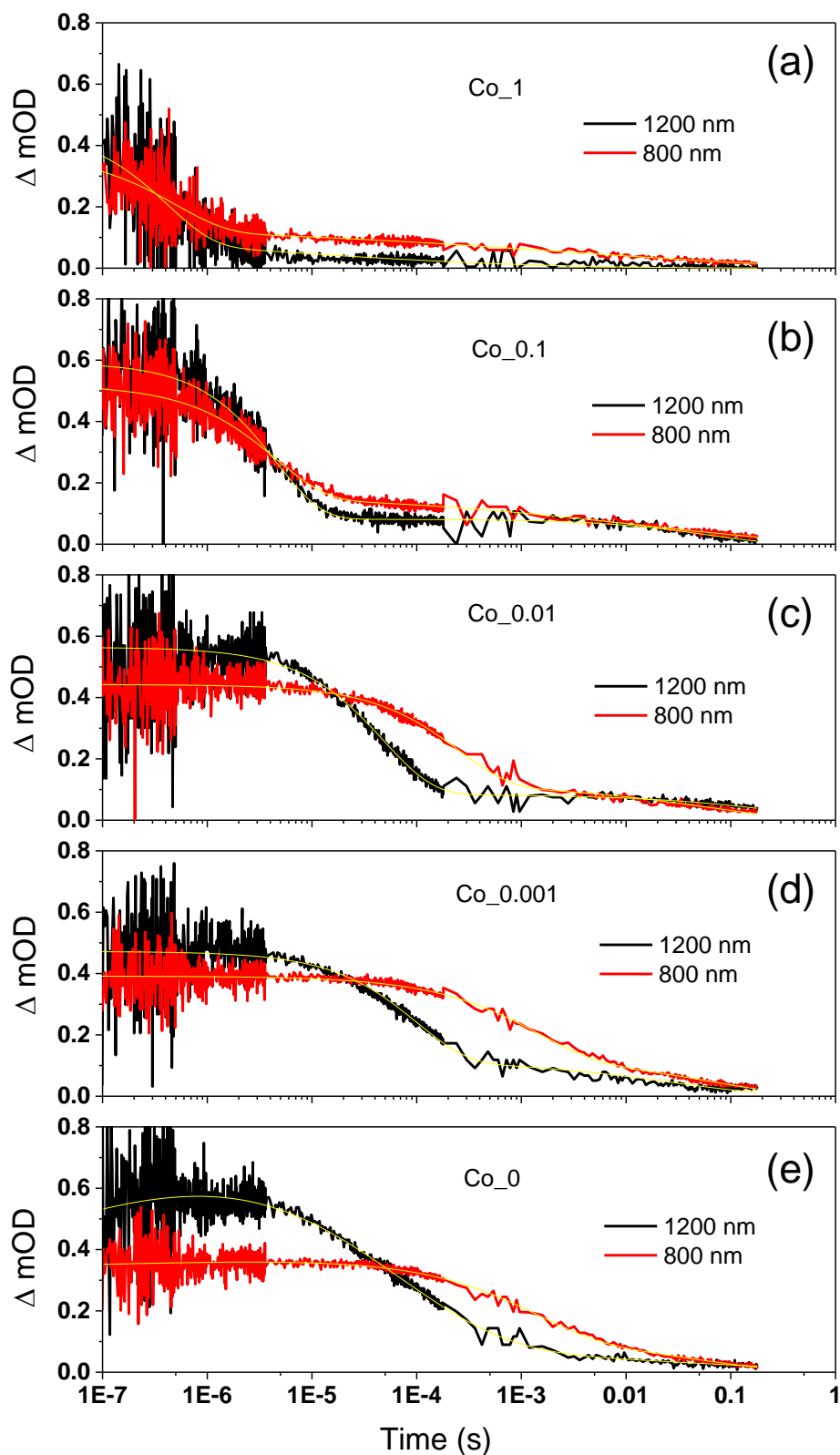


Figure 9.16 Time-resolved transient absorption decay and fitted curves of PorY1 / TiO₂ using the five cobalt electrolyte conditions after pulsed 532 nm laser irradiation probing at 1200 nm and 800 nm, respectively. (a) 0.11 M Co(dmbpy)₃²⁺, (b) 0.011 M Co(dmbpy)₃²⁺, (c) 0.0011 M Co(dmbpy)₃²⁺, (d) 0.00011 M Co(dmbpy)₃²⁺ and (e) Co₀.

9.9.2 Faster regeneration of PorY1 than Por

The regeneration rate constant of Por and PorY1 on TiO₂ is plotted versus the concentration of Co(dmbpy)₃²⁺ (Fig. 9.17). The regeneration rate constants of Por⁺ / TiO₂ and Por⁺-(Cb-TPA) / TiO₂ using 0.00011 M Co(dmbpy)₃²⁺ cannot be measured, hence they are not shown here.

The regeneration rate constants of Por⁺-(Cb-TPA) / TiO₂ are clearly larger than that of Por⁺ / TiO₂ when using 0.011 M and 0.11 M Co(dmbpy)₃²⁺ electrolytes. Similar to that using the iodine electrolyte, this is due to the partial intramolecular hole transfer from the porphyrin to the carbazole triphenylamine chromophore in PorY1. The regeneration rate constant of Por⁺-(Cb-TPA) / TiO₂ reduces by an order of magnitude when using 0.0011 M Co(dmbpy)₃²⁺ electrolyte compared to the other two conditions, which may be due to the steric effect of the carbazole chromophore that blocks the pathway of Co(dmbpy)₃²⁺ to the porphyrin. The steric effect was not observed in iodine conditions, which may relate to the smaller molecule size of I⁻ compared to that of Co(dmbpy)₃²⁺.

Faster regeneration of Por-(Cb-TPA)⁺ than Por⁺-(Cb-TPA) is only observed when using 0.0011 M Co(dmbpy)₃²⁺ compared to the iodine conditions (Fig. 9.17). The regeneration of either cation species in PorY1 displays similar rate constant when using 0.011 M and 0.11 M Co(dmbpy)₃²⁺ electrolytes. The regeneration rate constant of Por-(Cb-TPA)⁺ / TiO₂ ($\sim 2 \times 10^7 \text{ M}^{-1} \text{ s}^{-1}$) is five times faster than that of Por⁺ / TiO₂ ($\sim 4 \times 10^6 \text{ M}^{-1} \text{ s}^{-1}$) by Co(dmbpy)₃²⁺.

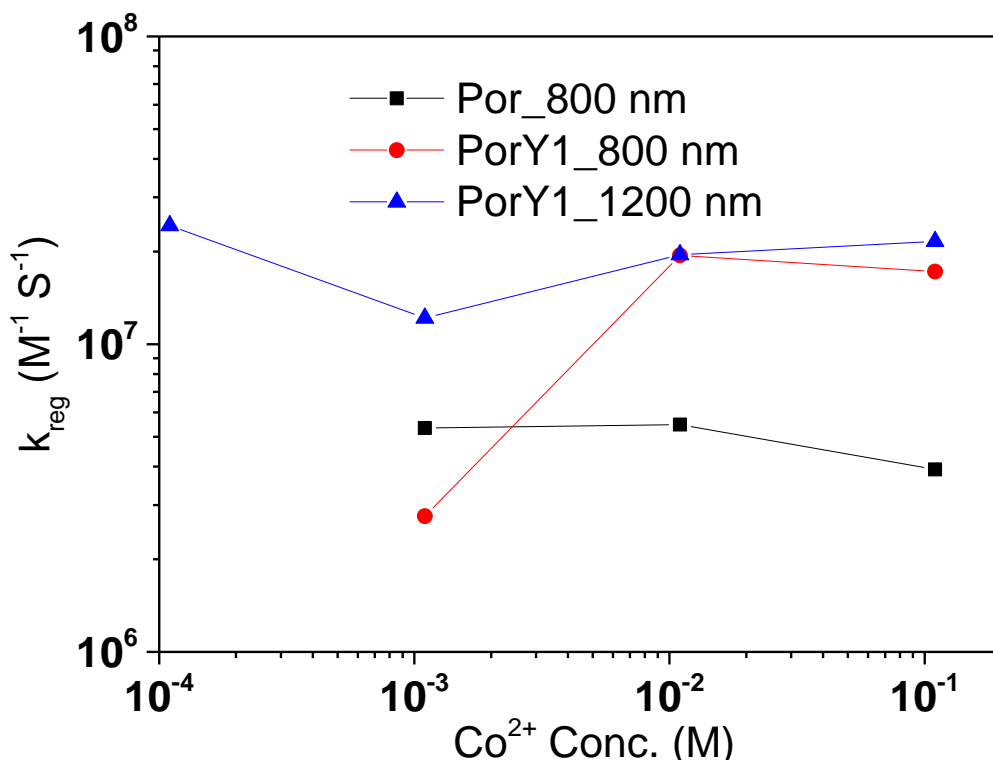


Figure 9.17 Regeneration rate constant of Por and PorY1 on TiO₂ with different concentrated cobalt electrolytes.

9.10. Comparison of regeneration rate between iodine- and cobalt-based electrolytes

Faster regeneration of Por-(Cb-TPA)⁺ / TiO₂ than Por⁺ / TiO₂ was obtained using both iodine- and cobalt-based electrolytes. Regeneration rate constants nearly fifteen times larger were observed in PorY1 compared to Por when using the iodine-based electrolyte. Regeneration rate constants five times larger were observed in PorY1 compared to Por when using the cobalt-based electrolyte. The regeneration rate constants of Por-(Cb-TPA)⁺ / TiO₂ were $\sim 2 \times 10^7 \text{ M}^{-1} \text{ s}^{-1}$ and $\sim 1 \times 10^7 \text{ M}^{-1} \text{ s}^{-1}$ using the cobalt- and iodine-based electrolytes, respectively.

The typical regeneration rate constants of Por⁺-(Cb-TPA) / TiO₂ using the cobalt complex were close to $10^7 \text{ M}^{-1} \text{ s}^{-1}$ when using 0.011 M and 0.11 M Co(dmbpy)₃²⁺ electrolytes, while those were $\sim 2 \times 10^6 \text{ M}^{-1} \text{ s}^{-1}$ when using the iodine-based electrolyte. Faster regeneration of Por⁺ / TiO₂ was also observed when using the cobalt-based electrolyte compared to that using the iodine-based electrolyte ($\sim 4 \times 10^6 \text{ M}^{-1} \text{ s}^{-1}$ vs. $\sim 0.6 \times 10^6 \text{ M}^{-1} \text{ s}^{-1}$, respectively).

The faster regeneration rate constant using Co(dmbpy)_3^{2+} is possibly due to three factors: 1) the reorganization energy; 2) the molecule size and 3) the different concentrations of *t*BP in the electrolytes. The driving force for dye regeneration is ~0.15 eV less in the cobalt-based electrolyte compared to that in the iodine-based electrolyte (the energy diagram in Chapter 3 Fig. 3.2), which may hinder the regeneration rate of the former.^{11,12}

- 1) The reorganization energy of the one-electron reaction cobalt complex is supposed to be smaller compared to that of the two-electron reaction iodine / triiodide redox couple, which may lead to faster dye regeneration kinetics of the former.¹³⁻¹⁶ During the reaction between oxidized dye and iodine, this two-electron reaction may lead to an intermediate species diiodide radicals ($\text{I}_2^{\bullet-}$).^{1, 14, 15} Hence, there are two redox couples participating in the regeneration reaction, i.e. I_2^-/I^- and $\text{I}_3^-/\text{I}_2^-$. The latter couple possessing larger reorganization energy slows the entire reduction reaction.¹⁴ The reorganization energy effect on dye regeneration has been introduced in Chapter 1 Section 1.11.2.
- 2) Co(dmbpy)_3^{2+} with bigger molecule size compared to I^- may also lead to faster dye cation regeneration using the former since more chances for the two reaction species (dye cation and $\text{Co(dmbpy)}_3^{2+} / \text{I}^-$) to be electronic coupled in the cobalt electrolyte.
- 3) The concentration of *t*BP in the two electrolytes are different: 0.1 M in the cobalt electrolyte and 0.5 M in the iodine electrolyte. The component *t*BP can coordinate with the zinc core in the porphyrin.^{17,18} The dye cation regeneration kinetics might be affected due to two possible mechanisms: i) a sub-ns time scale recombination between the injected electron in TiO_2 and the dye cation may happen when less *t*BP was employed in the electrolyte.¹⁹⁻²¹ ii) the energetics of the porphyrin might be slightly changed due to the coordination with *t*BP, which might affect the driving force for regeneration.

9.11. Conclusions

The effect of the organic chromophore on the dye cation regeneration kinetics was investigated using transient absorption spectroscopy. In tandem with the spectroelectrochemical measurement in solution, the transient absorption spectrum of the

dye cation radicals on TiO_2 suggested that the two possible cation radical locations in PorY1 showed two distinct spectral features. Two probe wavelengths were chosen to determine the decay kinetics of the dye cations, 800 nm for the location on porphyrin and 1200 nm for the location on the carbazole moiety. The main findings are:

1. Similar energy levels of the two chromophores in the di-chromophoric dye were suggested by the electrochemistry / spectroelectrochemical measurements.
2. In absence of redox couple, the recombination kinetics in PorY1 was similar to that in the single chromophoric porphyrin on TiO_2 films, which may be due to that this recombination is controlled by the release of electrons from electron traps and not by the interfacial electron transfer.
3. An intramolecular hole transfer from the porphyrin to Cb-TPA was observed on sub-nanosecond to microsecond time scale in PorY1 / TiO_2 when using the inert electrolyte (Fig. 9.18). Such slow intramolecular hole transfer was observed for the first time. This hole transfer occurs only on some of dye molecules. An estimation suggested the hole transfer quantum yield of $\sim 30\%$.
4. In the presence of redox couple, fifteen times faster regeneration rate of $\text{Por}-(\text{Cb-TPA})^+$ were obtained in the di-chromophoric dye compared to the single chromophoric porphyrin on TiO_2 films when using the iodine-based electrolytes. Five times faster regeneration rate of $\text{Por}-(\text{Cb-TPA})^+$ were obtained in the di-chromophoric dye compared to the single chromophoric porphyrin on TiO_2 films when using the cobalt-based electrolytes (Fig. 9.18).
5. The regeneration rate constants of $\text{Por}^+-(\text{Cb-TPA}) / \text{TiO}_2$ are slightly larger compared to that of $\text{Por}^+ / \text{TiO}_2$ (Fig. 9.18). This might be due to the partial intramolecular hole transfer from $\text{Por}^+-(\text{Cb-TPA})$ to $\text{Por}-(\text{Cb-TPA})^+$, the latter has a faster regeneration rate, in the di-chromophoric dye.
6. The regeneration rate constants of $\text{Por}^+ / \text{TiO}_2$, $\text{Por}^+-(\text{Cb-TPA}) / \text{TiO}_2$ and $\text{Por}-(\text{Cb-TPA})^+ / \text{TiO}_2$ were all observed larger when using $\text{Co}(\text{dmbpy})_3^{2+}$ compared to I^- , suggesting the utility of cobalt electrolyte in porphyrin sensitizers.

The faster regeneration kinetics in di-chromophoric porphyrin without sacrificing of the electrochemical energy provides a new sight in dye molecule engineering towards the application in varied photoinduced charge transfer processes.

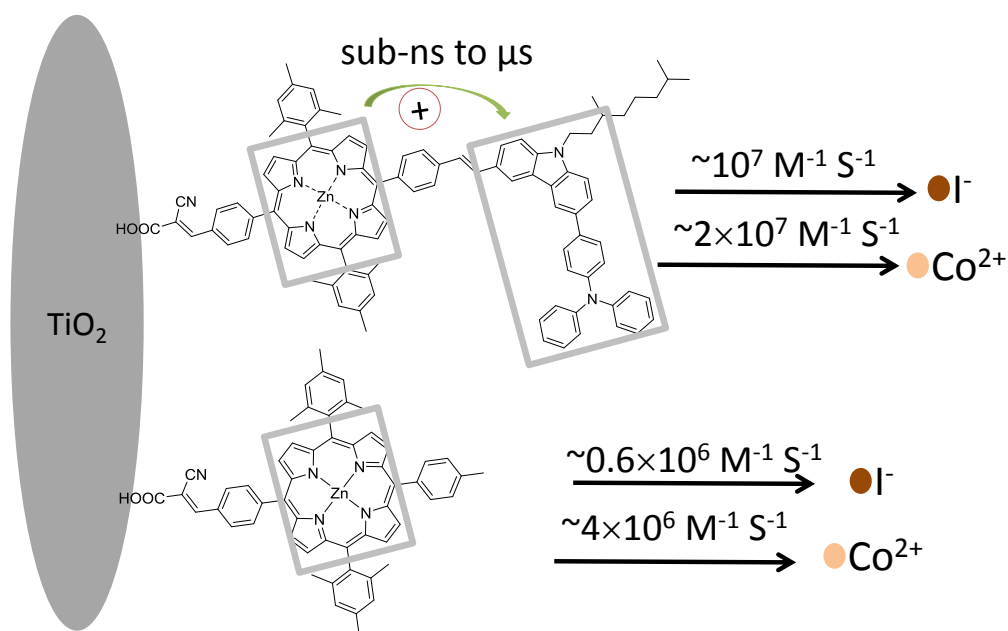


Figure 9.18 Regeneration rate constant of Por and PorY1 on TiO_2 with the I^-/I_3^- and cobalt electrolytes.

9.12. References

- (1) Anderson, A. Y.; Barnes, P. R. F.; Durrant, J. R.; O'Regan, B. C. *J. Phys. Chem. C* **2011**, *115*, 2439.
- (2) Anderson, A. Y.; Barnes, P. R. F.; Durrant, J. R.; O'Regan, B. C. *J. Phys. Chem. C* **2010**, *114*, 1953.
- (3) Argazzi, R.; Bignozzi, C. A.; Heimer, T. A.; Castellano, F. N.; Meyer, G. *J. J. Am. Chem. Soc.* **1995**, *117*, 11815.
- (4) Bonhôte, P.; Moser, J.-E.; Humphry-Baker, R.; Vlachopoulos, N.; Zakeeruddin, S. M.; Walder, L.; Grätzel, M. *J. Am. Chem. Soc.* **1999**, *121*, 1324.
- (5) Hirata, N.; Lagref, J.-J.; Palomares, E. J.; Durrant, J. R.; Nazeeruddin, M. K.; Grätzel, M.; Di Censo, D. *Chem. Eur. J.* **2004**, *10*, 595.
- (6) Hu, K.; Robson, K. C. D.; Beauvilliers, E. E.; Schott, E.; Zarate, X.; Arratia-Perez, R.; Berlinguette, C. P.; Meyer, G. J. *J. Am. Chem. Soc.* **2013**, *136*, 1034.
- (7) Moia, D.; Vaissier, V.; Lopez-Duarte, I.; Torres, T.; Nazeeruddin, M. K.; O'Regan, B. C.; Nelson, J.; Barnes, P. R. F. *Chem. Sci.* **2014**, *5*, 281.
- (8) Hu, K.; Robson, K. C. D.; Johansson, P. G.; Berlinguette, C. P.; Meyer, G. J. *J. Am. Chem. Soc.* **2012**, *134*, 8352.

- (9) Kroeze, J. E.; Hirata, N.; Koops, S.; Nazeeruddin, M. K.; Schmidt-Mende, L.; Grätzel, M.; Durrant, J. R. *J. Am. Chem. Soc.* **2006**, *128*, 16376.
- (10) Ogawa, J.; Koumura, N.; Hara, K.; Mori, S. *Jpn. J. Appl. Phys.* **2014**, *53*, 127301.
- (11) Daeneke, T.; Mozer, A. J.; Uemura, Y.; Makuta, S.; Fekete, M.; Tachibana, Y.; Koumura, N.; Bach, U.; Spiccia, L. *J. Am. Chem. Soc.* **2012**, *134*, 16925.
- (12) Feldt, S. M.; Wang, G.; Boschloo, G.; Hagfeldt, A. *J. Phys. Chem. C* **2011**, *115*, 21500.
- (13) Feldt, S. M.; Lohse, P. W.; Kessler, F.; Nazeeruddin, M. K.; Gratzel, M.; Boschloo, G.; Hagfeldt, A. *Phys. Chem. Chem. Phys.* **2013**, *15*, 7087.
- (14) Boschloo, G.; Hagfeldt, A. *Acc. Chem. Res.* **2009**, *42*, 1819.
- (15) Clifford, J. N.; Palomares, E.; Nazeeruddin, M. K.; Grätzel, M.; Durrant, J. R. *J. Phys. Chem. C* **2007**, *111*, 6561.
- (16) Oskam, G.; Bergeron, B. V.; Meyer, G. J.; Searson, P. C. *J. Phys. Chem. B* **2001**, *105*, 6867.
- (17) Sunahara, K.; Griffith, M. J.; Uchiyama, T.; Wagner, P.; Officer, D. L.; Wallace, G. G.; Mozer, A. J.; Mori, S. *ACS Appl. Mater. Interfaces* **2013**, *5*, 10824.
- (18) Liu, Y.; Lin, H.; Dy, J. T.; Tamaki, K.; Nakazaki, J.; Nishiyama, C.; Uchida, S.; Segawa, H.; Li, J. *J. Phys. Chem. C* **2014**, *118*, 1426.
- (19) Imahori, H.; Kang, S.; Hayashi, H.; Haruta, M.; Kurata, H.; Isoda, S.; Canton, S. E.; Infahsaeng, Y.; Kathiravan, A.; Pascher, T.; Chabera, P.; Yartsev, A. P.; Sundstrom, V. *J. Phys. Chem. A* **2011**, *115*, 3679.
- (20) Chang, C.-W.; Luo, L.; Chou, C.-K.; Lo, C.-F.; Lin, C.-Y.; Hung, C.-S.; Lee, Y.-P.; Diau, E. W.-G. *J. Phys. Chem. C* **2009**, *113*, 11524.
- (21) Griffith, M. J.; Sunahara, K.; Wagner, P.; Wagner, K.; Wallace, G. G.; Officer, D. L.; Furube, A.; Katoh, R.; Mori, S.; Mozer, A. J. *Chem. Commun.* **2012**, *48*, 4145.

CHAPTER 10. CONCLUSIONS AND OUTLOOK

10.1. Conclusions

In summary, three series of di-chromophoric dyes have been investigated in terms of their spectroscopic, electrochemical and photovoltaic properties in dye-sensitized solar cells (DSSCs). The investigated dyes consisted of a zinc porphyrin and an additional organic chromophore. The additional chromophores were carbazoles (the PorY dyes), carbazole-fused thiophenes (the PorO dyes) and carbazole-thiophene benzothiadiazole thiophene (PorR). Phenylethenyl group was used to link the porphyrin and the organic chromophore, which suppresses electronic communication between the two chromophores in the ground state as suggested by the electrochemical studies, density functional theory calculations, UV-visible absorption and resonance Raman spectroscopy measurements due to a dihedral angle between two chromophores. The main findings of this thesis are graphically summarized in Fig. 10.1.

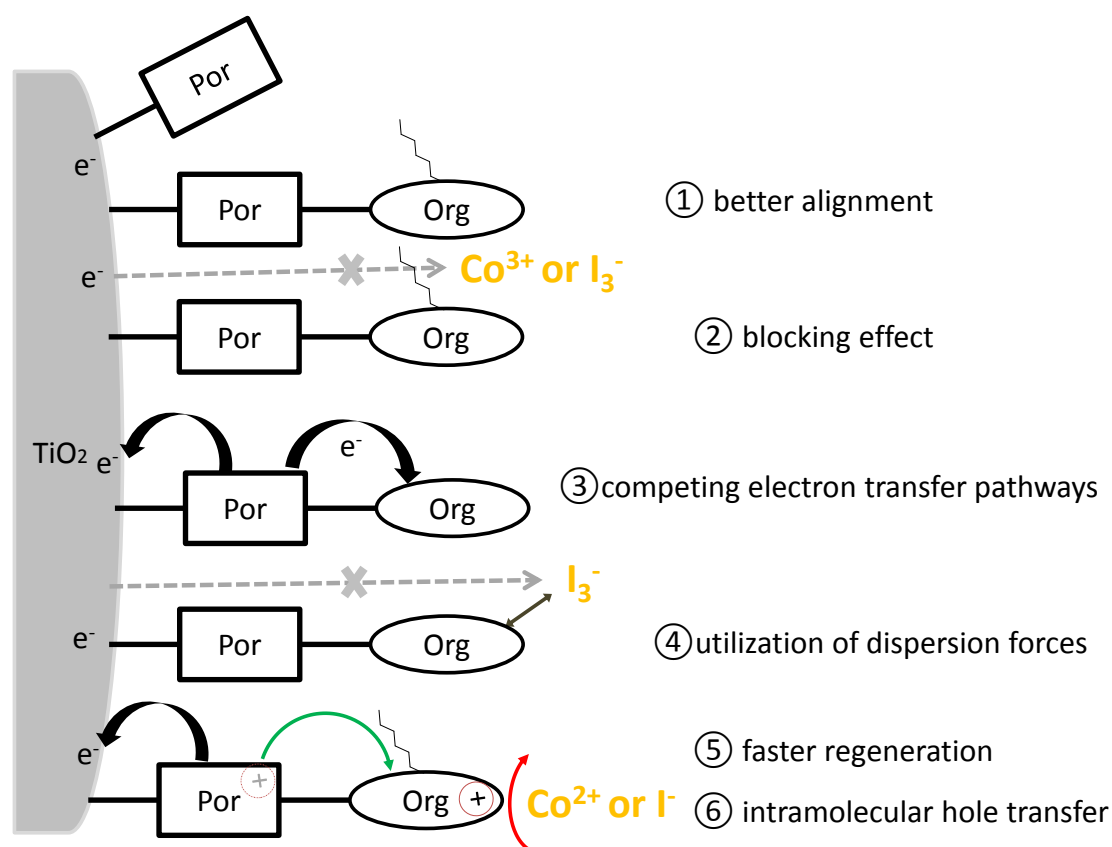


Figure 10.1 Summary of the main findings using di-chromophoric dyes in dye-sensitized solar cells in this thesis

1. Regarding the PorY and PorO dyes, the insertion of the additional organic chromophore revealed an enhanced device performance, in terms of photocurrent and photovoltage, compared to the single chromophoric porphyrin. The power conversion efficiency of PorY1 was improved up to 30% respect to the single chromophoric porphyrin in DSSCs using the iodine electrolyte. Nearly doubled power conversion efficiency was obtained by PorO2 compared to the DSSCs using the single chromophoric porphyrin using the cobalt electrolyte.

a) The enhanced photocurrent observed in PorY dyes was ascribed to the enhanced light harvesting and electron injection efficiencies. i) The carbazole unit in PorY dyes produced a distortion of the porphyrin structure, broadened the Soret band and increased the absorption in Q bands, which in turn improved light harvesting. ii) The bulky carbazole chromophore suppressed dye aggregation and eliminated non-injecting dyes, better dye layer morphology is suggested to be the reason for the enhanced electron injection efficiency (factor ① in Fig. 10.1).

b) In the case of PorO dyes, the improved photocurrent was mainly attributed to the complementary absorption of the carbazole-fused thiophene chromophore (450 - 550 nm) to the porphyrin. More importantly, the utility of di-chromophoric dyes using the cobalt electrolyte was also demonstrated.

2. The increased photovoltage in the PorY and PorO dyes originated from the longer electron lifetimes due to the steric blocking effect of the bulky organic chromophores. The alkyl chain of the organic chromophore blocks the pathway of conduction band electrons to the reduced species in the electrolyte and consequently increases the electron lifetime (factor ② in Fig. 10.1).

3. The use of PorR in DSSCs introduces two competing electron transfer pathways, suggesting a limitation of di-chromophoric dye using low band gap chromophore (factor ③ in Fig. 10.1). Comparisons were carried out within the single chromophoric dyes, PorR and mixed dyes (co-sensitization) in DSSCs. The DSSCs using mixed dyes showed slightly better power conversion efficiencies compared to that of the single chromophoric dyes, while nearly doubled compared to that of PorR. Nonetheless, PorR achieved larger dye loading on TiO₂ and increased light harvesting in most of the visible wavelength region as compared to the mixed dyes, suggesting the utility of di-chromophoric dye using thin photoanodes.

4. PorR dye, for the first time, demonstrated the possibility of utilizing intermolecular forces between the dye and I_3^- to extend the electron lifetimes. By linking a low band gap organic chromophore with increased dispersion forces (therefore attracting I_3^-) further away from the TiO_2 surface, the distance between TiO_2 and I_3^- is increased (factor ④ in Fig. 10.1). In turn, an increase of electron lifetime and consequently photovoltage was achieved, in contrary to what was observed in mixed dye-sensitized films. DSSC using PorR showed more than an order of magnitude longer electron lifetimes compared to that using the mixed dyes.

5. By attaching an organic chromophore to the porphyrin, the di-chromophoric dye PorY1 achieved more than five times faster dye cation regeneration rate constants compared to the single chromophoric porphyrin Por using both iodine- and cobalt-based electrolytes at a similar driving force on TiO_2 (factor ⑤ in Fig. 10.1). Such enhanced dye regeneration kinetics at a similar driving force has not been reported to date.

6. A partial intramolecular hole transfer from the porphyrin to the carbazole triphenylamine moiety in PorY1 / TiO_2 was also observed on the sub-nanosecond to microsecond time scale (factor ⑥ in Fig. 10.1). Such slow intramolecular hole transfer rate is also reported for the first time.

Two main limitations in di-chromophoric dyes that curb the further improvement in DSSC were also suggested by the present study: a) the limited electron injection efficiency (or the requirement of larger driving force for electron injection); b) the inefficient intramolecular electron / energy transfer. These two limitations would require further study.

10.2. Outlook

The present work highlights the potential of multi-chromophoric dyes in DSSCs, especially when using thin photoanodes due to their enhanced light harvesting ability. It has been shown that these dyes can improve the device performance in four ways: i) complementary light absorption; ii) blocking effect; iii) utilization of dispersion forces; iv) fast dye regeneration kinetics.

Based on the conclusions derived from this thesis, the design of more complex dyes featuring some of the concepts above mentioned, and the further improvement of

photoelectrochemical technology is enabled. Some structures of triads and tetrads that may further improve the power conversion efficiency are shown in Fig. 10.2.

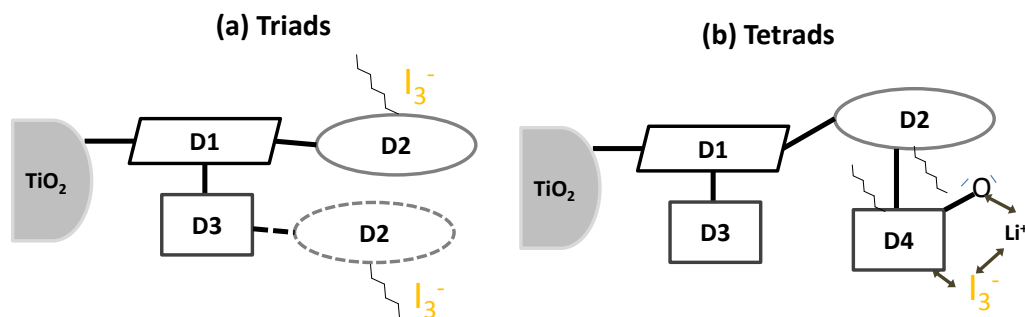


Figure 10.2 Molecular structures of further (a) triads and (b) tetrads.

For the chromophores in the triads (Fig. 10.2(a)), some considerations are listed as follows:

D1: This is the main light absorber. Efficient electron injection is expected from this chromophore to TiO_2 , hence requiring well electronic coupling with the conduction band of TiO_2 . The zinc porphyrin studied in this thesis might be a good choice.

D2: This is an additional light absorber. Alkyl chains are attached on this chromophore to block the recombination pathways. The band gap of this chromophore is larger than that of D1 to channel the energy transfer; the LUMO level of this chromophore is also more negative than that of D1 to channel the electron transfer. Moreover, this chromophore is expected to have faster regeneration kinetics, for example, the carbazole triphenylamine moiety used in this thesis. It can be attached to either D1 or D3 by considering the tridimensional structure of the triad since the dye loading on TiO_2 can be affected.

D3: This is an additional light absorber. The band gap of this chromophore is slightly larger compared to that of D1 but lower compared to that of D2, the LUMO level of this chromophore is also more negative than that of D1 but more positive compared to D2.

For the chromophores in the tetrads (Fig. 10.2(b)), the considerations for the chromophores D1, D2 and D3 are similar as that in the triads. The chromophore D4 is introduced as another additional light absorber. Some considerations on D4 are listed as follows:

- 1) Low band gap chromophore can be used to utilize the dispersion forces between D4 and the electrolyte to enlarge the distance between the TiO_2 surface and the oxidized species in the electrolyte (for example, I_3^-).
- 2) Since an energy transfer might occur from D2^* to D4, the distance between D2 and D4 should be large enough to hinder this energy transfer. Elongating the linker between D2 and D4 or attaching alkyl chains on D2 and / or D4 can fulfill the purpose.
- 3) Partial charge effect can be also used to attract I_3^- further away from the TiO_2 surface.

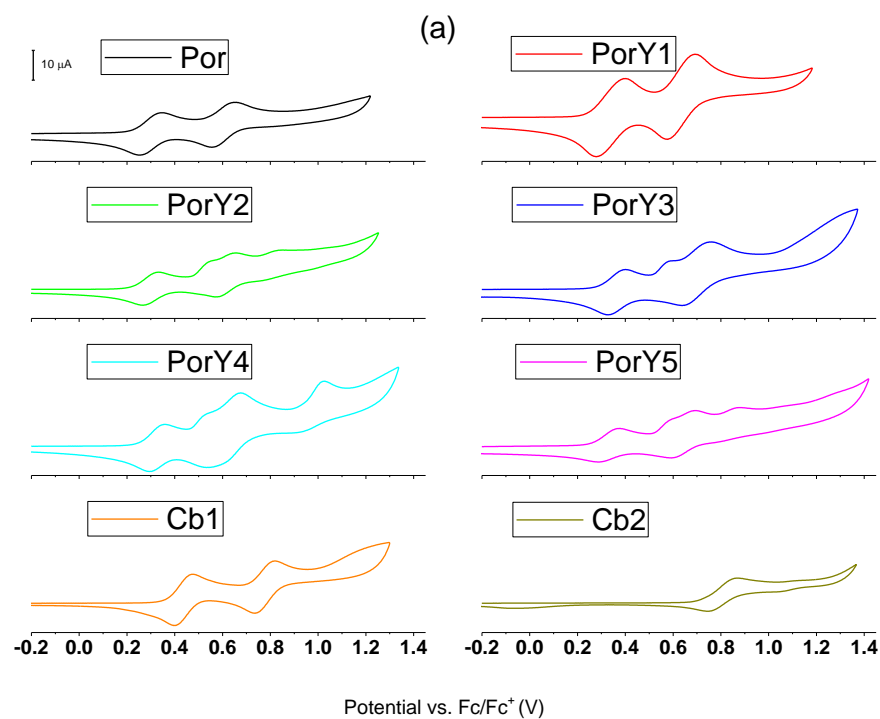
APPENDIX

A. UV-visible absorption spectroscopy: Dye loading calculation parameters

Table A1. Dye loading calculation parameters of the interested dyes in 0.033 M TBAOH in DMF

Chapters	Dye	Peak wavelength / nm	$\varepsilon / \times 10^6 \text{ M}^{-1}\text{cm}^{-1}$
4	Por	432	0.383
	PorY1	434	0.410
	PorY2	434	0.420
	PorY3	434	0.363
	PorY4	434	0.402
	PorY5	434	0.405
5	PorO1	434	0.281
	PorO2	433	0.266
	PorO3	434	0.396
8	CbBTD1	388	0.035
	PorR	433	0.370

B. Electrochemistry: Cyclic voltammetry of the investigated compounds



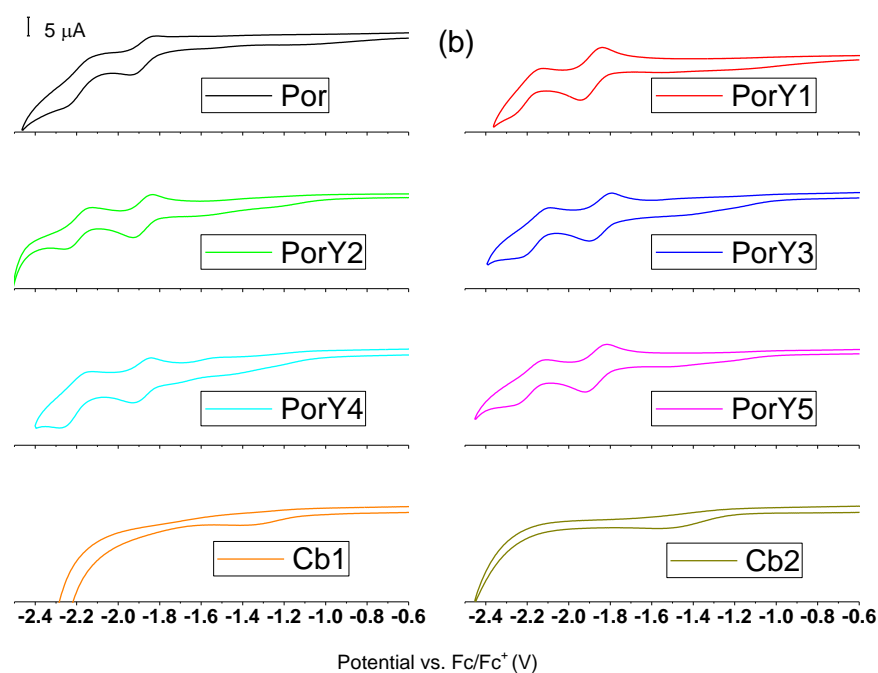


Figure A1. Cyclic voltammograms of the compounds in Chapter 4, (a) positive scan; (b) negative scan. Sample concentration: 0.5mM; solvent: DCM; supporting electrolyte: TBAP; Pt wire surface area: 6.6 mm²; scan rate: 100 mV s⁻¹.

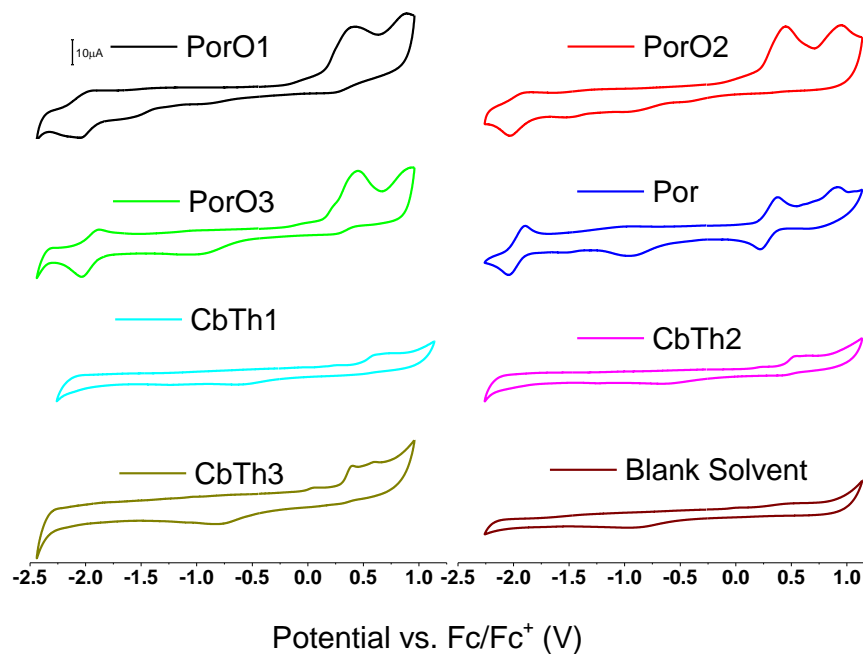


Figure A2. Cyclic voltammograms of the compounds in Chapter 5. Sample concentration: 0.5mM; solvent: DMF; supporting electrolyte: TBAP; Pt wire surface area: 6.6 mm²; scan rate: 100 mV s⁻¹.

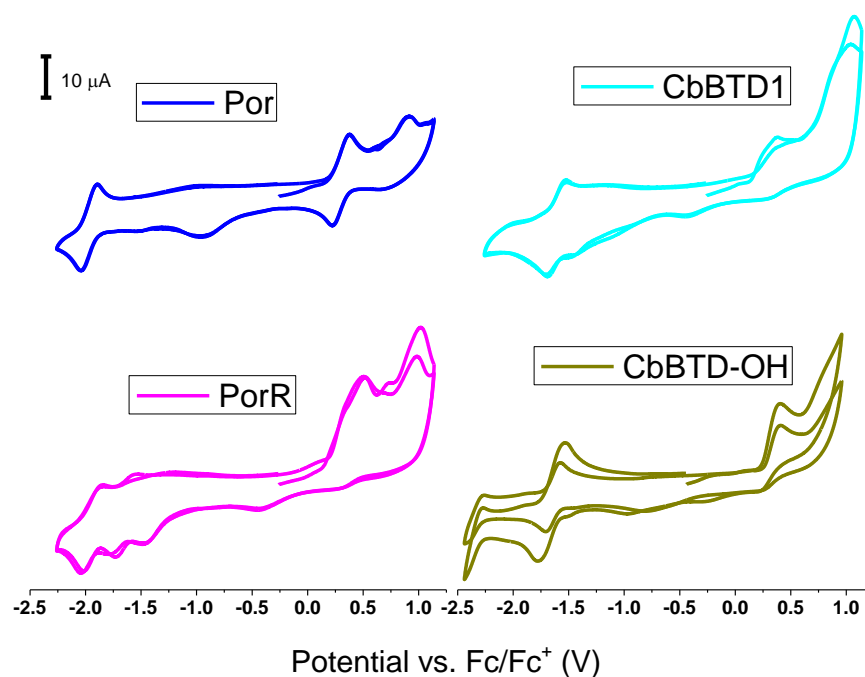


Figure A3. Cyclic voltammograms of the compounds in Chapter 8. Sample concentration: 0.5mM; solvent: DMF; supporting electrolyte: TBAP; Pt wire surface area: 6.6 mm²; scan rate: 100 mV s⁻¹. The first two cycles were displayed.

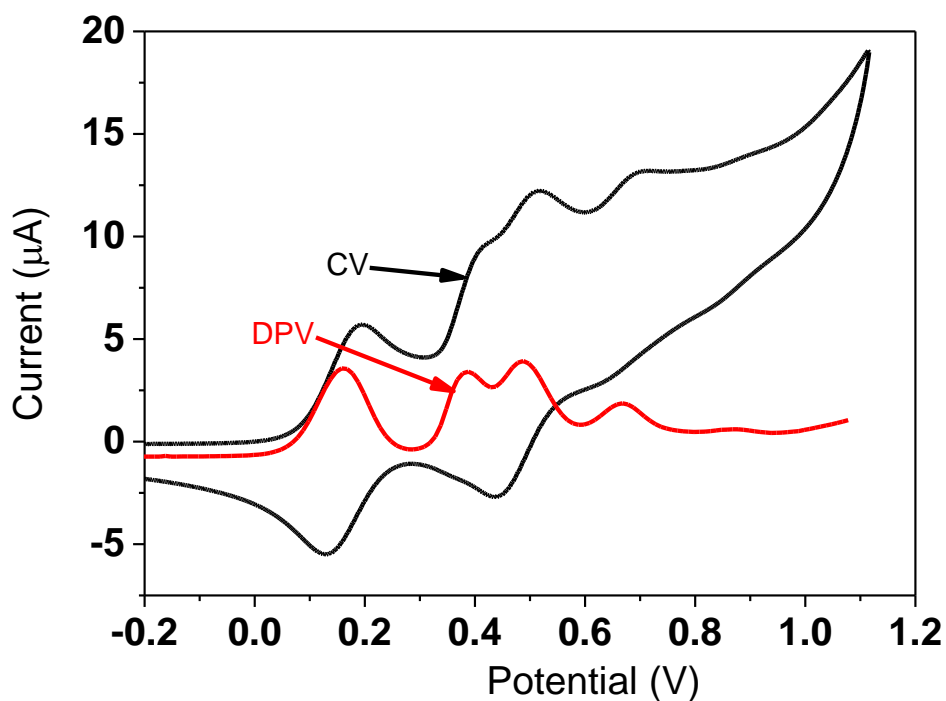


Figure A4. Differential pulse voltammetry (DPV) and cyclic voltammetry (CV) curves of PorY2 measured in DCM using 100 mV s⁻¹ scan rate.

C. Spectroelectrochemistry

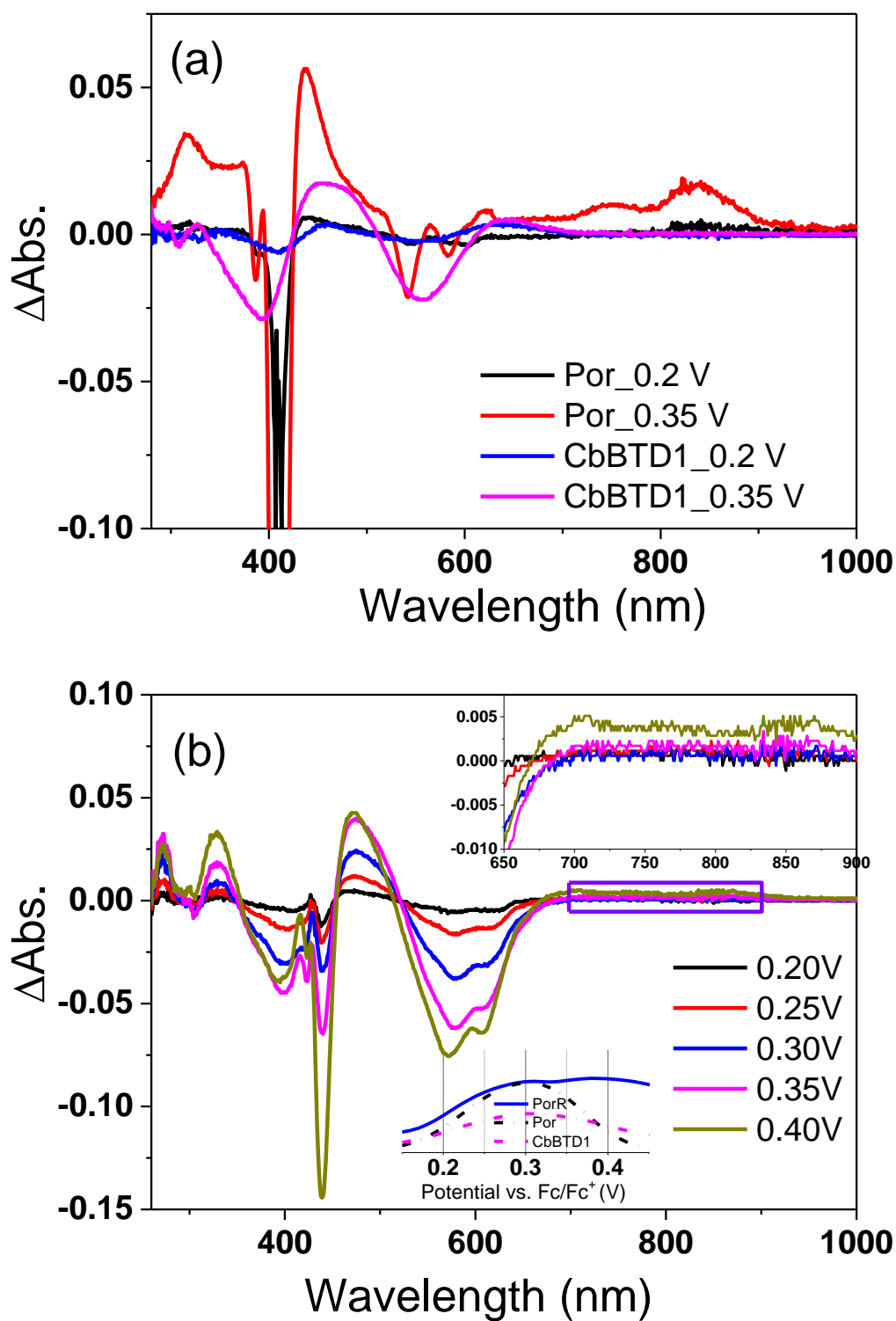


Figure A5. Spectroelectrochemical spectra of (a) Por and CbBTD1 and (b) PorR at different oxidation potentials vs. Fc/Fc^+ . The inset of (b) shows the DPV plots of the three compounds at the first oxidation peak.

Change of absorption is observed from 0.25 V vs. Fc/Fc^+ at wavelengths below 650 nm, indicating that the first oxidation occurs. No positive signal is observed beyond 600 nm before 0.4 V vs. Fc/Fc^+ , indicating that no porphyrin dye radical cation is formed at these applied potentials. The positive ΔAbs signals in the 680-900 nm wavelength range (assigned to the porphyrin radical cation absorption) are observed at 0.4 V vs. Fc/Fc^+ . The results indicate that, in the oxidation of the di-chromophoric dye, firstly the organic chromophore is oxidized at ~ 0.25 V vs. Fc/Fc^+ and secondly the porphyrin is oxidized at ~ 0.4 V vs. Fc/Fc^+ .

D. Photoluminescence

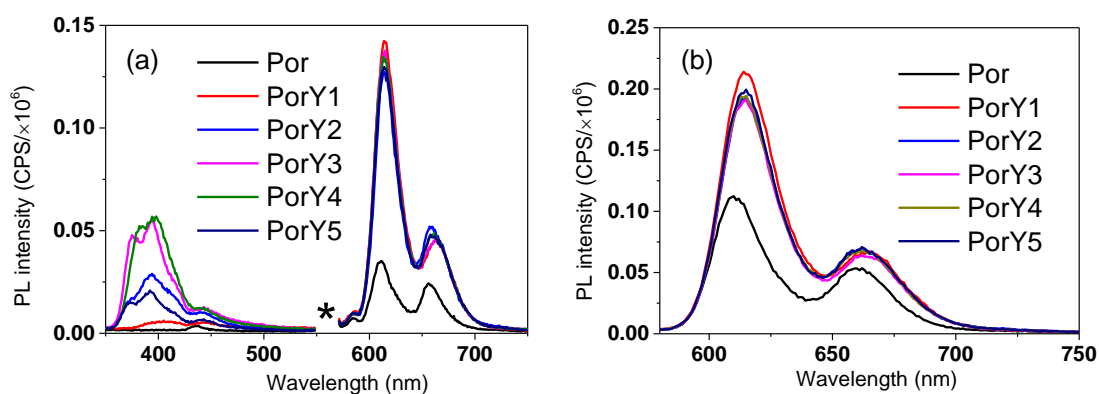


Figure A6. Photoluminescence spectra of the PorY dyes compared to Por in DMF with 1 μM concentration with excitation wavelength of (a) 280 nm and (b) 560 nm. The second harmonic of the excitation wavelength at 560 nm was deleted (indicated by a star) from (a).

E. SLIM-PCV and charge extraction measurements

E1. Electron diffusion length

Electron diffusion length (L) determines the average distance a photo-electron diffuses before recombining.¹ It is affected by both electron lifetime and electron diffusion coefficient (Eq. A1).

$$L = (D\tau_{sc})^{0.5} \quad (\text{A1})$$

where, τ_{sc} is the electron lifetime under the short circuit condition.

Charge collection efficiency (E_{coll}) could be estimated from the diffusion length according to Eq. A2.^{2,3}

$$E_{\text{coll}} = \tanh(\omega/L)/(\omega/L) \quad (\text{A2})$$

where, ω is the thickness of the TiO_2 film.

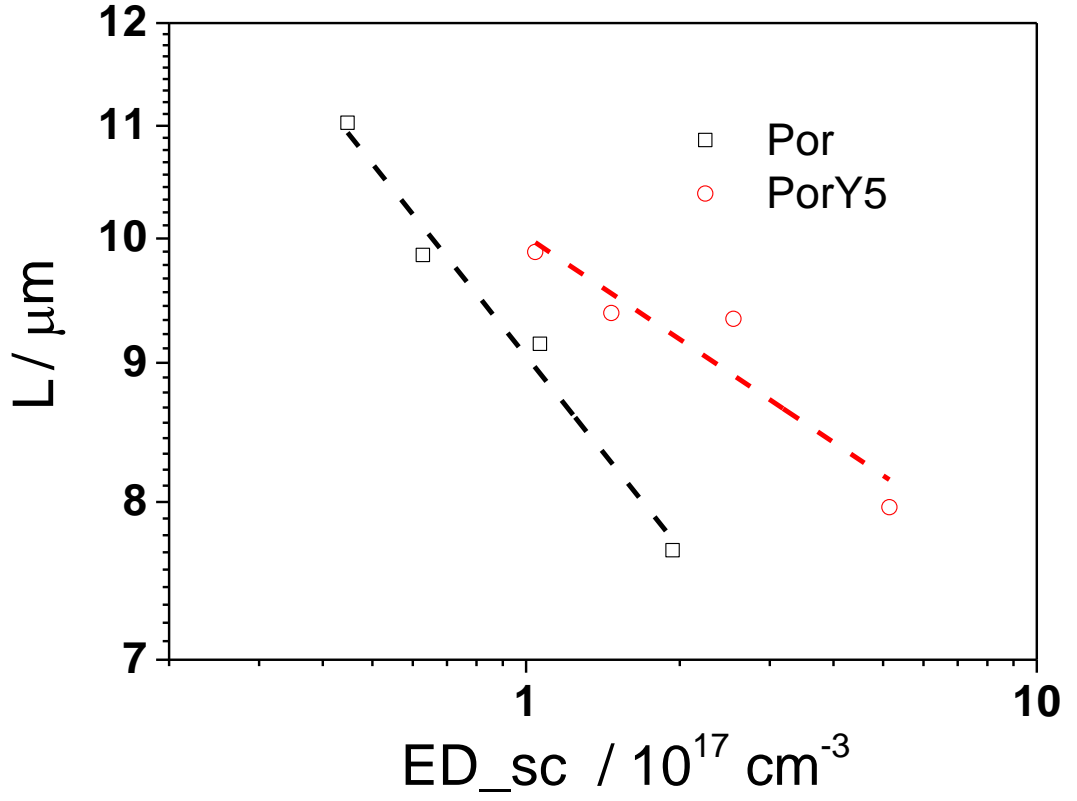


Figure A7. Diffusion length (L) versus electron density at short circuit (ED_{sc}) of DSSCs using Por and PorY5 using $3 \mu\text{m}$ TiO_2 films. The lowest charge collection efficiencies of Por and PorY5 are 95% and 96%, respectively.

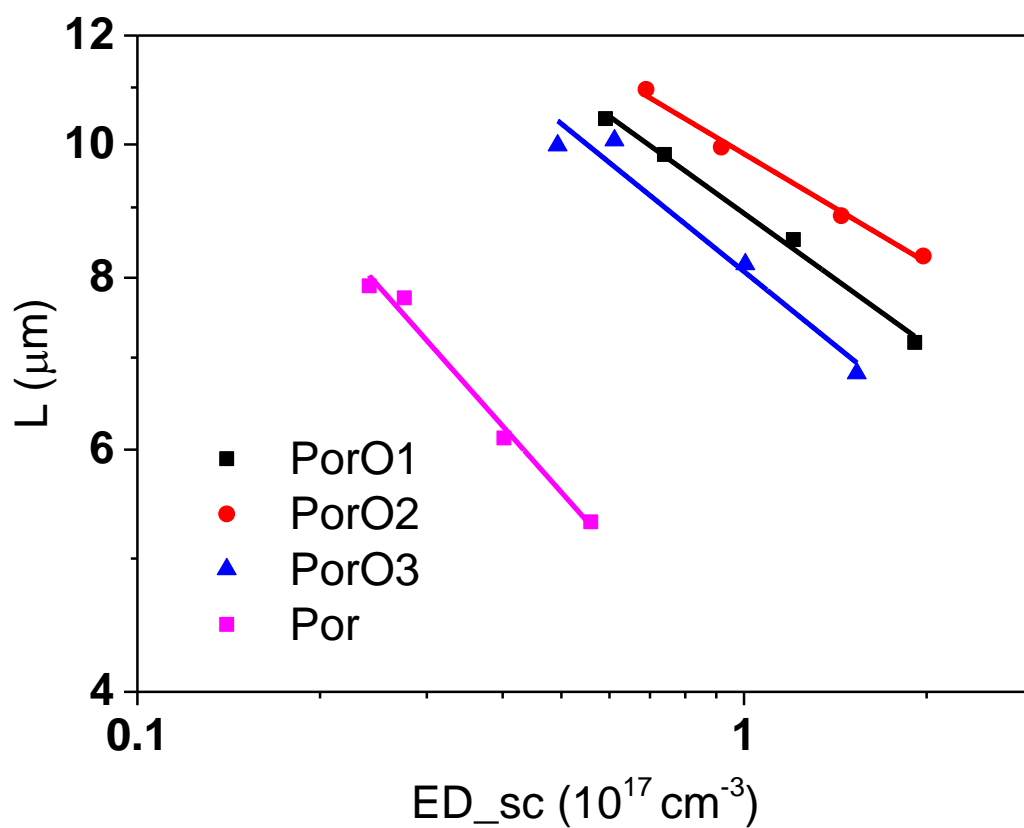


Figure A8. Diffusion length versus electron density at short circuit of DSSCs using the PorO dyes and Por using 3.1 μm TiO_2 films. The lowest charge collection efficiencies of PorO1, PorO2, PorO3 and Por are 94%, 96%, 94% and 90%, respectively.

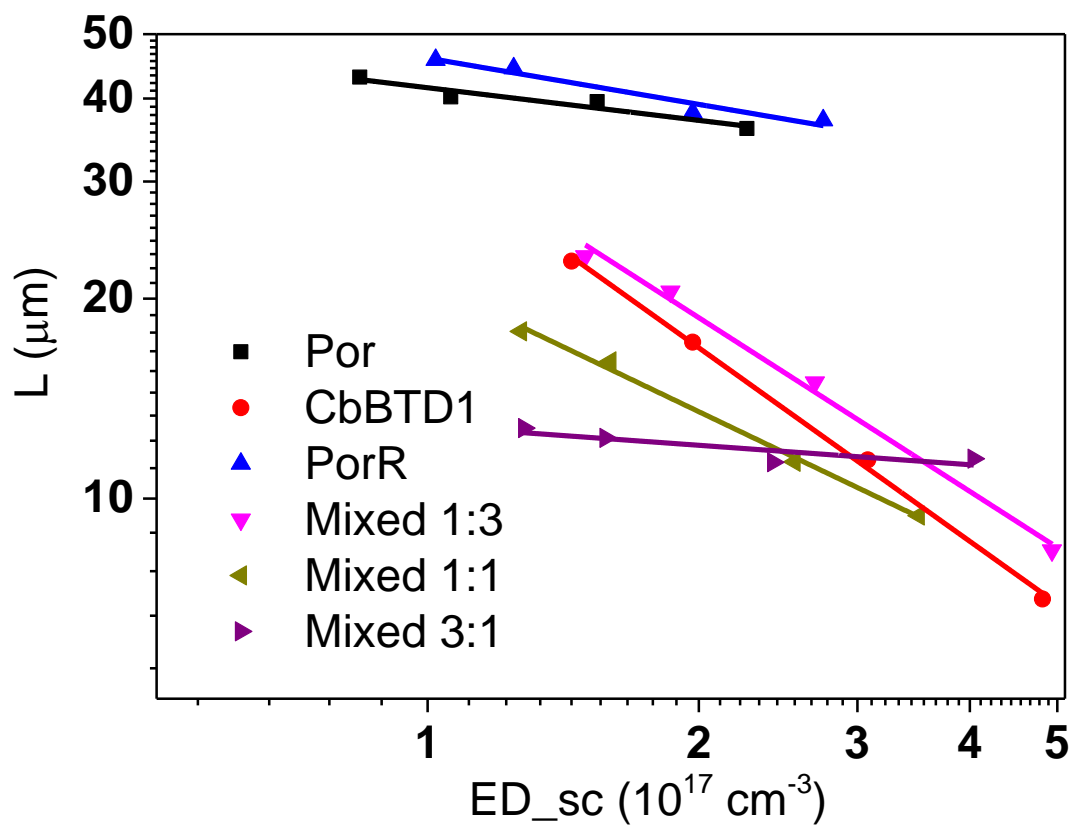


Figure A9. Diffusion length versus electron density at short circuit of DSSCs using Por, CbBTD1, PorR and the mixed dyes using 2.0 μm TiO_2 films. The lowest charge collection efficiencies of Por, CbBTD1, PorR, Mixed 1:3, Mixed 1:1 and Mixed 3:1 are 100%, 97%, 100%, 98%, 99% and 99%, respectively.

E2. Conduction band shift by removal of tBP from the cobalt electrolyte

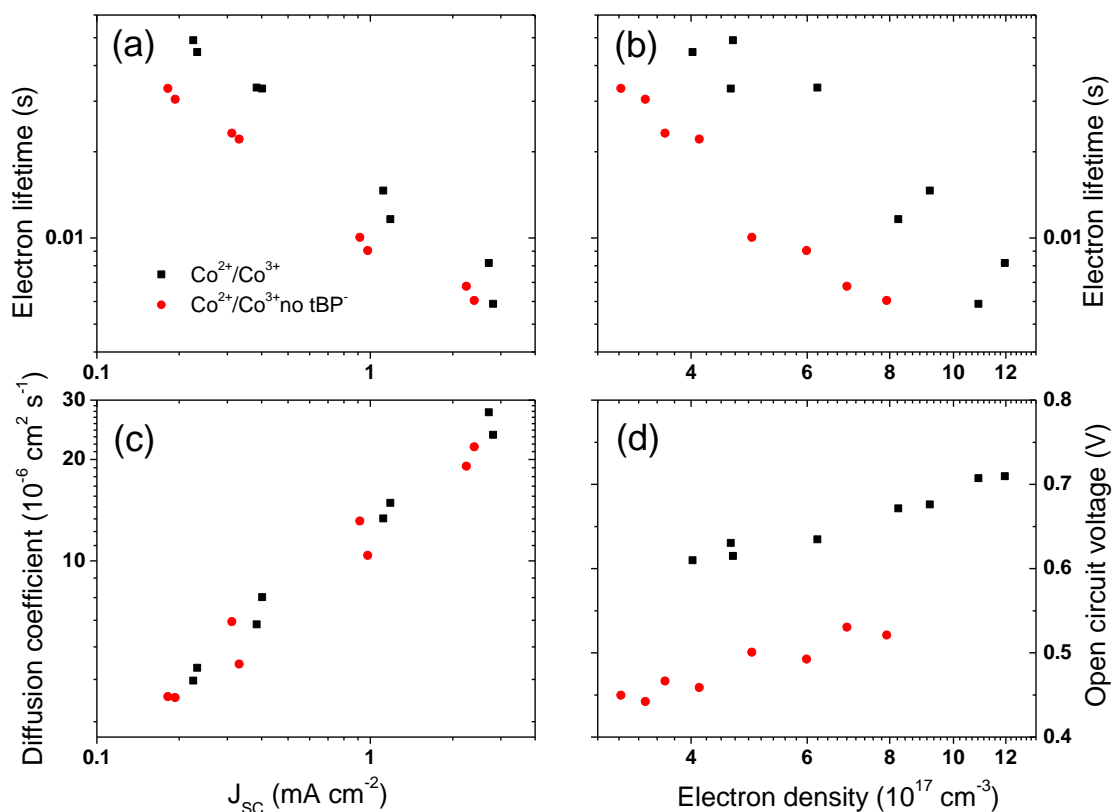


Figure A10. (a) Electron lifetime and (c) diffusion coefficient versus short circuit current density, (b) electron lifetime and (d) open circuit voltage versus electron density for DSSCs using PorO2 under different electrolytes (two samples for each condition).

Film thickness: $2.9 \pm 0.1 \mu\text{m}$ for cobalt, $3.2 \pm 0.2 \mu\text{m}$ for cobalt no tBP^- .

F. Transient absorption spectroscopy (INDI laser)

Table A2. Electron density calculation in TAS measurement

Pyroelectric/mV	16.7	Pyroelectric calibration/ V J^{-1}	335
Laser energy/ μJ	49.9	Pyroelectric area/ cm^2	0.95
Energy of 1 photon /J	3.7×10^{-19}	532 nm photon energy/eV	2.34
Porosity	0.6	LHE (assumed)	0.8
Electron density/ cm^{-3}	6.2×10^{17}	Film thickness/ μm	3

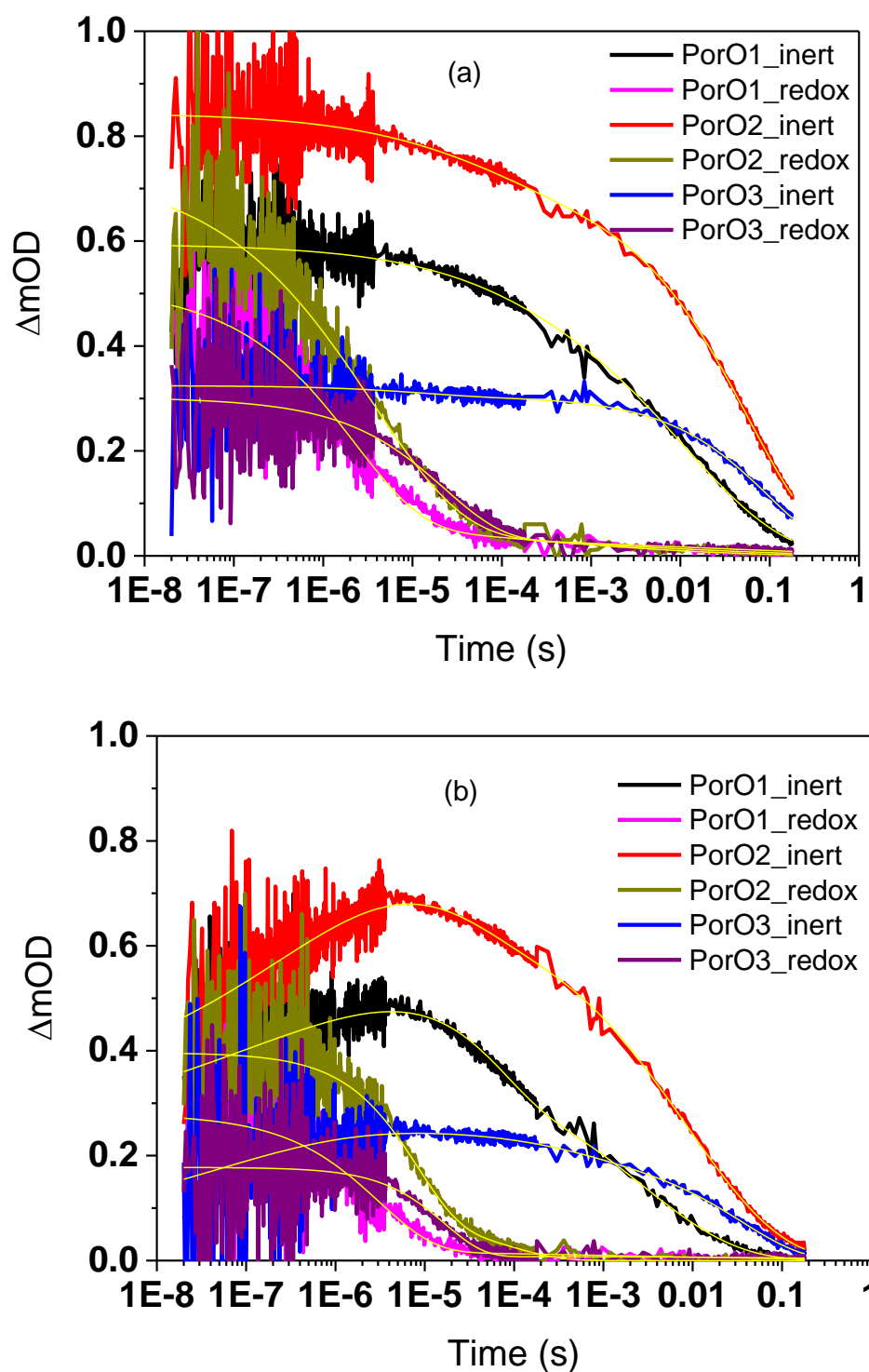


Figure A11. Time-resolved transient absorption decay and fit curves of the PorO dyes with the cobalt electrolyte monitored at (a) 800 nm and (b) 1300 nm after pulsed 532 nm laser irradiation. Laser energy: $\sim 10 \mu J cm^{-2} pulse^{-1}$; repetition frequency: 1 Hz. Inert: 0.05 M $LiClO_4$, and 0.1 M *t*BP in AN; Redox: 0.22 M $Co(dmbpy)_3^{2+}$, 0.05 M $Co(dmbpy)_3^{3+}$, 0.05 M $LiClO_4$, 0.1 M *t*BP and 1 mM CDCA in AN

Table A3. Fitted parameters for Figure A11.

(a) dye cation

Electrolyte	Wavelength (nm)	Sample	$\Delta OD_{D^+_{t=0}}$	$\tau_{ww_D^+}$ (s)	β_{D^+}	Γ_{D^+}	$\tau_{obs_D^+}$ (s)
Inert	800	PorO1	5.69E-04	1.10E-02	0.39	1.39	3.92E-02
		PorO2	7.10E-04	5.80E-02	0.54	0.95	1.02E-01
		PorO3	3.04E-04	1.00E-01	0.64	0.89	1.39E-01
	1300	PorO1	4.17E-04	2.34E-03	0.39	1.39	8.34E-03
		PorO2	7.05E-04	8.41E-03	0.41	1.27	2.61E-02
		PorO3	2.03E-04	3.50E-02	0.62	0.89	5.02E-02
Redox	800	PorO1	4.30E-04	2.26E-06	0.57	0.92	3.65E-06
		PorO2	6.80E-04	3.56E-06	0.43	1.18	9.77E-06
		PorO3	2.57E-04	2.28E-05	0.66	0.89	3.07E-05
	1300	PorO1	2.58E-04	3.09E-06	0.70	0.86	3.80E-06
		PorO2	3.15E-04	8.01E-06	0.90	0.94	8.37E-06
		PorO3	1.70E-04	1.69E-05	1.00	1.00	1.69E-05

(b) electron

Electrolyte	Wavelength (nm)	Sample	$\Delta OD_{e_{t=0}}$	τ_{ww_e} (s)	β_e	Γ_e	τ_{obs_e} (s)
Inert	800	PorO1	2.56E-05	1.04E-04	0.60	0.90	1.56E-04
		PorO2	1.34E-04	5.55E-05	0.44	1.15	1.45E-04
		PorO3	2.02E-05	1.21E-05	0.61	0.90	1.79E-05
	1300	PorO1	1.96E-04	6.16E-05	0.82	0.91	6.84E-05
		PorO2	3.03E-04	1.88E-05	0.55	0.94	3.21E-05
		PorO3	4.71E-05	4.73E-04	0.60	0.90	7.10E-04
Redox	800	PorO1	9.38E-05	1.08E-04	0.18	57.26	3.44E-02
		PorO2	6.06E-05	1.00E-03	0.18	57.26	3.18E-01
		PorO3	4.93E-05	6.80E-03	0.17	98.30	3.93E+00
	1300	PorO1	2.39E-05	2.05E-03	0.17	98.30	1.19E+00
		PorO2	8.16E-05	7.89E-05	0.72	0.89	9.75E-05
		PorO3	7.56E-06	1.26E+00	0.38	1.46	4.84E+00

(c) rise

Electrolyte	Wavelength (nm)	Sample	$\Delta OD_{D^+_{t=0}}$	$\tau l_{ww_D^+}$ (s)	βl_{D^+}	Γl_{D^+}	$\tau l_{obs_D^+}$ (s)
Inert	1300	PorO1	4.17E-04	4.53E-07	0.21	16.88	3.64E-05

		PorO2	7.05E-04	1.70E-06	0.29	3.14	1.84E-05
		PorO3	2.03E-04	5.08E-08	0.29	3.14	5.50E-07

Table A4. Regeneration yield of the PorO dyes monitored at both 800 nm and 1300 nm

(a) 800 nm

Description	Sensitizer	τ_{obs} (s)	k_{obs} (s^{-1})	ϕ_{reg}
TiO ₂ (e ⁻)-D ⁺ recombination	PorO1	3.92E-02	2.55E+01	-
	PorO2	1.02E-01	9.84E+00	-
	PorO3	1.39E-01	7.19E+00	-
D ⁺ regeneration	PorO1	3.65E-06	2.74E+05	1.00
	PorO2	9.77E-06	1.02E+05	1.00
	PorO3	3.07E-05	3.25E+04	1.00

(b) 1300 nm

Description	Sensitizer	τ_{obs} (s)	k_{obs} (s^{-1})	ϕ_{reg}
TiO ₂ (e ⁻)-D ⁺ recombination	PorO1	8.34E-03	1.20E+02	-
	PorO2	2.61E-02	3.84E+01	-
	PorO3	5.02E-02	1.99E+01	-
D ⁺ regeneration	PorO1	3.80E-06	2.63E+05	1.00
	PorO2	8.37E-06	1.20E+05	1.00
	PorO3	1.69E-05	5.92E+04	1.00

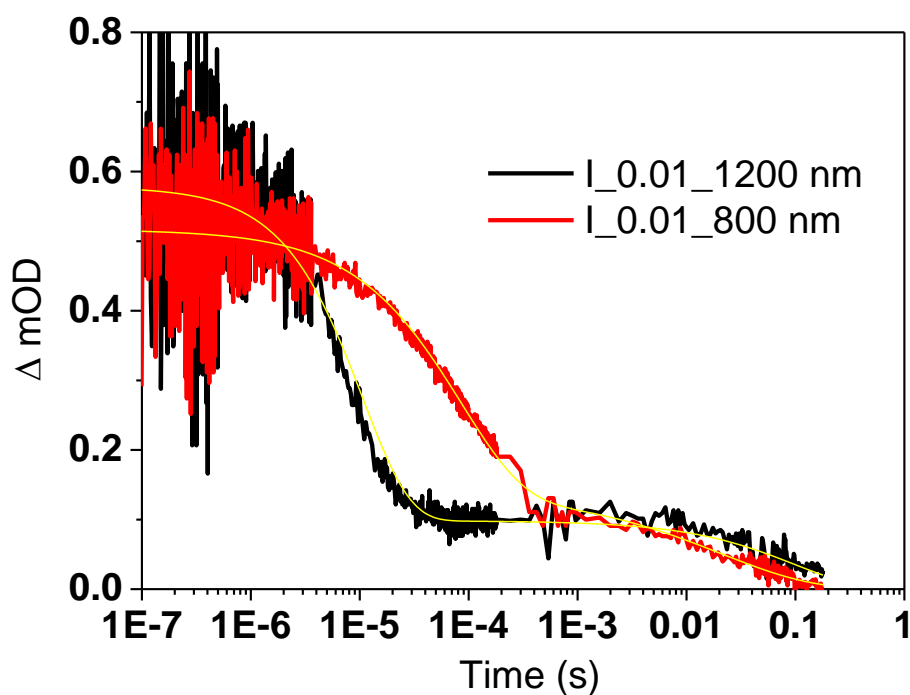


Figure A12. Time-resolved transient absorption decay and fitted curves of 35% dye loaded PorY1 on TiO₂ using 0.001 M LiI after pulsed 532 nm laser irradiation.

G. Transient absorption spectroscopy (Ekspla laser)

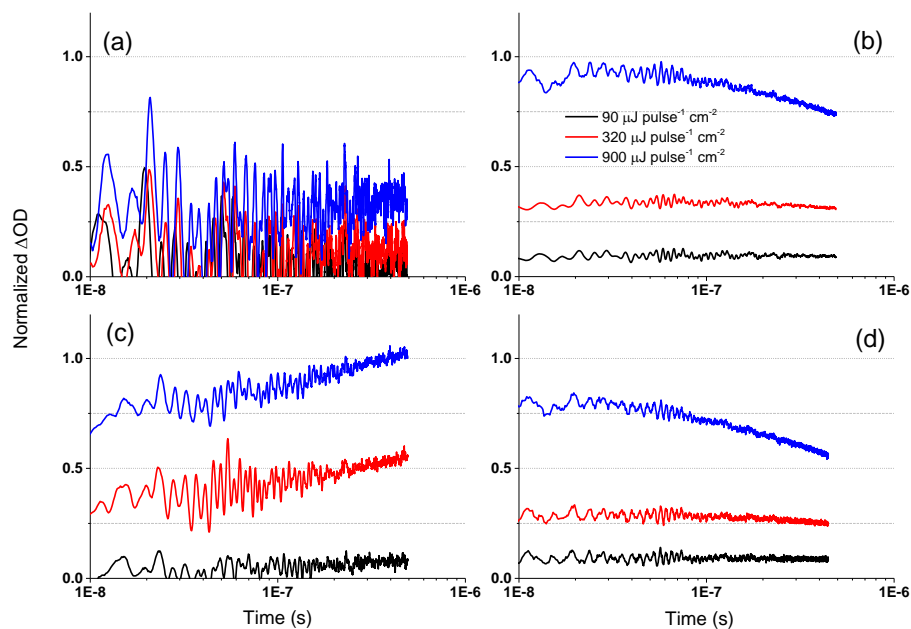


Figure A13. Time-resolved transient absorption decay with different laser intensities of (a) Por probed at 1200 nm, (b) Por probed at 730 nm, (c) PorY1 probed at 1200 nm, and (d) PorY1 probed at 730 nm with I₀ after pulsed 532 nm laser irradiation. Repetition

frequency: 1 Hz. I_0: 0.1 M LiClO₄, and 0.5 M *t*BP in AN: VN=85:15 (vol). The rise of ΔOD is observed in (c).

H. Fitting of the transient absorption decay curves

A stretched exponential decay of ΔOD described in Chapter 1 was applied for fitting. The fitted parameters of TiO₂(e⁻) at 1200 nm and 800 nm in both Por and PorY1 were treated individually, which is different from that in Ru-based dyes (the same parameters were employed at both 980 nm and 800 nm for electrons).^{4,5}

A clear rise feature was observed in PorY1 at 1200 nm when using I_0. Fitting this rise in the decay curve requires introducing the third stretched exponential term. The decay curve of PorY1 at 1200 nm was fitted using Eq. A3.

$$\Delta OD(Cb - TPA^+) = \Delta OD_{t=0}(Cb - TPA^+)e^{-\left(\frac{t}{\tau_{WW}(Cb-TPA^+)}\right)^{\beta(Cb-TPA^+)}} + \Delta OD_{t=0}(e^-)e^{-\left(\frac{t}{\tau_{WW}(e^-)}\right)^{\beta(e^-)}} - \Delta OD_{t=0}(Cb - TPA^+)e^{-\left(\frac{t}{\tau_{1WW}(Cb-TPA^+)}\right)^{\beta_1(Cb-TPA^+)}} \quad (A3)$$

Table A5. Fitted parameters for all the transient absorption curves measured in Chapter

9

(a) dye cation

Sample	Condition	Electrolyte	Wavelength (nm)	$\Delta OD_{D^+}_{t=0}$	τ_{ww-D^+} (s)	β_{D^+}	Γ_{D^+}	τ_{obs-D^+} (s)	k_{obs-D^+} (s ⁻¹)
PorY1	Full coverage	I_1	800	3.31E-04	1.59E-06	0.77	0.90	1.86E-06	5.37E+05
			1200	3.37E-04	1.45E-07	0.50	1.01	2.95E-07	3.39E+06
		I_0.1	800	3.10E-04	6.05E-06	0.96	0.98	6.13E-06	1.63E+05
			1200	5.12E-04	7.00E-07	0.65	0.89	9.49E-07	1.05E+06
		I_0.01	800	3.34E-04	1.57E-04	0.93	0.96	1.62E-04	6.19E+03
			1200	4.47E-04	1.59E-05	1.00	1.00	1.59E-05	6.29E+04
		I_0.001	800	2.90E-04	3.20E-04	0.95	0.97	3.26E-04	3.07E+03
			1200	3.84E-04	1.02E-05	0.68	0.89	1.32E-05	7.56E+04
		I_0	800	3.46E-04	6.37E-04	0.73	0.89	7.77E-04	1.29E+03

			1200	9.39E-04	3.42E-04	0.45	1.13	8.68E-04	1.15E+03
		Co_1	800	2.45E-04	4.95E-07	0.87	0.93	5.28E-07	1.90E+06
			1200	3.47E-04	4.20E-07	0.99	0.99	4.20E-07	2.38E+06
		Co_0.1	800	3.57E-04	4.46E-06	0.90	0.94	4.67E-06	2.14E+05
			1200	5.11E-04	4.52E-06	1.00	1.00	4.52E-06	2.21E+05
		Co_0.01	800	3.25E-04	2.50E-04	0.88	0.94	2.66E-04	3.76E+03
			1200	4.80E-04	4.83E-05	0.91	0.95	5.04E-05	1.98E+04
		Co_0.001	800	2.57E-04	1.34E-03	0.73	0.89	1.63E-03	6.15E+02
			1200	3.60E-04	9.80E-05	0.81	0.91	1.10E-04	9.13E+03
		Co_0	800	2.45E-04	1.30E-03	0.68	0.89	1.69E-03	5.91E+02
			1200	1.17E-03	2.78E-05	0.34	1.90	1.55E-04	6.46E+03
	Doctor-bladed reduced dye	I_0	1200	1.15E-03	2.32E-04	0.52	0.97	4.33E-04	2.31E+03
	Doctor-bladed CDCA-introduced		1200	9.50E-04	6.42E-04	0.86	0.93	6.92E-04	1.45E+03
	35%-coverage	I_0.01	800	3.78E-04	8.33E-05	0.75	0.89	9.88E-05	1.01E+04
			1200	4.80E-04	1.06E-05	1.00	1.00	1.06E-05	9.43E+04
		Co_0.01	800	2.03E-04	1.25E-04	0.80	0.91	1.42E-04	7.03E+03
			1200	4.56E-04	5.36E-05	1.00	1.00	5.36E-05	1.87E+04
Por	Full coverage	I_1	800	3.52E-04	2.19E-06	0.61	0.90	3.23E-06	3.09E+05
		I_0.1		2.54E-04	7.47E-06	0.85	0.92	8.09E-06	1.24E+05
		I_0.01		2.50E-04	4.68E-04	0.91	0.94	4.83E-04	2.07E+03
		I_0.001		2.96E-04	7.18E-04	0.64	0.89	9.98E-04	1.00E+03
		I_0		1.90E-04	2.20E-03	0.94	0.96	2.26E-03	4.43E+02
		Co_1		2.79E-04	9.79E-07	0.46	1.09	2.32E-06	4.31E+05
		Co_0.1		2.32E-04	1.39E	0.75	0.89	1.65E	6.06E+

					-05			-05	04
		Co_0.01		2.23E-04	1.57E-04	0.94	0.97	1.61E-04	6.22E+03
		Co_0.001		1.54E-04	3.59E-03	0.84	0.92	3.94E-03	2.54E+02
		Co_0		1.67E-04	2.61E-03	0.84	0.92	2.86E-03	3.50E+02

(b) electron

Sample	Condition	Electrolyte	Wavelength (nm)	$\Delta OD_{e_{t=0}}$	$\tau_{ww,e}$ (s)	β_e	Γ_e	$\tau_{obs,e}$ (s)
PorY1	Full coverage	I_1	800	2.50E-04	1.16E-03	0.15	389.00	3.008
			1200	5.73E-05	7.40E-02	0.55	0.94	0.127
		I_0.1	800	2.24E-04	9.36E-03	0.30	2.95	0.094
			1200	8.77E-05	1.52E-01	0.78	0.90	0.175
		I_0.01	800	1.43E-04	9.48E-03	0.48	1.04	0.021
			1200	8.58E-05	7.65E-02	0.57	0.92	0.123
		I_0.001	800	1.12E-04	6.48E-02	0.50	1.00	0.130
			1200	1.34E-04	5.04E-02	0.26	4.63	0.894
		I_0	800	1.16E-04	4.70E-02	0.44	1.15	0.123
			1200	3.53E-05	6.30E-02	0.54	0.95	0.112
		Co_1	800	1.41E-04	3.05E-03	0.20	29.16	0.456
			1200	1.87E-04	1.10E-06	0.15	389.00	0.003
		Co_0.1	800	1.67E-04	1.42E-02	0.26	4.63	0.249
			1200	8.14E-05	6.15E-02	0.71	0.89	0.078
		Co_0.01	800	1.18E-04	5.73E-02	0.48	1.04	0.124
			1200	8.40E-05	2.83E-01	0.56	0.93	0.470
		Co_0.001	800	1.35E-04	6.00E-02	0.51	0.98	0.115
			1200	1.26E-04	2.30E-02	0.38	1.50	0.092
		Co_0	800	1.28E-04	3.70E-02	0.46	1.09	0.088
			1200	1.05E-04	1.52E-02	0.21	16.87	1.210

	Doctor-bladed reduced dye	I_0	1200	2.72E-04	1.43E-03	0.34	1.90	0.010
	Doctor-bladed CDCA-introduced		1200	2.91E-04	6.00E-02	0.20	24.00	7.200
	35%-coverage	I_0.01	800	1.39E-04	2.10E-02	0.52	0.97	0.039
			1200	9.83E-05	9.60E-02	0.74	0.89	0.115
		Co_0.01	800	2.15E-04	1.04E-02	0.49	1.02	0.022
			1200	8.45E-05	7.35E-02	0.53	0.97	0.135
Por	Full coverage	I_1	800	1.12E-04	1.73E-01	0.69	0.89	0.223
		I_0.1		1.07E-04	5.73E-02	0.55	0.94	0.098
		I_0.01		1.02E-04	3.17E-02	0.41	1.28	0.099
		I_0.001		9.67E-05	2.51E-02	0.48	1.04	0.054
		I_0		9.27E-05	3.00E-03	0.30	2.78	0.028
		Co_1		6.60E-05	3.20E-02	0.42	1.21	0.091
		Co_0.1		1.36E-04	1.57E-02	0.20	24.00	1.856
		Co_0.01		9.72E-05	1.19E-01	0.44	1.14	0.308
		Co_0.001		9.94E-05	6.00E-02	0.64	0.89	0.083
		Co_0		1.29E-04	6.00E-02	0.47	1.06	0.135
		I_0	1200	7.63E-05	1.10E-03	0.28	3.76	0.015

(c) rise of PorY1

Condition	Electrolyte	Wavelength (nm)	$\Delta OD_{D^+_{t=0}}$	$\tau_{1_{ww_D^+}} (s)$	$\beta_{1_D^+}$	$\Gamma_{1_D^+}$	$\tau_{1_{obs_D^+}} (s)$	$k_{1_{obs_D^+}} (s^{-1})$
Full coverage	I_0	800	2.19E-04	2.80E-08	0.24	7.60	8.90E-07	1.12E+06
		1200	9.39E-04	2.80E-08	0.24	7.60	8.90E-07	1.12E+06
	Co_0	800	4.90E-05	1.99E-07	0.21	15.32	1.43E-05	6.99E+04
		1200	8.24E-04	1.99E-07	0.21	15.32	1.43E-05	6.99E+04
Doctor-bladed reduced	I_0	1200	1.15E-03	8.50E-08	0.35	1.76	4.27E-07	2.34E+06

dye								
Doctor-bladed CDCA-introduced		1200	9.50E-04	8.50E-08	0.37	1.51	3.47E-07	2.88E+06

Table A6. Hole transfer yield in PorY1 / TiO₂ calculation form

Experimental		Calculated	
Peak Δ Abs. at 700-900 nm	0.05	Δ Abs(Por) ⁺⁺ / Δ Abs(Cb-TPA) ⁺⁺	0.23
Peak Δ Abs. at 1100-1300 nm	0.22	Δ mOD(Por ⁺ -(Cb-TPA)) / Δ mOD(Por-(Cb-TPA) ⁺)	0.23
Δ mOD _{t=2μs} at 800 nm#	0.43	Numbers ratio of Por ⁺ -(Cb-TPA) / Por-(Cb-TPA) ⁺ at t=2 μ s	2.25
Δ mOD _{t=2μs} at 1200 nm#	0.83	Hole transfer yield %	31
Assumption: Δ mOD at 800 nm was only attributed by Por ⁺ -(Cb-TPA); the ratios of Δ Abs(Por) ⁺⁺ / Δ Abs(Cb-TPA) ⁺⁺ and Δ mOD(Por ⁺ -(Cb-TPA)) / Δ mOD(Por-(Cb-TPA) ⁺) are the same.			

I. Photovoltaic performance

TableA7. Photovoltaic performance of the devices fabricated by the investigated sensitizers for checking dispersion forces in Chapter 7.

Thickness (μ m)	Dye	J_{SC} mA cm ⁻²	V_{OC} mV	FF	η %	Dye loading Γ ($\times 10^{-4}$ mol cm ⁻³)	τ (s) at $ED=1.5 \times 10^{18}$ cm ⁻³
2.8	Por_4%	0.91	540	0.69	0.34	0.05	0.001
	Por_12%	2.63	605	0.63	1	0.14	0.012
	Por_full	6.67	705	0.56	2.64	1.2	0.053
	PorR_4%	0.96	630	0.68	0.41	0.06	0.03
	PorR_12%	2.15	655	0.67	0.94	0.16	0.052
	PorR_full	5.91	695	0.66	2.7	1.4	0.117

J. References

- (1) Barnes, P. R. F.; Liu, L.; Li, X.; Anderson, A. Y.; Kisserwan, H.; Ghaddar, T. H.; Durrant, J. R.; O'Regan, B. C. *Nano Lett.* **2009**, 9, 3532.

- (2) Halme, J.; Boschloo, G.; Hagfeldt, A.; Lund, P. *J. Phys. Chem. C* **2008**, *112*, 5623.
- (3) Barnes, P. R. F.; Miettunen, K.; Li, X.; Anderson, A. Y.; Bessho, T.; Grätzel, M.; O'Regan, B. C. *Adv. Mater.* **2013**, *25*, 1881.
- (4) Anderson, A. Y.; Barnes, P. R. F.; Durrant, J. R.; O'Regan, B. C. *J. Phys. Chem. C* **2011**, *115*, 2439.
- (5) Anderson, A. Y.; Barnes, P. R. F.; Durrant, J. R.; O'Regan, B. C. *J. Phys. Chem. C* **2010**, *114*, 1953.